Solid Form Selectivity in Multi-Component Molecular Crystals: from Batch to Continuous

Lunt, Ruth

Award date:
2019

Awarding institution:
University of Bath

Solid Form Selectivity in Multi-Component Molecular Crystals: from Batch to Continuous

Ruth Angharad Lunt

A thesis submitted for the degree of Doctor of Philosophy

University of Bath

Department of Chemistry

Supervisor: Professor Chick Wilson

June 2019

Abstract

The work presented in this thesis encompasses the crystallisation of multi-component crystalline systems, including co-crystals and salts, for solid form control, focusing on a transfer from batch to continuous crystallisation. The work forms part of the EPSRC funded Future Manufacturing Hub in Continuous Manufacturing and Advanced Crystallisation (CMAC).

The opening chapters introduce the background to the project, including the broader context in which the project sits, with the move towards developing continuous crystallisation and manufacturing of pharmaceuticals. Accounts of the methodology used are given, including the importance of the solid-state, crystallisation methods, polymorphism and co-crystallisation and salt formation for multi-component molecular materials.

Chapters 4-5 introduce the primary model system under investigation, urea barbituric acid (UBA), and document the work conducted on the system to further understand the polymorphism of the co-crystal system, achieve selective control of production of two of the UBA polymorphs, including the metastable form III (the relative thermodynamic stabilities of forms I and III are established, through competitive slurrying experiments) and the access of a novel polymorphic form. Chapter 5 discusses the use of seeding in batch cooling crystallisation to allow for control over the resultant solid form as well as demonstrating the transfer of UBA crystallisation, to yield metastable form III, from batch to continuous. Two continuous crystallisation platforms, the Continuous Oscillatory Baffled Crystalliser (COBC) and the Kinetically Regulated Automated Input Crystalliser (KRAIC) are described and their use investigated.

Chapter 6 focuses on the crystallisation of two novel multi-component systems using the barbituric acid derivative thiobarbituric acid (TBA) as the target compound. These multi-component systems are shown to be salt systems, with hydrogen transfer occurring from the target molecule, TBA, to the counter-ion. Their crystallisation is shown to be transferable from evaporative to slurrying and cooling crystallisation techniques in batch. Chapter 6 also demonstrates the successful transfer of the crystallisation of these two salt systems from batch to continuous platforms, using both the COBC and KRAIC.

Acknowledgements

Firstly I would like to thank Prof. Chick Wilson for giving me the opportunity to study for a PhD within his group and for all his support over the last four years.

Thank you to everyone in the Wilson group, past and present for making the last four years an enjoyable experience. I owe a huge thank you to Lauren Agnew who has been the most incredible support, I could never have stuck with it without you! (You were the best fake post doc I could have ever asked for.) Thank you, Anneke, for making my master's project so enjoyable that I decided to stick around for another four years. Your help and support throughout my masters and PhD has been incredible. Here's to many more years of friendship. To my little protégés, Lois and Polly, you're the best distractions I could ever have asked for, and if I can make it through this, so can you. Finally, to Lauren Hatcher, you joined our group at the perfect time to help me over the last few hurdles. Thank you for all your help and advice over the last year, especially all the help with my thesis. Thank you Rich, for being a great masters student and smashing out some great work and being a great continuous crystallisation partner.

To everyone in the particle sciences team at GSK, especially Dr Mei Lee, for allowing me to come and use your kit, thank you. It was an amazing opportunity and I don't think I have ever worked so hard in my life. Without your help and instruments this thesis would have some huge gaps! Thank you Mei, for all our Skype calls and all of the help you have given me over the last few years, it has made a huge difference and I am very grateful. Thank you to everyone in the particle sciences team for making me feel so welcome and always being willing to lend a hand, especially Amy Woods for all your help with the understanding UBA's thermal behaviour.

Thank you to everyone at Pfizer in the CTL and FAST teams for giving me the amazing opportunity to come out to the US for placement. I learnt more in those 11 weeks than I could ever have imagined and had an amazing time. Thank you Dr Kevin Girard, for all your help and support during my time at Pfizer, as well as when I got back home. Thank you Karen Sutherland, for Thanksgiving and looking out for me during my time in the US and after I got home.

Finally, thank you so much to all of my family and friends for all the support they have given me during my studies. Especially my Mum, Dad and Dan, I couldn't have done it without you.

This thesis is dedicated to Daniel Rixson

'I am glad that you are here with me. Here at the end of all things.'

Table of Contents

List of Figures

List of Tables

List of Abbreviations

API	Active pharmaceutical ingredient
BFDH	Bravais-Friedel-Donnay-Harker
CCD	Charged coupled device
CCDC	Cambridge Crystallographic Data Centre
CLD	Chord length distribution
CMAC	Continuous Manufacturing and Advance Crystallisation
CNT	Classical nucleation theory
COBC	Continuous oscillatory baffled crystalliser
CRD	Cambridge Reactor Designs
CSD	Crystal size distribution
CSD	Crystal Structure Database
DoE	Design of experiments
DSC	Differential scanning microscopy
EMA	European Medicines Agency
EtOH	Ethanol
FDA	Food and Drug Administration
FBRM	Focused beam reflectance measurements
FEP	Fluorinated ethylene propylene
Galden	Perfluoropolyether Galden SV110
IPA	Isopropanol
KRAIC	Kinetically Regulated Automated Input Crystalliser
LAG	Liquid assisted grinding
MSMPR	Mixed suspension mixed product removal
MSZ	Metastable zone
MSZW	Metastable zone width
NMR	Nuclear magnetic resonance
OFR	Oscillatory flow reactor
PAT	Process analytical technologies
PSD	Particle size distribution

PVM	Particle vision and measurement
PXRD	Powder X-ray diffraction
RBF	Round bottom flask
RT	Residence time
RTD	Residence time distribution
R&D	Research and design
STR	Stirred tank reactor
TBA	Thiobarbituric acid
TBAISNAM	Thiobarbituric acid isonicotinamide
TBANAM	Thiobarbituric acid nicotinamide
TGA	Thermogravimetric analysis
TST	Two step theory
T_{sat}	Saturation temperature
UBA	Urea barbituric acid
VT PXRD	Variable temperature powder X-ray diffraction

Chapter 1 - Introduction

1.1 Context of Research

Crystallisation is one of the most important steps in the manufacture of commercially available compounds, especially within the pharmaceutical industry, allowing for both separation and purification of the active pharmaceutical ingredient (API) from the final reaction mixture. A large proportion (> 80 %) of commercially available APIs are marketed in their solid form, and must therefore be subsequently crystallised post synthesis.[1] To ensure the high levels of purity needed for a marketed drug product, as well as ensuring the correct solid form is acquired, careful control over the crystallisation process is vital. This control over the crystallisation process not only allows for selective crystallisation in terms of the resultant solid form, but can also yield the desired level of uniformity throughout the crystalline material; uniform crystalline product allows for improved flow properties as well as increased ease of handling for secondary processes including filtration, drying and tablet formation.[2-6]

When compared to other unit operations and processing steps such as distillation and extraction, the level of understanding and generalisation of crystallisation is not of the same degree. In recent years, however, the study of crystallisation has become a major research area,[7, 8] with several national centres focused on the study of crystallisation being established and funded both by research councils and industrial partners. One of these centres is the EPSRC funded Future Manufacturing Hub in Continuous Manufacturing and Advanced Crystallisation (CMAC); a collaboration between seven UK universities and eight tier one industrial sponsors. This research forms part of that program. Nevertheless, there is still a long way to go before the fundamentals of nucleation and crystal growth, as well as the issues associated with scale up, are fully understood.[9]

1.2 Types of Crystalline Compounds

Crystals are a class of solids that possess long range order throughout the entirety of the solid phase, and can be defined by their characteristic repeating array of molecules. The way in which the molecules arrange themselves within these repeating arrays can significantly modify the physical properties of the solid.[10, 11] Many pharmaceutical compounds can exist in multiple solid forms, including both amorphous (no long range order) and crystalline forms. If a molecular entity can exist in more than one crystalline packing arrangement in the solid state, it exhibits polymorphism. Crystalline states of a compound may also incorporate solvent molecules, to form a solvate, or a secondary or tertiary molecular species to yield a multi-component crystal such as a salt or a co-crystal. In some cases solvates and hydrates (where the solvent in the crystal is water)

are referred to as pseudopolymorphs.[12, 13] Figure 1.1 displays a pictorial representation of the different types of solid forms.

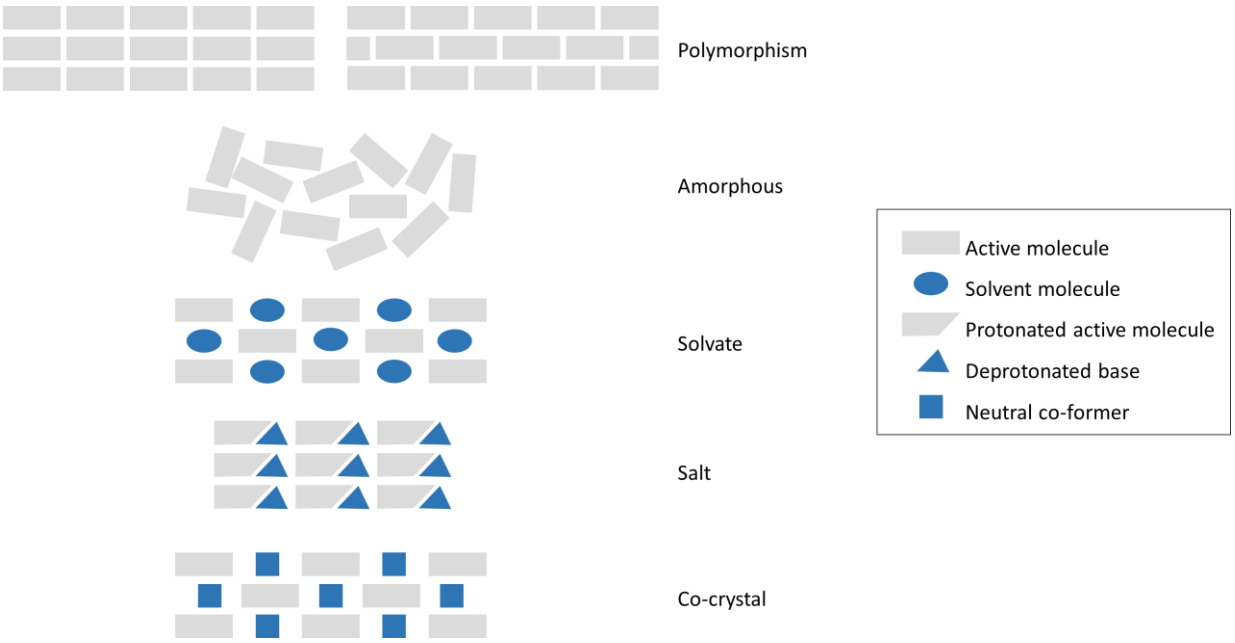

Figure 1.1: Pictorial representation of solid forms.

1.2.1 Polymorphism

Polymorphism is the ability for a chemical species to exist in multiple crystalline forms and arises when the molecular building blocks that make up the crystalline solid pack together differently within the crystalline structure (Figure 1.1). This difference in packing arrangements can lead to differences in the physical properties of the solid due to the variances in the free energies of each solid form. Properties such as solubility, bioavailability and thermal stability can all be affected by polymorphism.[14-17] In pharmaceutical production the ultimate goal is to find the solid form of the API with the optimal qualities for the proposed use, and to deliver a crystallisation process that yields the selective crystallisation of the chosen form. In order to determine the optimal polymorphic form of an API, polymorph screening is usually conducted in an aim to identify all relevant solid forms of the drug. The choice of which polymorphic form is to be used commercially is usually governed by a balance between its thermodynamic stability, solubility and bioavailability. The thermodynamically stable polymorph, the only form that will not convert to a different form over time, is usually chosen for the API product. However, in some cases a metastable form may be chosen due to it possessing enhanced physical properties such as a significantly higher solubility, and hence often increased bioavailability in comparison to the thermodynamically stable form.[2, 14, 16, 17]

The thermodynamic relationship between polymorphs with regards to temperature dependence must also be determined, as this can have a significant impact on

polymorphic transitions. Figure 1.2 below displays phase diagrams for monotropic and enantiotropic polymorphs. If a dimorphic system is monotropic then one polymorph will be the thermodynamically stable form, regardless of the temperature. However, if the polymorphic forms display enantiotropy then at a specific temperature, T_t, the relative stability of the two polymorphs will switch. At the transition temperature (T_t) the two polymorphs have the same free energy and can reversibly transform into one another. The enantiotropic example depicted in Figure 1.2 shows that at any temperature below T_t, form II is the thermodynamically stable polymorph, but above this temperature form I becomes the more stable form. If the transition temperature, T_t, is below the respective melting points of the polymorphs a transition between the two forms may be seen upon heating, depending on kinetics. However, if the melt of form II is lower than T_t the transition from form II to form I would not be observed upon heating form II. [18-22]

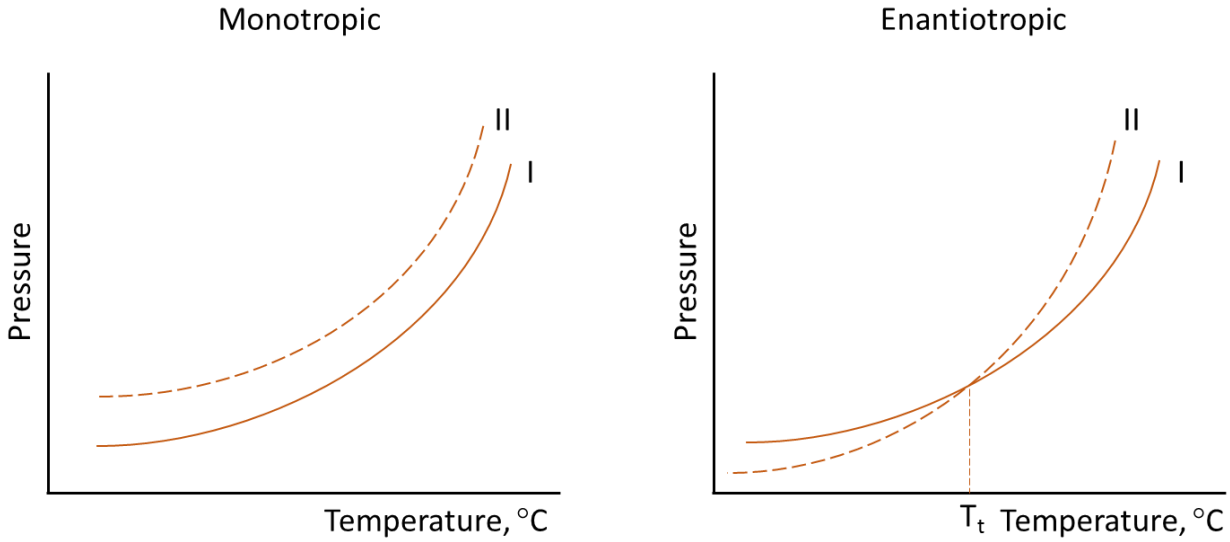

Figure 1.2: Phase diagrams of monotropic and enantiotropic polymorphs.

Polymorph screening to attain an advanced knowledge of an API's polymorphic behaviour, as well as the relationship between these polymorphs, before it is made commercially available is unsurprisingly critical. The late appearance of an additional polymorph can have detrimental effects to the future production of the API.[14] An example of this is the case of Ritonavir, a drug used in the treatment of HIV. The discovery of the thermodynamically stable form of the API was not made until two years after the drug became commercially available. The marketed form, form I, was metastable and soon became impossible to access from crystallisation processes and, as a result, the drug had to be withdrawn from the market until an appropriate crystallisation route to the thermodynamically stable form could be identified. This not only had a large financial cost to the manufacturer, Abbot Laboratories, but it also resulted in a period of several years where the drug was no longer available for patients.[23-25] The discovery of all polymorphic forms of an API and their thermodynamic relationship is therefore of the upmost importance before a drug goes to market; as well as the selection of the appropriate polymorphic form required for the desired purpose.

Careful design and control over the crystallisation process of the API is necessary for guaranteed production of the desired form.

1.2.2 Solvates

A solvate is defined as a crystalline solid that incorporates solvent molecules into its crystal structure.[13, 26] The most common form of solvate is a hydrate, where water molecules are incorporated into the molecule's crystal structure. The ease of incorporating water molecules into a structure, in comparison to organic solvents, arises from the small size of the water molecule, as well as its high propensity to form hydrogen bonds. The production of solvated forms of an API may, in some cases, be desirable, with the solvates occasionally possessing enhanced properties such as greater thermal stability, higher solubility in certain solvents or ease of handling. However, solvates can often have issues with solvent loss over time and subsequent degradation or change of solid form, which can significantly reduce their shelf-life. In cases where a solvate is unavoidable, but not the desired outcome, drying may be used to remove the solvent molecules from the crystal structure. However, in some cases this can have detrimental effects on the structural integrity of the crystalline compound, with removal of solvent often destroying the crystal structure.[20, 26-28]

1.2.3 Salts

A salt is defined as a crystalline solid containing more than one type of ion. In pharmaceutical salts, at least one of the ionic components comprises an API.[13] Salt formation is a well-established practice to alter the physical properties of a substance. For many years pharmaceutical products have been dispensed in salt form as these can often possess much higher solubility, thermal stability and/or chemical stability in comparison to the pure API form(s).[29] Over 50 % of the APIs approved within the US in 2013 were pharmaceutical salts.[30] A drawback of salt formation, however, is that it relies on the API being ionisable and therefore requires careful selection of appropriate counter-ions with complementary pKa values.[31] The general rule when seeking applicable counter-ions is that the pKa values should differ by at least two pH units, however pKa values of acids and bases can differ depending on the solvent medium, and this can further complicate the counter-ion selection.[32-34] This being said, the most common method for increasing an acidic or basic drug's solubility and bioavailability is by salt formation.[35]

1.2.4 Co-crystals

A molecular co-crystal is defined as a multi-component crystal system containing two or more uncharged molecular compounds that are solids under ambient conditions. The production of pharmaceutical co-crystals, where at least one of the components is an API, is a relatively new field that has started to attract increased interest in both academia and industry in recent years.[13, 32, 36-38] Many pharmaceutical compounds do

not make it to the commercial market due to their low solubility levels, and in some cases co-crystallisation could be a means of increasing this solubility and hence the bioavailability of the drug.[39, 40] The difference in the solubility of the different polymorphic forms of a single component system is typically up to a factor of two. However, incorporation of a co-former into the API crystal matrix can result in significantly higher solubility levels in comparison to the pure API.[31]

Enhancement of other physical properties of a compound, without interfering with the chemical behaviour, can also be achieved by co-crystallisation, as with salt-formation.[41, 42] In some instances, however, co-crystallisation may be seen as more desirable than salt formation, in part due to the need for an API to be ionisable in order to form a salt. Co-crystallisation, on the other hand, relies purely on intermolecular interactions and it therefore opens up a new range of potential API – co-former combinations to be investigated.[31] The recent upsurge in the growth of pharmaceutical co-crystallisation, not only arising from the opportunity for API property enhancement, but also the re-patentability of co-crystal drug products, has led to significant concerns over the regulatory status resulting in new regulations and guidance being published by the Food and Drug administration (FDA) and the European Medicines Agency (EMA) to clarify the status of co-crystals.[43, 44]

It is important to bear in mind that, similar to single component systems, co-crystals, salts and solvates all possess the ability to display polymorphism, and this in itself can lead to further changes in the physical properties of the system.[45-47] Discovery of all polymorphic forms, and determination of relative stabilities, of both the single and any multi-component pharmaceutical crystals is therefore vital before a drug is made commercially available.

1.3 Crystal Engineering and Intermolecular Interactions

Crystal engineering is defined by Desiraju as '*the understanding of intermolecular interactions in the context of crystal packing and in the utilisation of such understanding in the design of new solids with desired physical and chemical properties'*.[48] It uses the concept of molecular synthons – molecular fragments and the intermolecular interactions between them – to predict and design crystalline systems that have molecular packing arrangements which may encourage desirable properties such as a heightened solubility or an increase in thermal stability. Crystal engineering is based upon the assumption that these synthons are regularly occurring building units in the crystal and will therefore likely define the entire crystal structure. The ability to be able to predict and control the physical properties of a system through its crystal structure is unsurprisingly appealing and there has been significant growth and development in this field over the past 50 years. There are numerous reported cases were there has been significant success with engineering of crystal structures to improve particular properties of the target material.[36, 49-53] Recently, the use of computer modelling to predict crystal structures has increased, with the ability to accurately describe a range

of potential crystal structures and their properties for molecular compounds in the solid state. However, there is a still a long way to go until the challenges regarding crystal structure prediction are overcome.[54-56]

1.3.1 Hydrogen Bonding

Within crystal structures the intermolecular interactions present are largely dominated by hydrogen bonds. Hydrogen bonds are formed when a hydrogen atom is covalently bonded to an electronegative atom (A), such that the hydrogen becomes partially positively charged ($H^{\partial+}$). This hydrogen atom can then go on to form an attractive interaction with a second atom (B) which possesses either a lone pair of electrons or polarizable π-electrons. The resulting, bridging interaction, A-H···B, is neither covalent nor simply a London / van der Waals interaction and lies somewhere between these two extremes.

The strength of the bonding interaction will be determined by the nature of both A and B.[57] A wide variety of hydrogen bonds can be seen in the solid state and range in energies between 1 - 170 kJ mol^{-1}, with strong hydrogen bonds (60 - 170 kJ mol^{-1}) acting almost as covalent bonds with very strong directionality, and weak hydrogen bonds (< 17 kJ mol^{-1}) more akin to van der Waals forces of attraction, showing less directionality.[58] The growth of a crystal is largely dominated by the formation of moderate and strong hydrogen bonds and molecules will likely arrange themselves within a crystal in an attempt to maximise the formation and strength of these interactions.[56]

Table 1.1: Classification of hydrogen bonds.[56]

	Strong	Moderate	Weak
A-H···B interaction	Mostly covalent	Mostly electrostatic	Electrostatic
H···B bond length (Å)	~1.2 - 1.5	~1.5 - 2.2	~2.2 - 3.2
A·····B bond length (Å)	2.2 - 2.5	2.5 - 3.2	3.2 - 4.0
A-H···B bond angle (°)	175 - 180	130 - 180	90 - 150
Bond energy (kJ mol^{-1})	60 - 170	17 - 60	< 17

Hydrogen bonds can form between a multitude of functional groups, and the functionalities of both the donor and the acceptor groups will determine the resultant strength of the hydrogen bond. Hydrogen bond strength tends to be classified by the intermolecular bond lengths and angles, as can be seen in Table 1.1.[57] They can also be classified by the position of the hydrogen atom within the bond, for example, weak or moderate hydrogen bonds have the hydrogen atom residing mostly on the donor atom (A). With strong hydrogen bonds, however, the hydrogen atom will be more equally attracted to both the donor and the acceptor atoms.[59] Strong hydrogen bonds will arise when the acceptor atom is electron rich and/or when the donor group is electron

deficient.[57] Due to the positioning of the hydrogen atom in a strong hydrogen bond, there is no longer a clear A-H covalent bond and subsequently the definition must be altered. In strong hydrogen bonds the H···B interaction is now of almost equal strength to A-H and this consequently results in the overall A-B distance being almost equal to the sum of the two atomic radii; this is only true in the case of strong hydrogen bonds.[60]

It is unsurprising that within a crystal structure the molecules with appropriate functionalities will arrange themselves in a packing arrangement in an attempt to maximise the number and strength of the hydrogen bonding interactions within the solid state crystal.

1.3.2 π- π Stacking Interactions

Another important class of intermolecular interactions that can play a substantial role in crystal structure formation is π- π stacking. The strong attractive interactions between adjacent π systems, such as aromatic rings, arises from attractive interactions between π-electrons and the σ-framework outweighing the repulsive forces between π-electrons. Aromatic rings of neighbouring molecules can arrange themselves in a variety of different orientations, each of which can allow for π- π stacking interactions to form. The way in which the aromatic rings arrange themselves with respect to one another can be influenced by the substituents on the rings, due to the resultant polarisation of the electron cloud. For example, species with unsubstituted aromatic rings tend to form edge-on stacking, whereas rings with large substituents form parallel stacking arrangements such as offset π- stacking – face-to-face stacking is rarely observed. [61-63]

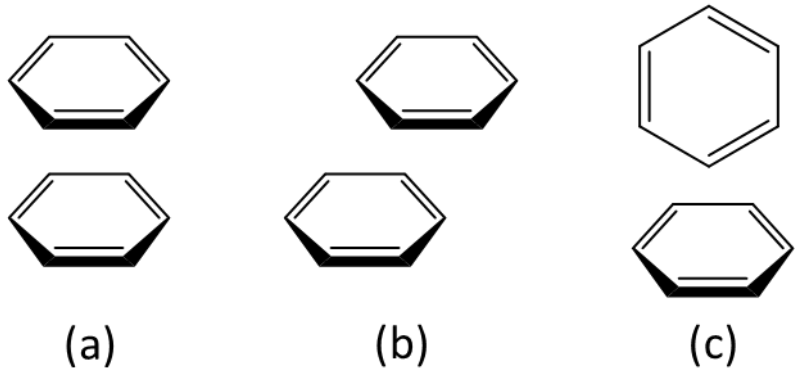

Figure 1.3: (a) Face-to-face π -stacking, (b) offset π -stacking and (c) edge-on π -stacking.

1.4 Crystallisation

Crystallisation describes the process that allows access to the phase transitions that yield crystalline solids from either a liquid solution or gaseous phase. Careful control over the crystallisation process can allow for direct control over the resultant crystal structure of the solid (otherwise known as the solid form), which is of high importance in both the pharmaceutical and fine chemicals industry. There are many methodologies by which to conduct a crystallisation process, each displaying varying levels of

sophistication. However, regardless of the methodology used to achieve crystallisation, all processes require the generation of supersaturation within the system.[64, 65]

1.4.1 Supersaturation

To design a successful crystallisation process a thorough understanding of the solubility of the system is required. The solubility of a solute is defined as the maximum amount of solute that will dissolve in a given solvent at a given temperature and pressure; Figure 1.4 below shows a typical solubility curve. Below the solubility curve the solution is undersaturated and more solute can dissolve into the solution.

For crystallisation to occur, supersaturation must be achieved within the system as this is the thermodynamic driving force for the crystallisation process. Supersaturation is defined as the point at which a solution has a higher concentration than that of its equilibrium solubility – the amount of solute that can dissolve at a given temperature and pressure (Figure 1.4 – solid line).

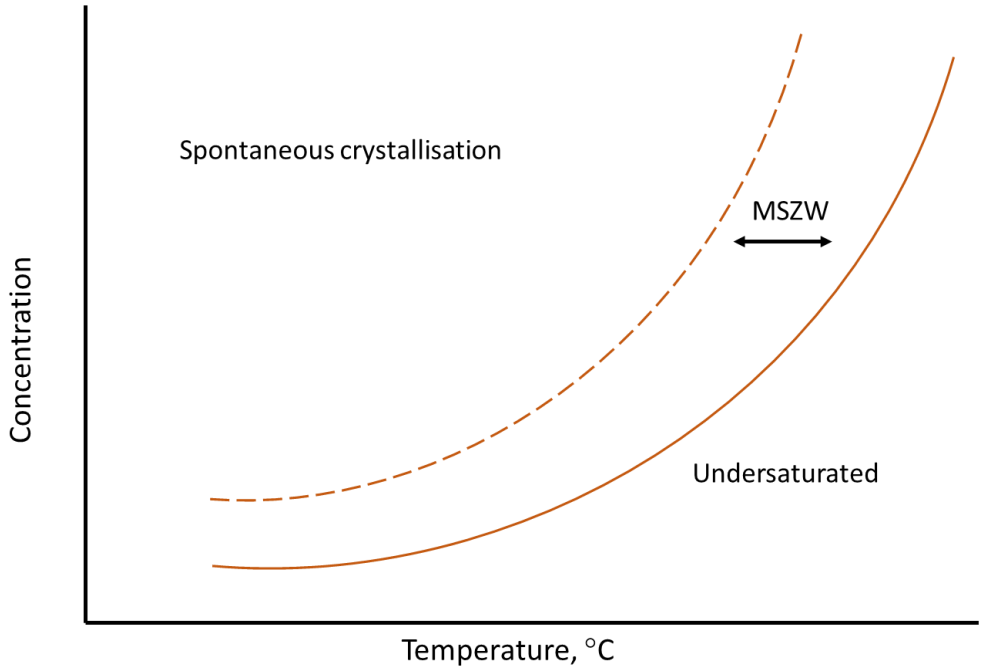

Figure 1.4: Equilibrium solubility curve - concentration of solute in solvent versus temperature. The solid line represents the solubility whilst the dashed line represents the metastable zone boundary.

Supersaturation can be expressed in a number of ways with regards to the solution concentration (c) and the solubility concentration (c*). Equation 1.1 describes the difference in solution concentration (c) and the equilibrium solubility concentration (c*), with the difference between the values, ΔC, representing the driving force for crystallisation: the larger the value of ΔC, the greater the driving force for crystallisation. The supersaturation ratio, S (Equation 1.2), between the two concentration values can also be used to describe supersaturation; the value of S will always be greater than 1 when the system is supersaturated. Equation 1.3 defines the relative supersaturation,

σ, and is dimensionless. Supersaturation can also be determined thermodynamically by the difference between the chemical potential of a molecular system in its equilibrium state and its supersaturated state ($\Delta\mu = \mu_{ss} - \mu_{eq}$).[3, 66, 67]

$$\Delta C = c - c^* \qquad \text{(Equation 1.1)}$$

$$S = \frac{c}{c*} \qquad \text{(Equation 1.2)}$$

$$\sigma = \frac{\Delta C}{C*} = S - 1 \qquad \text{(Equation 1.3)}$$

There are many ways in which supersaturation can be achieved in a system, but all systems will possess an inherent kinetic barrier to crystallisation and supersaturation must surpass this for spontaneous nucleation to occur. This region where a supersaturated system can exist, undisturbed, without nucleating is known as the metastable zone (MSZ). For spontaneous nucleation to occur the system must move past this limit by an increase in supersaturation. The equilibrium solubility of a system is governed by thermodynamics and for each solute-solvent system the solubility values will not change based on the crystallisation environment. However, nucleation is governed by kinetics and these kinetics determine the metastable zone width (MSZW) and hence, how much supersaturation is required within the system to generate nuclei. As nucleation and the MSZW are kinetic factors they possess an innate variability depending on the crystallisation environment, with factors such as impurities, stirring and scale having profound effects on the MSZW.

1.4.2 Nucleation

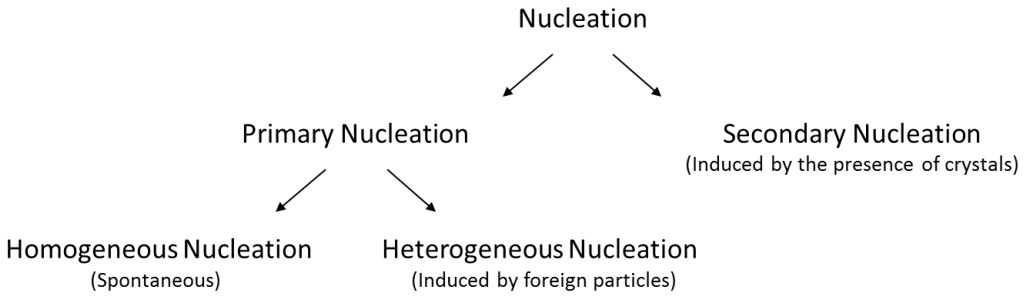

Figure 1.5: Nucleation mechanisms.

Once supersaturation has been achieved the formation of crystal nuclei can occur within the system and it is these nuclei that go on to grow during the crystallisation process. Within a crystallisation process there are several classes of nucleation (Figure 1.5) that can occur, with the main mechanisms being primary and secondary nucleation. Primary

nucleation occurs in a system without presence of any crystalline solute particles and can be either homogeneous or heterogeneous. Homogeneous primary nucleation is entirely spontaneous and arises in a system once the concentration of the solution has surpassed the metastable limit. Due to this spontaneity, little control can be exerted over the nucleation and subsequent crystal growth.[65, 66, 68-70]

The exact mechanism of how nuclei are formed within a homogeneous solution is not known; the difficulty in studying nucleation arises from the size of the nuclei falling in the range of ten to several thousand molecules, as well as the variable time scales for the formation of nuclei (from seconds to day).[5] However, there are two main theories: classical nucleation theory (CNT) and the two step theory (TST). The former theory assumes that within a solution minute clusters of solute are formed by sequential collisions of molecules. Once a pair of molecules has come together in solution in a preferential orientation, a third molecule then adds onto the pair and so on until a cluster is formed. During the formation of this cluster the overall free energy (ΔG) is a balance between the free energy of the surface, $\Delta G_{surface}$, and the free energy of the phase transformation, ΔG_{volume}. As the size of the cluster increases the surface area/volume ratio is decreased and a point will be reached where the dissolution of the cluster becomes less favourable than the addition of new molecules. This point is known as the critical size (r_c) and it is where the intermolecular forces within the nuclei begin to outweigh the effect of the surrounding particles. Once the nuclei has reached critical size it is now stable, and the propensity for it to dissolve back into solution has been overcome; the free energy of the nuclei decreases and crystallisation via growth of the cluster now becomes favourable. [21, 64, 71-73]

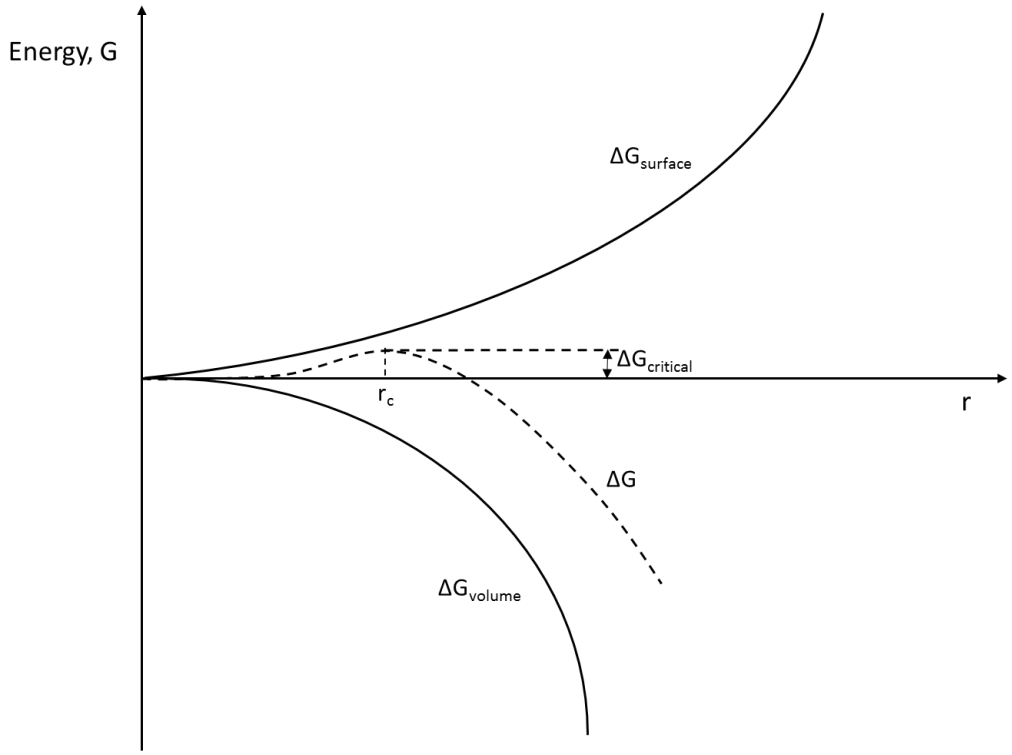

Figure 1.6: Free energy diagram for nucleation.

Figure 1.6 depicts the free energy diagram for nucleation in a homogeneous solution, and displays how a nuclei of a size greater than the critical size is stable in the solution. It can be seen, however, that there is an energy barrier to this stability, $\Delta G_{critical}$. In a homogeneous solution this energy barrier can be overcome by the natural fluctuations of energy that would be present in the system. Once supersaturation is reached these fluctuations can give rise to the spontaneous formation of nuclei and hence lead to crystallisation of the solute from the solution.[21, 71, 72]

The classical nucleation theory does, however, possess limitations due to the assumptions made when designing the model. The main drawback of this theory is that in reality, individual molecules are unlikely to add onto a cluster one at a time, and instead it is much more likely that these clusters rearrange whilst being assembled. The two step nucleation theory (TST) builds upon this assumption. The TST was initially used in the understanding and description of the crystallisation of proteins, however studies have shown that this model holds for the crystallisation of some small organic molecules as well.[5, 72] TST suggests that an initial disordered solute cluster, of sufficient size, forms which then undergoes reorganisation to yield the ordered structure of the crystal, as can be seen in Figure 1.7 below. It dictates that liquid-like clusters of solute form in areas of high solute concentration within the solution due to natural concentration fluctuations. These droplets, which are highly disordered in terms of the solute molecules, can undergo a reorganization to yield crystalline nuclei that are larger than critical size. These nuclei then undergo growth and result in crystallisation of the system.[5, 72, 74]

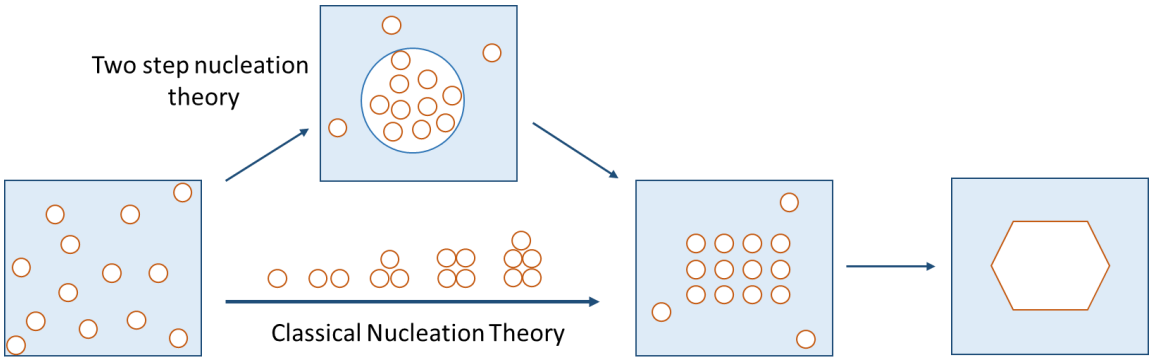

Figure 1.7: Pathways depicting classical nucleation theory (CNT) and the two step theory (TST).

Within a crystallising system, the level of supersaturation required for spontaneous primary nucleation is determined by $\Delta G_{critical}$; the larger the value for $\Delta G_{critical}$, the higher the level of supersaturation required in the system to achieve homogeneous nucleation. Heterogeneous nucleation, however, tends to require lower levels of supersaturation as it results from nuclei forming on already present surfaces. It can either be as a result of foreign particles (primary) or solute crystals (secondary) being present in the crystallisation media. The presence of foreign surfaces within a solution reduces the energy barrier, $\Delta G_{critical}$, for nucleation, as crystalline material can adsorb onto the available surfaces, thereby reducing the energy required to make new surfaces ($\Delta G_{surface}$). This consequently requires lower levels of supersaturation, in comparison to

spontaneous nucleation and unlike homogeneous nucleation, heterogeneous nucleation can occur within the MSZ.

Nucleation that is induced by the presence or addition of crystalline particles of the same species as the solute being crystallised is called secondary nucleation. The crystalline particles act as interfaces for further nucleation and can encourage the nucleation and growth of their crystalline form at the expense of other solid forms that could also be produced within the system. There are several different mechanisms by which secondary nucleation can transpire. One mechanism is when dry seeds are added to a supersaturated solution. Crystalline dust is often shed from the seed crystals and these small particles act as secondary nuclei and subsequent centres for growth. Shear nucleation is used to describe the case when secondary nuclei are produced from the surface of seed crystals as a result of the imposed shear forces in the system. The most common secondary nucleation mechanism, however, is the contact mechanism where secondary nuclei are created from crystal-crystal, crystal-wall and crystal-impeller collisions.[73, 75, 76]

1.4.3 Crystal Growth

Once nucleation has successfully occurred in the system, the stable nuclei will begin to grow into crystals that are visible to the naked eye. The level of growth in a system will be determined by the number of nuclei formed, the width of the metastable zone, and where the system lies within this zone when nucleation occurs. For example, Figure 1.8 below depicts a situation where a solution of concentration A is cooled until the metastable zone limit, B, is reached. At this point, spontaneous nucleation can occur, resulting in the concentration of solution dropping. If there is no further change in temperature, the concentration of solution will fall vertically once the stable nuclei are formed and subsequently grow. Growth will continue until the concentration of solution reaches that of the equilibrium concentration (point C).[3]

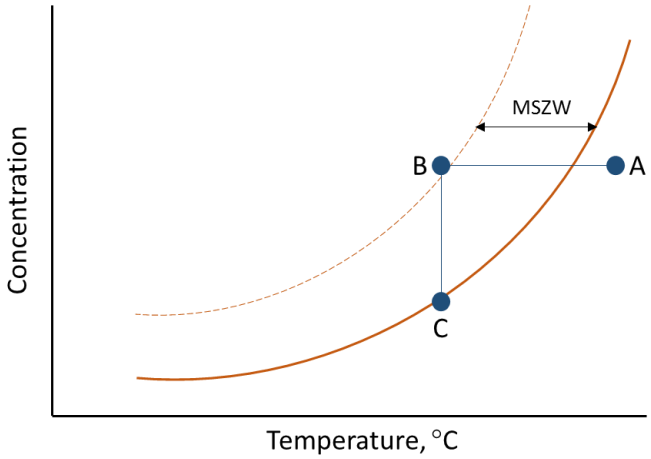

Figure 1.8: Solubility curve showing metastable zone (MSZ).

During the crystallisation process nuclei will have their crystalline surfaces exposed to a supersaturated solution. If the flux of molecules, or growth units, towards the surface is

greater than that of molecules leaving the surface, net growth of the crystalline particle will result. The incorporation of additional molecules onto the crystal surface, leading to growth, is dependent on both the strength and number of interactions forming between the surface and the arriving growth unit. Hartmann and Perdock introduced a classification system for how many interactions a growth unit makes with the crystal surface: when a surface is flat it is assumed that the number of interactions formed between this growth unit and the surface is one, when there is a step in the surface two interactions are assumed to be formed, and three interactions when there is an available kink site on the surface. [64, 71, 73, 77] Figure 1.9 below depicts a growing crystal surface with flat faces, steps and kinks.

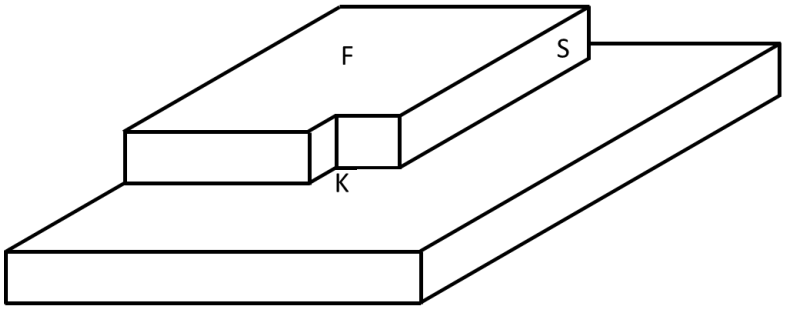

Figure 1.9: A three dimensional crystals showing flat faces (F), steps (S) and kinks (K).

Crystal growth theories are governed by the growth of flat faces, F. However, as these faces offer just one intermolecular interaction, of a greatly reduced strength in comparison to covalent bonds, addition of single molecules to these surfaces would not happen at a rate fast enough to explain the measurable rate of crystal growth. Instead, the growth rate is also governed by the generation of steps and kinks on these faces.[64] The Gibbs-Volmer theory suggests that during growth of a crystal solute molecules initially adsorb onto the flat face of a crystals surface, losing only one degree of freedom. These molecules then diffuse over the surface to a step or kink site before they are integrated into the crystal structure. This adsorption and subsequent surface diffusion results in the crystal growing in a layer-by-layer fashion.[78] However, for this to occur, steps and kink sites must be available on the crystal's surface. These sites can be created by the removal of a growth unit from the surface to start a new layer and this process will have an energy change attributed to it, ΔE. Equation 1.4 defines the α-parameter which describes how easy it is for a crystal surface to create steps and kinks in order to promote crystal growth. If the value for the α-parameter is low then the formation of steps and kinks on the surface will be fast, resulting in a fast growth rate as there will be many favourable binding sites.[77]

$$\alpha = \frac{\Delta E}{kT} \qquad \text{(Equation 1.4)}$$

There are several mechanisms by which crystal growth can occur: continuous growth, surface nucleation and spiral growth. The mechanism by which growth occurs for a crystallising system will be determined by the α-parameter. If the parameter is low the crystallising system will possess high surface roughness, with many kinks and steps on

the surface. These sites will act as binding sites and, as there are many of them, all approaching growth units will bind onto the surface. As the crystal grows by the addition of these growth units, new kinks and steps will be produced and so the growth is continuous and linearly proportional to the supersaturation in the system. This continuous growth occurs for systems when α is less than 3.[73, 77]

The second growth mechanism is known as surface nucleation, or the birth and spread model, and occurs when the value for α is between 3 and 5. As this value increases, the ease of creating a rough surface is decreased and the crystal surface tends to be much smoother, this results in much fewer kinks and steps, and hence, not every approaching growth unit can add onto the surface as with continuous growth. In this mechanism it is thought that some of these incoming growth units will simply return back to the solution phase, whereas others may attach to the surface to form two-dimensional nuclei. These nuclei will then spread across the surface as further molecules add onto the step points they create to build an additional layer. [64, 73, 77] This mechanism is depicted in Figure 1.10 (a).

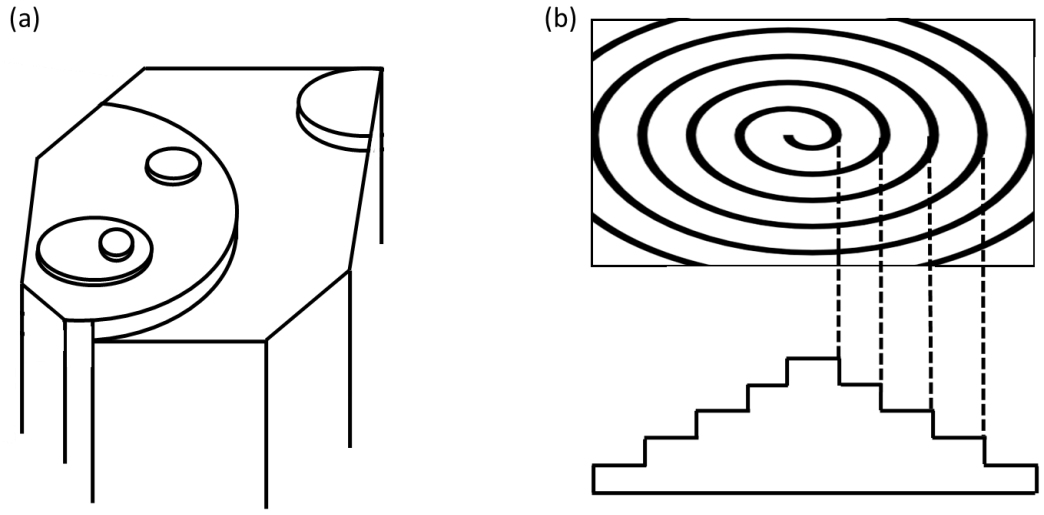

Figure 1.10: Two dimensional surface nucleation (a) and spiral growth (b) mechanisms.[77]

The final growth mechanism, the Burton-Cabrea-Frank model (BCF) occurs by spiral growth, or screw dislocation (Figure 1.10 (b)). As the α-parameter for a system increases above 5 the surface of the growing crystal is likely to be smooth due to the increased difficulty of creating steps and kinks. For sufficient crystal growth to occur in these instances a step must be created by an energetically cheap process to which approaching units can bind. As no crystal is perfect, each one will possess an array of defects and it is therefore incredibly unlikely that any crystal face will be perfectly flat and require completely fresh two-dimensional nucleation in order to grow. Frank *et al.* discuss the concept that crystals may inherently possess what is known as a screw dislocation, resulting in a self-generated step.[79, 80] These dislocations can arise as a result of stresses in crystal growth and remove the need for two-dimensional nucleation on the surface. Once the dislocation has permeated to the surface then the crystal face can grow in a spiral fashion eradicating the need for fresh two-dimensional nucleation on the surface as the surface will never be flat.[64, 73, 77]

1.4.4 Crystal Morphology

Crystal morphology, or habit, describes the crystal in terms of its external appearance. It quantifies the crystal in terms of both the size and shape of the crystal's external faces. The morphology of a crystal is a direct result of the relative growth rates of each of the crystal faces, with slow growing faces being expressed to a much greater extent than fast growing faces. As crystal growth is dominated by the formation of intermolecular interactions, the difference in the growth rates of each crystal face is largely dominated by what interactions are forming on that face. The formation of strong interactions, such as hydrogen bonds, results in fast growth rates, whereas much weaker interactions, such as van der Waals forces of attraction, lead to much slower growth rates. The type and strength of intermolecular interactions which form on each face is determined by the inherent molecular structure as well as the intrinsic crystalline structure. This means that the resultant crystal morphology is directly influenced by the molecular structure of the crystallising species.[81, 82] Several theories exist, such as the BFDH theory, that predict crystal morphology based on the intrinsic crystal structure of a system.

Crystal morphology can, however, be greatly influenced by environmental factors and in some cases the same solid forms of a chemical species can exhibit vastly different morphologies when crystallised under different conditions. The crystallisation method used, solvent medium, temperature, pressure, pH and the presence of impurities can all have a significant effect on the resultant crystal morphology.[81, 83, 84] Polymorphic forms of the same species can also display different habits due to the difference in intermolecular interactions within the crystal structures.

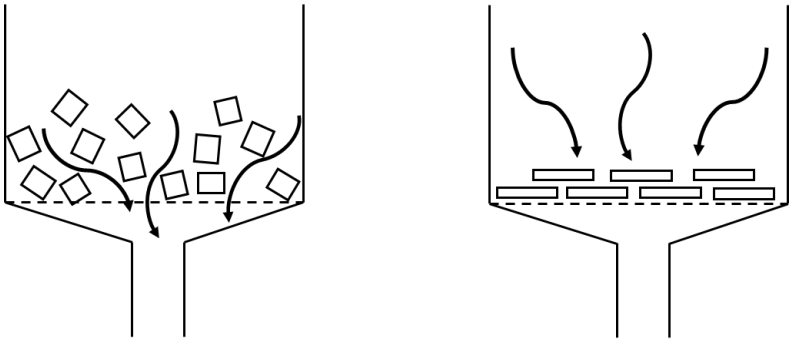

Figure 1.11: Ease of filtration for block and needle morphologies.

The morphology of a crystal is very important in the fine chemicals and pharmaceutical industry as the shape and size of crystals can vastly affect the ease of processing and formulation of the product. The flowability of the system, compressibility, bulk density and downstream processes, such as filtration and drying, are all influenced by morphology and it is therefore imperative that the resultant shape of the product is controlled. Figure 1.11 demonstrates the effect morphology has on filtration. When the crystallisation produces fine needle crystals they knit together during filtration and can cause an impenetrable layer. If the crystals are block like in shape, however, the filtration is much more efficient.[81, 85]

Crystal size distribution (CSD) is also directly affected by the morphology and growth of the crystals and is a very important aspect as it significantly affects not only the further processing and storage of a product, but also the general appeal of the product to potential customers.[81] In the pharmaceutical industry small uniform particles with narrow CSD are required in order to allow for a uniform dissolution of particles in the body as well as ease of compaction for tableting.[86] When the desired size and CSD cannot be achieved during the crystallisation, milling is employed, however, this incurs additional steps in the manufacturing process and is usually undesirable.[87]

1.4.5 Crystallisation Methods

Crystallisation can be achieved via many different methods, for example, crystallisation from the melt, reactive crystallisation, vapour diffusion and crystallisation from solution; the chosen method will greatly depend on the type of material one is trying to crystallise. In the pharmaceutical industry, crystallisation from solution is the most common method utilised and once the desired solid form for the active pharmaceutical ingredient (API) has been chosen, a crystallisation method must be designed. In order to design an efficient crystallisation process the solubility of the API in the chosen solvent medium must be fully characterised. Once these values have been determined the method of crystallisation can be chosen. Here, three methods will be discussed: evaporative crystallisation, cooling crystallisation and solution-mediated (slurry) crystallisation.[32, 88]

1.4.5.1 Evaporative Crystallisation

The choice of crystallisation method will be greatly influenced by the temperature dependence of the solubility of the system. For example, if a system's solubility has a weak temperature dependence and only slightly increases upon significant increases in temperature, then evaporative or anti-solvent crystallisation are likely to be the most appropriate choices for the crystallisation. Figure 1.12 illustrates an evaporative crystallisation process in terms of the solubility, MSZW and system solution concentration. For evaporative crystallisation, an amount of solute is fully dissolved in the chosen solvent so that the solution concentration lies below that of the equilibrium solubility, as represented by point A: the system is undersaturated. The system is then left open to the environment so that over time the solvent can evaporate, subsequently increasing the concentration of solute in solution. As evaporation of solvent continues the solution concentration will increase and move upwards from point A until it reaches point B, the equilibrium solubility of the system: the solution is now saturated. Solvent will continue to evaporate and the solution concentration will continue to increase past point B, into the MSZ. Whilst in the MSZ the solution is supersaturated and, although its concentration has surpassed that of the equilibrium solubility, it will not nucleate spontaneously. If left undisturbed, the evaporation will continue until the solution concentration reaches the MSZ limit, point C. At this point the supersaturation within the system has reached a value whereby spontaneous nucleation can occur. Nuclei will grow, depleting the supersaturation in the system, until the solution concentration

returns to point B. As further evaporation occurs, creating additional supersaturation in the system, the crystals will continue to grow. The crystals will continue to grow until all the solvent has evaporated or the system is filtered.[4, 32, 89, 90]

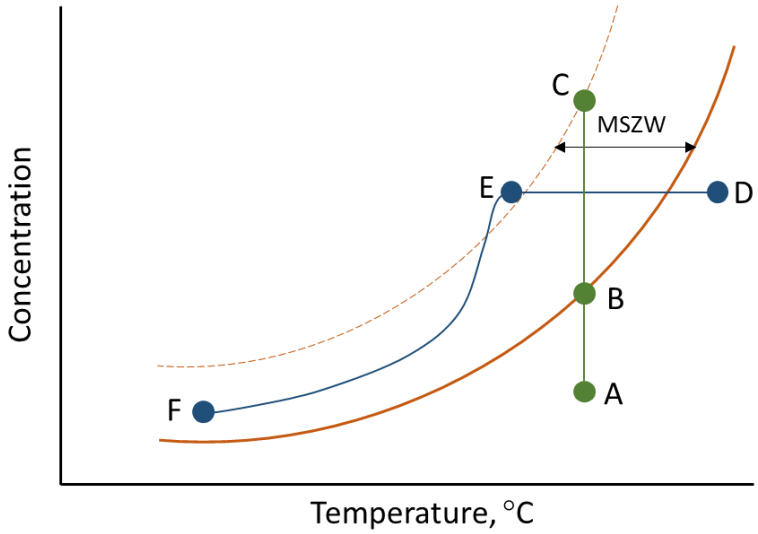

Figure 1.12: Solubility curve representing evaporative crystallisation (green line, points A-C) and cooling crystallisation (blue line, points D-F). Solid orange line represents the solubility curve with the MSZ represented by the dashed orange line.

1.4.5.2 Cooling Crystallisation

If a system's solubility has a strong dependence on temperature cooling crystallisation methods can be used. In batch crystallisation cooling crystallisation is the preferred method as it can allow for improved control over the crystallisation outcome in comparison to evaporative crystallisation. Using the solubility curve an appropriate cooling profile can be designed for the crystallisation process. Figure 1.12 above depicts a cooling crystallisation process (blue line). An undersaturated solution is prepared by dissolving an amount of solute in solution at an elevated temperature, point D. In a closed system, the solution is then cooled down, resulting in the concentration surpassing the equilibrium solubility and becoming supersaturated. If left undisturbed, the system will not nucleate until the concentration of the solution reaches the MSZ limit, point E. At this point homogeneous primary nucleation can occur. The concentration of the solution will decrease upon nucleation and subsequent crystal growth. As the system is cooled further, more supersaturation will be generated which will then be depleted by the growing crystals. For a successful process, the temperature profile should be designed such that after initial nucleation the concentration remains within the MSZW for the remainder of the process (for example, the path from E to F) in order to avoid any subsequent primary nucleation as well as prioritising the crystal growth.[4, 9, 32, 89]

1.4.5.3 Solution-mediated Crystallisation (Slurry Techniques)

Solution-mediated crystallisation techniques (slurry techniques) build upon solution-mediated phase transformations and they can be an efficient method for identifying

new polymorphic forms of a substance, or for screening for novel multi-component systems. This method of crystallisation is a suspension technique and is based upon the thermodynamic relationships between different crystalline species, such as polymorphs, solvates and multi-component crystals. If a system possesses two monotropic polymorphs, form I and form II, with form II being the metastable form, conversion to form I from II can be accomplished using solution-mediated phase transformations. If an excess of form II is added to a chosen solvent the solution will become saturated and an excess of solid will be present as a suspension (or slurry). As form I is more stable in comparison to form II it will be less soluble and hence the solution will be supersaturated with respect to form I. This supersaturation can subsequently lead to nucleation of form I. Once this initial nucleation of the more stable form has occurred the solution concentration has decreased, resulting in more form II now being able to dissolve. This in turn leads to more form I nucleation and growth and so the cycle continues until complete conversion of form II into form I is achieved.[32, 70, 91-94]

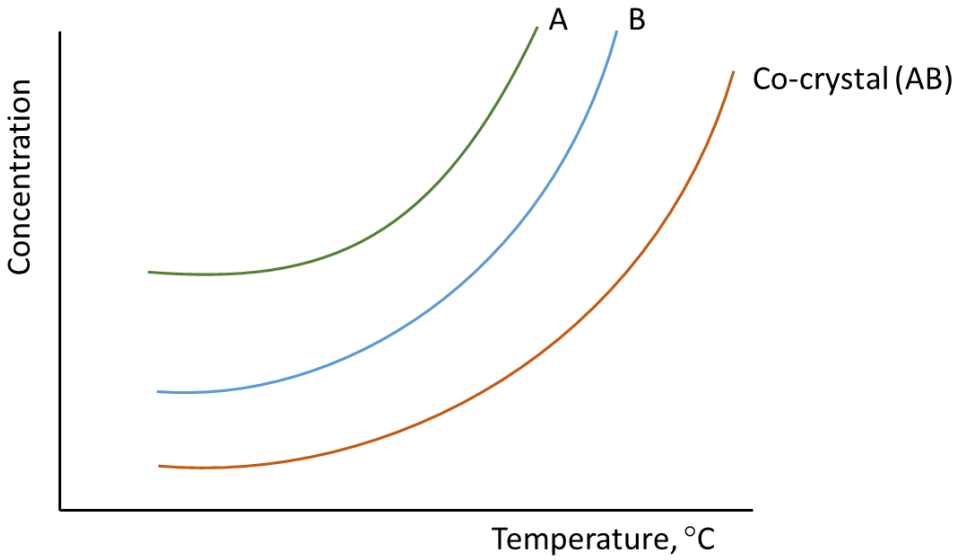

Figure 1.13: Solubility curves of starting components A and B and the co-crystal AB.

This same principle can also be applied to the formation of multi-component systems such as co-crystals. Figure 1.13 displays the solubility curves of two starting components, A and B and of their co-crystal form, AB. It can be seen that, in the chosen solvent system, the co-crystal has a lower solubility than its two starting components and it is this thermodynamic relationship that allows for the crystallisation of the multi-component system to occur. Formation of this co-crystal from this solvent system could be achieved via the use of solution-mediated phase transformations (slurrying) techniques. If an excess of both solid A and B was added to a small amount of the chosen solvent system then both components would dissolve into the solution and result in the solution being saturated with respect to both components. Excess solid of both A and B would then be suspended in the solution as a slurry. As the system is saturated with respect to both A and B, it will therefore be supersaturated with respect to the co-crystal, AB (as long as the co-crystal has a lower solubility than the individual

components). Hence, nucleation of AB can occur (as long as the supersaturation is beyond the MSZW of AB). Once nucleation of the co-crystal has occurred, A and B will be depleted from the solution, resulting in more A and B dissolving from the suspension. This in turn leads to further nucleation and growth of AB. This cycle will continue until all starting material has been converted into the more stable, less soluble co-crystal, AB.[91]

1.4.5.4 Mechano-chemcial Crystallisation

Mechano-chemical crystallisation is a technique that utilises grinding to access new solid forms of a system. It is often used in multi-component crystallisation where the two components are ground together to allow for the formation of a new crystalline form which incorporates both the starting components in the crystal structure. The technique can be conducted neat (with no solvent) or with small amounts of solvent, known as liquid assisted grinding (LAG). LAG uses only small amounts of solvent to lubricate the system and to encourage the phase transitions. Due to the technique using very little amounts of solvent for the access of a crystalline form, it is deemed a green crystallisation process. The grinding method can be conducted by hand using a pestle and mortar or mechanically with apparatus such as ball mills and jet mills.[95-97]

1.5 Crystallising the Desired Polymorph

In industry an enormous amount of work goes into the careful selection of the desired polymorph for commercial production. Once the solid form landscape for an API has been determined, the most appropriate form will be chosen for commercial manufacture. Once the desired polymorph has been selected, a selective, reproducible and robust crystallisation route must then be achieved. Accessing a crystallisation route to yield the desired solid form selectively can pose great difficulty, but there are numerous factors that can be manipulated in order to achieve selective crystallisation.

Many methods and variables exist that, upon altering, can result in the selective formation of different polymorphs.[98] One way to manipulate the process in order to access a specific polymorph is by consideration of Ostwald's law of stages. This law states that if a system displays more than one polymorphic form the least stable form will nucleate first. This metastable form will then undergo a solution mediated phase transformation to yield a more thermodynamically stable polymorph.[16, 64] This rule suggests that the polymorph obtained may be controlled by the time at which the solid is harvested. A fast crystallisation has a higher chance of yielding the metastable form due to the minimal time available for polymorphic transitions to occur. Alternatively, a slow crystallisation is more likely to yield the thermodynamically stable form.[99] However, this is not always the case as many other environmental factors can influence the polymorphic outcome.

Different crystallisation methods such as evaporative, cooling, mechano-chemical, crystallisation from the melt and slurry techniques can all lead to the formation of different polymorphs. In the pharmaceutical industry, where crystallisation from solution is the most common means of producing crystalline compounds, employing different solvents, changing the pH of the crystallizing solution or varying the environmental conditions such as pressure and/or temperature can all have profound effect on the polymorphic outcome.[100] These environmental factors can not only affect the polymorphism of the material, but also the resultant crystal morphology and particle size distribution (PSD).[28]

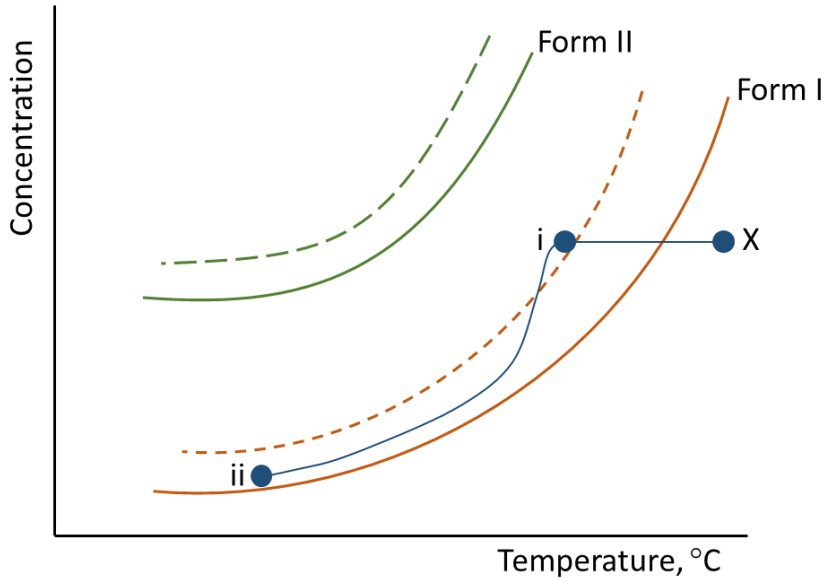

Figure 1.14: Solubility curves (solid lines) of monotropic polymorphs. Form I is the thermodynamically stable form, form II is the metastable form. The dashed lines display the metastable zone widths for each polymorph.

Control of supersaturation within a crystallising system can allow for control over the polymorphic outcome, as can be visualised in Figure 1.14. If the thermodynamic form, form I, is the desired polymorph then control over the supersaturation may be implemented to selectively crystallise this form. If a solution of concentration X is cooled to point i the solution becomes supersaturated with respect to form I, but not form II. Once the MSZW of form I is exceeded, spontaneous nucleation of this form can occur, resulting in a drop in the solution concentration. The cooling profile can be designed to keep the solution concentration within the MSZW of form I for the remainder of the crystallisation (path from i to ii). This method is effective in controlling the polymorphic outcome and eliminating the chance of form II being crystallised. However, if the metastable form, form II, is desired this method cannot be utilised.[101]

The choice of solvent can also have a significant influence on the polymorphic outcome, with some solvents stabilising the formation of particular polymorphs. Solvent-solute interactions can interfere with crystallisation and can inhibit the formation of specific solid forms.[100, 102, 103] The presence of impurities or additives in a system can also have profound effects on the resultant crystallisation; not only can they have a large influence

on the solubility of the solute, but they can also influence the growth rates, resultant crystal habit and polymorphic outcome.[83, 104] There are several reported cases where new polymorphs have been serendipitously accessed as a result of co-crystallisation screens, with the co-former acting as an additive and forcing the crystallisation of a specific polymorphic form.[105, 106] The solute-additive interactions that can be formed in the solution can lead to the inhibition of nucleation and/or growth of a specific polymorph, seemingly driving the formation of another polymorphic form.[104, 107]

1.5.1 Seeding for Solid Form Control

In industry the most commonly employed method for manipulating the polymorphic outcome during a solution crystallisation process is seeding. Seeding refers to the process where crystalline particles of the desired solid form are added to the supersaturated solution to induce secondary nucleation and growth. Not only is it the only reliable way to access a desired polymorph in many cases, it can also offer a pathway to controlling particle size distribution (PSD) and product uniformity.[32, 88, 108-110] There are multiple cases in the literature where seeding has been successfully implemented to control the polymorphic outcome of a crystallisation.[111-113] Although in many cases seeding with the desired form can result in growth of this polymorph at the expense of others, this is not always the case. In some instances, seeding with one solid form can lead to the selective formation of an alternative sold form.[32, 114]

The technique of seeding builds upon the concept of secondary nucleation. Usually, crystalline particles of the crystallising solute are added to a supersaturated homogeneous solution within the metastable zone of the system. These seeds then deplete the supersaturation of the system, either by growth or by secondary nucleation. As seeding avoids the need for spontaneous nucleation the level of control over the system is significantly increased. Spontaneous nucleating systems have large batch to batch variation as a result of several factors. Firstly, the variation in impurity level and type that occurs from batch to batch can have a significant impact on the outcome of the crystallisation, as well variations in initial concentration of solute and subsequent rate of generation of supersaturation. The presence of foreign particles or seed particles within the batch crystalliser from a previous crystallisation can also have an effect, resulting in primary heterogeneous nucleation or secondary nucleation, respectively, of an undesired form. The implementation of seeding into a process can help eradicate all these issues and provides a pathway for secondary nucleation and growth of the desired solid form. A seeded crystallisation also provides a well-defined starting point for the crystallisation process resulting in a higher level of reproducibility.[88, 109]

The amount of seed crystals added into a crystallising system in order to exert control over the polymorphic outcome can be critical.[115] For full control over polymorph selection, a sufficiently large amount of seeds is required in order to promote growth as opposed to inducing secondary nucleation, as well as attempting to supress any polymorphic phase transitions that may occur. A small seed loading of less than 1 % can

aid in controlling unwanted nucleation of other forms, but may not be enough to achieve predominantly crystal growth within the system. Amounts between 5-10 % will increase the probability of growth and help prevent secondary nucleation occurring. The size and amount of the seed particles added have a direct effect on the resultant size of the final crystal particles, with a lesser seed loading resulting in larger particles: there are less nuclei so the growth per nucleus is larger. In some cases, where very small crystal sizes are required a large amount of seeds can be added in order to ensure this.[88, 109, 116]

As the employment of seeding means one can avoid spontaneous nucleation, a narrowing of the PSD, in comparison to non-seeded crystallisations, is usually observed. Complete elimination of nucleation to yield an all-growth crystallisation process, however, is unlikely, with a small level of secondary nucleation being present in all crystallisation processes to some degree. Secondary nuclei can be created from the seed particles during the process due to attrition and fragmentation of particles due to impact with the impeller, or 'initial breeding' where the seed crystals have an amount of seed dust that comes away upon addition to the crystallising system and acts as secondary nuclei.[117]

This nucleation will result in the formation of much smaller particles, which can widen the PSD. Seed ageing during a crystallisation process can be employed to counteract this and give an overall narrowing of the PSD. A seed ageing step in a cooling crystallisation requires the temperature to be temporarily held at a constant value for a set period of time. This allows for seed growth and subsequent depletion of the supersaturation before continuation of the crystallization process. During this seed ageing, not only will the seed crystals grow, but Ostwald ripening will also occur. This is where the smallest crystals within the system will dissolve and redeposit onto the larger crystals, narrowing the PSD. Temperature cycling is another method that can be used to encourage dissolution of fines (very small crystallites) in order to narrow the PSD.[73, 109 118]

How effective seeding is in a process will be determined not only by the seed loading, but also the seed surface, the timing of addition and the method of addition. Each factor can significantly influence the resultant product. The addition of seeds needs to be at a point in the crystallisation where the solution is supersaturated, so that the seed will not dissolve, but not so supersaturated that primary nucleation can occur; a general rule is that seeding one third of the way into the MSZW is sufficient to ensure the seed holds. In some cases, however, seeds can be added up to 5 °C below the saturation temperature, assuming that enough seed is added so that some will remain undissolved and suspended in the solution. This method may be implemented into a crystallisation system that has a very narrow MSZW. Figure 1.15 depicts a typical seeded cooling crystallisation. The system is cooled from A to B, where seed crystals are then added. At this point the solution is supersaturated, but still remains within the MSZW; the seeds will not dissolve and there is no chance of primary nucleation occurring. The temperature is then held for a small period of time to allow for seed ageing and

depletion of the supersaturation before cooling is continued to point C to allow for further seed growth.[32, 88, 109]

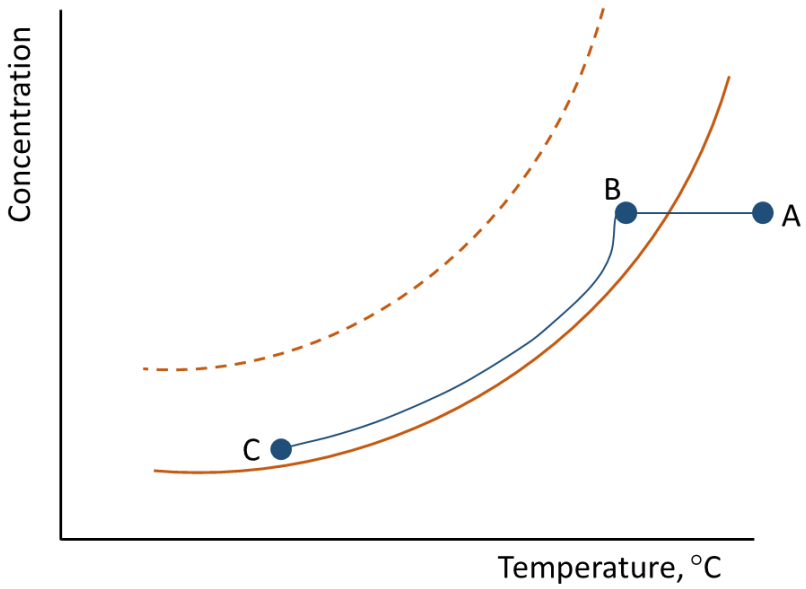

Figure 1.15: A typical seeded cooling crystallisation concentration-temperature profile.

The method of seed addition is also a key factor. The addition of a dry powder was the common procedure in the past, however this method is now usually replaced by the addition of seed slurries. This is due partly to exposure risk when using a dry powder, but also because seed slurries can allow for activation of the seed surface. The condition of the seed surface is an important factor, if dry seed is used the surfaces may be damaged and there may be a large amount of crystalline dust causing 'initial breeding' and/or agglomeration of the seed crystals. The crystalline dust particles will likely act as secondary nuclei within the system, hence widening the PSD. If a slurry is prepared these dust particles will dissolve, as well as some slight dissolution of the larger particle. This slight dissolution, however, will reveal cleaner surfaces and hence allow for better growth of the seeds. However, if one is seeding with a metastable polymorph, the generation of a seed slurry may lead to the transformation of this polymorph into the thermodynamic form; in this case dry seeds would be the preferred choice for addition.[88, 109]

The application of seeding to a crystallisation process relies on a small quantity of seed material being readily available at the start of development. The initial production of the seed particles can in some cases be a major cause of difficulty as selective formation of the desired form must somehow be achieved before a seeded operation can be carried out. In some cases a small amount of product may be available from a previous polymorph screening, or by a different crystallisation route such as evaporative crystallisation or crystallisation from the melt. Once suitable seed crystals are prepared a seeded crystallisation will hopefully give rise to the desired product in a much larger quantity. Further seed crystals can then be obtained from this product.[32]

1.6 Industrial Crystallisation – Batch versus Continuous

In the pharmaceutical industry crystallisation is traditionally carried out using large scale batch processes, usually in stirred tasks producing huge volumes at a time. Batch crystallisation and synthesis can, however, be very slow and result in long lead times and large inventory costs. Due to the increasing pressure on the industry to move towards more sustainable, cheaper manufacturing methods, whilst still producing products of high quality, there is currently a significant drive towards more continuous routes, including the implementation of flow synthesis and continuous crystallisation.[119-123] In 2013, Mascia *et al.* published the first example of an end-to-end continuous manufacturing process for a pharmaceutical product (aliskiren hemifumerate) with the final tableted product meeting the required specifications for the drug product qualtiy.[124] In recent years research into flow chemistry and continuous manufacturing platforms and processes has significantly increased[123] with several national centres such as the Future Manufacturing Hub in Continuous Manufacturing and Advanced Crystallisation (CMAC) being established and supported by both industry and academic funding bodies. Continuous manufacturing has both advantages and disadvantages over batch, as summarised in Table 1.2 below.

Table 1.2: Advantages and disadvantages of continuous crystallisation versus batch crystallisation.

Advantages	Disadvantages
• Shorter cycle times • Lower solvent use • Easier to scale up • Better mixing and heat transfer • Less space requirements • Low cost of inventory • Better control over crystal size distribution	• High capital costs • Most plants have existing batch equipment • Technology is not fully developed • Still issues with fouling and encrustation for many of the continuous technologies

The reliance of the pharmaceutical industry on large scale batch production is an arguably out of date structure, which results from the industry working on a 'push driven process' where forecasts about future demand have to be decided before production, due to the long life-cycle of the drugs. The 'blockbuster' drug model is one that pharmaceutical companies have thrived on in the past, resulting in high turnovers and allowing for good reinvestment into further research and development (R&D). However, as patents run out and more niche products and personalised medicines become the norm, the blockbuster model is becoming less feasible and the pharmaceutical companies no longer have the profit margins they once had.[121, 125]

Continuous manufacturing and crystallisation could significantly benefit the pharmaceutical industries, providing the opportunity to move to a more 'made-to-order' model; this would allow a significantly easier start-up/shut-down of manufacturing processes, as well as providing much more flexibility in the product

quantities produced.[120, 126] The implementation of new continuous technologies not only has an advantage for the supply chain of pharmaceuticals, it can also provide significant improvements over the nature of the resultant product. Continuous crystallisation technologies have significantly better heat transfer than large batch crystallisers, as well as resulting in much more efficient mixing. They can also allow for an increased level of control over the particle size and size distribution.

1.7 Systems of Interest

The work presented in this thesis focuses on the crystallisation of model organic compounds; the main systems of interest being urea barbituric acid (UBA) and thiobarbituric acid (TBA).

1.7.1 Urea Barbituric Acid

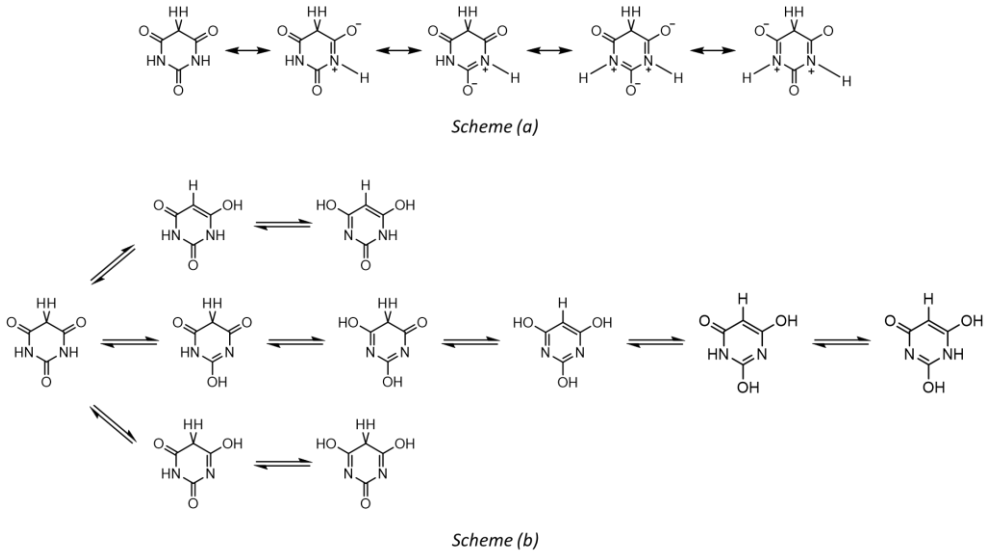

Figure 1.16: Resonance structures (scheme (a)) and tautomeric structures (scheme (b)) of barbituric acid.

Barbituric acid is a precursor for the barbiturate family of compounds which act as central nervous system depressants. Due to barbiturates possessing large addiction potential and overdose risks, many have now been replaced by benzodiazepines, especially in the treatment of anxiety. However they are still widely used for a variety of purposes, such as in the treatment of epilepsy, migraines and as general anaesthesia.[127] Barbituric acid is known to display polymorphism, with two known polymorphs as well as two dihydrate forms.[128-131] It can exist in 10 different keto/enol tautomeric structures, as well as possessing the capability to form several resonance structures (Figure 1.16). This, coupled with its hydrogen bond donor and acceptor capability make it an ideal candidate molecule for co-crystallisation and polymorph studies.[132] Within the Cambridge Structural Database (CSD) there are 18 organic multi-component structures for barbituric acid, including salts, co-crystals and hydrates. One of these is the co-crystal urea barbituric acid (UBA) which is one of the systems of interest in this work.

UBA is utilised as a model system and consists of a 1:1 stoichiometric ratio of the two components. The co-crystal was first discovered by Gryl *et al.*[133] in 2008 and was reported to have three polymorphic forms, form I, II and III. Form I and II crystallise in monoclinic space groups $P2_1/c$ and Cc respectively, with form III crystallising in triclinic $P\bar{1}$. The three polymorphs differ not only by their hydrogen bonding, but also by the mesomeric behaviour of the barbituric acid molecules within the crystal structure. The three solid forms are all shown to have layered crystal structures, however the layers in each form differ by the species from which they are built. Form I consists of chains of urea-urea hydrogen bonded dimers as well as barbituric acid molecule chains. Form II does not display any hydrogen bonding interactions between molecules of the same type. Similarly to form I, form III possesses hydrogen bonded urea dimers as well as barbituric acid dimers in alternate chains. [133, 134] Form I and form III have been shown to be very close in energy, with form II being highly metastable in comparison to these two forms.[135] A reason for this may be due to the hydrogen bonded urea dimers seen in both form I and III as well as the mesomeric forms barbituric acid takes in the crystal structures of form I and III in comparison to form II; form III possess the same mesomeric form as seen in form I as well as an additional mesomeric form, whereas in form II the barbituric acid takes on an entirely different mesomeric form. [133, 134]

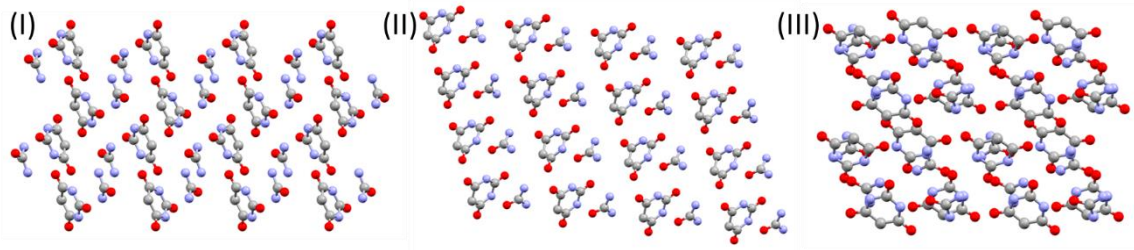

Figure 1.17: The three polymorphic forms of urea barbituric acid (UBA).

The UBA system is of interest as it presents challenges in the selective crystallisation of the three polymorphic forms. When first discovered, each form was accessed via small scale evaporative crystallisation with the outcome dependent on the solvent used and the stoichiometric ratio of the starting components (Table 1.3).

Table 1.3: Crystallisation parameters for evaporative crystallisation of the three solid forms of urea barbituric acid.

Parameter	UBA I	UBA II	UBA III
Solvent	Methanol	Ethanol	Methanol
Ratio of U:BA	1:2 or 1:3	2:1	2:1

Upon transfer of the crystallisation of this system to cooling crystallisation by Wittering it was found that form II was elusive, likely due to its high metastability in comparison to the other two forms.[135] The work showed that form I could be accessed selectively using cooling crystallisation techniques from methanol, but the selective crystallisation

of pure form III was not achieved. Powell *et al.* successfully transferred the selective crystallisation of UBA form I into cooling crystallisation from methanol and subsequently determined the experimental conditions to produce pure form I via continuous crystallisation in a periodic mixed suspension mixed product removal (PMSMPR) crystalliser cascade. During this work they found that pure form III remained elusive, with form I always being present.[136]

Solubility analysis of form I and form III in both water and methanol indicated that the two forms have very similar free energy, with their solubilities being almost identical to one another, regardless of the solvent.[135] This then leads to the question: which form is the thermodynamic form and how are these two forms related thermodynamically?

1.7.2 Thiobarbituric Acid

The second material of interest in this work is thiobarbituric acid (TBA). Due to its structural similarity to barbituric acid it was chosen as a target molecule for co-crystallisation studies. Similarly to barbituric acid, thiobarbituric acid has the propensity to form 10 keto/enol tautomers.[132] This results in a rich collection of polymorphs; there are six reported polymorphs of thiobarbituric acid in the CSD as well as a hydrate form. All six polymorphs contain one keto tautomer (Figure 1.18 isomer a), with form IV having both this keto tautomer as well as an enol/keto (Figure 1.18 isomer b) tautomer present in the crystal structure. Within the hydrate, thiobarbituric acid exists as the keto/enol tautomer seen in form IV. [137, 138] Surprisingly, there are only two reported co-crystals for thiobarbituric acid; one being a barbituric acid thiobarbituric acid system.[139] Due to the tautomerism and hydrogen bonding capabilities of the molecule thiobarbituric acid is an ideal candidate for multi-component crystallisation studies.

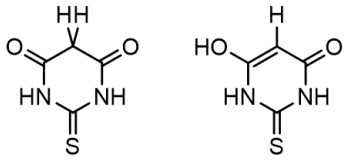

(a) *(b)*

Figure 1.18: Two tautomers of thiobarbituric acid which are present in the reported polymorphic forms.

1.8 Aims and Objectives

The majority of work presented in this thesis focuses on the urea barbituric acid (UBA) co-crystal system. The first aim of this research was to learn more about the relationships between the UBA polymorphs: which is the thermodynamically stable form; are they enantiotropic or monotropic?

The next aim of the current research project is to investigate ways of accessing form III selectively using cooling crystallisation techniques, with investigation into seeding to obtain this a significant objective. If the selective crystallisation of form III can be

achieved in batch cooling crystallisation studies, the next step will be its transfer into continuous methods and optimisation of this new process.

Another area of research covered within this thesis is the investigation into the multi-component crystallisation of thiobarbituric acid (TBA). The aim will be to produce novel multi-component systems using TBA as a target compound using simple co-crystal screening techniques and, if successful, scaling up the production of these novel forms into batch cooling crystallisation. If the scale up of these systems is successful, the further aim will be to then investigate their potential for continuous cooling crystallisation.

Chapter 2 – Theory of Analytical Techniques

2.1 X-ray Crystallography

X-ray crystallography encompasses a variety of techniques used to analyse the crystal structure of solid state materials. X-rays are diffracted by electrons within the crystal and the resulting diffraction pattern allows for the positions of the atoms as well as their bonding behaviour to be determined, giving an accurate depiction of the crystal structure. X-ray crystallography is undertaken through a range of techniques including powder X-ray diffraction and single crystal diffraction, both of which have been used for analysis within this thesis.

2.1.1 The Unit Cell

Within a crystal structure, the unit cell is the smallest repeating unit of the highest symmetry within the crystal; it is the building block for the entirety of the crystal structure. The unit cell is constructed by looking for areas of identical environment within a crystal structure; if each molecule is taken as a single motif then areas of identical environment, or lattice points, can be defined. Joining eight adjacent lattice points together yields a three-dimensional parallelogram - the unit cell. The unit cell is defined by the lengths of the three axes (*a*, *b* and *c*) and by the angles between these axes (α,β and γ).[140-142]

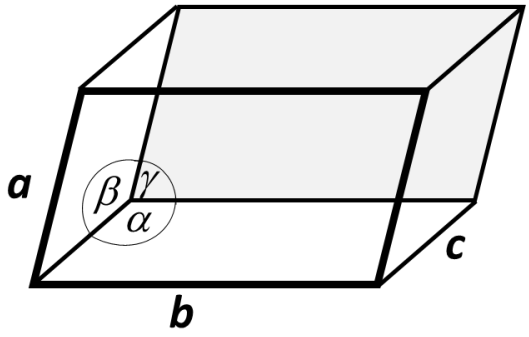

Figure 2.1: Unit cell diagram showing unit cell lengths (*a*, *b* and *c*) and angles (α, β and γ).

Due to the variance in the position of lattice points within crystal structures the relative unit cell lengths and angles will vary; taking this into account, each unit cell can be assigned to one of seven crystal systems, as seen below in Table 2.1. These crystal systems define the unit cell in terms of its parameters, for example, if the unit cell lengths are all equal and the angles between the axes are 90 °, then the unit cell is cubic. Whereas, if *a*, *b* and *c* are all different in length and none of the angles are equal to one another, or to 90 °, then the unit cell is triclinic.[143]

The arrangement of lattice points within a unit cell also gives rise to four different lattice types: primitive (P), body-centred (I), face centred (F) and base-centred (C). These different types are defined by the presence of lattice points on the unit cell faces (F and C), or in the middle of the unit cell (I). The presence of additional lattice points at the faces, or in the cell, results in each lattice type having a different number of lattice points per unit cell. It is important to stress here, however, that lattice points do not refer to individual molecules, but areas of identical electron environment and hence one lattice point can be made up of multiple molecules.[140-143]

Combining these four lattice types with the seven different crystal systems gives rise to fourteen Bravais lattices. Each crystal structure, regardless of its content's chemical makeup, belongs to one of these Bravais lattice types.

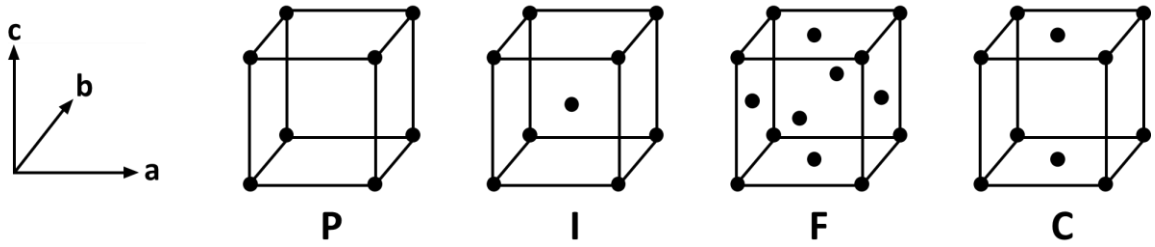

Figure 2.2: The four lattice types (filled circles signify lattice points).

Table 2.1: The unit call parameters and lattice types that lead to the 14 Bravais lattices.

Crystal system	Unit cell parameters	Lattice types
Cubic	$a = b = c \quad \alpha = \beta = \gamma = 90\,°$	P, I, F
Hexagonal	$a = b \neq c \quad \alpha = \beta = 90\,°, \gamma = 120\,°$	P
Trigonal	$a = b \neq c \quad \alpha = \beta = 90\,°, \gamma = 120\,°$ ($a = b = c \quad \alpha = \beta = \gamma \neq 90\,°$)	P, (R)
Tetragonal	$a = b \neq c \quad \alpha = \beta = \gamma = 90\,°$	P, I
Orthorhombic	$a \neq b \neq c \quad \alpha = \beta = \gamma = 90\,°$	P, C, I, F
Monoclinic	$a \neq b \neq c \quad \alpha = \gamma = 90\,°, \beta \neq 90\,°$	P, C, (I)
Triclinic	$a \neq b \neq c \quad \alpha \neq \beta \neq \gamma \neq 90\,°$	P

Lattice points can also be joined to form two-dimensional planes throughout the structure. These planes can be defined in terms of their intercepts with the three cell axes: Weiss indices (*x*, *y*, *z*). In crystallography these planes, however, are more commonly described by Miller indices (*h*, *k*, *l*) which are calculated by taking the reciprocal of the Weiss indices and clearing all fractions. Whereas Weiss indices refer to

individual planes within the crystal lattice, Miller indices refer to a set of parallel planes of characteristic spacing (d_{hkl}).[144]

Although the unit cell is the smallest unit of highest symmetry within the crystalline structure, it can be reduced further into asymmetric units. These are unique segments of the unit cell upon which any additional internal symmetry within the unit cell is performed to yield full the unit cell contents. Asymmetric units can be made up of several molecules, or be fragments of a molecule, depending on what symmetry operations are present within the molecule and the unit cell. The asymmetric unit undergoes certain symmetry operations to build up the unit cell and there are six different types of such symmetry elements. Of these six symmetry operations, four are non-translational and two are translational. The non-translational symmetry elements are reflection, rotation, inversion and rotation-inversion; these all describe a form of rotation of the asymmetric unit. The two translational operations do as the name suggests; they translate the object within the unit cell. Both the screw axis and glide plane combine a non-translational element with a translation of the object: a glide plane involves reflection and then translation of the unit, whereas a screw axis involves a rotation and translation. Within a crystal structure these simple symmetry elements can be combined to yield more complex symmetry. There are 32 different possible ways of combining the six symmetry elements whilst also maintaining the 3D translational symmetry required for a periodic crystals, and these are known as crystallographic point groups. Point groups describe the symmetry of an individual object and can be thought of as the complete collection of all the symmetry elements passing through a central point. Combining all 32 point groups with the fourteen Bravais lattices discussed earlier gives rise to 230 potential combinations; these are termed space groups. Every crystal structure will fall into one of these space groups, and with knowledge of the asymmetric unit and space group one can build up a picture of the entire structure.[141, 142]

2.1.2 X-ray Diffraction

Due to the long range order present in a crystalline material, such materials can diffract X-rays. The wavelength of X-rays is comparable to interatomic distances (0.8 – 3.0 Å) which enables the atomic contents of a crystalline structure to be determined. X-ray diffraction in the laboratory typically use X-rays of λ = 1.54045 or λ = 0.71073 Å accessed by using Cu and Mo- based sources, respectively.

During X-ray diffraction experiments, a crystal is irradiated with X-rays produced from a metal target. The X-rays interact with the electrons present in the crystal structure which causes the X-rays to be scattered/diffracted. Due to the crystal having a regular structure, a diffraction pattern results which consists of distinct diffraction spots. The scattering of X-rays is dependent on the number of electrons within an atom, hence hydrogen atoms have very weak scattering. This can often lead to difficulty in determining the position of hydrogen atoms in an X-ray crystal structure.

In 1912 W. L. Bragg studied X-ray diffraction and devised the geometric interpretation that the diffraction of X-rays by the electrons in a crystal can be regarded as reflection from sets of parallel planes, Miller planes. Bragg found that the diffraction of X-rays by a crystal is analogous to the reflection of light by a mirror, such that the angle of incidence of the X-ray with the Miller plane is equal to that of the angle of reflection. This finding led to the derivation of Bragg's law (Equation 2.1); for a reflection to be observed Bragg's law must be satisfied.[141, 145]

$$n\lambda = 2dsin\theta \qquad \text{(Equation 2.1)}$$

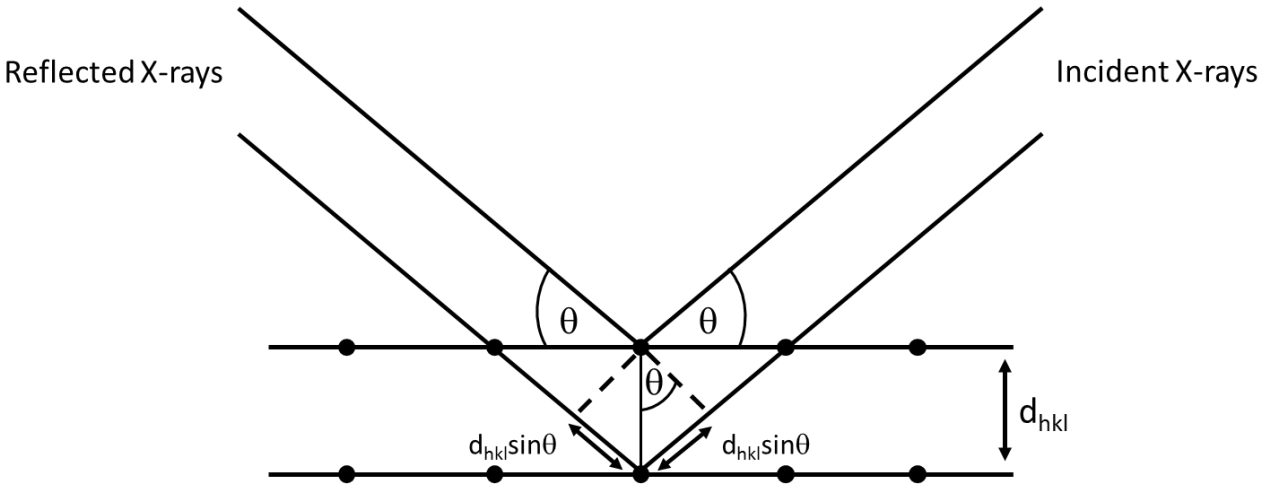

Figure 2.3: Pictorial representation of Bragg's law.

The law states that for a reflection to be observed, the path difference between two X-rays ($2d\sin\theta$) must be equal to an integer (n) number of wavelengths (λ). The value for n is typically set to 1 and the wavelength for an experiment remains constant. As a result, for a set of planes with characteristic spacing d_{hkl}, it is the angle between the incident X-ray and the planes that determines whether a reflection will be observed. During an experiment, diffraction spots will therefore occur when Bragg's law is satisfied.

Each spot on a diffraction pattern represents a specific set of Miller planes and hence a specific *hkl* value, measured at the relevant scattering angle. During data collection the intensity, I_{hkl}, of diffraction from each Miller plane is measured. The intensity of a diffraction spot is determined by the unit cell and the crystal contents.

2.1.3 The Reciprocal Lattice

To understand how the observed diffraction spots relate to their respective Miller indices, one must consider reciprocal space. Unit cells, Miller indices and their resultant *d*-spacing's are in real (or direct) space with units of Å. However, Bragg's Law states that $\sin\theta$ is directly proportional to $1/d$ (i.e. $Å^{-1}$). In a diffraction pattern $\sin\theta$ is proportional to the distance of each diffraction spot from the centre of the pattern and this results in $1/d$ also being proportional. As a diffraction pattern is based on the units of $1/d$, it is

said to be in reciprocal space. As a result, large unit cells, with large *d*-spacing, will have compressed diffraction patterns; whereas small unit cells, with small *d*-spacing, will have expanded diffraction patterns.[146-148]

Diffraction spots for specified Miller indices can subsequently be determined by moving $1/d$ away from the origin in a line perpendicular to the Miller planes. This therefore allows each diffraction spot in a pattern to be assigned easily to a set of Miller planes and the intensity, I_{hkl}, of each spot can be measured. It is the position of these spots and their I_{hkl} values that are measured in a data collection. The intensities are then used in order to create an electron density map in direct space for a portion of the unit cell, allowing for atom types and positions to be determined.[146-148]

2.1.4 Structure Solution using Single-crystal X-ray Data

In order to solve a crystal structure an electron density map (ρ_{xyz}) must be produced to allow for the location and type of atoms within the unit cell to be determined. The atom locations are determined in terms of areas of electron density: electrons per cubic Angstrom (e Å^{-3}) versus all locations (*x, y, z*) within the unit cell. In order to create an electron density map the structure factors (F_{hkl}) for each Miller set must be determined.[146]

$$I_{hkl} = (F_{hkl})^2 \qquad \text{(Equation 2.2)}$$

$$F_{hkl} = \sum_{j=1}^{j=n} f_j \cos 2\pi\left(hx_j + ky_j + lz_j\right) + i \sum_{j=1}^{j=n} f_j \sin 2\pi(hx_j + ky_j + lz_j)$$

(Equation 2.3)

Where *j* is the atom type and f_j is the atomic scattering factor for the atom in question.

The structure factor is the square root of the measured intensities for the associated Miller set (Equation 2.2) and allows for information to be gained about the Miller set of planes, the positions of all atoms (x_j, y_j, z_j) within the unit cell and all atom types. The magnitude of the structure factor can be easily calculated from I_{hkl} values. However, the sign (+ or −) of F_{hkl} (for centrosymmetric space groups), or more generally its phase, cannot be, leading to the phase problem. [145, 146] Ways in which the phase problem can be overcome will be discussed later.

F_{hkl} is dependent on atom type, atom positions and the atom scattering ability of all atoms in the unit cell (Equation 2.3). The atomic scattering, f_j, will vary dependent on the atom type due to all atoms having different electron clouds and subsequently scattering X-rays differently. At low Bragg angles the ability of an atom's electron cloud to scatter X-rays is much greater than at high angles and can be viewed as proportional to the number of electrons in the cloud, hence hydrogen atoms, with a single electron,

will have very low scattering and can be difficult to locate. The scattering ability drops off at higher Bragg angles, as can be seen in Figure 2.4.[145, 146, 149]

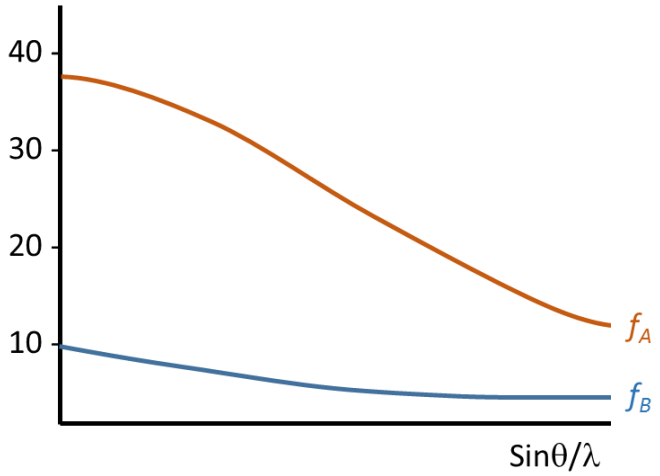

Figure 2.4: Representation of atomic scattering, f_j, of atoms A and B with respect to Sinθ/λ.

Once a full data collection has been conducted the unit cell parameters, crystal system and I_{hkl} for all *h, k, l* values (up to a specified θ value) are known. From this the magnitudes of the structure factors, F_{hkl}, can be determined. The space group can also be determined by looking for systematic absences in the data, *i.e*. where the I_{hkl} for some Miller indices equals zero. These absences arise when F_{hkl} equals zero for one of two reasons: lattice centring or the presence of translational symmetry elements in a space group. Lattice centring absences are caused when the lattice type is anything other than primitive, P. These absences extend across the whole data set, for example, if the lattice type is I then F_{hkl} = 0 when the sum of the indices (h + k + l) is odd. Systematic absences also arise from the presence of translational symmetry elements (glide planes and screw axes) within the space group. When these translational symmetry elements are present they result in subsets of reflections within the data set being absent, for example, if a 2_1 screw axis is present along the a axis then systematic absences will occur for Miller sets with *h, 0, 0* when *h* is odd.[146, 150, 151] (For full set of systematic absences refer to Appendix Table 9.1 - Table 9.3).

Determining which I_{hkl} values are absent within a data set is therefore an important element of determining the space group in which the system has crystallised. With this information one can determine where the asymmetric units within the unit cell are and how they relate to one another. As the magnitude of the structure factors has been determined from the I_{hkl} values, the electron density map can then be produced (Equation 2.4), where *V* is the volume of the unit cell.[142, 146]

$$\rho_{xyz} = \frac{1}{V}\sum_h \sum_k \sum_l F_{hkl} \cos 2\pi\,(hx + ky + lz) \qquad \text{(Equation 2.4)}$$

This can then be used in tandem with the knowledge of the space group in order to begin solving the crystal structure. Once some atom positions are known then analysis programs can calculate a structure factor for each Miller set (F_{hkl}^{calc}). These calculated

structure factors are used to then construct a calculated electron density map which is in turn compared with the electron density map yielded from the data collection. However, the phase problem must first be overcome in order to fully solve a crystal structure. In order to do this there are two distinct methods: Patterson methods and Direct methods. Which method is used will depend upon the atomic nature of the structure. If there are heavy metals then Patterson methods can be used, but if the system is purely organic with small atoms then Direct methods can be used.[146]

2.1.4.1 Patterson Methods

The Patterson series is generated as the initial step for structure solution. The series, or map, is a Fourier series and is based on $(F_{hkl}^{obs})^2$ as opposed to F_{hkl}.[146]

$$P_{xyz} = \frac{1}{V}\sum_h \sum_k \sum_l (F_{hkl}^{obs})^2 \cos 2\pi\,(hx + ky + lz) \quad \text{(Equation 2.5)}$$

A Patterson map is produced which is made up of a series of peaks. Each of these peaks represents a vector between two atoms. The largest peak is found at the origin (*0, 0, 0*), and is an overlap of all the vectors between an atom and itself; every pair of atoms (e.g. A and B) in the unit cell gives rise to two equal and opposite vectors (e.g. A→B and B→A). The peaks/vectors produced are proportional to the squares of the atomic numbers of the atoms which give rise to them. This therefore means that if a heavy atom (A) is present in the structure the peaks involving this atom can be easily identified due to their size. By knowing the vector positions and symmetry operations required for the space group, it is therefore possible to determine the position of the heavy atom (x_A, y_A, z_A). As the space group is known, all equivalent positions of the atom within the unit cell can be determined. The calculated locations for the heavy atom (A) within the unit cell, as well as its atomic structure factor f_A can then be input into the equation for F_{hkl} (Equation 2.3). This then yields a F_{hkl}^{calc} value based solely on the heavy atoms within the unit cell. As the scattering efficiency for heavy atoms is so high it has a significant impact on the phase of the overall structure factor and so one can be confident that the phases for the calculated structure factors are correct. The resulting F_{hkl}^{calc}values can then be used to create an initial electron density map which can subsequently be used for further structure solution, by least-square iterations to determine further atoms in the structure, and refinement.[146, 152, 153]

2.1.4.2 Direct Methods

When a structure consists of only organic molecules and has no heavy atoms present, Direct methods may be preferred to overcome the phase problem. For this method some of the phases for structure factors are assigned randomly based on linked mathematical inequalities. Strong reflections are chosen to have phases assigned and the phase that they are assigned will have mathematical implications on the strength and phases of other reflections. This Direct methods strategy is conducted only once as the initial step to yield structure factors that are then used to create an electron density map based solely on these F_{hkl} (Equation 2.4). This map usually contains a recognisable

fragment of a molecule, such as an aromatic ring. From this the positions of some of the atoms can be assigned correctly and inserted into Equation 2.3 to yield F_{hkl}^{calc} values with the correct phase. These are then subsequently used to create another electron density map which is used to locate further atoms and for structure refinement through least-square iterations, as with Patterson methods.[146, 154]

2.1.4.3 Dual-space Methods and Charge Flipping

Recently, new methods to overcome the phase problem have emerged and, unlike Patterson methods which work predominantly in direct-space and direct methods which work in reciprocal space, these methods are based on both direct and reciprocal space and subsequently denoted as dual-space iterative methods.[155, 156] These dual-space methods are computationally intensive, however, recent advantages in computer processing power has accelerated their use in structure solution in recent years.

Dual-space methods apply constraints in both reciprocal space (Fourier amplitudes impose a constraint on possible electron densities) and direct space (the requirement for the positivity of electron density). These constraints are properties that electron density must fulfil and the combination of these in both direct and reciprocal space allows for subsets of densities to be determined. These subsets are determined by looking at all possible electron densities and finding combinations of subsets that fulfil both constraints.[156] In order to do this, sophisticated algorithms are required; the main algorithm used is charge flipping. Charge flipping is an iterative method which allows for electron densities to be modelled until convergence is observed during the iterative process.[157, 158] This subsequently allows for the electron density map (in a P1 unit cell) to be determined which can then be used for both the crystal structure and space group determination. An advantage of charge flipping over direct methods is that no information about the chemical composition or symmetry is required.[156]

2.1.5 Least Square Iterations and Structure Refinement

Once initial F_{hkl}^{calc} have been calculated from either Direct methods, Patterson methods or Dual-space methods, new F_{hkl}^{calc} can be subsequently calculated using least square iterations. The initial F_{hkl}^{calc} are subsequently used to create an electron density map which is then subtracted from the one which arises from the measured experimental data. This then allows other regions of electron density to be assigned to other atoms within the molecule(s), allowing additional atomic positions and the relative atomic structure factors to be used to re-calculate F_{hkl}^{calc} values. Subsequently, an updated electron density map is calculated and is again subtracted from the one which arises from the experimental data set. This iterative process continues until all atoms have been located and all the electron density has been accounted for. Once all or most of the atoms are determined, this process also involves a least-squares fit of the proposed atom locations with the measured data set to help refine the atom positions. The structure refinement continues this least squares iteration process, allowing the atomic

positions, thermal vibration and other parameters to vary, until the magnitude for the F_{hkl}^{calc} values is close to the observed values. Once the refinement has converged, the R factor (Equation 2.6) gives a measure of the refinement quality; for a well refined structure the R factor should be between 2-6 %.[146, 159]

$$R = \frac{\Sigma \left| \left|F_{hkl}^{obs}\right| - \left|F_{hkl}^{calc}\right| \right|}{\Sigma |F_{hkl}^{obs}|} \qquad \text{(Equation 2.6)}$$

2.1.6 Powder X-ray Diffraction (PXRD)

The above discussion of structure solution is based upon the collection of X-ray diffraction from a single crystal. X-ray diffraction can also be used with a polycrystalline powder with each individual small crystallite giving its own diffraction pattern which are then superimposed onto one another. Due to the different orientation of the crystals, diffraction peaks are generated by each of the crystallites at different times as Bragg's law is satisfied for each. For each diffraction peak the 2θ value is the same, however the direction of the reflected X-rays will vary. This results in a cone of reflection being observed, as is shown in Figure 2.5.[160, 161]

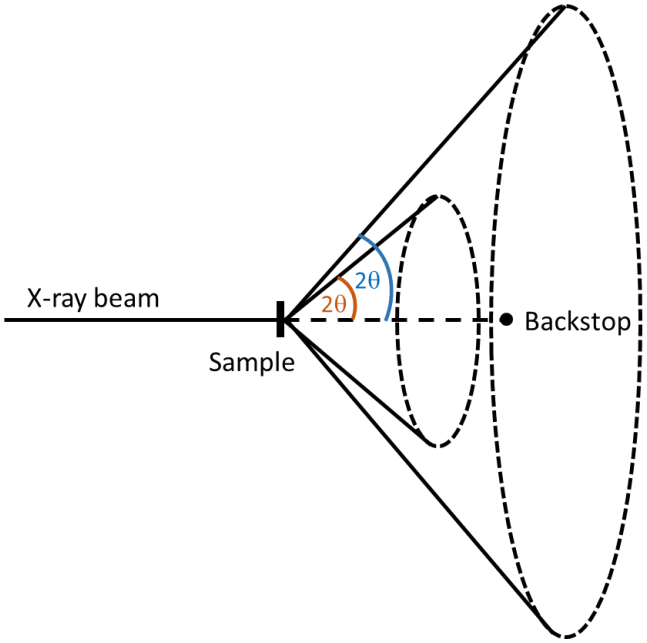

Figure 2.5: Schematic of powder X-ray diffraction (PXRD) showing two cones of diffraction resulting from a multi-crystalline powder sample.

The detector moves through 2θ values and measures the intensity of these cones of diffraction, resulting in a plot of intensity versus 2θ. The position of peaks in a PXRD pattern are unique to each crystal structure and are determined by the unit cell parameters and can therefore be used as fingerprinting tools. This is incredibly valuable when trying to differentiate between different solid forms of a system. With very well-resolved powder diffraction data, these plots, or powder diffraction 'patterns', can also

be indexed to determine the unit cell parameters, and even solve or refine the crystal structure using methods such as Rietveld refinement; the intensities of the peaks are determined by the unit cell contents. However, there can also be issues with PXRD data, such as, the simultaneous presence of diffraction from different Miller sets that satisfy Bragg's law at similar 2θ value, which can result in overlapping peaks in the PXRD patterns.[160, 162] The intensity of the rings of diffraction also may vary due to preferred orientation effects, increasing the intensity of some of the peaks; the sample is often rotated during the data collection to mitigate this. [161, 162]

2.2 Thermal Analysis Techniques

2.2.1 Differential Scanning Calorimetry (DSC)

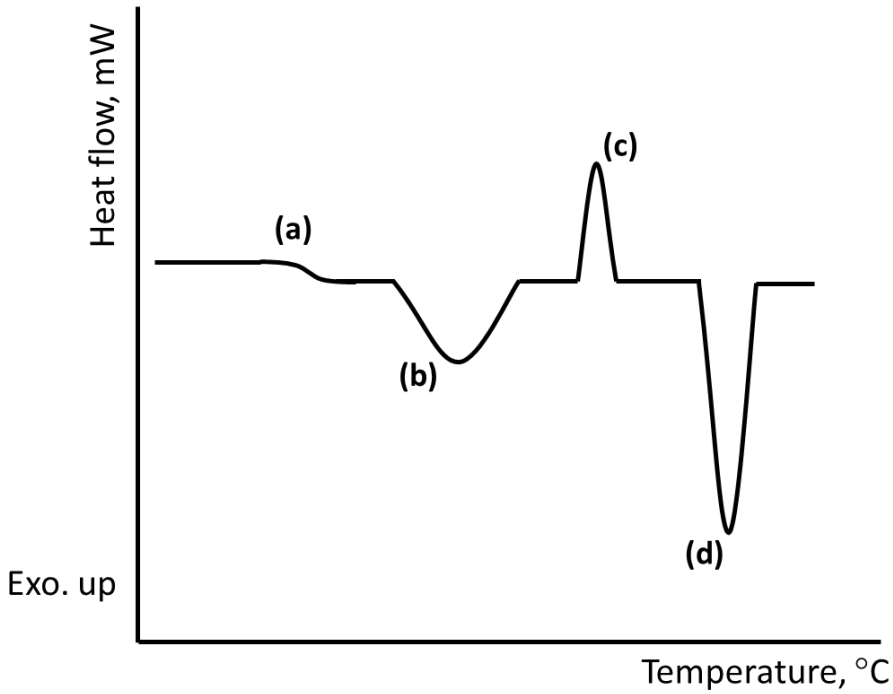

Figure 2.6: Diagram showing typical events in a DSC trace (exothermic up): (a) glass transition, (b) desolvation or phase transition, (c) re-crystallisation and (d) melting.

Differential scanning calorimetry (DSC) is an analytical technique that measures the difference in heat flow between a reference and the sample. During DSC a small amount of sample (1 – 10 mg) is placed inside an aluminium or ceramic pan. This pan is then placed inside the DSC instrument along with an empty reference pan. The sample and reference pan are then subject to the same heating/cooling profile and the difference in heat flow between the two is measured. This method can yield information about melting, decomposition, glass transitions, phase transitions and recrystallisation. During a thermal event the difference in heat needed to be given to the sample to keep it at the same temperature as the reference pan will be altered. If an endothermic event, such as melting occurs upon heating the sample, the heat flow required by the sample pan to keep it heating at the same rate as the reference pan will be higher than is

required by the reference. If an exothermic event, such as recrystallization occurs, the opposite will be true. Typically, a DSC trace will consist of a plot of the overall heat flow versus temperature and can give valuable information about the thermal behaviour of a system. An example of a DSC trace displaying typical thermal events can be seen in Figure 2.6 .[163, 164]

2.2.2 Thermogravimetric Analysis (TGA)

Thermogravimetric Analysis (TGA) measures mass loss as a function of temperature. It can be used to investigate the stoichiometry of solvates as well as investigation into the decomposition behaviour of a material. A sample pan (aluminium or ceramic) is prepared with a known quantity of material (typically a few mg) which is then placed onto a hanging balance within the instrument. A heating profile is designed to which the pan is then subjected. A weak flow of nitrogen can be applied over the sample chamber to provide an inert atmosphere if required. As thermal events, such as solvent loss, melting and decomposition occur, mass may be lost from the sample in the form of vapour. This mass loss is measured and plotted against the temperature. The resulting trace allows for calculation of percentage mass loss of the total sample mass. TGA can also be coupled with a mass spectrometer in order to further analysis the gaseous phase given off during the heating. A typical TGA trace can be seen in Figure 2.7.[163, 164]

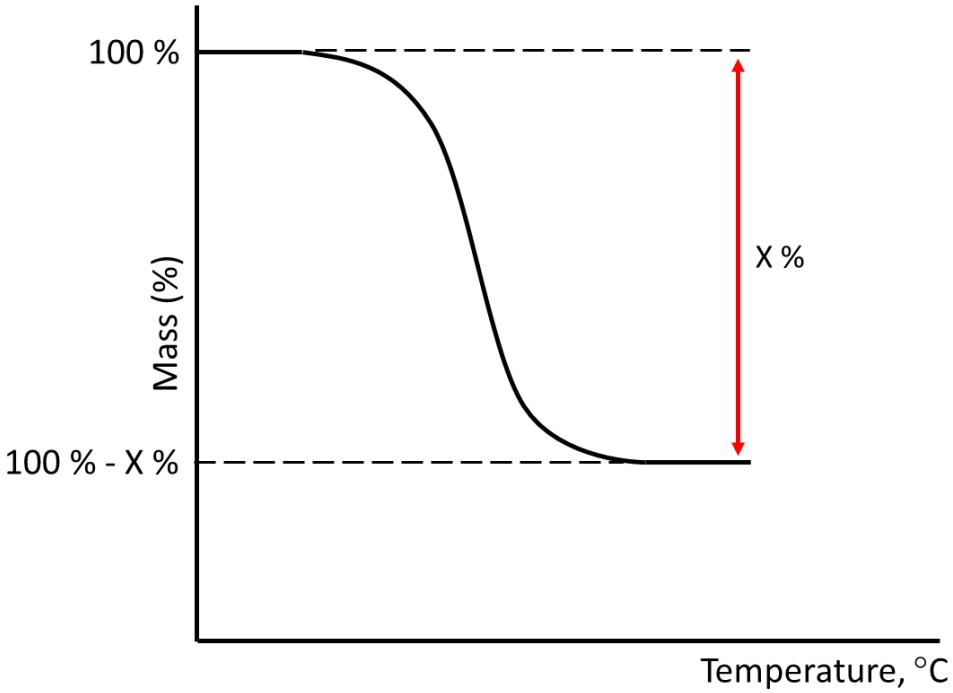

Figure 2.7: A typical TGA trace.

2.3 Process Analytical Technologies (PAT)

The FDA process analytical technologies (PAT) initiative defines process analytical technologies as a way of *'designing, analysing, and controlling manufacturing through timely measurements (i.e., during processing) of critical quality and performance*

attributes of raw and in-process materials and processes, with the goal of ensuring final product quality.'[165] The use of PAT over the past 20 years has increased significantly, with the FDA developing an initiative in 2002 to promote its uptake in the pharmaceutical industry and publishing a guidance for industry in 2004.[166] The FDA states that the goal of PAT is to control the manufacturing process and enhance one's understanding – '*quality cannot be tested into products; it should be built-in or should be by design.'*[165] The utilisation of *in-situ* analytics in a process provides the potential for a much faster and more enhanced understanding to be gained of the process and allows for better design and control. The use of 'real time' analytical measurements to be taken during a manufacturing process allows for quick intervention and correction if the results are not within the required specification.[167] PAT instruments encompass measuring conditions such as pressure, pH and temperature as well as utilising spectroscopic analytical techniques such as infrared (IR), Raman and UV/vis. Other PAT techniques allow for particle size measurements such as focused beam reflectance measurement (FBRM) and particle vision and measurement (PVM) probes.[166-168]

2.3.1 Focused Beam Reflectance Measurement (FBRM)

The predominant PAT method used in this project will be focused beam reflectance measurement (FBRM). This method allows for *in situ* measurements of the particle characteristics to be taken. It is often used in crystallisation to measure the chord length of the crystalline particles (in the range of 0.5 – 2000 μm) and to give information on the chord length distribution (CLD), both of which can be related to the particle size and particle size distribution. It can also provide valuable information about when nucleation and growth occur within the system. Empirical and theoretical methods of obtaining conventional diameter distributions of the particles from the chord length distributions are available.[169, 170]

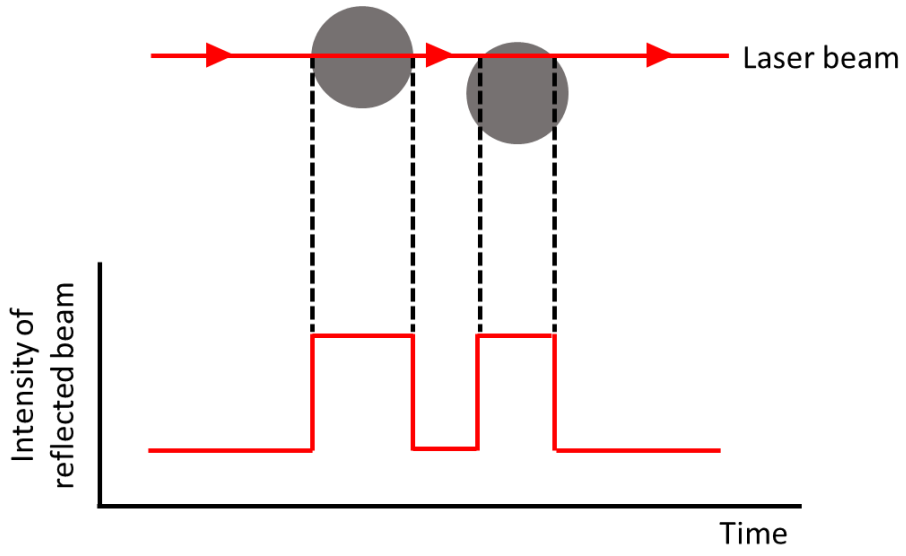

Figure 2.8: Pictorial representation of how FBRM works: intensity of reflected laser beam is measured to determine chord length. Chord lengths will vary with size of particles, where the laser crosses the particle and the shape of particles.

FBRM probes work by the use of a laser that rotates at a specified velocity and gives a beam of highly focused light at a point near the probe window. When rotating, the laser interacts with particles in the solution and when the beam crosses over a particle the light is reflected back to the instrument and is detected. As the velocity of the rotating beam is known then the duration of the reflected light pulse can be directly correlated to the width of the particle the beam crossed. As it is unlikely that the beam will have crossed through the centre of the particle, giving the diameter, a chord length is measured (Figure 2.8). The data collected during an FBRM experiment is typically plotted as counts (the number of particles in a specified chord length range per second) versus time. The chord length ranges can be set by the user to give an accurate representation of the measured chord lengths and CLD with time. [169, 170]

2.4 Continuous Crystallisation Platforms

There are many variations of continuous crystallisation platforms available, some utilising tubular designs (for example the Continuous Oscillatory Baffled Crystalliser, COBC), and some being made form a cascade of stirred tanks (for example the Mixed Suspension Mixed Product Removal, the MSMPR). Different designs of reactor can be beneficial for different reactions, and each possesses their own advantages and disadvantages.

In a flow environment there are different types of flow possible, depending on the conditions. Laminar flow, as shown in Figure 2.9, has an uneven dispersion of velocity depending on where in the pipe the solution is: solution in the middle has the highest velocity, with velocity decreasing as the solution gets closer to the walls. Plug flow, however, is when the velocity is the same regardless of the position. Plug flow results in the entire solution experiencing the same conditions and also results in a much narrower residence time (RT) distribution. The residence time is defined as the time it takes for a particle to travel the entire length of the crystalliser. For uniformity in a flow process the residence time distribution (RTD, the spread of residence times observed in the crystalliser) should be as narrow as possible.[171-173]

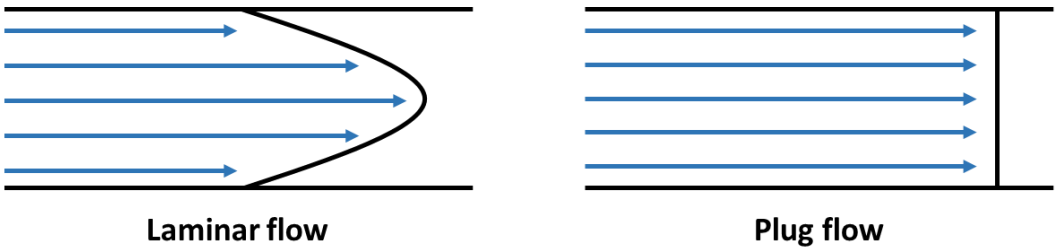

Figure 2.9: Pictorial representation of laminar flow and plug flow.

In a tubular reactor the residence time is directly related to the internal diameter of the tubing and the flow rate. To achieve plug flow high flow rates are required coupled with small internal diameters. However, this results in short residence times which may not allow enough time for the process to complete. To overcome the need for fast flow rates

and small internal diameters, internal mixing apparatus can be utilised with the aim to achieve more turbulent mixing within the tubing, allowing for plug flow to be accessed more easily.[171, 172]

Continuous flow platforms do not, however, have to be tubular and can be made from a cascade of stirred tank reactors (STR). A Mixed-Suspension Mixed-Product Removal (MSMPR) set up utilises a cascade of stirred tanks that flow into one another either continuously, or periodically, in order to mimic a continuous process. The residence times in each reactor, the temperatures and stirring can all be controlled separately allowing for sophisticated temperature profiles to be attained. MSMPRs have been shown to achieve higher production capacity in comparison to equivalent batch processes with shorter residence times and comparable yields.[173-175]

2.4.1 Continuous Oscillatory Baffled Crystalliser (COBC)

Oscillatory flow reactors (OFRs) are types of tubular reactors that contain periodic restrictions (often baffles joined via constrictions) combined with oscillation of the fluid. These reactors inherently have efficient mixing due to the constant generation and cessation of eddies formed from the interaction of the oscillating flow with the baffles.[176-179] Figure 2.10 demonstrates the formation of eddies in an OFR. As solution passes through the constrictions on an upstroke, eddies are formed downstream of each baffle joint. On the down-stroke, the solution is forced backwards through the same constrictions causing eddies to be formed on the opposite sides of the baffle joints. As the oscillation continues the eddies from both the upstroke and down-stroke collide within the baffles, thereby producing mixing similar to what is obtained in a well-mixed stirred tank reactor.[178]

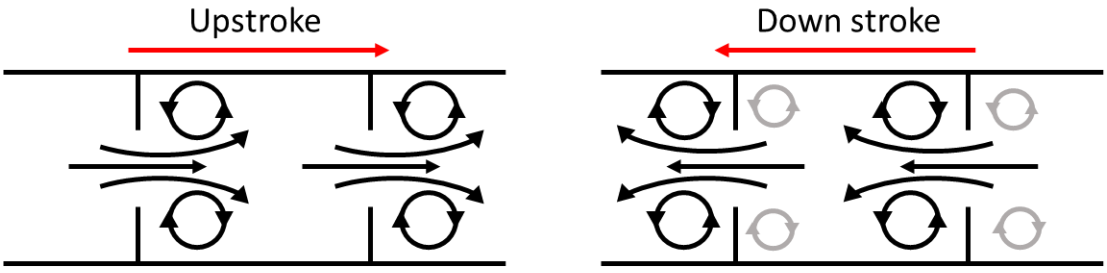

Figure 2.10: Eddies formed in an oscillatory baffled reactor (OFR) on the upstroke and down stroke oscillations.

The flow within an OFR is governed by three main equations (below) which yield dimensionless constants that describe the flow conditions. Firstly, the oscillatory flow Reynolds number (Re_o) quantifies the oscillation behaviour within the system and the intensity of mixing applied to the tube. The net flow Reynolds number (Re_n) quantifies the overall flow and the Strouhal number (St) is the ratio of tubing diameter and oscillatory stroke length and quantifies the propagation of eddies inside the baffles.[176, 177 179]

$$Re_o = \frac{2\pi f \rho d \chi_o}{\mu} \qquad \text{(Equation 2.7)}$$

$$Re_n = \frac{\rho u d}{\mu} \qquad \text{(Equation 2.8)}$$

$$St = \frac{d}{4\pi\chi_o} \qquad \text{(Equation 2.9)}$$

Where f is the frequency of oscillation (Hz), ρ is the density of solution, d is the tubing diameter (m), χ_o = centre to peak amplitude (m), μ is the viscosity of solution (kg m^{-1} s^{-1}), u is the mean velocity (m s^{-1}).

The velocity ratio (φ) can be determined from the ratio of the oscillatory Reynolds number and the net flow Reynolds number:

$$\varphi = \frac{Re_o}{Re_n} \qquad \text{(Equation 2.10)}$$

In order to access plug flow operation there are general limits for the above values: $Re_o \geq 100$, $St \leq 0.5$ and $Re_n \geq 50$. The velocity ratio (φ) should always be greater than 1 (the oscillation velocity should exceed the net flow velocity) with values of 2 to 10 advised for plug flow operation.[177]

The continuous oscillatory baffled crystalliser (COBC) is an OFR designed and marketed by NiTech solutions, founded by Professor Xiong-Wei Ni in 2004.[180] The crystalliser is of a tubular design and utilises the design of OFRs. The COBC is comprised of a number of straights and bends allowing for flexibility in the length of the crystalliser. The COBC has been shown to offer improved control over the size and shape of crystals as well as also significantly reducing crystallisation time by up to 97 %. It has also been shown to allow for near plug flow conditions when operating under steady state.[172, 181]

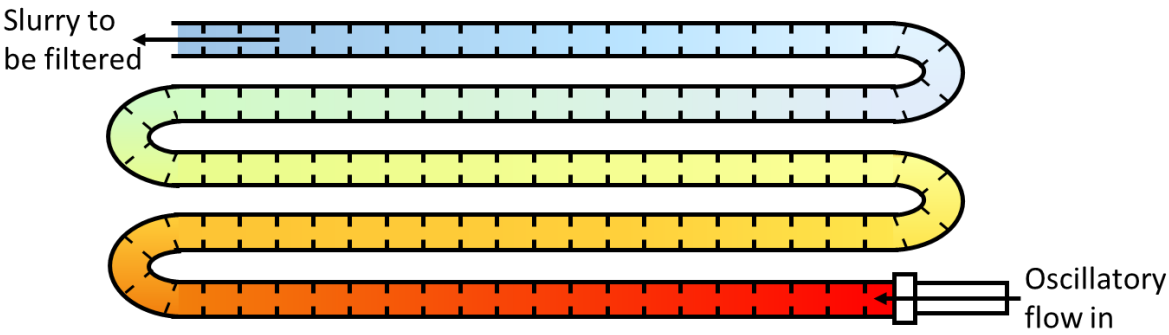

Figure 2.11: Diagram of a continuous oscillatory baffled crystalliser (COBC).

The COBC can be used for cooling crystallisation processes, with the temperature profile being controlled by the jacket temperatures via the use of external chillers. An external bellows is attached to provide the oscillation of the flow. The amplitude and frequency of the oscillation can be altered to allow for optimal mixing within the system, resulting in full suspension of the solid particles in solution. The hot feed solution is pumped into the crystalliser and is cooled as it is flowed through the length of the tubing, as

demonstrated in Figure 2.11. The system can be left to spontaneously nucleate, or seeding can be implemented to allow for secondary nucleation. The volume, and hence residence time, of the crystalliser can be manipulated by the addition or removal of straights from the set-up.[182, 183]

2.4.2 Kinetically Regulated Automated Input Crystalliser (KRAIC)

The Kinetically Regulated Automated Input Crystalliser (KRAIC), designed at the University of Bath, works on the premise of segmented flow to achieve plug flow conditions throughout the reactor length.[184] Liquid segmented flow uses an immiscible liquid (carrier fluid) to created discrete segments, or slugs, within the reactor. Within the flow set up, these slugs can move through under plug flow conditions and act as mini batch reactors. The mixing generated in the flow conditions is gentle and bolus in nature. Under these conditions, it has been shown that narrow PSDs can be accessed. Gas segmentation can also be utilised in some cases, however can result in fouling issues, which are a major downfall for continuous flow reactors and crystallisers. [185-188]

In segmented flow reactors/crystallisers the chosen immiscible medium, whether a liquid or gas, is brought to the reaction or crystallisation solution via a mixer piece. When the two media come into contact segmentation occurs resulting in discrete slugs of the solution medium and slugs of the chosen segmenter. Figure 2.12 demonstrates segmented flow using a Y mixer piece. The carrier fluid is chosen so that it also preferentially wets the crystalliser walls, resulting in the solution slugs only having solution-solution interfaces. As the solution slugs should never touch the crystalliser walls, encrustation should be prevented. In the KRAIC, the implementation of a cross mixer piece, to introduce not only the chosen carrier fluid, but also air allows for tri-segmented flow to be achieved. [184]

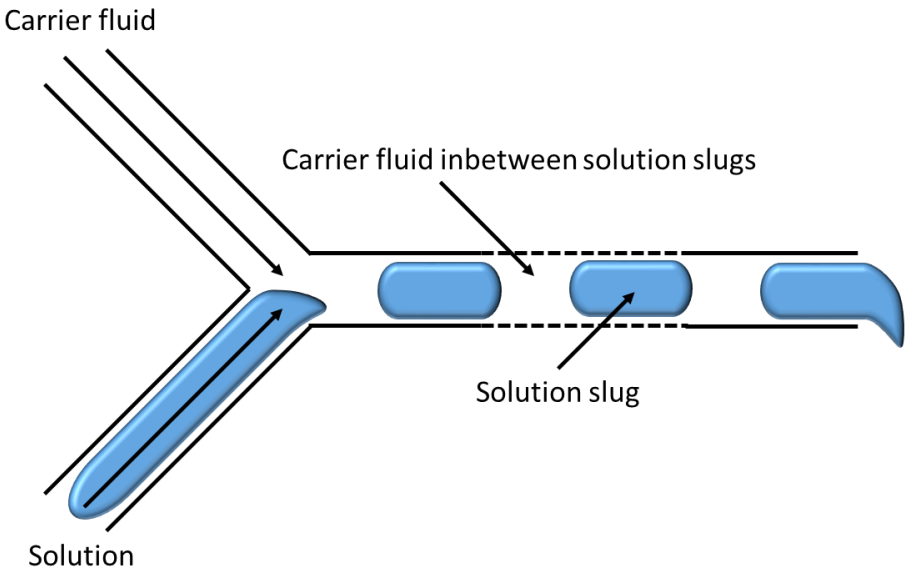

Figure 2.12: Representation of liquid segmented flow using a Y-mixer piece.

The KRAIC is set-up to have a 15 m crystalliser length and an internal diameter of 3.2 mm. The tubing is made of fluorinated ethylene propylene (FEP) and both peristaltic and gear pumps are used to flow the solution, carrier fluid and air into the system. The tubing is coiled around to form three discrete coils for ease of temperature control (Figure 2.13). Each coil is made up of 10-11 rungs and the system flows from the bottom of the coil to the top. Each coil can be heated via use of a Drysyn hot plate or can be cooled using an ice bath to access the desired temperature profile.

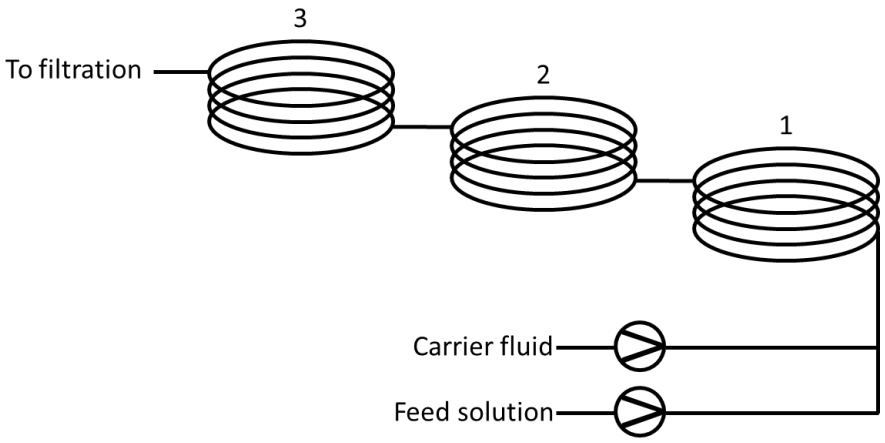

Figure 2.13: Schematic of the Kinetically Regulated Automated Input Crystalliser (KRAIC) set-up.

The platform, similarly to the COBC, utilises cooling crystallisation with the hot feed solution being pumped in and allowed to cool and subsequently crystallise as it travels through the reactor. Tubing jackets for the tubing running from the feed solution to coil 1 can also be implemented to either provide additional heating of the feed solution to keep it at the feed temperature, or they can be used after segmentation to cool the solution in order to help to induce spontaneous nucleation. At the end of coil 3 the exit tubing carries the slurry to the end of the crystalliser where it is filtered using vacuum filtration techniques. The carrier fluid is separated from the segmented flow at the end piece, immediately before filtration, to be recycled back into the crystalliser. The crystallisation platform has been successfully used for continuous crystallisation of a variety of materials including succinic acid, paracetamol and UBA.[135, 184, 189, 190]

Chapter 3 – Experimental Techniques and Instrumentation

3.1 Solubility Measurements

For this work, three methods for solubility measurements were used: turbidity measurements using the Technobis Crystal16 were conducted at the University of Strathclyde and at GSK, Stevenage, whilst at the University of Bath gravimetric solubility measurements and solubility measurements by observation were conducted using the Cambridge Reactor Designs (CRD) Polar Bear Plus apparatus.

3.1.1 Turbidity Measurements using the Crystal16

Figure 3.1: The Technobis Crystal16.

The Technobis Crystal16 (Figure 3.1) works on the basis of measuring the transmissivity of a laser through a sample in order to determine clear points (when transmissivity reaches 100 %) as well as cloud points (when transmissivity drops from 100 %). Solutions of known concentrations are prepared in 1.5 mL vials by weighing a known amount of the target solid and adding 1 mL of the chosen solvent. These vials are then placed into the Crystal16 and magnetic bottom stirring is used to agitate the system. Up to 16 vials can be investigated in parallel, with the flexibility to have four separate temperature profiles investigated simultaneously (4 x 4). A temperature profile is designed to allow for specific cooling and heating of the system during which the transmissivity of a laser through the solutions is measured. Upon heating of the system, when all solid has dissolved, the transmissivity reaches 100 %, yielding the clear points. These clear points are taken as the solubility points for the solutions. Multiple concentrations can be measured at once allowing for a solubility curve to be plotted. The system can then be cooled down and the transmissivity is again measured. Once nucleation occurs within the system the transmissivity will drop below 100 %, giving the cloud point (representing the metastable limit as this is the region where spontaneous nucleation occurs). An accumulation of cloud points will allow for the metastable zone width to be measured for the system in question.

All data were analysed using CrystalClear v.1.0.1.614 from Avantium Technologies. An example of a resultant plot of transmissivity versus temperature versus time can be seen below in Figure 3.2. The clear and cloud points can be clearly determined from the data to give the solubility and MSZ. Further details of the temperature profiles used for individual studies can be found in the relevant chapters. For each concentration, one replicate was conducted and both sets of data points were used to create the solubility curves.

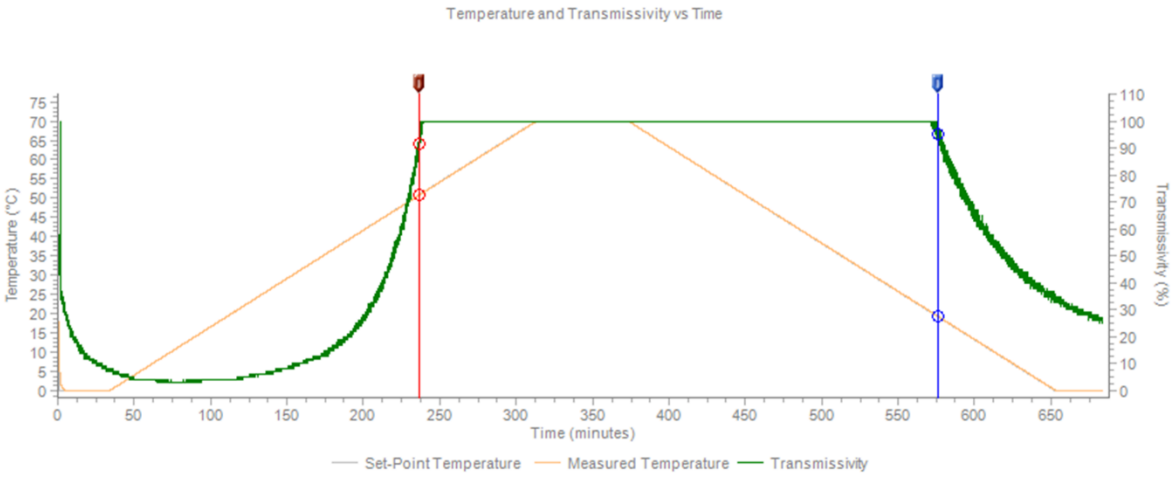

Figure 3.2: CrystalClear plot of data obtained from a Crystal16 experiment: green line represents the transmissivity and the orange line indicates the temperature. Red and blue vertical lines represent the clear and cloud points, respectively.

3.1.2 Gravimetric Measurements

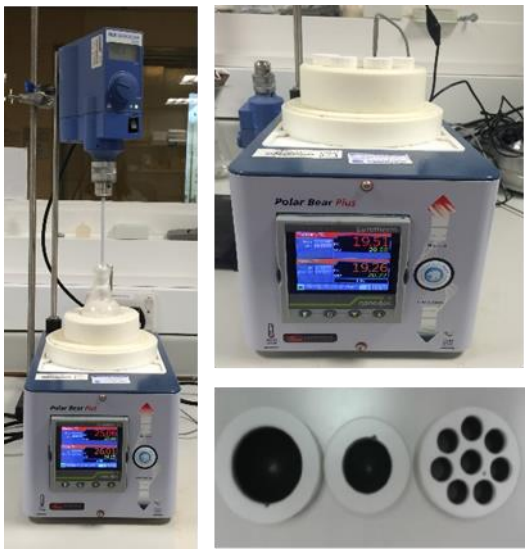

Figure 3.3: The Cambridge Reactor Designs (CRD) Polar Bear Plus Crystalliser.

Gravimetric solubility measurements of UBA form I and form III in both ethanol and isopropanol (IPA) were conducted using the Cambridge Reactor Designs (CRD) Polar Bear Plus Crystalliser (Figure 3.3). The Polar Bear Plus provides a platform for controlled heating/cooling of samples in a temperature range of -40 °C to 150 °C. It has

interchangeable inserts to allow for gradual scale up of systems from 1.5 mL vials to 250 mL round bottom flasks (RBF).

The gravimetric solubility measurements were carried out using a 100 mL RBF with a working volume of 50 mL of solvent. Excess solid was added to the solvent to create a suspension which was kept at a pre-determined constant temperature. Overhead stirring of the suspension was provided by an external motor and shaft and set to 350 rpm. 2 mL aliquots of the slurry were taken at set time intervals (after 15 minutes, 30 minutes, 1 hour, 2 hours and 4 hours). The aliquots were filtered through a syringe to remove any solid present and placed into pre-weighed, clean vials. These vials were then weighed before being left undisturbed at 30 °C (on a Drysyn hot plate) to allow for the solvent to evaporate. The vials were weighed daily for the next four days, or until the mass stabilised. The concentration of solute in the 2 mL aliquots was calculated allowing for the equilibrium solubility at that temperature to be determined. These experiments were conducted at 20 °C, 30 °C, 40 °C, 50 °C and 60 °C to obtain solubility curves.

3.1.3 Solubility by Observation

The solubilities of UBA form I and form III in both ethanol and isopropanol (IPA) were also measured using observation techniques. For these experiments the CRD Polar Bear Plus was used to allow for controlled heating of the sample. 25 mL of the chosen solvent was allowed to equilibrate at 0 °C before any solid was added. Magnetic bottom stirring was used and set to a stirring rate of 700 rpm. Once the solvent had reached 0 °C, small increments of solid were added and allowed to dissolve. The quantity of solid added until no more would dissolve into the solvent was noted; this value gives the solubility at 0 °C. If the first addition of solid did not dissolve, the sample was heated slowly until the solid went into solution, giving the first solubility point. The solution was heated up at a rate of 0.2 °C min^{-1} and further increments of solid (of known mass) were added to the solution. As the temperature of solution increased the additional solid dissolved and the temperature at which all the solid had dissolved was noted before subsequent increments were added. This process was repeated until the solution reached a temperature of 60 °C. The masses added were used to calculate the concentration of solution and this, with the observed dissolution temperatures, yielded solubility curves.

3.2 Metastable Zone Width Measurements

Metastable zone width measurements for the cooling crystallisation of UBA from both ethanol and IPA were conducted using the CRD Polar Bear Plus with a 250 mL RBF. The experiments were conducted with a working volume of 150 mL of the chosen solvent and the starting concentrations of UBA was chosen based on the measured solubility data. The mass of the starting components (urea and barbituric acid) were calculated to result in the desired concentration of the 1:1 UBA co-crystal in the system. Several different saturation temperatures were investigated (20 °C to 60 °C) in order to obtain

a MSZW with at least three points. The starting components were added to the solvent separately (barbituric acid was added first and allowed to dissolve before the urea was added) and overhead stirring at 400 rpm was used to suspend the slurry. The system was heated to 15 °C above the saturation temperature and held for 1 hour to allow for full dissolution of the barbituric acid starting material before the urea was added and allowed to dissolve (< 15 minutes). The system was then cooled down at a rate of 1 °C min^{-1} and filmed using a GoPro $Hero3^{+}$. Once nucleation had been observed the crystallisation was halted and the slurry filtered and dried. The resulting crystalline powder was then analysed using PXRD to determine the polymorphic form. The nucleation temperature was determined by watching the video and observing when crystals can first be seen in the solution. Obtaining spontaneous nucleation temperatures for a variety of concentrations allowed for a MSZW to be plotted.

3.3 Crystallisation Techniques

For this work, a variety of different crystallisation techniques were used: evaporative crystallisation, slurry techniques, cooling crystallisation (in both batch and continuous platforms) and mechano-chemical crystallisation.

3.3.1 Evaporative Crystallisation

For this study evaporative multi-component crystallisations were conducted for urea with barbituric acid as well as thiobarbituric acid with a variety of co-formers. In 7 mL vials, small amounts of the chosen solids (10-20 mg) were added in a variety of different molar ratios: 1:1, 2:1, 3:1, 1:2 and 1:3. The chosen solvent was then added in small quantities (mL) until full dissolution of the solid material was observed. In some cases, a small amount of heating coupled with sonication of the sample was used to aid dissolution. Once the solid was fully dissolved, plastic caps were placed on the sample vials which had approximately six small holes pierced in them. The samples were then left undisturbed to allow for solvent evaporation and subsequent crystallisation. All crystallisations conducted in this way were set up to contain both the target material and co-former, with the intention of forming a multi-component system. In addition to the different stoichiometries of starting materials, a variety of different evaporation temperatures were also investigated: 5 °C (placed in fridge) and room temperature, 30 °C, 40 °C and 50 °C. For the elevated evaporation temperatures Drysyn hot plates were used for temperature control. The samples were observed for any crystallisation and the crystals were harvested before the samples completely dried out, in an aim to keep any unwanted impurities in the solution phase. The crystals were analysed via optical microscopy as well as DSC and PXRD in order to determine if a new phase (or in the case of UBA, the desired phase) had been accessed. If a new form had been accessed single crystals were harvested for single crystal X-ray diffraction analysis.

3.3.2 Solution-mediated Crystallisation Techniques (Slurry Techniques)

Slurry techniques can be an efficient means of probing polymorphic phase transformations as well as investigations into multi-component crystallisation. In this thesis multi-component screening was conducted using slurry techniques as well as competitive slurrying between polymorphic forms of UBA to investigate stability relationships.

3.3.2.1 Multi-component Slurrying Experiments

Small scale slurries were prepared by using ~200 - 400 mg of target compound and the chosen co-formers in corresponding molar ratios: 1:1, 2:1, 1:2 and 1:3. A small amount of solvent (a few mL) was then added to the solid materials in 7 or 20 mL vials (depending on the scale) ensuring that not all the solid dissolved and an excess remained, forming a suspension. The samples were placed in the CRD Polar Bear Plus or a Drysyn hot plate for temperature control (20 °C or 30 °C). Magnetic bottom stirring (250 – 350 rpm) was used for agitation. A variety of solvent media were used (ethanol, methanol, IPA and water), depending on the specific study being undertaken. The systems were left slurrying for a predetermined amount of time before being filtered and dried at room temperature. The slurry product was then analysed for solid form identity by PXRD and DSC. Full experimental parameters can be found in the relevant chapters.

For investigations into larger scale slurries (for the crystallisation of UBA from ethanol) 100 mL RBFs were used with overhead stirring (400 rpm) as opposed to flat bottom vials with magnetic bottom stirring. The CRD Polar Bear Plus was used for temperature control, as well as an adapted water bath set up that utilised an external circulator for temperature control. At this scale, 5 g of urea was used with barbituric acid being weighed in its corresponding molar ratio (1:1 or 2:1). These slurries were then subject to a Design of Experiments study, full details of which can be found in Section 3.4.2.

3.3.2.2 Competitive Slurrying

For competitive slurries two polymorphic forms of UBA were mixed together to create a 1:1 solid mixture. 150 mg of this mixture was placed into 1.5 mL glass vials and 1 mL of the chosen solvent (ethanol) was added. The CRD Polar Bear Plus was used to allow for both magnetic bottom stirring (set at 1500 rpm – experimentally at 1429 rpm) and temperature control (20 °C, 40 °C, 50 °C and 75 °C). The slurries were left mixing for a pre-determined amount of time (between 24 hours and 2 weeks). The slurries were then filtered via vacuum filtration and left to dry at room temperature before being analysed by PXRD. Full details can be found in the relevant chapters.

3.3.3 Cooling Crystallisation

Cooling crystallisations were conducted in both batch and continuous platforms. For batch crystallisations the CRD Polar Bear Plus and the Mettler Toledo Easymax platforms

were used. For continuous cooling crystallisations two platforms, the COBC and KRAIC, were utilised.

3.3.3.1 Unseeded Batch Cooling Crystallisation

Small scale cooling crystallisations (1 – 10 mL) were conducted using the CRD Polar Bear Plus with magnetic bottom stirring. 1.5 mL or 20 mL vials were used depending on the scale of crystallisation. Solid was weighed into the vials and the appropriate amount of chosen solvent added. The vials were placed in the Polar Bear Plus and stirred at 400 rpm. Cooling profiles were designed based on the solvent used and the solubility data obtained for the system of interest. The systems were heated to the initial temperature at a rate of 10 °C min^{-1} and held for a specified amount of time (usually 1 hour) to allow for the solid to dissolve fully. Once all the starting components had dissolved the system was then cooled to the final temperature with a predetermined cooling rate. Once at the final temperature the systems were left to dwell for a specific amount of time before being filtered via vacuum filtration, dried at room temperature and then analysed for solid form identity. Full experimental details on individual systems can be found in the relevant results chapters.

For larger scale batch cooling experiments (50 – 150 mL), the CRD Polar Bear Plus was used with RBFs. Overhead stirring was provided by an external motor and shaft. The starting components were weighed and added to the solvent in the RBF and heated at 10 °C min^{-1} to the starting temperature. In the case of UBA crystallisations, barbituric acid was added to the solvent and heated to the starting temperature and left for 1 hour to allow for full dissolution. The urea was then added and left for approximately 15 minutes to dissolve. For all other systems, once the starting temperature had been reached the system was held for 30 minutes – 1 hour to allow for full solvation. Once all the starting components had fully dissolved the system was then cooled, via the same profile used for the corresponding small scale experiment and held at the final temperature for a specified length of time. Full experimental details on individual systems are provided in the relevant results chapters.

3.3.3.2 Seeded Batch Cooling Crystallisation

Seeded cooling crystallisations were conducted at GlaxoSmithKline's Stevenage site using their Mettler Toledo Easymax system coupled with the Lasentec FBRM probe. The Easymax is a platform that allows for sophisticated heating/cooling programs to be conducted between -40 °C and 180 °C. The platform has two parallel reactors (these can be 50 mL or 100 mL vessels), allowing for two crystallisations to be conducted in tandem. The set-up also allows for overhead mixing, solvent dosing and the use of PAT probes. For this work, a Mettler Toledo Lasentec FBRM probe was used to investigate nucleation and growth during the seeded cooling crystallisations.

Both ethanol and IPA were used as solvent media in the seeded cooling crystallisations of urea barbituric acid, along with both UBA form I and form III seeds. For the seeded cooling crystallisations the solution concentration was based on measured solubility for

UBA in both solvents. Both the solvent and barbituric acid were added and the system was heated to 70 °C (as fast as possible) and held until full dissolution of the barbituric acid was observed (as shown by the FBRM counts). The urea was then added to the system and allowed to dissolve. Once the FBRM data showed full dissolution of both starting components, the system was cooled to 60 °C at a rate of either 0.5 °C min^{-1} or 1 °C min^{-1}, depending on the experiment being conducted. At 60 °C the seed material was added (1 %, 5 % and 20 % seed loadings were investigated) and the system was held for a 15 minute seed age. Cooling then continued at the same rate as pre-seeding until the final temperature of 0 °C was reached. The system was held at the final temperature for 1 hour before being filtered via vacuum filtration and dried at room temperature. For some experiments, the system was held at the final temperature overnight before being filtered.

During the crystallisations, small samples were taken every 10 minutes in order to follow the supersaturation during the crystallisation process. A plastic pipette was used to take a small slurry sample from the system, which was then put into a syringe with a filter tip. The sample was filtered via the syringe and the solution was collected in a pre-weighed 1.5 mL vial. The mass was taken and then the samples were left at 50 °C in a vacuum oven overnight for solvent evaporation. The dry vials were then weighed and the concentration of the solution sample calculated. This was then plotted alongside the solubility to allow for the supersaturation to be followed throughout the experiment.

The FBRM probe was set up to take a measurement every 15 seconds in order to determine the number of particle counts and the chord length distribution in the system. It was used for the entirety of the experiment.

3.3.3.3 Continuous Cooling Crystallisation in the COBC

The COBC was used in a 12 straight set up, resulting in an internal volume of 1.66 L. The peristaltic pump used for the introduction of the feed solution into the COBC was set to 4.1 rpm, which corresponds to a net flow rate of 50 mL min^{-1-}. The oscillation was supplied by external bellows and set to a frequency of 2 Hz with an amplitude of 25 mm. The residence time for the set up was 33.3 minutes (33 minutes and 20 seconds).

A Drysyn hot plate was used to heat the feed solution in a 5 L RBF and provide magnetic bottom stirring. Four external chillers were used for temperature control with chiller 1 linking to straights 1 and 2; chiller 2 linking to straights 3-6; chiller 3 to straights 7-10; and chiller 4 to straights 11 and 12. Fluorinated ethylene propylene (FEP) tubing was connected to the end piece to provide transfer of the slurry to the filtration set up. Vacuum filtration was used to isolate the solid product and the filter paper was changed every residence time. The product was left to dry at room temperature before being analysed for solid form identity.

In order to prime the COBC before a continuous crystallisation was initiated, pure solvent was flowed through the entirety of the crystalliser to flush it out and ensure no

impurities remained. The solvent was flowed through until all air had been pushed out from the crystalliser.

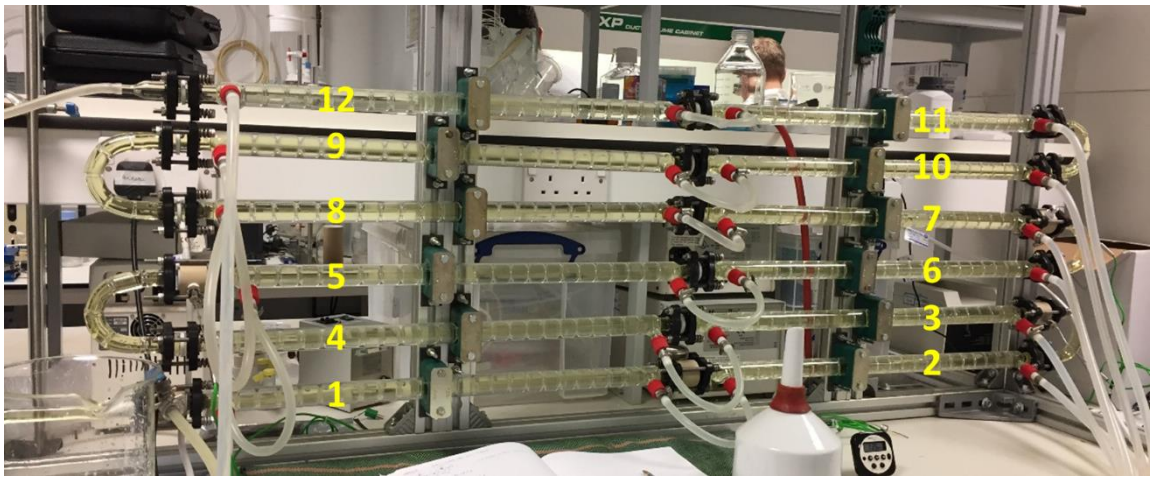

Figure 3.4: Experimental COBC set-up.

Continuous crystallisations of both UBA and two thiobarbituric acid (TBA) multi-component systems were conducted using the COBC. For the continuous crystallisation of UBA, ethanol was used as the solvent medium; for the TBA crystallisations water was the solvent medium of choice. Full details of experimental conditions are given in the relevant results chapters.

3.3.3.4 Continuous Crystallisation in the KRAIC

Continuous crystallisations of UBA from both ethanol and IPA, as well as continuous crystallisations of multi-component TBA systems from water, were carried out using the KRAIC. For the production of segmented flow, a cross mixer piece was utilised to allow for tri-segmented flow to be achieved within the system. Both air and an immiscible carrier fluid were introduced to the feed solution at the mixer piece resulting in the formation of alternating solution slugs and air slugs. The chosen carrier fluid, perfluoropolyether Galden SV110 (Galden) preferentially wets the crystalliser walls and as a result sits above, below and between the solution and air slugs. This results in no liquid-solid interfaces being present in the crystalliser for the crystallising solution, only liquid-liquid interfaces.

The feed solution was heated and stirred in a 3 L RBF using a Drysyn hot plate and was transferred to the mixer piece via a heated jacketed tube. The jacketed tubing was controlled by an external circulator in order to keep the feed solution hot as it flowed from the RBF to the mixer piece. The cross mixer piece was kept in a water bath to keep the feed solution at temperature; the temperature of the water bath was externally controlled by a Drysyn hot plate. Three pumps were used in this set up: a peristaltic pump for the feed solution and two gear pumps, one for the carrier fluid and one for the air. The flow rates on all pumps are moderated separately allowing for ease of fine tuning to get desirable flow and slug formation. The crystalliser length is 15 m and has an internal diameter of 3 mm, resulting in a volume of 106 mL. For each experiment the

residence time was measured in order to get an accurate value for each crystallisation, due to the variation of flow rates used. For this work the systems were allowed to cool naturally after the slugs left the mixer piece, with no external temperature control being exerted on the system. At the end of the crystalliser the slurry was collected over a vacuum filtration set up and the filter paper was changed each residence time. The product was allowed to dry at room temperature before being analysed for solid form identity via PXRD.

In order to prime the system, pure solvent and Galden is pumped through the entire length of the crystalliser to allow for segmentation to occur and to equilibrate as well as to flush out any impurities from inside the crystalliser. Once the system is primed the input is switched from the priming solvent to the feed solution. Once the feed solution has been depleted, the input is switched back to the priming solution to push the last residence time of material out of the crystalliser. The system is then flushed with pure solvent to remove all Galden before being emptied of all material. The experimental conditions for each experiment varied and can be found in the appropriate results chapters.

3.3.4 Mechano-chemical Crystallisation

Figure 3.5: Retsch PM100 Planetary Ball Mill.

Multi-component grinding experiments of TBA were conducted with chosen counter-ions. These experiments were carried out both by hand, using a pestle and mortar, as well as mechanically using a Retsch PM100 Planetary Ball Mill (Figure 3.5). Initial experiments used a 1:1 molar ratio of the components (using ~40 mg of TBA) and were ground for 15 minutes by hand using a pestle and mortar. Subsequent experiments utilised the ball mill, in which 15 x 3 mm ball bearings were used with a rotation speed

of 500 rpm. The grinding time was varied between 15 minutes and 1 hour. The resultant product was isolated and analysed using both PXRD and DSC.

3.4 Design of Experiments (DoE)

Design of Experiments (DoE) is a statistical method that is used to sample the entire problem space of a multi-parameter experiment in a systematic and even manner. In an experiment, one or more process variables (or factors) are normally changed, in order to observe the effect the changes have on one or more measured response variables. DoE is an efficient procedure for planning experiments so that the data obtained can be analysed to yield valid and objective conclusions.[191, 192] DoE begins with determining the objectives of an experiment and selecting the process variables for the study. It provides an effective method of exploring process variables as it uses a computer enhanced, systematic approach to experimentation that considers all factors simultaneously. DoE provides information about the interaction of factors, and their effect on the whole system, while also showing how interconnected factors respond over a wide range of values. Crucially, DoE achieves this without requiring the testing of all possible values, making it an efficient way of exploring a complex parameter space.

3.4.1 DoE for UBA III Formation using Solution-mediated Phase Transformations (Slurry Techniques)

Table 3.1: Experimental conditions for the solution-mediated phase transformation DoE - UBA in ethanol.

Exp No	Exp Name	Run Order	Incl/Excl	Temperature (°C)	Stirring rate (rpm)	Time (hours)
1	N1	10	Included	20	200	24
2	N2	7	Included	50	200	24
3	N3	11	Included	20	400	24
4	N4	2	Included	50	400	24
5	N5	1	Included	20	200	72
6	N6	9	Included	50	200	72
7	N7	8	Included	20	400	72
8	N8	5	Included	50	400	72
9	N9	6	Included	35	300	48
10	N10	4	Included	35	300	48
11	N11	3	Included	35	300	48

A full factorial DoE was conducted for the investigation of UBA formation using solution-mediated phase transition (slurry) techniques. The experiments were conducted at a 50 mL scale with ethanol as the solvent medium and a 1:1 ratio of urea: barbituric acid. For this investigation the chosen variables were the temperature of the slurry, the stirring rate and the length of time for which the sample was left slurrying. Table 3.1

outlines the experimental conditions for each of the eleven experiments. The response factors measured for this DoE study were the yield and the polymorphic outcome. Again, as numerical values must be assigned to the measured response factors, a pure product of form I was assigned the value 1, a pure product of form II was assigned the value 2, a pure product of form III was assigned the value 3 and a mixture of any of the polymorphic forms was assigned the number 4.

For these experiments a 100 mL RBF was used with 50 mL of ethanol, 5 g of urea and 10.66 g of barbituric acid. Unlike with previous slurry investigations, the CRD Polar Bear Plus was not used and instead an adapted water bath set up was used. This platform linked a water bath with an external chiller allowing for temperature control. The RBF was immersed in the water and overhead stirring was implemented via an external motor and shaft. Once the slurry experiment was complete the product was filtered via vacuum filtration and allowed to dry at room temperature before being analysed by PXRD.

3.4.2 DoE for Cooling Crystallisation of UBA from Ethanol

Table 3.2: Experimental conditions for cooling crystallisation DoE - UBA from ethanol.

Exp No	Exp Name	Run Order	Incl/Excl	Cooling rate (°C/min)	Dwell time (min)	Stirring rate (rpm)	SM ratio (stoichiometric)
1	N1	11	Included	0.5	10	200	1:1
2	N2	9	Included	1	10	200	1:1
3	N3	12	Included	0.5	60	200	1:1
4	N4	13	Included	1	60	200	1:1
5	N5	17	Included	0.5	10	400	1:1
6	N6	3	Included	1	10	400	1:1
7	N7	19	Included	0.5	60	400	1:1
8	N8	10	Included	1	60	400	1:1
9	N9	4	Included	0.5	10	200	2:1
10	N10	14	Included	1	10	200	2:1
11	N11	15	Included	0.5	60	200	2:1
12	N12	7	Included	1	60	200	2:1
13	N13	2	Included	0.5	10	400	2:1
14	N14	16	Included	1	10	400	2:1
15	N15	1	Included	0.5	60	400	2:1
16	N16	8	Included	1	60	400	2:1
17	N17	18	Included	0.75	35	300	1:1
18	N18	5	Included	0.75	35	300	1:1
19	N19	6	Included	0.75	35	300	1:1

A full factorial DoE study of UBA batch cooling crystallisation from ethanol was conducted using the MODDE 11 software to analyse the results and produce a model for the system. A summary of the experimental conditions for which individual experiments were undertaken can be seen in Table 3.2. The polymorphic form and yield

were the measured responses, with numerical values being assigned to the polymorphic outcome. A pure product of form III was assigned the value 3, with pure form I being assigned the value 1 and pure form II assigned the value 2. An experiment that yielded a mixture of the polymorphic forms was assigned the numerical value of 4. Pure form III (3) was the target response for the polymorphic outcome.

All DoE runs were conducted using the CRD Polar Bear Plus and a 100 mL RBF with a working volume of 50 mL of solvent. Overhead stirring was used throughout the entirety of the crystallisation, provided by an external motor and shaft. The initial and final temperatures remained constant (70 °C and 5 °C respectively) for all runs. Upon heating, the system was held at 70 °C for one hour to ensure full solvation of the starting components before being cooled. After each experiment, the samples were filtered using vacuum filtration and left to dry at room temperature before analysis. Once dry, the products were analysed using PXRD and DSC. The stirring rate, cooling rate, starting material ratio (urea: barbituric acid) and dwell time at the final temperature (5 °C) were the factors chosen for this DoE investigation.

3.5 Analytical methods

3.5.1 Optical Microscopy

A microscope fitted with a polarising lens was used to determine the crystallinity of solid; when viewed under polarised light, a single crystal will 'extinguish' when rotated as the high degree of order within the crystalline structure leads it to act as a polariser. Optical microscopy is also a useful tool for assessing a crystal's size and shape (morphology) which can sometimes be an indicator of a particular solid form.

3.5.2 Powder X-ray Diffraction (PXRD)

For the majority of the work, a Bruker D8 Advance Diffractometer equipped with monochromatic Cu-$K_{\alpha 1}$ radiation (λ = 1.54045 Å) was used to analyse powder samples. The crystalline samples were lightly ground (when required) and placed onto a glass slide with the use of a low-diffracting oil, fomblin. The slide was then mounted onto a glass flat-plate with a non-diffracting adhesive substance. The sample was evaluated at room temperature (298 K) and a diffraction pattern obtained between $2\theta = 5 - 40$ °. The resulting diffraction patterns were compared against those obtained from the pure starting materials and/or known multi-component systems in order to characterise the products of the crystallisation experiments.

For the seeded cooling crystallisation work conducted at GSK, Stevenage, a Panalytical Empyrean DY0669 Diffractometer was used with Cu-$K_{\alpha 1}$ radiation (λ = 1.54045 Å). Samples were prepared by using a small amount of low-diffracting grease to secure the sample onto a non-diffracting silicon wafer. The samples were evaluated at room temperature (298 K) and a diffraction pattern was collected between $2\theta = 5 - 40$ °.

These were then compared against known patterns to determine the solid form identity of the product.

Subsequent work conducted at the University of Bath (in 2019) used a STOE STADI P diffractometer with Cu-$K_{\alpha1}$ radiation (λ = 1.54045 Å). The samples were prepared by placing some crystalline powder onto a transparent, zero-diffracting foil in the sample holder. A secondary foil was placed over the top of the sample, before being secured in the sample holder. The samples were evaluated at room temperature (298 K) and a diffraction pattern was obtained for 2θ = 2 – 75 °. The resultant patterns were compared to known patterns to evaluate the identity of the crystallisation product.

Variable temperature PXRD was conducted on Bruker D8 ADVANCE A25 diffractometer on behalf of the author at Astra Zeneca, Macclesfield. The samples were prepared by placing 2 – 3 mg of the powder sample is onto a non-diffracting silicon wafer to form a flat homogeneous layer. The sample was then analysed using Cu-$K_{\alpha1}$ radiation (λ = 1.54045 Å) and evaluated at predetermined temperatures (full details to be found in the relevant chapters). Diffraction patterns were collected between 2θ = 5 – 40 °.

A high resolution PXRD pattern for a sample of UBA was collected at a synchrotron source (Diamond Light Source, Beamline I11). A powder sample was loaded into a borosilicate glass capillary which was secured in a brass holder using an adhesive, allowing for automatic sample changing using a robot. A diffraction pattern was collected using synchrotron radiation, passed through a Si (111) monochromator crystal (λ = 0.82483 Å), between 2θ = 5 – 93 °.

3.5.3 Single Crystal X-ray Diffraction

Both a Rigaku Oxford Diffraction SuperNova and a Rigaku Oxford Diffraction Xcalibur Single Crystal X-ray diffractometer were used in this work. The SuperNova diffractometer is dual source with both Cu-$K_{\alpha1}$ radiation (λ = 1.54045 Å) and Mo-$K_{\alpha1}$ radiation (λ = 0.71073 Å) with microfocus sources allowing for high X-ray flux to be delivered to the sample. The Xcalibur is single source, using Mo-$K_{\alpha1}$. Both diffractometers utilise a graphite monochromator and have a four-circle kappa goniometer and an Eos S2 detector. The four-circle goniometer allows for movement through all the diffractometer angles (κ, φ, ω, 2θ) allowing for a complete set of diffraction data to be collected.

All single crystals were isolated from the batch before being mounted onto a looped filament attached to the goniometer head. The mounted crystal was then subject to X-ray diffraction experiment at 150 K where the temperature was maintained by a flow of liquid nitrogen, controlled by an Oxford Cryostreams Cryostream 700 series. The exposure times for each data collection were dependent on which system was being analysed (full details can be found in the relevant results chapters). The initial data obtained was processed via use of the CrysAlisPro 171.37.33. software. Once a full data

set had been collected, the crystal structures were solved and refined by the use of SHELX-2013[193] via the WinGX[194] interface, and visualised in Mercury.[195]

3.5.4 Differential Scanning Calorimetry (DSC)

For DSC measurements, 1 - 10 mg of powdered sample was weighed and placed into a Tzero aluminium pan. Aluminium lids were placed on the pans and then sealed using a clamping device. The pan was then placed into the instrument alongside an empty Tzero aluminium pan and lid (the reference pan). A TA instruments Q20 DSC equipped with a Thermal Advanced Cooling System 90 was used with a dry nitrogen purge gas flow at a rate of 18 mL min^{-1}. Heating programmes were devised using the TA software, allowing for specific heating and cooling rates and temperature limits. The resultant endothermic and exothermic events that occurred during the programmed runs were recorded using the software Advantage for Qseries version 5.4.0 © 2001-2011 TA Instruments-Waters LLC. Universal Analysis software[196] was used to evaluate the resulting DSC traces.

3.5.5 Thermogravimetric Analysis (TGA)

In this work TGA analysis was conducted using a Setsys Evolution TGA 16/18 in tandem with a mass spectrometer. Once the instrument had been calibrated, a small powdered sample (1 - 5 mg) was placed into a 170 μL aluminium crucible which was placed onto the internal instrument balance. The sample was then subject to a pre-programmed heating profile and the mass loss of the sample was recorded with respect to the temperature. The data collection and processing was carried out using Calisto. Any evolved gas was run through the attached mass spectrometer for analysis. For some data collections, an argon flow was passed over the sample at a rate of 20 ml min^{-1}.

3.5.6 Nuclear Magnetic Resonance (NMR)

A Bruker 500 MHz NMR was used for the collection of ^{13}C NMR spectra. Samples were prepared by dissolving a small amount of the solid in deuterated water. The experiment was conducted at 298 K. The resultant spectra were processed using Topspin 3.5.

Chapter 4 - The Polymorphic Forms of Urea Barbituric Acid

4.1 Introduction

The co-crystal system urea barbituric acid (UBA) has three known polymorphic forms; I, II and III.[133] Form II is known to be highly metastable with respect to the other two forms and DSC data shows that upon heating form II transforms to form III at 117 °C.[135] The DSC data of both forms I and III show that they have very similar thermal behaviour, both displaying exothermic peaks immediately followed by endothermic events at 188 °C and 196 °C respectively. Within this chapter the stability relationship between form I and form III is investigated with an aim to determine which is the thermodynamically stable form. To do this, solubility analysis, thermal analysis and competitive slurries were all investigated.

4.2 The Relative Stability of UBA Form I versus Form III

It is known that form I and form III are very close in energy, displaying very similar solubility to one another in both water and methanol. Previous work has suggested that UBA form III may be the thermodynamically stable form due to its access from a six month quiescent experiment with a 2:1 urea: barbituric acid composition in methanol.[135] However Zhang *et al.* contradict this, suggesting that form III is metastable at ambient conditions and the two forms are enantiotropic.[197] Due to the conflicting conclusions as to which form is more stable, further work was conducted in order to elucidate which form is the thermodynamically stable form.

4.2.1 Thermal Analysis of UBA Form I and Form III

4.2.1.1 DSC Analysis

The DSC data for both form I and form III were collected independently in the range of 20 °C to 350 °C (Figure 4.1). The DSC data show that form III undergoes thermal events at a slightly higher temperature to form I (196 °C vs 188 °C). Initially the traces suggest that the systems melt and then recrystallise to yield a high temperature solid form.[135] If this was the case, the higher temperature for the UBA form III melt would suggest that at these elevated temperatures, UBA form III is the thermodynamically stable form and form I is metastable. However, upon further investigation into the thermal behaviour of the two solid forms, the endothermic event was found not to be resulting from melting of the co-crystal.

The initial DSC traces (Figure 4.1) were obtained using a heating ramp of 10 °C min^{-1}. Subsequent experiments were conducted using greater heating rates of 50 °C min^{-1} to

200 °C min^{-1}. The traces obtained showed that upon increasing the heating rate, the temperature at which the thermal events occurred shifted to higher temperatures (see Appendix Figure 9.1 and Figure 9.2). The Wunderlich definition for a true thermodynamic melt states that it must be at a single, time independent (heating rate independent) temperature at which the solid and amorphous liquid are in equilibrium and there must be no chemical change.[198, 199] As the temperature at which the endothermic event occurs is dependent on the heating rate it cannot be a true melt as previously postulated.

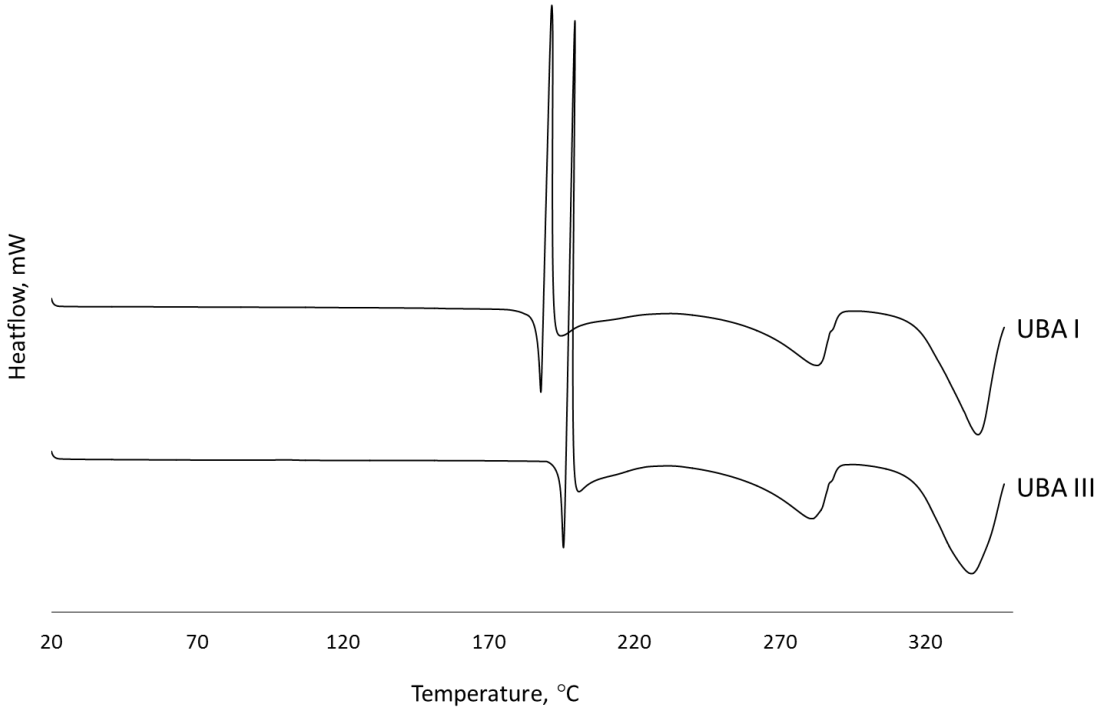

Figure 4.1: DSC traces of UBA form I and form III, obtained with a 10 °C min^{-1} heating ramp. (Exothermic up.)

Heating the two forms to 300 °C (at a rate of 20 ° min^{-1}), using a melting point apparatus, showed that the solids do not melt; instead a solid-state phase transformation was observed at approximately 200 °C for both forms. The phase transition was determined by a change in size, shape and packing of the crystals in tandem with a clouding of the capillary. Zhang *et al.* report that upon heating UBA form I and form III, the co-crystal decomposes into urea and barbituric acid and the urea subsequently vaporises and decomposes into ammonia and cyanic acid.[197] This behaviour would account for the observed solid state phase transformation and the endothermic event which occurs in the DSC traces (previously assumed as a melting event). The nature of this event is largely kinetic, due to the decomposition of the co-crystal and subsequent vaporisation and decomposition of urea, and this explains why the temperature at which this event occurs is dependent on the heating rate used. As the co-crystal decomposes into the individual components, the barbituric acid remains in the solid phase and as a result a recrystallisation event must occur almost simultaneously with the UBA decomposition. This recrystallisation event is likely the cause of the significant exothermic peak observed in the DSC.

4.2.1.2 TGA Analysis

The DSC data suggests that upon heating, the UBA co-crystal breaks down into its individual components. Schaber *et al.*[200] showed that urea starts to decompose between 152 - 190 °C and one of its decomposition products, biuret, decomposes between 190 - 250 °C. TGA data of barbituric acid obtained by Wittering[135] shows that it begins to decompose around 180 °C.

TGA experiments conducted on both form I and form III with a heating rate of 10 °C min^{-1} showed that there is a mass loss at the approximate temperatures seen for the endothermic events in the DSC for both UBA form I and form III (see Appendix Figure 9.3 and Figure 9.4). This is conducive to the theory proposed by Zhang *et al*., suggesting that that the co-crystal breaks down to the individual parts and at the elevated temperatures of this decomposition, urea is lost to vaporisation and decomposition events. High resolution TGA experiments with both UBA form I and form III, conducted at GSK, Stevenage, show that the mass loss during the apparent melt is approximately 35 % for UBA form I and 26 % for form III (Figure 4.2 and Figure 4.3). As the percentage mass of urea in the co-crystal is 32 %, these experiments provide further evidence that upon heating the co-crystal breaks down into its individual components and as a result the urea decomposes. When comparing the TGA data collected at both Bath and GSK, there is a significant difference in the mass losses (35 % versus 15 % for UBA form I and 25 % versus 17 % for UBA form III). These discrepancies arise form the differences in the experiments, with the high-resolution experiments being conducted under a nitrogen flow at GSK, and the Bath experiments not being conducted under the nitrogen flow. High resolution experiments also allow the system more time to equilibrate due to the heat rate altering to a lower value once mass loss occurs.

At the University of Bath, TGA-MS experiments were conducted in order to identify the nature of the evolved gas. When the mass spectrometry (MS) data is analysed it can be seen that upon melting of the sample the ion current corresponding to the ionic mass of ammonia (NH_3^+) increases showing that the urea in the sample, once the co-crystal has broken down, is decomposing and giving off ammonia and cyanic acid (Figure 4.4). The shape of this MS peak mirrors the mass loss steps observed in the TGA and shows that ammonia is still being lost from the sample during the recrystallisation event and then again when further decomposition of the high temperature solid form of barbituric acid occurs. Interestingly, the MS response for the ion mass corresponding to biuret is zero for the duration of the experiment showing that upon decomposition of urea, biuret is not formed. The spectra corresponding to cyanic acid ions ($NHCO^+$), the fragment that remains of urea after NH_3 is lost, can be seen to have the same shape as the ammonia peak, which is to be expected. It can be seen that the ion current corresponding to the loss of carbon dioxide (CO_2) increases during the co-crystal melt event and then again during the final thermal decomposition event of the recrystallised solid form(s).

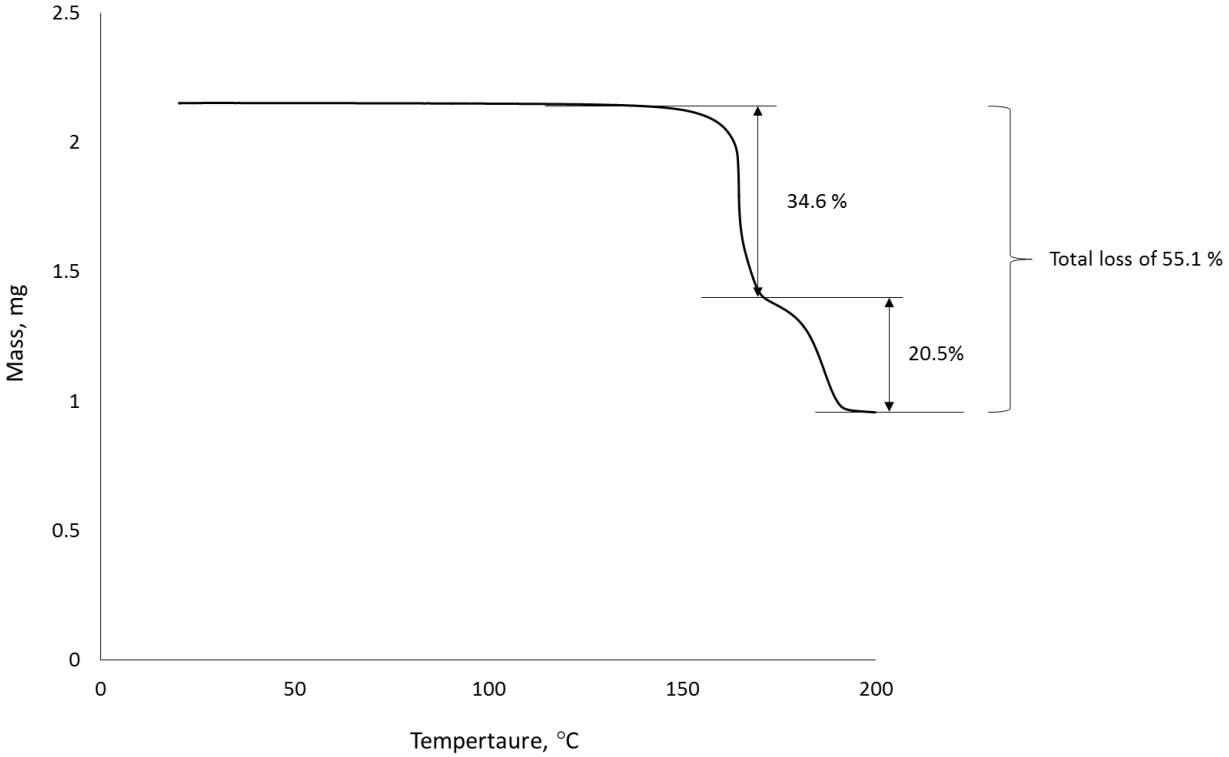

Figure 4.2: High resolution TGA spectra for UBA form I (20 °C min^{-1} heating rate, under N_2).

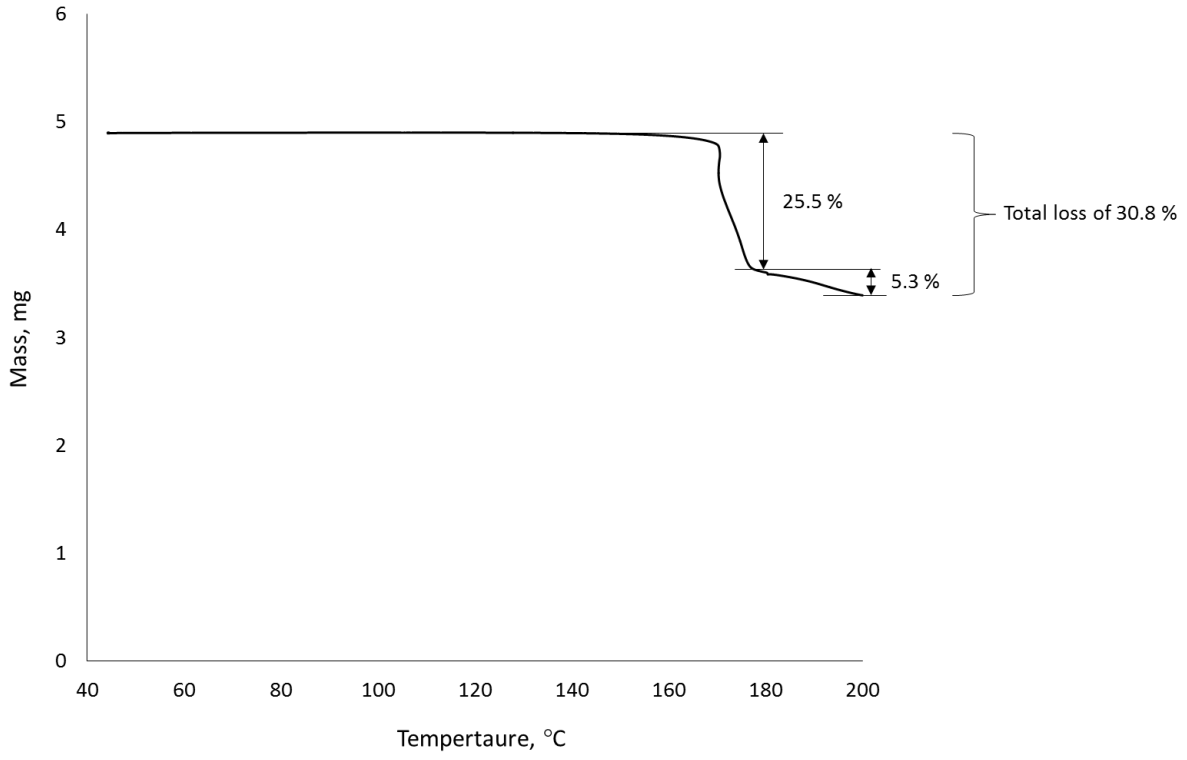

Figure 4.3: High resolution TGA spectra for UBA form III (20 °C min^{-1} heating rate, under N_2).

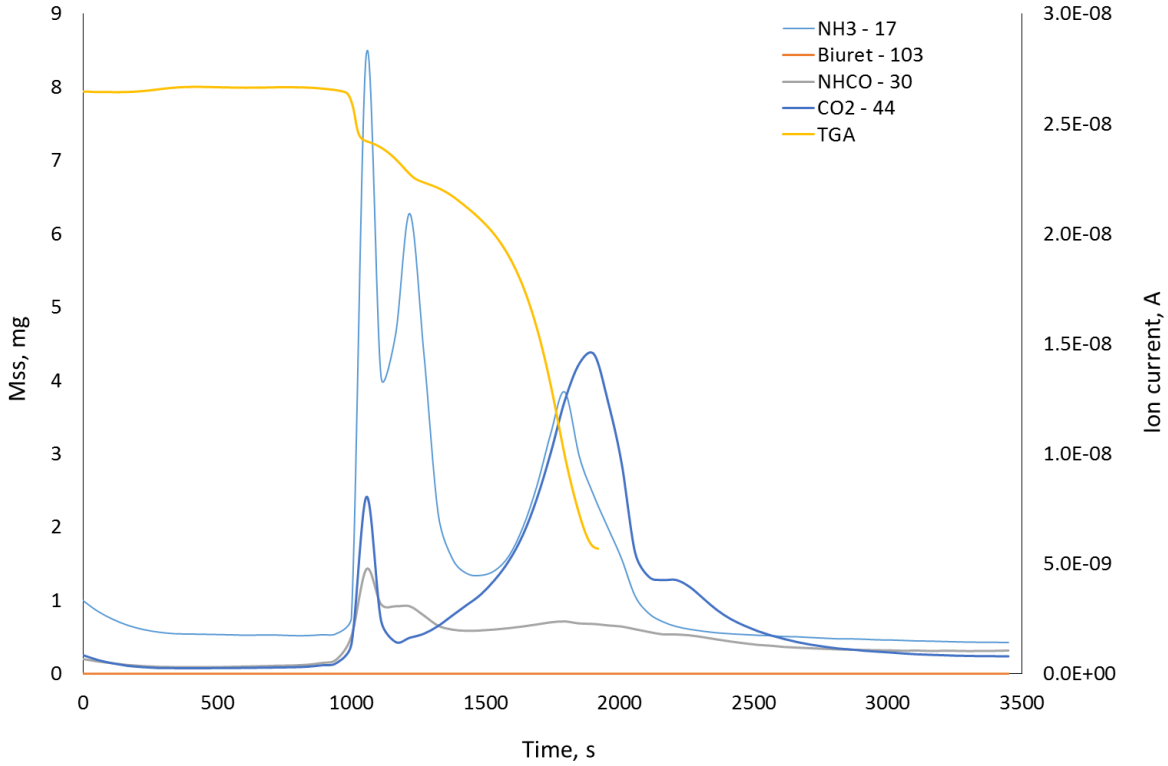

Figure 4.4: Mass spectrometry spectra for TGA-MS experiment of UBA form I (10 °C min^{-1} heating rate).

After the decomposition of the co-crystal and loss of urea from the system, a white solid remains: barbituric acid. The remaining solid produces a PXRD pattern that does not match any of the known barbituric acid solid forms suggesting that a high temperature form is accessed under these conditions. The full VT PXRD study will be discussed further in section 4.4.

As the UBA system does not melt, it cannot be stated as to which form has a higher melting point and hence stability. However, the slightly higher temperatures required to break down UBA form III into its individual components could suggest that this form is more stable than UBA form I at these elevated temperatures. However, no information can be gained from the thermal behaviour as to how these polymorphs relate to each other in terms of their stability dependence with temperature; whether they are enantiotropic or monotropic polymorphs. When looking at the DSC traces obtained from heating the two forms it can be seen that no solid state phase transformations occur upon heating. If two forms of a system are enantiotropic, the stable form at lower temperatures (below the transition temperature, T_t) may undergo a solid state phase transformation at this transition temperature to yield the newly stable form. As can be seen from the DSC traces, the traces remain stable up to the decomposition of the solid form with no evidence that any phase transformations occur. This may initially suggest that the two forms are monotropic in nature and as a result, form III is the more stable form, however, the relative energies are still very close for each form. Further analysis of this system (see below), however, suggests that this may not be the case and that the two polymorphs are in fact enantiotropic in nature.

4.2.2 Solubility Analysis of UBA Form I and Form III

For a large number of systems, the relative stability of two polymorphic forms can be determined with ease by looking at their solubility data: the more stable form will be less soluble. Solubility data for form I and form III in methanol collected using a Crystal16 by Wittering (Figure 4.5) shows that the solubility of the two forms is very similar, not allowing one form to be confidently termed the thermodynamically stable form within that temperature range.[135] This is also the case for the solubility of the two forms in water. This then suggests that the two forms are very close in energy and this may be a reason for the difficulty of accessing pure form III during previous work.

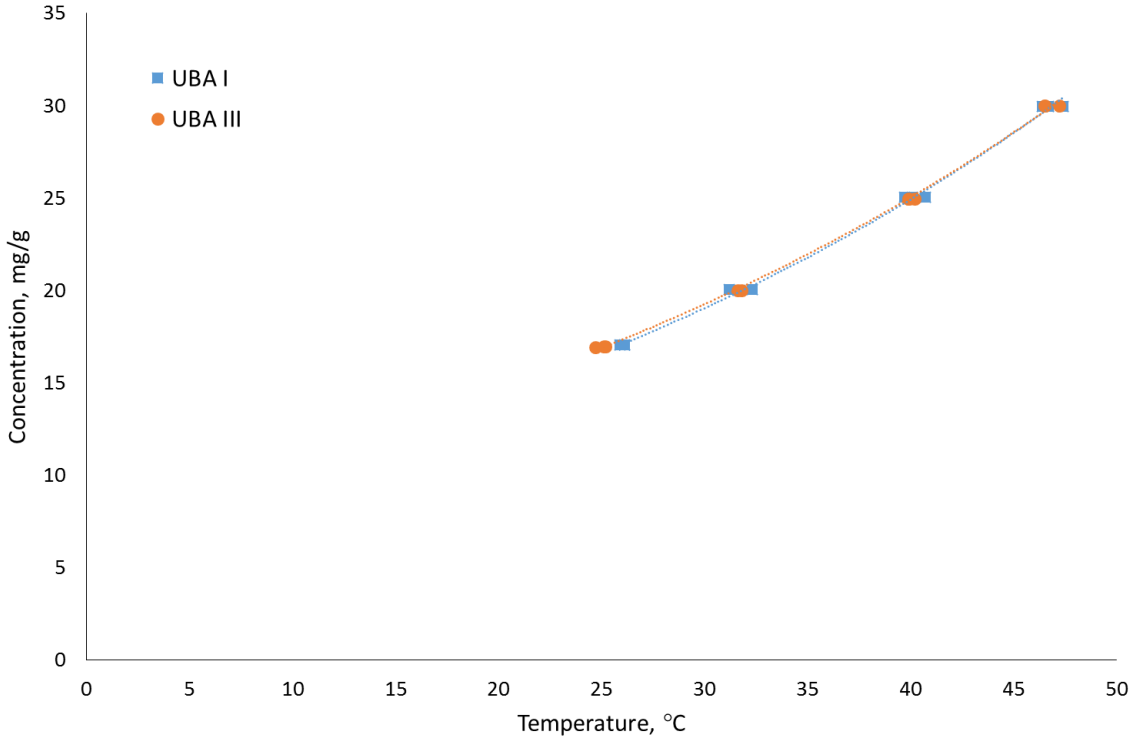

Figure 4.5: Solubility of UBA forms I and III in methanol (using the Crystal16 with a 0.5 °Cmin^{-1} heating rate).[135]

4.2.2.1 Turbidity Solubility Measurements in Ethanol (Crystal 16)

Pudipeddi *et al.* stated that the '*polymorph solubility ratio is independent of the solvent used*'.[201] As the solubility ratio of UBA form I and form III is almost one, this would indicate that the solubility of these forms should be almost identical in whichever solvent was used. To investigate this point, the solubility of forms I and III were measured in ethanol using the Technobis Crystal16 apparatus at GSK, Stevenage. Two different heating rates were used for the experiments, 1 °C min^{-1} and 0.2 °C min^{-1} (Figure 4.6). The data shows that when a 0.2 °C min^{-1} cooling rate was used, the solubilities for the two forms are very similar to one another. However, it can be seen that with a heating rate of 1 °C min^{-1} the solubility curves for the two forms are significantly different. The curve obtained for UBA form I with this heating rate is closer in value to the curves obtained with the slower cooling rate.

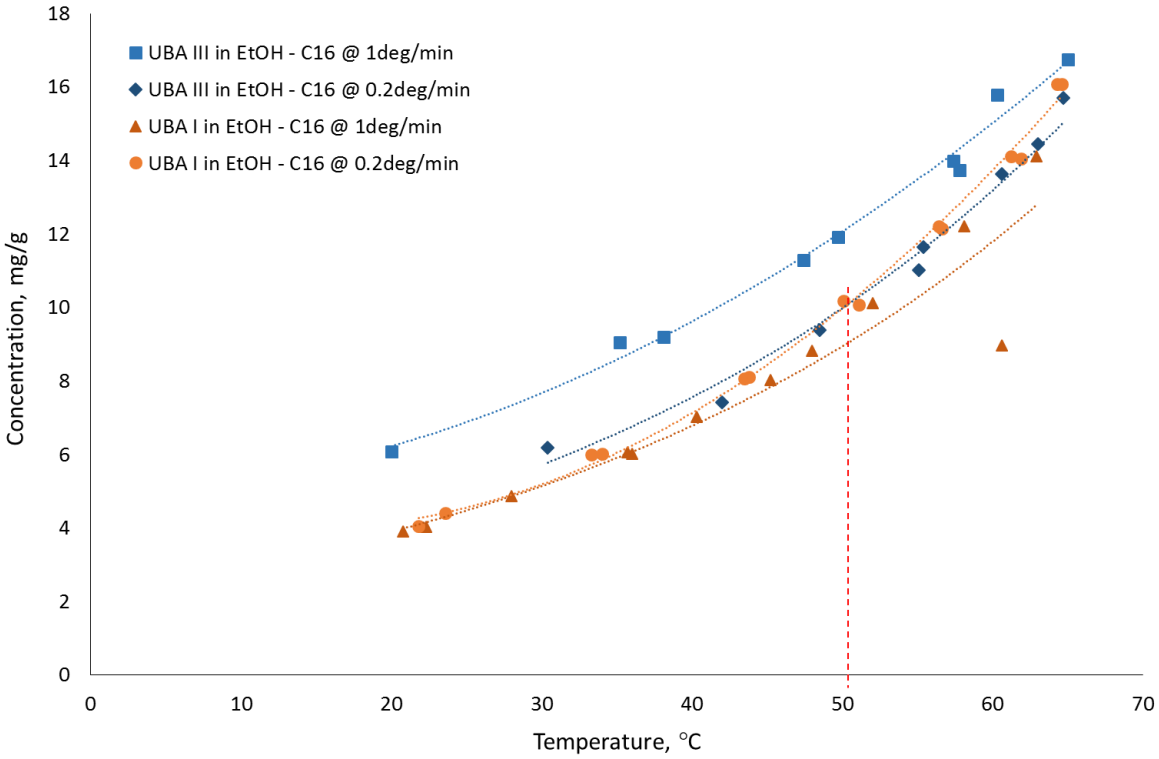

Figure 4.6: Solubility data of UBA form I and III in ethanol using turbidity methods (Crystal16).

The apparent discrepancy of the form III solubility when the faster heating rate is used, however, could be a result of the limitations of the method used to collect data. During the turbidity measurements, a system can appear more soluble than the actual value due to solid particles still being present in the solution when the transmissivity reaches 100 %. This issue is quite common when using the Crystal16 and will result in a solubility curve higher than the true values. One way to get around this issue is to check the samples by eye once the system has recorded that the transmissivity is 100 %. If solid particles can still be seen the instrument can be re-calibrated to minimise this effect. Another limitation for the Crystal16 is that a heating profile must be set for the experiment. When dealing with systems with a slow rate of dissolution, this can result in inaccurate solubility data that is shifted to higher temperatures, suggesting that system is less soluble than it is. If the system has a solution concentration that would ordinarily dissolve at 40 °C in the chosen solvent medium, but has a slow rate of dissolution and therefore does not all dissolve until, for example, five minutes after the system has reached 40 °C, the turbidity measurements will be affected. As a result, the transmissivity will not reach 100 % until the system reaches 45 °C (for a 1 °C min^{-1} heating rate) , giving an inaccurate temperature for the clear point and hence solubility. This results in the system appearing to dissolve at higher temperatures than its true solubility, i.e. the measured solubility is less than the thermodynamic value. This is sometimes referred to a system's kinetic solubility. The solubility curve obtained for UBA form I at the faster heating rate displays a slightly lower solubility than that obtained at 0.2 °C min^{-1}, which may be a result of a slow rate of dissolution for this form. One way to overcome this issue is to reduce the rate of heating for the experiment to give the

system more time to equilibrate and dissolve. However, when working with metastable polymorphs this can result in solution-mediated phase transformations of a metastable form to the more stable form and as a result the solubility of a different form will be measured, not the form intended.

When looking only at the data obtained using the 0.2 °C min^{-1} heating rate, it can be seen that the solubility curves for the two forms intersect one another. This suggests that the two systems are enantiotropic; although they are very close in solubility, there is a distinct cross-over in their relative solubilities and hence stabilities. The transition temperature, T_t, is at approximately 50 °C. Below T_t, form III is more soluble and hence less stable, with the opposite being true when the temperature surpasses T_t. Zhang *et al.*[197] collected solubility data of the two forms in water using gravimetric techniques and the data shows an intercept of the two solubility curves with the T_t for the two forms shown be approximately 33-35 °C. Below this temperature, UBA form III is more soluble and hence metastable, and above the opposite is true. In terms of the enantiotropic relationship between these two forms, these results agree with the turbidity solubility. However, there is a significant difference in the values obtained for T_t.

4.2.2.2 Gravimetric Solubility Measurements in Ethanol

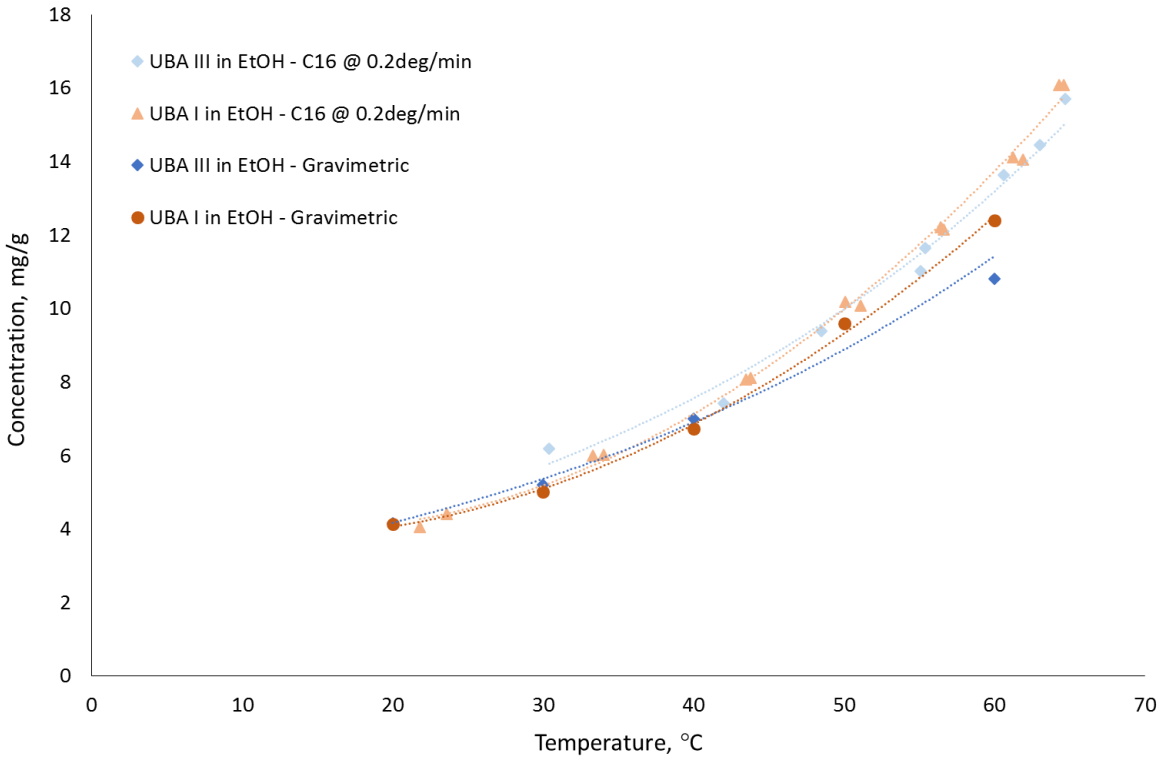

Figure 4.7: Solubility data of UBA form I and form III in ethanol obtained from both turbidity measurements (Crystal16, 0.2 °C heating rate) and gravimetric experiments.

Due to the inconsistencies in the Crystal16 solubility data, specifically when a heating rate of 1 °C min^{-1} is used, the solubility of both form I and form III in ethanol were next measured using gravimetric techniques. These experiments were conducted at the

University of Bath using the CRD Polar Bear Plus. The resultant solubility data from both the Crystal16 and gravimetric experiments can be seen in Figure 4.7. It can be seen that the gravimetric solubility data of the two forms appears very similar to the Crystal16 turbidity data obtained for both forms with a 0.2 °C min^{-1} heating rate. It can also be seen that the gravimetric solubility curves obtained for form I and form III are very to each other, as was seen for their solubility data in methanol and water. These solubility measurements, upon initial observation, suggest that the turbidity measurement of UBA form I in ethanol using the Crystal16 with a 1°C min^{-1} heating rate is inaccurate for the reasons discussed previously. Conversely, the gravimetric results align well with the 0.2 °C min^{-1} heating rate turbidity data, indicating that both methods provide an accurate assessment the solubility.

Upon closer inspection of the gravimetric solubility data it can be seen that there is an interception of the experimental solubility lines of form I and form III, agreeing with the relative solubilities observed with the turbidity data. However, the temperature of this interception is approximately 37 °C, significantly lower than that seen with the previous (Crystal16) data. Interestingly, this value of T_t is much closer to that obtained by Zhang *et al.*[197] (35 °C), who also used gravimetric techniques.

4.2.2.3 Observation Solubility Measurements in Ethanol

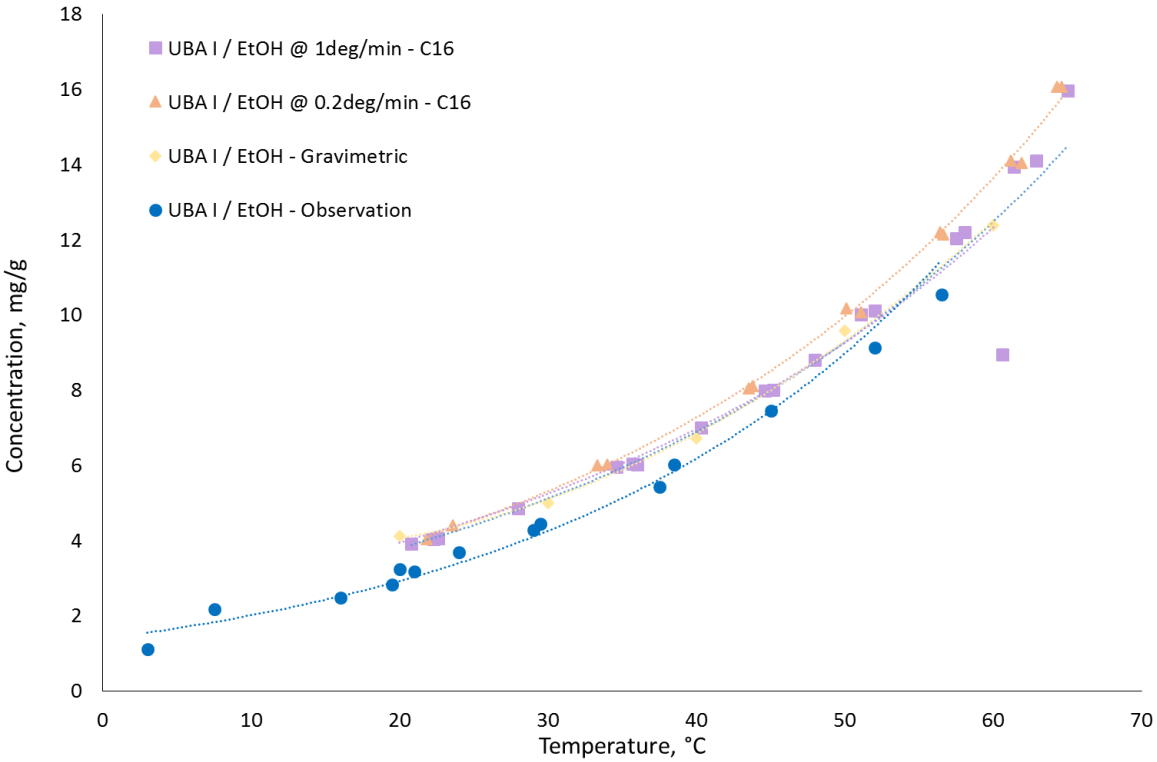

Figure 4.8: UBA form I solubility in ethanol, measured using a variety of techniques.

Further solubility measurements of UBA form I and form III in ethanol were also conducted at the University of Bath using observation techniques (Figure 4.8 and Figure 4.9 respectively). These experiments resulted in solubility curves not too dissimilar to

the curves obtained from the gravimetric solubility experiments. However, at lower temperatures the observation solubility data gave slightly lower values than those obtained from gravimetric measurements, but conversely gave solubility values greater than the gravimetric values upon increasing the temperature. This result could arise from a slow rate of dissolution of the sample in the observation measurements at lower temperatures: the system was heated at a rate of 0.2 °C min^{-1} and the solid may have been slow to dissolve, resulting in it appearing to dissolve at higher temperatures than the true thermodynamic value; this would therefore result in the measured data points suggesting a lower solubility. Upon increasing the temperature in the system the rate of dissolution may increase and the issues associated with this will be reduced, resulting in the values becoming closer in accuracy to the true solubility values.

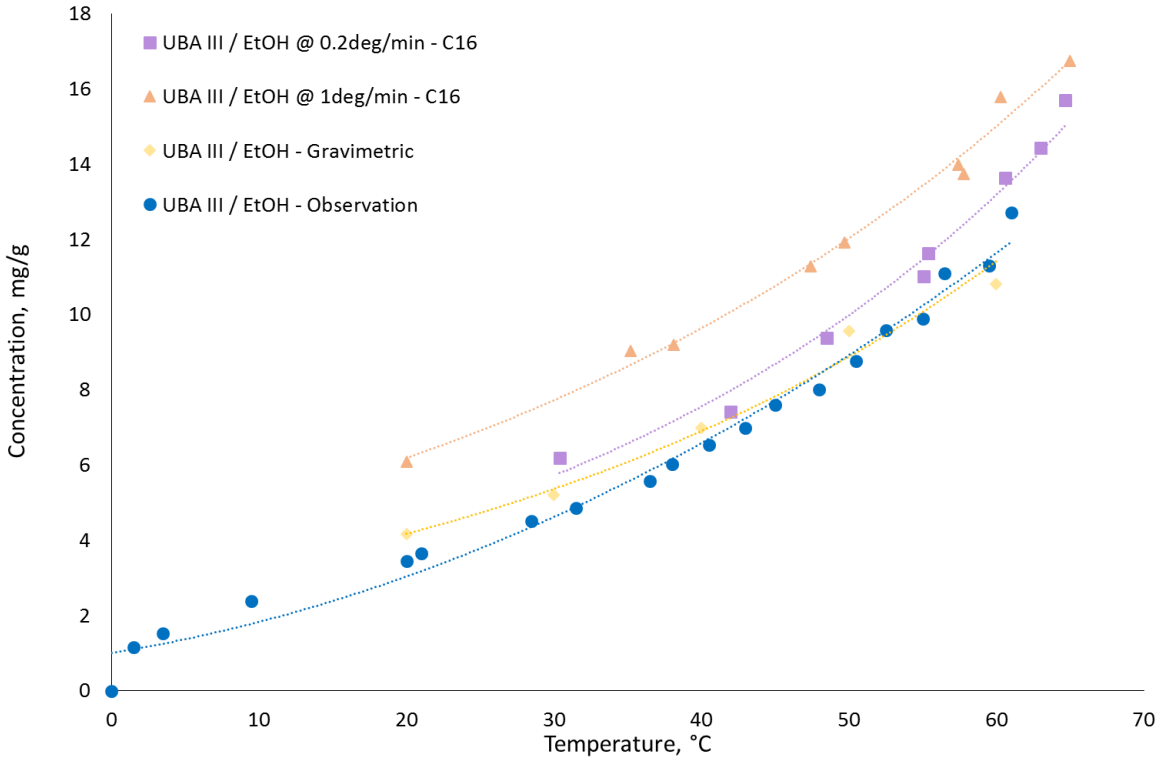

Figure 4.9: UBA form III solubility in ethanol, measured using a variety of techniques.

The solubility data obtained using observation methods was chosen as the data to be taken forward into subsequent crystallisation work of UBA from ethanol as it was deemed the most accurate. When comparing the observation solubility curves of both form I and form III in ethanol it can be seen that they are very similar, as is seen with the solubility data previously obtained in both methanol and water. On close inspection of the solubility curves it appears that they cross over one another at a T_t of approximately 42 °C, as indicated by the dashed red line in Figure 4.10. This suggests again that the two forms are enantiotropic, with form I being the stable form below this transition temperature and form III becoming the stable form above the transition temperature. The transition temperature from these solubility curves is approximately 5 °C higher than that estimated from the gravimetric solubility curves and 8 °C lower than the

turbidity solubility data. As there is a significant degree of error associated with solubility analysis, the transition temperature cannot be determined solely by the solubility curves, especially when different methods of solubility analysis yield significantly different results.

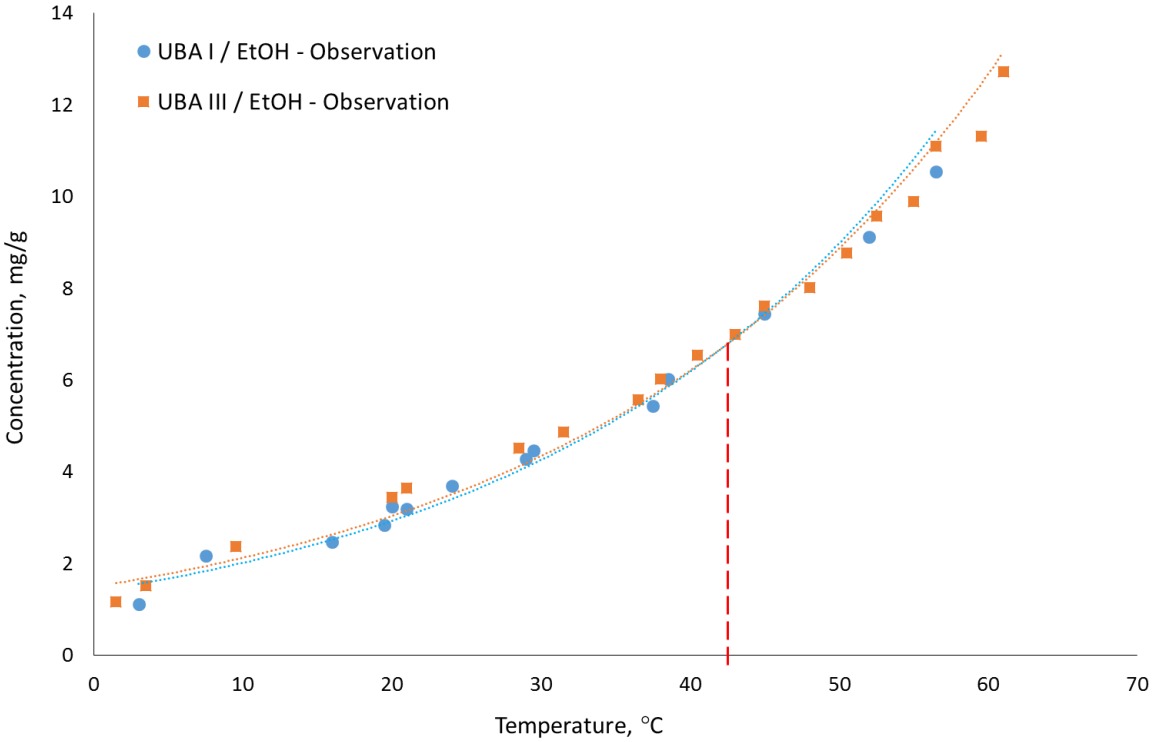

Figure 4.10: Observation solubility data for both UBA I and UBA III in ethanol.

4.2.2.4 Solubility in IPA

The solubility of both UBA form I and form III in IPA was also measured using gravimetric and observation techniques at the University of Bath, as well as using turbidity techniques with the Crystal16 at GSK, Stevenage. Figure 4.11 shows the solubility curves obtained for UBA form I in IPA. It can be seen that the turbidity data is similar, regardless of the heating rate used for the experiment. The solubility data obtained using observation techniques is, however, significantly lower than that from the turbidity data obtained using the Crystal16 at GSK. The gravimetric solubility data points lie at intermediate values. There may be several reasons for the difference in the measured solubility values for UBA I in IPA. Firstly, the data obtained using the Crystal16 could be higher than the actual values due to the system reading 100 % transmissivity when particles still remain in solution. The data obtained via gravimetric methods can have a large error associated with it, especially as the vials of solution are left exposed on a bench top for up to four days. There are also errors associated with observation techniques, such as not allowing the system enough time to equilibrate at a set temperature resulting in the system appearing to not dissolve until higher temperatures, resulting in an apparently lower solubility.

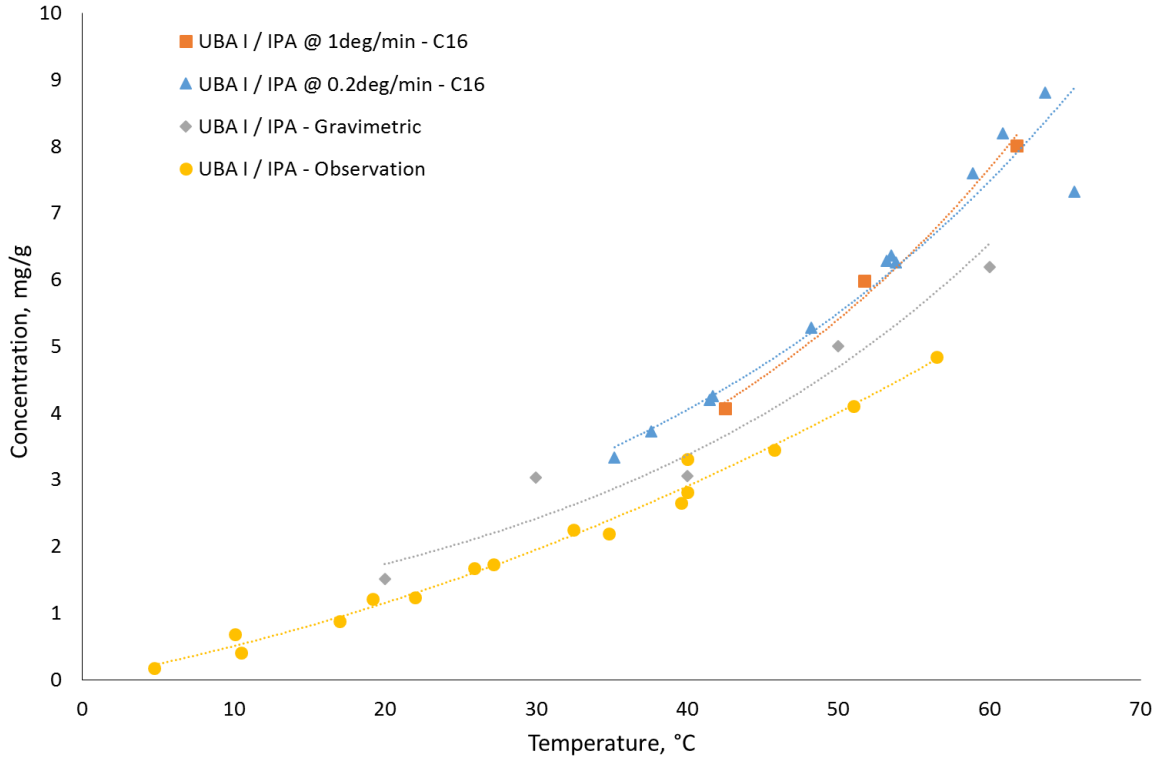

Figure 4.11: Solubility data of UBA I in IPA measured using gravimetric, observation and turbidity techniques.

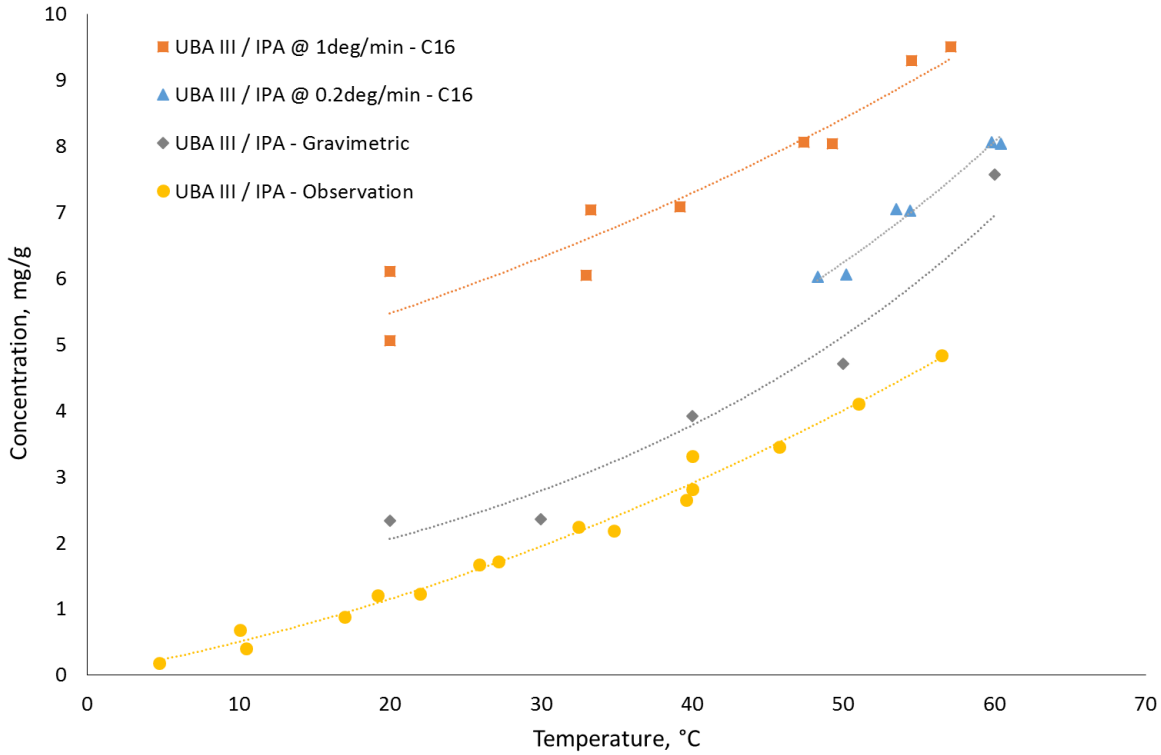

Figure 4.12: Solubility data of UBA form III in IPA measured using observation, gravimetric and turbidity techniques.

Figure 4.12 shows the solubility data obtained for UBA form III in IPA using the Crystal16 at GSK, gravimetric techniques and observation techniques. The solubility curves obtained for UBA form III in IPA are all significantly different, with the turbidity data obtained at 1 °C min^{-1}, being approximately five times higher at 20 °C and two times higher at 60 °C than that obtained using observation methods. The reasons for the difference in the measured solubility values using the different methods can be assumed to be similar to those discussed previously in this chapter. When compared to the data collected for UBA form III, the average values of the solubility data for both forms is similar, as was seen in both methanol and ethanol. This is again unsurprising, as the solubility ratio of the two polymorphic forms should remain constant, irrespective of the solvent medium. However, the data clearly shows that there is a significant drop in the solubility of the two forms when moving from ethanol to IPA (Figure 4.13). In comparison to the solubility values of the two UBA forms in methanol it can be seen that moving from methanol to ethanol reduces the solubility approximately three fold. The move from ethanol to IPA subsequently reduces the solubility a further two fold. This result is possibly unsurprising and may be explained by the fact that increasing the size of the alcohol solvent results in a reduction in polarity of the solvent molecule. As UBA contains molecules with polar functionalities, it is expected to be more soluble in more polar solvents.

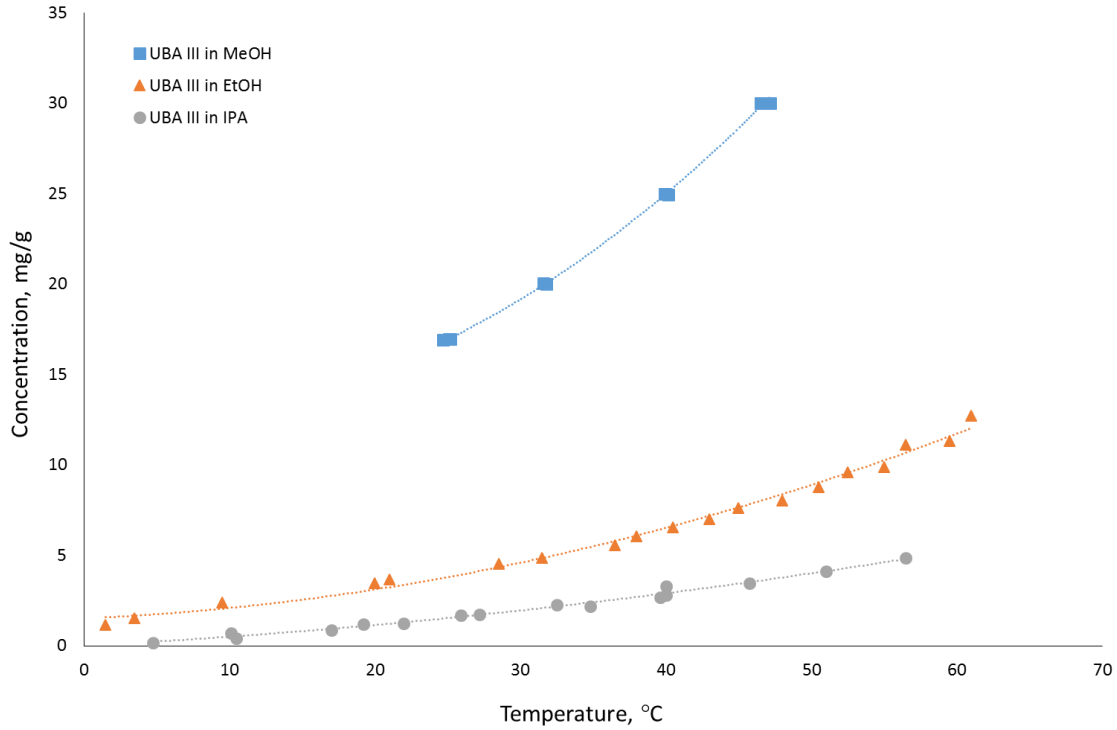

Figure 4.13: Observation solubility for UBA form III in ethanol and IPA with Crystal16 data for UBA form III in methanol.

The solubility data obtained in both ethanol and IPA shows a significant variation between the values obtained depending on the method used to obtain the data. The measurement of solubility of a multi-component system is inherently difficult, due to

not definitively knowing whether the system may in fact be breaking down into its individual components and hence the solubility measured being that of the individual components. This combined with the errors and issues associated with each method result in relatively inaccurate values being obtained. Gravimetric and observation methods in ethanol suggested that the two forms were enantiotropic with their transition temperature occurring between 37 °C and 42 °C. Zhang *et al.*[197] reports an intersection in the gravimetric solubility curves of the two forms in water at approximately 35 °C. However, no intersection of curves was observed in IPA and so the transition temperature for the two forms cannot be confidently determined using these data.

4.2.3 Competitive Slurrying of UBA Form I and Form III

To further evaluate the stability relationship between UBA form I and form III, competitive slurry experiments were conducted. The premise behind these experiments is that if two polymorphic forms of a system are mixed together with a small amount of solvent, the system will undergo a solution-mediated phase transformation to yield the more stable form. If a more stable form is present in the suspension this will seed the transformation of the metastable form to the stable form and the mixture will convert to the stable form over time.

Competitive slurries of form I and form III were conducted using the CRD Polar Bear Plus for both mixing and temperature control. For initial investigations into which form was the thermodynamically stable polymorph under ambient conditions, competitive slurrying was conducted at 20 °C. 150 mg of a 1:1 form I: form III mixture was added to 1.5 mL vials to which 1 mL of ethanol was then added. The vials were then placed into the CRD Polar Bear and left mixing for 24 – 120 hours. Every 24 hours, a sample was removed from the CRD Polar Bear, filtered using vacuum filtration, dried at room temperature and then analysed using PXRD to determine the solid form. Each experiment was conducted in triplicate.

As can be seen in Figure 4.14, the PXRD pattern of the initial dry 1:1 mixture of the two forms is a combination of the patterns obtained from both form I and form III. The PXRD analysis of the slurry products shows that, under these conditions, full conversion of the 1:1 mixture to yield pure form I is achieved within 24 hours and remains UBA form I for the remaining slurry time. It can be seen that the longer slurry times (120 hours) result in a slight broadening of the peaks in the PXRD pattern. However, this is unsurprising as the samples will likely reduce in size after being slurried for such a long period of time due to the grinding associated with the magnetic bottom stirring. The full conversion of the mixture to yield pure form I indicates that form I is more stable than form III at 20 °C. This result supports the conclusions drawn from the solubility analysis and further reiterate that the two forms, I and III, are enantiotropic.

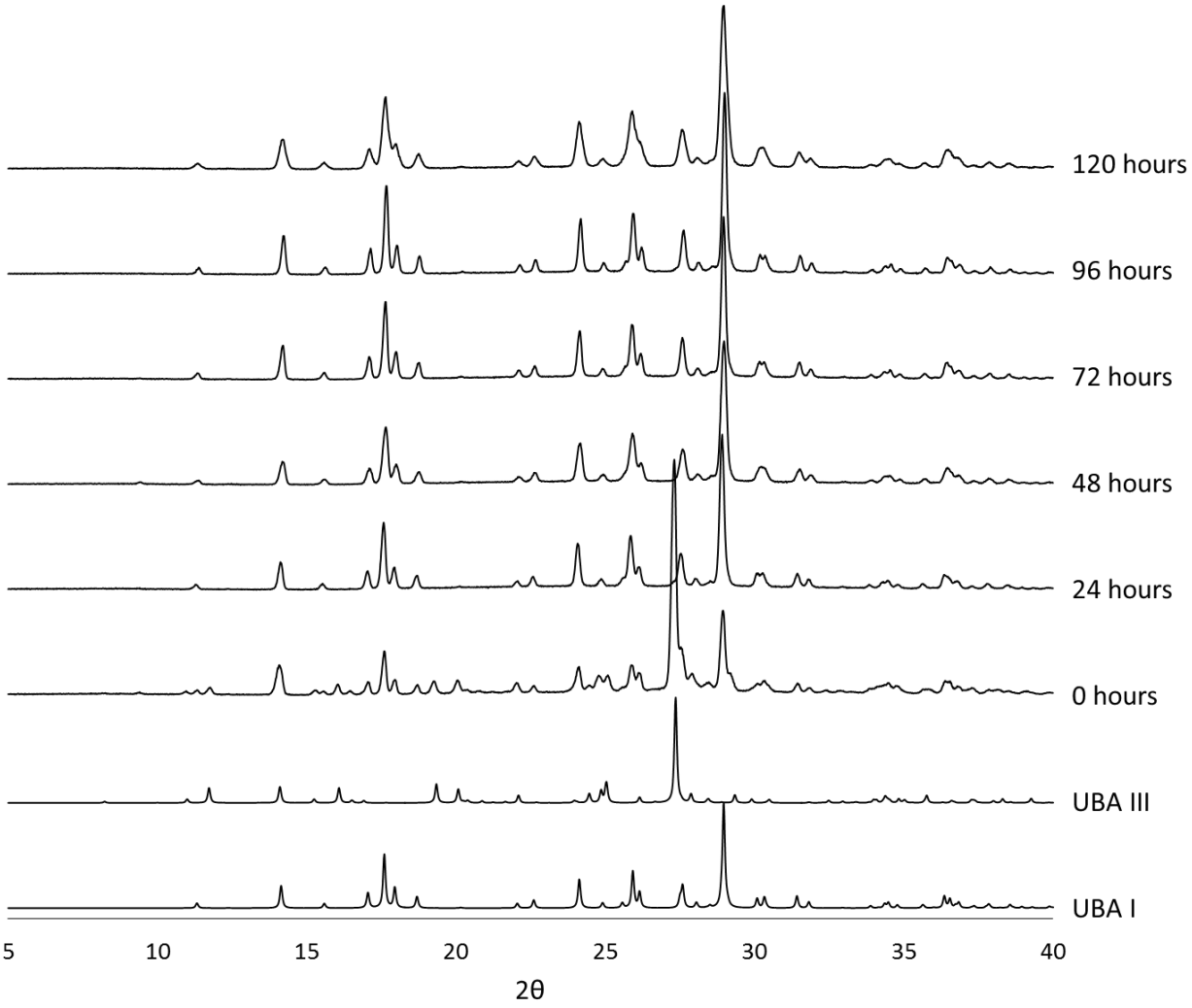

Figure 4.14: PXRD patterns of competitive slurries of UBA form I and form III in ethanol at 20 °C.

As the solubility data obtained by both gravimetric and observation methods suggests that the transition temperature, T_t, is in the approximate range of 35 °C – 42 °C, a competitive slurry was conducted at 40 °C in order to investigate which form is more stable at this elevated temperature, as well as to distinguish which value of T_t is more accurate. At this temperature the mixture of the two forms converted to yield pure form I within 48 hours (Figure 4.15 (a)), indicating that at 40 °C, form I is still the stable polymorph. This finding shows that the transition temperature estimated from the gravimetric solubility data of UBA in ethanol is inaccurate. This is unsurprising however; as the solubilities for the two forms are so close and, due to the significant error associated with the solubility measurement, the solubility curves estimated from the measured data points are therefore likely to propagate that error. A competitive slurry of form I versus form III was then conducted at 50 °C to investigate which form is stable at this temperature; if one was to assume that the transition temperatures estimated from the gravimetric and observation solubility analysis are relatively accurate it would be predicted that at this elevated temperature form III is likely to be more stable. However, it can be seen from the PXRD patterns collected for the competitive slurry

products that at 50 °C the mixture fully converts to form I within 48 hours (Figure 4.15 (b)). These experiments show that form I remains the thermodynamically stable form until at least 50 °C, indicating the inaccuracy with the solubility data and the transition temperatures obtained from it.

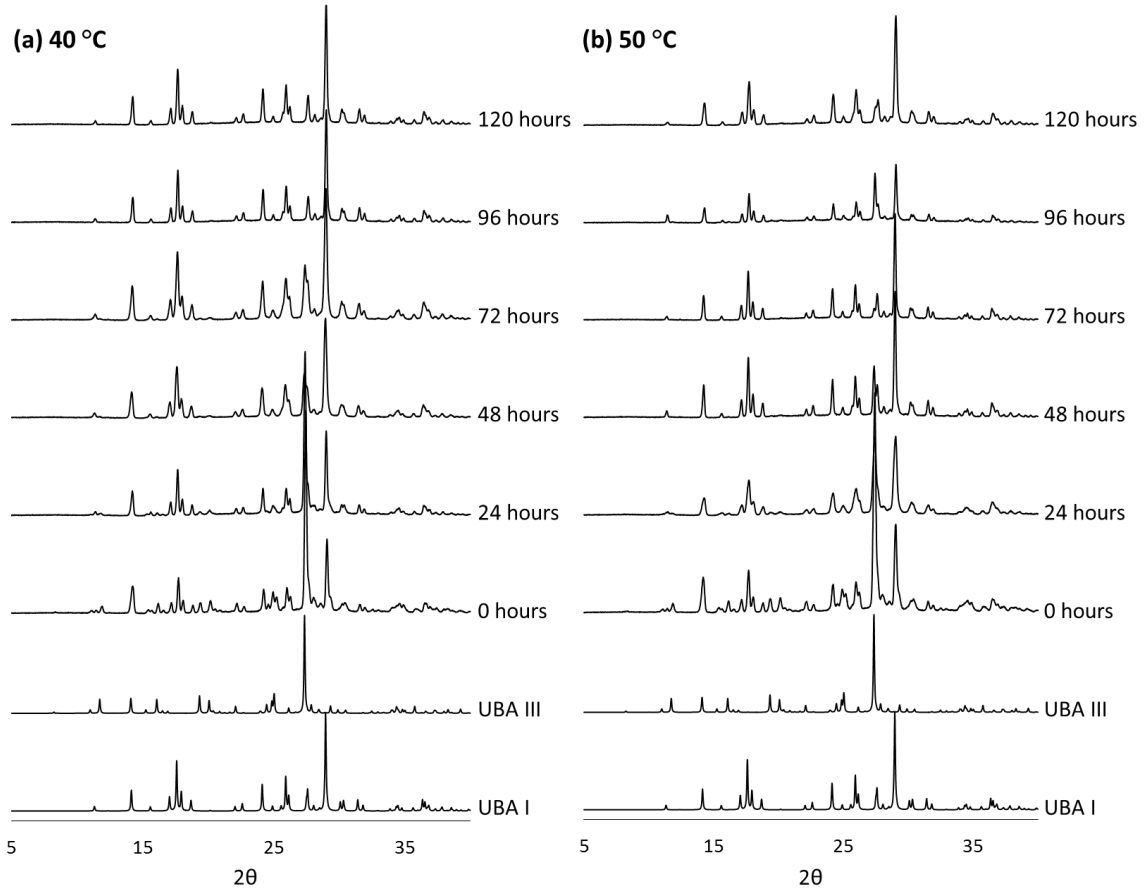

Figure 4.15: PXRD patterns of competitive slurries of UBA form I and form III in ethanol at (a) 40 °C and (b) 50 °C.

Competitive slurries were then investigated at 75 °C due to this being the highest temperature that any further crystallisation processes would encounter. However, at this temperature the solvent evaporated from the slurries during the experiment and some decomposition of the system occurred resulting in the white slurry becoming pale orange in colour. Due to the solvent evaporation and decomposition of the sample at these temperatures, the slurry product was removed after 48 hours. PXRD data obtained for the slurry product suggested conversion of the mixture to yield UBA form I, however some of the data collected for some of the samples suggested a significant reduction in the level crystallinity of the sample. (See Appendices Figure 9.5.)

These results all demonstrate that UBA form I is the thermodynamically stable polymorph, up to at least 75 °C, and that UBA form III is a metastable form, although the two forms are very close in energy. Though solubility data suggests that the two polymorphs are enantiotropic in nature this could not be confirmed by competitive slurrying in the accessible temperature range. However, the higher temperature needed

for the decomposition of the co-crystal into its individual components for UBA form III may suggest that at elevated temperatures UBA form III is more stable, and hence the two systems are enantiotropic.

4.2.4 Crystallographic Analysis of UBA Form I and Form III for Stability Justification

When looking at the crystal structures of UBA form I and form III, the relative stability of the two forms can be justified in terms of the individual crystal structures. For example, Gryl *et al.* calculated the crystal density of the three forms of UBA, I, II and III to be 1.593, 1.556 and 1.586 Mg m^{-3} respectively.[133] The density rule for polymorph stability proposes that the most stable polymorph will have the highest density (at 0 K), however for hydrogen bonded systems this becomes more complicated and may only serve as a rough estimation.[202] It is known that form II is highly metastable in comparison to both form I and form III, and the much lower density of this form therefore aligns well. Although the densities for form I and form III are very close, form I is slightly denser, aligning with the experimental data that shows form I is the thermodynamically stable form at ambient conditions. However, it must be noted that the densities for these three forms are calculated for 293 K, not 0 K and are therefore not a perfect representation.

Form I

Form III

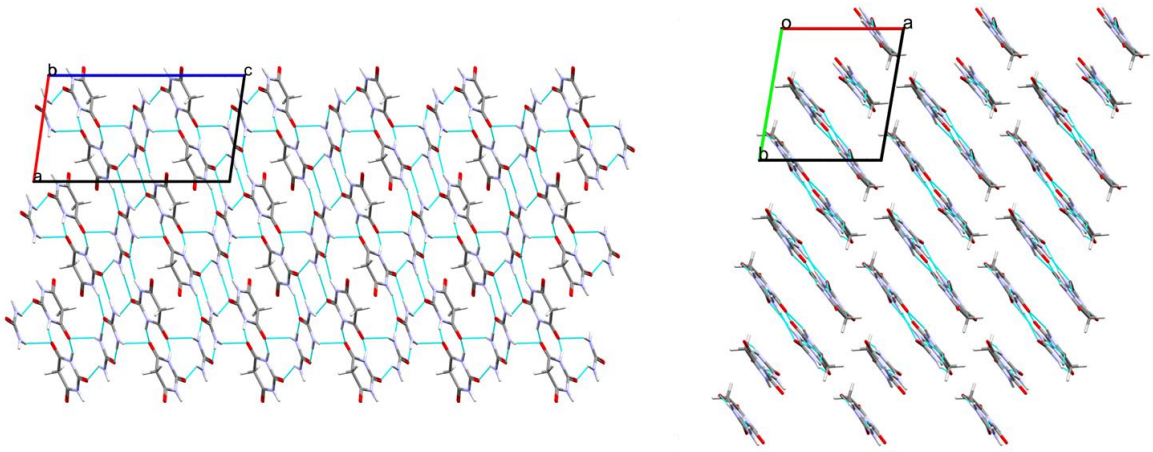

Figure 4.16: Crystal packing of (left) UBA form I (viewed down the *b* axis) and (right) UBA form III (viewed down the *c* axis).

When looking at the crystal structures for form I and form III significant differences can be seen in the hydrogen bonding and subsequent crystal packing. Figure 4.16 shows the crystal structures for the two forms and it can be seen that in form I a three dimensional hydrogen bonding network is present, unlike in form III. In form III the hydrogen bonds result in the formation of one dimensional chains of molecules that run parallel to the *c* axis. These chains lie adjacent to one another and result in a layered structure. The one dimensional hydrogen bonding that occurs in the structure of form III may be a reason as to why it has a lower stability at ambient conditions, to form I. The three

dimensional hydrogen bonding in form I, linking each molecule together throughout the entirety of the structure may give the system additional stability.

Full interaction map calculations, performed using the CCDC crystal data visualisation software Mercury, allow for areas to be mapped in which hydrogen bonding interactions are likely to form for a given molecule (or collection of molecules).[203] The likelihood of an interaction is determined in reference to similar interactions observed in the many 100,000s of crystal structures contained in the Cambridge Structural Database (CSD). Figure 4.17 shows the full interaction maps for both UBA form I and form III. The full interaction maps show the preferred positions of interactions (hot spots) and are calculated by defining the distinct functional groups in the molecules and calculating their interaction preferences using the IsoStar interaction data collected from all the structures in the CSD.[203-205] Factors such as steric hindrance are automatically taken into account and an interaction space is mapped around the functionalities. The red areas in the map depict regions in which hydrogen bonds are likely to form with an incoming hydrogen bond accepting group, with the blue areas depicting regions where hydrogen bond donors are likely to interact. The full interaction maps can be calculated with a varying number of contours set to different levels, with each contour level indicating an area mapped out by a certain interaction likelihood. The numerical value for the level indicates how many more times you would expect an interaction to happen within that region than at random.

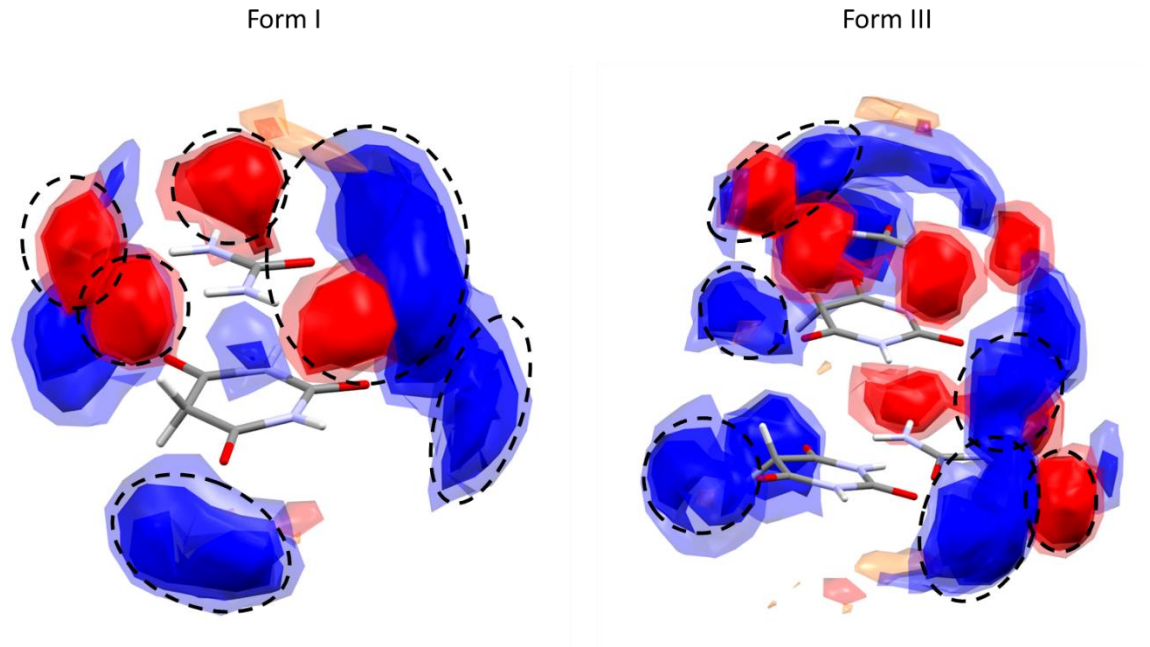

Figure 4.17: Satisfaction of hotspots in full interaction maps for molecules in UBA form I (left) and UBA form III (right) – satisfied hot spots circled. The full interaction maps are made of three contours set at levels 2, 4 and 6.

When looking at the crystal structure of form I it can be seen that all of the hydrogen bond donors are involved in hydrogen bonds, but not all of the acceptor atoms. One carbonyl oxygen (O6) on the barbituric acid molecule does not form any hydrogen bonds

within the structure. Looking at the hydrogen bonds that do form, in terms of their donor and acceptors and their geometries, it is seen that they all form within the full interaction map hot spots (Figure 4.17 left). The same investigation into form III indicated that, although every hydrogen bond donor and acceptor functionality is involved in hydrogen bonding interactions, the geometries of some of the hydrogen bonds do not form in favourable positions, resulting in many not forming at the hot spots (Figure 4.17 right). This suggests that the hydrogen bonds forming, and the resulting packing arrangements, in UBA form III are less likely to form than those in UBA form I, indicating that they may be less stable. This full interaction analysis may give some justification as to why form I is the experimentally determined thermodynamically stable form.

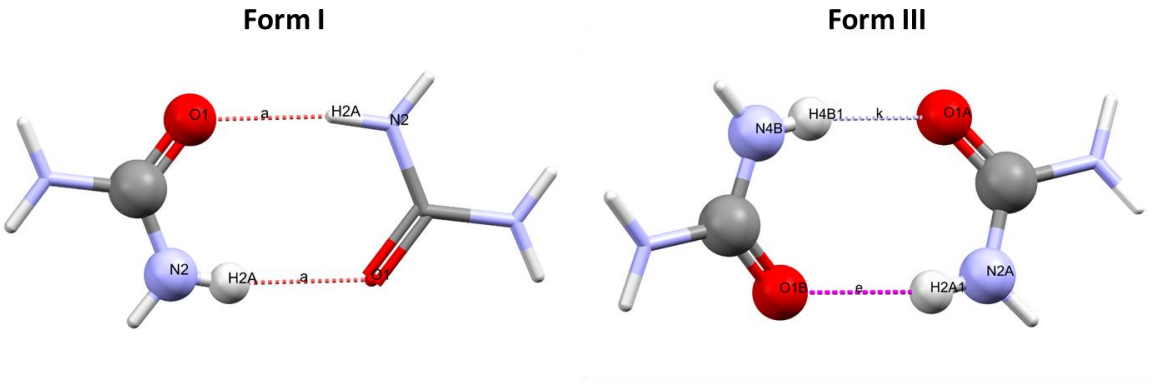

R2,2(8)
O1···H2A-N2 = 2.903(2) Å
O1···H2A = 2.055 Å
O1···H2A-N2 angle = 168.4 °

R2,2(8)
O1B···H2A1-N2A = 3.077(2) Å
O1B···H2A1 = 2.238 Å
O1B···H2A1-N2A angle = 165.3 °
O1A···H4B1-N4B = 3.055(2) Å
O1A···H4B1 = 2.212 Å
O1A···H4B1-N4B angle = 166.6 °

Figure 4.18: Urea-urea hydrogen bonded dimers in UBA form I (left) and UBA form III (right).

When looking at the hydrogen bonding networks that exist in the three polymorphs of UBA it is seen that both form I and form III possess a urea-urea hydrogen bonded dimer and UBA form II does not.[133] The presence of these urea-urea dimers that exist in form I and form III may be a reason as to why these two forms are significantly more stable than form II. When looking at the hydrogen bonds responsible for the formation of these dimers it can be seen that in UBA form I, the dimer forms with two hydrogen bonds of equal strength, yielding a symmetrical hydrogen bonded ring network (Figure 4.18 left). In form III, however, this is not the case and the dimer has two unique hydrogen bonds. These two hydrogen bonds differ subtly from one another in terms of both their atomic distance and angles (Figure 4.18 right). When comparing the bond distances and angles of these with the hydrogen bond seen in the form I dimer, it can be seen that they are slightly longer and more acute, suggesting that the bond that forms in form I is slightly stronger. The uniformity of the dimer in form I, combined with the stronger hydrogen

bond would suggest that this dimer is stronger and may contribute to the slightly higher stability of form I in comparison to form III.

It has been seen that, in comparison to form III, form I has a higher density; it contains a three dimensional hydrogen bonded network, as opposed to discrete one dimensional chains; satisfies the full interaction map hotspots to a greater extent; and has a stronger urea-urea hydrogen bonded dimer. All these factors help to rationalise the structural basis for the higher stability of form I over form III that was experimentally determined and provide some justification for this observed stability relationship of the two forms.

4.3 A Novel Solid Form of UBA

4.3.1 The Formation of the Novel Solid Form of UBA

A novel solid form of UBA was discovered during slurry experiments utilising a 2:1 ratio of urea: barbituric acid. Small scale slurry experiments (2 mL solvent) using both methanol and ethanol as the solvent medium yielded slurry products that displayed unique peaks in their PXRD patterns (Figure 4.19). The slurry experiments were conducted using the CRD Polar Bear Plus for temperature control and magnetic bottom stirring (250 rpm) and were left mixing at 20 °C for a predetermined time. Once the experiment time was complete, the slurries were filtered using vacuum filtration, dried at room temperature and analysed for solid form identity using both PXRD and DSC.

The resultant slurry product was a white crystalline powder regardless of the solvent medium used for the experiment. Both the ethanol and methanol mediated slurry products exhibit very similar PXRD patterns, which are unique in comparison to the known polymorphs of UBA and the starting components. As can be seen in Figure 4.19, the methanol mediated slurry product has a few additional peaks in its PXRD pattern in comparison to the ethanol mediated slurry product. However, these match peaks corresponding to UBA form I, suggesting that some form I impurities are present when methanol is used as the solvent medium and not when ethanol is used.

The unique PXRD patterns obtained from the slurry products indicate that a new solid form has been accessed during these experiments. As there is no evidence in the PXRD patterns of residual urea or barbituric acid, this suggests that this new solid form is a multi-component system combining both starting materials. This implies that the new solid form could be a novel polymorphic form of UBA, a co-crystal with a different stoichiometry, or a solvated/hydrated form. However, as this solid form is accessed using two different solvents it is less likely that a solvate has been accessed. The nature of this solid form will be discussed in more detail in subsequent sections in this chapter.

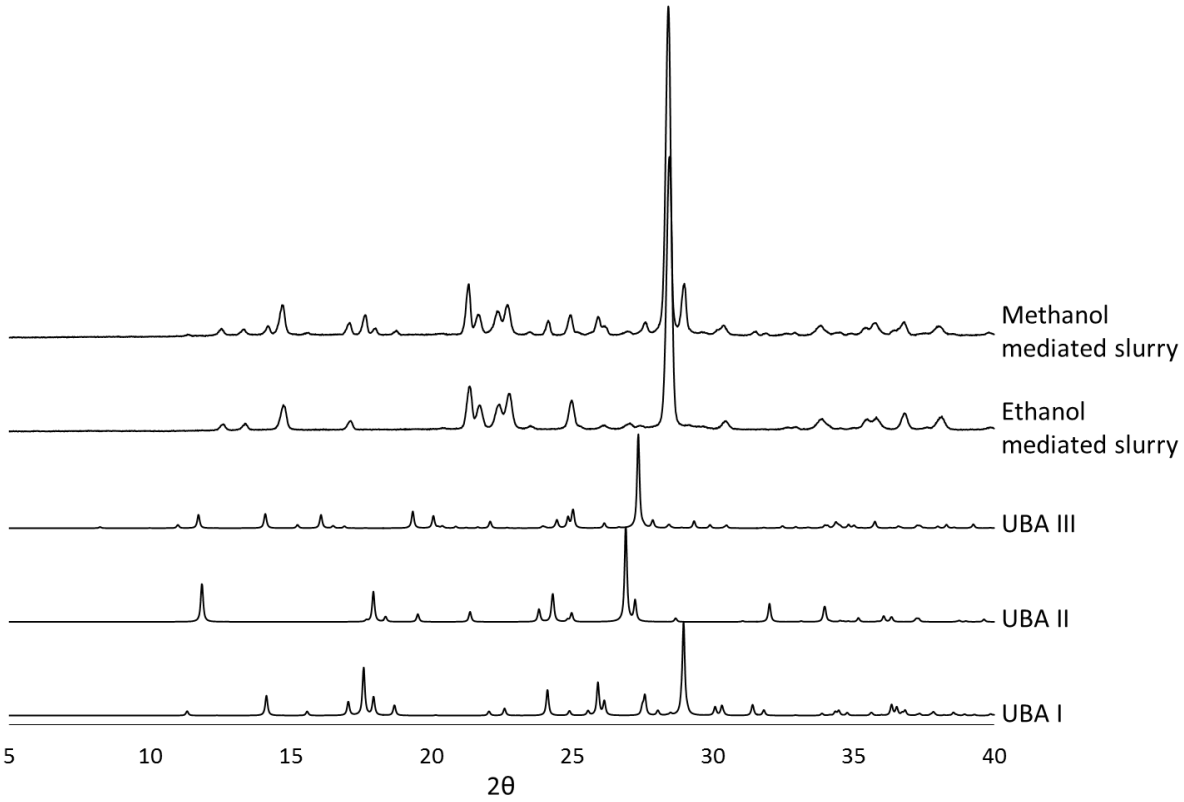

Figure 4.19: PXRD patterns for the methanol and ethanol mediated 2:1 urea: barbituric acid 24 hour slurry products.

4.3.1.1 Investigation into Time of Formation for the Novel Solid Form

The initial slurry experiments were conducted for a duration of 24 hours before the slurry product was isolated via vacuum filtration. Subsequent experiments were conducted in order to investigate if this new solid form could be accessed at shorter slurry times with both ethanol and methanol as the solvent media. For ethanol mediated slurries the experiment time was initially reduced down to 2 hours. However, PXRD patterns of the resultant slurry product (Figure 4.20) showed the presence of additional peaks in comparison to the 24 hour slurry product (2θ = ~14.2 °, ~16.1 °, ~17.8 °, ~18.3 °, 19.4 °, ~21.1 ° and 20.5 °). Upon analysis of these peaks it was observed that they match peaks found in the PXRD patterns of the barbituric acid starting material (form II). This therefore suggests that upon significantly reducing the slurry time down to 2 hours, full conversion of the starting components to yield the new solid form was not achieved.

After slurrying the system for 4 hours, the barbituric acid starting material peaks still remain, but are reduced in intensity. Longer slurrying times of 8, 16 and 22 hours were also investigated, which revealed that full conversion of the starting components to the new form was complete within 8 hours (Figure 4.20).

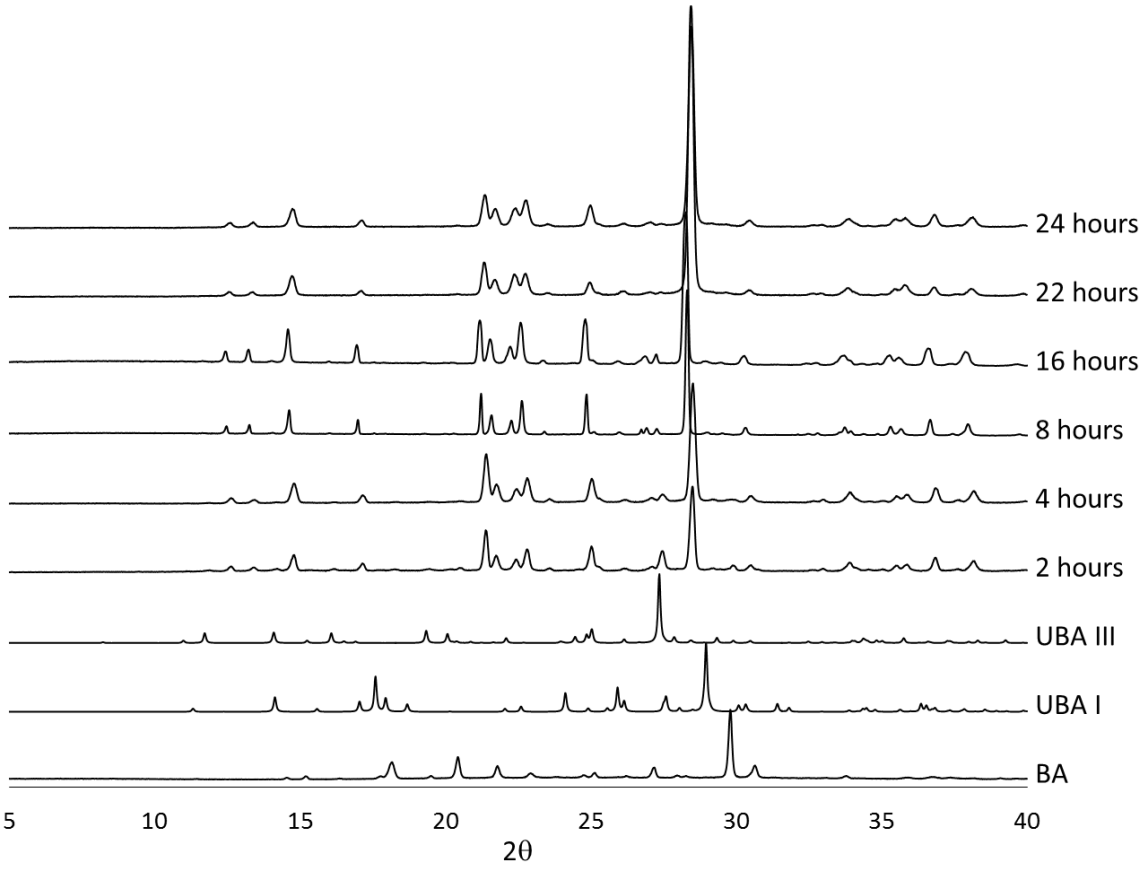

Figure 4.20: PXRD patterns of 2:1 urea: barbituric acid ratio ethanol mediated slurries with different experimental slurry times.

The same investigation was subsequently conducted using methanol as the solvent medium instead of ethanol. When the slurry time was reduced down to 2 hours, the PXRD pattern (Figure 4.21) of the resulting slurry product exhibited additional peaks (2θ = ~11.9 °, ~16.2 °, ~19.5 °, 20.1 °, 20.5 °, 24.5 ° and 27.2 °) in comparison to the 24 hour slurry product. The positioning of these peaks in the PXRD pattern matches peak positions found in the PXRD pattern of UBA form III, indicating that at shorter slurry times, when methanol is the chosen solvent medium, UBA form III is produced alongside both the novel solid form and form I impurities. As the slurry time is increased to 4 hours, the peaks corresponding to UBA form III impurities still exist with similar intensity, suggesting that increasing the slurry time to 4 hours is not sufficient to remove these form III impurities. When the system is slurried for a period of 8 hours some additional peaks at 2θ = ~16.2 °, ~19.5 °, ~20.5 °and 27.2 ° which correspond to the presence of UBA form III, still exist, however some of the UBA form III peaks observed in shorter slurry times are no longer present. The PXRD data for the 16 hour slurry time only has two peaks corresponding to UBA form III showing that the longer slurry times are resulting in the amount of UBA form III decreasing, likely due to its conversion to UBA form I. Slurries with a 22 hour experiment time resulted in very trace amounts of UBA form III impurities, with peaks corresponding to both the novel form and form I. The difference in the PXRD patterns of the 22 hour and 24 hour slurry is very slight, with only two very small peaks at 2θ = ~16.2 ° and 2θ = ~19.5 °signifying the presence of UBA form

III impurities. The reduction in the intensity of the UBA form III peaks in the PXRD pattern suggest that increasing the experiment time for this system allows for a solution-mediated phase transformation of form III to yield form I. As UBA form I is the stable form it is likely that the form III that is produced early on in the experiment (whether this is due to its nucleation or phase transformation from another solid form, for example UBA form II or the novel form), transforms over time to yield UBA form I. The presence of UBA form III in short slurry times in methanol, compared to the presence of residual barbituric acid in short ethanol slurry times, highlights the slower rate of production of UBA in ethanol in comparison to methanol.

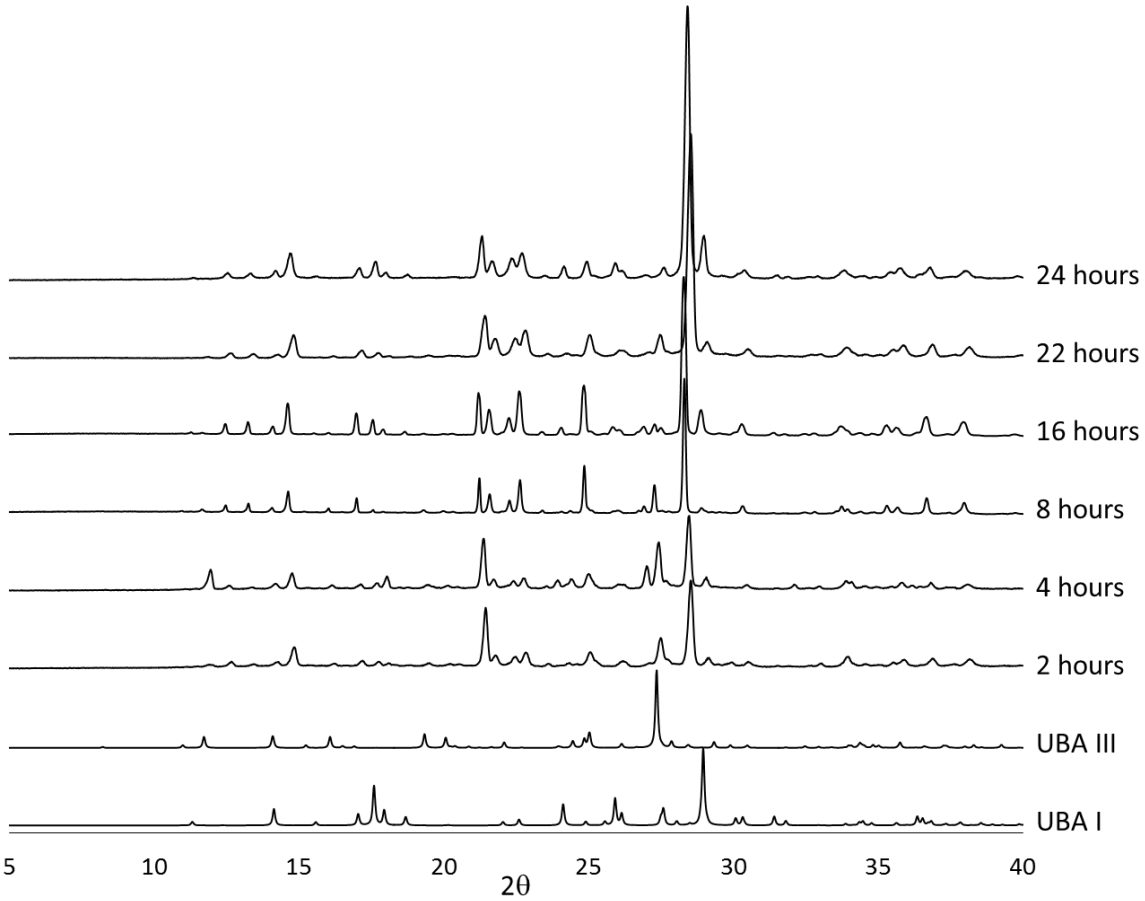

Figure 4.21: PXRD patterns of methanol mediated 2:1 urea: barbituric acid slurries with different experimental slurry times.

The presence of UBA form III in the methanol mediated slurries with experiment times of less than 24 hours, but not in small scale ethanol mediated slurries, suggests that the novel solid form may undergo a solution-mediated phase transformation to yield form III (and subsequently form I) in methanol at these small scales. This outcome could be due to the significantly higher solubility of the UBA system in methanol in comparison to ethanol: a greater solubility will result in much faster solution-mediated phase transformations. Investigations into significantly longer slurry times (up to 1 month) for the ethanol mediated system were then conducted to probe whether additional UBA forms could be accessed from solution-mediated phase transformations of the novel solid form in ethanol.

The small scale (2 mL) ethanol mediated 2:1 urea: barbituric acid slurries were set up and left mixing for a prolonged period (1 week – 1 month) at room temperature. Unlike with previous experiments, magnetic bottom stirring was set to 350 rpm (not 250 rpm) and was provided by a Drysyn hot plate and not the CRD Polar Bear Plus. Heating was turned off for the duration of the experiment; no temperature control was utilised and the systems were left at room temperature. Samples were removed at designated time periods (1 week, 2 weeks and 1 month) and were isolated via vacuum filtration, left to dry at room temperature and then analysed using PXRD to identify the solid form present. After an experimental slurry time of 1 week, the PXRD data (Figure 4.22) showed that only the novel solid form was accessed: there were no additional peaks when compared to the 24 hour ethanol mediated slurry product. After the system had been slurried for 2 weeks, two additional peaks were observed in the PXRD pattern at 2θ = ~17.6 ° and ~18.0 °. These peaks correspond to UBA form I. After slurrying for a month the additional peaks observed after two weeks had increased in intensity, as well as a small additional peak at 2θ = ~15.6 ° being evident, corresponding to UBA form I. This suggests that when ethanol is used as the solvent medium under these conditions the novel form can be accessed to high purity with slurry times of 24 hours to 1 week (168 hours). However, when left for experimental times between one week and two weeks UBA form I impurities begin to be produced in the system, likely due to solution-mediated phase transformations of this novel solid form to the thermodynamically stable form I.

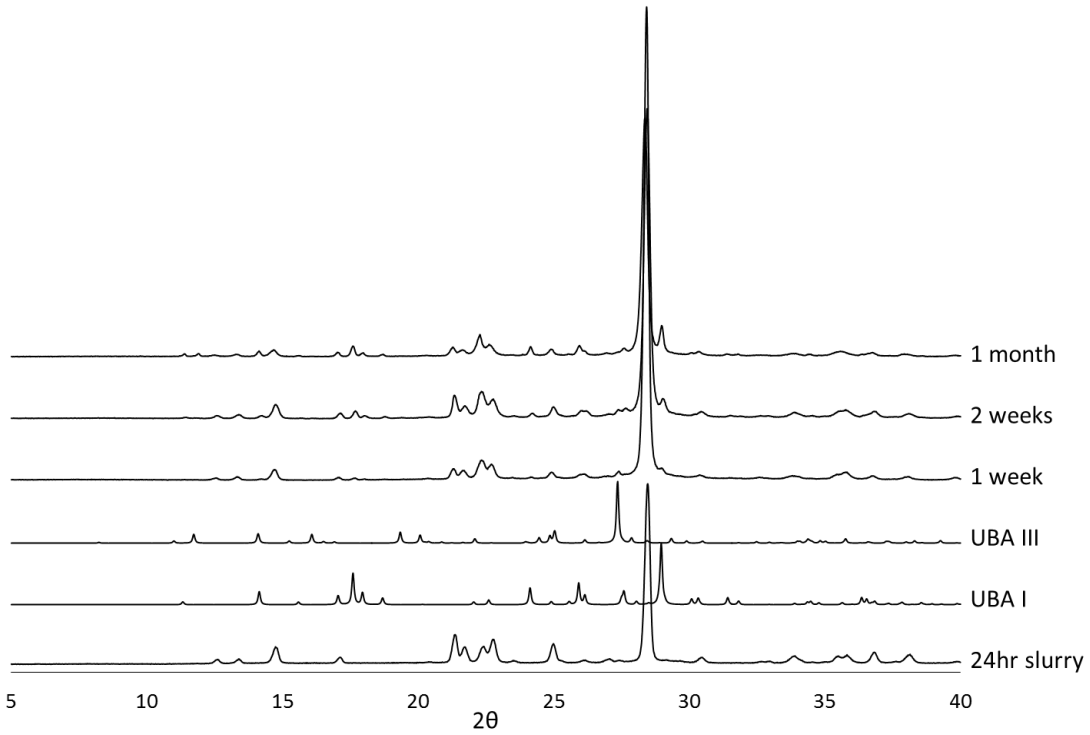

Figure 4.22: PXRD patterns of ethanol mediated 2:1 (urea: barbituric acid) room temperature slurries.

When methanol is used as the solvent medium, form I impurities are seen in the product even with short with slurry times of 2 hours. However when ethanol is used, slurry times

of greater than 1 week are required before any form I impurities are observed. This suggests that under these conditions the solution-mediated phase transformation of the novel form to yield form I is significantly hindered when using ethanol in comparison to methanol. It must be noted, however, that for these prolonged experiments a Drysyn hot plate was used to provide the magnetic bottom stirring, not the CRD Polar Bear Plus. The mixing provided by the hot plate set up is significantly less uniform than that provided using the Polar Bear and this is likely to have an impact on the phase transformation observed in the slurries. If the mixing is less uniform and less intense then it would be unsurprising for the solution-mediated phase transitions to happen at a reduced rate and it may be the case that if the experiments were conducted using the Polar Bear, the transformation to give UBA form I may have happened much quicker. That being said, the novel form to form I transition is significantly slower in ethanol than methanol, as expected due to the much lower solubility of the UBA system in ethanol.

4.3.1.2 Investigation into Scale up of the Production of the Novel Solid Form

Investigations into the scale up of the production of this novel solid form were conducted. All the above experiments used 2 mL of solvent and 200 mg of urea, with barbituric acid weighed in a 2: 1 molar ratio (426.5 mg). 50 mL slurries were investigated to see if the novel solid form could be accessed at this larger scale. For these experiments the CRD Polar Bear Plus was used with a 100 mL RBF. Overhead stirring was utilised at 400 rpm and provided by an external motor and shaft. Both ethanol and methanol mediated slurries were investigated.

For the ethanol mediated slurry, experiments conducted for 24 hours at this scale resulted in conversion of the starting components to yield the novel solid form. However, when looking at the PXRD pattern obtained from the 50 mL slurry, a few additional peaks (2θ = ~16.2 °, ~19.5 °, ~20.1 ° and ~21.5 °) can be seen (Figure 4.23). The position of these peaks matches those of UBA form III showing that at this scale a 24 hour slurry time is insufficient to access solid form purity of the novel solid form. When methanol is used as the solvent medium, peaks corresponding to form III can also be seen in the PXRD pattern, as well as the same peaks from UBA I impurities that are present in the small scale slurries for this solvent system at this experimental time. The presence of form III impurities in both the ethanol and methanol mediated slurries suggests that at this scale the formation of UBA form III is heightened, regardless of the solvent medium, unlike at the 2 mL scale.

Upon increasing the scale, many experimental factors are altered which can in turn alter the crystallisation and metastable zone width for each of the solid forms. There is a significant difference in mixing between magnetic bottom stirring and overhead stirring which can contribute to a difference in both heat and mass transfer in the larger slurry. Magnetic bottom stirring also has a grinding effect associated with it which can often lead to secondary nuclei being formed more readily than with overhead stirring. The change from a flat bottom vial to a RBF may also have an impact on the metastable zone and hence crystallisation of the two forms due to differences in the flow of solution

within the vial. The larger scale of the system itself will inherently have a different level of mass and heat transfer which will influence the rate of crystallisation for each of the solid forms. It may be the case that at this scale, with ethanol as the solvent medium the rate of potential transformation of the novel solid form to UBA form III is increased and this is why UBA form III is seen in the slurry product. It may also be that at this scale the rate of transformation of UBA form III to form I is reduced and this is why UBA form III is present, and not form I as was seen in smaller scale slurries for ethanol with long slurry times.

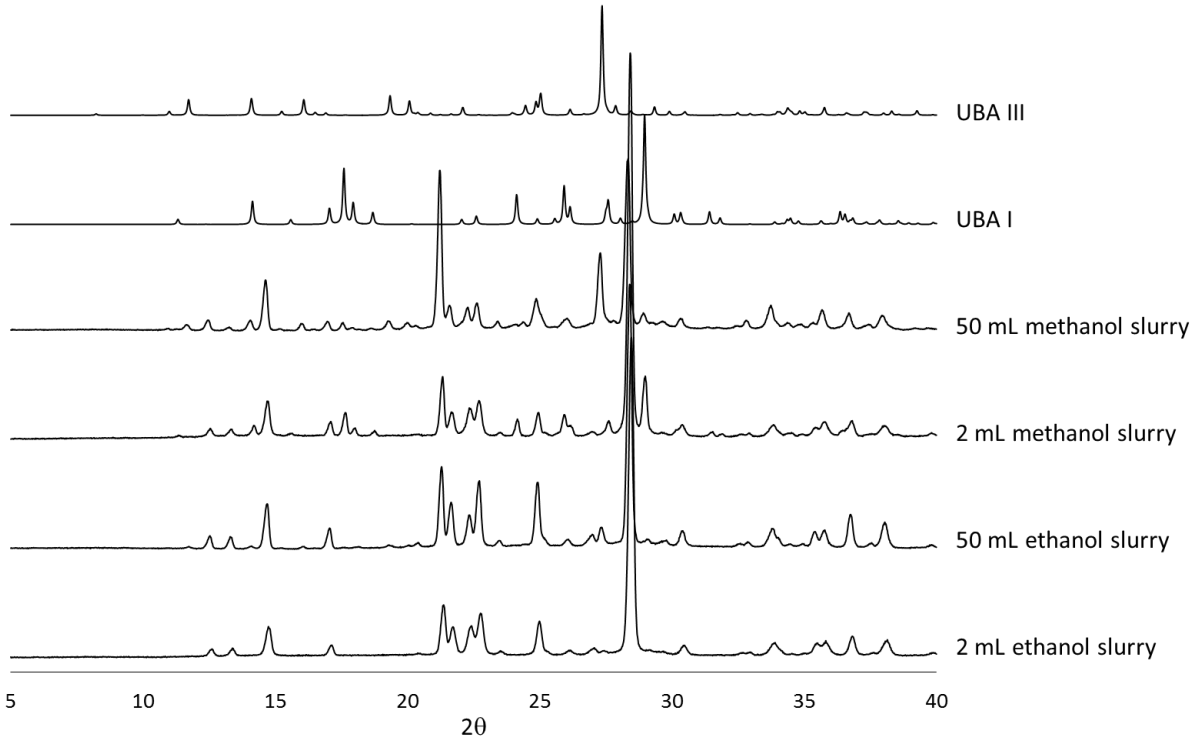

Figure 4.23: PXRD patterns for both 2 mL and 50 mL ethanol and methanol mediated slurries with a 24 hour slurry time.

During these experiments the solid state relationship between this novel form and the known forms of urea barbituric acid was unknown. It may be that form I and form III spontaneously nucleate during the slurry process, or that they are formed as a result of solution-mediated phase transformations of this novel solid form to yield the known solid forms. The stability relationship of the novel form in comparison to both UBA form I and form III is discussed in section 4.3.5.

4.3.2 The Thermal Behaviour of the Novel Solid Form of UBA

4.3.2.1 DSC Analysis

The unique PXRD data obtained from the slurry experiments discussed above indicated that a novel solid of UBA may be being accessed under these conditions. The data suggested that 24 hour slurry times yield this new solid form in the highest purity when ethanol is used as the solvent medium. With methanol mediated slurries, the product

contains some UBA form I impurities after this slurry time (24 hours). The slurry products were analysed using DSC to investigate the thermal behaviour of the potential new solid form. Figure 4.24 shows the DSC traces obtained for both the 24 hour ethanol and methanol mediated slurry products. It can be seen that the thermal behaviour of the two slurry products is very similar, both displaying an endothermic event, followed by an exothermic event. The DSC trace for the ethanol mediated slurry has a small endothermic peak at approximately 133 °C which can be explained by a small level of residual urea being present in the slurry product. The presence of urea was not observed using PXRD techniques, however PXRD has a lower level of sensitivity in comparison to DSC. It could also be due to the remaining urea no longer being very crystalline and as a result contributing to the PXRD background. The presence of this small endothermic event at the melting temperature of urea suggests that there are low levels of urea impurity in the ethanol mediated slurry product. This urea impurity is not seen in the methanol mediated slurry DSC trace, but this can be easily explained due to the much higher solubility of urea in methanol than ethanol resulting in any urea impurities being in the solution phase of the methanol mediated slurry and not the solid phase.

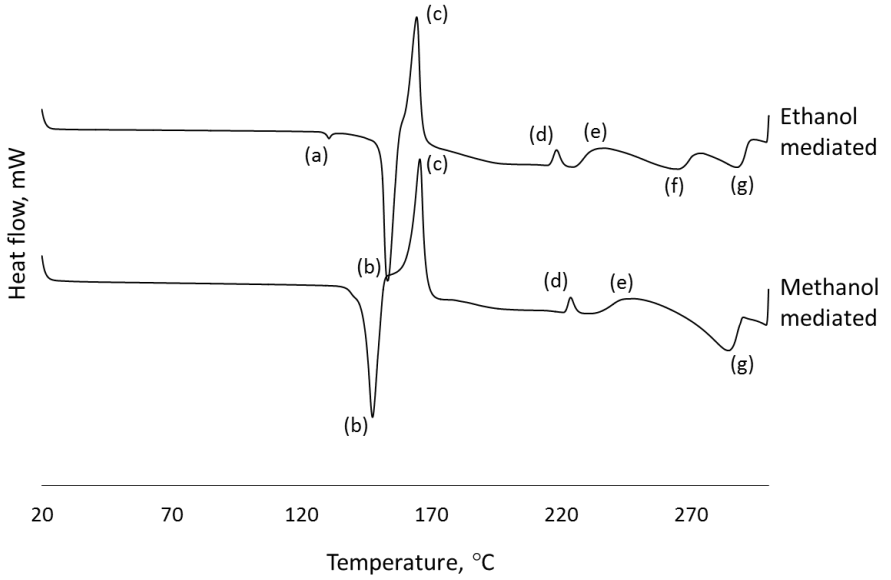

Peak	Ethanol mediated	Methanol mediated
(a)	131 °C	-
(b)	153 °C	147 °C
(c)	164 °C	165 °C
(d)	218 °C	224 °C
(e)	234 °C	248 °C
(f)	265 °C	-
(g)	287 °C	286 °C

Figure 4.24: DSC traces of the 24 hour ethanol and methanol mediated 2:1 (urea: barbituric acid) slurry products (10 °C min^{-1} heating rate, exothermic up).

The temperature for the large endothermic event (Figure 4.24 (b)) observed in both DSC traces varies slightly between each system; for the ethanol system it is at 153 °C and for the methanol system it is at 147 °C. This event signifies an apparent melting of the slurry products. From the PXRD data we know that the methanol mediated slurry product is less phase pure than the ethanol mediated slurry, displaying some additional peaks corresponding to UBA form I. It may be this phase impurity that results in the lower melting temperature for the methanol mediated slurry product. Or it could arise from systematic error within the DSC measurements. Both slurry products exhibit a large exothermic peak after the apparent melt event at approximately 164 - 165 °C, suggesting that a recrystallisation event is occurring (Figure 4.24 (c)). After this

recrystallisation event both DSC traces display very similar thermal behaviour upon the continuation of heating. A small exothermic peak (Figure 4.24 (d)) can be seen for both traces, occurring at similar temperature for both the slurry products. After this the trace becomes significantly uneven, displaying broad exothermic and endothermic events (Figure 4.24 (e), (f) and (g)). It is likely that these exothermic and endothermic events are a result of decomposition within the sample. TGA experimental analysis to help determine the nature of these peaks and understand the nature of the recrystallized high temperature solid form is discussed in section 4.3.2.2.

The DSC trace of the ethanol mediated slurry product is plotted against the DSC traces for both UBA form I and form III in Figure 4.25 below. It can be seen that the overall shape of the DSC traces is very similar for all three solid forms which would not be unexpected if the novel solid form is a new solid form of UBA as theorised. Due to the similarity in the thermal behaviours of the three solid forms, it is likely that the endothermic peak (peak (a)) for the novel form is decomposition of the co-crystal to the individual components, coupled with loss of urea, and the exothermic event is the recrystallisation of the residual barbituric acid (peak (b)).

Peak	UBA I	UBA III	Novel solid form
(a)	188 °C	196 °C	153 °C
(b)	192 °C	200 °C	164 °C
(c)	283 °C	281 °C	287°C

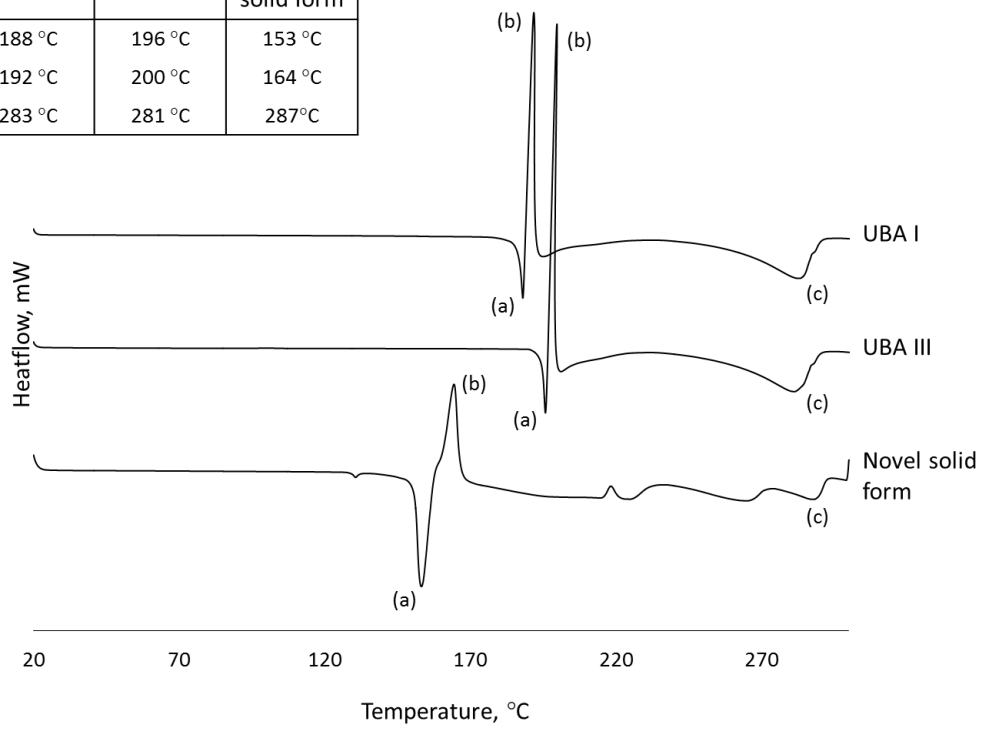

Figure 4.25: DSC traces of UBA I, UBA III and the novel solid form of UBA (10 °C min^{-1} heating rate, exothermic up).

After the large exothermic peak (peak (b)), the UBA form I and form III traces display a broad endothermic hump (peak (c)) at a similar temperature to endothermic events observed in the slurry product. The decomposition of the co-crystal and recrystallisation event observed for the novel solid form, however, appear at a much lower temperature

than for form I and form III (153 °C versus 188 °C and 196 °C respectively) suggesting that this novel solid form is metastable with respect to both form I and form III.

If the novel solid form is a novel form of the UBA co-crystal system then it would be likely that the same high temperature form of barbituric acid is accessed after the initial decomposition event, if this is the case then the thermal events after this form have been accessed should be the same for all of the samples. For UBA I and III it can be seen that the events post recrystallisation are the same for each, however there is a difference in the shape of the trace after the recrystallisation of the novel solid form. This may suggest that the high temperature form accessed from the decomposition of the novel solid form is different. The nature of this high temperature form will be further discussed in section 4.4 below.

4.3.2.2 TGA Analysis

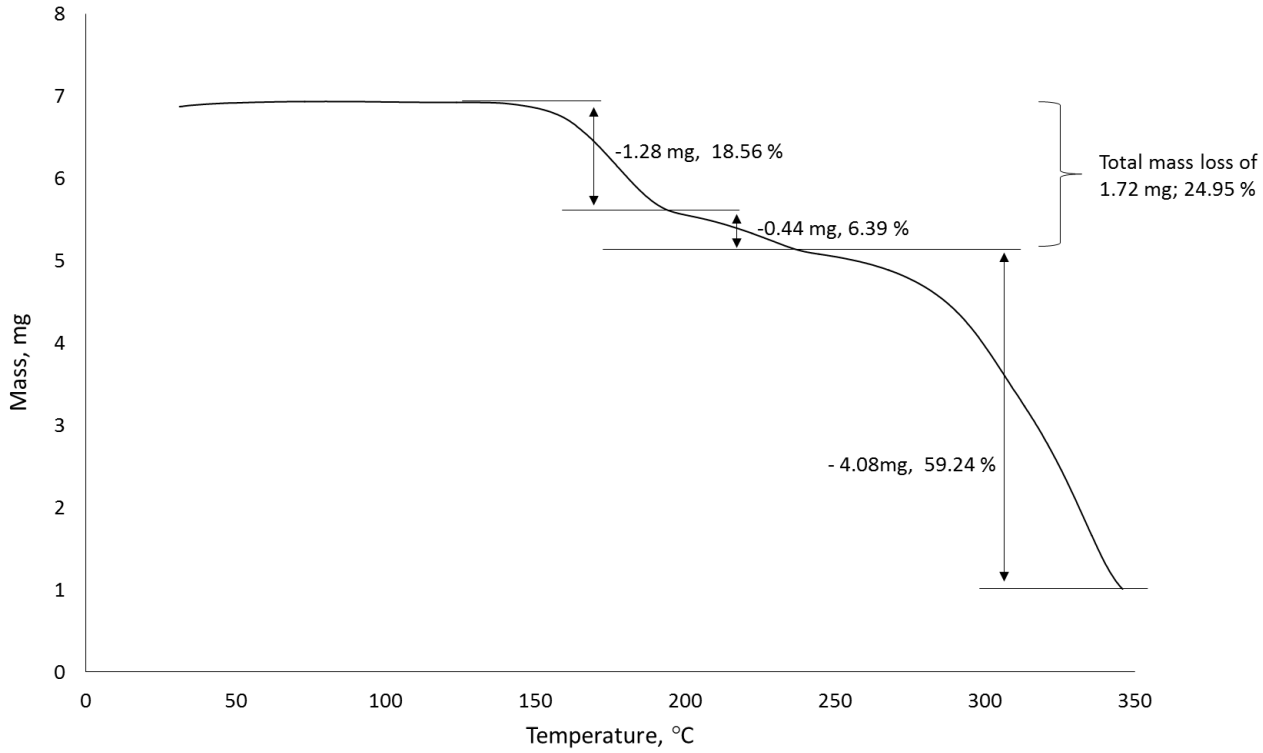

Figure 4.26: TGA spectra of the novel solid form of UBA (10 °C min^{-1} heating rate, under air).

For the novel solid form the TGA trace is again very similar in shape to those from the other UBA solid forms (I and III), giving three distinct mass losses of 18.6 %, 6.4 % and 59.2 % and a total mass loss of 84.2 % (Figure 4.26). During the breakdown of the co-crystal and subsequent recrystallisation event for barbituric acid the total mass loss varies between 24.95 % (novel solid form) and 34.6 % (UBA form I), with UBA form III giving a mass loss of 25.5 %. As previously discussed, upon decomposition of the co-crystal into its individual components, the urea will begin to decompose and ammonia (NH_3) and cyanic acid (NCOH) will be evolved from the sample. The percentage mass of urea in the UBA co-crystal system is 32 % and so these initial mass losses can be

attributed to the decomposition of the urea within the sample, suggesting that upon recrystallisation only barbituric acid will be present.

4.3.3 Solubility of the Novel Solid Form of UBA

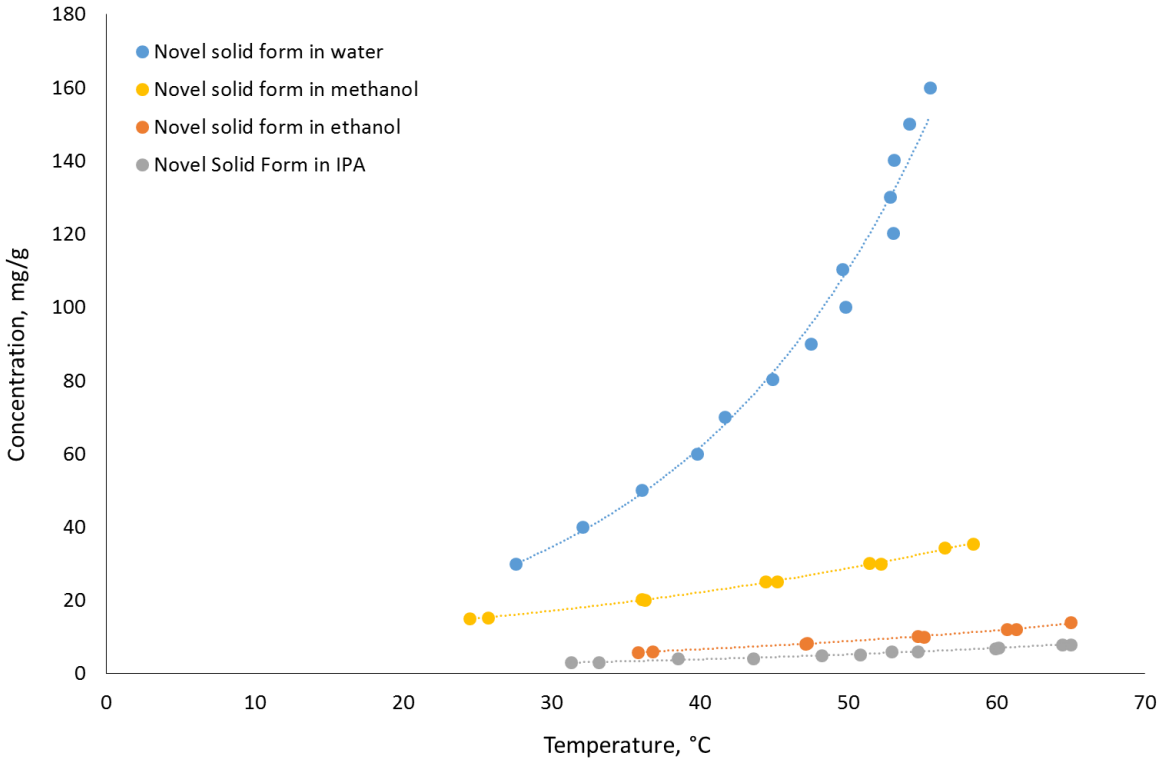

Figure 4.27: Solubility curves of the novel solid form of UBA in water, methanol, ethanol and IPA. Measured using turbidity methods (Crytsal16).

The solubility of the novel solid form in water, methanol, ethanol and IPA was measured using the Crystal16 at GSK, Stevenage (Figure 4.27). As with UBA form I and form III, the solubility of this solid form significantly reduces when increasing the size of the solvent molecule and hence reducing the polarity. The system's solubility reduces approximately three fold when moving from methanol to ethanol and then again by a factor of two going from ethanol to IPA, as is seen with UBA form I and form III. Figure 4.28 shows the solubility of the novel solid form in comparison to both form I and form III in ethanol and IPA. It can be seen that the solubility in ethanol for all three solid forms is very similar, with the curves almost overlapping. It could be argued that the solubility for the novel form in ethanol is greater than both form I and form III, as would be expected for a metastable form. However, the solubility curves are only an estimate based on the measured solubility points which carry their own errors and so the curves are essentially overlapping at the level of accuracy of the determination. It does appear that the solubility for the novel solid form in IPA is significantly higher than that of form I and form III, however. Although, this should be treated with caution and may again be an artefact of the errors associated with the techniques used as the data obtained for the novel solid form used turbidity measurements which, as discussed previously

(section 4.2) have inherent problems, as opposed to observation methods which were used for the below solubility data of both form I and form III. The similarity in the solubility curves for all three forms in ethanol suggests that, although the novel form is likely metastable due to its lower melt, there may only be a slight energy difference between this form and the two known polymorphic forms.

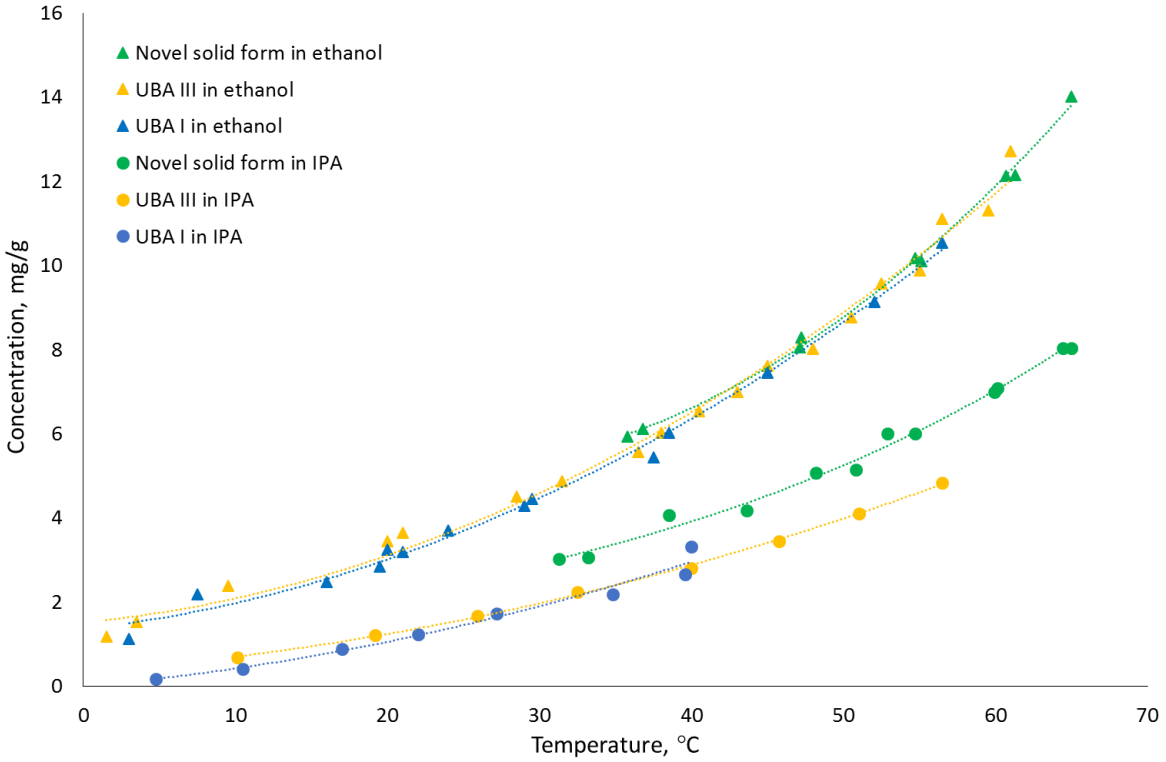

Figure 4.28: Solubility of the novel solid form and UBA form I and III measured using turbidity techniques and observation techniques respectively.

4.3.4 Investigation into the Identity of Novel Solid Form of UBA

The PXRD and DSC data suggest that a novel solid form of UBA has been accessed under these experimental conditions (2:1 ratio urea: barbituric acid slurries). Unfortunately, the crystals accessed from the slurry experiments are not conducive to single crystal analysis due to them being a crystalline powder and so no single crystal X-ray diffraction experiments to obtain the crystal structure have been made. However, attempts at determining the contents of the crystal structure have been made.

4.3.4.1 NMR Analysis of the Novel Solid Form

Solution NMR analysis on the slurry product was conducted in order to determine the contents of the crystal structure in terms of its chemical components. As no significant amount of the starting components was observed with PXRD or DSC analysis it is likely that the crystal structure contains both urea and barbituric acid. Due to the same solid

form being accessed using both ethanol and methanol as the solvent medium it seems unlikely that a solvate had been formed from two different solvents. However, the solid form could be a hydrate due to water impurities present in the alcohol solvents used. A 2:1 molar ratio of urea: barbituric acid was used to access this solid form and as no significant amount of residual urea was observed using PXRD, and only a small amount was observed in the DSC for the ethanol mediated slurry product, it could be that the new solid form could contain a 2:1 ratio of urea: barbituric acid and hence be a stoichiometrically different co-crystal to the known system.

Initially, ^{1}H NMR was used with deuterium oxide as the solvent, however due to the lability of the hydrogens in urea, the urea could not be seen in the NMR spectra. Subsequently, ^{13}C NMR was conducted, again using deuterium oxide as the solvent. The resulting NMR spectra (Figure 4.29) showed the presence of both urea and barbituric acid in the crystal and showed that the ratio of the two molecules was 1:1. The ^{13}C NMR shows no sign of solvent molecules (either ethanol or methanol), suggesting that the novel solid form is not a solvate and may be a polymorph of the UBA co-crystal system. However, the ^{13}C NMR cannot show the presence of water and consequently it cannot confirm that the solid form is not a hydrated form of UBA. That being said, hydrated forms tend to show a broad endothermic peak in their DSC traces around 80 – 100 °C, where the water molecules are lost from the structure and the solid is desolvated. As there is no evidence of any desolvation in the DSC or TGA it suggests that this solid form is not a hydrated form.

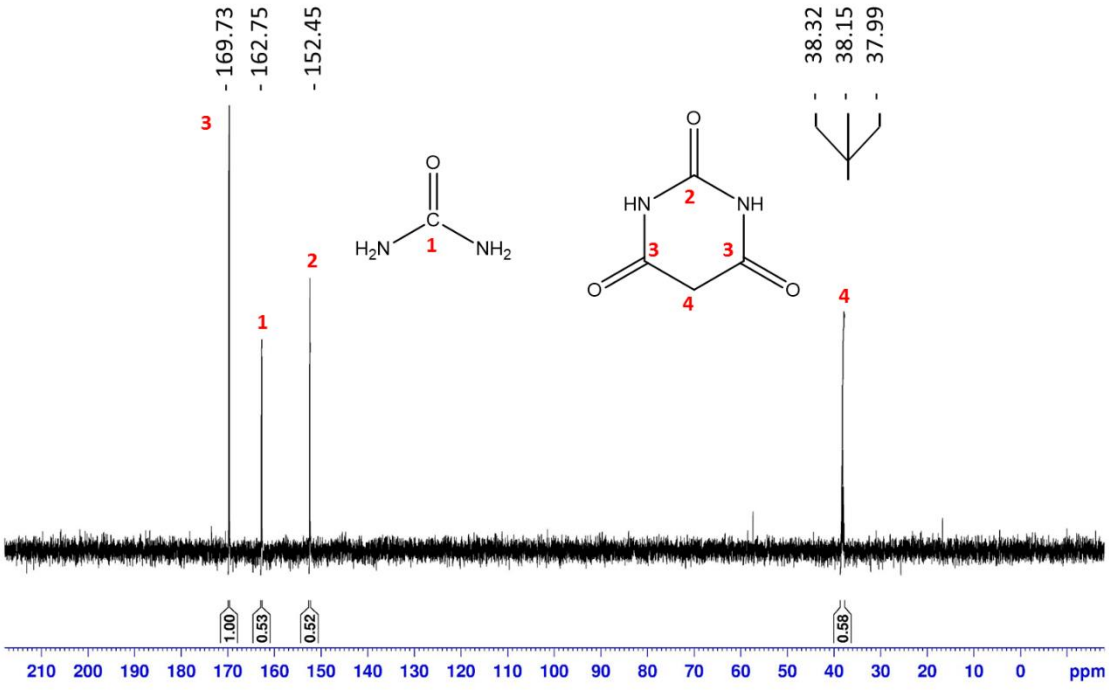

Figure 4.29: ^{13}C NMR spectra of novel solid form of UBA.

The PXRD, DSC and ^{13}C NMR analysis all provided evidence that a new solid form has been accessed during these experiments and that it is likely to be a novel 1:1 solid form

of the UBA co-crystal system. The results suggests that the solid form is likely to be a novel polymorph of UBA, not a solvate or hydrated form.

4.3.5 Stability of the Novel Solid Form of UBA

4.3.5.1 Solid State Stability of the Novel Solid Form

Due to the novel solid form of UBA having a significantly lower decomposition temperature than form I and form III (153 °C versus 188 °C and 196 °C respectively) it can be predicted that the novel form of UBA is metastable in comparison to both form I and form III. Investigations into the solid state stability of the novel form were conducted by analysing samples via PXRD over a period of 2.5 years to investigate if any solid-state phase transformations into more stable forms had occurred.

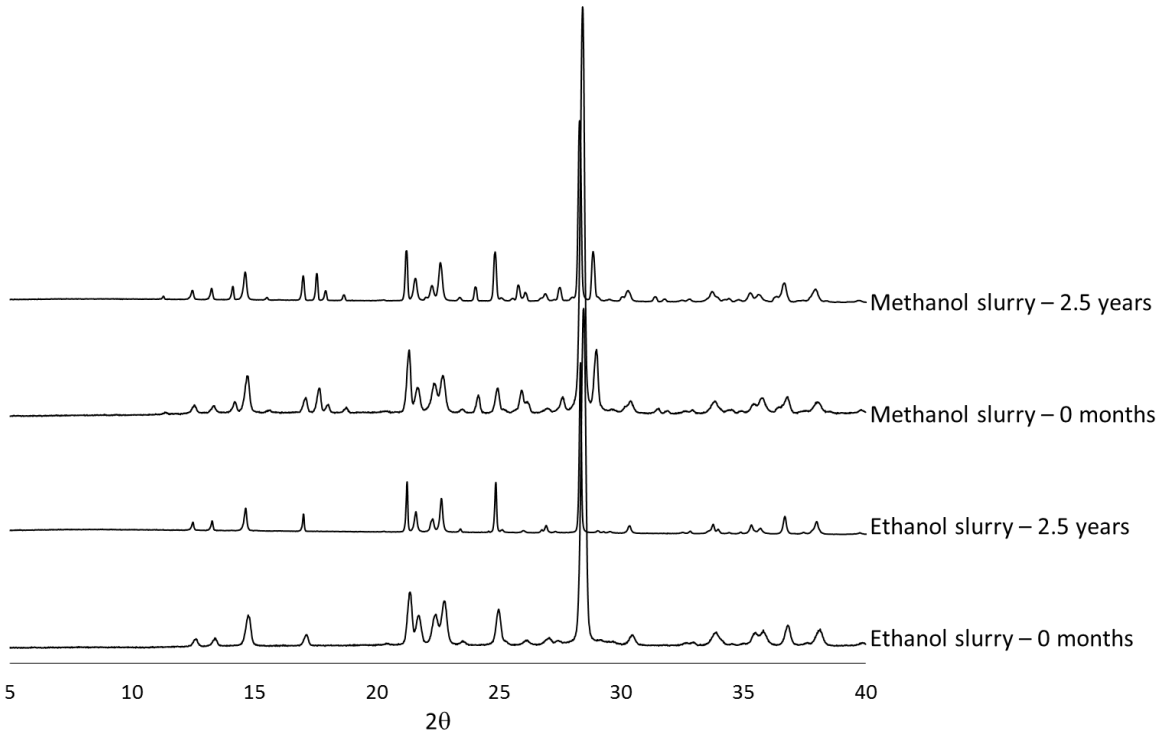

Figure 4.30: PXRD patterns of the novel solid form obtained from both ethanol and methanol mediated slurries measured at time of formation and 2.5 years after.

The PXRD patterns in Figure 4.30 show that the novel solid form (obtained from ethanol mediated slurries) is stable in the solid state under ambient conditions for a period of at least 2.5 years, with no observable changes in the PXRD patterns during this time. Samples where UBA form I impurities were present in the initial experimental product (methanol mediated slurry products) were also investigated to see if the presence of these form I impurities would seed the transformation of the novel form to the more stable form. The PXRD analysis shows that for samples of this type the presence of UBA form I did not seed any solid-state phase transformations and the product remains the same after being left under ambient conditions for 2.5 years. These results show that under ambient conditions the novel solid form does not transform to any of the known

solid forms via any solid phase transformations, with solid state stability established to be greater than two and a half years.

4.3.5.2 Competitive Slurries of the Novel Solid Form with Form I and Form III

Competitive slurries of the novel solid form with both form I and form III were conducted in order to investigate the solution-mediated phase transitions between the systems. The competitive slurries were carried out using ethanol as the solvent medium (1 mL) and the CRD Polar Bear Plus for both temperature control and mixing. The slurries were formed using 150 mg of a 1:1 mixture of the novel form with either form I or form III and left to mix (1500 rpm) at 20 °C for a predetermined amount of time (24 hours – 1 week). PXRD analysis was used to identify the solids present in the competitive slurry products once they had been isolated using vacuum filtration and dried at room temperature.

As the thermal behaviour suggests that both form I and form III are more stable than the novel solid form, one might expect that the competitive slurries would yield a full conversion of the novel form to either form I or form III, depending upon which other solid form was present in the competitive slurry. For competitive slurries with a mixture of UBA form I and the novel solid form, full conversion of the mixture to yield the more stable form I was not achieved within a two week time period. Figure 4.31 shows the PXRD patterns for the competitive slurry samples and it is evident that even after two weeks peaks still remain that correspond to the novel solid form as highlighted.

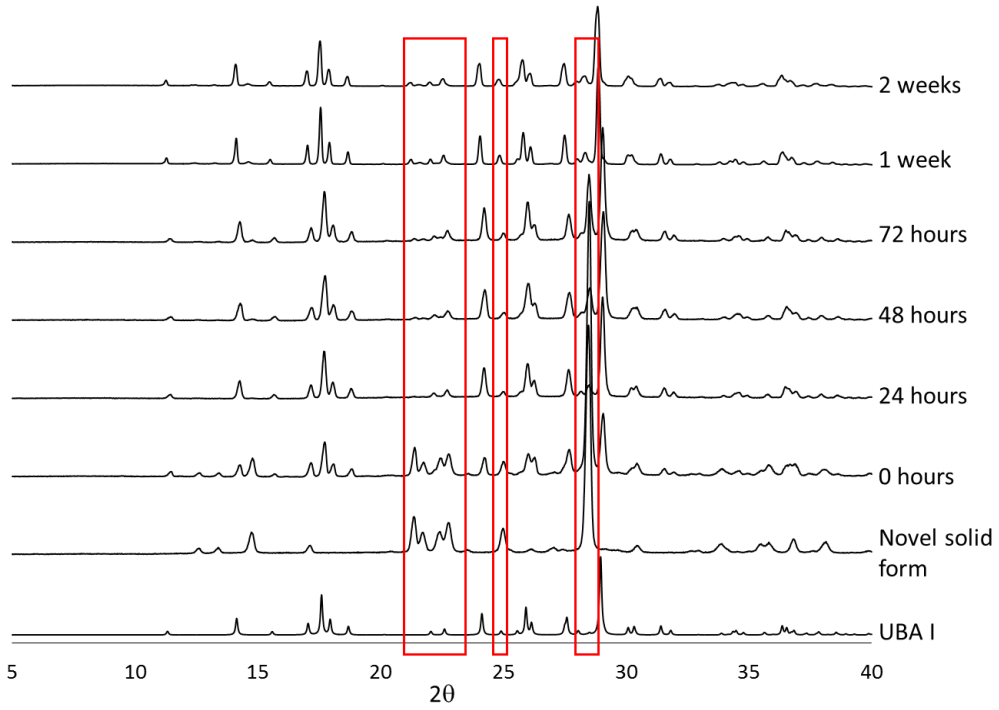

Figure 4.31: PXRD patterns of competitive slurries of UBA form I and the novel solid form. Red boxes highlight peaks unique to the novel solid form.

It can be seen from the PXRD data that the peaks corresponding to the novel solid form decrease in intensity, suggesting that there is less of that form in the slurry product.

However, the intensity of these peaks decreases within the first 24 hours and then remains of a similar intensity for the remaining experiment time. This suggests that between 24 hours and 2 weeks little to no conversion of the remaining novel solid form in the slurry mixture occurs. The initial reduction in the intensity of the peaks corresponding to the novel solid form in the first 24 hours may be due to partial conversion of this form to the more stable form I. However, as it appears that no further conversion happens after this initial 24 hour period, and some novel solid form still remains in the mixture, it seems unlikely that an initial conversion would occur within the first 24 hours and then stop. The reduction in intensity may therefore be due to preferential dissolution of this solid form over form I once the slurry has been formed. The 0 hour PXRD pattern is obtained from the dry mixture of the two forms before any solvent has been added. Once the ethanol is added forming the slurry, and the system is left stirring for the first 24 hours, some of the solid will dissolve into the ethanol. As the novel solid form is metastable with respect to UBA form I and appears to have a slightly higher solubility, more of this form will dissolve into the ethanol, thus reducing the solid ratio of novel form: form I in the slurry and resulting in the PXRD peaks for this form being reduced in intensity in comparison to the form I peaks.

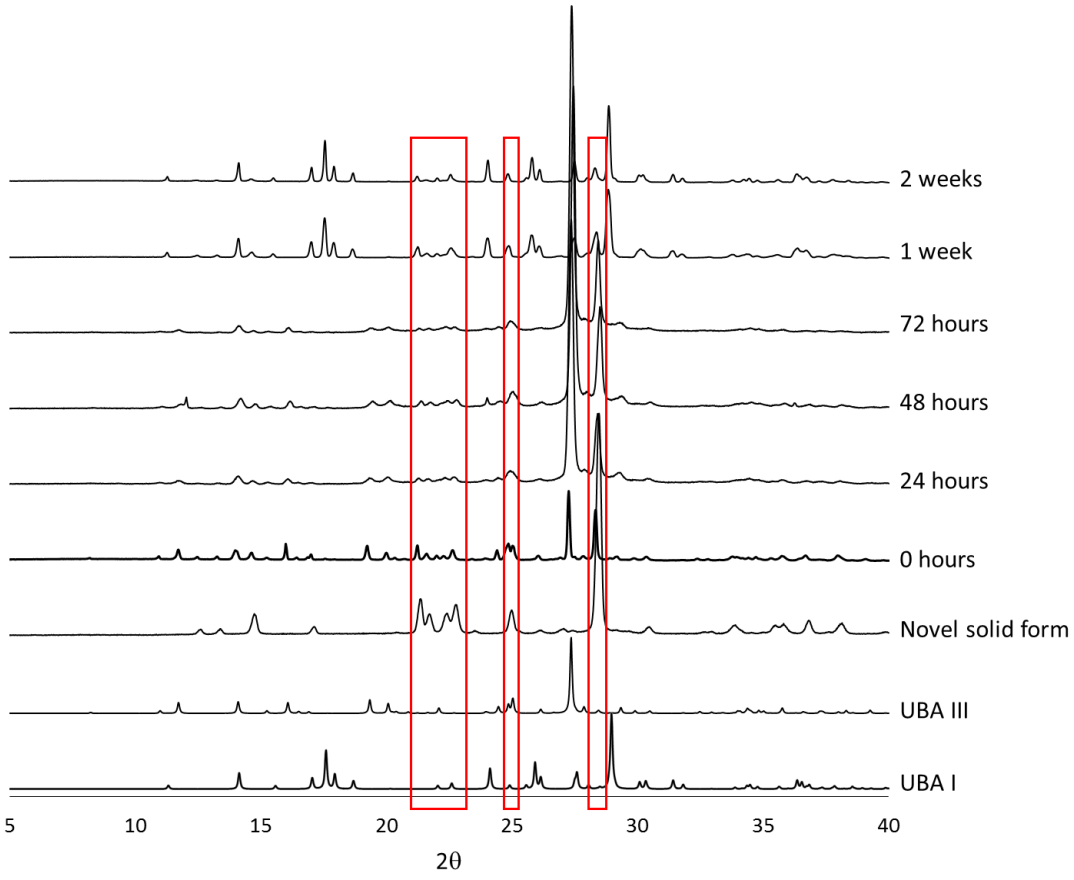

Figure 4.32: PXRD patterns of competitive slurries of UBA form III and the novel solid form. Red boxes highlight peaks unique to the novel solid form.

As it appears that little to no conversion of the novel solid form to the stable form has occurred within two weeks it can be concluded that the kinetic energy barrier between

the novel solid form and form I is sufficiently high that under these conditions it is not overcome. This large kinetic energy barrier between these two forms may be due to a large amount of energy being initially required for the rearrangement of molecules between the two crystal structures and the breaking of the intermolecular bonds present in the novel solid form. The lack of conversion may also be due to ethanol seemingly stabilising the novel solid form whilst in solution.

When competitive slurries of UBA form III and the novel solid form were conducted a similar outcome was observed with respect to the novel solid form not converting to the more stable form (Figure 4.32). Interestingly, when the slurries were left for 1-2 weeks the resultant product was a mixture of the novel solid form and UBA form I; the UBA form III had transformed to yield form I in the slurry, but the novel solid form had not converted and remained unchanged in the slurry. The arguments for why the novel solid form does not convert in this competitive slurry, whilst UBA form III does, are the same as discussed previously: it is likely that the kinetic barrier between the novel solid form and form I is too high to be overcome under these conditions.

4.4 The High Temperature Solid Form

Upon heating of each UBA form I, form III, and the novel solid form, the co-crystal decomposes and urea is lost from the system. As a result, the remaining barbituric acid re-crystallises into an assumed high temperature form. Little is known about the nature of this solid form and it was previously been predicted to be a high temperature form of UBA.[135] However, this work has shown that the urea is lost from the system upon the decomposition of the co-crystal and so the resultant high temperature form is unlikely to be a multi-component system involving urea. Investigations into whether the recrystallisation product of the novel solid form matches that of the product from both form I and form III were conducted as well as further investigation into the nature of the high temperature solid form.

4.4.1 Variable Temperature PXRD (VT PXRD) Analysis

Variable temperature PXRD (VT PXRD) data were collected for UBA form I, form III and the novel solid form at AstraZeneca, Macclesfield, UK on behalf of the author. PXRD patterns were collected for each form at predetermined temperatures based on events observed in the DSC traces. For each system, PXRD patterns were collected at 20 °C, a temperature immediately before the co-crystal decomposition, temperatures during and after the re-crystallisation event, and at 25 °C after the system had been cooled back down. This allowed the identity of the solid state material to be followed during the thermal transitions which occur upon heating as observed in the DSC traces.

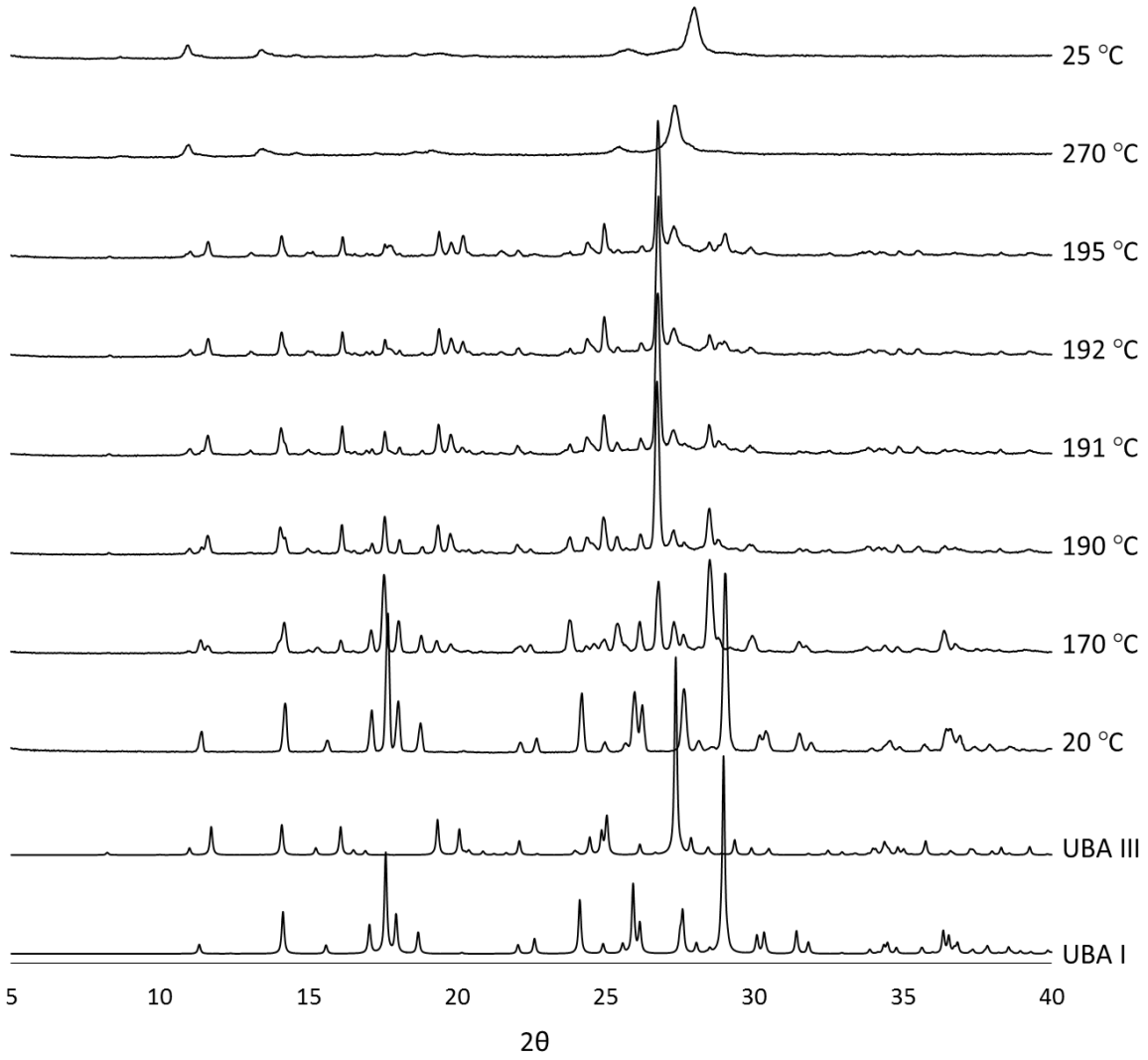

Figure 4.33: VT PXRD patterns obtained for UBA form I.

For UBA form I, the VT PXRD patterns show that there is a change in the solid form upon heating (Figure 4.33). It can be seen that at 170 °C, before the co-crystal system has broken down, the collected PXRD pattern has additional peaks in comparison to the pattern collected at 20 °C. These additional peaks can be attributed to the presence of form III in the sample. This result shows that upon heating a pure sample of form I, a solid-state phase transformation to form III occurs before 170 °C. This partial transformation of form I to form III at this elevated temperature provides evidence that at 170 °C, form III is the more stable form. However, this phase transformation cannot be observed in the DSC data and so the exact onset of this transition cannot be determined. Three PXRD patterns were collected at temperatures during the recrystallisation event (190 °C, 191 °C and 195 °C) and show that a new crystalline state is accessed after the co-crystal breaks down and urea is lost. The PXRD patterns at each of these three temperatures are the same and do not match any known forms of BA. As the system is heated further (to 270 °C) it can be seen that the level of crystallinity in the sample is significantly reduced and only a few peaks are present in the PXRD pattern,

indicating a loss in crystallinity of the sample. Upon cooling of the sample, DSC data shows that no further thermal events take place and the high temperature solid form remains at these lower temperatures. This is supported by there being no change in the last PXRD pattern that was collected at 25 °C after the system had been cooled from 270 °C, showing that the transformation to this high temperature form is irreversible.

Figure 4.34 shows the VT PXRD data obtained for UBA form III. It can be seen that heating UBA form III to 170 °C does not cause any change in the solid form to occur, which is as expected due to form III being the more stable form at this temperature. PXRD patterns were collected at 199 °C, 200 °, 201 °C and 203 °C in order to follow the decomposition and recrystallisation event. At 199 °C the PXRD pattern is slightly changed from that of UBA form III, with additional peaks occurring at approximately 2θ = 13 °, 15 ° and 17.5 °, 22.5 °, 25.5 °, 27 ° and 28.5 °. As the temperature is increased from 200 °C to 203 °C the PXRD pattern remains mostly the same, but with some peak broadening and loss of intensity. At 270 °C there is a further loss in the intensity, as well as a broadening in the PXRD peaks showing a loss in crystallinity of the sample. Upon cooling back to 25 °C, the PXRD shows a slight change in some of the peak positions, especially at higher 2θ values. However, this peak shift is likely due to a contraction of the unit cell with temperature and hence a reduction in the d-spacing.

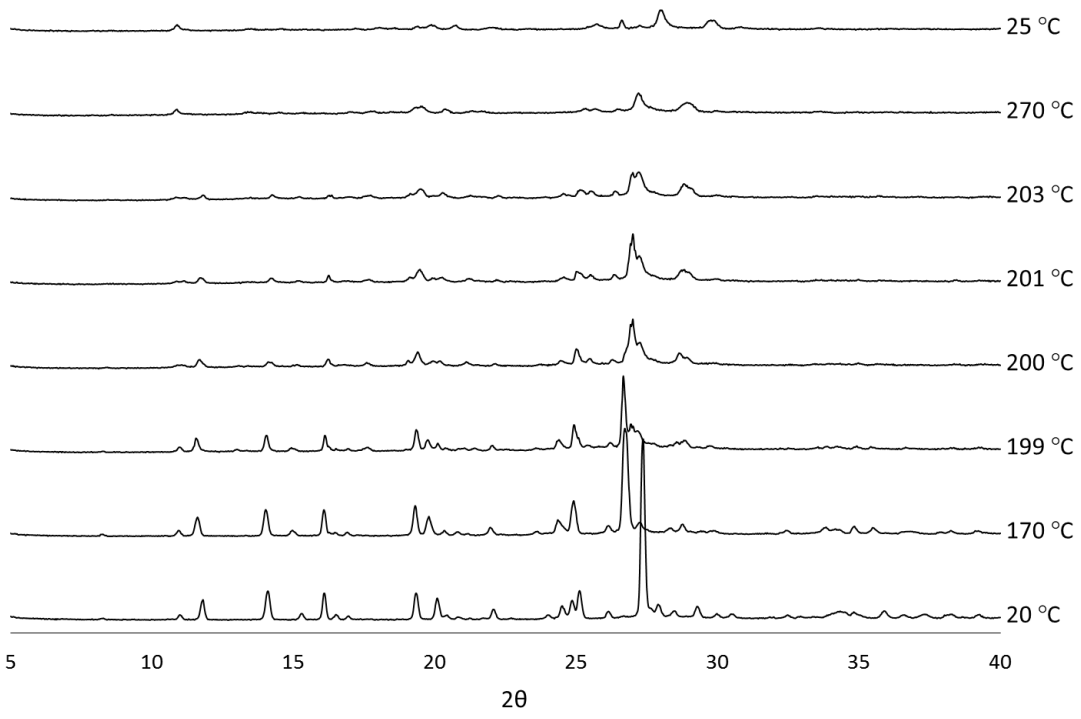

Figure 4.34: VT PXRD patterns obtained for UBA form III.

Figure 4.35 shows the VT PXRD data obtained for the novel solid form of UBA. At 125 °C, approximately five degrees before a small melt occurs that is assumed to be a melt of residual urea in the sample, a small change in the PXRD pattern for the novel solid form can be seen. The peaks at 2θ = 21.3 ° and 21.7 ° (at 20 °C) now appear as one peak at 2θ = 21.25 ° with a shoulder at 2θ = 21.45 °. The peaks at 2θ = 22.3 °and 22.7 ° appear

to be more separated and slightly shifted towards lower 2θ values. The peaks at larger 2θ values have shifted to lower values due to the unit cell increasing in size with temperature and hence the d-spacing between Miller planes increases. The PXRD pattern obtained at 135 °C, before the decomposition of the novel solid form into the individual components, matches that at 125 °C as expected as the only event observed in the DSC between these two points is that of the melt of the residual urea that was present in the sample. The PXRD pattern collected at 164 °C, the recrystallisation temperature, is significantly different to the starting PXRD pattern, showing a new solid form has been accessed. As the sample is heated further the PXRD patterns exhibit only a small amount of change: the peaks broaden, specifically the two at 2θ = 26.7 ° and 27.3 ° which are no longer resolved from one another. Once the system is cooled back down to 25 °C the PXRD pattern remains the same showing no change in solid form.

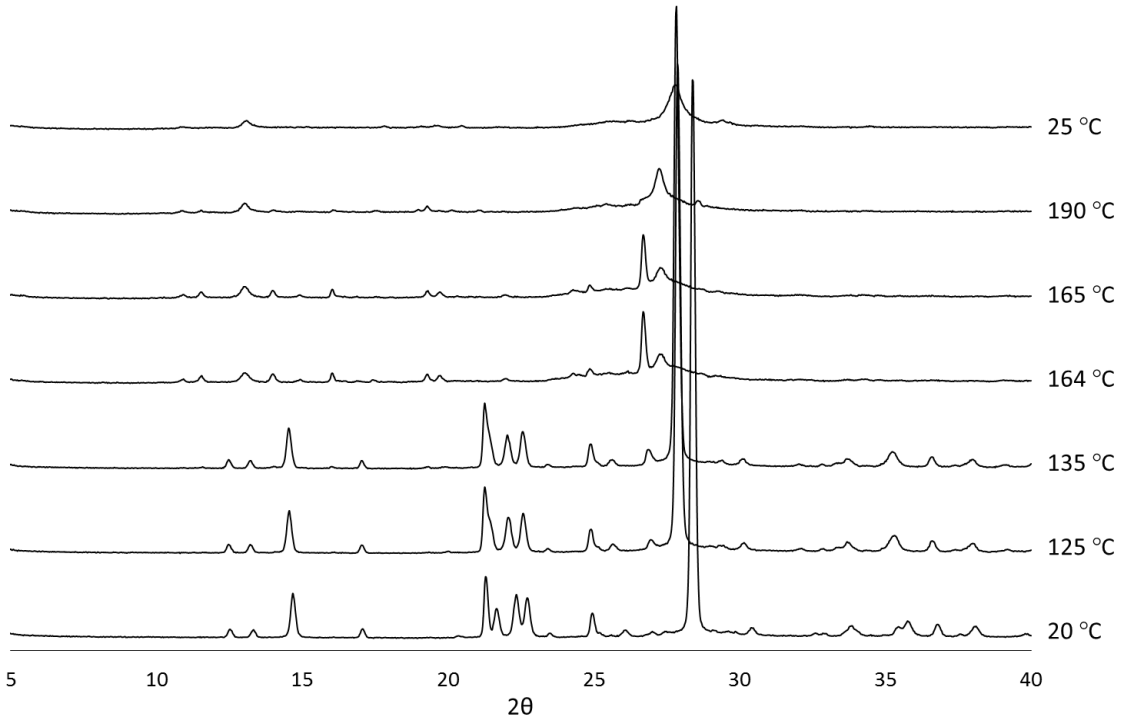

Figure 4.35: VT PXRD patterns obtained for the novel solid form of UBA.

All three solid forms undergo a solid form change upon heating, Figure 4.36 shows the PXRD patterns obtained for each sample after the recrystallisation event. The peak positions in each pattern are the same, but it can be seen that the patterns obtained for UBA form III and the novel solid form display a much lower level of crystallinity: the peaks are much broader and less intense than those seen for the UBA form I recrystallisation product. This suggests that the recrystallisation of barbituric acid, once the co-crystal has broken down and urea has decomposed, for both UBA form III and the novel solid form produces a less crystalline product than the recrystallisation of form I. Specific temperatures for PXRD data collection for each solid form were chosen based on the thermal events observed in the DSC patterns and as a result the PXRD patterns for the recrystallisation events were collected at a different temperatures. This may be

one of the reasons for the differences observed in the peak sharpness and intensity between the systems. The decomposition of the co-crystal for each form also occurs at a different temperature and hence the temperature at which this high temperature form is crystallised is also different. This could lead to the differing levels of crystallinity observed. The VT PXRD data shows that the exothermic events observed after the melts in the DSC traces do result in a crystalline solid form, however there is also presence of amorphous material. Upon further heating of this high temperature form it is seen that in all three samples the level of crystallinity of the samples is reduced.

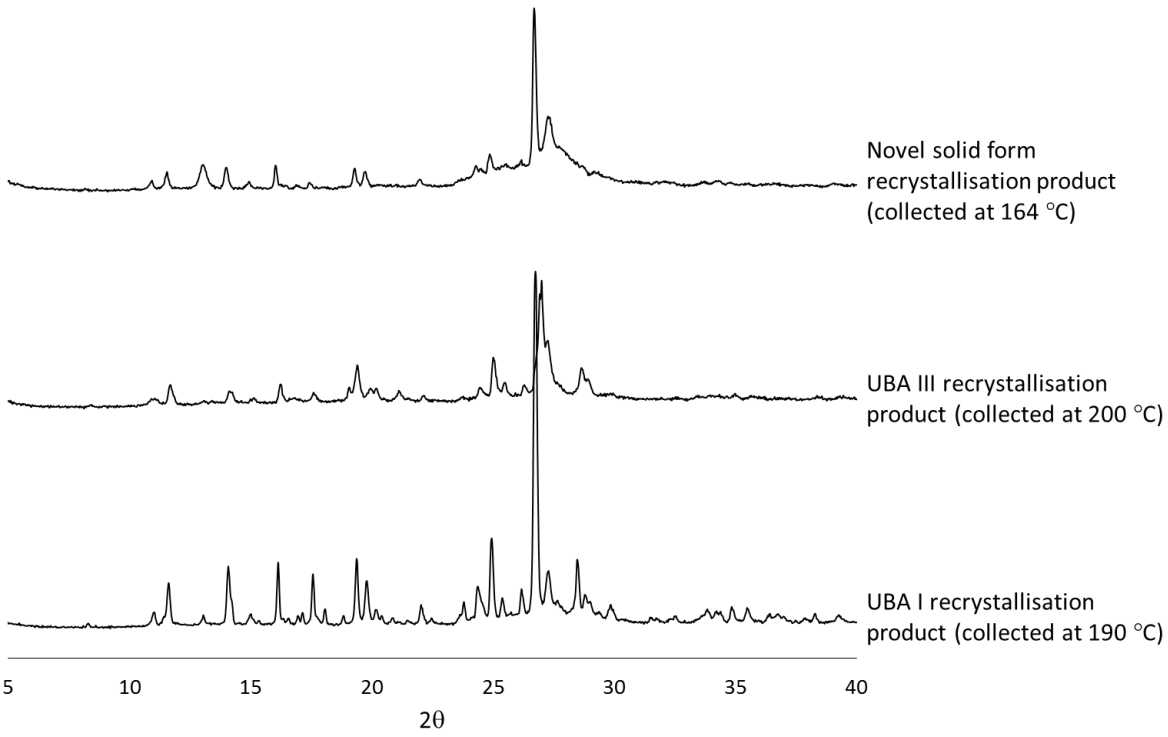

Figure 4.36: VT PXRD patterns of the high temperature solid form accessed upon heating UBA I, UBA III and the novel solid form of UBA.

Unfortunately, the nature of the recrystallised solid form has yet to be identified, with ^{13}C NMR experiments not yielding any measurable peaks and unable to provide information on the chemical contents of the resultant solid. The solid obtained is also not conducive to single crystal X-ray analysis, so no single crystal structure can be obtained.

4.5 Chapter Conclusions

The work discussed in this chapter focused on determining the relative stability and stability relationship of UBA form I and form III, as well as looking further into the polymorphism and solid form landscape of the UBA co-crystal system. During this work, a novel solid form of UBA was accessed using small scale slurrying techniques (2:1 ratio of urea: barbituric acid in ethanol or methanol). The novel solid form was identified via its unique PXRD pattern and thermal behaviour. Solution ^{13}C NMR analysis showed that

the novel solid form contained a 1:1 ratio of urea: barbituric acid, suggesting a novel polymorph had been accessed. Unfortunately, a crystal structure of this solid form could not be accessed.

Upon heating, samples of UBA form I and form III do not undergo a melt and subsequent recrystallisation as previously thought. Instead, TGA data shows that in each polymorph the co-crystal breaks down into the individual components resulting in the vaporisation and decomposition of urea. As the urea is lost during the decomposition, the residual barbituric acid rearranges to access a high temperature form. The VT PXRD data obtained for UBA form I and form III show that upon the decomposition of the co-crystal, the same high temperature solid form is obtained. Thermal analysis of the novel solid form of UBA, along with VT PXRD, showed that the novel solid form undergoes a decomposition event into the individual components and loses the urea, as was seen for both UBA form I and form III, however this thermal event occurs approximately 50 °C lower in temperature indicating that this solid form is metastable in comparison to both form I and form III.

Competitive slurries of the novel solid form and UBA form I and form III did not result in conversion of the novel solid form to either of the two forms. These results suggest that, although metastable, the kinetic barrier between the novel solid form and form I/III was too high to be overcome during the slurrying experiments.

The temperature at which the co-crystal decomposition occurs is slightly higher for UBA form III than UBA form I. This may suggest that at these elevated temperatures, UBA form III is the thermodynamically stable form. Solubility data obtained for both form I and form III in ethanol using gravimetric and observation techniques suggests that the polymorphs are enantiotropic, with a transition temperature (T_t) in the range of 37 °C – 42 °C. Below T_t, the solubility for form III was higher, suggesting that form I was the thermodynamically stable form, with the opposite being true once the temperature surpassed T_t. This result aligns with Zhang *et al.* who stated that in water, there is an interception of the solubilities at approximately 35 °C.[197] The measured solubility data in both ethanol and IPA highlighted the difficulty of accessing accurate solubility of a co-crystal system, which, combined with the limitations of each method results in the propagation of these errors into the determination of T_t.

Competitive slurry experiments of UBA form I and form III conducted at 20 °C confirm that form I is the thermodynamically stable form. Competitive slurry experiments conducted at 50 °C, however, showed full conversion of the mixture to form I, not form III. This indicated that UBA form I still remains the thermodynamically stable form at 50 °C and that the T_t obtained from solubility data is inaccurate. Further experiments conducted at 75 °C suggested that conversion of the mixture to yield form I was still occurring at these elevated temperature, implying that form I is the thermodynamically stable form until at least 75 °C, resulting in form III being a metastable form in this temperature range. Crystallographic analysis of the two forms provides some justification as to form I being the thermodynamically stable form, with form I having a

higher density, a three dimensional hydrogen bonded network and a stronger urea-urea hydrogen bonded dimer. Form I was also shown to satisfy more of the full interaction map hotspots than form III.

Chapter 5 – The Selective Crystallisation of UBA Form III

5.1 Introduction

The three solid forms of UBA can be accessed selectively using small scale evaporative co-crystallisation techniques depending on the solvent medium (ethanol or methanol) and the ratio of the starting components used in the crystallisation process (Table 1.3). Previous work investigating the transfer of this selective crystallisation into cooling techniques showed that form II was elusive in cooling crystallisation and that form I could be accessed selectively when using methanol as the solvent medium and a 2:1 ratio of urea: barbituric acid in the cooling process. This contradicted the evaporative crystallisation conditions needed to access form I selectively; with ratios of 1:2 or 1:3 being needed for the selective access of form I and a 2:1 ratio yielding form III. This work also showed that the selective formation of UBA form III, now known to be the metastable form, could not be achieved using methanol as the solvent system with a 2:1 ratio of urea: barbituric acid in cooling crystallisation, as form I was always present in the crystallisation product.[135, 136]

This chapter covers the experiments conducted in order to achieve selective crystallisation of the metastable form III of UBA. It covers initial steps taken using small scale slurrying techniques and the subsequent transfer of slurrying methods into cooling crystallisation to access pure UBA form III and the scale up of these techniques in batch cooling crystallisation. Both unseeded and seeded cooling crystallisation experiments are conducted and their results discussed. The batch cooling crystallisation of UBA form III is subsequently transferred to continuous crystallisation, utilising both the KRAIC and COBC platforms. The results of these experiments are discussed in detail in this chapter.

5.2 Multi-component Solution-mediated Phase Techniques (Slurry Techniques)

Initial steps in attempting to access pure UBA form III were taken using slurrying experiments. The small scale (2 mL) slurry experiments were conducted using the CRD Polar Bear Plus for both temperature control (constant temperature of 20 °C) and magnetic bottom stirring (250 rpm). The slurries were left mixing for pre-determined experimental times before the product was isolated using vacuum filtration and dried at room temperature. The slurry products were analysed using PXRD for solid form identity.

Initial slurry experiments were conducted using both ethanol and methanol as solvent media, and utilised a variety of urea: barbituric acid ratios that were shown to access

UBA in evaporative techniques (1:1, 1:2, 1:3 and 2:1). When a 2:1 ratio was used a novel solid form of UBA was accessed as previously discussed in Chapter 4. Experiments using both 1:2 and 1:3 ratios of urea: barbituric acid with ethanol or methanol as the solvent medium did not yield pure UBA solid product, with significant amounts of residual barbituric acid starting material being present after slurry times of 24 hours (see Appendix Figure 9.6). UBA form III was accessed alongside the residual barbituric acid when ethanol was used as the solvent medium and UBA form I was accessed alongside the residual barbituric acid when methanol was used. Due to the significant amounts of barbituric acid still present in the slurry product these ratios were not taken forward for any further investigations.

When a 1:1 ratio of urea: barbituric acid was used in the slurry experiments, it was found that when using methanol as the solvent medium, UBA form I was selectively accessed with slurry times of 22 – 24 hours. This outcome aligns well with previous crystallisation work conducted on this system by Wittering[135] where methanol was the solvent taken forward to produce UBA form I selectively in cooling crystallisation under batch conditions, as well as on a variety of different continuous crystallisation platforms. When shorter slurry times were investigated the resultant product was a mixture of UBA form I and form III as shown by the PXRD data in Figure 5.1.

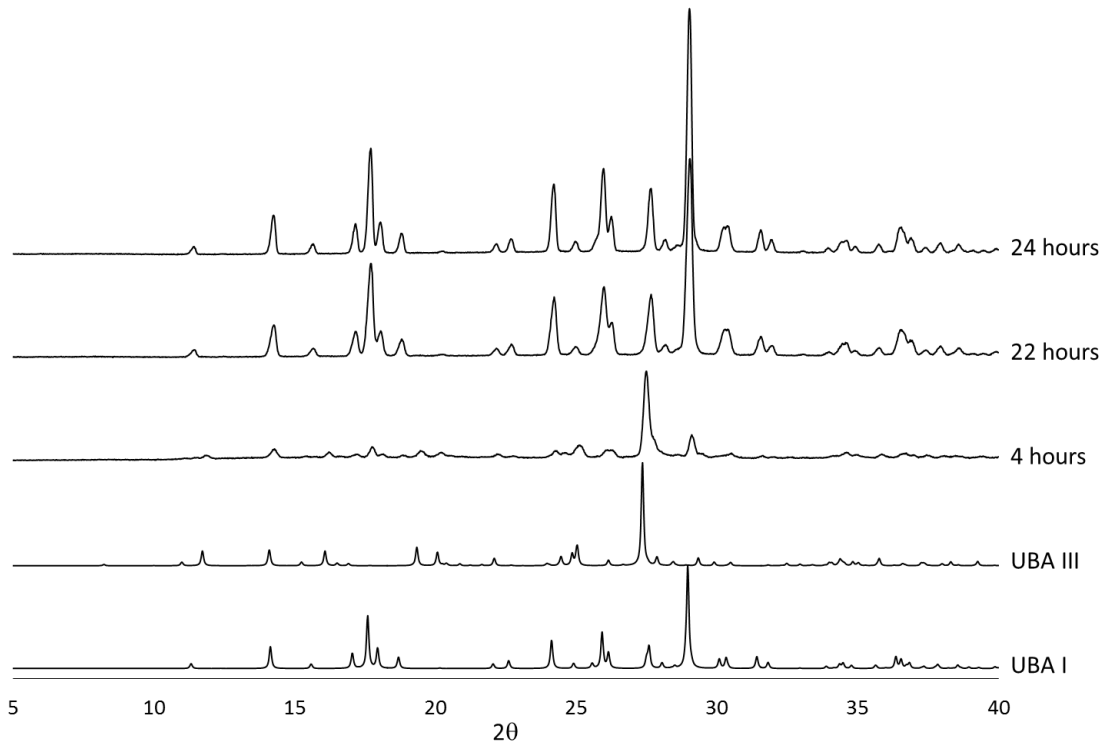

Figure 5.1: PXRD patterns of 1:1 urea: barbituric acid slurries in methanol.

The presence of UBA form III in shorter slurry times (4 hours), but not in longer slurry times (22 – 24 hours), allows for the conclusion that, upon slurrying the two starting components in methanol at 20 °C, initial co-crystallisation results in the nucleation of the metastable form, form III, which then undergoes a solution mediated phase

transformation to yield the thermodynamically stable form, form I, as the systems are left mixing.

When the same 1:1 ratio of urea: barbituric acid was used, but with ethanol as the solvent medium, it was observed that UBA form III could be accessed to relatively high polymorphic purity (Figure 5.2). Slurries with experimental times of 16 – 24 hours resulted in a product that was predominantly UBA form III, with only very small amounts of UBA form I present. Shorter slurry times of 2 hours produced UBA form III with no presence of UBA form I, however significant amounts of residual barbituric acid were observed in the PXRD data. Slightly longer slurry times of 4 – 12 hours gave a mixture of UBA form III, residual BA and trace amounts of UBA form I.

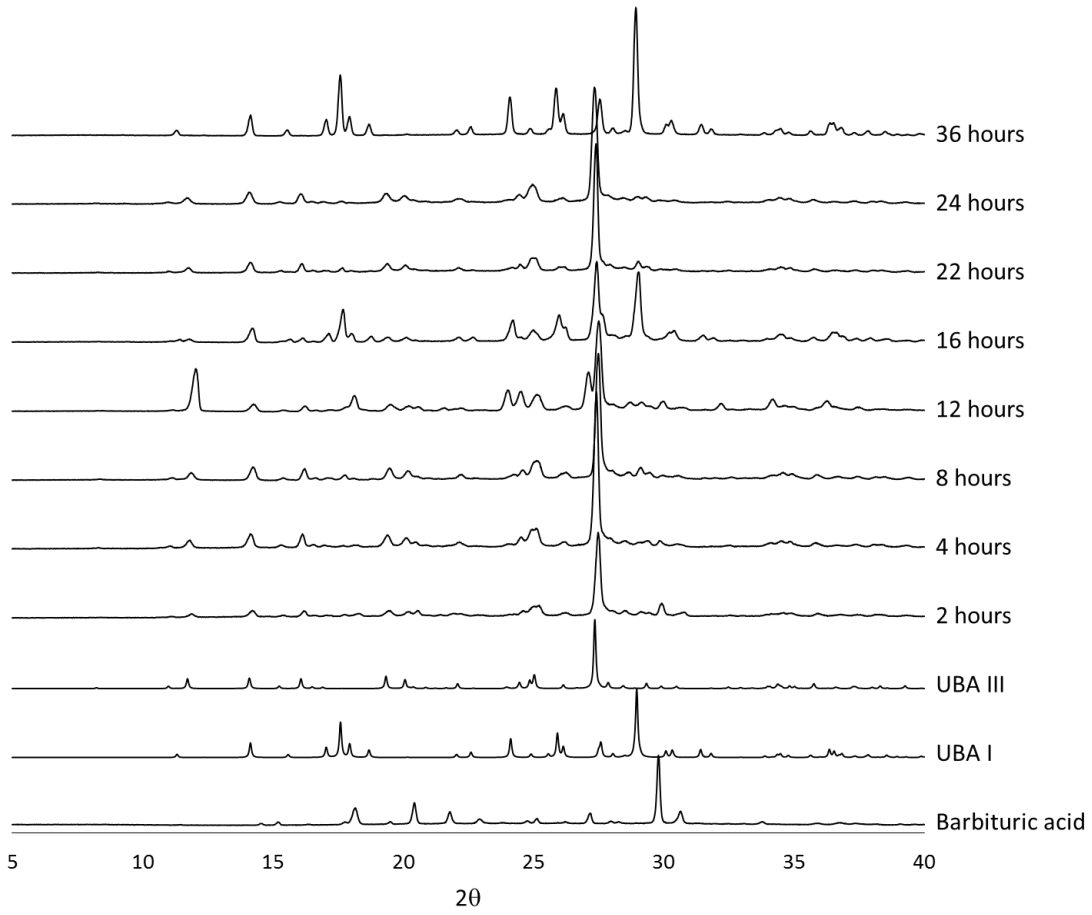

Figure 5.2: PXRD patterns from 1:1 urea: barbituric acid slurry products in ethanol.

These results (Figure 5.2) show that for full conversion of the starting materials to the co-crystal an experimental slurry time of 16 hours is required to ensure that no barbituric acid remains in the product. However, slurry times of greater than 2 hours result in form III to form I conversion in the slurry and as a result, small amounts of UBA form I impurities are obtained. When the slurry time was increased to 36 hours the resultant product was pure form I. This gives further evidence that during the slurrying process co-crystallisation occurs to yield form III, which then undergoes solution-mediated phase transformations to the stable form, form I. The time scale for this

transformation to occur is significantly increased in ethanol in comparison to the methanol mediated slurries discussed earlier. This is very likely due to the significant reduction in solubility of the UBA co-crystal system in ethanol, resulting in a reduction in the rate at which the phase transformations occur in solution.

5.2.1 Scale up of UBA Form III Formation using Slurry Techniques

Small scale slurries using 2 mL of ethanol and a 1:1 ratio of urea: barbituric acid, resulted in UBA form III being accessed with high polymorphic purity when slurry times of 16 – 24 hours were used. Investigations into the scale up of these slurries were carried out. An initial increase from 2 mL to 3 mL was conducted, now using 400 mg of urea and 852 mg of BA. At this scale the slurries were still prepared in 20 mL vials and magnetic bottom stirring at 250 rpm was used. The slurry experiments were executed using the CRD Polar Bear Plus and kept at a constant temperature of 20 °C. The slurries were left stirring for 4 hours before being isolated by vacuum filtration, dried at room temperature and then analysed using PXRD. The PXRD patterns showed that the resultant slurry products were a mixture of UBA form III and barbituric acid starting material (see Appendix Figure 9.7). The presence of barbituric acid at this time scale would be expected as it was seen that at the 2 mL, 200 mg urea scale, slurry times of 16 hours were needed in order to achieve full conversion of starting components to the co-crystal. As crystallisation and solution-mediated phase transitions are kinetically governed, it would therefore be expected that equal or greater slurry times would be needed to achieve full conversion of the starting materials to the co-crystal at this larger scale.

The slurries also had a greater solid loading, having double the amount of solid and only 1.5 times the amount of solvent. This will have an effect on mass transfer as well as the rate of solution-mediated phase transformations in the system, likely reducing the rate of conversion. Subsequent scale up was investigated, using 1 g of urea, 2.13 g barbituric acid and 6 mL of ethanol. The slurries were stirred at 350 rpm and kept at 20 °C for a duration of 5 hours. The resultant slurry product was a mixture of UBA form III, residual barbituric acid and small amounts of UBA form I. This suggested that at this scale full conversion of the starting components to yield UBA was not achieved before UBA form III started to transition to UBA form I. There are a number of ways in which to attempt to increase the conversion of the starting components to the co-crystal, such as increasing the stirring rate to allow for better mass transfer, adding additional solvent to create a less dense suspension and increasing the temperature to increase the rate of conversion. These could, however, all have detrimental effects on the form III to form I conversion, resulting in a reduced selectivity to form III. Longer slurry times of 24 - 48 hours were investigated, with all other experimental parameters remaining constant. The resultant PXRD data (Figure 5.3) showed that at this scale, with a slurry time of 24 hours, UBA form III could be accessed to high polymorphic purity with only a few additional peaks being observed in the PXRD patterns indicating small amounts of UBA form I. Upon further increasing the slurry time to 48 hours, peaks corresponding to

the presence of UBA form I in the slurry product had increased. These results show that UBA form III can still be accessed to relatively high polymorphic purity at a larger scale via the slurrying techniques.

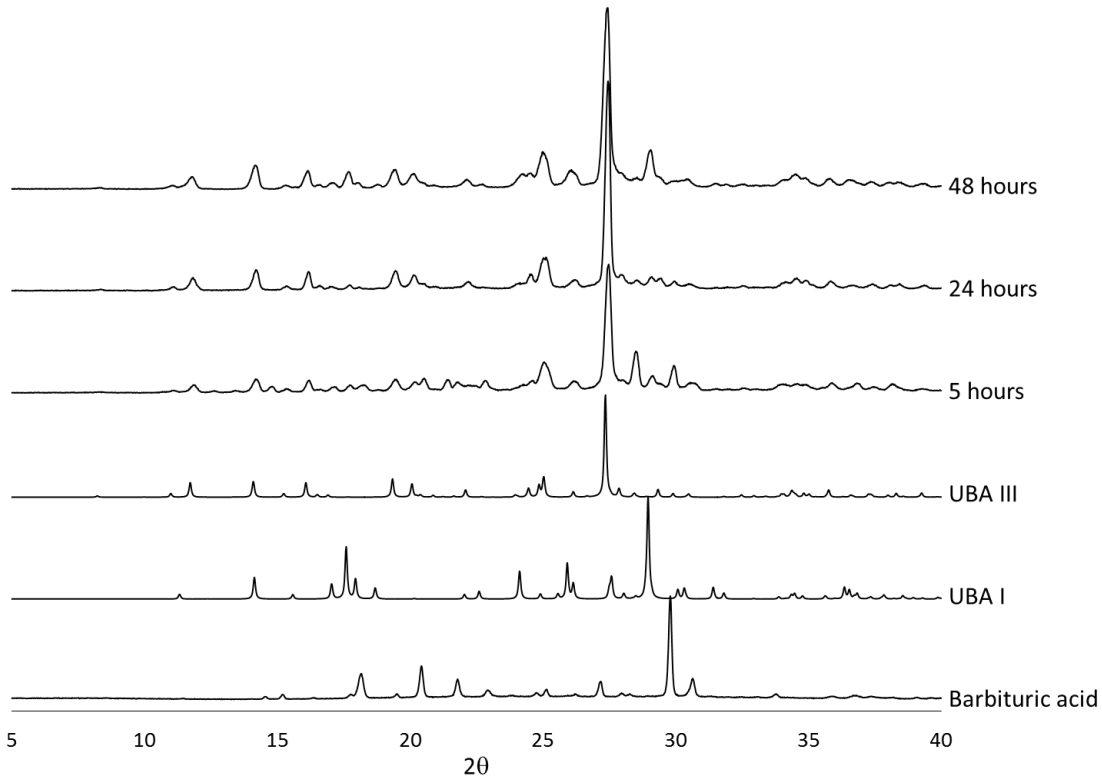

Figure 5.3: PXRD patterns for ethanol mediated 1:1 urea: barbituric acid slurries - 1 g urea, 2.13 g barbituric acid and 6 mL ethanol.

Further scale up of this system to 50 mL was conducted to investigate whether a significant change in scale, solid loading and mixing would have an effect on the selective formation of UBA form III. At this scale, a 100 mL RBF was used with overhead stirring, supplied by an external motor and shaft. Two temperatures (20 °C and 25 °C) were investigated and the stirring was set to 400 rpm. 5 g and 10.65 g of urea and barbituric acid were used respectively at this scale. At 20 °C, when the system was slurried for 24 hours the PXRD pattern of the resultant slurry product showed a mixture of UBA form I and form III had been accessed. When the system was slurried for 24 hours at 25 °C a mixture of form I and form III was again accessed, with little to no difference in the PXRD patterns of the products at the two different temperatures (see Appendix Figure 9.8).

The lack of selectivity at this scale, and the increased levels of UBA form I in the system, may be due to a number of factors. The mixing environment at this scale is significantly different as overhead stirring, not magnetic bottom stirring, is used. This may be resulting in increased mass transfer, allowing for an increased rate of polymorphic conversion within the system. The solid loading of the slurry is also less than in comparison to the smaller scale slurries, which could allow for a faster conversion due to increased mass transfer.

5.2.1.1 Design of Experiments (DoE) Study for 50 mL Ethanol Mediated Slurries

A full factorial Design of Experiments (DoE) study was conducted for the ethanol mediated 1:1 ratio slurry system to probe whether access to UBA form III to high polymorphic purity at this scale could be achieved and whether UBA form I could also be accessed selectively depending on the experimental parameters. Three variables were chosen for this study: temperature, stirring rate and slurry time. The measured responses chosen were the polymorphic outcome and the yield and PXRD was used to identify the resultant solid form(s). Eleven experiments were conducted as part of the full factorial study; their experimental parameters and measured responses are summarised in Table 5.1.

Table 5.1: Summary of experimental parameters and measured responses for the DoE study on the 50 mL ethanol mediated 1:1 ratio (U:BA) slurry.

Exp No	Exp Name	Run Order	Incl/Excl	Temperature (°C)	Stirring rate (rpm)	Time (hours)	Polymorphic form	Quantitative Polymorphic response	Yield (%)
1	N1	10	Included	20	200	24	Form III + BA	4	94.48
2	N2	7	Included	50	200	24	Form III, form I + BA	4	80.18
3	N3	11	Included	20	400	24	Form III, form I + BA	4	93.11
4	N4	2	Included	50	400	24	Form III + BA + trace form I	4	91.05
5	N5	1	Included	20	200	72	Form III + BA	4	75.14
6	N6	9	Included	50	200	72	Form III + BA	4	90.45
7	N7	8	Included	20	400	72	Form III + form I	4	94.90
8	N8	5	Included	50	400	72	Form III + BA	4	90.10
9	N9	6	Included	35	300	48	Form III + BA	4	91.34
10	N10	4	Included	35	300	48	Form III + BA	4	81.72
11	N11	3	Included	35	300	48	Form III + BA	4	87.60

Due to the nature of the DoE software, only quantitative responses can be used and as result the polymorphic outcome, which is qualitative, must be assigned a numerical value. For this DoE study a product of pure UBA form I was assigned the value 1, pure UBA form II was assigned the value 2, pure UBA form III was assigned the value 3 and a mixture of solid forms was assigned the value 4. It can be seen from Table 5.1 that none of the experiments yielded the target response of pure form III (3). In seven of the eleven experiments (N1, N5, N6, N8, N9, N10, N11) a mixture of UBA form III and barbituric acid was produced (Figure 5.4). For these systems the qualitative response was assigned the value 4; although it is not a mixture of UBA polymorphs, it is not a pure UBA outcome. In three of the remaining four experiments (N2, N3, N4) a mixture of form III, barbituric acid and form I was obtained, whilst a mixture of form I and form III was obtained in experiment N7 (Figure 5.4). As all these outcomes were mixtures of solid forms, they were all assigned the numerical outcome of 4 for the polymorphic form response.

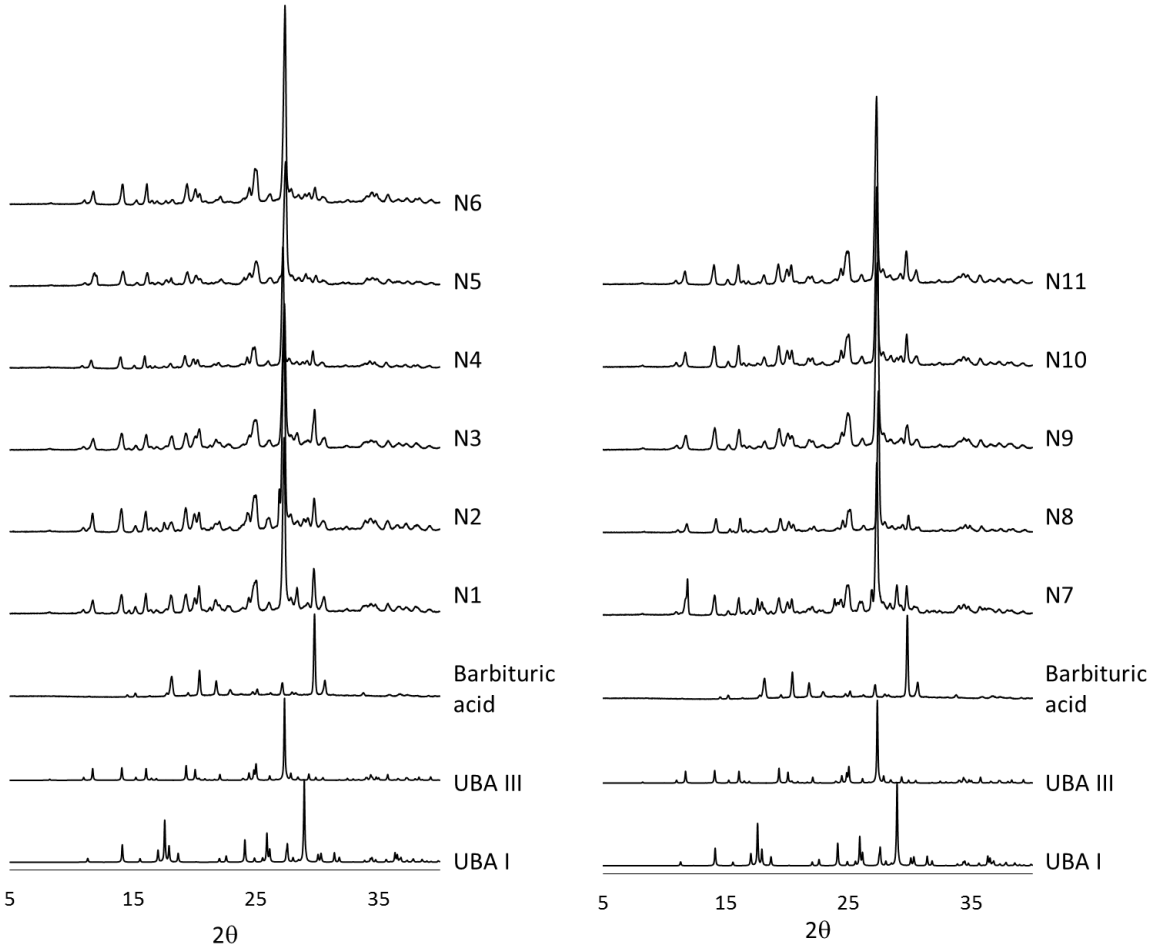

Figure 5.4: PXRD patterns for the 50 mL ethanol mediated slurry DoE products.

In this case, assigning the qualitative responses as numerical values leads to significant issues. The MODDE 11 software works on the premise that the measured responses are all related to one another on a numerical scale and in this case the qualitative results cannot be related by this same scale; Figure 5.5 helps illustrate this point.

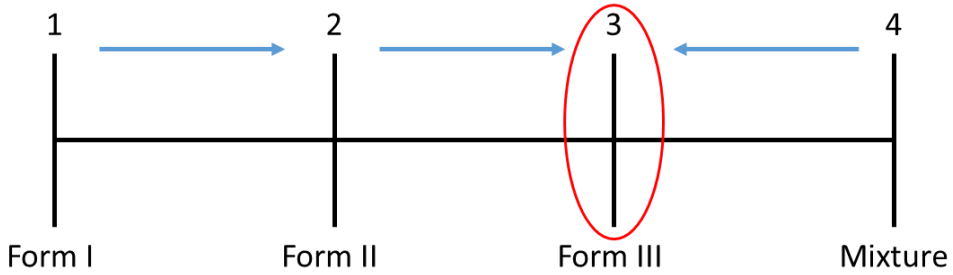

Figure 5.5: Quantitative scale used for the polymorphic response in the MODDE DoE software.

The software assumes that if a certain set of parameters give rise to the pure formation of UBA form II (2) and another set of conditions lead to a mixture of solid forms (4) then the conditions in the middle of these two will likely lead to the formation of UBA form III (3); it assumes that the closer in numerical value we get to the target value, the more likely we are to access the target response. However, this is not how this system works

in reality. A value of 2 (form II) does not necessarily mean that the outcome is closer to the desired target of 3 (form III) than a value of 1 (form I).

The system then meets additional issues as the value 4 is assigned to a variety of different outcomes. This results in a lack of differentiation between the measured outcomes when a mixture of solid forms has been obtained from the experiment. If different numerical values were assigned to each type of mixture, however, the numerical scale would become even more inaccurate. For example, if a mixture of form III and barbituric acid was assigned the value 4 and a mixture of form I and form III was assigned the value 5, the software would assume that the barbituric acid and form III product (4) is closer to the desired outcome than a mixture of form I and form III, however this is not the case. This would only be complicated further if a separate value was also assigned to a mixture of form I, form III and barbituric acid.

As each experiment was assigned the value 4 for the polymorphic outcome response, the MODDE 11 software cannot created a model for the system with respect to this response. It can, however, still use the measured responses for yield to create a model in an attempt to determine if, and how, the various factors influence the resultant yield. The summary of fit plot for the yield response can be seen below in Figure 5.6. This plot displays the R^2, Q^2, model validity and reproducibility for the yield response. The R^2 value represents the goodness of fit; it represents the variation in measured responses to the predicted model responses. An R^2 value of 1 would represent a perfect model, where all the measured responses fit perfectly. For the model to be deemed informative, the value of R^2 must be greater than 0.5. It can be seen that the R^2 value for the yield response in this DoE study is 0.55, showing that this model is informative. If the R^2 value is above 0.75, the model is considered 'good'. As the R^2 value obtained from this study for the yield response is below 0.75 but greater than 0.5, it demonstrates that the model is informative, but not stable.

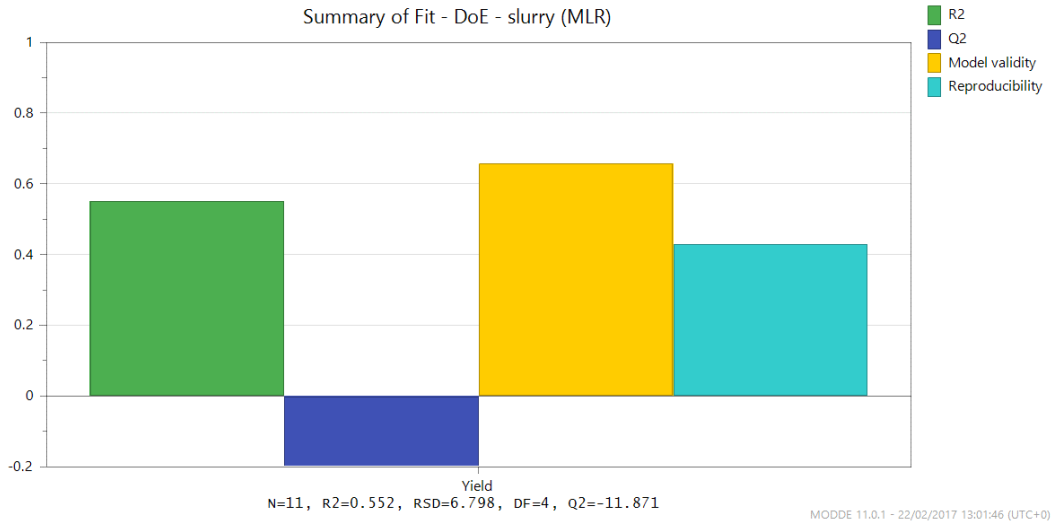

Figure 5.6: Summary of fit plot for the yield response for the slurry DoE study.

The Q^2 factor is a representation of the goodness of future prediction and indicates how well the proposed model can predict what will happen in future experiments. It can be seen that for this model, the value of Q^2 is negative (-0.2), indicating that this model has no capacity to predict accurately any future outcomes for the percentage yield for this slurry system. It should be taken into account, however, that there is a large error associated with the measured yield due to the potential for product loss during the vacuum filtration step used to isolate the slurry products.

For a model to be valid the value for model validity must be greater than 0.25. It can be seen that the value for the yield response is 0.66, suggesting that the model is a relatively good fit to the process. The reproducibility value for this system is determined to be 0.43. The highest value that this factor can take is 1, achieved when the system is 100 % reproducible. This factor is determined by the three control experiments that were conducted as part of the study (N9, N10 and N11). The value obtained is relatively low, but it can be understood by looking at the yield values for these three control experiments. For all three of these experiments the experimental parameters were kept the same, however there is a variation in percentage yield of approximately 10 %. It is this variation that leads to the reproducibility value being low. The design space in Figure 5.7 shows the probability of failure of accessing the target yield (99 %). The green areas show parameters that are likely to result in the desired percentage yield; the probability of failure in these areas is less than 1 %. However, it is important to note that although the yield can be measured, the contribution of each solid form to the total mass is not accessible and so a higher yield is not necessarily a better outcome as this may incorporate a higher percentage of an undesired solid form.

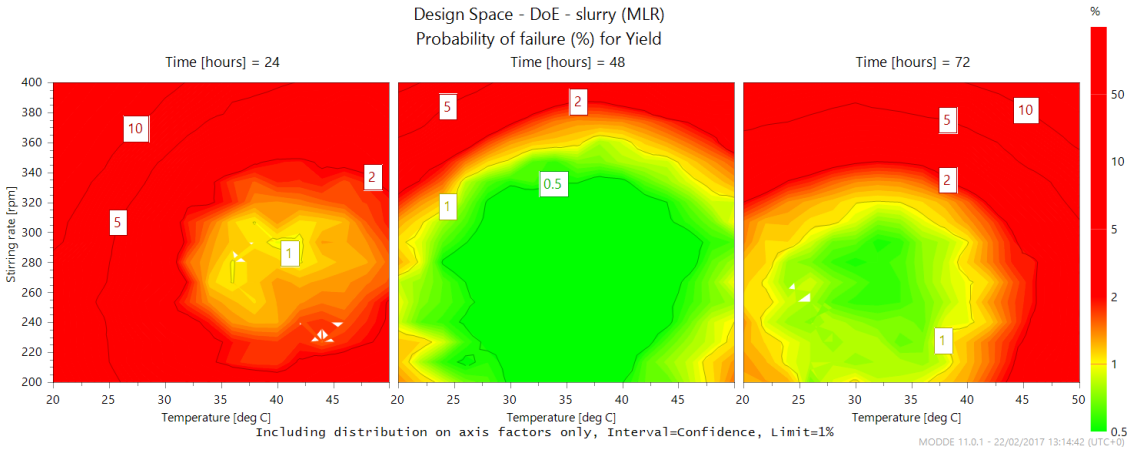

Figure 5.7: Design space for the percentage yield outcome for the slurry DoE.

For this system, the DoE approach is inadequate in determining any optimisation parameters for the polymorphic outcome. It is also inadequate at analysing the yield dependence on the experimental parameters as we cannot be sure of the percentage contributions that each solid form makes to the total mass/yield. The formation of pure UBA form III using this slurry system requires further optimisation. Optimisation at a smaller scale (the 2 mL slurries) may be more beneficial in this case, however, as they

demonstrate less variation in the solid form outcome at timescales of 22 hours and above.

5.3 Unseeded Batch Cooling Crystallisation of UBA Form III from Ethanol

Due to ethanol showing an enhanced selectivity towards the metastable form III in the slurrying experiments, this solvent system was taken forward into both seeded and unseeded batch cooling crystallisation techniques.

5.3.1 Small Scale (10 mL) Unseeded Batch Cooling Crystallisations

For the initial transfer of UBA crystallisation from ethanol from slurrying to cooling crystallisation techniques, 10 mL crystallisations were conducted. These crystallisation experiments were carried out using the CRD Polar Bear Plus with magnetic bottom stirring. The concentration used for these crystallisations was determined from the measured solubility data; 7.858 mg/g of UBA in ethanol was used (corresponding to an approximate saturation temperature of 50 °C). The starting materials were added to the solvent in 20 mL flat bottom vessels and screw cap lids were secured in place. Magnetic bottom stirring was used at a rate of 400 rpm. The systems were heated to 65 °C and left for approximately 60 minutes to allow for full dissolution of the starting material. They were then cooled down to 5 °C at a rate of 0.5 °C min^{-1}. Once the final temperature had been reached the systems were left to dwell for 5 minutes before being filtered using vacuum filtration and left to dry at room temperature. All systems were then analysed using PXRD in order to determine the solid form of the product.

Both 1:1 and 2:1 ratios of urea: barbituric acid were investigated at this scale. For the 1:1 ratio crystallisations the weights of each individual components were calculated from the desired UBA concentration. When a 2:1 ratio was used, the mass of urea was doubled. Previous cooling crystallisations utilising methanol as the solvent system, conducted by Wittering, utilised a 2:1 ratio of urea: barbituric acid in order to access the co-crystal system due to the significantly higher solubility of urea in comparison to barbituric acid in methanol. As urea maintains a much higher solubility in comparison to barbituric acid in ethanol both ratios were investigated.

The PXRD patterns obtained for the crystallisation products (Figure 5.8) show that when a 2:1 ratio of urea: barbituric acid was used in the cooling process at this scale, the resultant product was either pure UBA form I or a mixture of UBA form I and form III; it was not selective to the desired metastable form, form III. Interestingly, when a 2:1 ratio was used in the slurrying techniques a novel polymorphic form of UBA was accessed (Section 4.3), however this was not found to be the case upon transfer into cooling crystallisation. When a 1:1 ratio was used, however, the PXRD patterns show that the desired form III was accessed either pure or to very high polymorphic purity, with only a few, very small, additional peaks appearing that correspond to UBA form I (highlighted peaks in Figure 5.8 (b)).

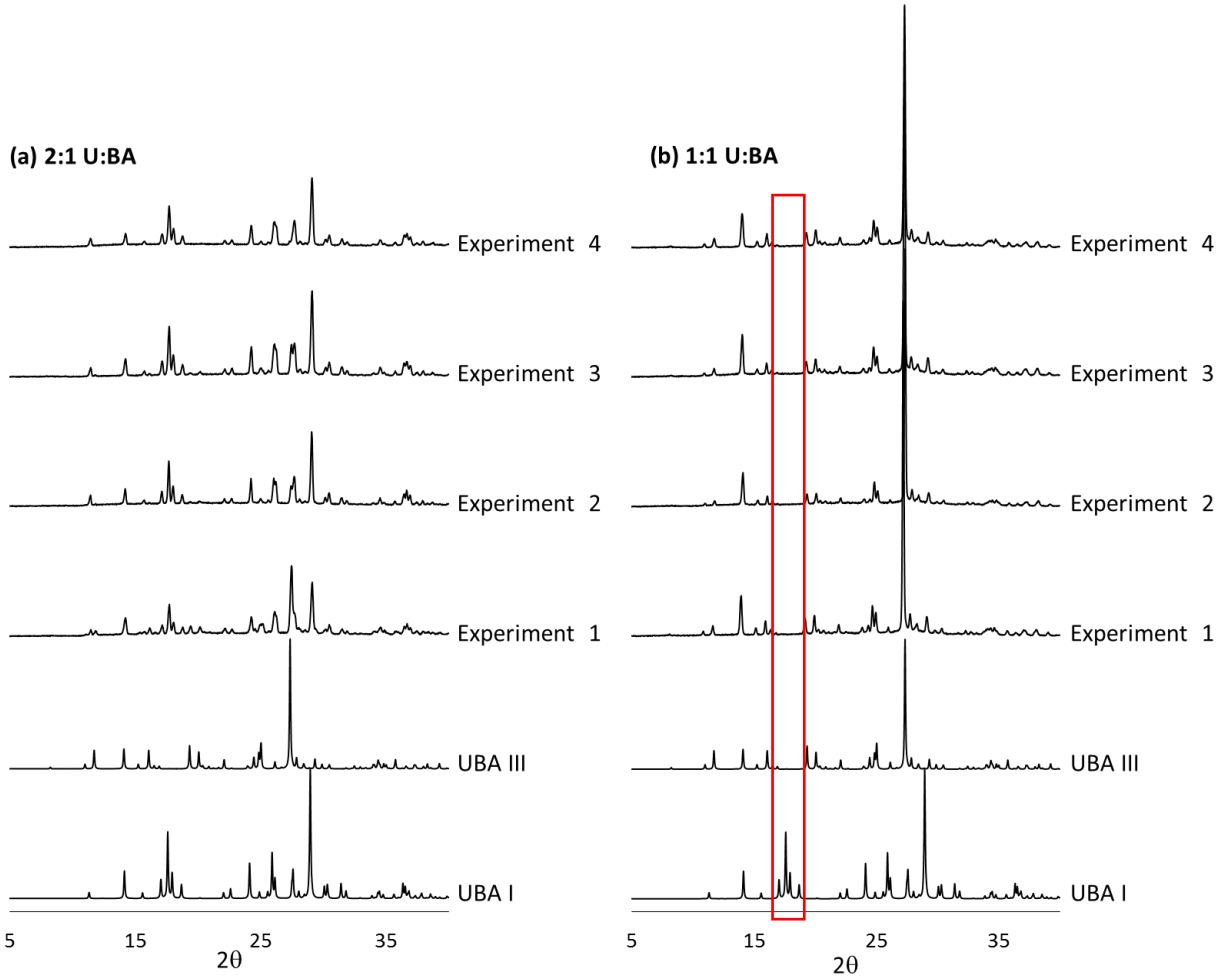

Figure 5.8: PXRD patterns of products from the 10 mL cooling crystallisations from ethanol with (a) 2:1 and (b) 1:1 ratios of urea: barbituric acid. Red box highlights peaks corresponding to UBA form I.

5.3.2 50 mL Unseeded Batch Cooling Crystallisations

Due to the success of accessing UBA form III selectively at the 10 mL scale using unseeded cooling crystallisation from ethanol, investigations into the scale up of this system were conducted. The system was scaled up from 10 mL to 50 mL. Due to this increase in solvent volume a 100 mL RBF had to be used for the process, replacing the smaller flat bottom vials. Overhead stirring was then implemented into the system via the use of an external motor and shaft. This change in crystallisation environment, as well as the increase in scale would likely have a significant impact on the overall crystallisation procedure and may have an effect on the resultant polymorphic outcome. Because of this, both the 2:1 and 1:1 urea: barbituric acid ratios were investigated at this scale.

For these crystallisations the same saturation (T_{sat} = 50 °C, 7.858 mg/g) was used along with the same temperature profile (70 °C to 5 °C at a rate of 0.5 °C min^{-1}). Once the systems had cooled to the final temperature they were left to dwell for 30 minutes. Overhead stirring, set at 400 rpm, was used throughout the duration of the experiments.

At this scale, under these conditions, regardless of the ratio of the starting components in the crystallisation process, pure UBA form III was accessed selectively as shown by PXRD analysis (Figure 5.9).

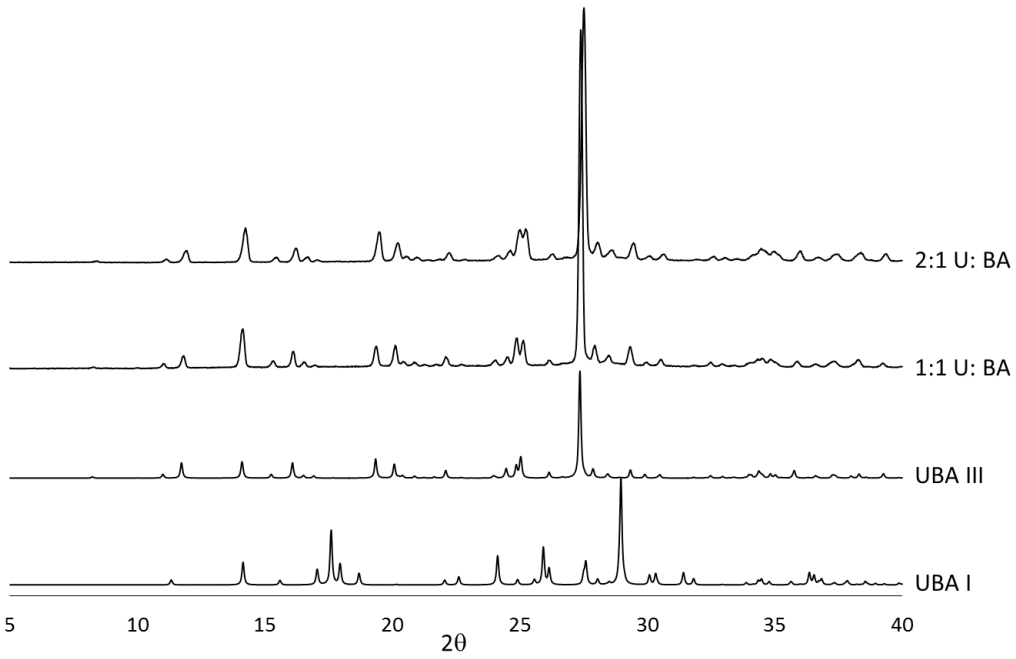

Figure 5.9: PXRD patterns of products from 50 mL cooling crystallisation from ethanol..

5.3.2.1 Design of Experiments (DoE) Study on 50 mL Unseeded Cooling Crystallisation

Previous work scaling up the unseeded cooing crystallisation of pure UBA form III from ethanol, from 10 mL to the 50 mL scale, suggested that UBA form III could be accessed selectively regardless of the ratio of the starting components used in the crystallisation process. A DoE study on the crystallisation of UBA from ethanol at the 50 mL scale was conducted in order to investigate how some of the experimental factors would affect the crystallisation in terms of solid form and yield. A full factorial DoE study was conducted investigating four variables: stirring rate, cooling rate, dwell time at the final temperature and the ratio of urea: barbituric acid used. As with the previous DoE study (section 5.2.1.1) the polymorphic response was qualitative and the outcomes needed to be assigned to a numerical value. A response of pure form I was assigned the value 1, pure form II the value 2, pure form III the value 3 and any mixture of solid forms was assigned the value 4. The yield was reported in terms of percentage yield, calculated from the mass put in and the mass out of the crystallisation. For this study nineteen experiments were run, including the three control experiments. A summary of the experimental parameters and measured responses can be seen in Table 5.2.

Table 5.2: Summary of experimental parameters and measured responses for the DoE study on cooling crystallisation of UBA from ethanol (50 mL).

Exp No	Exp Name	Run Order	Incl/Excl	Cooling rate (°C/min)	Dwell time (min)	Stirring rate (rpm)	SM ratio (stoichiometric)	Polymorphic form	Quantitative polymorphic response	Yield
1	N1	11	Included	0.5	10	200	1:1	Form III + Form I	4	45.48%
2	N2	9	Included	1	10	200	1:1	**Form III**	3	44.11%
3	N3	12	Included	0.5	60	200	1:1	**Form III**	3	58.72%
4	N4	13	Included	1	60	200	1:1	Form III + Form I	4	59.03%
5	N5	17	Included	0.5	10	400	1:1	**Form III**	3	48.26%
6	N6	3	Included	1	10	400	1:1	**Form III**	3	50.48%
7	N7	19	Included	0.5	60	400	1:1	**Form III**	3	46.84%
8	N8	10	Included	1	60	400	1:1	**Form III**	3	8.29%
9	N9	4	Included	0.5	10	200	2:1	Form III & trace form I	4	79.65%
10	N10	14	Included	1	10	200	2:1	Form III + Form I	4	66.97%
11	N11	15	Included	0.5	60	200	2:1	**Form III**	3	64.94%
12	N12	7	Included	1	60	200	2:1	Form III & trace form I	4	70.26%
13	N13	2	Included	0.5	10	400	2:1	Form III & form I	4	16.16%
14	N14	16	Included	1	10	400	2:1	Form III & trace form I	4	60.16%
15	N15	1	Included	0.5	60	400	2:1	**Form III**	3	31.30%
16	N16	8	Included	1	60	400	2:1	**Form III**	3	72.35%
17	N17	18	Included	0.75	35	300	1:1	Form III & trace form I	4	49.39%
18	N18	5	Included	0.75	35	300	1:1	**Form III**	3	17.13%
19	N19	6	Included	0.75	35	300	1:1	**Form III**	3	13.06%

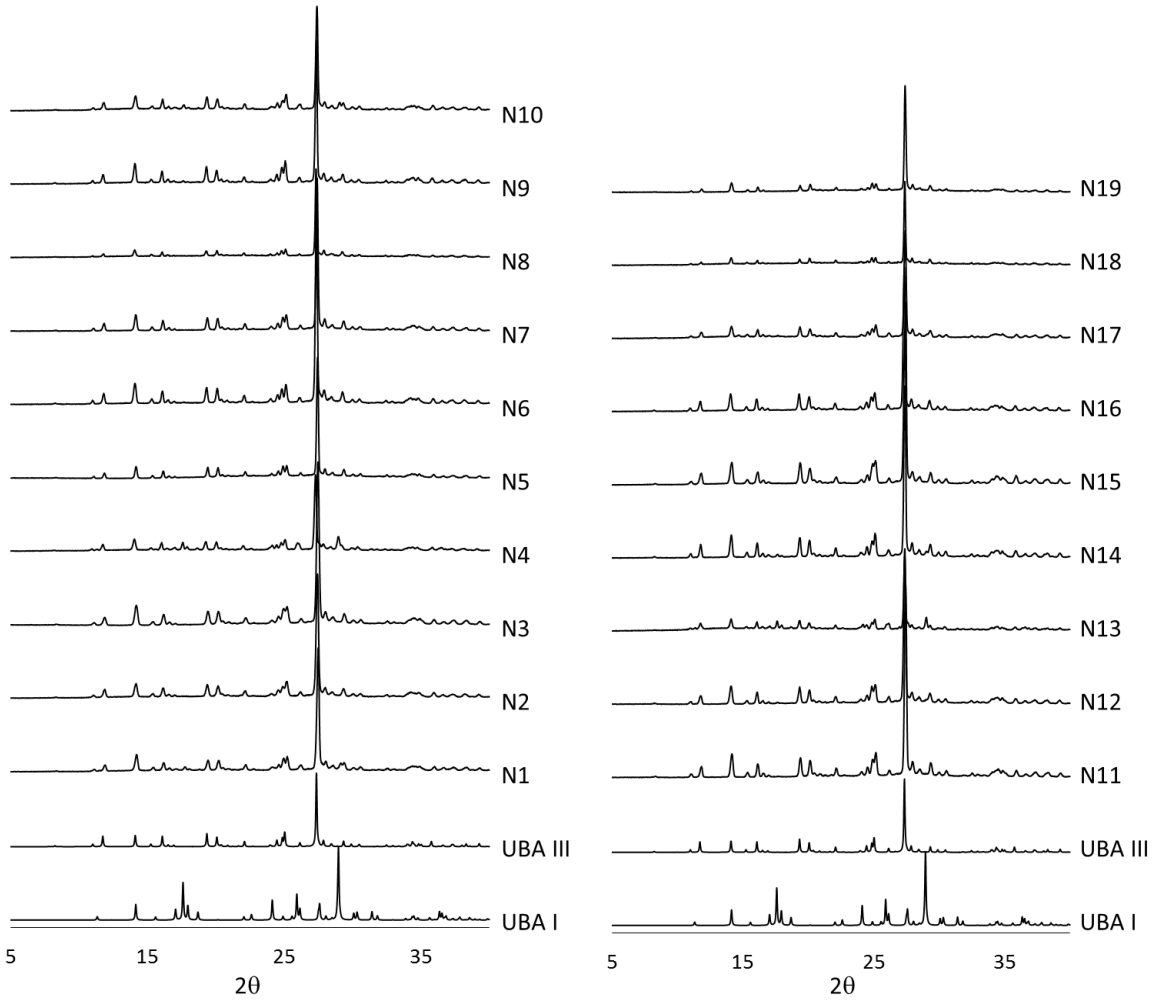

Figure 5.10: PXRD patterns of products from the 50 mL cooling crystallisation from ethanol DoE study.

It can be seen that eleven of the nineteen experiments gave rise to UBA form III selectively, with no other solid phase impurities. The other eight experiments resulted in UBA form III with small amounts of UBA form I impurities present, as seen by the PXRD data (Figure 5.10). The measured responses for both the polymorphic outcome and the percentage yield were input into the MODDE 11 software to allow for a model of the system to be created in order to determine if, and how, the variables influence these responses. The summary of fit plot for the polymorphic outcome response can be seen in Figure 5.11 below and displays the R^2 and Q^2 factors, the model validity and the reproducibility for this response. The R^2 factor represents the goodness of fit; for the polymorphic response it can be seen that the R^2 factor is 0.67 (67 %). This value is relatively low, but it can be attributed to the nature of this response. As discussed previously with the slurry DoE study, the polymorphic responses were assigned numerical values in order for the DoE to be conducted. However, this results in the measured responses being placed on a numerical scale that does not fit with the inherent qualitative nature of this measured response. For this DoE the only outcomes were pure form III (3) and a mixture of form I and form III (4). This resulted in the measured responses only ever being one of two values, with no quantitative variation depending on the amount of form I present in the product. This lack of variation in measured responses is likely the reason behind the low R^2 value.

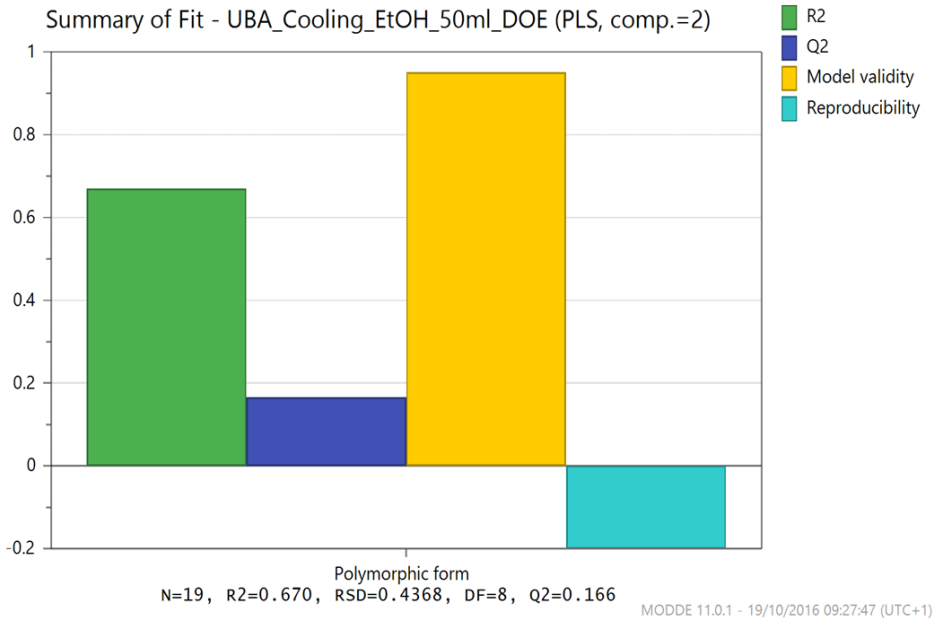

Figure 5.11: Summary of fit plot for the polymorphic outcome response for the cooling crystallisation DoE study.

The Q^2 factor gives information about the goodness of prediction of the model and; for the polymorphic outcome response it can be seen that the Q^2 value is 0.17 (1.7 %), showing that future prediction of polymorphic outcome using this model is very poor. Interestingly, the model validity for the polymorphic response for this system is 0.95 (95 %). For a model to be considered 'valid' this value must be greater than 0.25. The value for the polymorphic response is significantly higher than this, and very close to the

maximum value of 1. This high value may initially seem to contradict the low values seen for goodness of prediction (Q^2), however the low value of Q^2 is likely a direct result of the poor level of reproducibility of the system. As can be seen in Figure 5.11, the reproducibility for the polymorphic response is negative. This value is determined by the variation of the measured response under the same conditions (the pure error) compared to the total variation of the response. If the reproducibility is below 0.5 (50 %) it indicates a large pure error and poor control over the experimental procedure.

The poor reproducibility can be understood by referring to Table 5.2. As can be seen, N17, N18 and N19 are the three control experiments, each with identical experimental parameters. However, in one of the three experiments (N17) a mixture of UBA form I and form III was accessed, whilst the other two gave pure UBA form III. This lack of consistency in the solid form result explains why the reproducibility for the polymorphic response was so low, and indicates that full control over the crystallisation process has not yet been achieved in terms of polymorphic selectivity. This low value for reproducibility will have an effect on the Q^2 response, resulting in poor response prediction as was previously discussed.

The lack of consistency in the polymorphic outcome in the three control experiments can be attributed to the unseeded system and the stochastic nature of spontaneous nucleation. Primary nucleation is inherently difficult to control, especially in polymorphic systems. Although the likelihood of initial nucleation of the metastable form is higher than that of the more stable form, it may not always be the case and in some experiments the thermodynamically stable form may also nucleate.

The coefficient plot for the polymorphic form response can be seen in Figure 5.12. This plot displays if, and how, each factor affects the measured responses. The size of the coefficient bar represents how much a variation in the experimental factor will affect the measured response. The value for the coefficient factors vary between values of 1 and -1, with a positive value usually indicating that an increase in that factor will result in an increase in the response. A negative value for the coefficient will indicate that the opposite is true; an increase in the factor will result in a decrease in the measured response. However, for the polymorphic outcome, the presence of pure form III was assigned the value 3, with a mixture of form I and form III being assigned the value 4. Therefore, a negative effect on polymorphic form actually corresponds with an increased tendency to for the production of form III with no form I present. It is important to note, however, that each coefficient has an error bar associated with it and for the polymorphic response outcome all of these error bars cross zero. If an error bar crosses zero, the effect of the associated factor on the response is said to be insignificant. As this is the case for each of the experimental factors and the interaction of factors, it is not possible at this stage to deduce if any of the factors play a specific role in the polymorphic outcome. This result highlights the difficulty in the selective production of UBA form III for this system. Crystallisation is an inherently difficult process to control due to the stochastic nature of nucleation; it is a kinetically driven

process and is therefore unpredictable in nature. In this case, the difficulty in control over the polymorphic outcome is not only due to the nature of the process, but is also enhanced by the closeness in energies of the two solid forms (I and III).

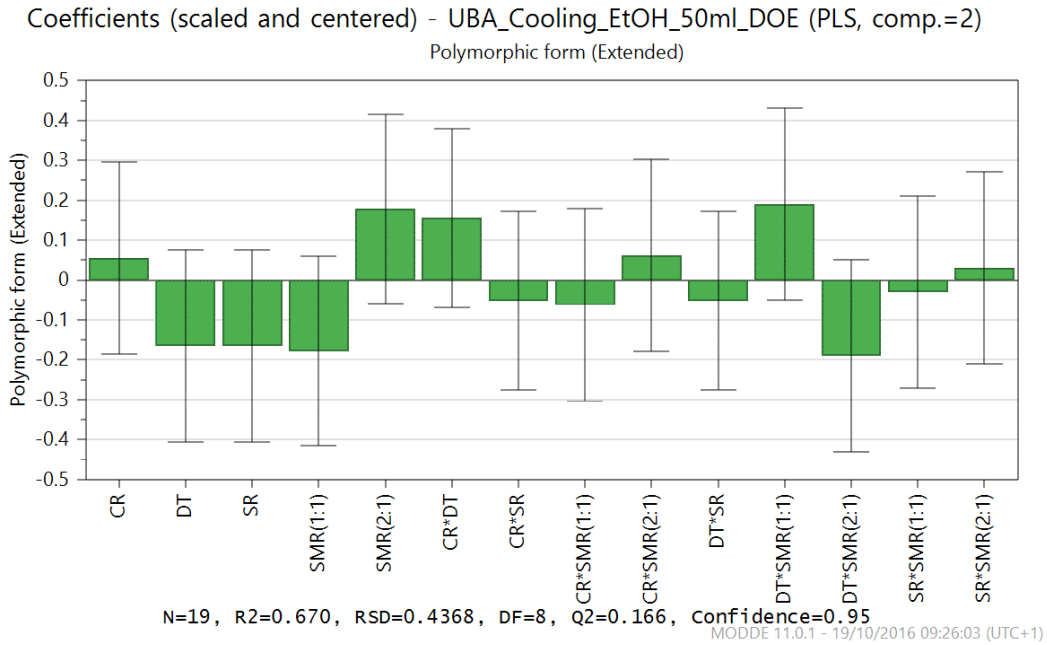

Figure 5.12: Coefficient plot for the polymorphic outcome response of the cooling crystallisation DoE study.

The design space for the cooling crystallisation of the UBA form III from ethanol can be seen in Figure 5.13. The design space shows the probability of failure for the polymorphic outcome; any form present in the product that is not UBA form III. The green areas depict regions where the likelihood of not obtaining pure UBA form III is very low (less than 1 %). The red depicts regions where the percentage failure is greater than 2 %. The design space suggests that in order to crystallise pure form III, a stirring rate of 200 rpm should not be used, with higher stirring rates such as 300 - 400 rpm being required. Similarly, a 1:1 ratio of urea: barbituric acid gives a much larger design space where pure form III should, in theory, be accessible as long as the other parameters are chosen carefully. For experiments using a 1:1 ratio of starting components, with a stirring rate of 300 - 400 rpm, the dwell time at the final temperature seems to have little effect on the resultant solid form. However, intermediate cooling rates may be preferred. In using these conclusions to guide subsequent experimental design, it is important to bear in mind the Q^2 factor and the reproducibility values previously discussed, as these suggested that the model lacks reproducibility and it is therefore difficult to be confident that using the parameters suggested by the design space will yield pure form III.

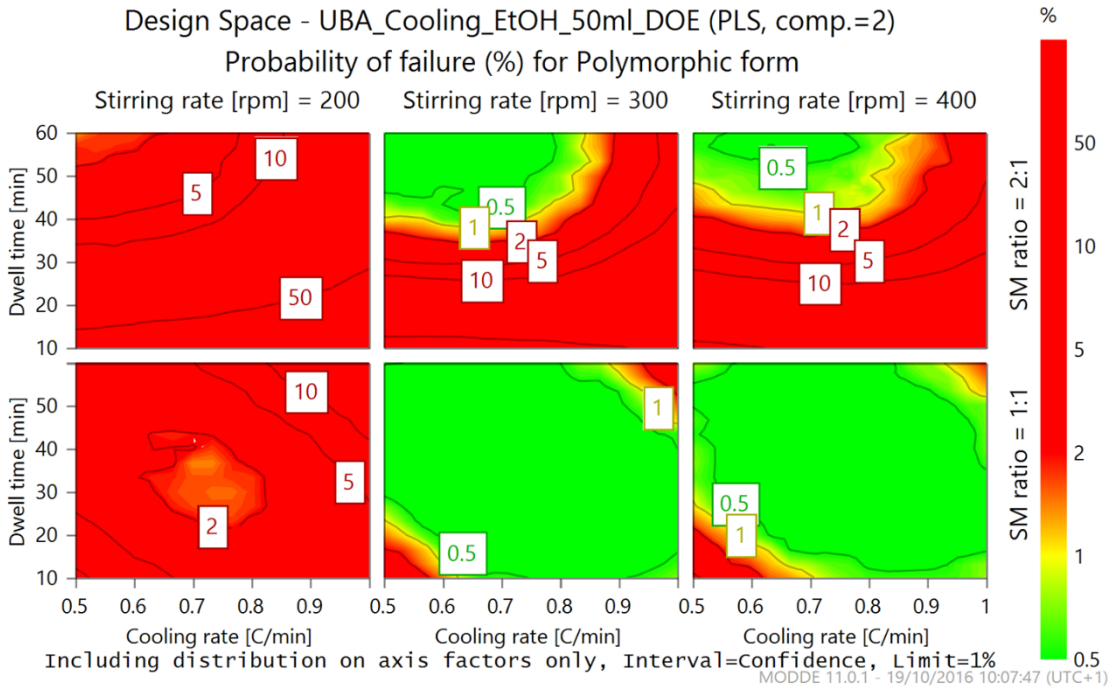

Figure 5.13: Design space for the polymorphic outcome of the cooling crystallisation obtained from the DoE study.

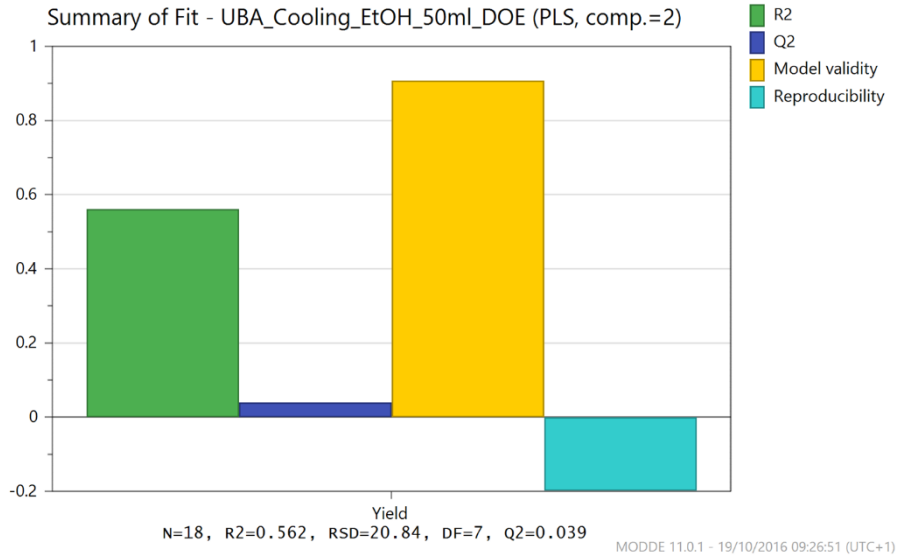

Figure 5.14: Summary of fit plot for the yield response of the cooling crystallisation DoE study.

The percentage yield for the cooling crystallisations was also measured as a response for the DoE study, and a model produced. The summary of fit plot for this response can be seen in Figure 5.14. The R^2 factor is 0.56 (56 %), indicating that the goodness of fit of the measured response to the model is not a good fit, but may still possess some indicative value. The Q^2 value is very low for the yield, at 0.04 (4 %). This indicates that the prediction of the yield outcome for subsequent experiments will be very poor. As

with the polymorphic outcome, the low value for Q^2 cannot result from poor model validity, as the model validity in this case is 0.9. It must therefore arise from the poor reproducibility, which is negative (-0.2). It can be seen in Table 5.2 that for the three control experiments (N17, N18 and N19) the yields are significantly different to one another, even though the same experimental parameters were used. The poor reproducibility here may arise from each system undergoing nucleation at a different point in the crystallisation, resulting in more or less time for the system to crystallise. It may also be a result of the large errors associated with the vacuum filtration method used for the isolation of the solid products.

Each factor and combination of factors in the coefficient plot for the yield response (Figure 5.15) has error bars passing through zero, as was seen with the polymorphic response outcome. As each error bar crosses zero it can be concluded that the effect that each factor has on the resultant yield is insignificant.

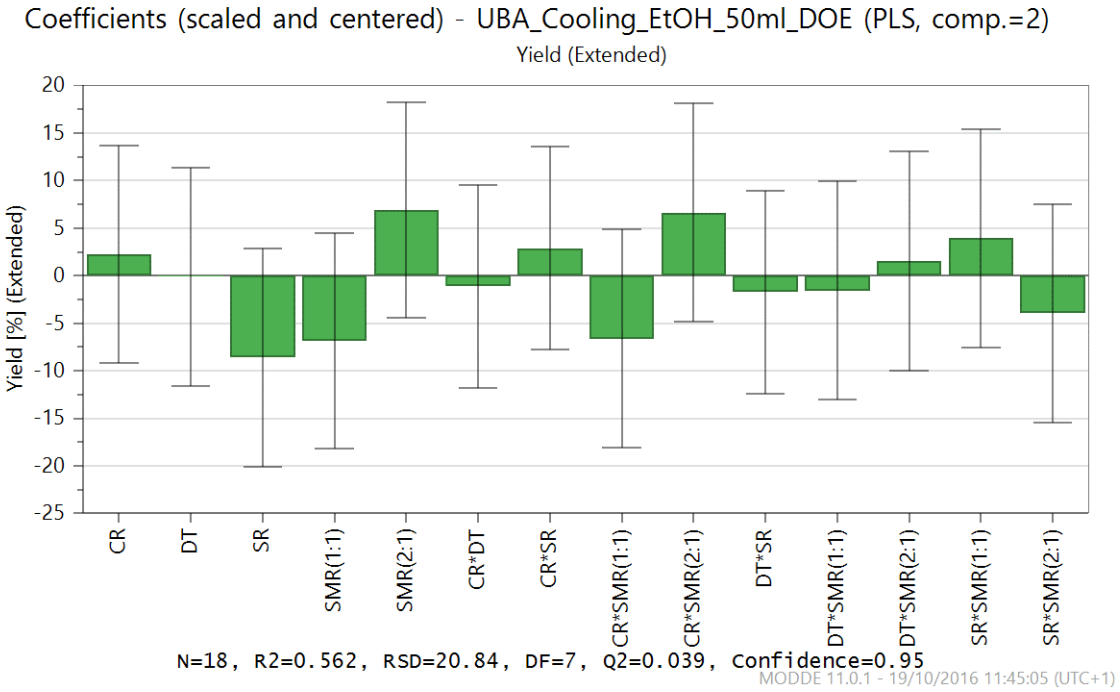

Figure 5.15: Coefficient plot for the percentage yield of the cooing crystallisation from the DoE study.

The design space for the yield can be seen in Figure 5.16. This is a landscape displaying the probability of failure of achieving the targeted response. For the yield, the target response was chosen as 50 %. It can be seen that to achieve a yield of 50 % or greater there is a relatively large design space to work within, especially when intermediate stirring rates of 300 rpm are used. A starting material ratio of 1:1 unsurprisingly gives a larger design space for a higher yield than a ratio of 2:1, due to the smaller starting material masses in the crystallisation ratio.

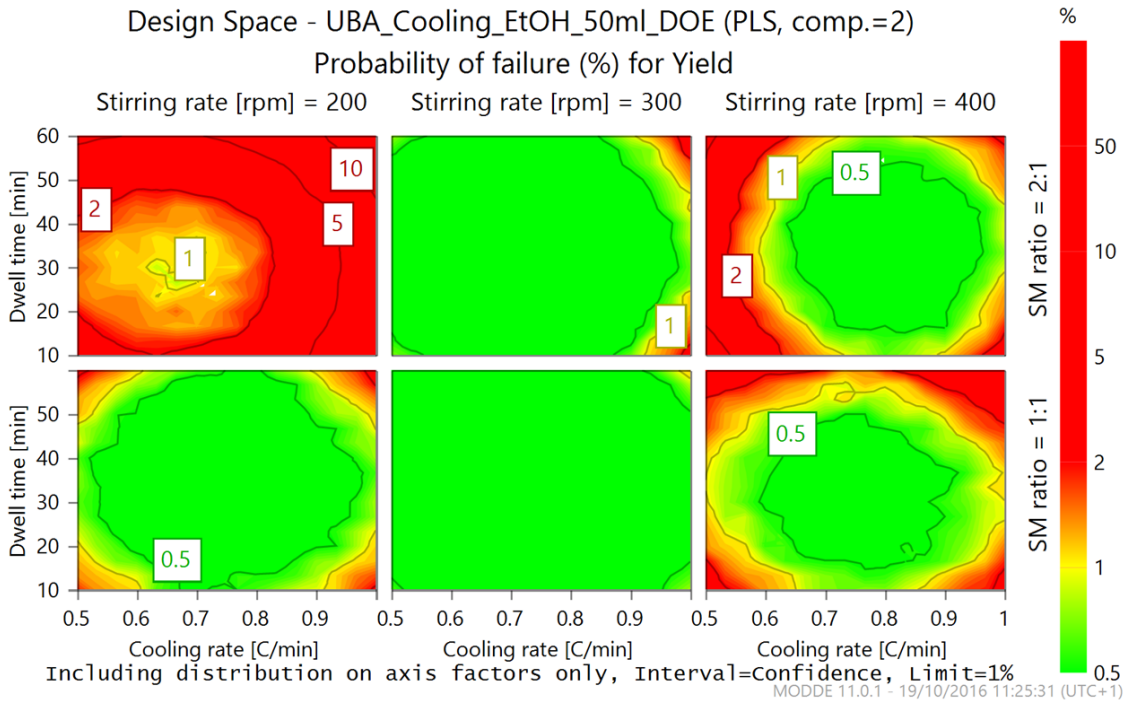

Figure 5.16: Design space for the percentage yield from the cooling crystallisation DoE study.

Overall, this DoE study has allowed for exploration of the cooling crystallisation of UBA from ethanol at the 50 mL scale. The resultant design spaces for both polymorphic form and yield obtained from the study allow for parameters to be chosen for subsequent experiments that have the highest chance of producing pure UBA form III, the desired solid form. However, the poor predictability (Q^2) and reproducibility values obtained from the models highlights the difficulty in the selective formation of UBA form III, giving evidence that a method such as seeding may be required to enable the reproducible crystallisation of pure UBA form III.

5.3.2.2 Subsequent 50 mL Cooling Crystallisations

Further 50 mL cooling crystallisations of UBA from ethanol were conducted using parameters chosen from the polymorphic outcome design space in order to determine the optimal parameters for the system. The parameters were chosen so that they corresponded to points within the design space that had a percentage failure for the resultant solid form of less than 1 % for cool 1 and cool 2 and less than 0.5 % for cool 3. The experiments, unsurprisingly given the low Q^2 and reproducibility values, had varied success in accessing UBA form III selectively. Table 5.3 summaries the experimental parameters used in these subsequent studies.

Two of the three experiments (cool 1 and cool 3) yielded UBA form III selectively, with no other solid forms present. Cool 2, however, a direct repeat of cool 1, resulted in trace amounts of UBA form I being present in the product (see Appendix Figure 9.9). The experimental parameters for cool 1 and cool 2 were identical and this difference in outcome further supports the lack of reproducibility observed in the DoE study. These

parameters however, may give an appropriate starting point for subsequent seeded crystallisations.

Table 5.3: Experimental parameters for subsequent 50 mL cooling crystallisations of UBA from ethanol.

Parameters	Cool 1	Cool 2	Cool 3
Urea: barbituric acid ratio	1:1	1:1	1:1
Cooling rate ($°Cmin^{-1}$)	1	1	0.75
Stirring rate (rpm)	400	400	300
Dwell time at final temperature (min)	30	30	30

5.3.3 150 mL Unseeded Batch Cooling Crystallisations

Due to the relative success with accessing pure UBA form III from ethanol at the 50 mL scale, the system was further scaled up to 150 mL. For these crystallisations a 250 mL RBF was used with overhead stirring. The CRD Polar Bear Plus was used for temperature control. At this scale, UBA form III could be accessed selectively, however, the issues with reproducibility observed at the 50 mL scale still remained, with a large proportion of experiments yielding UBA form I impurities alongside form III (see Appendix Figure 9.10).

5.3.3.1 Metastable Zone Width Measurement of UBA Cooling Crystallisation from Ethanol

In order to understand the cooling crystallisation of UBA from ethanol further, attempts were made to measure the metastable zone width (MSZW) of UBA in ethanol. For this, the 150 mL scale cooling crystallisation set up was used. The determination of the MSZW for this system would allow for not only an increased understanding of the system, but also for efficient design of subsequent seeded cooling crystallisations. In order to determine the MSZW, solutions of different UBA saturations were produced, heated to 10 °C above the saturation temperature to ensure full solvation and then cooled at a rate of 1 °C min^{-1}. A GoPro $Hero3^{+}$ was used to film the crystallisation experiments and record when nucleation happened within the system; the films were watched back and the nucleation/cloud point determined. Three repeat experiments at each saturation were conducted which allowed for the calculation of error bars for the cloud points (Figure 5.17).

The error bars on the MSZW plot are three standard deviations as calculated by the measured cloud points. It can be seen that although the error bars are quite significant, an approximate MSZW was determined for the system. The MSZW of this system is approximately 25 °C when compared with the observed solubility of UBA in ethanol. These solubility data and MSZW were used to design subsequent seeded crystallisations of UBA from ethanol.

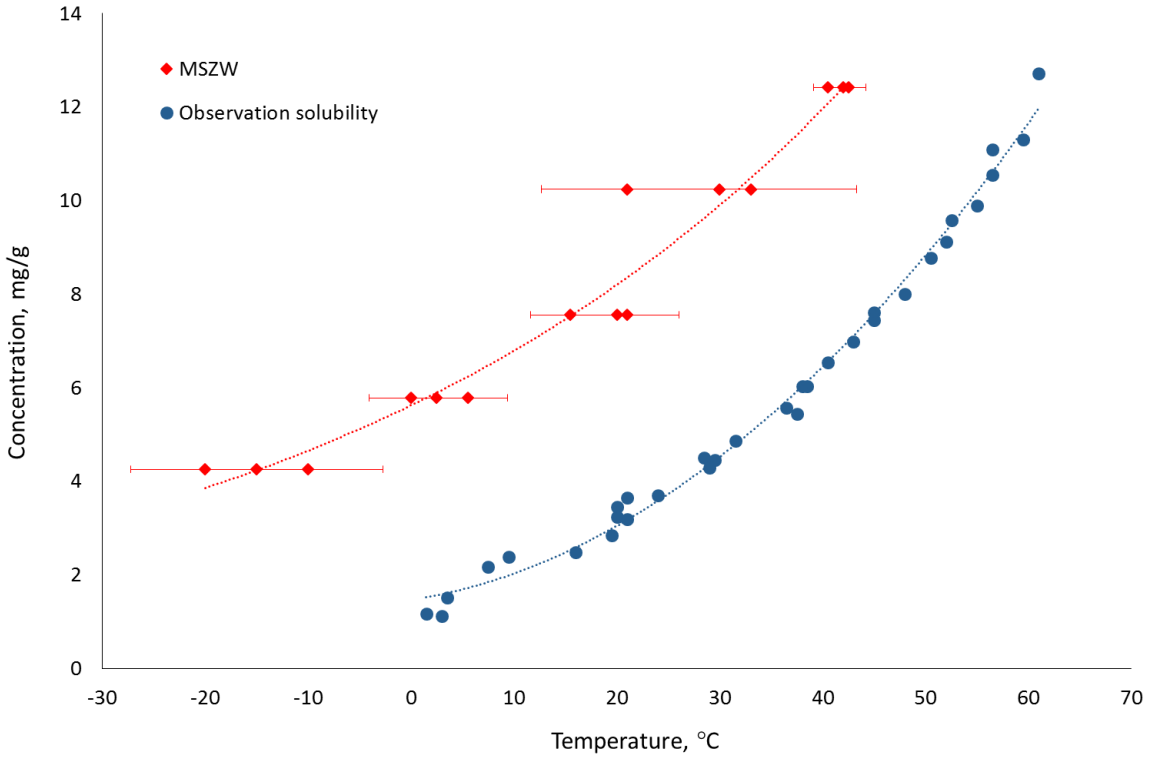

Figure 5.17: Metastable zone and solubility (by observation methods) of UBA form III in ethanol.

5.4 Seeded Batch Cooling Crystallisation of UBA from Ethanol

Due to the lack of reproducibility and robustness of the unseeded cooling crystallisation of UBA form III from ethanol, seeding methods were investigated. The seeding experiments were designed to investigate the effect of seeding with both form I, the thermodynamically stable form, and form III, the metastable form. These experiments investigated different seed loadings (1 %, 5 % and 20 %) and two different cooling rates (0.5 °C min^{-1} and 1 °C min^{-1}). The experiments were conducted at GSK, Stevenage using the Mettler Toledo Easymax with a Mettler Toledo Lasentech FBRM probe. The FBRM probe was used to follow the reaction in terms of dissolution, nucleation and crystal growth. Due to the size of the Easymax set up, the crystallisations were conducted at the 100 mL scale with overhead stirring at 500 rpm.

The saturation temperature of the systems was chosen to be 60 °C which corresponded to an approximate UBA concentration of 13 mg/g (327.4 mg of urea and 698.3 mg of barbituric acid). The barbituric acid was added to the ethanol and the system was heated to 70 °C to allow for full dissolution. Once full solvation of the barbituric acid had occurred (as shown by the FBRM counts) the urea was added and allowed to dissolve. Once full solvation of the starting components had been achieved the cooling crystallisation was conducted. The systems were cooled from 70 °C to 60 °C at the appropriate rate (as noted above) at which point dry seed was then added. For unseeded experiments the cooling continued to 0 °C (Figure 5.18 (a)). In seeded experiments, once the seed was added the system was held for a 15 minute seed age before the cooling was commenced (Figure 5.18 (b)). Once all systems had reached their final temperature

of 0 °C they were left to dwell for an hour. FBRM was used throughout to follow the particle counts and chord lengths for the duration of the experiment. Once cooling had begun a sample was taken from the system every 10 minutes for gravimetric analysis in order to follow the concentration of the solution throughout the experiment.

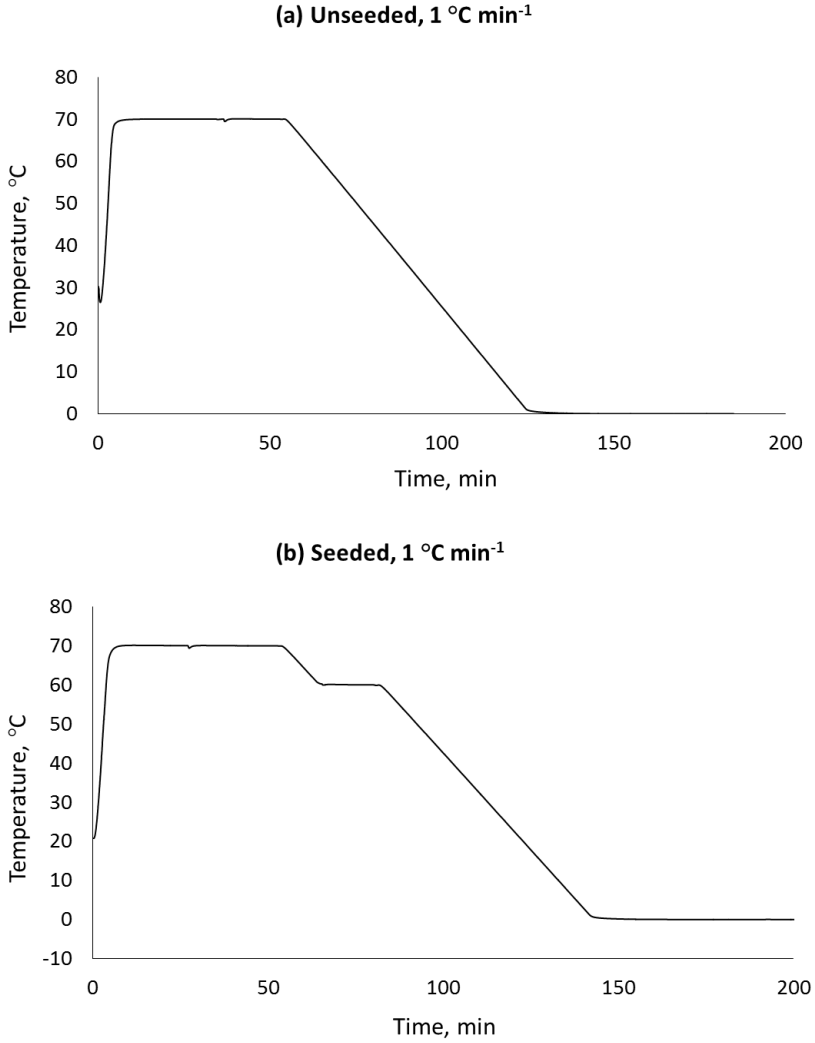

Figure 5.18: Example temperature profiles of unseeded (a) and seeded (b) cooling crystallisation of UBA from ethanol, cooling rate of 1 °C min^{-1}.

Table 5.4 summarises the twelve seeded experiments conducted and their outcomes. The systems were filtered using vacuum filtration and the solids left to dry at room temperature before being analysed by PXRD. It can be seen that, for this system, the polymorphic outcome is independent of the cooling rate. When seeding with UBA form I, the thermodynamically stable form, a seed loading of 5 % was required to access this form selectively with no form III impurities. When seeding with the metastable form, form III, a higher seed loading of 20 % was required in order to access pure form III. Unseeded crystallisations using this platform lead to the production of a mixture of UBA form I, form III and residual barbituric acid unlike the previous work using the CRD Polar Bear Plus. This is likely due to the changes in the experimental set up including size and shape of the crystallisation vessel, size and shape of impeller, the difference in stirring rate and the presence of the FBRM probe. All of these would likely result in different

mixing conditions as well as changes in the mass and heat transfer and could alter the kinetics of the system.

Table 5.4: Seeding parameters and outcomes for the seeded cooling crystallisation experiments of UBA from ethanol: (a) 0.5 °C min^{-1} cooling rate, (b) 1 °C min^{-1} cooling rate.

(a) 0.5 °C min^{-1} cooling rate

Seed type	Seed loading			
	0%	1%	5%	20%
UBA I	UBA III/I/BA	UBA I/III	UBA I	UBA I
UBA III		UBA I/III	UBA I/III	UBA III

(b) 1 °C min^{-1} cooling rate

Seed type	Seed loading			
	0%	1%	5%	20%
UBA I	UBA III/I/BA	UBA I/III	UBA I	UBA I
UBA III		UBA I/III	UBA I/III	UBA III

The FBRM data collected for the unseeded cooling crystallisations can be seen in Figure 5.19 and Figure 5.20. The vertical green lines represent the point at which the cooling crystallisation process was started. The three horizontal lines represent the recorded counts of three different size (chord length) classes of particles (blue < 10 μm, green 10 - 100 μm and red 100 - 1000 μm). The point at which the counts start to increase is the point at which spontaneous nucleation occurs within this system. Regardless of the cooling rate, the nucleation temperature for each experiment is approximately 45 °C. Once initial nucleation has occurred the number of counts continues to increase due to secondary nucleation and growth effects.

Solution samples were taken every ten minutes throughout the cooling crystallisations; corresponding to every 10 °C for the 1 °C min^{-1} cooling profile and every 5 °C for the 0.5 °C min^{-1} cooling profile. The concentrations of UBA in each sample were determined gravimetrically and allowed for the concentration of the system to be followed for the duration of the process (Figure 5.21). It can be seen that for each unseeded crystallisation experiment the concentration of solution is below the solubility curve at the initial temperature of 70 °C; the solution is undersaturated. As the system is cooled to 60 °C the concentration remains the same and the system passes into the metastable zone. Further cooling then results in spontaneous nucleation at approximately 45 °C as observed with the FBRM. It can be seen that for both cooling experiments the concentration in the solution significantly decreases between 50 °C and 40 °C due to the occurrence of this nucleation event. Once the initial nucleation event has occurred the concentration follows the trend of the solubility curve. The systems were left at the final temperature of 0 °C in an attempt to mitigate any remaining supersaturation in the system. It can be seen that during this period the concentration of the solution does drop further towards the solubility line, but full desupersaturation of the solution is not achieved.

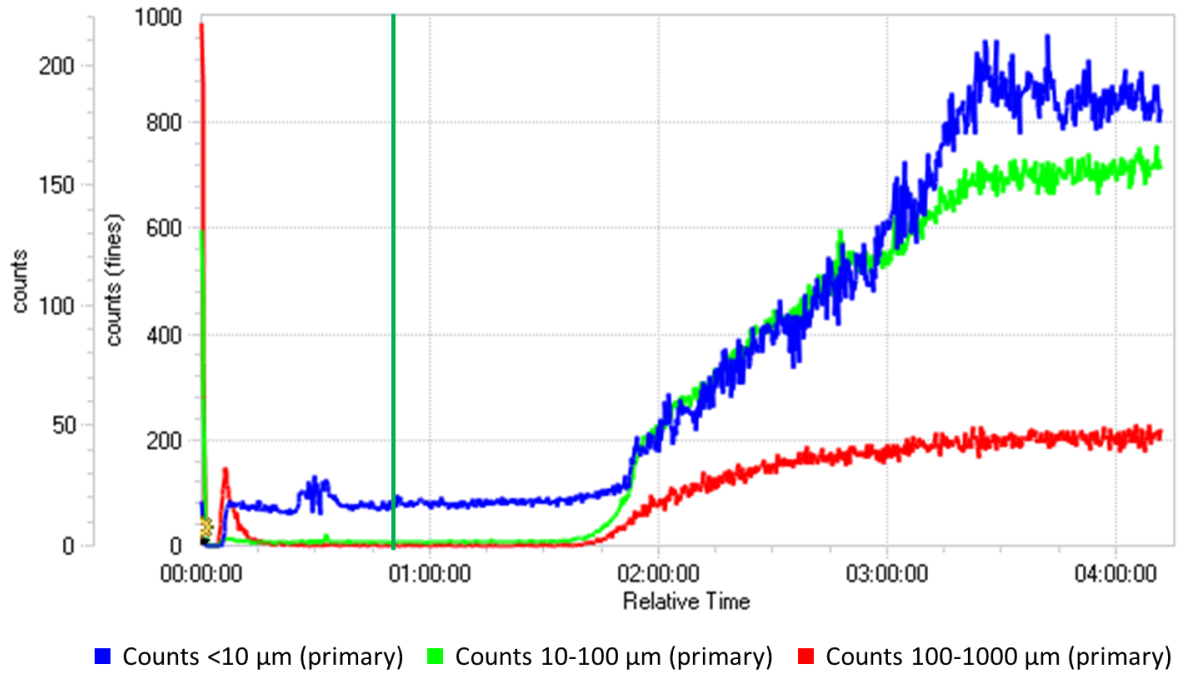

Figure 5.19: FBRM trace of unseeded Easymax cooling crystallisation of UBA from ethanol; 0.5 °C min^{-1} cooling rate. Vertical green line represents the start of the cooling process.

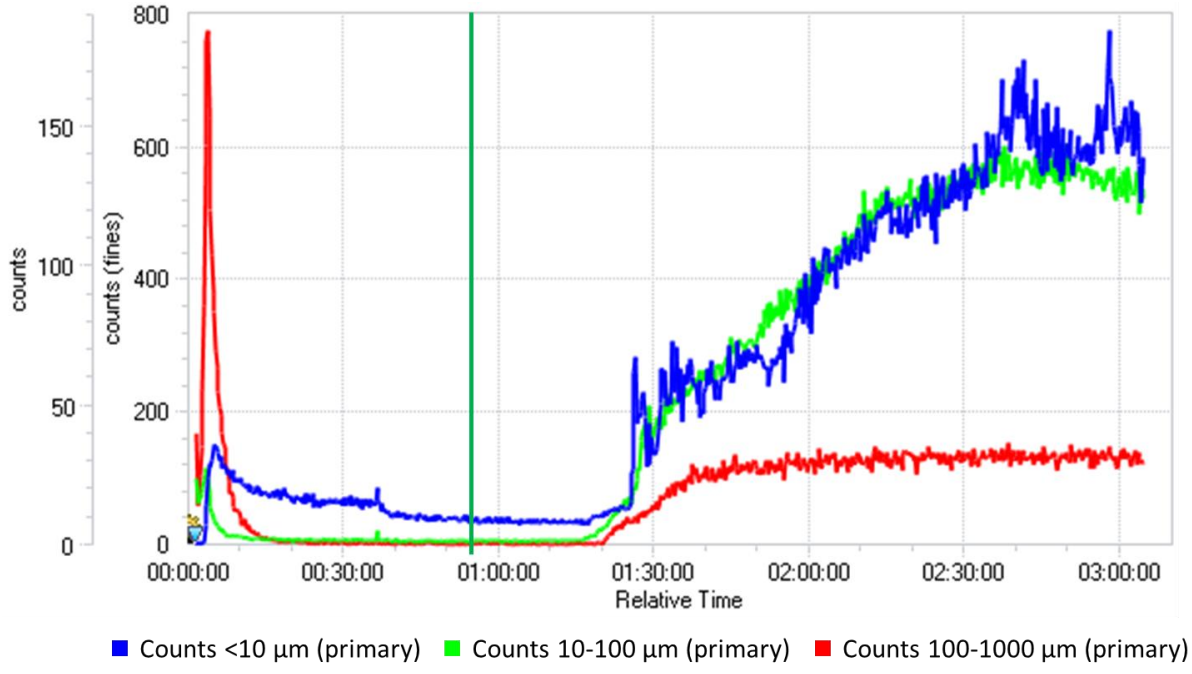

Figure 5.20: FBRM trace of unseeded Easymax cooling crystallisation of UBA from ethanol; 1 °C min^{-1} cooling rate. Vertical green line represents the start of the cooling process.

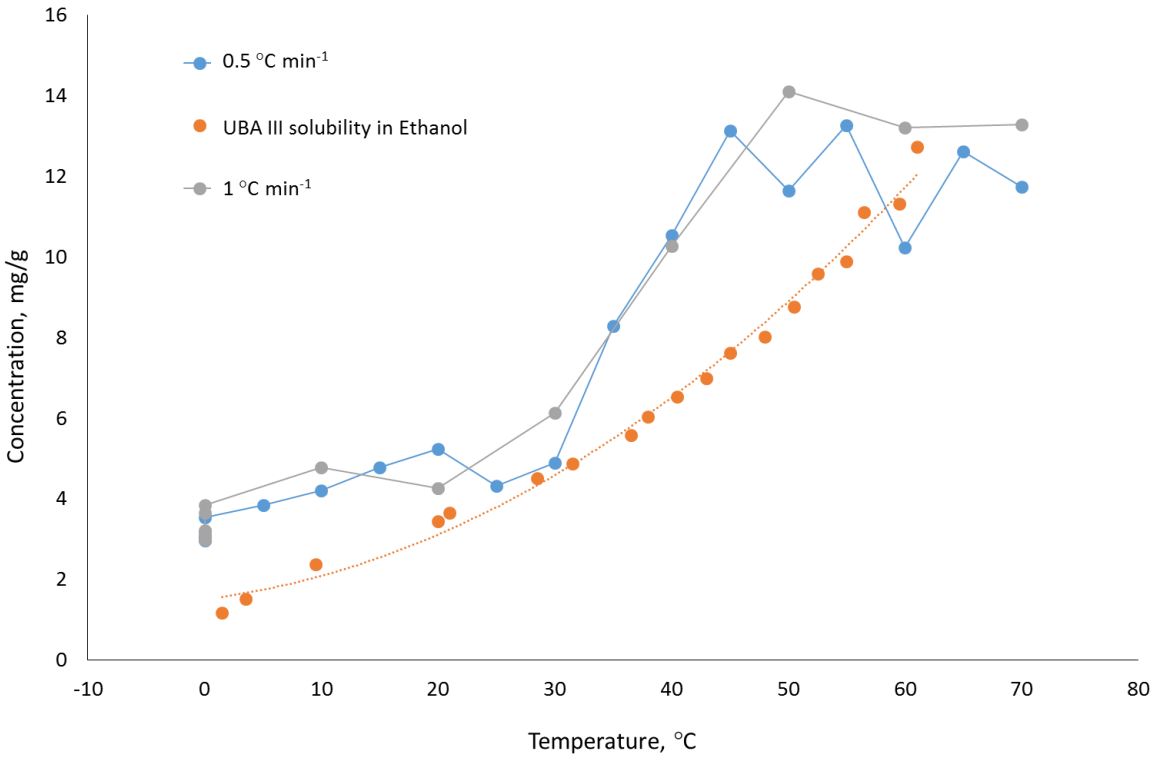

Figure 5.21: Concentration curves of the unseeded Easymax cooling crystallisations of UBA from ethanol plotted alongside the observation solubility of UBA form III in ethanol.

5.4.1 UBA Form I Seeded Batch Cooling Crystallisations

For the introduction of seeding to the system, dry seed was added at 60 °C, once the system had entered the metastable region. The seed addition temperature was chosen based on the concentration profiles obtained from the unseeded experiments. The system was held at 60 °C for a duration of 15 minutes to allow for a seed ageing step in order to encourage the seed to take in the solution and reduce the supersaturation. The cooling of the system was then resumed and continued in the same way as the unseeded experiments. Upon analysing the FBRM data for the seeded crystallisations unexpected trends were observed.

Figure 5.22 to Figure 5.24 show the FBRM data obtained from the UBA form I seeded crystallisations with a cooling rate of 0.5 °C min^{-1}. For these graphs, the vertical solid green line indicates when seed was added to the system, with the vertical dashed green line representing the end of the seed hold and the continuation of cooling. It can be seen, that with seed loadings of 1 % and 5 %, once the seed is added to the system, the counts remain constant. It can also be seen that there is no change in counts even once the cooling crystallisation proceeds; the counts remain constant until the vertical dashed blue line is reached. At this point in the process the number of counts, especially those representing the number of fine particles in the system, significantly increases. This behaviour suggests a nucleation event is occurring. When seed loadings of 5 % and 20 % are used it can be seen that the number of counts corresponding to chord lengths of 100 - 1000 µm begins to reduce over time once the cooling is resumes. This can be

attributed to breakage of the larger seed particles during the crystallisation process due to collision with the impeller and vessel walls.

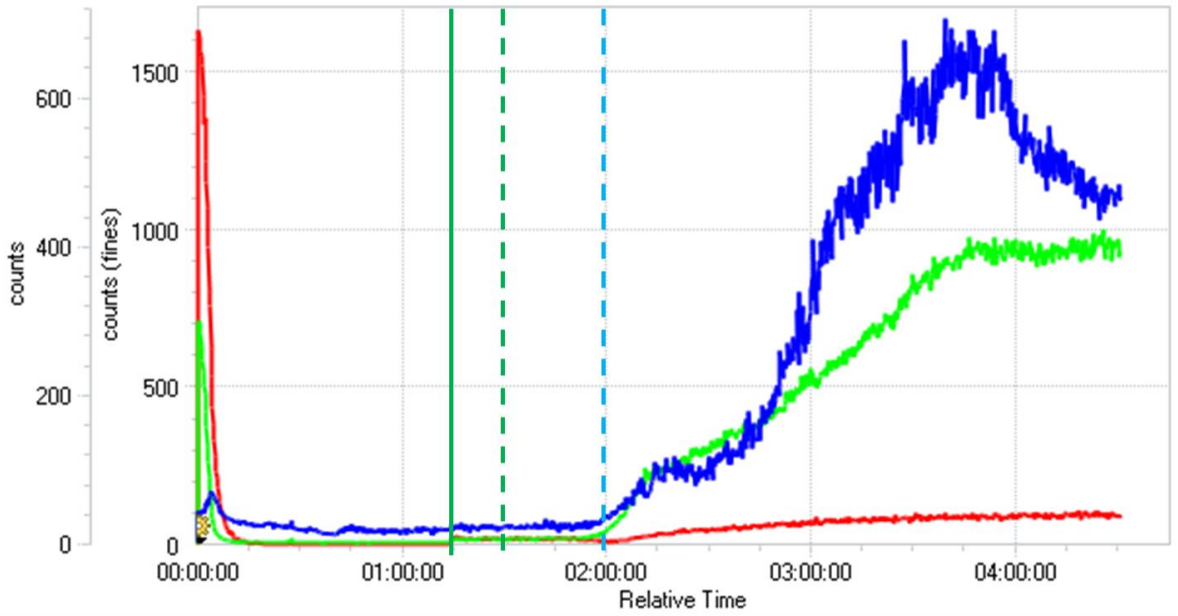

Figure 5.22: FBRM trace of 1 % UBA form I seeded Easymax cooling crystallisation of UBA from ethanol; 0.5 °C min^{-1} cooling rate. Solid green line represents seed addition, dashed green line shows end of the seed hold and the dashed blue line shows start of nucleation event.

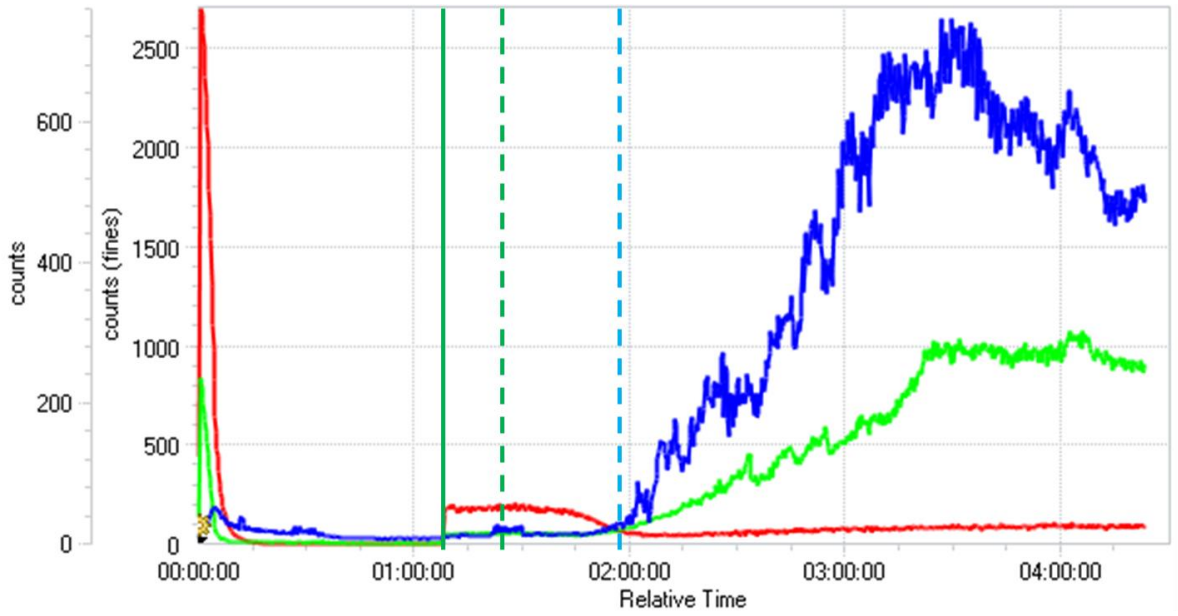

Figure 5.23: FBRM trace of 5 % UBA form I seeded Easymax cooling crystallisation of UBA from ethanol; 0.5 °C min^{-1} cooling rate. Solid green line represents seed addition, dashed green line shows end of the seed hold and the dashed blue line shows start of nucleation event.

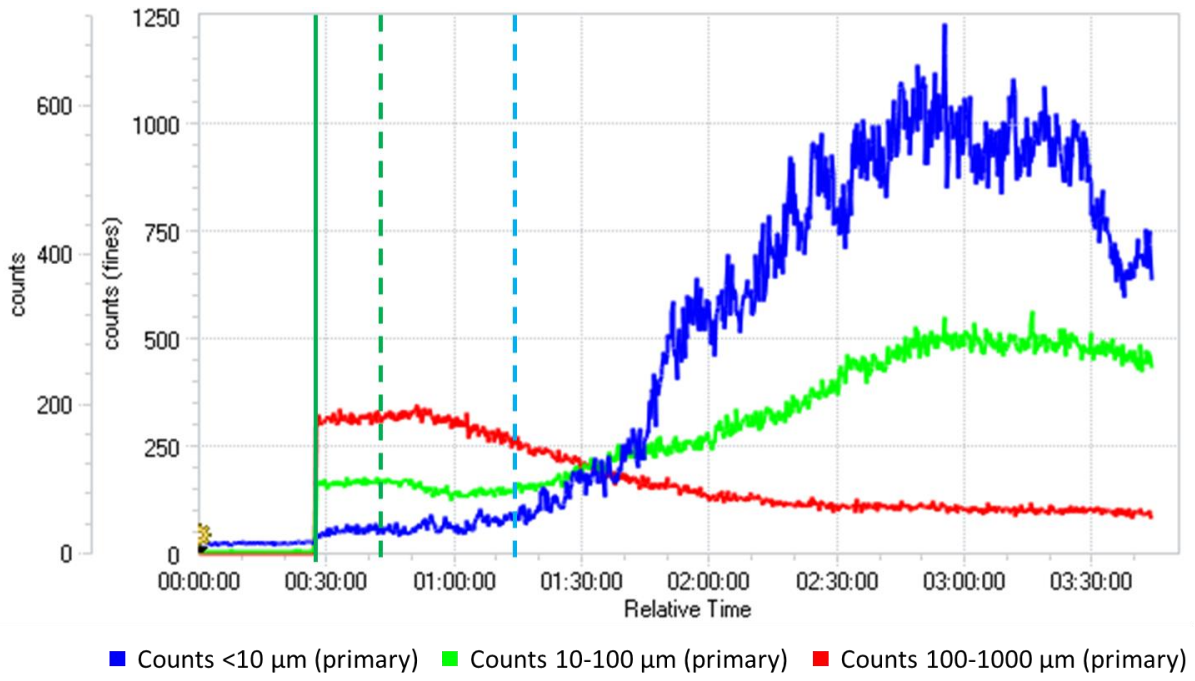

Figure 5.24: FBRM trace of 20 % UBA form I seeded Easymax cooling crystallisation of UBA from ethanol; 0.5 °C min^{-1} cooling rate. Solid green line represents seed addition, dashed green line shows end of the seed hold and the dashed blue line shows start of nucleation event.

For all seed loadings the overall trend is the same and the temperature at which these nucleation events occur is approximately 45 °C for each system. This suggests that upon the addition of the seed crystals they do not take to the solution and no growth or secondary nucleation events occur upon the addition or during the seed hold. The systems appear to act in a very similar way to the unseeded crystallisations, displaying a nucleation event at the same temperature as when no seed is present.

The concentration of the solutions for each crystallising system further confirms the theory that the seed particles are not taking to solution and that no growth or secondary nucleation occurs due to their presence in the solution. Solution samples were taken before seed addition (at 60 °C) and after the 15 minute seed hold (at 60 °C). It can be seen that for each of the seed loadings there is no significant drop in concentration after the seed hold, suggesting that the seed is not absorbing any of the supersaturation within the system; no growth or secondary nucleation is occurring. It can also be seen that the concentration trends for the seeded experiments are very similar to the unseeded system showing that the presence of seed is having no effect on the solution concentration and subsequent nucleation events.

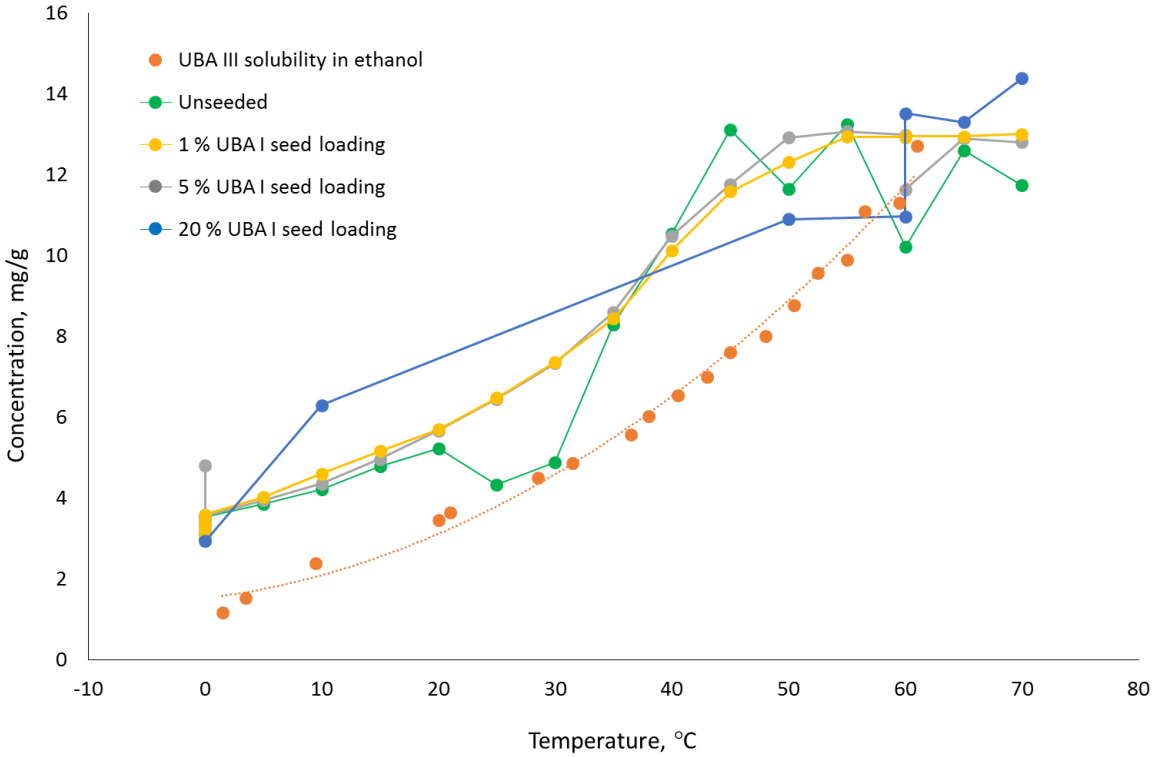

Figure 5.25: Concentration profiles of unseeded and UBA form I seeded cooling crystallisations of UBA from ethanol with a cooling rate of 0.5 °C min^{-1}.

The FBRM and concentration data for the UBA form I seeded crystallisations with a 1 °C min^{-1} cooling rate show the same trends as seen with the 0.5 °C min^{-1} crystallisations (see Appendix Figure 9.12 to Figure 9.15). This suggests that regardless of the cooling rate or seed loading, the seed crystals added make no difference in the overall crystallisation process in terms of nucleation events. However, the PXRD analysis of the collected products suggests that upon addition of 5 % UBA I seed, UBA form I is accessed selectively as opposed to a mixture of UBA form I and form III, regardless of the cooling rate used. As it has been concluded that no growth or secondary nucleation of the seed occurs during the process as would have been expected. This solid form control therefore must occur for a different reason.

As the system begins to nucleate it is likely that, due to Ostwald's law of stages the metastable form III will nucleate first. However, this does not mean that form I nucleation will not also occur concurrently. As further growth and nucleation continue during the cooling process there is an inherent competition between nucleation of the two forms and the solution-mediated phase transformation of form III to form I. It seems likely that, upon the addition of UBA form I seed, the presence of form I in the solution will increase the tendency of UBA form I to nucleate as well as increase the tendency and rate of UBA form III to form I phase transformations; hence allowing for form I to be accessed selectively with higher seed loadings.

5.4.2 UBA Form III Seeded Batch Cooling Crystallisations

When UBA form III seed was used, regardless of the cooling rate used, a seed loading of 20 % was required to gain solid form control and access pure UBA form III. When looking at the FBRM data collected from the 0.5 °C min^{-1} cooling rate experiments (Figure 5.26 - Figure 5.28) a similar trend to the UBA form I seeded experiments is observed.

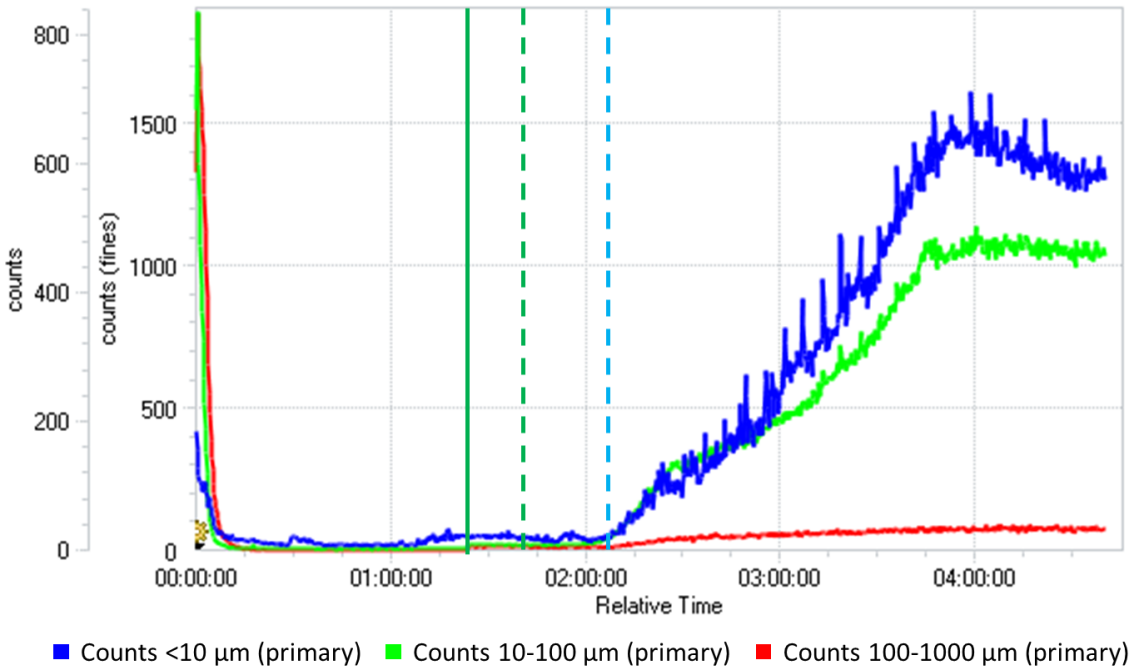

Figure 5.26: FBRM trace of 1 % UBA form III seeded Easymax cooling crystallisation of UBA from ethanol; 0.5 °C min^{-1} cooling rate. Solid green line represents seed addition, dashed green line shows end of seed hold and the dashed blue line shows the start of the nucleation event.

Again, the vertical solid green line indicates the point of seed addition and the dashed vertical green line the end of the seed hold period. It can be seen that during the seed hold, no growth or secondary nucleation occurs within the system, and the seed material remains unchanged in the crystallisation vessel. The system remains unchanged upon subsequent cooling of the system, until a significant increase in the number of counts occurs after approximately 30 minutes, represented by the vertical dashed blue line. The same trend is observed regardless of the seed loading, with the temperature at which these nucleation events occur being approximately 45 °C for each experiment. Again, this data suggests that addition of the UBA form III seed crystals has had little effect and the system acts in a very similar manner to the unseeded system.

Concentration analysis for these experiments further confirmed the inactive nature of the seeds (Figure 5.29). It can be seen that the concentration trends observed in the seeded experiments with a 0.5 °C min^{-1} cooling rate remain relatively unchanged in comparison to the unseeded experiment; there is no significant drop in concentration after the seed hold and the concentration remains relatively constant until approximately 45 °C where the nucleation event is observed with the FBRM data. The

same trends are seen in both the FBRM and concentration data for the seeded experiments conducted at 1 °C min^{-1} (see Appendix Figure 9.16 to Figure 9.19).

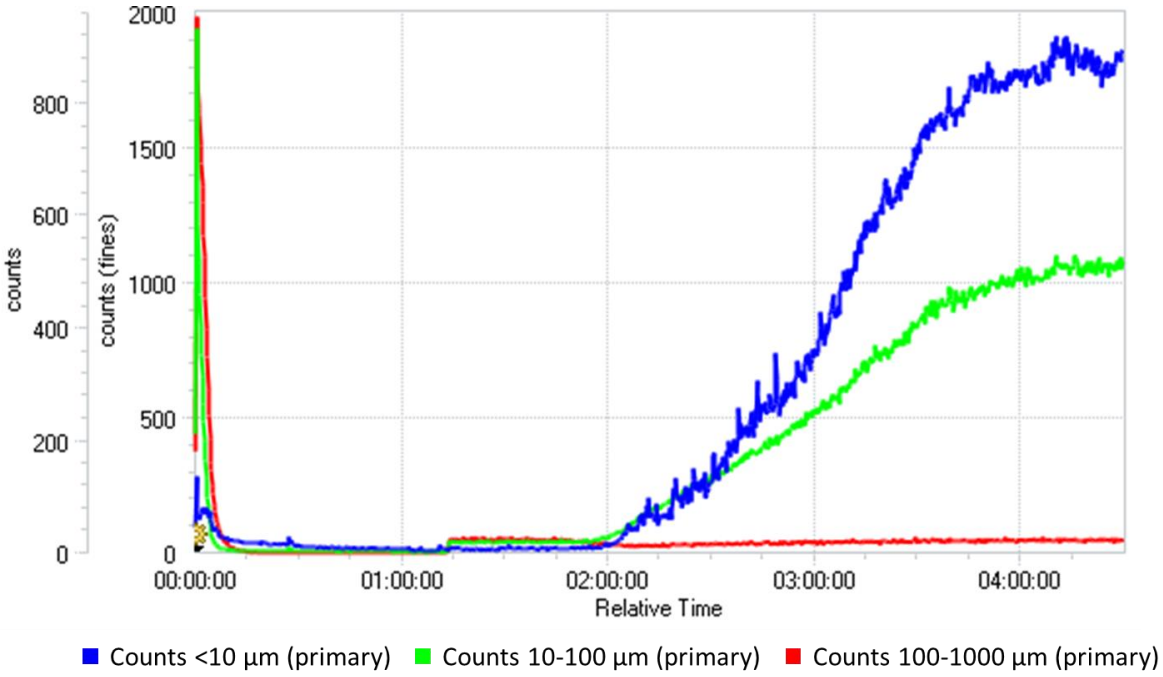

Figure 5.27: FBRM trace of 5 % UBA form III seeded Easymax cooling crystallisation of UBA from ethanol; 0.5 °C min-1 cooling rate. Solid green line represents seed addition, dashed green line shows end of seed hold and the dashed blue line shows the start of the nucleation event.

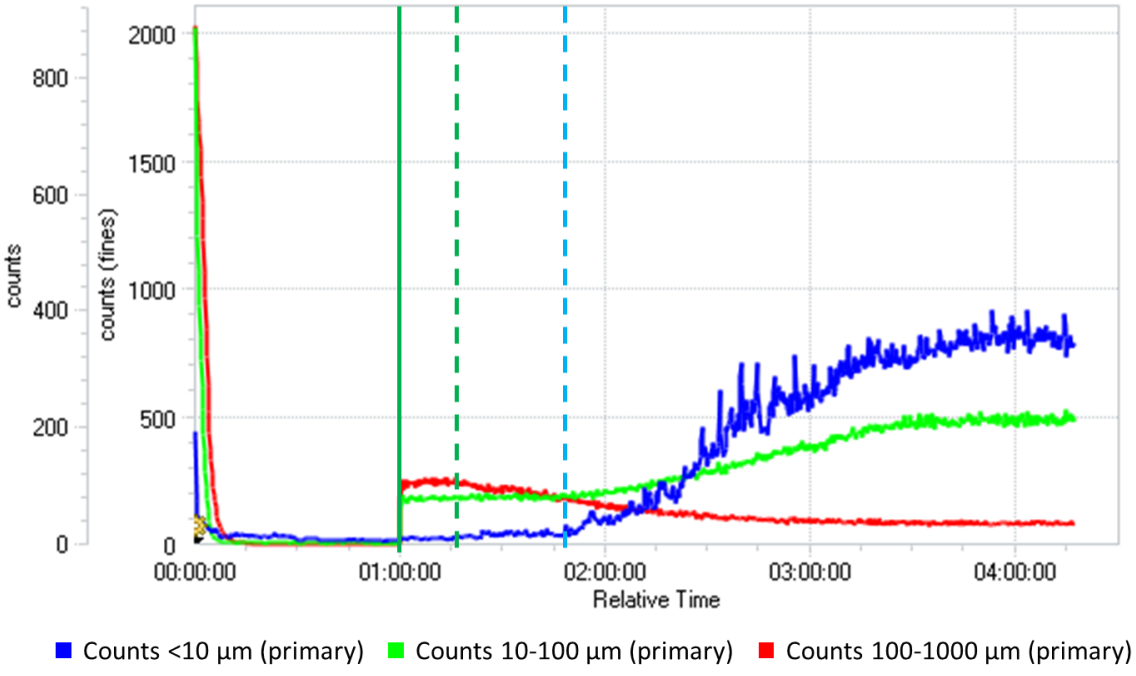

Figure 5.28: FBRM trace of 20 % UBA form III seeded Easymax cooling crystallisation of UBA from ethanol; 0.5 °C min-1 cooling rate. Solid green line represents seed addition, dashed green line shows end of seed hold and the dashed blue line shows the start of the nucleation event.

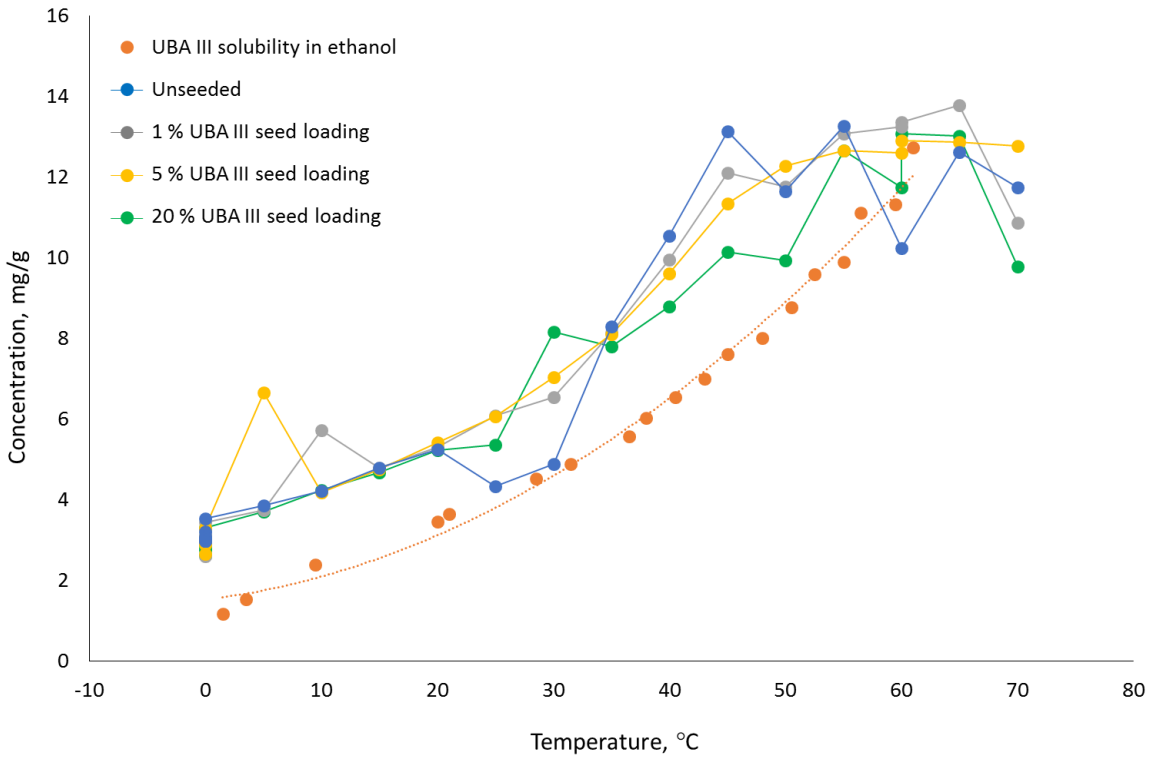

Figure 5.29: Concentration profiles of unseeded and UBA form III seeded cooling crystallisations of UBA from ethanol with a cooling rate of 0.5 °C min^{-1}, plotted alongside the observation solubility of UBA form III in ethanol.

It can be concluded that the addition of seeds in these cooling crystallisation experiments is not having the expected effect; no growth of the seeds occurs upon addition and they do not encourage any secondary nucleation events. Solid form control, is however, achieved with the large seed loading of 20 % when using UBA form III. As previously discussed with the form I seeding experiments, the competition between form I and form III nucleation may be being affected by the presence of one of these solid forms in the solution. The large amount of UBA form III present (at a 20 % seed loading) may result in a templating effect upon the observed nucleation events; it may encourage the nucleation of UBA form III and effectively drown out any nucleation of UBA form I that may occur in the system when unseeded (or with less seed). This suggests why a large amount of seed is required as the volume of solid present in the system when the nucleation event occurs must be significant enough to 'drown out' any form I nucleation in the system.

There could be several reasons as to why the seed crystals did not take to the solution. One of these is that the seeds could be damaged and hence not have any clean surfaces available for further growth. The outside of the particles may have become amorphous and therefore no crystal faces were available for the addition of solute molecules, or the crystals may have already reached a morphology whereby there were no longer any fast growing faces available on the habit, resulting in no further growth. One way in which this could be overcome would be to add the seeds in a slurry, as opposed to a dry powder. This would allow for some initial dissolution of the seed crystals before their

addition to reveal clean surfaces available for growth and hence activate the seeds. However, in some cases adding the seed in a slurry can allow for solution-mediated phase transformation to occur before the seed addition and can therefore be problematic when seeding with a metastable form, such as UBA form III.

The point of seed addition may also be a reason as to why the seed did not take. The seeds may have been added too close to the solubility curve and as a result there would not be enough supersaturation available in the system for any measureable secondary nucleation or growth. An addition point of 60 °C was chosen for this work based on the unseeded experiments concentration profiles, however this is very close to the solubility curve obtained from observation methods and so lower seed addition temperatures should be investigated.

Overall, the introduction of seeds to access a more robust crystallisation route for the selective formation of UBA form III proved not to be successful in terms of controlling the outcome via growth of the seed crystals and secondary nucleation upon their addition to the system. Large seed loadings of 20 % did allow for the formation of pure form III, however due to time constraints this work could not be repeated and so the robustness of this method could not be established.

5.5 Unseeded Batch Crystallisation of UBA from IPA

Due to the lack of robustness of the selective UBA form III crystallisation from ethanol, investigation into a different solvent system was conducted. It was previously discussed that upon moving from methanol to ethanol the solubility of the co-crystal system was significantly reduced and this in turn allowed for a higher level of selectivity towards the metastable form, form III. Thus moving to the use of IPA represents a logical next step in the search for even better polymorphic control. The solubility of the UBA co-crystal (form I and form III) was determined in IPA, compared to that of methanol and ethanol and shown to be significantly reduced, as discussed in section 4.2.2 (Figure 4.13). Due to this reduction in solubility IPA was taken forward for subsequent investigation into the potential metastable form selectivity that this solvent may yield.

5.5.1 Solution-mediated Phase Transformation Techniques (Slurry Techniques) in IPA

Small scale (2 mL) slurrying experiments were conducted to investigate whether the reduced solubility of UBA in IPA would result in a higher level of selectivity for the metastable form III. The experiments were conducted in the same manner as the previously discussed ethanol and methanol slurry experiments (Section 5.2) and utilised a 1:1 urea: barbituric acid molar ratio. Three experimental slurry times (8 hours, 16 hours and 24 hours) were investigated and the PXRD patterns of the resultant slurry products can be seen in Figure 5.30.

It can be seen from the PXRD data that after slurrying urea and barbituric acid in IPA for a period of 8 hours the resultant product is a mixture of UBA form II and form III. UBA form II is the highly metastable form of the co-crystal system and has only ever been previously accessed using small scale evaporative crystallisation techniques. Although this slurry experiment does not selectively access UBA form II, the presence of PXRD peaks corresponding to this form in the slurry products indicates that during the slurrying experiment the highly metastable form II is initially produced and this then undergoes solution-mediated phase transformations to the more stable forms of UBA, as per Ostwald's law of stages. As UBA form II is not observed in either the ethanol and methanol mediated slurry products, but is present when IPA is used, this gives confirmation that the reduced solubility of the co-crystal in IPA has resulted in a significant reduction in rate of the solution-mediated phase transformations. As the slurry time is increased to 16 hours the PXRD pattern shows peaks corresponding to the presence of UBA form I, as well as both form II and form III. As the time is further increased to 24 hours, the PXRD pattern again shows a mixture of the three forms of UBA (I, II and III).

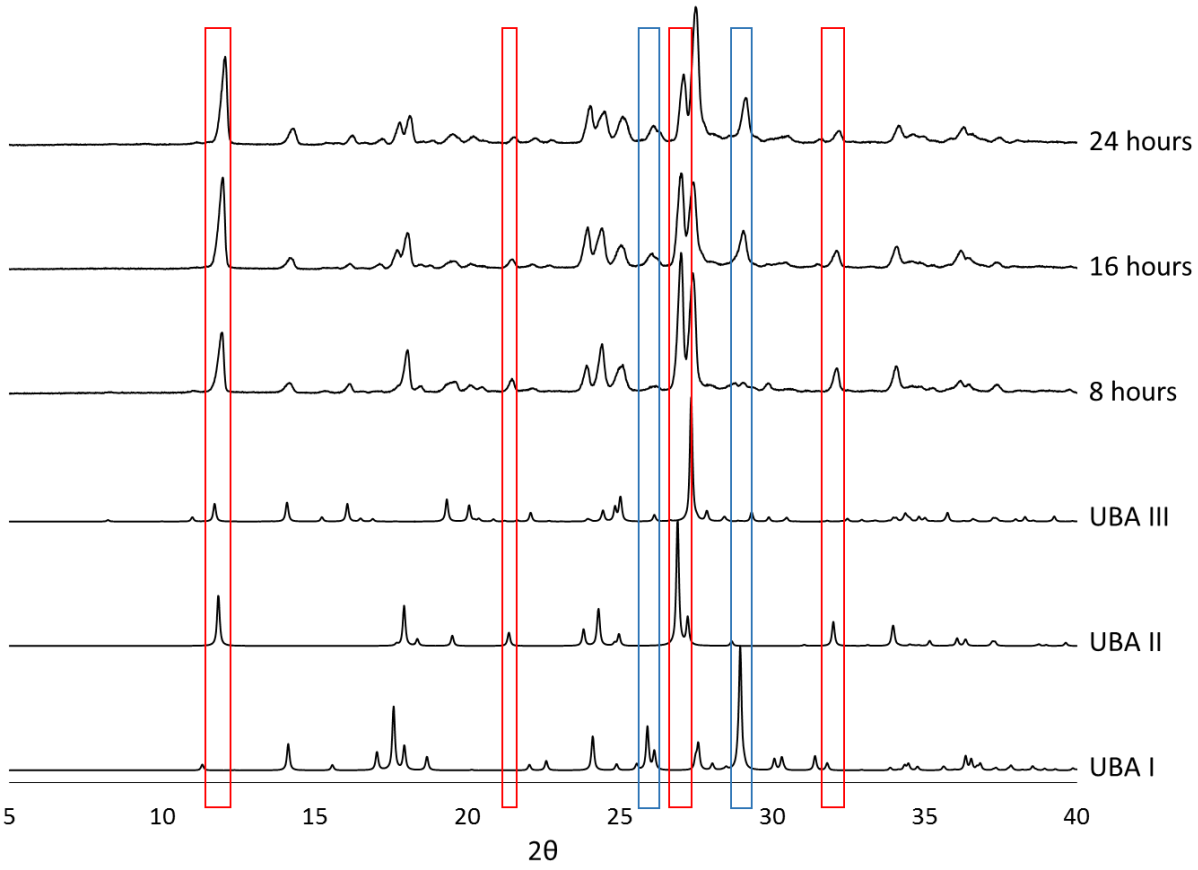

Figure 5.30: PXRD of 2 mL IPA mediated urea barbituric acid (1:1 ratio) slurry products. Red boxes show peaks unique to UBA form II with the blue boxes showing peaks unique to UBA form I.

Although the slurry technique is not selective to any one form in particular, the presence of UBA form II in all three slurry times confirms that the solution-mediated phase transformations for this system have been significantly reduced in rate upon moving to the IPA solvent system as predicted.

5.5.2 Batch Cooling Crystallisation of UBA from IPA

Due to the phase transformations between the solid forms of UBA being slowed down when IPA was used in slurrying, the transfer of this solvent system into cooling crystallisation was investigated. 150 mL scale cooling crystallisations were conducted using the CRD Polar Bear Plus with a 250 mL RBF and overhead stirring (400 rpm). Initial experiments (experiments 1 – 3) were conducted at a saturation temperature of T_{sat} = 60 °C and were cooled from 75 °C to 5 °C at a rate of 1 °C min^{-1}. The dwell time at the final temperature was varied between 0 minutes and 30 minutes and shown to have no effect upon the resultant outcome. PXRD analysis of the isolated solid products showed that pure UBA form III had been accessed (Figure 5.31). Further cooling crystallisations of this system were conducted using lower saturation temperatures to investigate whether the saturation had an effect on the resultant solid form.

Table 5.5: Summary of experimental parameters and outcomes for 150 mL unseeded cooling crystallisations of UBA from IPA.

Experiment	Saturation Temperature, °C	Initial Temperature, °C	Final Temperature, °C	Cooling Rate, °C min^{-1}	Dwell Time at Final Temperature, min	Outcome
1	60	75	5	1	0	Form III
2	60	75	5	1	0	Form III
3	60	75	5	1	30	Form III
4	50	65	5	1	0	Form III & trace I
5	50	65	5	1	0	Form III & trace I
6	50	65	-10	1	30	Form III
7	50	65	-10	1	30	Form III & Form I
8	40	55	-20	1	30	Form I
9	40	55	-20	1	30	Form I

Table 5.5 summarises the experimental parameters and the resultant solid form outcome of these experiments. It can be seen that when the saturation in the system was reduced to T_{sat} = 50 °C (experiments 4 – 7) the selectivity towards UBA form III was reduced. Two of the three experiments at this saturation cooled the system down to 5 °C and had dwell times of 0 minutes. For both of these cases UBA form III was accessed, but trace amounts of UBA form I impurities could be seen from the PXRD patterns (Figure 5.31). When the system was cooled to a lower temperature of -10 °C and a dwell time of 30 minutes was used form III could be accessed without trace amounts of UBA I being present, however upon repeating this experiment, trace amounts of form I were then observed. This outcome is likely a result of the lack of control exerted over systems when relying on primary nucleation and shows that at this saturation temperature there is a lower level of reproducibility of the system to access form III selectively. Further reducing the saturation temperature of the system to T_{sat} = 40 °C (experiments 8 and 9) resulted in form I being accessed selectively. These results show that for this solvent system a higher saturation level is required for the access to the desired metastable

form, form III and that upon reducing this saturation the system becomes selective to the thermodynamically stable form.

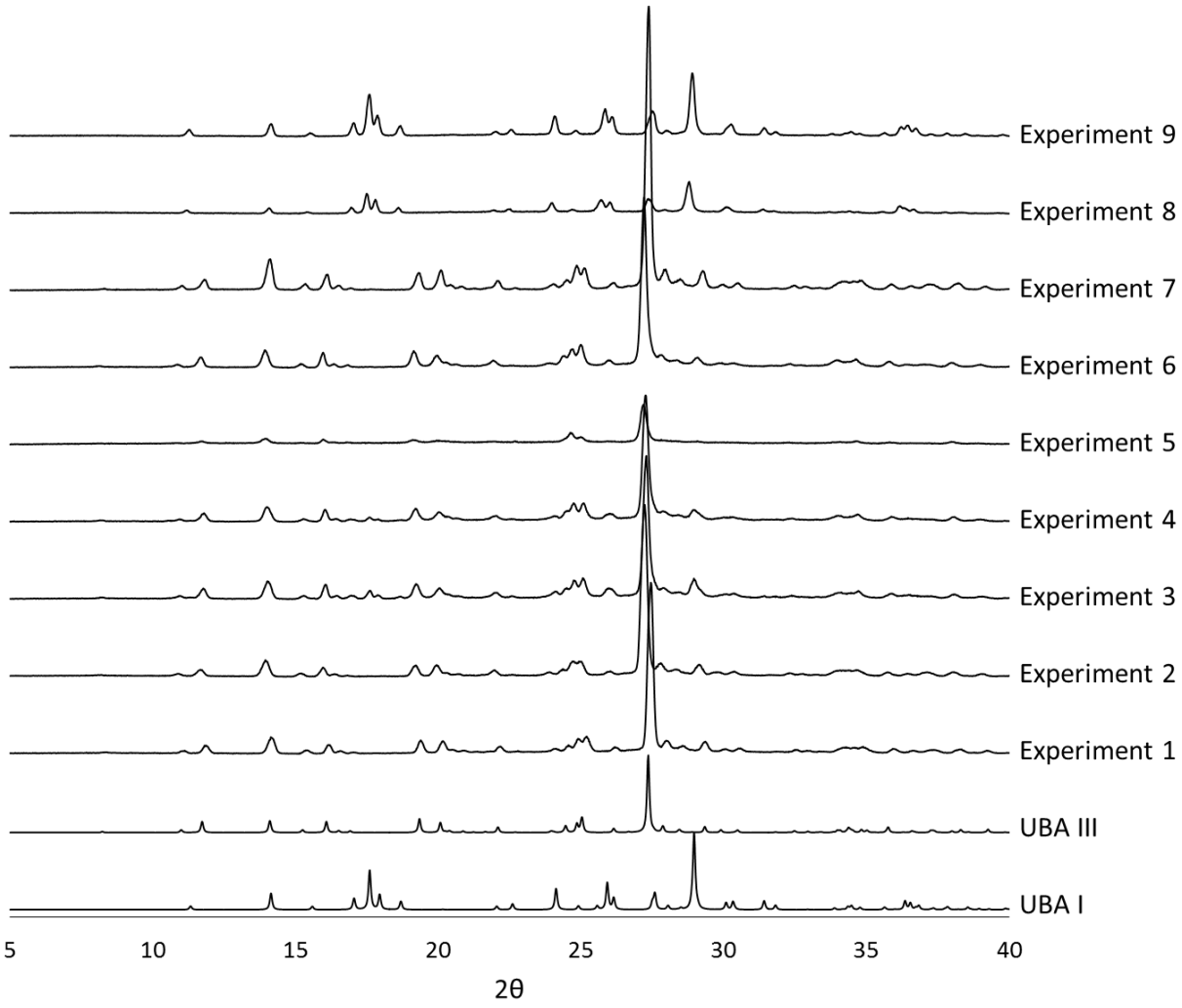

Figure 5.31: PXRD patterns for the 150 mL unseeded cooling crystallisations of UBA from IPA as summarised in Table 5.5.

Repeat cooling crystallisations using the desirable experimental parameters (T_{sat} = 60 °C or 75 °C to 5 °C, cooling profile at 1 °C min^{-1}), but with a larger dwell time of 1 hour were conducted to test the reproducibility of the system. The process was shown to be very reproducible, resulting almost exclusively in pure UBA form III, with very few experiments giving rise to any form I impurities. Overall, the experiments showed that using IPA resulted in a far more robust unseeded cooling crystallisation of UBA form III. It is likely that this increased level of reproducibility accessed using IPA as the solvent medium arises from the reduction in rate of UBA form III to form I transformation during the crystallisation process.

5.5.2.1 Metastable Zone Width Measurement of Cooling Crystallisation of UBA from IPA

Table 5.6: Summary of experiments to determine the metastable zone of UBA form III from IPA.

Tsat, °C	Concentration, mg/g	Nucleation temperature, °C	Form
60	8.39	38.00	UBA III
60	8.39	41.00	UBA III & trace BA
60	8.39	39.50	UBA III
55	6.37	27.00	UBA III & trace BA
55	6.37	30.00	UBA III
55	6.37	24.00	UBA III
50	4.83	15.00	UBA III & trace BA
50	4.83	14.00	UBA III
50	4.83	16.00	UBA III
45	3.67	5.00	UBA III
45	3.67	-2.00	UBA III
45	3.67	3.00	UBA III & UBA I
40	2.78	-18.50	UBA III & trace BA
40	2.78	Did not crystallise	N/A
40	2.78	Did not crystallise	N/A

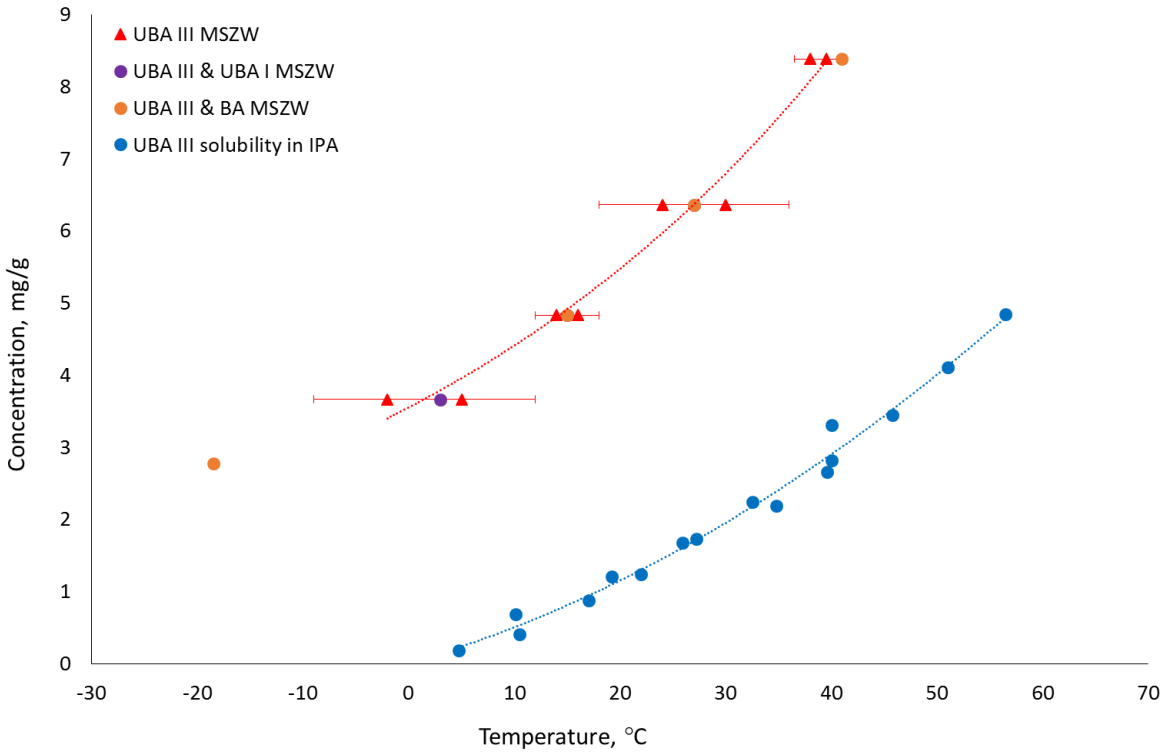

Figure 5.32: Metastable Zone Width of UBA form III in IPA (red) plotted with UBA form III solubility in IPA. Blue and orange points are nucleation points when pure form III was not obtained.

The metastable zone width (MSZW) of UBA from IPA was measured using unseeded cooling crystallisations at the 150 mL scale. Cooling crystallisations of solutions with different saturations were conducted using a 1 °C min^{-1} cooling rate and the CRD Polar Bear Plus. The systems were filmed using a GoPro Hero3^{+} enabling the crystallisations to be watched back and the nucleation point determined. Once nucleation had occurred within the system, the solid was isolated by vacuum filtration for solid form analysis. It

can be seen from Table 5.6 that some of the experiments gave rise to a mixture of UBA form III and barbituric acid, or UBA form I and form III, but only the crystallisations giving rise to pure form III were used to calculate the MSZW for UBA form III and the associated error bars (Figure 5.32).

As previously discussed, the likelihood of gaining form I impurities is significantly reduced when having a higher saturation within the system. It can be seen however, that in four of the experiments, residual barbituric acid remained in the system. This could be due to inefficient dissolution of the starting material resulting in some of the barbituric acid remaining in the system for the duration of the experiment. Alternatively, it could be due to some barbituric acid nucleating during the process which would then normally re-dissolve back into solution or convert to the co-crystal during the cooling process, however, as solid was collected quickly after the nucleation event it may not have had time to convert/re-dissolve.

5.6 Seeded Batch Cooling Crystallisation of UBA from IPA

As with the ethanol mediated system (Section 5.4), seeding techniques were introduced into the IPA system in order to investigate whether a more robust crystallisation system could be accessed for the selective crystallisation of a metastable form of UBA, form III. For this study the Easymax platform was used at GSK, Stevenage with the use of a Lasentech FBRM probe. The crystallisations were conducted at the 100 mL scale with overhead stirring at 500 rpm. Seeding experiments using seeds of both UBA form I (the thermodynamically stable form) and UBA form III (metastable) were investigated as well as two different cooling profiles (1 °C min^{-1} and 0.5 °C min^{-1}) and seed loadings of 1 %, 5 % and 20 %. The FBRM was used for the duration of the cooling crystallisations to monitor dissolution, nucleation and growth. The concentration of the systems was monitored for the duration of the cooling process by gravimetric techniques; solution samples were taken every ten minutes during the cooling process.

The saturation temperature of the systems was chosen to be 60 °C which corresponded to an approximate UBA concentration of 7.5 mg/g (188.2 mg of urea and 401.3 mg of barbituric acid). The barbituric acid was added to the IPA and the system was heated to 70 °C to allow for full dissolution. Once full solvation of the barbituric acid had occurred (as shown by the FBRM counts) the urea was added and allowed to dissolve. Once full solvation of both starting components had been achieved the cooling crystallisation was conducted. The systems were cooled from 70 °C to 60 °C at the appropriate rate at which point dry seed was added. If no seed was to be added, the cooling process continued to 0 °C (Figure 5.33 (a)). If seed was added, the system was then held for a 15 minute seed age before the cooling was commenced (Figure 5.33 (b)). Once all systems had reached their final temperature of 0 °C they were left to dwell for an hour. FBRM was used throughout to follow the particle counts and chord lengths for the duration of the experiment. Once cooling had begun a sample was taken from the

system for gravimetric analysis in order to follow the concentration of the solution throughout the experiment.

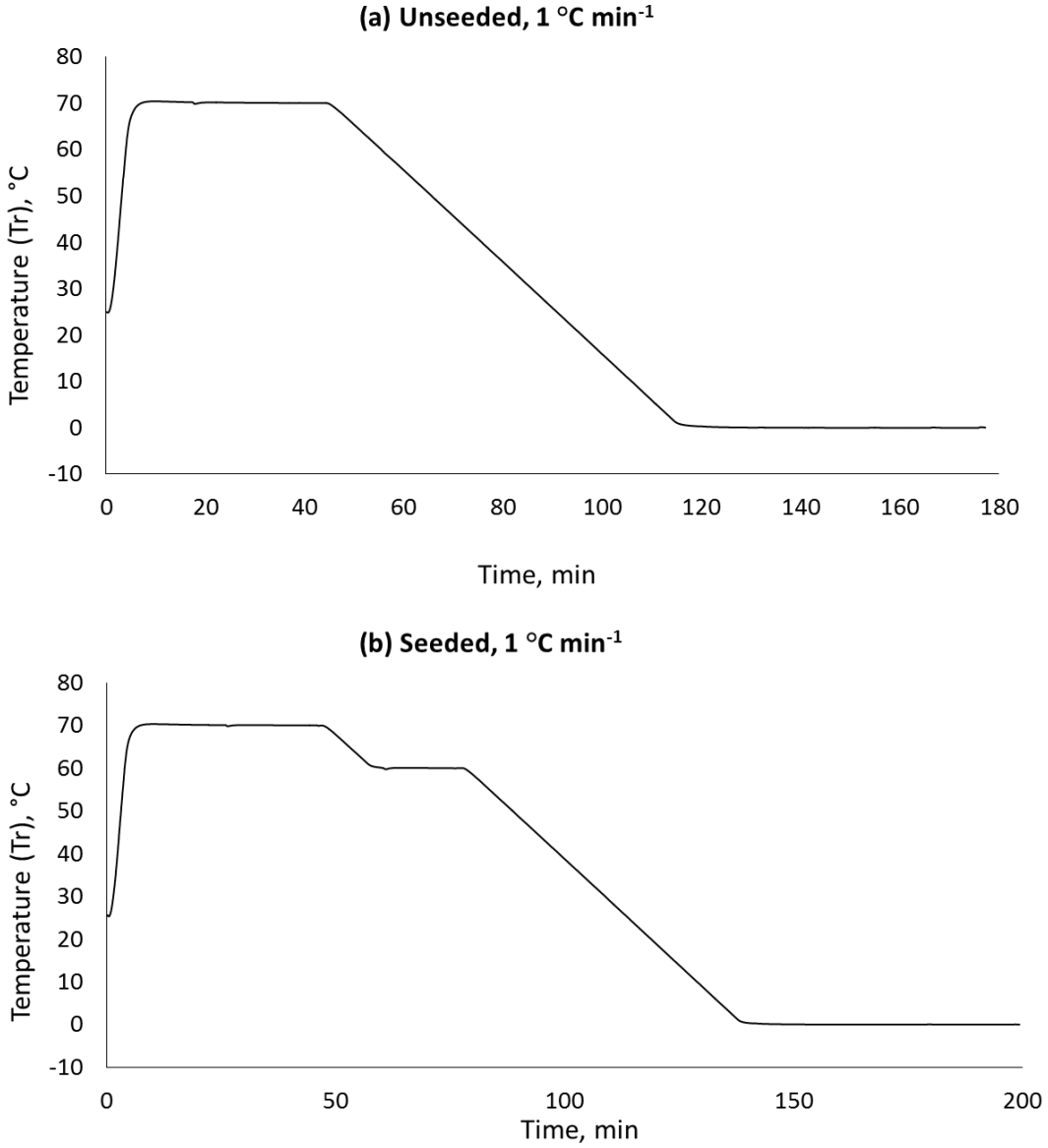

Figure 5.33: Example cooing profiles of unseeded (a) and seeded (b) cooling crystallisation of UBA from IPA using the Easymax set up at GSK, Stevenage.

When no seeds were introduced to the system and it was allowed to spontaneously nucleate, the resultant product depended on the cooling rate used. When the slower cooling rate of 0.5 °C min^{-1} was used a mixture of UBA form I and form III resulted, however when the faster 1 °C min^{-1} cooling rate was used UBA form III resulted. This suggests that the slower cooling rate allows for form III to form I conversion to occur, whereas the fast crystallisation process prevents this from happening. However as repeat crystallisations were not conducted it cannot be concluded with certainty that this is not an artefact of the lack of control over the spontaneous nucleation.

These outcomes differed in comparison to the previous work conducted at 150 mL at the University of Bath using the CRD Polar Bear Plus, where a mixture of form I and

form III was very rarely observed for this system. However, the difference in scale, shape and size of the vessel, stirring and the presence of FBRM probe are all likely to have an effect on the crystallisation process. It is therefore unsurprising that the outcome under these new conditions was slightly different, giving reduced selectivity to UBA form III.

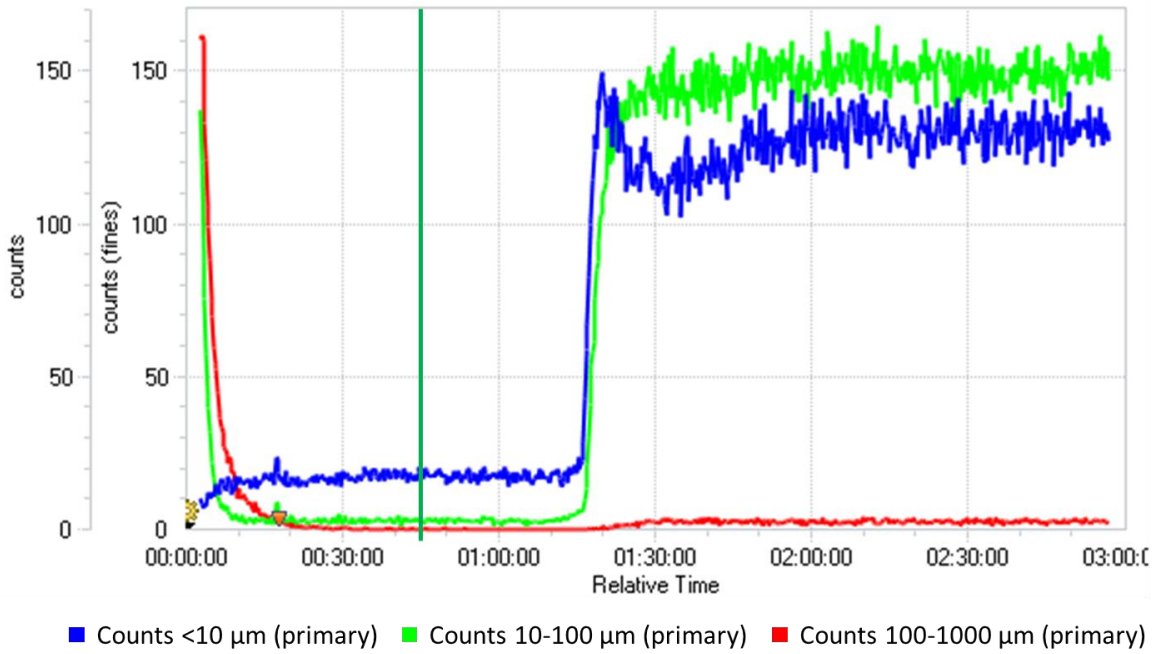

Figure 5.34: FBRM trace of the unseeded Easymax cooling crystallisation of UBA from IPA; 1 °C min^{-1} cooling rate. Vertical green line shows start of cooling.

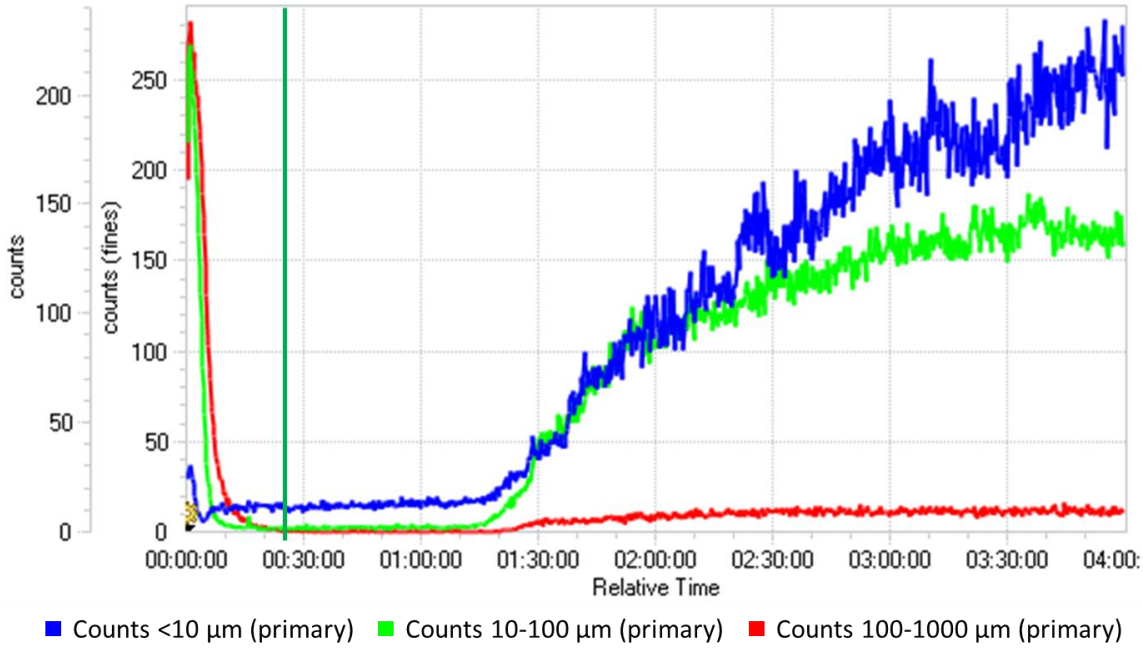

Figure 5.35: FBRM trace of the unseeded Easymax cooling crystallisation of UBA from IPA; 0.5 °C min^{-1} cooling rate. Vertical green line shows start of cooling.

The FBRM traces obtained for the two unseeded cooling crystallisations (Figure 5.34 and Figure 5.35) show that spontaneous nucleation occurs at approximately 40 - 45 °C. This aligns relatively well with the measured MSZW discussed earlier (Section 5.5.2.1), which suggests that the nucleation for a solution of concentration 7.5 mg/g should occur at approximately 40 °C. During each crystallisation process, solution samples were taken every 10 minutes for gravimetric concentration analysis to allow for the concentration of solution to be followed throughout the crystallisations. It can be seen in Figure 5.36 that the concentration of the solutions remains relatively steady from 70 °C to 50 °C/45 °C for the 1 °C min^{-1} and 0.5 °C min^{-1} cooling rate respectively. The drop in solution concentration as a result of nucleation within the system can be seen to occur between 40 °C and 50 °C, as was observed with the FBRM traces. The concentration then continues to decrease as the cooling process continues, following the trend of the solubility curve and dropping towards the solubility line as the system is left to dwell at 0 °C at the end of the cooling process, to allow for full desupersaturation of the solution to be achieved.

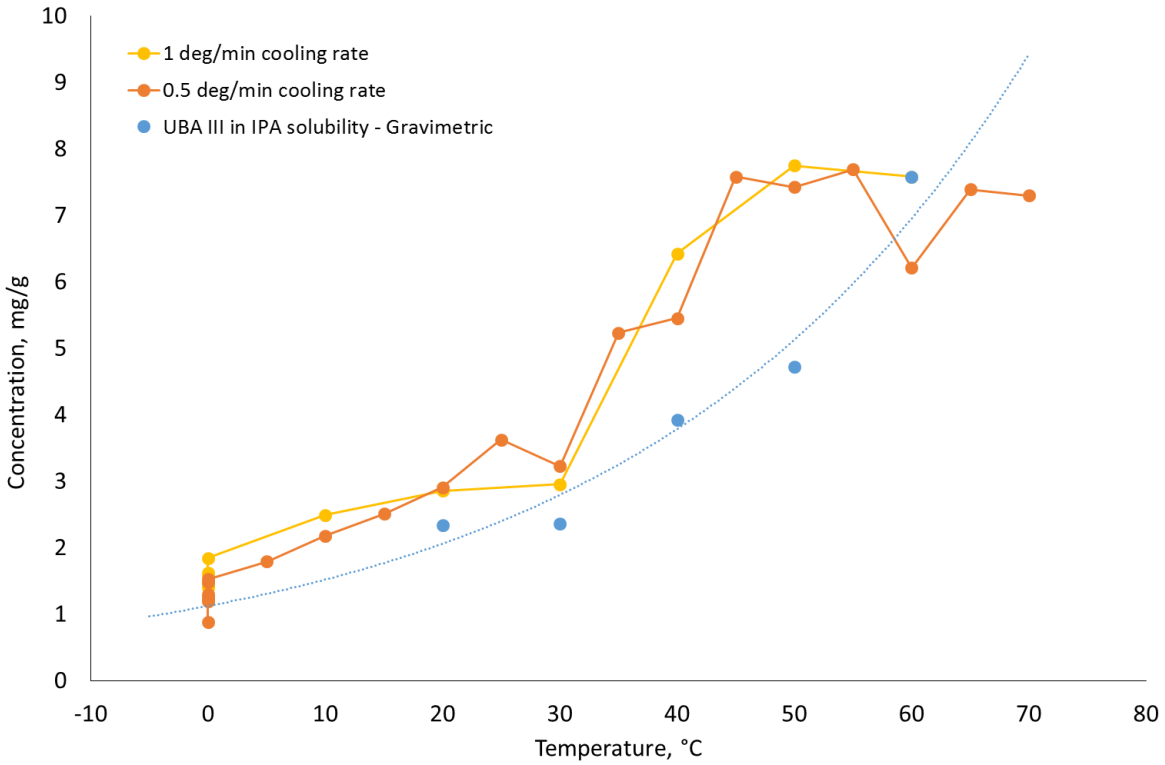

Figure 5.36: Concentration graphs of the unseeded Easymax cooling crystallisations of UBA from IPA.

5.6.1 UBA Form I Seeded Easymax Cooling Crystallisation

Table 5.7 summarises the seeding experiments parameters and the solid form outcomes. It can be seen that for this solvent system, the cooling rate does have an effect on the amount of seed required for solid form control when seeded with UBA form III.

Regardless of the cooling rate used, all seed loadings gave solid form control when seeding with UBA form I, the thermodynamically stable form. However, when looking at the FBRM traces obtained for the 0.5 °C min^{-1} cooling crystallisations with a seed loading of 1 % it can be concluded that, although having the form I seeds does access apparent solid form control, the seed crystals do not take to the solution as expected.

Table 5.7: Summary of Easymax seeded cooling crystallisations of UBA from IPA.

(a) 0.5 °C min^{-1}

Seed type	Seed loading			
	0%	1%	5%	20%
UBA I	UBA I/ UBA III	UBA I	UBA I	UBA I
UBA III		UBA I/ UBA III	UBA I/ UBA III	UBA III

(a) 1 °C min^{-1}

Seed type	Seed loading			
	0%	1%	5%	20%
UBA I	UBA III & UBA I/ UBA III with hold	UBA I	UBA I	UBA I
UBA III		UBA I/ UBA III	UBA III	UBA III

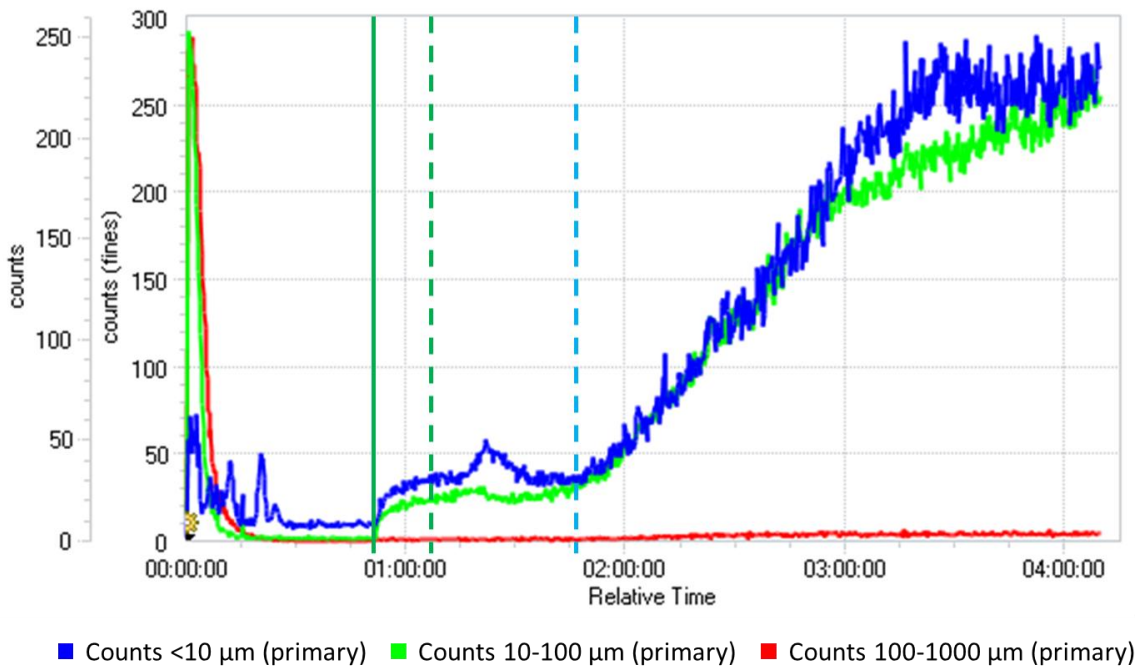

Figure 5.37: FBRM trace obtained from the 1 % UBA form I seeded Easymax cooling crystallisation of UBA from IPA; 0.5 °C min^{-1} cooling rate. Solid green line shows seed addition, dashed green line represents the end of seed hold and the dashed blue line shows nucleation event.

It can be seen in Figure 5.37 that upon addition 1 % seed loading, no growth or secondary nucleation events occur. The solid vertical green line represents the point of seed addition, with the vertical dashed green line representing the end of the 15 minute seed hold. It can be seen that during this seed aging step the number of counts remains relatively constant showing that there is no increase in the number of particles within the system as would be expected with secondary nucleation. It also shows that no growth is occurring within the system which would be represented by a decrease in the

counts corresponding to fines within the system (blue line) and an increase in the counts representing larger particles (green and red). Instead, no observable changes occur during this 15 minute hold, suggesting that seed particles are not taking to the solution. After this seed hold, once the cooling process resumes, it can be seen the FBRM counts remain fairly constant until a significant increase is observed (at the vertical dashed blue line). This increase in counts can be attributed to a nucleation event and the temperature at which this nucleation event occurs is approximately 40 °C. This is the same temperature at which the nucleation event is observed for the unseeded crystallisations, suggesting that the addition of seed is having little to no effect on the crystallisation process.

When looking at the concentration profile for the 1 % UBA form I seeded crystallisation it can be seen that it is not too dissimilar to that of the unseeded crystallisation (Figure 5.38). A sample was taken before the seed addition and after the 15 minute seed hold (both at 60 °C), and it can be seen that there is no significant decrease in concentration during this seed hold, further confirming that the seed does not take to the solution. The solution concentration trend is very similar to that obtained from the unseeded crystallisation, further indicating that at this seed loading the crystallisation behaved as if unseeded. If the seed took to solution it would be expected that the concentration would reduce during the seed hold due to a decrease in saturation arising from growth of the seeds or secondary nucleation events.

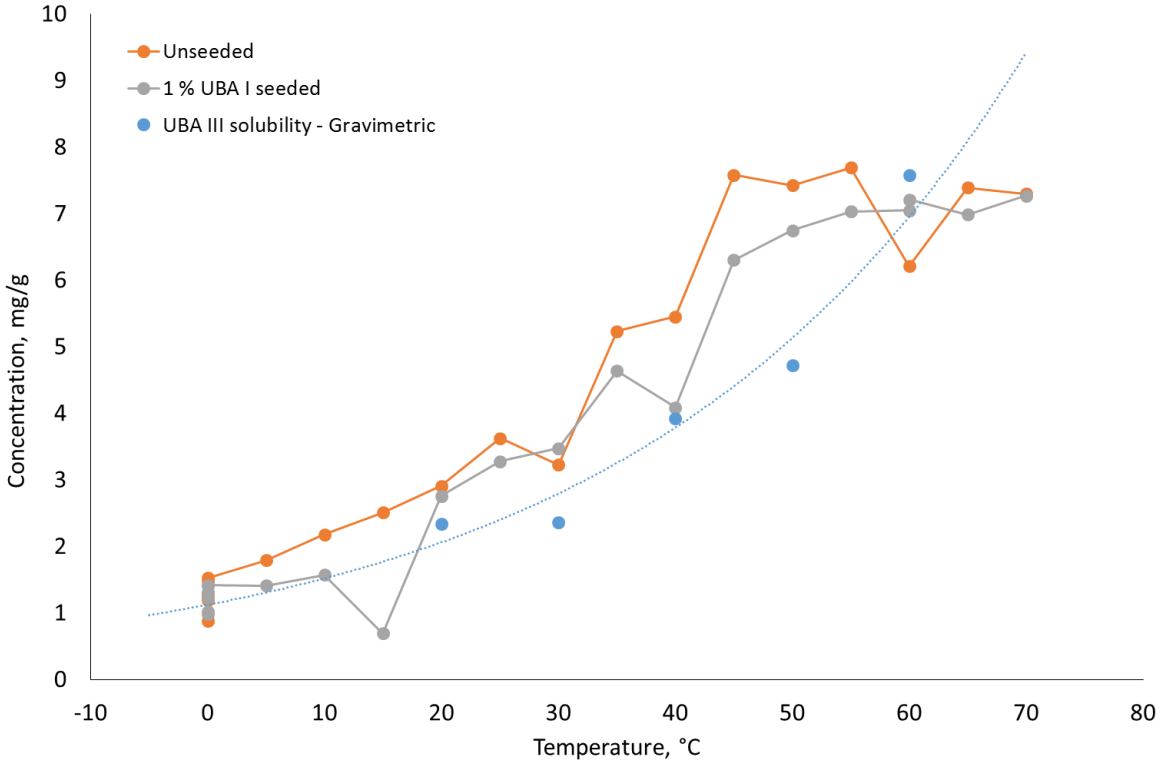

Figure 5.38: Concentration profiles of the unseeded and 1 % UBA form I seeded Easymax cooling crystallisations of UBA from IPA; 0.5 °C min^{-1} cooling rate.

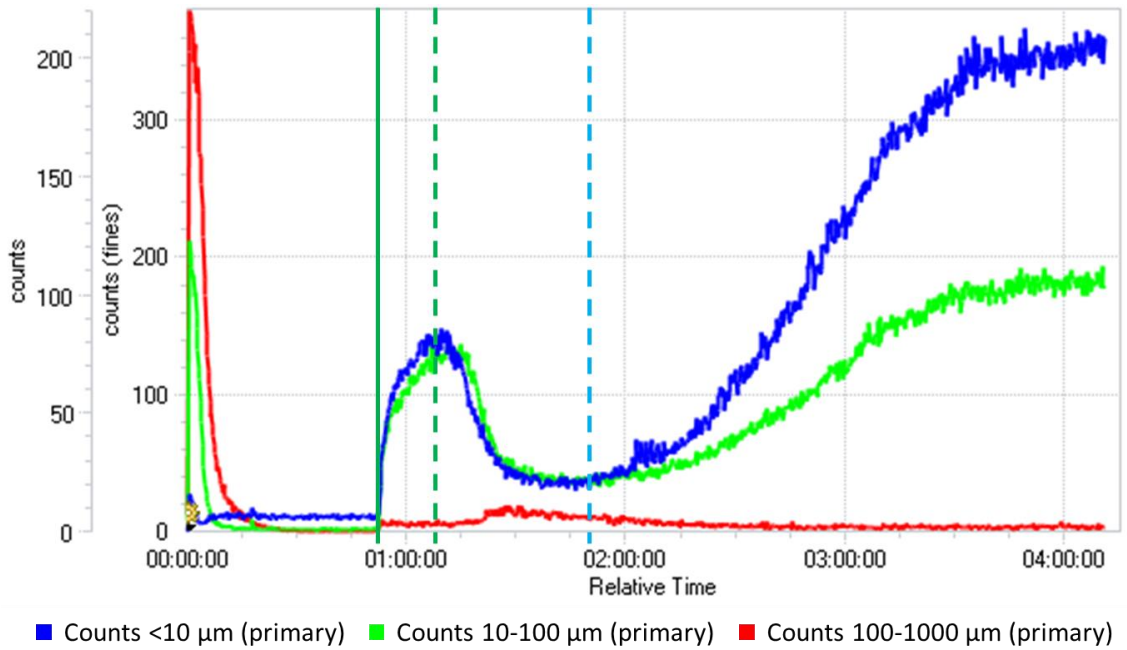

Figure 5.39: FBRM trace obtained from the 5 % UBA form I seeded Easymax cooling crystallisation of UBA from IPA; 0.5 °C min^{-1} cooling rate. Solid green line shows seed addition, dashed green line represents the end of seed hold and the dashed blue line shows nucleation event.

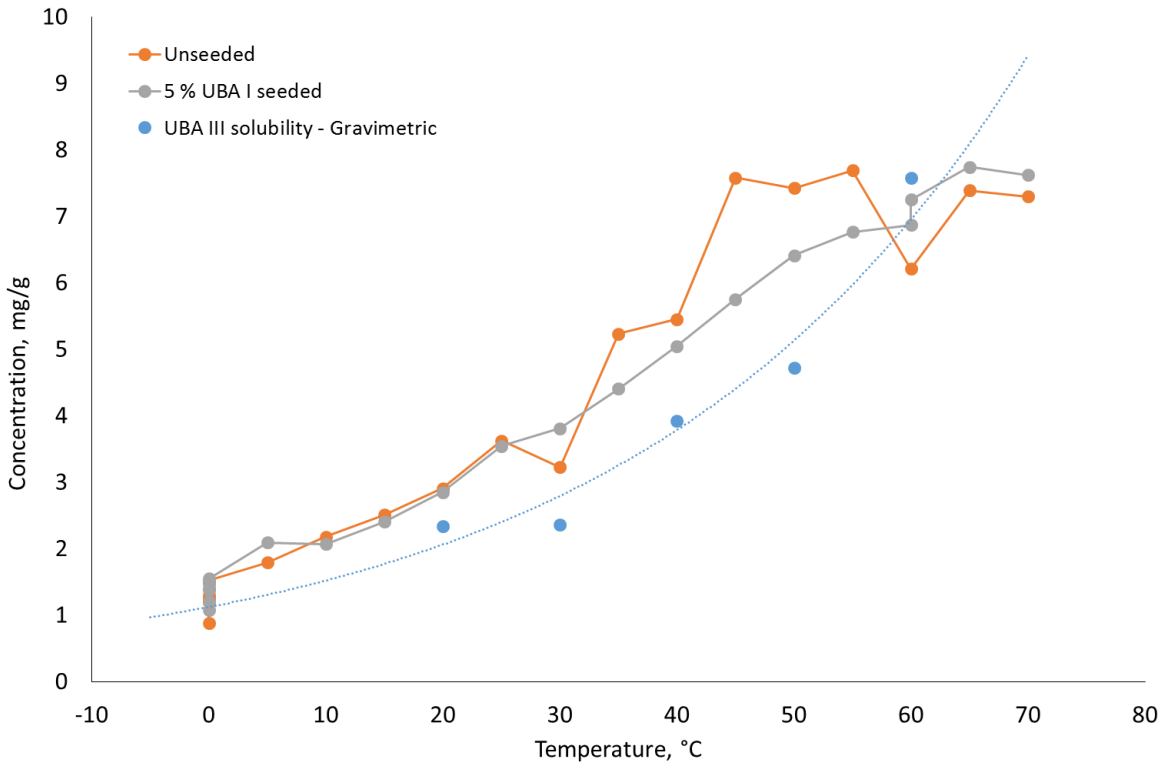

Figure 5.40: Concentration profiles of unseeded and 5 % UBA form I seeded Easymax cooling crystallisations with a 0.5 °C min-1 cooling rate.

When a 5 % seed loading was used (Figure 5.39) the FBRM trace suggests that a small level of secondary nucleation may have occurred during the seed hold, indicated by a gradual increase in counts for chord lengths of <10 – 100 μm (blue and green lines). Once the seed hold ends, and the cooling continues, the number in counts corresponding to this size range significantly reduces. This may be due to growth of the particles upon cooling, as the counts corresponding to larger particles (100-1000 μm) increase as the counts for the smaller chord lengths decrease, or this may be arising from the formation of agglomerates in the system. The blue dashed line however, signifies a point at which a nucleation event occurs, as is seen in the 1 % seed loading experiments and the unseeded experiments. Again, the temperature at which this nucleation event occurs is approximately 40 °C.

When looking at the concentration profile for the 5 % UBA form I seeded crystallisation it can be seen that upon the addition of seed and for the duration of the seed hold the concentration of the solution appears to be reduced, suggesting absorption of some of the supersaturation by the seed (Figure 5.40). Once cooling is resumed the concentration reduces gradually and follows the line of the solubility curve for the duration of the process unlike with the unseeded system where a large drop in concentration is observed around 45 °C. This, in tandem with the FBRM trace, suggests that upon addition of the seed secondary nucleation occurs within the system resulting in the observed reduction in solution concentration.

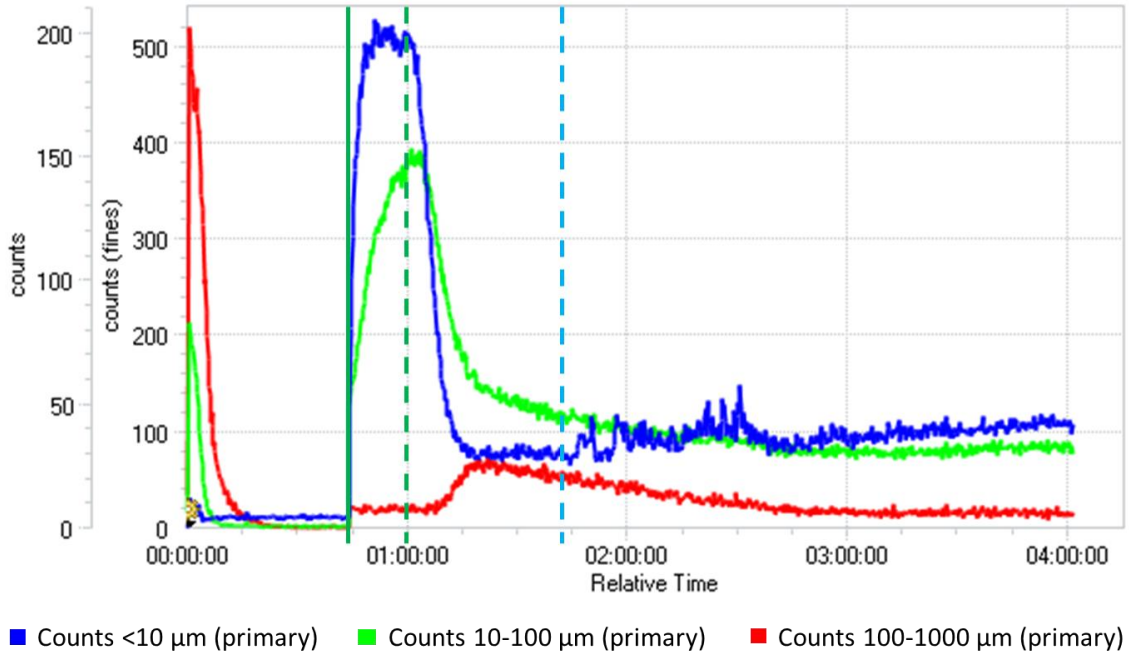

Figure 5.41: FBRM trace obtained from the 20 % UBA form I seeded Easymax cooling crystallisation of UBA from IPA; 0.5 °C min^{-1} cooling rate. Solid green line shows seed addition, dashed green line represents the end of seed hold and the dashed blue represents when the system reaches 40 °C.

When a seed loading of 20 % is used the FBRM data shows a significant increase in the number of counts upon the seed addition which then level out and remain fairly constant for the duration of the seed hold. Once cooling resumes, post seed hold, the

counts corresponding to chord lengths of <10 – 100 μm drop significantly over a short period of time (approximately 15 minutes). It can be seen that during this time the counts for the larger chord lengths (100 – 1000 μm) increase. The nature of this trend suggests that upon reinitiating the cooling process the seed crystals begin to grow, or agglomerate, resulting in a decrease of the number of smaller particles and an increase in the number of larger ones. As the cooling continues the counts for the larger particles starts to slowly decrease and the counts for fines (< 10 μm) begin to increase slowly. This may be due to secondary nucleation within the system increasing the number of fines as well as breakage and attrition of the larger crystals. The vertical blue dashed line in Figure 5.41 represents when the system reaches 40 °C, the temperature at which spontaneous nucleation occurs in the unseeded system. Unlike with the lower seed loading experiments, at this point there is no significant increase in the number of counts suggesting that with this high seed loading of 20 % the system is encouraged to deposit the supersaturation on the seeds via growth of the seed particles as opposed to acting similarly to when no seeded is added.

The concentration profile of the 20 % seed loading experiment with UBA form I seeds can be seen in Figure 5.42. A significant drop in solution concentration can be seen at 60 °C post seed hold, suggesting that the seed crystal must be growing or some secondary nucleation must be taking place within the system. Upon the resumption of cooling of the system, the concentration is shown to reduce slowly and follow the same line as the solubility curve.

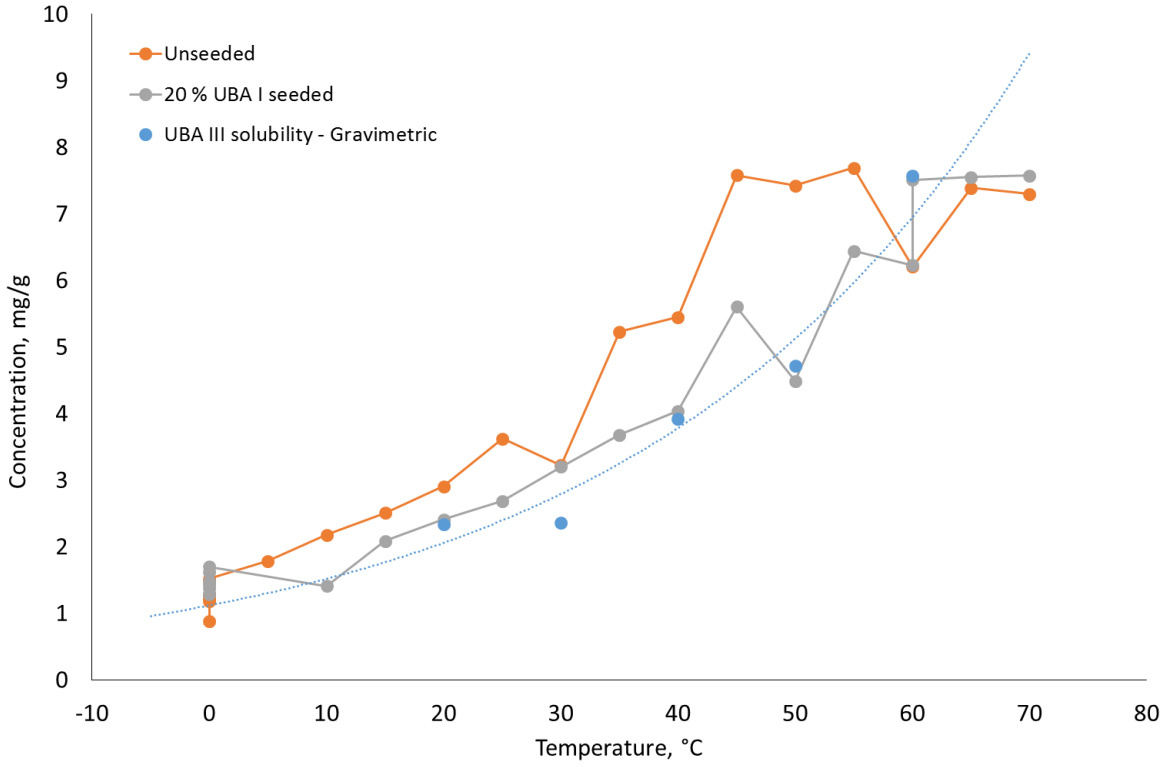

Figure 5.42: Concentration profile of unseeded and 20 % UBA form I seeded Easymax cooling crystallisations of UBA from IPA with a 0.5 °C min^{-1} cooling rate.

These results suggest that upon the increase of seed loading for this system the seeds start to be more active. When a low seed loading (1 %) was used the system appeared to behave as if no seed had been introduced. However, upon increasing the amount of seed added the seeds begin to take to the solution and growth and secondary nucleation occurs. Although even the 1 % seed loading resulted in the access of UBA form I selectively, the seeds did not behave as would be desired in a robust seeded cooling crystallisation, with a significant nucleation event occurring at a similar temperature as the unseeded systems. Increasing the seed loading appears to allow for growth of the seeds and some secondary nucleation to occur within the system, as well as solid form control.

The same FBRM trends are seen in the UBA form I seeded crystallisations using a 1 °C min^{-1} cooling rate (see Appendix Figure 9.21 to Figure 9.23). When a seed loading of 1 % is used the seed appears not to take and no seed growth or secondary nucleation is observed during the seed hold or once the system resumes cooling. There is a significant increase in the counts for the number of fines after the system has been cooled for approximately 20 minutes, which corresponds to a temperature of 40 °C, the same temperature at which the unseeded system nucleated. When a seed loading of 5 % is used there is again an increase in the number of counts for the smaller particles within the system during the seed hold, suggesting secondary nucleation. Once the cooling process is resumed the counts for the finer particles reduces and there is a slight increase in the counts for larger particles, suggesting growth of the particles within the system. However, this seed loading is again seen to be insufficient to control the system completely, and at 40 °C there is a significant increase in counts corresponding to a nucleation event, as was seen in the unseeded crystallisations and the 1 % seed loading experiments. When the seed loading is increased to 20 % a similar outcome is seen as with the slower cooling rate. Upon the addition of seeds some secondary nucleation occurs shown by the gradual increase in the number of counts during the seed hold. When the seed hold ends and the cooling is continued the number of fines within the system reduces significantly whilst there is an initial increase in the counts corresponding to larger particles; this shows that upon cooling of the system, growth is the predominant factor. Over time the counts corresponding to the larger particles start to reduce showing breakage and attrition occurring within the vessel and the number of fines begins to slowly increase. All three seed loadings gave solid form control and UBA form I was accessed, however the control over nucleation of the system was not accessed at the lower seed loadings and a seed loading of 20 % was required to realise this.

There could be several reasons as to why the lower seed loadings resulted in the seeds not taking to the solution, for example it may be due to there not being sufficient surface area available for seed growth and this was overcome by increasing the seed loading. It could also be due to a large percentage of the seeds having damaged or amorphous surfaces, resulting in a high proportion of the seeds not taking to the solution; increasing the seed loading increased the number of seeds available for growth.

5.6.2 UBA Form III Seeded Easymax Cooling Crystallisation

When UBA form III seeds were used with a 0.5 °C cooling rate, solid form control was only accessed when a seed loading of 20 % was used. When 1 % and 5 % seed loadings were used the resultant product was UBA form III with UBA form I impurities. The FBRM data for the 1 % and 5 % seed loading experiments suggests that the added seed did not take to the solution and did not undergo any growth or induce secondary nucleation. It can be seen in Figure 5.43, where the 1 % seed loading was used, that during the seed hold and even once the cooling resumes, no change in the number of counts is observed. This suggests that adding the seed (vertical solid green line) has no observable effect on the system, which then proceeds to act as if unseeded. The FBRM counts remain constant for the duration of the seed hold (vertical dashed green line) and during the resumption of the cooling, until the vertical dashed blue line. At this point there is a sudden and significant increase in the number of counts, especially for the smaller sized particles (blue and green lines), indicating a nucleation event within the system. This nucleation event occurs approximately 40 minutes after the seed hold has ended and the cooling process has resumed, corresponding to a temperature of approximately 40 °C. This temperature is similar to that seen for the spontaneous nucleation event in the unseeded crystallisation discussed earlier and implies that the seed is not taking to the solution and the system is acting as if unseeded.

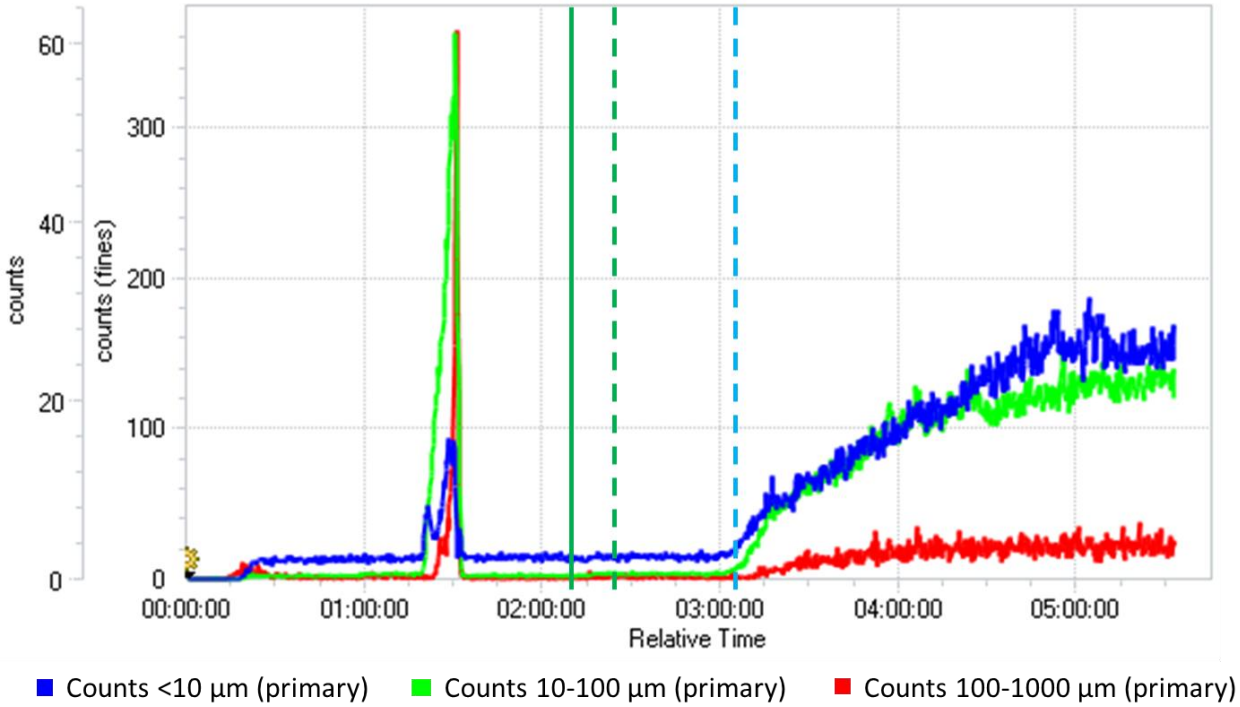

Figure 5.43: FBRM trace obtained from the 1 % UBA form III seeded Easymax cooling crystallisation of UBA from IPA; 0.5 °C min^{-1} cooling rate. Solid green line shows seed addition, dashed green line represents the end of seed hold and the dashed blue represents nucleation event.

When a 5 % seed loading is used, the same situation is observed as for a seed loading of 1 % (Figure 5.44). Upon the addition of the seed crystals the FBRM counts increase as would be expected as there is now solid within the system. During the seed hold

(between the solid and dashed vertical green lines) the counts remain constant showing that no growth of the seeds is occurring as well as no secondary nucleation. Once the cooling process is continued, the FBRM counts remain constant until the dashed blue line, where there is a sudden and significant increase in the counts for the smaller particles (blue and green lines), suggesting a nucleation event. The temperature at which this event happens is approximately 50 °C. This is 10 °C higher than was seen with the 1 % seed loading experiment, however due to there being no change in FBRM counts until this point in the crystallisation process it therefore implies that upon the addition of the seed crystals to the system they do not take and the system largely mimics the behaviour of the unseeded system.

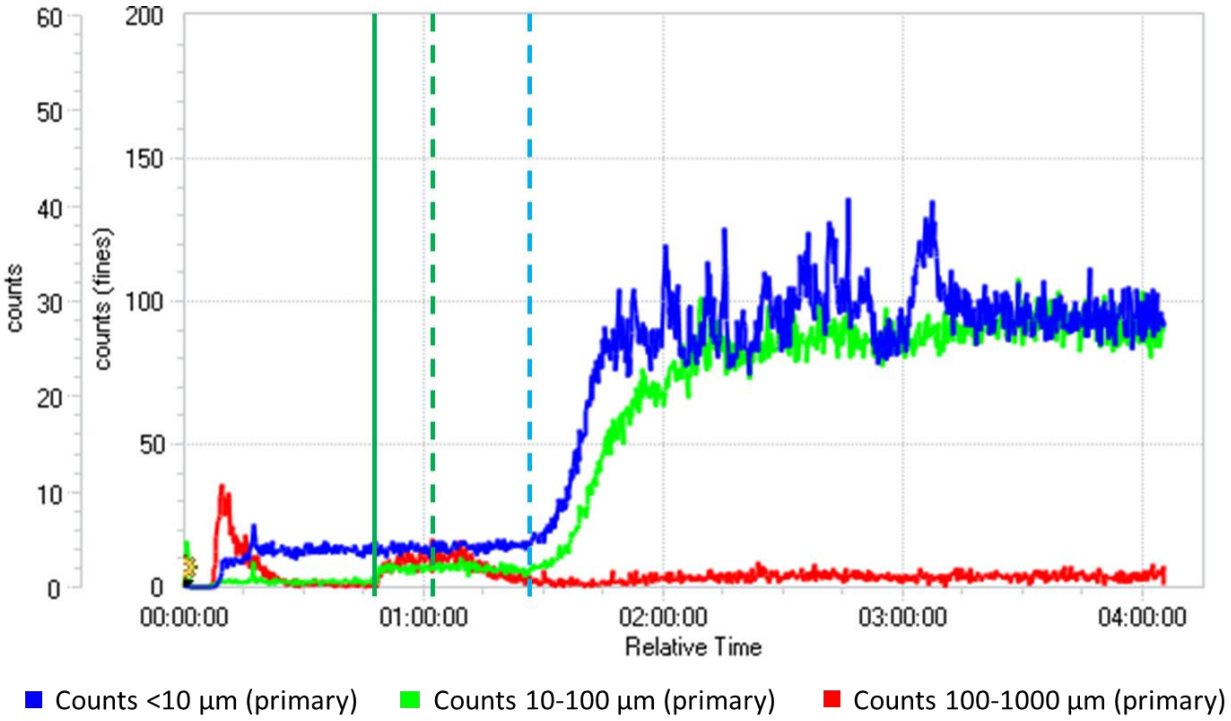

Figure 5.44: FBRM trace obtained from the 5 % UBA form III seeded Easymax cooling crystallisation of UBA from IPA; 0.5 °C min^{-1} cooling rate. Solid green line shows seed addition, dashed green line represents the end of seed hold and the dashed blue represents nucleation event.

Upon the addition of a 20 % seed loading the resultant solid form was pure UBA form III, suggesting that solid form control had been achieved by the introduction of the seed crystals. When looking at the FBRM data obtained for the 20 % seed loading experiment, however, it can be seen that the system behaves in a very similar manner to both the 1 % and 5 % seed loading experiments (Figure 5.45). Upon the addition of the seed and during the 15 minute seed age no change in the FBRM counts is observed. The counts remain upon the recommencement of the cooling process until the blue dashed line, where the counts start to increase. The increase in counts is not as sudden as with the smaller seed loadings, however the temperature at which it occurs is approximately 40 °C, as seen with the other seed loadings and the unseeded system. This suggests that

again, the seeds are not taking to the solution and the system acts largely as if the seed crystals are not present.

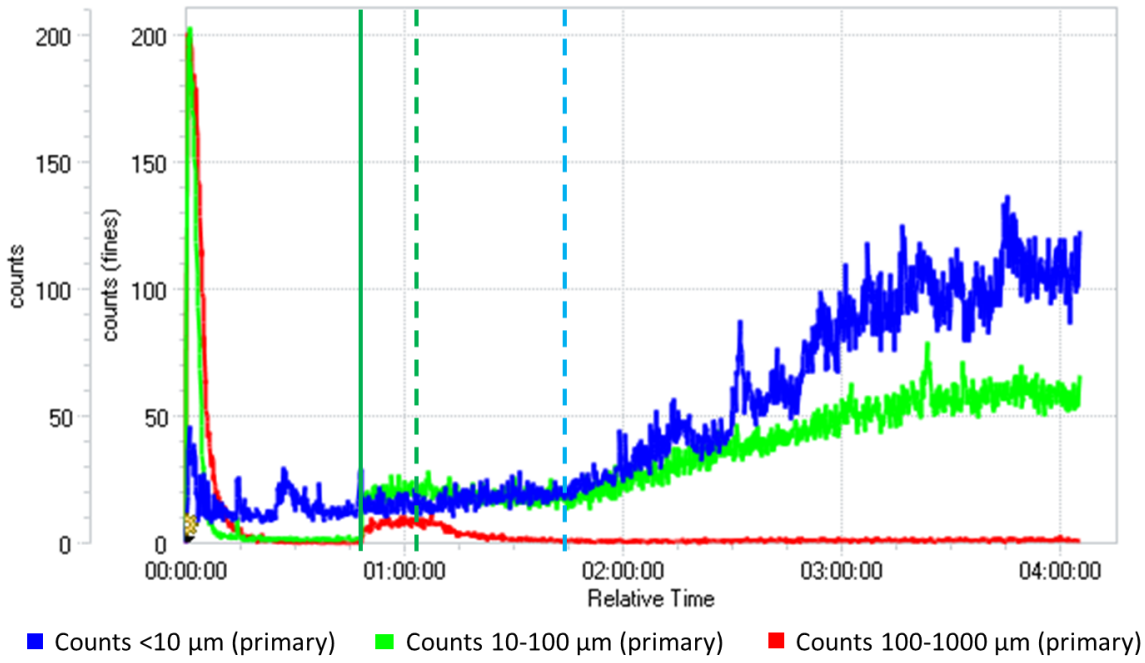

Figure 5.45: FBRM trace obtained from the 20 % UBA form III seeded Easymax cooling crystallisation of UBA from IPA; 0.5 °C min^{-1} cooling rate. Solid green line shows seed addition, dashed green line represents the end of seed hold and the dashed blue represents nucleation event.

When looking at the concentration profiles (Figure 5.46) for the three UBA form III seeded experiments and the unseeded experiment when a 0.5 °C min^{-1} cooling rate was used, it can be seen that for each of the cooling crystallisations display very similar concentration profiles both to one another and to that of the unseeded system. For the seeded experiments a solution sample was taken at 60 °C before the seed addition and then again at 60 °C after the 15 minute seed hold. It can be seen that for all seed loadings there is no significant decrease in concentration between these two points, suggesting that during the seed hold there is no desupersaturation of the system. This further confirms what was observed in the FBRM traces: upon the addition of the seed crystals, they do not take to the solution and none of the supersaturation within the system is adsorbed. All three concentration profiles exhibit a significant reduction in concentration between 50 ° and 40 °C, similar to what is seen for the unseeded system. This aligns well with the FBRM as at these temperatures there is a significant increase in counts suggesting a nucleation event has occurred. The similarity in the concentration profiles for all three seed loadings, as well as with the unseeded crystallisation indicate that these seeding experiments were unsuccessful and did not proceed as would be expected in 'normal' seeded crystallisations.

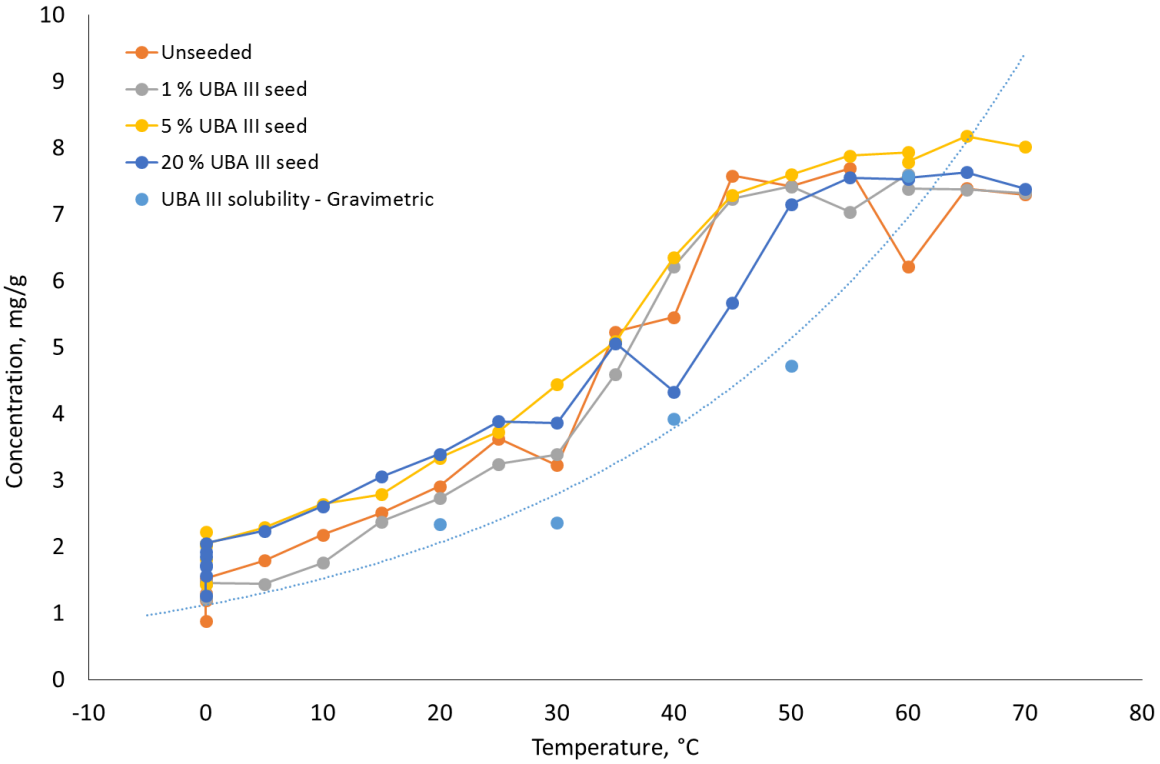

Figure 5.46: Concentration profiles for the three UBA form III seeded and the unseeded Easymax cooling crystallisation of UBA from IPA with a 0.5 °C min^{-1} cooling rate.

Although the seeds appear not to have taken in the solution, resulting in no growth of the seed crystals and no secondary nucleating events, the high seed loading did appear to enable solid form control and access pure UBA form III. In successful seeding experiments, the addition of seeds tends to result in either growth of the seed particles by absorbing the supersaturation, or induction of secondary nucleation of the desired solid form (usually the same form as the seed type). Solid form control is usually accessed via the growth of the seeds resulting in growth of crystals of that solid form, or by inducing secondary nucleation of the seed type. However, this is not the case for these seeding experiments; it can be seen that the addition of 20 % seed crystals does not cause growth or secondary nucleation. It can be postulated that the solid form control gained with the high seed loading is more of a secondary effect, with the large amount of UBA form III present when the system 'spontaneously' nucleates resulting in a larger amount of UBA form III being nucleated due to templating effects and 'drowning out' the UBA form I nucleation, as was discussed in the ethanol mediated seeding experiments (Section 5.4).

When the seeding experiments were conducted for the Easymax cooling crystallisations using a cooling rate of 1 °C min^{-1}, it was shown that both seed loadings of 5 % and 20 % gave rise to UBA form III selectively, unlike with the slower cooling rate of 0.5 °C min^{-1} which required a seed loading of 20 %. When looking at the FBRM obtained from these seeded experiments (see Appendix Figure 9.25 - Figure 9.27), the trends observed are the same as those observed with the slower cooling rate. Upon addition of the seed crystals, regardless of the seed loading used, no growth or secondary nucleation events

were observed. The FBRM counts remain constant for the duration of the seed hold and continued to remain unchanged once the cooling process was resumed, up until a point at which all systems showed a significant increase in the number of counts for the finer particles. The point at which the three seeded systems displayed this increase in counts was very similar for each seed loading and came at approximately 40 °C. As discussed previously, the unseeded system undergoes spontaneous nucleation at approximately 40 °C, suggesting that the seed crystals are not taking to the system and the crystallisation is displaying similar behaviour to the unseeded system.

Again, when looking at the concentration profiles for the three seeded systems with a 1 °Cmin^{-1} cooling rate they are all very similar and display a very similar trend to that of the unseeded system (Figure 5.47). Regardless of the seed loading used, there is no significant reduction in the concentration of the system after the seed hold (as seen by the similarity in values for the concentrations taken before seed addition and after the seed hold, both at 60 °C). This suggests that upon the addition of the seed particles no desupersaturation occurs within the systems. The concentration profiles continue to follow the same trend as the unseeded system, all displaying a drop in solution concentration between 50 °C and 40 °C as a result of the nucleation events observed in the FBRM data.

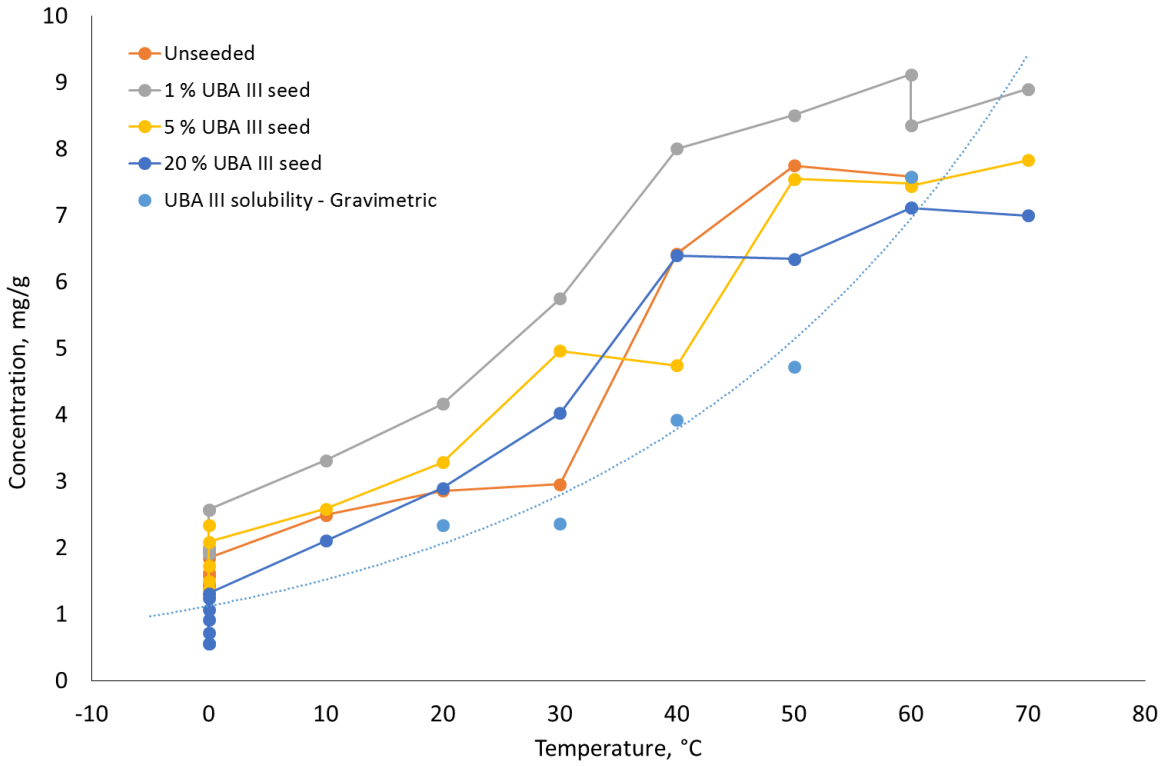

Figure 5.47: Concentration profiles of UBA III seeded and unseeded Easymax cooling crystallisations of UBA from IPA with a 1 °C min^{-1} cooling rate.

It can be concluded that when seeding with UBA form III the seed particles did not take to the solution and as a result no growth or secondary nucleation events occurred. It was seen however that a smaller level of seed loading was required to access pure UBA form III when the faster cooling rate of 1 °C min^{-1} was used. This is likely due to the

presence of UBA form III seeds encouraging the nucleation of that form over the nucleation of form I once these nucleation events occur. As the seed loading is increased a larger amount of the desired form is present and 'drowns out' the nucleation of the unwanted form I. During the crystallisation process the transformation between form III and form I is likely to occur, and so a faster cooling rate will reduce the chance for this phase transformation resulting in a lower seed loading being required. However, it must be noted that when no seed was used, UBA form III was accessed selectively with a cooling rate of 1 °C min^{-1}, but when 1 % seed was added a mixture of form III and form I was obtained. This suggests that the outcome of the crystallisation is serendipitous due to the stochastic nature of the nucleation events occurring, with and without seeding. In order to establish confidently if the seeding does give solid form control for these systems repeat experiments need to be conducted.

5.6.2.1 UBA Form III Seeded Easymax Cooling Crystallisations with Overnight Hold

Due to pure UBA form III being accessed using a 20 % seed loading with both the 0.5 °C min^{-1} and 1 °C min^{-1} cooling rates, as well as with a 5 % seed loading for the faster cooling rate, it was hypothesised that solid form control using a lower seed loading with a faster cooling rate occurs due to their being less time for UBA form III to form I conversion to occur within the system. With this in mind several experiments, seeded and unseeded, were conducted in order to investigate the effect of an overnight hold at the final temperature on resultant solid form. The experimental parameters and polymorphic outcome for these experiments is summarised in Table 5.8.

Table 5.8: Summary of UBA form III seeded and unseeded Easymax cooling crystallisation of UBA from IPA experiments with and without an overnight hold.

Cooling rate	Seed Loading	Overnight hold?	Outcome
0.5 °C min^{-1}	0 %	Yes	UBA III
0.5 °C min^{-1}	0 %	No	UBA III & I
0.5 °C min^{-1}	20 %	Yes	UBA III
0.5 °C min^{-1}	20 %	No	UBA III
1 °C min^{-1}	0 %	Yes	UBA III & I
1 °C min^{-1}	0 %	No	UBA III
1 °C min^{-1}	5 %	Yes	UBA III & I
1 °C min^{-1}	5 %	No	UBA III

For the 0.5 °C min^{-1} cooling rate, both the unseeded experiment and that with 20 % UBA III seed loading were repeated allowing for the system to hold at the final temperature (0 °C) for 16 hours (overnight). In contrast to the unseeded crystallisation

with no overnight hold, the unseeded system with overnight hold resulted in pure UBA form III, not a mixture of form I and form III (Figure 5.48). It initially seems unexpected that the system without the extended hold period produced a mixture of the metastable form and the stable form, whereas the system with the 16 hour hold resulted in pure form III. However, this is likely an artefact of the lack of control over solid form within the unseeded system and not a direct result of the experimental time. When a 20 % UBA form III seed loading was used with no extended hold, UBA form III was produced. When the same experiment was repeated, but with the 16 hour hold period, UBA form III was still accessed. However, due to the access of pure form III from the unseeded system with the extended hold period it cannot definitively be concluded that the presence of seed within the system is what is resulting in the solid form control.

It was previously discussed (Section 5.6.2) that upon the addition of the UBA form III seed to the system, the seed did not take to the solution and no growth or secondary nucleation occurred due to the presence of the seed; the crystallisation proceeded as if unseeded. It cannot therefore be concluded that the presence of the seed does offer a level of control over the solid form and repeat experiments are required to asses this. Solid form control may not be being accessed by the present of the seed crystals and the polymorphic outcome may be due to the stochastic, uncontrolled nature of the nucleation occurring within the system.

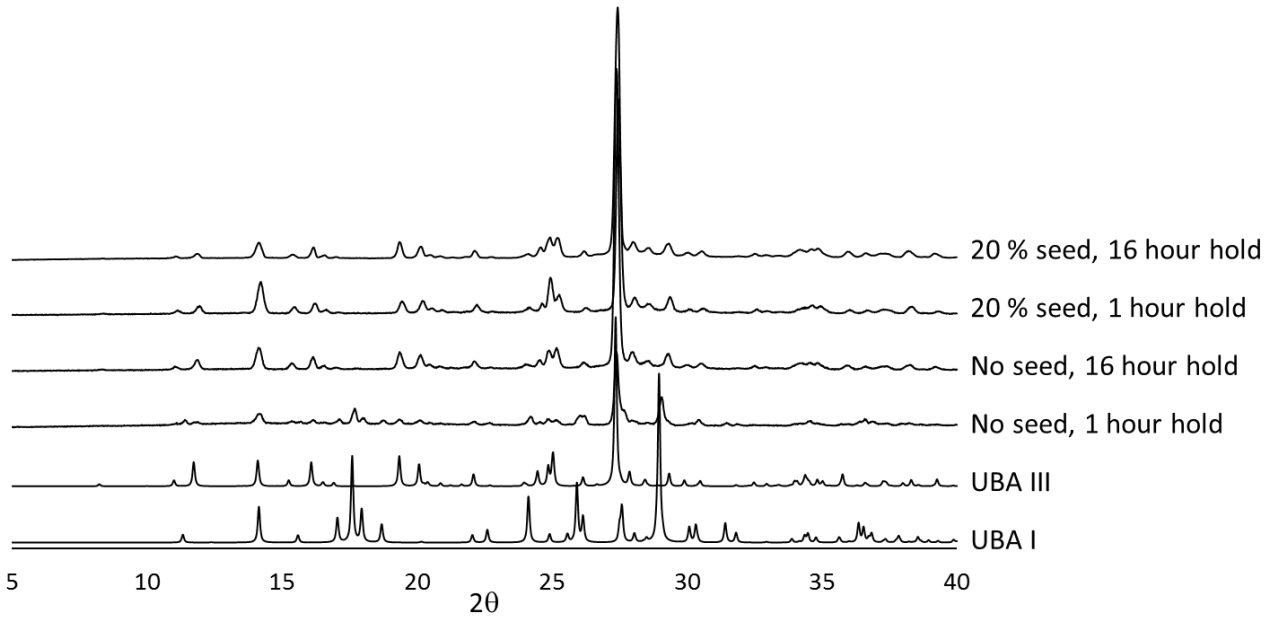

Figure 5.48: PXRD patterns of 0.5 °C min^{-1} Easymax cooling crystallisations of UBA from IPA, with and without UBA form III seed.

When a cooling rate of 1 °C min^{-1} was used, the unseeded experiment with no overnight hold gave rise to UBA form III, with the unseeded experiment with an overnight hold producing a mixture of UBA form I and form III. This suggests that during the overnight hold, partial conversion of form III to form I occurred. The introduction of 5 % UBA form III seed gave rise to pure form III being accessed in the experiment with no

overnight hold. The experiment was repeated, but with an extended hold period at the end of the process (16 hours); the result of this experiment was a mixture of UBA form III and form I, again suggesting that during the overnight hold some of the form III underwent a conversion to yield form I. This conversion could be due to a natural solution-mediated phase transition occurring within the system, or could be a result of UBA form I nucleation occurring during the crystallisation process. As previously discussed, it cannot be confidently assumed that the presence of seed is resulting in solid form control, as opposed to the stochastic and uncontrolled nature of the nucleation within the system, which is giving rise to these results. Further repeat experiments would be required to test the seeding and to see if it does result in robust solid form control.

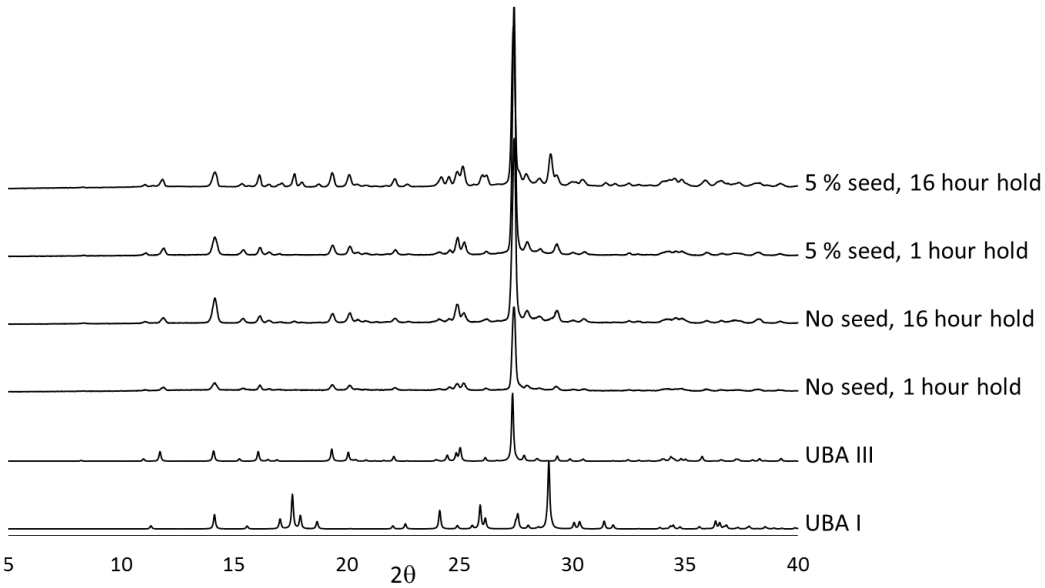

Figure 5.49: PXRD patterns of 1 °C min^{-1} Easymax cooling crystallisations of UBA from IPA, with and without UBA form III seed.

5.7 Continuous Crystallisation of UBA

Due to the limited success of pure UBA form III formation in batch crystallisation using both ethanol and IPA as solvent media, but using the information obtained from these, investigations into continuous crystallisation were conducted. Two tubular continuous crystallisers were used for this work: the COBC and the KRAIC. Both the ethanol and IPA solvent systems were taken forward into the continuous crystallisation studies with ethanol being used in both the COBC and KRAIC and IPA being used in the KRAIC.

5.7.1 Continuous Crystallisation of UBA from Ethanol in the COBC

The continuous crystallisation of UBA from ethanol was investigated using the COBC. For this study three experiments were conducted to attempt to optimise the crystallisation. The experimental parameters for each experiment are summarised in Table 5.9.

The experimental parameters used for the COBC (Table 5.9), such as the flow rate and oscillation parameters, were taken from previous work conducted using this set-up.[189] The chiller temperatures were chosen based on the batch cooling crystallisation process as well as the concentration of UBA used (11.43 mg/g, T_{sat} = 57 °C). Three experiments were conducted in an attempt to optimise the system and access UBA form III, with changes made to the straight temperatures and solution saturation.

It can be seen that the Reynolds oscillatory (Re_o) number, the Reynolds net flow (Re_n) number and Strouhal number are 1737, 52 and 0.1 respectively, indicating that plug flow should be achieved in these experiments: Re_o and Re_n must be equal or greater than 100 and 50 respectively and the Strouhal number (St) must be equal to or less than 0.5.

5.7.1.1 COBC 1 – UBA from Ethanol

During COBC 1 nucleation was not achieved within the first residence time (RT); after 44 minutes (RT2) the temperature for chiller 3 (straights 7-10) was reduced to 20 °C in an attempt to induce nucleation within the crystalliser. After 52 minutes a single crystal was observed in straight 10, with multiple small crystals being observed in straights 9-12, the end piece and on the filter paper 54 minutes into the experiment time. However, at 56 minutes into the experiment, crystallisation was observed to the left of the feed inlet, in the bellows connector pipe. This indicated that the membrane between the bellows and the crystalliser was no longer intact and feed solution was entering the pipe, cooling down and crystallising. The presence of these crystals either induced nucleation in straight 1 of the COBC, or were transferred from the bellows to the COBC. However, these crystals then dissolved back into solution in straights 2-4. After 1 hour and 5 minutes crystals were observed in straight 7. Due to the undesired crystallisation occurring in the bellows pipe, the process was terminated at 1 hour and 6 minutes (after two RTs), resulting in solid from RT 1 only being collected (during RT2).

The solid collected was analysed using PXRD and the results showed that UBA form I had been accessed during this process, not the desired UBA form III (Figure 5.50).

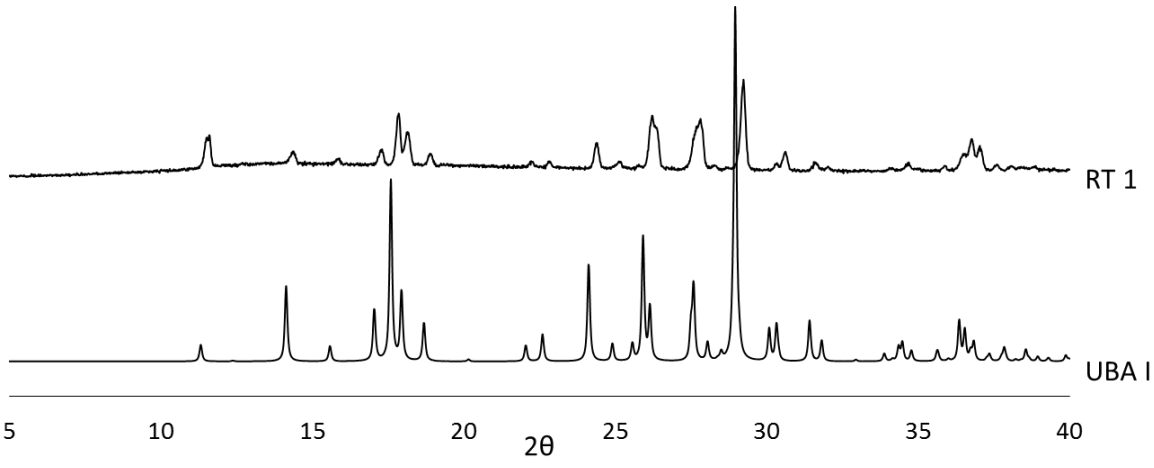

Figure 5.50: PXRD pattern of solid sample from RT 1 of COBC 1.

Table 5.9: Summary of COBC continuous crystallisation experimental parameters.

Experiment	Concentration (mg/g)	Flow rate (ml min^{-1})	RT (mins)	Oscillation					Temperature (°C)				
				Frequency (Hz)	Amplitude (mm)	Re_o	Re_n	St	Feed	Straight 1 & 2	Straight 3 - 6	Straight 7 - 10	Straight 11 & 12
COBC 1	11.43	50	33.2	2	25	1737	52	0.10	70	60	45	30/20*	20
COBC 2	11.43								70	60	45/30†	30/20††	20/15‡
COBC 3	11.9								70	60	30	20	15

* Temperature reduced to 20 °C after 44 minutes to induce nucleation
† Temperature reduced to 30 °C after 43 minutes to induce nucleation
†† Temperature reduced to 20 °C after 38 minutes to induce nucleation
‡ Temperature reduced to 15 °C after 38 minutes to induce nucleation

5.7.1.2 COBC 2 – UBA from Ethanol

Due to the crystallisation occurring in the bellows in COBC 1, a new membrane was fitted to prevent feed solution getting into this area of the set up. A second COBC experiment was then run, initially with the same set up as the first (Table 5.9). After 38 minutes no nucleation had occurred within the system and as a result chiller 3 (straights 7-10) and chiller 4 (straights 11-12) temperatures were reduced to 20 °C and 15 °C respectively. After 43 minutes there was still no presence of crystallisation in the crystalliser and so chiller 2 (straights 3-6) was reduced to a temperature of 30 °C. As no nucleation had occurred in the system at 54 minutes, the temperatures in chiller 3 (straights 7-10) and 4 (straights 11-12) were further reduced to 10 °C. This reduction in temperature worked as desired, inducing nucleation within the system; at 55 minutes, crystals were observed in straights 8-12. Correspondingly, the temperatures for chiller 3 (straights 7-10) and chiller 4 (straights 11-12) were subsequently raised again to 20 °C and 15 °C.

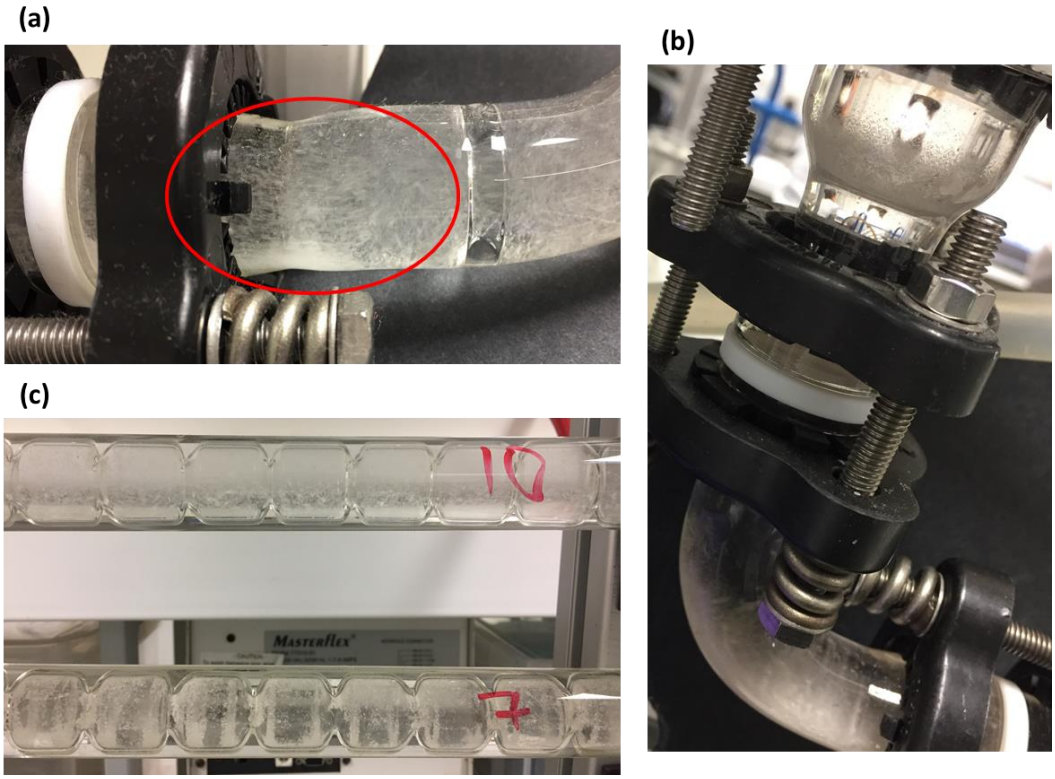

Figure 5.51: Pictures from COBC 2: (a) sedimentation in bend between straights 10 and 11, (b) crystallisation in bellows, (c) encrustation in straight 7 and crystallisation in straight 10.

During the run, approximately 57 minutes into the process, issues with sedimentation were observed in some of the bends between straights, specifically the bend between straights 10 and 11 (Figure 5.51 (a)), with some slight sedimentation also occurring in the bend between straights 8 and 9. Such sedimentation can cause issues with subsequent blockages forming between the baffle constrictions, as well as resulting in a spread of the residence time distribution (RTD) and crystal size distribution (CSD). 1 hour into the crystallisation, sedimentation was observed in the exit tubing resulting in a significant amount of crystals remaining in the tubing and not being collected; again this

can cause blockages and a spread of RTD and CSD. It was also seen that, as with COBC 1, crystallisation had occurred in the bellow tubing, as a result of the membrane again breaking (Figure 5.51 (b)). A heat gun was used in an attempt to heat the solution and dissolve the solid, however this was unsuccessful. Any crystallisation induced in straight 1 due to the crystallisation in the bellows dissolved back into solution in the next few straights (2-4).

As the process continued, encrustation started to occur on the walls of straights 8 (1 hour and 5 minutes), 7 and 9 (1 hour 9 minutes), with the encrustation in straight 7 worsening with time (Figure 5.51 (c)). Throughout the duration of the run, the point at which nucleation/crystallisation first occurred within the crystalliser moved back from straight 8, to earlier straights. After 1 hour and 22 minutes a few fine crystals could be seen as early as straight 4. This shows that back mixing was occurring within the crystalliser set up, with the already present crystals inducing secondary nucleation earlier in the crystalliser. After three RTs (approximately 1 hour 40 minutes), the input was changed to pure ethanol and RT 3 solid was collected.

The collected solid was subject to PXRD analysis to investigate the solid form identity obtained in each RT. The PXRD data for each RT showed that again, UBA form I was accessed selectively, with no peaks corresponding to the desired metastable form, form III (Figure 5.52).

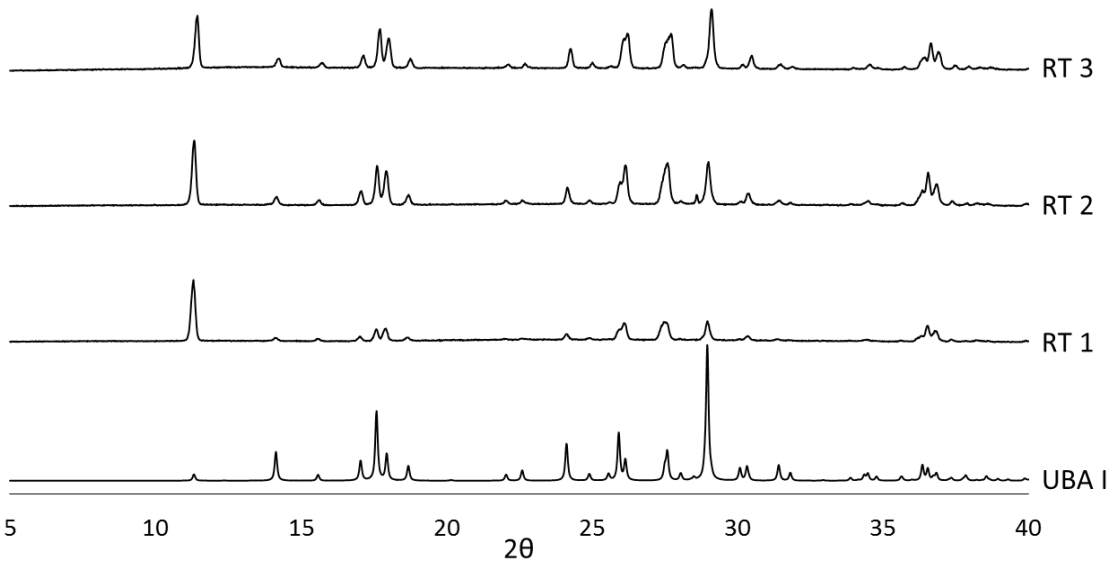

Figure 5.52: PXRD patterns of samples from each RT of COBC 2.

It can be concluded from both COBC 1 and COBC 2 that a lower temperature is required in the later straights in order to induce nucleation within the system. Each system gave rise to the thermodynamically stable form selectively, unlike in the batch crystallisation set up which showed more selectivity towards the metastable form. There could be several reasons why this is the case. The crystallisation kinetics are likely to be significantly altered upon transfer of the crystallisation from relatively small scale batch experiments to larger scale continuous crystallisation. This could result in the MSZW for

each solid form of UBA being altered and hence the point at which each form will nucleate may be significantly different. Once initial nucleation has occurred within the system, the COBC is then self-seeded. As a result if any form I has nucleated initially in the system the process will then be seeded with this thermodynamically stable form.

5.7.1.3 COBC 3 – UBA from Ethanol

Due to the selective formation of UBA form I in the two previous COBC runs, the temperature of straights 3 - 12 were set to the final temperatures at which the straights in COBC 2 were set (Table 5.9). This was done in an attempt to nucleate the system earlier in the crystalliser, as well as induce the nucleation at a lower temperature in an attempt to access the metastable form over the thermodynamic form.

The concentration used for this COBC run was also increased slightly (11.9 mg/g, T_{sat} = 58 °C) in the hope that a slightly higher level of saturation will also favour the formation of UBA form III. Once the process was started it became apparent that again there was some diffusion of the feed solution into the bellows piping, as after 47 minutes crystals could be seen in this tubing. Again, as with COBC 2, a heat gun was used in an attempt to heat up this area (as it is unjacketed) and this allowed for dissolution of the crystals. Although the transfer of feed to the bellows piping is unwanted and should be prevented by an adequate membrane, in this case the crystallisation was kept under control via the use of a heat gun for the duration of the crystallisation. After 40 minutes crystals were observed in straights 7 - 9 showing that nucleation had occurred within the system. After 52 minutes some very small crystals were observed in straight 1 due to the crystallisation occurring in the bellows; however, as with COBC 2, these were seen to dissolve back into solution over the next few straights. Once nucleation had initially occurred the solid loading in the crystalliser increased rapidly and after 55 minutes sedimentation of the crystals was observed to occur in the bends between straights 8 and 9 and 10 and 11 (Figure 5.53 (a)), as seen in COBC 2. Encrustation could also be seen on the walls of the crystalliser in straights 5-8 and crystals appeared to be settling towards the bottom of the straights in 9 - 12.

The issues with encrustation continued to worsen, with evidence of encrustation occurring in straights 3 - 4, much earlier in the crystalliser than seen with the previous run (Figure 5.53 (b)). The solid loading in straights 4 - 6 was observed to be significantly higher than that seen in COBC 2. As the crystallisation proceeded, it was seen that large ‘flakes’ of encrustation were detaching from the tubing walls in straight 4 and travelling through the crystalliser (1 hour 48 minutes). After three RT quantities of feed had been flowed into the crystalliser, the feed was switched to primer solution (pure ethanol) and solid from RT 3 was collected.

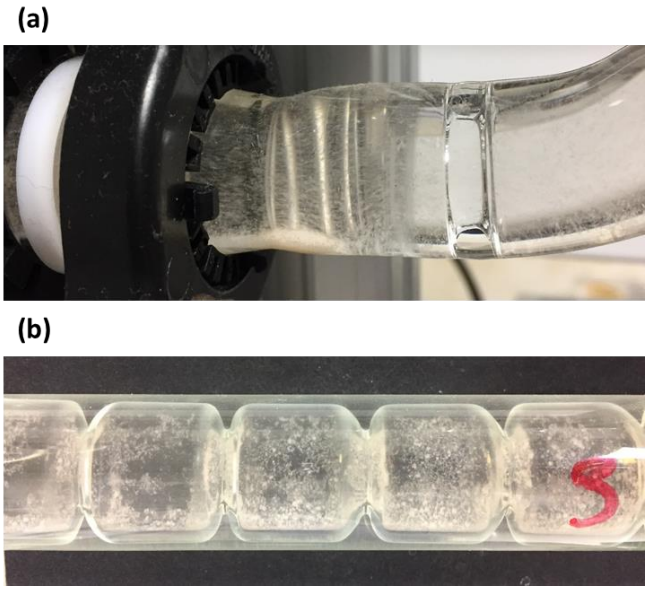

Figure 5.53: Pictures from COBC 3: (a) sedimentation in bend between straights 10 and 11, (b) encrustation in straight 3.

The PXRD data patterns obtained for product from all three RTs show peaks corresponding to both UBA form I and form III (Figure 5.54). The peaks corresponding to UBA form III are low intensity but show that under the conditions chosen for this COBC run, there is less selectivity towards UBA form I. This may be due to the slightly higher saturation used for this run, or the change in temperature of the straights, but does suggest that upon further optimisation UBA form III may be able to be accessed selectively from ethanol using the COBC.

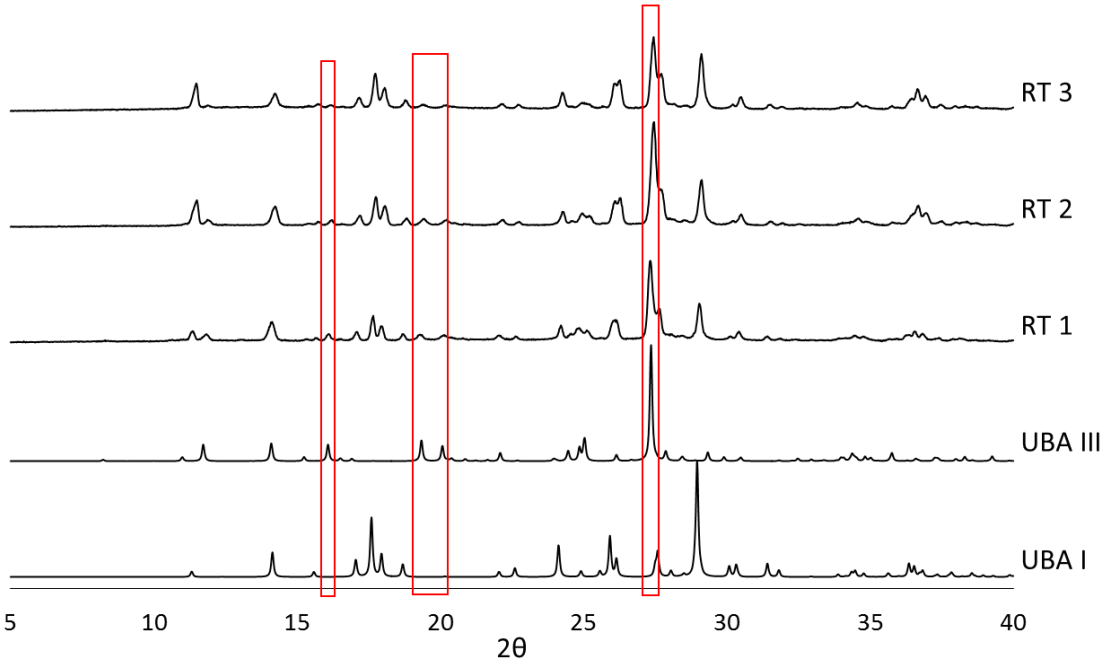

Figure 5.54: PXRD patterns of solid samples from each RT of COBC 3. Red boxes highlight peaks unique to UBA form III.

5.7.1.4 COBC Conclusions

Attempts to access UBA form III selectively from ethanol in continuous cooling crystallisation using the COBC were unsuccessful, with two out of the three experiments resulting in pure UBA form I and one resulting in UBA form I with small amounts of form III. It was seen that reducing the temperature of the later straights resulted in less selectivity towards the more stable form and more selectivity towards the metastable form, form III. Further experiments should investigate the effect of reducing the temperature of the straights further as well as different solution concentrations. Another approach that may enable form III to be accessed to a higher purity is reducing the RT of the system, and hence reducing the amount of time available for UBA form III to form I solution-mediated phase transformations. One way in which this could be achieved is by increasing the flow rate for the system. Another is by reducing the length of the crystalliser (i.e. removing straights).

One of the main issues seen in these experiments was the transfer of feed solution into the bellows tubing. This could be overcome in future experiments by implementing an adequate membrane in the system to prevent any feed solution entering the bellows tubing. The second issue was the observed encrustation on the crystalliser walls. The level of encrustation was worse in COBC 3 then COBC 2, spanning straights 3 - 8 versus straights 7 - 9. This may be a direct result of the increase in concentration of the feed resulting in a higher level of supersaturation in the system.

Experiments to investigate the transfer of the selective formation of UBA form III from batch cooling crystallisation using IPA as the solvent medium were not conducted in the COBC due to safety issues in this large volume crystalliser. However, the transfer of this system into continuous was investigated using the KRAIC, as was the ethanol solvent system (Section 5.7.3)

5.7.2 Continuous Crystallisation of UBA from Ethanol in the KRAIC

The KRAIC operates on the premise of segmented flow, using an immiscible carrier fluid to dissect the feed stream into discrete segments (or slugs). For this work tri-segmented flow was achieved using both an immiscible carrier fluid (Galden) and air. Three KRAIC runs of UBA in ethanol were conducted as part of the study to optimise the continuous crystallisation and to test the robustness of the system. The experimental parameters for each KRAIC run are summarised in Table 5.10. For this work, once the slugs left the mixer bath they were allowed to cool naturally, with no external temperature control being applied in the three coils.

5.7.2.1 KRAIC 1 – UBA from Ethanol

The first KRAIC run (KRAIC 1) was successfully run for four residence times (RTs), equating to a run time of approximately 36 minutes (RT = 9 minutes). The RT for the system was directly determined by the sum of the individual flow rates of the feed solution (peristaltic pump), Galden (gear pump) and air (gear pump). As the feed flow

Table 5.10: Summary of KRAIC continuous crystallisation experimental parameters.

Experiment	Solvent medium	UBA concentration (mg/g)	Flow rate (mL min-1)			Residence time	Set Temperature (°C)		
			Feed solution	Carrier Fluid	Air		Feed	Transfer tube	Mixer bath
KRAIC 1	Ethanol	12.42	4	4.18	4.18	9 minutes	70	65	60
KRAIC 2	Ethanol	11.43	4	4.18	4.18	9 minutes 50 seconds	75	65	60
KRAIC 3	Ethanol	11.43	4	4.18	4.18	11 minutes 30 seconds	75	70	65
KRAIC 4	IPA	7.5	4.2	4.18	4.18	9 minutes 40 seconds	75	70	65
KRAIC 5	IPA	7.5	4.2	4.18	4.18	11 minutes	75	70	65

rate was set to 4 mL min^{-1}, approximately 36 mL of feed solution should have been flowed through the system each RT. Solid from each RT was collected on pre-weighed filter paper to allow for solid form to be determined.

During the crystallisation process, nucleation was first witnessed at 8 minutes and 40 seconds into the run (in RT1). It was first observed in the 5th rung of coil 2. During the next few minutes the point of nucleation moved backwards, ending up in the bottom rung in coil 2; nucleation occurred earlier in the crystallisation process over time. After approximately 11 minutes the point of nucleation remained steady at the start of coil 2, implying that the system was reaching steady state. Once four RTs worth of feed had been pumped from the feed vessel (approximately 144 mL), the solution input was then changed back to heated (75 °C) primer solution (pure ethanol) to allow for the continuous process to carry on in order to collect the solid product from the fourth RT.

Figure 5.55 shows the PXRD patterns obtained for solid obtained from each RT for this run, and show that in this crystallisation the desired outcome was achieved and UBA form III was accessed selectively in each RT.

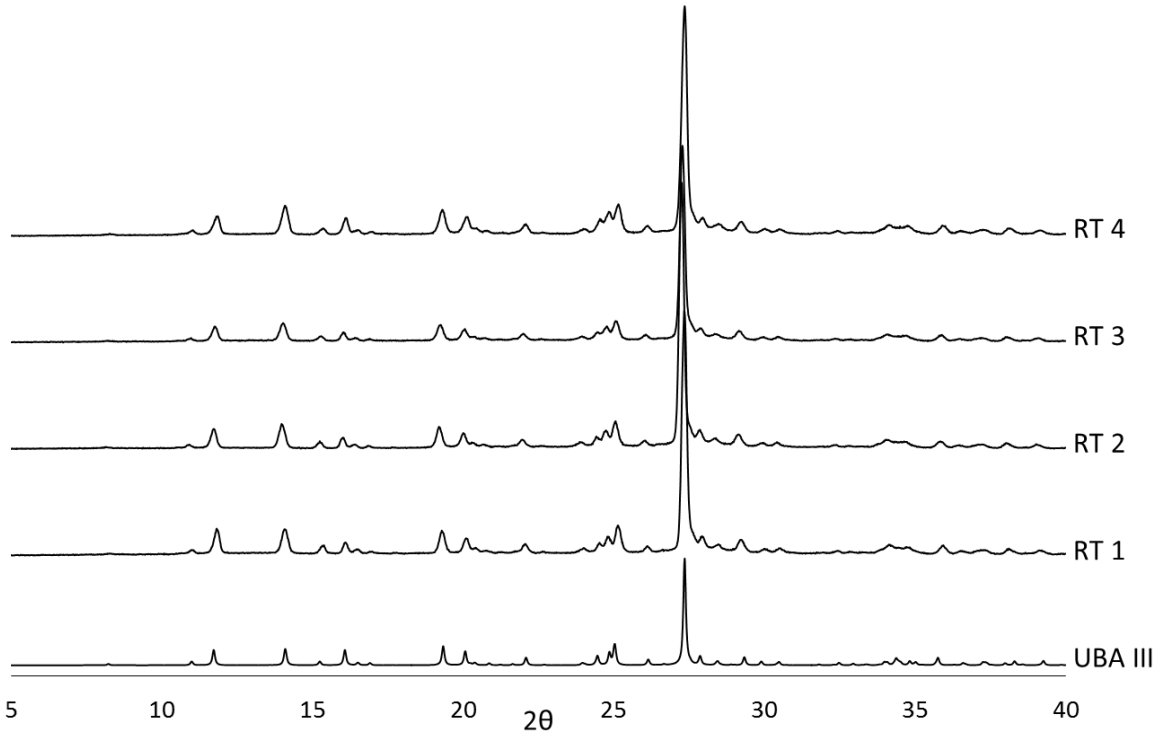

Figure 5.55: PXRD patterns of samples from each RT of KRAIC 1.

During the run, the system was left to cool naturally once segmentation had occurred and the slugs left the heated mixer bath. As the RT was 9 minutes, and the mixer bath was set at a temperature of 60 °C, the system cooled from 60 °C to approximately 20 °C in 9 minutes (approximately 4.4 °C min^{-1}). This is a much faster rate than used in the batch crystallisation experiments (either 0.5 °C min^{-1} or 1 °C min^{-1}). This faster cooling rate is likely a factor in the selective crystallisation of the metastable form, form III; at higher cooling rates nucleation of the metastable form will be preferential over

nucleation of the thermodynamically stable form. Using this continuous crystallisation platform with the chosen parameters results in the RT, and hence the crystallisation time for the system, being very short (under 10 minutes). This means that once the system has nucleated in the solution slug, there is very little time available for form III to form I phase transformations to occur, which will also contribute to the selectivity towards pure UBA form III.

Overall, the continuous process ran very smoothly with no issues arising from sedimentation, encrustation or blockages. These are often issues observed in tubular flow crystallisers. However, the use of Galden allows for preferential wetting of the walls by this carrier fluid and so the solution slugs should not come into contact with the solid interface. This can help prevent encrustation and subsequent blocking.

5.7.2.2 KRAIC 2 – UBA from Ethanol

Due to the successful formation of pure UBA form III from ethanol using the KRAIC set up, a longer run was conducted in order to further investigate the robustness of the system. As can be seen in Table 5.10, the temperatures of the jacketed tube and the mixer bath were kept the same, but the feed temperature was increased to 75 °C. The solution concentration was also reduced slightly to 11.43 mg/g. This was done to in an attempt to better mimic the batch cooling crystallisation experiments. The pumps were all set at the same rates (mL min^{-1}) as KRAIC 1, however, upon measuring the RT for this run, there was a slight increase from 9 minutes to 9 minutes and 50 seconds. This increase in RT was unexpected due to the flow rates being unchanged, however it arises from issues with the pumping of air into the system. The gear pump used is not specifically made for pumping gasses, it is tailored for solutions and as a result of this the actual flow rate of air is reduced over time, if not regularly primed.

For this experiment, the crystallisation was run for a total of 12 RTs (solid from the first 11 RTs was collected) which corresponds to an experimental time of approximately 1 hour and 58 minutes. During this experiment however, unlike with the first run, some issues with blocking were encountered. After running for approximately 55 minutes, a small blockage in the mixer piece resulted in almost no Galden getting into the cross mixer and hence only air slugs were formed with the solution acting as a carrier fluid. The input was swapped over from the feed solution to the primer fluid to prevent any encrustation occurring due to the solution now being in contact with the crystalliser tubing walls. The blockage was removed successfully and slug formation resumed with the Galden now wetting the tubing walls. At 1 hour and 5 minutes into the run the input was changed back from the primer solution to the feed solution and the crystallisation resumed. However, approximately 40 minutes later (1 hour and 44 minutes into the run) the mixer piece blocked again, resulting in a lack of Galden in the system. The flow rate for the Galden was increased for 30 seconds to flush out the small blockage and then reduced back down to 4.18 mL min^{-1}. After 1 hour and 48 minutes the input was changed to the primer solution to allow for the final RTs worth of solid (RT 11) to be collected before the crystallisation was stopped.

The solid was collected for each residence time and a sample from each was subject to PXRD analysis. It can be seen in Figure 5.56 that pure UBA form III was accessed selectively in all RTs. This shows that a high level of robustness is achieved upon the transfer of the crystallisation from batch to continuous using this crystallisation platform. Unlike in batch, UBA form III is produced reproducible, with no form I impurities being observed.

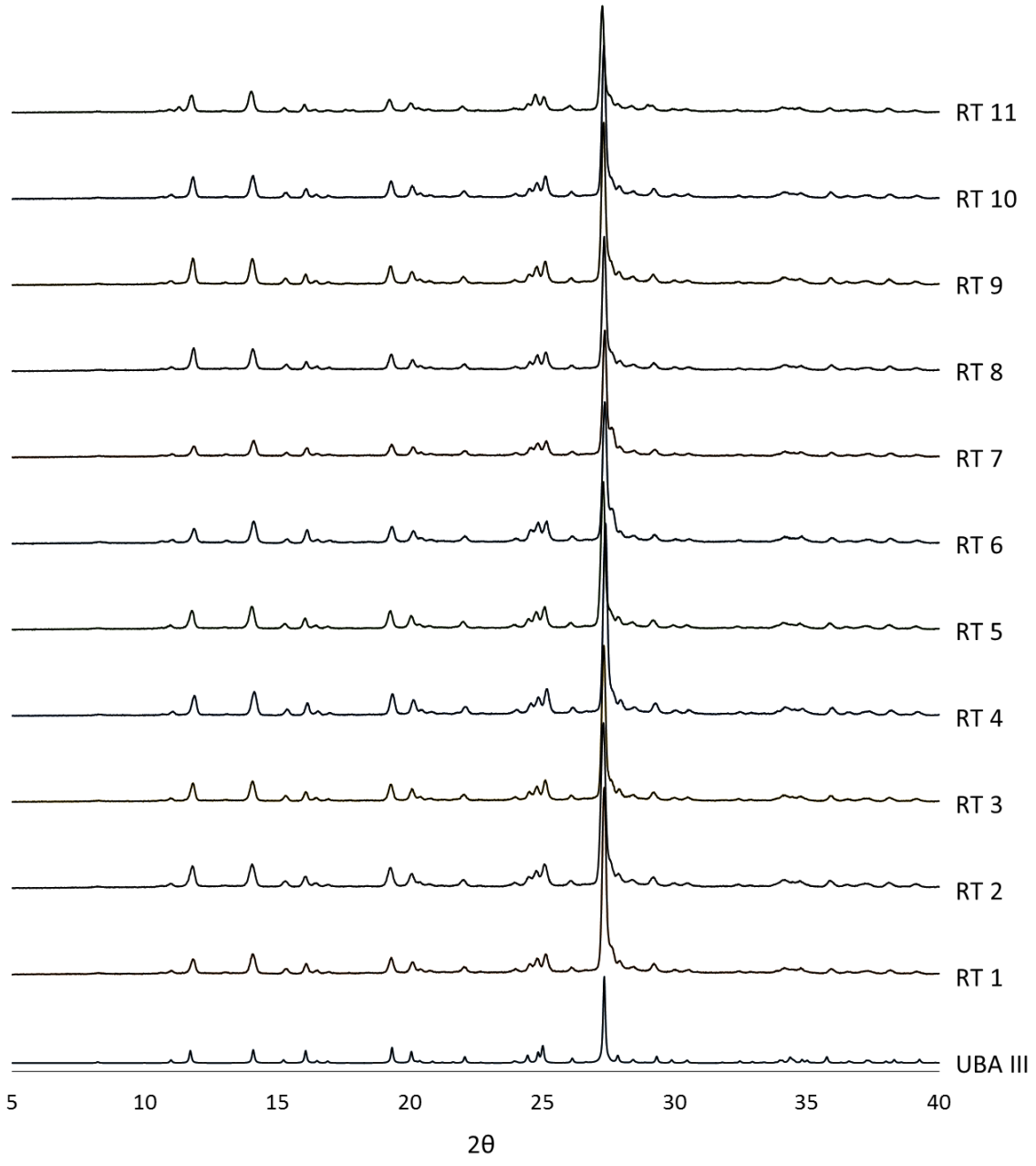

Figure 5.56: PXRD patterns of samples from each RT of KRAIC 2.

During the crystallisation process, initial nucleation in the system was observed 5 minutes into the run (RT), with the point of nucleation being in the 4th rung of coil 1. This is at an earlier point in the crystallisation than observed in KRAIC 1, and may be due to the greater drop in temperature of the system as it moves from the feed vessel to the

mixer piece (10 °C versus 5 °C) resulting in supersaturation being reached faster. As the mixer bath was kept at 65 °C and the system was cooled to ambient temperatures (approximately 20 °C), the cooling rate was approximately 4 °C min^{-1}, slightly slower than in KRAIC 1. However, the blockages occurring in the mixer bath suggest that some nucleation was occurring in the mixer piece before segmentation implying that this temperature profile results in cooling of the solution, accessing the supersaturation too quickly. A higher temperature of the transfer tube and mixer bath would likely overcome this.

5.7.2.3 KRAIC 3 – UBA from Ethanol

A third KRAIC run of UBA from ethanol was conducted in order to further optimise the continuous crystallisation of UBA using the KRAIC. The previous run (KRAIC 2) resulted in some slight blockages in the mixer piece and as a result the temperatures of the jacketed transfer tube and the mixer piece for this run were increased, as can be seen in Table 5.10. Due to the inherent issues with the air pump, the RT for this run was significantly higher than the previous two runs, being 11 minutes and 30 seconds.

The experiment was conducted for a total of 11 RTs (for 10 of which solid was collected), resulting in an experimental time of approximately 2 hours and 6 minutes. Nucleation was first observed approximately 9 minutes into the run in rung 7 of coil 1. PXRD analysis (Figure 5.57) of solid collected from each RT showed that UBA form III was accessed selectively in every RT as with the previous two runs.

After 34 minutes the amount of crystals observed in the solution slugs in coil 2 seemed to be reducing. As the crystallisation proceeded the number of crystals appeared to reduce with a large proportion of slugs having none at all in coils 2 and 3. At 53 minutes into the process the temperatures of water bath and transfer tube were turned down to 60 °C and 65 °C, respectively, in an attempt to increase the amount of nucleation within the system. At 58 minutes crystals were observed in slugs in rung 6 of coil 1, showing that nucleation was again being induced within the system. However, the lower temperature of the water bath resulted in the system blocking at the mixer piece and the Galden not getting into the system, as was seen in KRAIC 2. The blockage was cleared by increasing the Galden flow rate for 30 seconds and the temperature of the water bath was increased to 63 °C. This increase in temperature did not seem to affect the nucleation within the system and crystals were observed in rung 3 of the first coil. However, the issues with the Galden flow remained for the duration of the run, with the flow having to be intermittently ramped up to remove any blockages. The temperature of the water bath was increased back to 65 °C however this resulted in a lack of crystals in being observed in coil 1. At 1 hour 39 minutes the bath was reduced to 63 °C in an attempt to induce the nucleation earlier on in the system and resulted in crystals being observed in rung 6 of coil 1. However, the issues with the Galden flow persisted. After 1 hour and 55 minutes the input was changed from the feed solution to the primer solution and the last RT's (RT10) worth of solid was collected.

For this experiment the increase in temperature of the transfer tube and water bath resulted in little nucleation occurring early in the crystallisation, and as a result the temperatures were decreased. However, this led to the previously seen issues with Galden flow. Although the system was not optimised in terms of the water bath temperatures to control the nucleation point or to prevent any blocking, UBA form III has been shown to be reproducibly accessed using this set up.

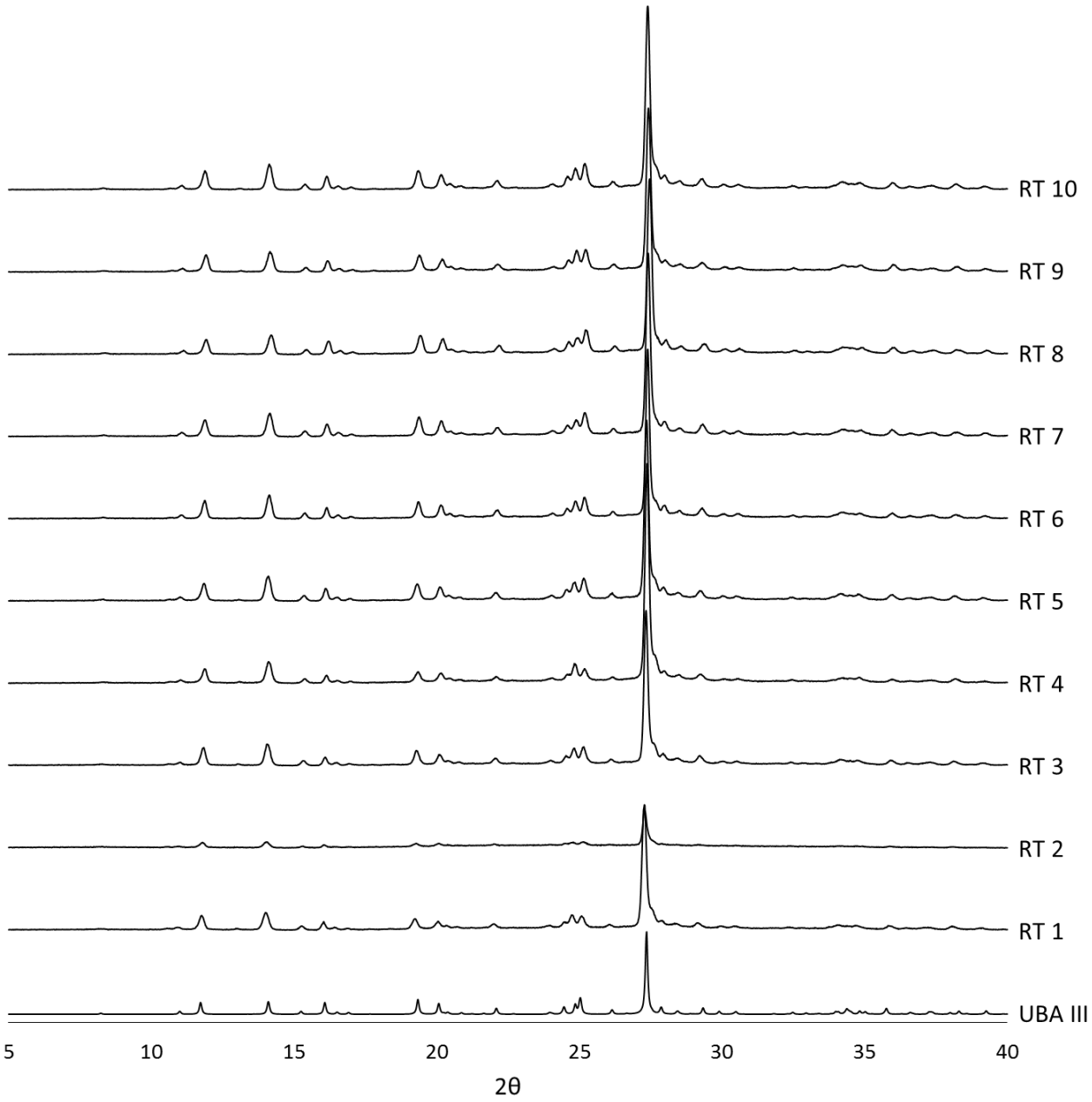

Figure 5.57: PXRD patterns of samples from each RT of KRAIC 3.

The robustness of the crystallisation of UBA from ethanol in batch crystallisation was a major issue, with some experiments yielding pure form III, but others having small quantities of UBA form I present (as seen via PXRD analysis). Upon transfer of the cooling crystallisation from batch to continuous, using the KRAIC set up, it has been shown that

pure UBA form III was accessed in every RT in all three experiments, regardless of the slight changes in RT and temperature.

Using the KRAIC for continuous crystallisation of UBA from ethanol allows for selective formation of the desired metastable solid form, unlike the findings from the COBC. This is likely due to a number of factors such as the short RT accessed using this platform, the faster cooling rate achieved and the lack of back mixing due to the segmented flow. The KRAIC allows for a reproducible and robust method to access UBA form III from cooling crystallisation with ethanol as the solvent medium that has not been achieved using batch crystallisation techniques.

5.7.3 Continuous Crystallisation of UBA from IPA in the KRAIC

Due to the success of accessing UBA form III selectively from ethanol in the KRAIC, as well as the much more robust batch cooling crystallisation of UBA form III from IPA, investigations into the continuous cooling crystallisation of UBA from IPA were conducted. As with the ethanol mediated system, the concentration/saturation temperature used was taken directly from the batch cooling crystallisation experiments (7.5 mg/g, T_{sat} = 60 °C). For these crystallisations the system was left to cool naturally once the slugs left the vicinity of the mixer bath. The experimental parameters for the IPA mediated KRAIC crystallisations (KRAIC 4 and 5) can be seen in Table 5.10. The same temperatures were used for the feed solution, tubing jacket and mixer bath as were used in the ethanol mediated crystallisation run KRAIC 3 due to the relative success with this system. The same flow rates were also utilised due to their success in accessing uniform slugs and short residence times.

5.7.3.1 KRAIC 4 – UBA from IPA

In this experiment, the residence time was 9 minutes and 40 seconds and the crystallisation was run for a total of 13 RTs (2 hours 6 minutes) with solid collected for 12 RTs. During the crystallisation nucleation was first observed 16 minutes and 30 seconds into the experiment in the 5th rung of coil 2. During the run, the point of nucleation moved backwards to rung 2 of coil 2. The crystallisation ran smoothly with no issues of sedimentation, encrustation or blockages.

The solid was collected for each residence time and analysed for solid form identity using PXRD. Figure 5.58 shows that UBA form III was accessed selectively in each RT, with no solid form impurities being present in the PXRD patterns. This result was unsurprising due to IPA allowing for solid form selectivity in unseeded batch cooling crystallisations to a relatively robust level.

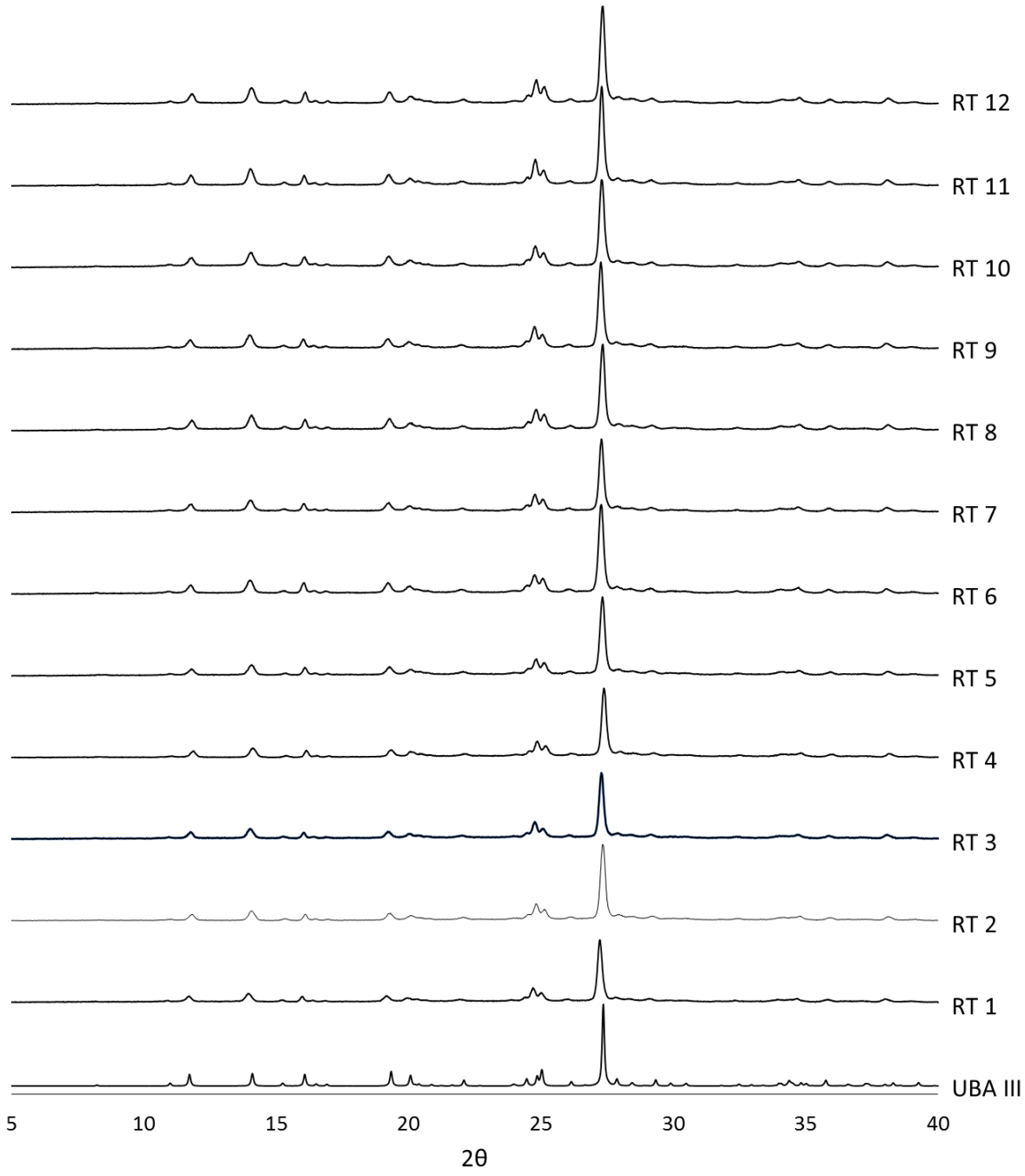

Figure 5.58: PXRD patterns of samples from each RT of KRAIC 4.

5.7.3.2 KRAIC 5 – UBA from IPA

In order to investigate whether the selective crystallisation of UBA from IPA using the KRAIC was reproducible, a repeat experiment was conducted with the same experimental parameters. However, for this experiment the residence time was 11 minutes, due to issues with the air pump not introducing as much air into the system as expected. Again, the continuous crystallisation was run for 13 residence times, which for this experiment equates to 2 hours and 23 minutes. The solid form for each RT was analysed using PXRD and it can be seen (Figure 5.59) that in each RT UBA form III was accessed selectively.

For this run, nucleation was first witnessed after approximately 5 minutes into the crystallisation, in the second rung of coil 1. This is significantly earlier than was observed in KRAIC 4 and as a result the overall size of the crystals once the slugs reached coil 2 were larger than in KRAIC 4. During this run no issues with blockages were observed and it ran smoothly as was seen with the previous run using IPA.

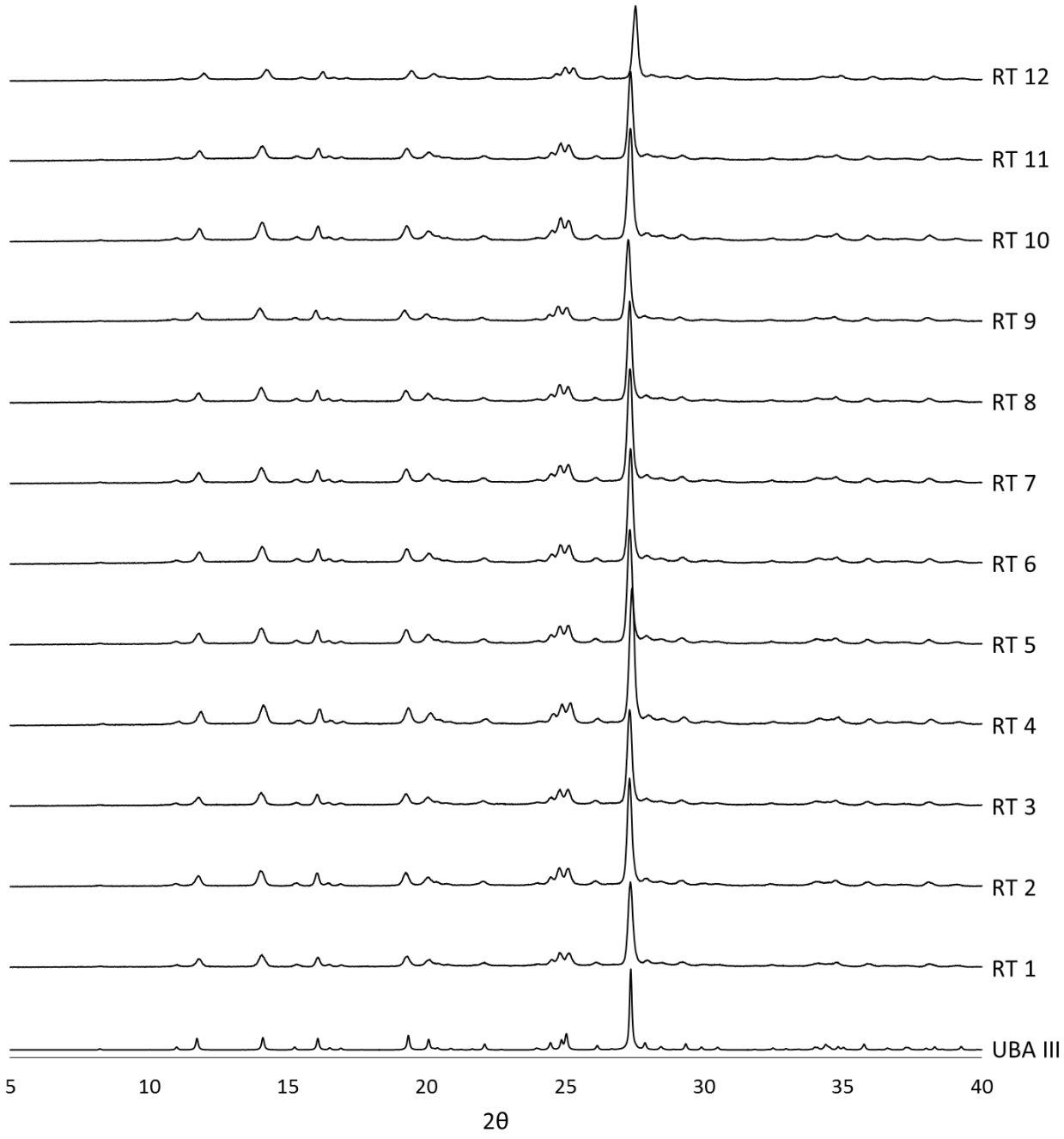

Figure 5.59: PXRD patterns of samples from each RT of KRAIC 5.

Even though both runs had the same experimental parameters they had slightly different residence times. However, it can be seen that regardless of the RT the same outcome was achieved, showing that this crystallisation is robust. UBA form III was

accessed selectively with no other solid forms present (as seen by PXRD analysis) as was expected due to the previous results from the batch crystallisation process.

5.7.3.3 KRAIC Conclusions

Regardless of the solvent medium used, ethanol or IPA, UBA form III was accessed selectively from continuous crystallisation using the KRAIC. The short RT and fast cooling rates are likely the reasons why UBA form III was accessed selectively in ethanol in the KRAIC when this was not the case using the COBC. Both solvent systems showed that the crystallisations using the KRAIC platform were robust and reproducible. However, when using ethanol issues with blockages in the mixer piece were encountered. Further work is required in order to optimise the temperature profile for the ethanol mediated systems in order to access nucleation, but reduce the blocking in the mixer piece. One way this could be done is to keep the mixer bath and transfer tube at the same temperature as the feed solution, so that it remains undersaturated, and then implement a cold tube post mixer bath to cool down the system and induce nucleation.

5.8 Chapter Conclusions

The work presented in this chapter focused on the development of the selective crystallisation of metastable UBA form III in both a batch and continuous cooling crystallisation environment. UBA form III was shown to be accessed to high polymorphic purity using small scale slurry techniques with ethanol as the solvent medium and a 1:1 stoichiometric ratio of the starting components. Experimental times of 16 – 24 hours yielded form III with only trace amounts of form I impurities (as shown by PXRD). Slurry times below this had residual barbituric acid present indicating that full conversion of the starting material to the co-crystal does not occur in these times. Longer slurry times (36 hours) resulted in the production of UBA form I, indicating that upon slurrying for a prolonged period UBA form III transforms to UBA form I, supporting the conclusion that form I is the thermodynamically stable form. When methanol was used for the slurry experiments UBA form I was accessed with a 22 hour slurry time; below this time, UBA form III was also observed in the product. This work suggests that upon slurrying the two components, urea and barbituric acid, the metastable UBA form III is formed which then undergoes a solution mediated phase transition to yield UBA form I. The rate at which this transition occurs is faster in methanol than in ethanol due to the higher solubility of the system in methanol.

Investigations into the scale up of the slurry for UBA form III formation indicated that UBA form III could still be accessed to high polymorphic purity, but at larger scales UBA form I impurities were still present in the slurry product. A design of experiments (DoE) study was conducted at the 50 mL scale to investigate the effect of several experimental parameters on the polymorphic outcome and yield. It was seen that none of the variables (stirring rate, temperature or experimental slurry time) had an effect on the polymorphic outcome and each experiment yielded UBA form III with either UBA form I or barbituric acid impurities.

The slurry experiments indicated that crystallisation from ethanol was more selective towards UBA form III due to the lower solubility of the system resulting in a reduced rate of form III to form I solution-mediated phase transformations. Cooling crystallisations conducted at the 10 mL scale showed that UBA form III could be accessed selectively when using a 1:1 molar ratio of the starting components. When a 2:1 ratio was used the system was more selective to UBA form I. Scale up of this cooling crystallisation to 50 mL showed that UBA form III could be accessed selectively regardless of the starting material ratio (1:1 or 2:1) used. A DoE study conducted on the cooling crystallisation at this scale highlighted that the system had an inherent lack of reproducibility. Two of the three control experiments resulted in pure UBA form III, but one resulted in UBA form III with form I impurities. The study also suggested that the variables chosen (stirring rate, cooling rate, starting material ratio and dwell time at the final temperature) had little to no effect on the polymorphic outcome. Further scale up of the cooling crystallisation, using a 1:1 urea: barbituric acid ratio, to 150 mL was successful in accessing UBA form III selectively. However, the issues with reproducibility of the system still persisted at this scale.

Seeding experiments conducted at GSK, Stevenage showed that when seeding with UBA form I, the thermodynamically stable form, solid form control could be accessed with a seed loading of at least 5 %. However, the FBRM data and concentration profiles obtained for the experiment indicated that the seed did not take to the solution as expected; upon the addition of seed no growth or secondary nucleation events occurred and the system acted largely as if unseeded. The observed solid form 'control' was likely an artefact of the UBA form I being present and promoting the UBA form III to form I transformation to occur once the system had nucleated. When UBA form III seed was used a seed loading of 20 % was required to access solid form control. Again, the FBRM data and concentration profiles indicated that the added seed did not take to solution and the system acted largely as if no seed had been added, nucleating at the approximate temperature at which spontaneous nucleation is observed. The apparent solid form control accessed from high seed loadings is likely due to the large amount of UBA form III being present 'drowning out' any form I nucleation or form III to form I phase transformations that may occur.

Small scale slurry experiments using IPA as solvent medium and a 1:1 urea: barbituric acid ratio indicated that upon moving to IPA, in which the UBA system has a lower solubility than in ethanol, the solution mediated phase transitions were reduced in rate. PXRD analysis of the slurry product showed that UBA form II was present with slurry times of at least 24 hours. The presence of this highly metastable form indicated that the rate of solution-mediated phase transitions had been significantly reduced. Peaks corresponding to UBA form I did not appear in the PXRD patterns until slurry times of 16 hours, further indicating that the rate of phase transformations had been reduced; in ethanol, in contrast, trace UBA form I was observed with slurry times of 4 hours.

Cooling crystallisation of a 1:1 mixture of urea: barbituric acid from IPA resulted in UBA form III being accessed selectively at scales of 10 mL – 150 mL. The experiments showed that the access of UBA from IPA was far more reproducible than seen with ethanol, a direct result of the reduction in rate of the form III to form I solution-mediated phase transformations using this solvent system. Seeding experiments were conducted at GSK, Stevenage to probe as to whether complete solid form control could be achieved. When the system was seeded with the thermodynamically stable form, form I, solid form control was achieved using 1 % seed loading. Analysis of the experimental FBRM data, along with the concentration profiles showed that larger seed loadings (20 %) were required for full control over the crystallisation process, regardless of the cooling rate used; experiments using smaller seed loadings (1 % and 5 %) resulted in a nucleation event at approximately the same temperature at which spontaneous nucleation was observed. When the system was seeded with UBA form III, the amount of seed required to access solid form control was dependent on the cooling rate. A smaller seed loading of 5 % allowed for access of pure UBA form III with the faster cooling rate, but 20 % seed was required with the slower cooling rate. This indicated that the faster cooling rate reduces the time available for solution-mediated form III to form I transformations to occur and as a result less seed is required. From the FBRM data and concentration profiles obtained for each experiment, however, it was seen that, as with the ethanol seeded experiments, the form III seed did not take. The FBRM and concentration profiles indicated that the system acted largely as if unseeded, with the seed not absorbing any of the supersaturation in the system and as a result a nucleation event occurred at approximately the same temperature at which spontaneous nucleation occurs. The observed solid form 'control' is likely an artefact of a significant amount of UBA form III being present at the time of the nucleation event, promoting form III nucleation and reducing the rate at which form III transforms to form I.

Having achieved UBA form III selectively in batch cooling crystallisations, a number of investigations were carried out to explore the transfer of the crystallisation of this metastable form to the continuous environment. It was not possible to access UBA form III selectively using continuous crystallisation from ethanol in the COBC, however. The first experiment yielded UBA form I, but with optimisation of the temperature/cooling rate and saturation of the feed solution a mixture of UBA form I and form III was obtained. Further work to optimise this set up could potentially allow for UBA form III to be accessed from ethanol via continuous crystallisation in the COBC. However, during each experiment, issues with encrustation of the crystalliser walls were encountered, with the level of encrustation worsening with an increase in cooling rate and saturation. Continuous crystallisation of UBA from ethanol was also conducted in the KRAIC, and unlike in the COBC, UBA form III was accessed selectively; this represents successful transfer of crystallisation of this metastable form to a continuous environment. Again, some issues with encrustation were encountered with this platform. The issues did lead to small blockages at the mixer piece which had to be removed periodically by an intermittent increase in carrier fluid flow. The process

requires further optimisation in order to prevent these blockages, but in terms of solid form control and reproducibility the runs were a success. Continuous crystallisation of UBA from IPA using the KRAIC also allowed for the selective and reproducible crystallisation of UBA form III, with form III being accessed in each residence time (RT) of each experiment. The use of IPA also lead to the previously observed blocking issues being removed, and the process ran very smoothly. The selective continuous crystallisation of metastable UBA form III from IPA was thus found to be more robust than from ethanol, mirroring findings of the batch cooling crystallisation experiments.

Overall, selective crystallisation of metastable UBA form III has been achieved using continuous crystallisation from ethanol in the KRAIC as well as from batch cooling and continuous (KRAIC) crystallisation from IPA.

Chapter 6 – Crystallisation of Novel Multi-Component Systems of Thiobarbituric Acid: from Batch to Continuous

6.1 Introduction

This chapter details the discovery of two novel salt systems of thiobarbituric acid (TBA) with isonicotinamide and nicotinamide acting as counter ions. The systems are crystallised using small scale evaporative crystallisation techniques as part of a multi-component crystalline materials discovery project using TBA as a target compound. The crystal structures of each solid form are discussed along with their thermal behaviour. Investigations into the transfer of crystallisation of these systems from evaporative to slurrying, mechano-chemical and cooling techniques are discussed. To achieve this, scale up of cooling crystallisation is investigated up to a 150 mL scale before transfer from batch techniques to continuous techniques using both the COBC and KRAIC platforms.

6.2 Materials Discovery via Multi-Component Evaporative Crystallisation

A materials discovery project was undertaken using TBA as the target compound. TBA was chosen due to its structural and tautomeric similarity to barbituric acid, one component of the main system examined in the overall project. Small scale evaporative crystallisations were conducted using a variety of solvents, a range of co-formers/counter-ions, different starting material ratios and a variety of evaporation temperatures, as detailed in Table 6.1. Any crystalline solid obtained from these crystallisations was analysed using both DSC and PXRD to investigate if a new solid form had been accessed.

Table 6.1: Summary of small scale multi-component evaporative crystallisations with TBA.

Co-former/ counter- ion	Urea, biuret, oxalic acid, nicotinic acid, isonicotinic acid, 2-picolinic acid, nicotinamide, isonicotinamide
Ratio (TBA: co-former/counter ion)	1:1, 1:2, 1:3, 2:1
Solvent	Water, ethanol, methanol, IPA
Evaporation temperature	4 °C, RT

During the subsequent analysis of the obtained solids from this multi-component crystallisation screen, two novel salt forms of thiobarbituric acid were identified with nicotinamide and isonicotinamide as the counter-ions.

6.3 The Novel Thiobarbituric Acid Isonicotinamide (TBAISNAM) Salt System

6.3.1 Evaporative Crystallisation of the TBAISNAM Salt System

A novel multi-component crystalline system of thiobarbituric acid and isonicotinamide (TBAISNAM) was discovered via small scale evaporative crystallisation techniques. The novel system can be accessed using either water, ethanol, IPA or methanol as the solvent media, when a 1:1 ratio of the two components are put into the crystallisation process. The evaporation temperature (2 °C or room temperature) had no effect on the crystallisation outcome. The resultant crystals were orange in colour and block-like in shape. The novel salt was identified via both a unique PXRD pattern and unique thermal behaviour, which will be discussed in sections 6.3.2 and 6.3.3 respectively.

6.3.2 The Crystal Structure of the TBAISNAM Salt System

Single crystal X-ray diffraction experiments were conducted on the resultant solid, indicating that a new unit cell had been obtained. A single crystal data collection was then run on the solid using the Rigaku Oxford Diffraction Xcalibur diffractometer with Mo-$K_{\alpha 1}$ radiation (λ = 0.71073 Å).

Solving the crystal structure for this novel salt system showed that the system has a 1:1 ratio of the two starting components within the crystal structure and that hydrogen transfer occurred between these molecules resulting in the formation of a salt. The TBA moieties in the crystal exist in the enol tautomer with both nitrogen atoms protonated, along with a carbonyl group and a deprotonated hydroxyl group. In turn, the isonicotinamide moiety is protonated at the pyridine nitrogen. The TBAISNAM salt crystallises in the $P2_1/c$ space group with a single TBA ion and a single isonicotinamide ion in the asymmetric unit (Figure 6.1). Within this asymmetric unit a single hydrogen bond forms between the two components, along the hydrogen transfer pathway; bridging a hydroxyl group of the TBA and the protonated nitrogen of the isonicotinamide.

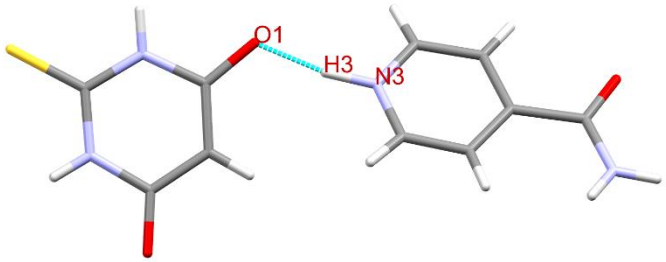

Figure 6.1: Asymmetric unit of TBAISNAM and hydrogen bond parameters.

Within the crystal structure a total of nine hydrogen bonds form, with four of these utilising C-H donor groups. Table 6.2 summarises the hydrogen bonds in terms of their donor atoms (D and H) and their acceptor atoms (A), along with bond distances and angles.

Table 6.2: Table of hydrogen bonds in the TBAISNAM crystal structure.

D	H	A	d(D-H)/Å	d(H-A)/Å	d(D-A)/Å	D-H-A/°
N1	H1	O2[1]	0.87(2)	1.93(2)	2.804(2)	177(2)
N2	H2	O1[2]	0.85(2)	2.13(2)	2.965(2)	169(2)
C3	H3A	O3[3]	0.94(2)	2.62(2)	3.503(2)	157(2)
N3	H3	O1	1.05(2)	1.54(2)	2.590(2)	170(2)
N4	H4A	S1[4]	0.85(2)	2.68(2)	3.497(2)	161(2)
N4	H4B	O2[5]	0.90(2)	2.03(2)	2.929(2)	174(2)
C5	H5	S1[1]	0.94(2)	2.82(2)	3.371(2)	118(2)
C8	H8	S1[4]	0.91(2)	2.91(2)	3.785(2)	161(2)
C9	H9	O3[3]	0.97(2)	2.28(2)	3.022(2)	132(2)

[1]1-X, -1/2+Y, 1/2-Z;
[2]1-X, 1/2+Y, 1/2-Z;
[3]2-X, 1/2+Y, 3/2-Z;
[4]1+X, 1/2-Y, 1/2+Z;
[5]2-X, -1/2+Y, 3/2-Z

Expanding the crystal structure beyond the asymmetric unit, the oxygen involved in the hydrogen bonding between the two components in the asymmetric unit (O1) forms an additional hydrogen bond that is involved in a hydrogen bonded dimer ring ($R_2^2(8)$) between two adjacent TBA ions. The formation of these hydrogen bonded TBA dimers gives rise to a one-dimensional TBA chain network throughout the crystal structure, running parallel to the *b* axis (Figure 6.2). The dimers form between the NH units of the ring and the adjacent carbonyl unit (N2-H2···O1 and N1-H1···O2).

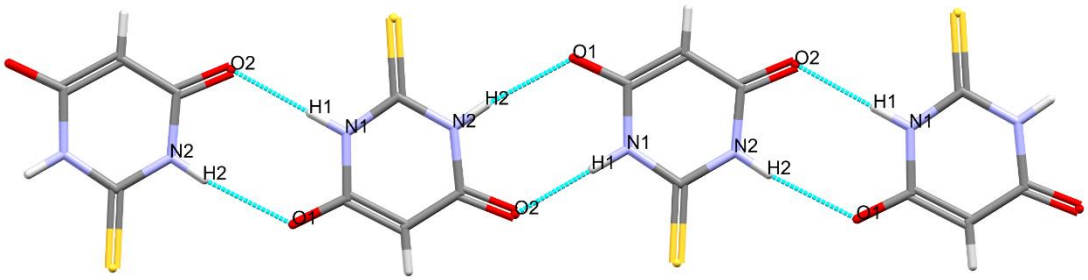

Figure 6.2: One dimensional TBA chain network formed from TBA-TBA hydrogen bonded dimers.

Each TBA ion also forms another hydrogen bond to a further isonicotinamide unit, forming between O2 of the TBA ion and the N4-H4B functionality of the isonicotinamide.

This hydrogen bond, in addition to the hydrogen bond forming in the asymmetric unit (O1···N3-H3), results in the isonicotinamide ions linking adjacent TBA chains and leading to the formation of a two-dimensional sheet network within the crystal structure (Figure 6.3). These sheets form diagonally across the unit cell and give rise to the overall packing seen in Figure 6.4.

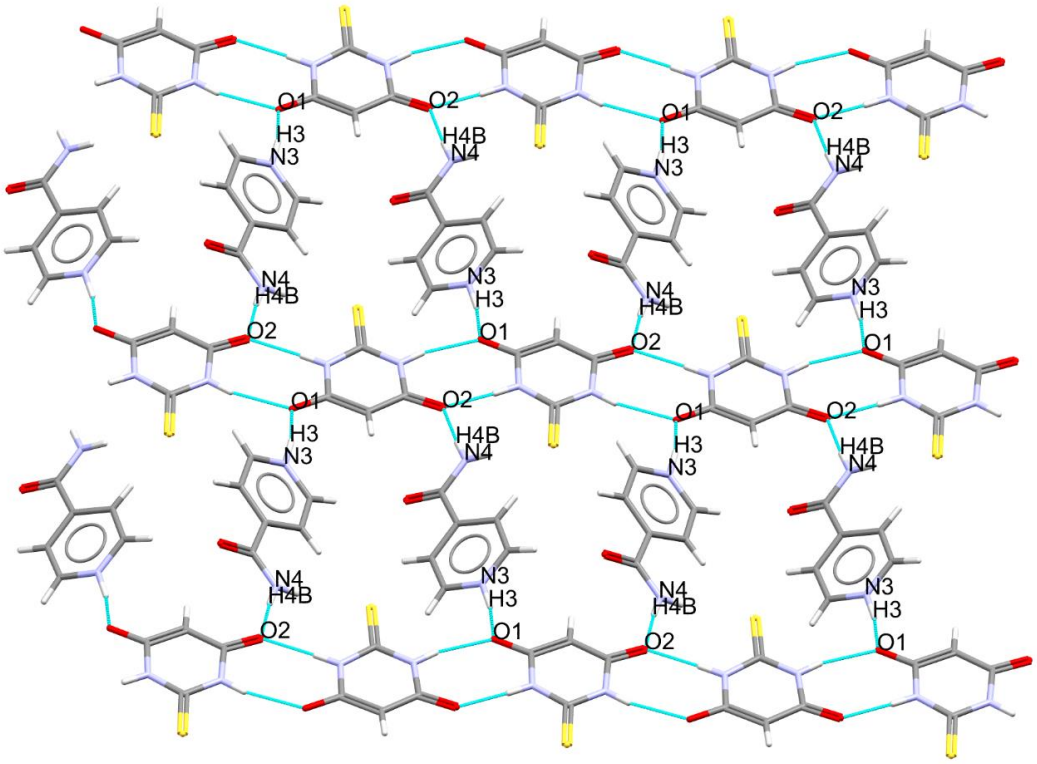

Figure 6.3: Two-dimensional sheet formation in the TBAISNAM crystal structure.

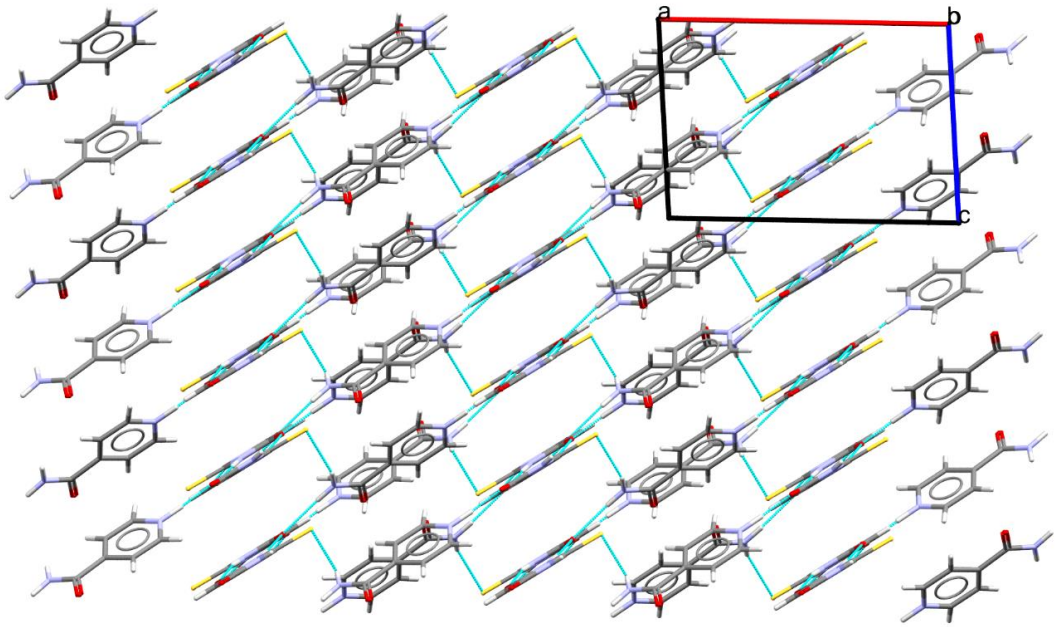

Figure 6.4: The packing arrangement in the TBAISNAM crystal structure (viewed along the *b* axis).

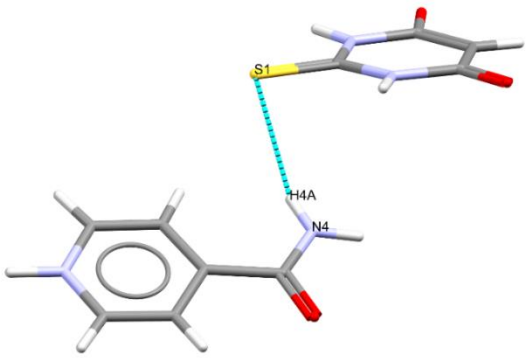

Figure 6.5: The inter-layer hydrogen bond that forms in the TBAISNAM crystal structure.

A further hydrogen bond forms within the crystal structure, linking together these two-dimensional sheets, yielding a three-dimensional hydrogen bonding network as can be seen in Figure 6.4. The hydrogen bond forms between the sulphur atom (S1) of the TBA unit and the N4-H4A functionality of the isonicotinamide unit from a sheet above/below (Figure 6.5).

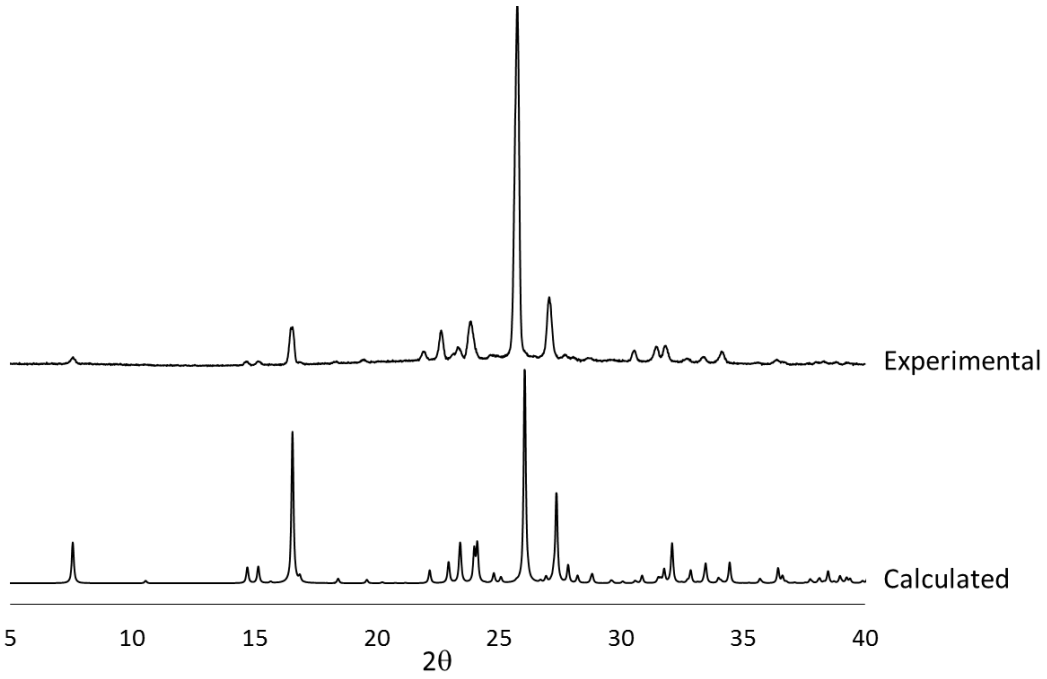

Figure 6.6: Calculated and experimental PXRD patterns of the thiobarbituric isonicotinamide (TBAISNAM) salt system.

The single crystal structure was used to calculate a PXRD pattern for the novel salt system. On comparison of this to an experimentally obtained pattern, it can be seen that the experimental PXRD pattern matches well to the calculated pattern; however some peak overlap can be seen along with some broadening of the peaks (Figure 6.6).

6.3.3 The Thermal Behaviour of the TBAISNAM Salt System

The thermal behaviour of the TBAISNAM system was investigated using DSC. It can be seen from the resultant DSC trace that the salt system melts at approximately 215 °C, an intermediate value between the two starting components (Figure 6.7). After the melt there is an immediate exothermic event; with the melting point of TBA being at 245 °C, this endothermic event could be arising from TBA recrystallising from the melt.

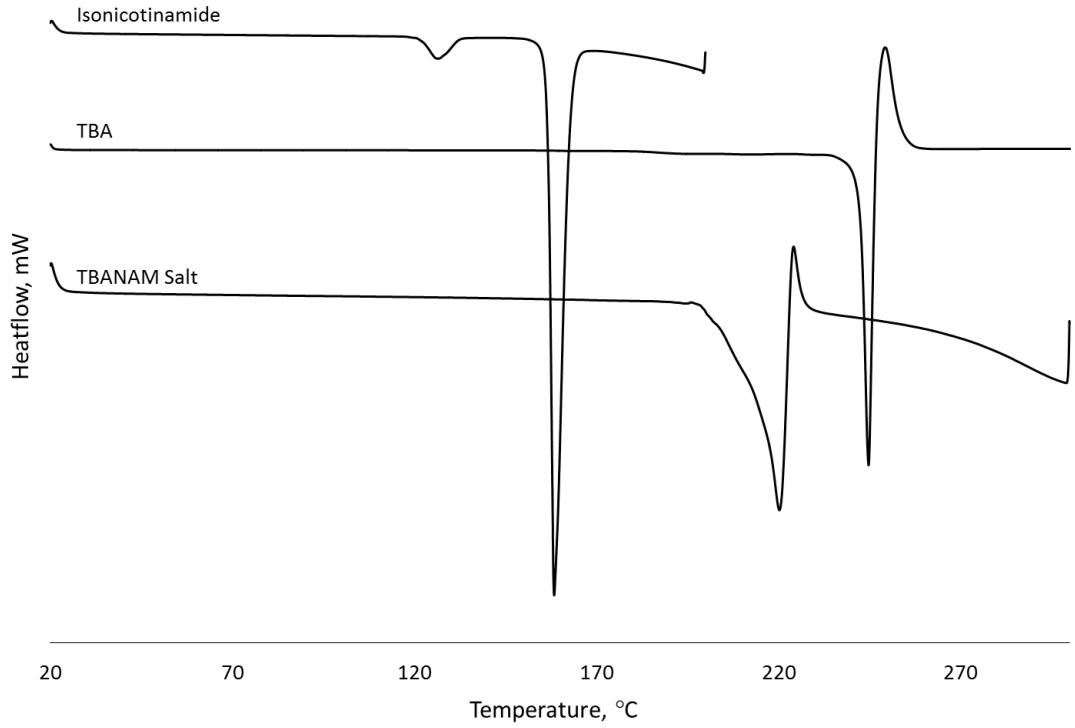

Figure 6.7: DSC traces of isonicotinamide, TBA and the TBAISNAM salt system (10 °Cmin^{-1} heating rate, exothermic up).

6.3.4 Solution-mediated Multi-Component Phase Transformations (Slurry Techniques) for the Access of the TBAISNAM Salt System.

Investigations into whether the novel salt system could be accessed using small scale slurry techniques were conducted using the same four solvents shown to access the system in evaporative crystallisation (water, ethanol, methanol and IPA). The slurries were conducted using a 1:1 ratio of the two components (150 mg of TBA) and 2 mL of solvent. The systems were left mixing (250 rpm) at 30 °C on a Drysyn hotplate for a period of one week. Once the experiment was completed, the product was isolated via vacuum filtration and left to dry at room temperature before being analysed by PXRD and DSC. The PXRD data in Figure 6.8 show that regardless of the solvent medium used for the slurry experiment, the salt system was accessed selectively. The DSC (see Appendix Figure 9.28) also shows that in each case the salt form was accessed selectively.

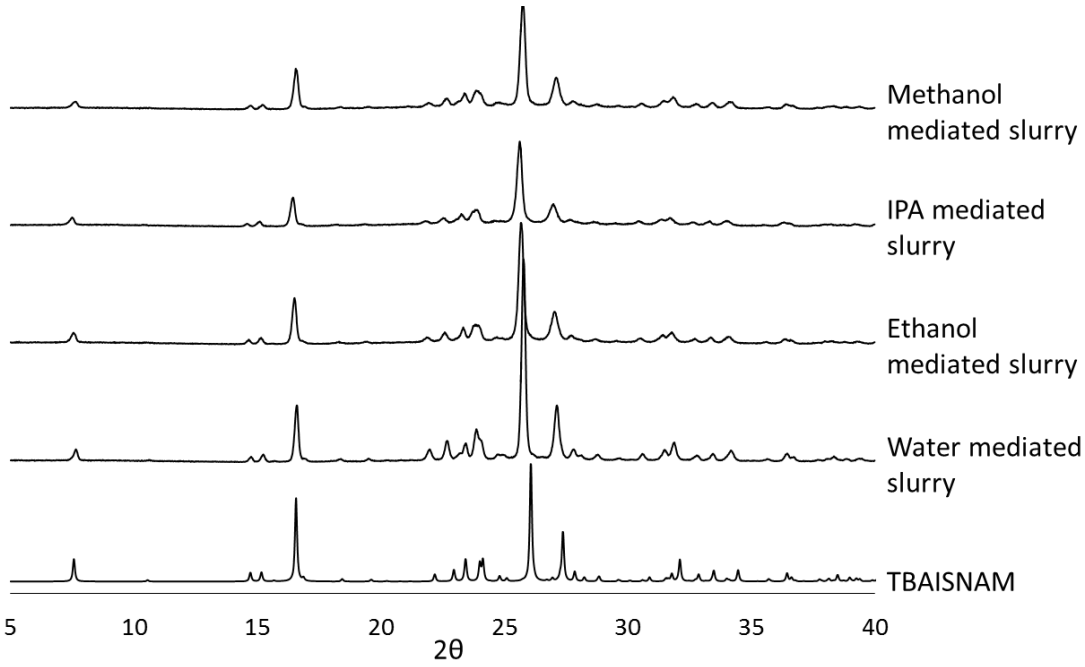

Figure 6.8: PXRD patterns of product from TBA isonicotinamide slurry experiments.

6.3.5 Mechano-chemical Grinding Experiments for the Access of the TBAISNAM Salt System.

The possibility of accessing the thiobarbituric acid isonicotinamide salt system using grinding techniques was studied using both a pestle and mortar and a Retsch PM100 Planetary Ball Mill. For each technique, a 1:1 ratio mixture of the two starting components was ground and the resulting solid analysed using PXRD and DSC. When the sample was ground by hand using the pestle and mortar, 40 mg of TBA and 34 mg of isonicotinamide was used and the sample was ground for 15 minutes. The PXRD pattern obtained from the product suggests that a mixture of the salt system and TBA has been obtained (Figure 6.9).

Upon transferring the grinding to the ball mill, an initial experiment was conducted using 10 mg of TBA and 8.5 mg of isonicotinamide. The system was ground for an hour and the PXRD data shows that the salt system, was accessed (Figure 6.9). However, it can be seen that the PXRD pattern for the experimental product has much more noise, suggesting that the solid is less crystalline than the hand ground sample.

Subsequent grinding experiments were conducted using the ball mill, but with 20 mg of TBA and 17 mg of isonicotinamide. The experimental time was varied between 15 minutes and 1 hour. Figure 6.9 also shows the PXRD patterns of solid obtained from these experiments and it can be seen that in all cases some starting material remains: a peak at 2θ = ~21 ° is seen in the PXRD patterns and corresponds to isonicotinamide.

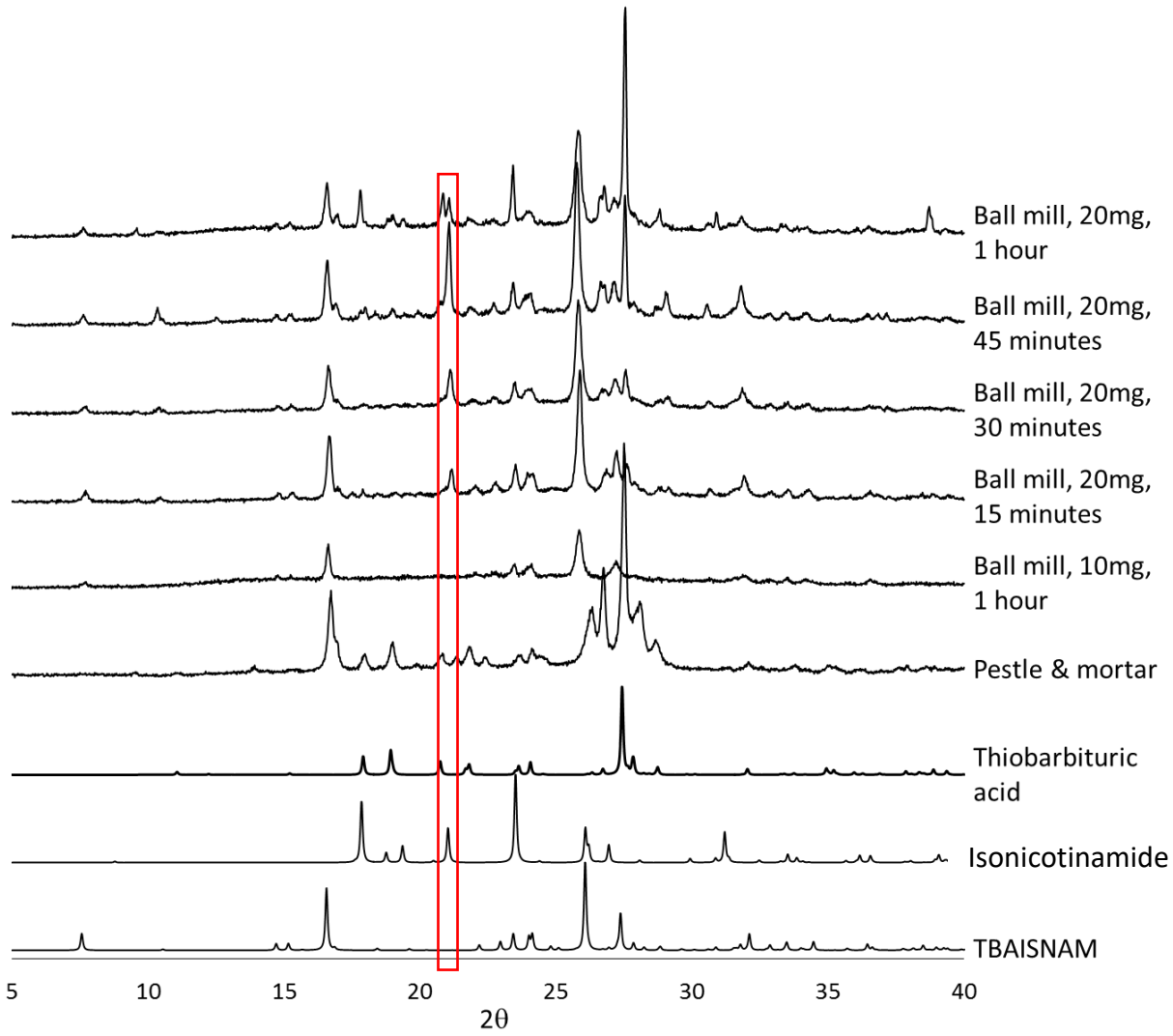

Figure 6.9: PXRD patterns of solid product from thiobarbituric acid isonicotinamide grinding experiments. Red box highlights peak corresponding to isonicotinamide.

The solid products were also analysed using DSC and the traces obtained from each sample can be seen in Figure 6.10. The trace obtained from the pestle and mortar sample confirmed the presence of a significant amount of residual TBA, and little salt. Endothermic peaks corresponding to the melting of isonicotinamide (at approximately 155 °C) could be seen in the ball mill samples. Surprisingly the peak corresponding to isonicotinamide appeared to get larger with longer grinding times. This may be a result of extended grinding accessing smaller, more uniform particle sizes, resulting in a more uniform melting and hence a sharper peak.

The PXRD and DSC data suggest that upon transfer to grinding, the access of the salt system is less selective. Further experiments looking into liquid assisted grinding (LAG) and/or longer experimental times could be conducted in an attempt to access the salt form selectively. However, as grinding is not the usual crystallisation method chosen for scale up, these experiments were not conducted as part of this work.

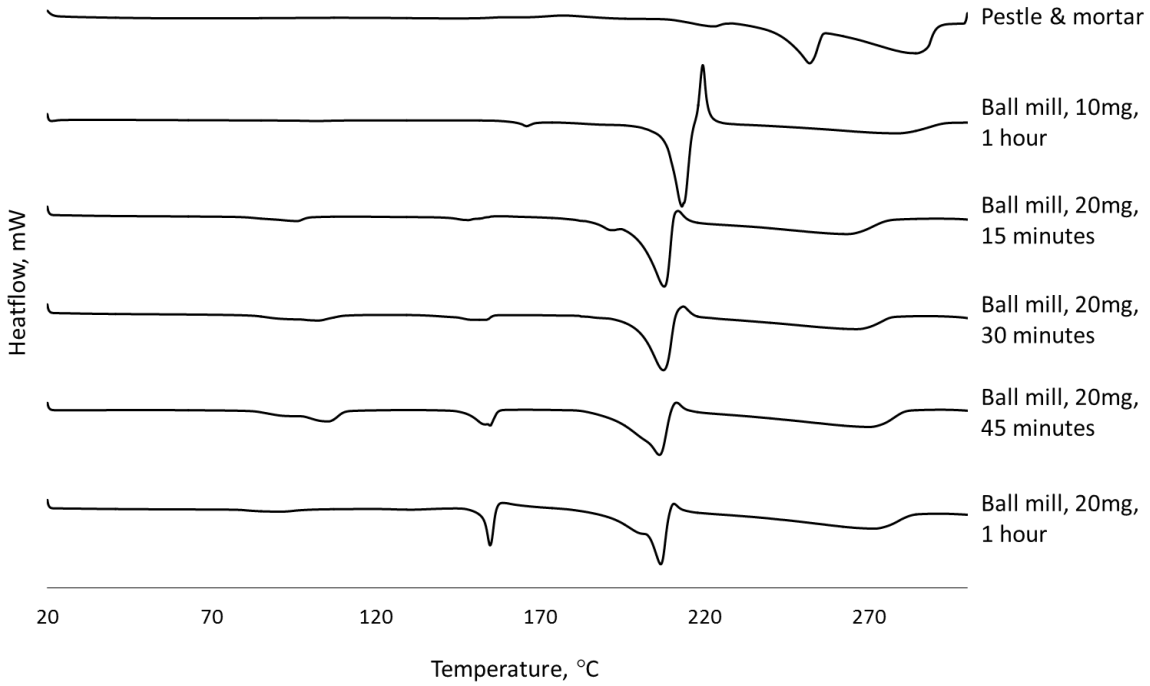

Figure 6.10: DSC traces of solid products from thiobarbituric acid isonicotinamide grinding experiments.

6.3.6 Solubility Analysis of the TBAISNAM Salt System

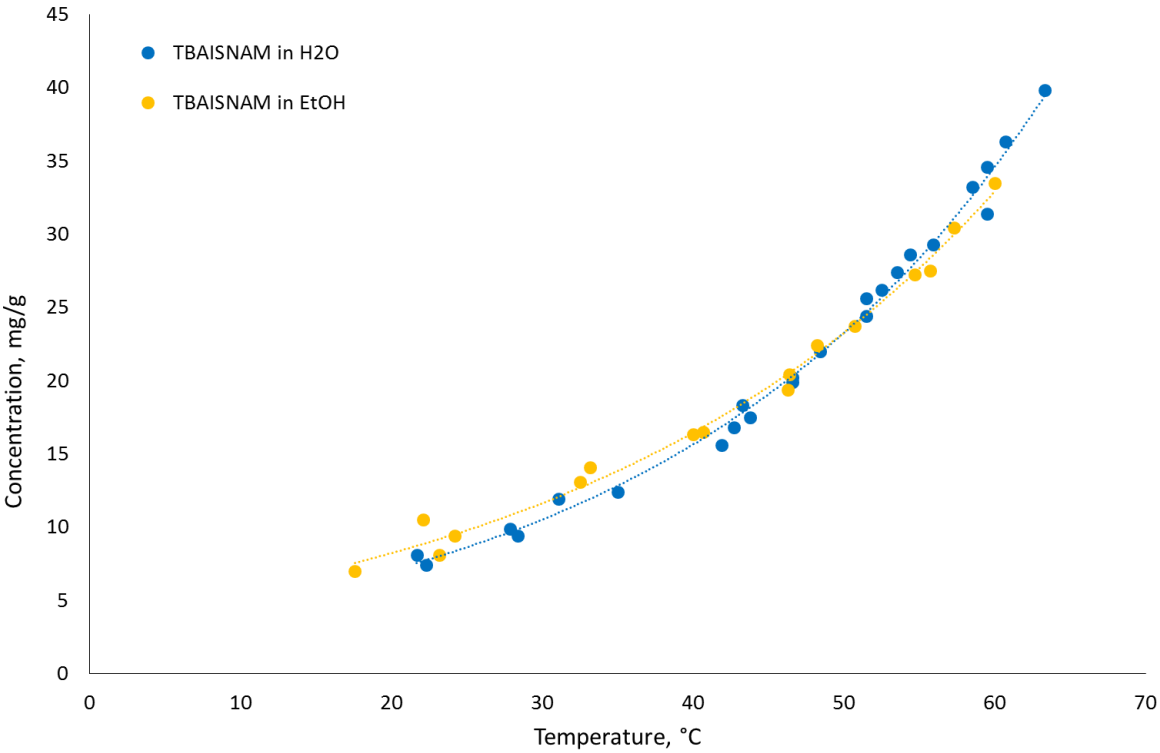

Figure 6.11: Solubility data of the TBAISNAM salt system in water (blue) and ethanol (yellow). Obtained from turbidity methods using the Crystal16.

Solubility analysis of the novel thiobarbituric acid isonicotinamide salt system in both water and ethanol was conducted using a Crystal16 device at the University of Strathclyde. The data were obtained using a heating rate of 1 °C min^{-1} and show very little difference in the solubility of the salt system in the two solvents (Figure 6.11).

6.3.7 Batch Cooling Crystallisation of the TBAISNAM Salt system

Investigations into the transfer of the crystallisation of the TBAISNAM salt system into batch cooling crystallisation and the subsequent scale up of this process were conducted by a final year MChem student, Richard Wilkinson, under the supervision of the author.

6.3.7.1 1 mL Cooling Crystallisation of TBAISNAM from Water

Initial investigations into the transfer of the crystallisation of the novel TBAISNAM salt system were conducted at the 1 mL scale. Two saturation temperatures (T_{sat} = 60 °C and 50 °C) were used, corresponding to concentrations of 34 mg/g and 23 mg/g, respectively. The CRD Polar Bear Plus was used to conduct these cooling crystallisations, with magnetic bottom stirring at 400 rpm. The systems were heated to 70 °C before being held for 30 minutes to ensure full dissolution of the starting components. The samples were then cooled to 5 °C at a rate of 1 °C and held at the final temperature for 30 minutes before the solid was isolated via vacuum filtration and dried at room temperature. PXRD analysis of the resultant solid showed that, regardless of the saturation temperature used, the desired salt system was accessed (Figure 6.12).

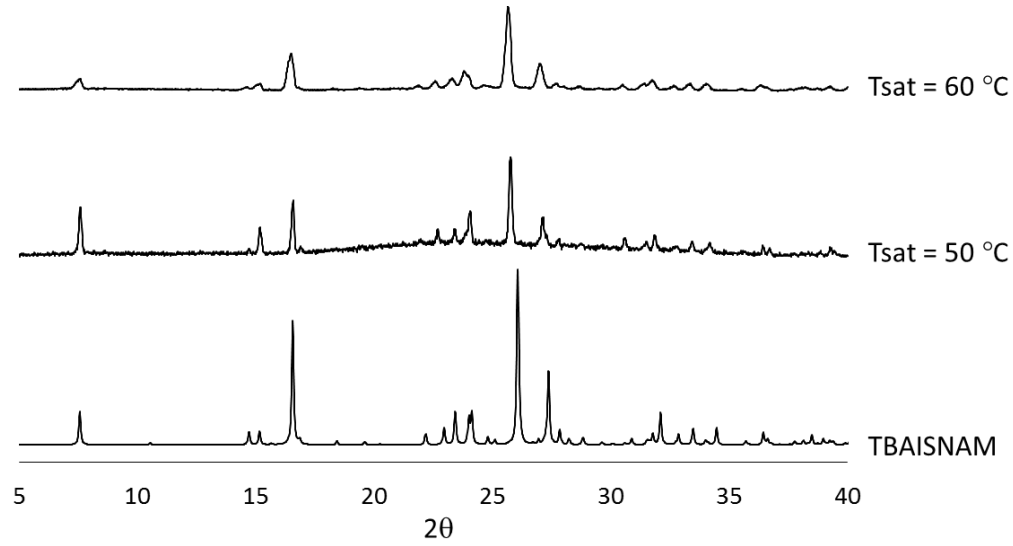

Figure 6.12: PXRD patterns of product obtained from 1 mL cooling crystallisations of thiobarbituric acid isonicotinamide from water.

6.3.7.2 Scale up of Cooling Crystallisations of TBAISNAM from Water to 150 mL

TBAISNAM was shown to be accessed selectively at the 1 mL scale via cooling crystallisation from water using two saturation temperatures (T_{sat} = 50 °C and 60 °C) and the crystallisations were subsequently scaled up to 150 mL. During this study several intermediate scales (5 mL, 10 mL, 50 mL and 150 mL) were investigated in order to

ensure that the salt system was being accessed selectively from the crystallisation at a variety of scales. All experiments were conducted using the same two saturation temperatures and cooling profile as the 1 mL system. Upon moving from the 10 mL scale upwards to the 150 mL scale, the crystallisations were no longer conducted using magnetic bottom stirring in flat bottom vials, and instead RBFs were used with overhead stirring. The product from each crystallisation experiment was isolated via vacuum filtration and left to dry at room temperature before being analysed for solid form identity.

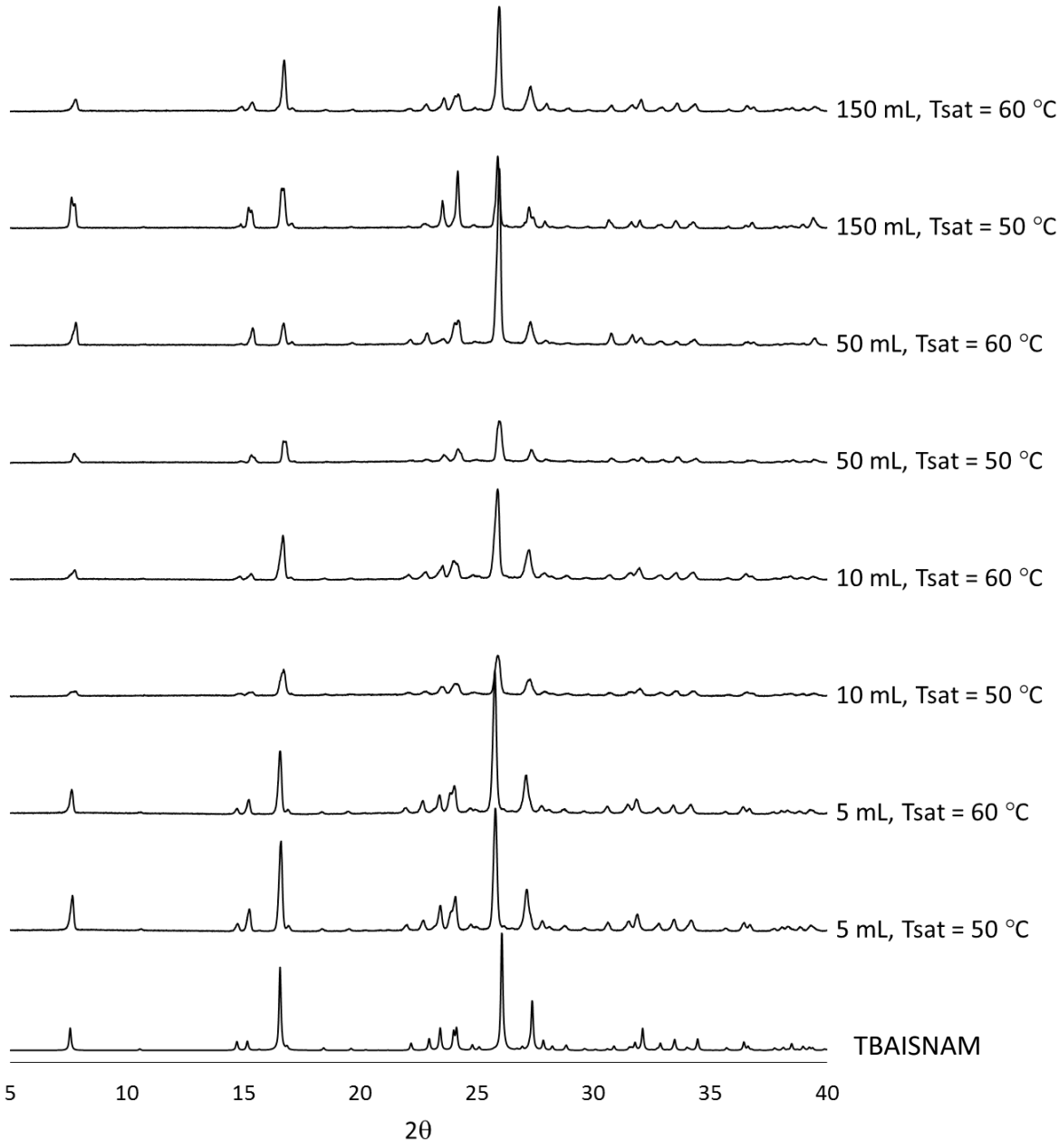

Figure 6.13: PXRD patterns of product obtained from cooling crystallisation experiments of thiobarbituric acid isonicotinamide from water.

PXRD analysis of the solid products shows that the TBAISNAM salt system was accessed selectively at each scale (Figure 6.13). Several of the PXRD patterns, however display a split peak at 2θ = ~7.5 °, where this is a single peak in the calculated pattern. However, the calculated PXRD pattern is determined form the single crystal structure, the data for which was collected at 150 K and the experimental PXRD patterns are collected at RT. This observed peak splitting may therefore be a temperature effect. Repeat experiments at the larger scales (50 mL and 150 mL) proved the crystallisation to be reproducible and robust, accessing the salt system every time.

6.3.8 Continuous Cooling Crystallisation of the TBAISNAM Salt System from Water

Due to success of accessing TBAISNAM from batch cooling crystallisation from water at a scale of 150 mL, investigations into the transfer into continuous cooling crystallisation from water were conducted using both the COBC and the KRAIC platforms.

6.3.8.1 Continuous Cooling Crystallisation using the COBC

Two continuous crystallisations using the COBC platform were conducted using the experimental parameters summarised in Table 6.3 and Table 6.4. A saturation temperature of 50 °C was used for the experiments, corresponding to a concentration of 23 mg/g. The same oscillation parameters were used as for the UBA continuous runs, and hence the Reynolds net flow and oscillation numbers and the Strouhal number, remain unchanged and sit within the limits for plug flow: Re_o = 1737, Re_n = 52 and St = 0.1.

TBAISNAM COBC 1

The continuous crystallisation was run for approximately 2.5 RTs (1 hour 17 minutes). The experimental parameter used care summarised in Table 6.3. After running for one RT (33 minutes 12 seconds) no nucleation had occurred within the system and as a result the temperature of the chillers controlling straights 7 – 12 was reduced to 15 °C, with the temperature of straights 3 – 6 being reduced to 30 °C. After approximately 40 minutes the temperature of straights 3 – 6 was further reduced to 20 °C, however nucleation was still not induced within the system and as a result the temperature was decreased further to 15 °C. After 50 minutes there was still no nucleation and the temperature of straights 7 – 12 was consequently reduced to 10 °C. This further reduction in the temperature of the later part of the system resulted in nucleation being induced and, 53 minutes into the run, crystals were observed on the filter paper and in the exit tubing of the crystalliser. After 57 minutes, large crystals were seen in the end piece of the COBC and by 59 minutes there was a large build-up of crystals in the end piece and exit tubing; these crystals were not seen earlier in the crystalliser in the main straights. At 1 hour and 4 minutes, severe encrustation had built up in the exit tubing and end piece of the system and was moving backwards into the end of straight 12 (Figure 6.14).

Table 6.3: Experimental parameters used for TBAISNAM COBC 1.

Feed concentration	23 mg/g
Flow rate	50 mL min^{-1}
Residence time (RT)	33 minutes 12 seconds
Feed temperature	60 °C
Straights 1 – 2 temperature	50 °C
Straights 3 – 6 temperature	35/30††/25‡/15‡‡/20‡‡ °C
Straights 7 – 10 temperature	25/15†/10‡/20‡‡ °C
Straights 11 – 12 temperature	20/15†/10‡/20‡‡ °C

† Temperature reduced at 33 minutes into run
†† Temperature reduced at 34 minutes into run
‡ Temperature reduced at 40 minutes into run
‡‡ Temperature reduced at 48 minutes into run
‡ Temperature reduced at 50 minutes into run
‡‡ Temperature increased at 1 hour 4 minutes into run

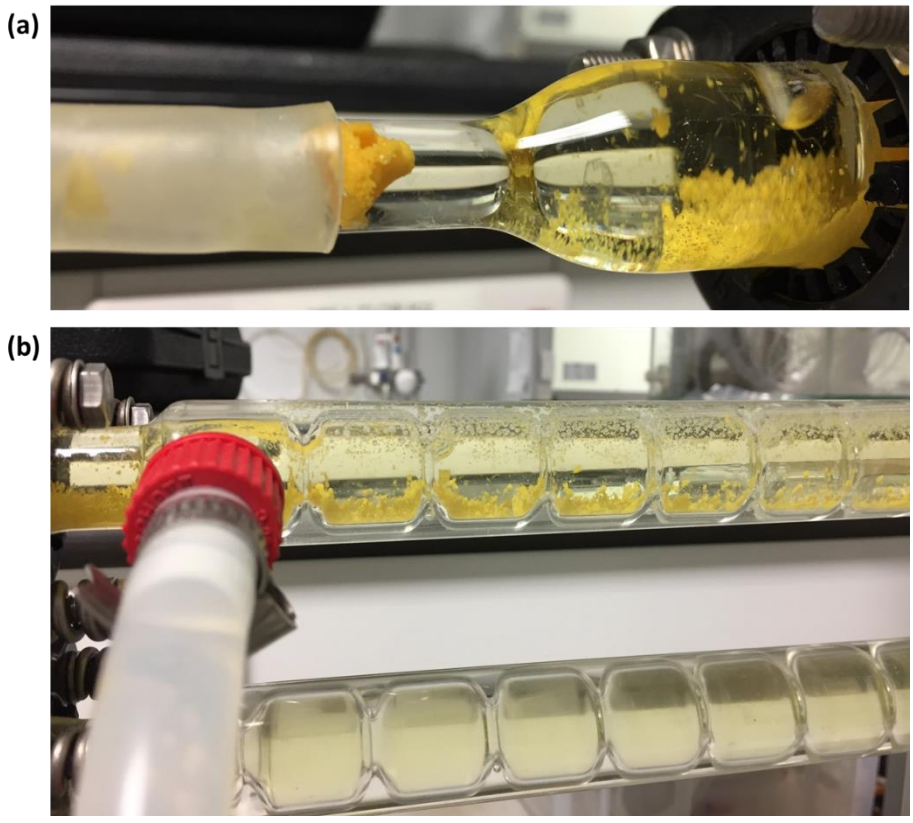

Figure 6.14: Images of TBAISNAM COBC 1: (a) encrustation and blockage in end piece and (b) encrustation in straight 12.

To prevent the certain worsening of this encrustation and the risk of a blockage, the temperature of straights 3 - 12 was increased to 20 °C. The heat gun was also utilised to help remove some of the encrustation in the end piece and the exit tubing was temporarily removed for cleaning. During this time the input was changed from the feed solution to primer solution (pure water). After 1 hour and 14 minutes small crystals were observed in straights 10 and 11, however after 1 hour 17 minutes the encrustation in straight 12 had worsened and all the chiller temperatures were increased to 60 °C. Due to the issues with severe encrustation, the input was not changed back to the feed once the chiller temperatures were increased to 60 °C.

Solid obtained from RTs 1 and 2 was analysed using PXRD from which it can be seen that the salt system was accessed during the continuous crystallisation (Figure 6.15).

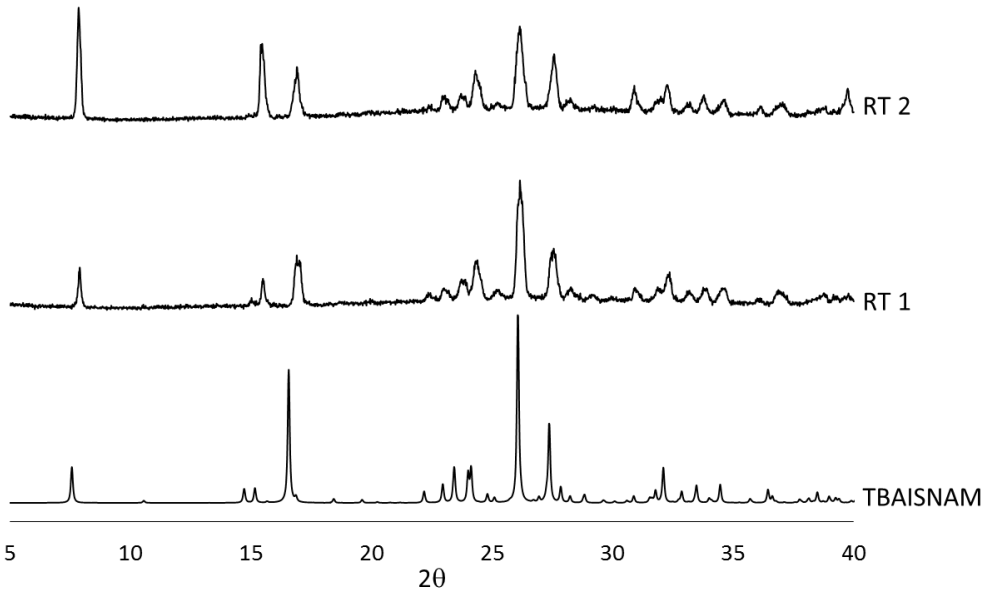

Figure 6.15: PXRD patterns of solid obtained from RT 1 and RT 2 of the continuous cooling crystallisation of thiobarbituric acid isonicotinamide from water using the COBC.

TBAISNAM COBC 2

A second COBC experiment was conducted in an attempt to optimise the process. The experimental parameters used are shown in Table 6.4. As can be seen, the initial straight temperatures used in this run were much lower than those used in the first run, due to the significant reduction in temperatures required to induce the nucleation in COBC 1. The crystallisation was run for approximately 3 RTs, with solid from RT 1 and 2 being collected. As with the first run, no crystallisation occurred within the first RT and as a result after 38 minutes the temperature of straights 7 – 12 was reduced to 10 °C. However, still no crystals were observed in the system and so after 45 minutes the temperature of straights 3 – 6 was also reduced to 10 °C. 53 minutes into the crystallisation, with straights 3 – 12 at 10 °C, crystals were observed on the filter paper and in the exit tubing. In an attempt to induce nucleation earlier on in the crystalliser, the temperature of straights 7 – 12 was further reduced to 7.5 °C. After 1 hour, crystals were observed in the end piece, however encrustation was also observed in the exit

tubing. After 1 hour and 16 minutes the input was changed from the feed to the primer solution due to the feed being depleted. Two minutes later, it was observed that there was severe encrustation in the exit tubing and end piece (Figure 6.16), with a small amount of encrustation in straight 12. After 1 hour and 21 minutes some large crystals were observed in straight 5, but not in any earlier or later straights. Two minutes later, the large crystals were observed in straight 6 and the bend between straights 6 and 7. A blockage in the join between straight 12 and the end piece was also observed and the temperature of straights 11 and 12 was increased to 60 °C in an attempt to clear the blockage, before being reduced back down to 7.5 °C once the blockage had cleared. After 1 hour and 33 minutes the solid product from RT 2 had been collected and the continuous run was terminated.

Table 6.4: Experimental parameters used for TBAISNAM COBC 2.

Feed concentration	23 mg/g
Flow rate	50 mL min^{-1}
Residence time (RT)	33 minutes 12 seconds
Feed temperature	60 °C
Straights 1 – 2 temperature	50 °C
Straights 3 – 6 temperature	15/10†† °C
Straights 7 – 10 temperature	15/10†/7.5‡ °C
Straights 11 – 12 temperature	15/10†/7.5‡ °C

† Temperature reduced at 38 minutes into run
†† Temperature reduced at 45 minutes into run
‡ Temperature reduced at 57 minutes into run

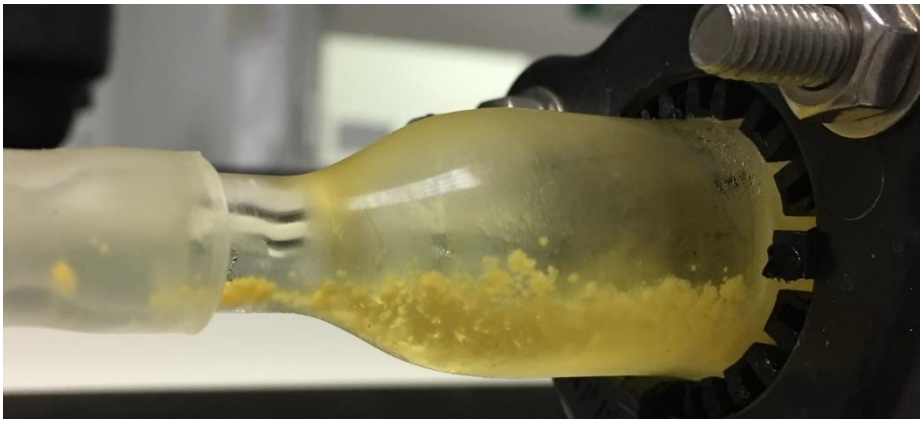

Figure 6.16: Encrustation in end piece of TBAISNAM COBC 2.

Samples from the solid product collected from RT 1 and RT 2 were analysed using PXRD. The patterns showed that during the continuous crystallisation, the desired salt form

had been accessed, as with the previous run (Figure 6.17). The second run showed that lower temperatures were still needed in order to nucleate the system earlier than in the exit tubing. However, nucleation was still not induced in the system until 53 minutes into the run (during the second RT). Further work should investigate using lower temperatures from the start of the run in an attempt to nucleate the system earlier in the crystalliser. An increase in residence time would allow the system a longer time to nucleate and crystalliser within the crystalliser, resulting in a higher yield. The most effective way of achieving this would be to extend the length of the crystalliser, as the alternative of reducing flow rates would impact the overall flow behaviour within the system and may result in plug flow no longer being achieved.

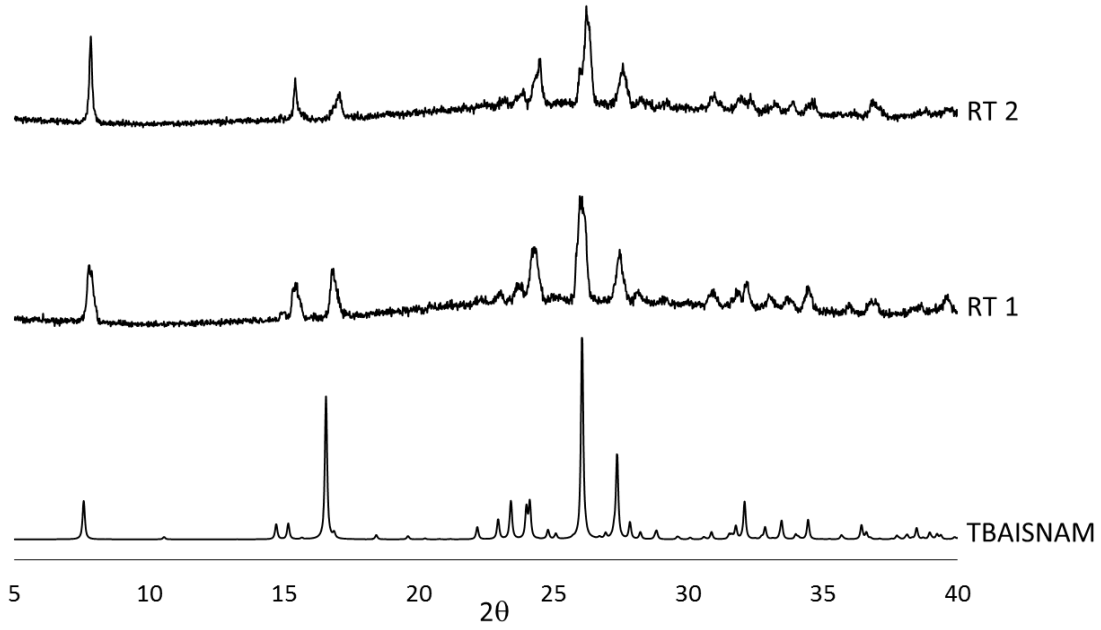

Figure 6.17: PXRD patterns obtained from samples from each RT of the continuous crystallisation of thiobarbituric acid isonicotinamide from water using the COBC.

6.3.8.2 Continuous Crystallisation using the KRAIC

The KRAIC platform was also used to investigate the continuous cooling crystallisation of TBAISNAM from water. Three runs were conducted in an attempt to optimise the crystallisation process. As with the UBA crystallisations in the KRAIC, tri-segmented flow was utilised, introducing both Gladen and air at the cross mixer piece. A jacketed transfer tube was used to take the hot feed solution to the mixer piece, the temperature of which was controlled by an external mixer bath. The mixer bath was kept at an elevated temperature by the use of a Drysyn hot plate.

TBAISNAM KRAIC 1

The first KRAIC experiment was run with T_{sat} = 50 °C and had a residence time of 17 minutes and 50 seconds, and was run for 53 minutes, approximately three residence times. The experimental parameters for the run can be seen in Table 6.5. After 18 minutes and 30 seconds no crystallisation had been observed in the crystalliser and the

temperature of the mixer bath and the transfer tube were reduced to 50 °C and 55 °C, respectively. The temperature of the Drysyn used to heat the feed was also reduced to 60 °C. 44 minutes into the run, there were still no crystals observed in the crystalliser and the feed solution, transfer tube and mixer bath were all further reduced to 55 °C, 50 °C and 45 °C respectively. After 49 minutes an ice bag was added to the middle of coil 3 to try to induce nucleation within the system. However, this was not effective and nucleation did not occur. After 3 RTs (53 minutes) the input was changed to primer solution and the system was run for an additional RT before being terminated.

Table 6.5: Summary of experimental parameters of TBAISNAM KRAIC 1.

Parameters	TBAISNAM KRAIC 1
Feed concentration	23 mg/g
Feed flow rate	2 mL min^{-1}
Carrier fluid flow rate	4.18 mL min^{-1}
Air flow rate	6.26 mL min^{-1}
Residence time (RT)	17 minutes 50 seconds
Feed temperature	65/60[†]/55[††] °C
Transfer tube temperature	60/55[†]/50[††] °C
Mixer bath temperature	55/50[†]/45[††] °C

[†] Temperature reduced 18 minutes into run
[††] Temperature reduced 44 minutes into run

TBAISNAM KRAIC 2

Unfortunately, during the first KRAIC run no crystallisation occurred, even with the introduction of ice into coil 3. As a result a second KRAIC run was conducted, using a higher saturation temperature (T_{sat} = 60 °C versus 50 °C). Again, an ice bag was placed into coil 3 to help reduce the temperature of the slugs and induce nucleation within the system. The initial temperatures of the feed solution, transfer tube and mixer bath were increased in the second run due to the higher concentration of solution being used. A summary of experimental parameters can be seen in Table 6.6.

Table 6.6: Summary of experimental parameters of TBAISNAM KRAIC 2.

Parameters	TBAISNAM KRAIC 2
Feed concentration	34 mg/g
Feed flow rate	2 mL min^{-1}
Carrier fluid flow rate	4.18 mL min^{-1}
Air flow rate	6.26 mL min^{-1}
Residence time (RT)	19 minutes 20 seconds
Feed temperature	65/60[††] °C
Transfer tube temperature	65/60[††]/55[‡]/50[‡‡] °C
Mixer bath temperature	60/50[†]/45[‡]/40[‡‡]/30[‡]/35[‡‡] °C

[†] Temperature reduced 20 minutes into run
[††] Temperature reduced 28 minutes into run
[‡] Temperature reduced 37 minutes into run
[‡‡] Temperature reduced 50 minutes into run
[‡] Temperature reduced 1 hour 5 minutes into run
[‡‡] Temperature increased 1 hour 27 minutes into run

The residence time for this run was 19 minutes and 20 seconds, one and a half minutes longer than in the first run. This is due to issues relating to the gear pump used for the introduction of air into the system; it is not made for gases and as a result requires regular priming and maintenance due to it becoming less effective over time. During the run, no nucleation was seen during the first residence time and after 20 minutes the temperature for the mixer bath was decreased to 50 °C. After 28 minutes the temperature for the feed solution and transfer tube was reduced to 60 °C. During the run the ice bag had to be removed from coil 3 due to issues with its leaking. After 37 minutes, as no crystallisation had occurred, the temperatures for the mixer bath and transfer tube were reduced further to 45 °C and 55 °C respectively. However, this reduction in temperature did not result in the system nucleating and at 50 minutes the temperatures were further reduced to 40 °C and 50 °C respectively. After 1 hour and 5 minutes there was still no sign of crystallisation in the system and as a result the temperature of the mixer bath was reduced to 30 °C. This reduction in temperature was successful in inducing nucleation within the system, as after 1 hour and 27 minutes a significant amount of crystals were observed in the crystalliser. The temperature of the mixer bath was subsequently increased to 35 °C and after 1 hour and 45 minutes crystals could be seen in the second rung in coil 1 (Figure 6.18). The input was changed from the feed solution to the primer at 1 hour 49 minutes and the crystallisation was terminated.

As the system nucleated 1 hour and 27 minutes into the run, the solid from this RT and the subsequent RTs (RT 4 and 5) was collected and analysed using PXRD. The obtained patterns show that the novel salt system was selectivity accessed during the continuous crystallisation (Figure 6.19).

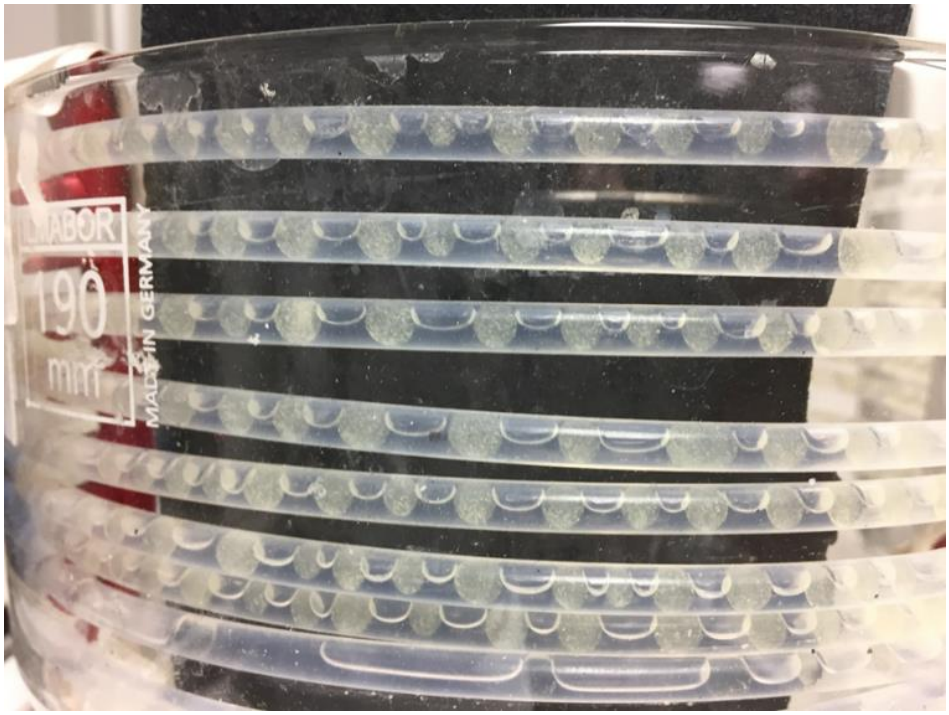

Figure 6.18: Crystallisation in coil 1 of the KRAIC (TBAISNAM KRAIC 2).

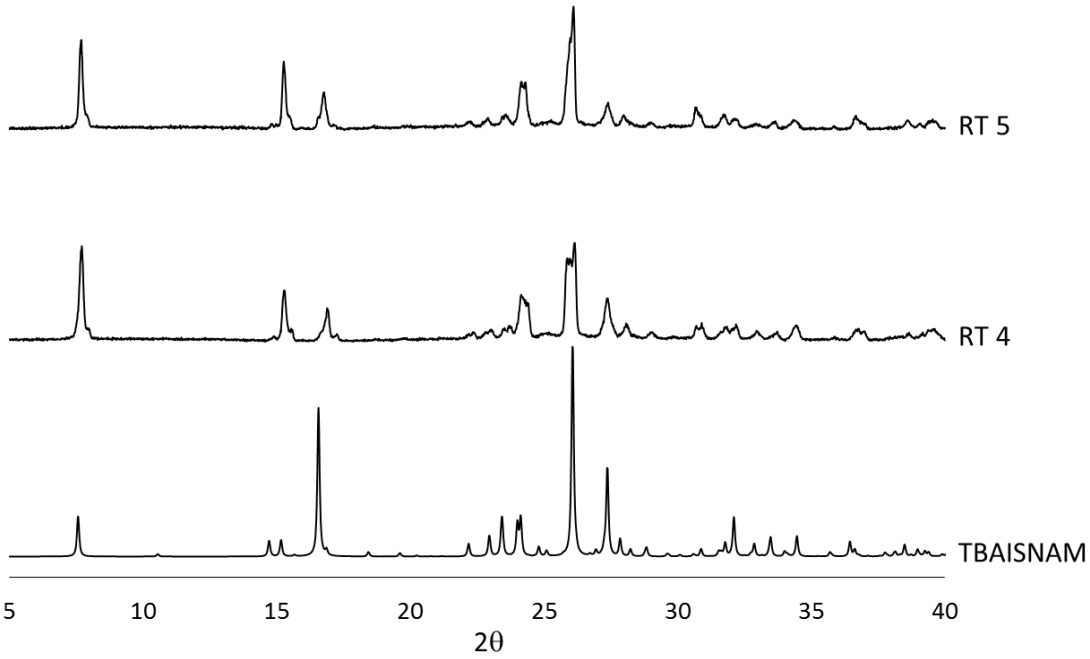

Figure 6.19: PXRD patterns of solid obtained from the TBAISNAM KRIAC 2 run.

Peak splitting can be observed in some of the PXRD peaks (2θ = ~7.5 ° and 26.0 °), however, this can be attributed to temperature effects due to the RT collection of experimental PXRD patterns in comparison to the 150 K collection of data for the calculated pattern.

TBAISNAM KRAIC 3

Table 6.7: Summary of experimental parameters for TBAISNAM KRAIC 3.

Parameters	TBAISNAM KRAIC 3
Feed concentration	34 mg/g
Feed flow rate	2 mL min^{-1}
Carrier fluid flow rate	4.18 mL min^{-1}
Air flow rate	6.26 mL min^{-1}
Residence time (RT)	21 minutes 16 seconds
Feed temperature	60 °C
Transfer tube temperature	45/40††/35‡‡ °C
Mixer bath temperature	40/35†/30‡/20‡/25‡‡/30* °C

† Temperature reduced 18 minutes into run
†† Temperature reduced 30 minutes into run
‡ Temperature reduced 49 minutes into run
‡‡ Temperature reduced 1 hour 2 minutes into run
‡ Temperature reduced 1 hour 14 minutes into run
‡‡ Temperature increased 1 hour 15 minutes into run
* Temperature increased 1 hour 20 minutes into run

A third KRAIC run was then conducted with this system, again with a saturation temperature of 60 °C. For this run the initial temperatures of the feed, transfer tube and mixer bath were at lower values compared to the KRAIC 2 due to the significant drop in temperatures required during this experiment to induce nucleation. For this run the residence time was again slightly longer, now being 21 minutes and 16 seconds. The other experimental parameters used during the run can be seen in Table 6.7.

No nucleation had been observed 18 minutes into the run and as a result the temperature of the mixer bath was reduced to 35 °C. However, this did not result in nucleation being induced and as a result the temperature of the transfer tube was reduced to 40 °C at 30 minutes into the run. These further reductions in temperature did not succeed in inducing nucleation within the system and the temperature of the mixer bath was reduced further to 30 °C 49 minutes into the run. After 1 hour and 2 minutes the transfer tube temperature was further reduced to 35 °C, however 1 hour and 14 minutes there were still no crystals in the crystalliser (the solution was not nucleating) so the temperature of the mixer bath was reduced to 20 °C. This reduction

in the temperature of the mixer bath and transfer tubing was now successful in inducing crystallisation, with crystals being observed in the first rung of coil 1 at 1 hour 15 minutes. As the nucleation was occurring very close to the mixer bath (observed in slugs as soon as they leave the mixer bath), the temperature of the bath was increased to 25 °C at 1 hour 15 minutes and then to 30 °C after 1 hour and 20 minutes. The run was continued until 1 hour 43 minutes (4 RTS) before the input was changed to primer solution and solid from the previous RT was collected.

The PXRD patterns obtained for the solid produced in the last two residence times (RT 4 and 5) show that again, the TBAISNAM salt was accessed during this continuous crystallisation. It can be concluded that further work is required in order to optimise the temperatures of the transfer tube and mixer bath for the continuous crystallisation of TBAISNAM from water using the KRAIC. One way in which more control could be exerted is to use a cold tube after the mixer bath. This could allow for higher temperatures to be used for both the mixer bath and transfer tubing as the system could be cooled quickly once the slugs have left the mixer bath, once they enter the cold tube. However, it has been shown that the TBAISNAM salt system can be accessed to high solid form purity using this continuous crystallisation apparatus.

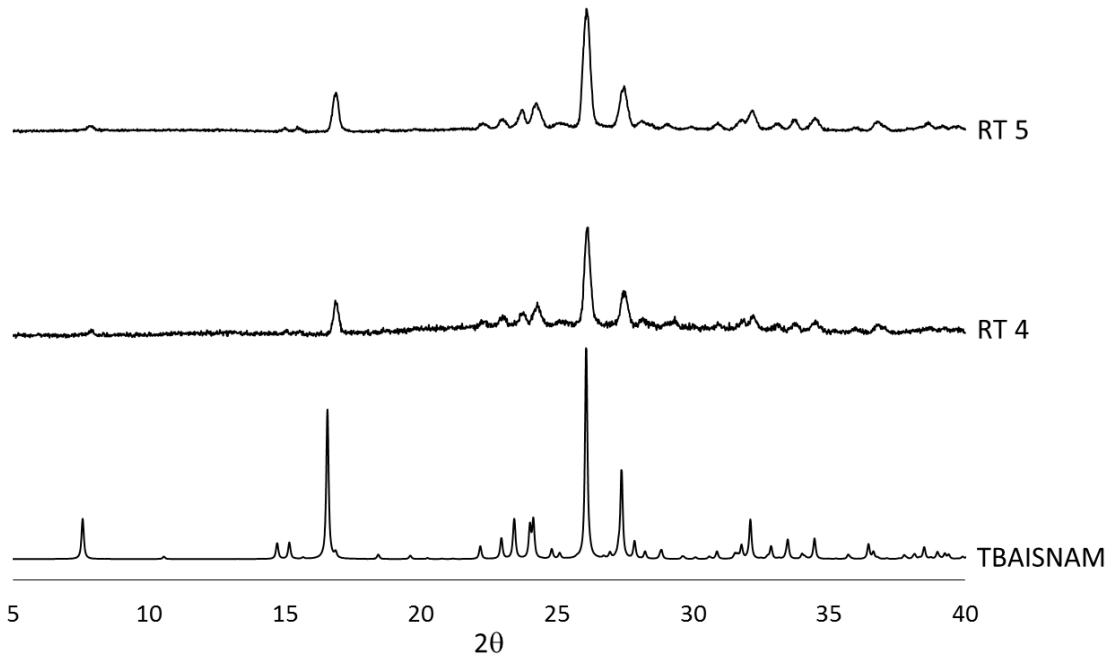

Figure 6.20: PXRD patterns of samples from TR 4 and RT 5 of TBAISNAM KRAIC 3.

6.4 The Novel Thiobarbituric Acid Nicotinamide (TBANAM) Salt System

6.4.1 Evaporative Crystallisation of the TBANAM Salt System

A second novel multi-component form of thiobarbituric acid was accessed, in this case with nicotinamide acting as the counter ion during the evaporative crystallisation experiments described above. The salt form was obtained utilising a 1:1 ratio of the two

starting components at both 5 °C and room temperature. The salt was accessed from all four solvent media investigated as part of this study (water, ethanol, IPA and methanol). The resultant solid was orange in colour and the crystals displayed a block-like habit. The systems were initially identified as novel due to their PXRD patterns not matching those of the starting components, as well as DSC experiments showing unique thermal behaviour with respect to the starting materials. The PXRD and DSC data will be discussed in section 6.4.2 and 6.4.3 respectively.

6.4.2 The Crystal Structure of the TBANAM Salt System

Single crystal X-ray diffraction experiments were conducted on the resultant solid, indicating that a new unit cell had been obtained. A single crystal data collection was then run on the solid using the Rigaku Oxford Diffraction Supernova diffractometer with Mo-$K_{\alpha 1}$ radiation (λ = 71073 Å).

The crystal structure shows that the TBA entities exist in their enol tautomer form, with both nitrogen atoms and one of the oxygen atoms being protonated, as was seen with the novel TBAISNAM salt above. A hydrogen atom is transferred from the hydroxyl group of the enol tautomer of TBA to the pyridine nitrogen of the nicotinamide, resulting in the system being a salt, not a co-crystal. Interestingly, only one of the two of the TBA ions within the asymmetric unit display a hydrogen bond along this hydrogen transfer pathway. It can therefore be possible that the hydrogen transfer occurs within the solution phase of the crystallisation process, and not as a direct result of the crystal packing. The bond length of each C-O bond in the deprotonated TBA ion is equal due to resonance within the structure. It is thus unclear which oxygen has been deprotonated and which was part of the original carbonyl functionality.

Within the crystal structure for the TBANAM salt system there are a total of 16 hydrogen bonds formed, summarised in Table 6.8. It can be seen that six of these involve a CH group, with the rest utilising the NH functionalities of the molecules.

The TBANAM salt system crystallises in the $P\bar{1}$ space group with two ions of each component present in the asymmetric unit (Figure 6.21 (a)). Within the asymmetric unit, the deprotonated TBA ions form a hydrogen bonded dimer ($R_2^2(8)$) with these two bonds forming between N2-H2 and O5 and N6-H6 and O2 (Figure 6.21). Two further hydrogen bonds are present in the asymmetric unit, forming between each carbonyl group on the TBA ion and the NH_2 group of each nicotinamide ion (N4-H4B···O5 and N4-H4B···O4; Figure 6.21).

Table 6.8: Summary of hydrogen bonds in the TBANAM crystal structure.

D	H	A	d(D-H)/Å	d(H-A)/Å	d(D-A)/Å	D-H-A/°
N1	H1	O4[1]	0.82(2)	2.00(2)	2.822(2)	179(2)
N2	H2	O5	0.85(2)	2.01(2)	2.864(2)	176(2)
N5	H5A	O1[2]	0.88(2)	1.95(2)	2.834(2)	178(2)
N6	H6	O2	0.86(2)	2.00(2)	2.862(2)	177(2)
N3	H3	O2[3]	0.98(3)	1.68(3)	2.657(2)	177(2)
N4	H4A	O6[4]	0.85(2)	2.12(2)	2.957(2)	174(2)
N4	H4B	O5	0.88(2)	2.06(2)	2.939(2)	172(2)
C5	H5	S2[3]	0.96(2)	2.60(2)	3.356(2)	136(2)
C5	H5	O5	0.96(2)	2.58(2)	3.314(2)	133(2)
C9	H9	S1[5]	0.99(2)	2.89(2)	3.686(2)	138(2)
N7	H7A	O1[3]	0.95(2)	1.74(2)	2.689(2)	177(2)
N8	H8A	O3[4]	0.92(2)	1.95(2)	2.857(2)	174(2)
N8	H8B	O4	0.87(2)	2.04(2)	2.891(2)	168(2)
C15	H15	O4	0.95(2)	2.33(2)	3.215(2)	155(2)
C19	H19	S2[6]	0.95(2)	2.71(2)	3.350(2)	125(2)
C19	H19	O5[5]	0.95(2)	2.35(2)	3.098(2)	135(2)

[1]-1+X, -1+Y, +Z;
[2]1+X, 1+Y, +Z;
[3]1-X, 2-Y, 1-Z;
[4]1-X, 2-Y, -Z;
[5]+X, 1+Y, +Z;
[6]2-X, 3-Y, 1-Z

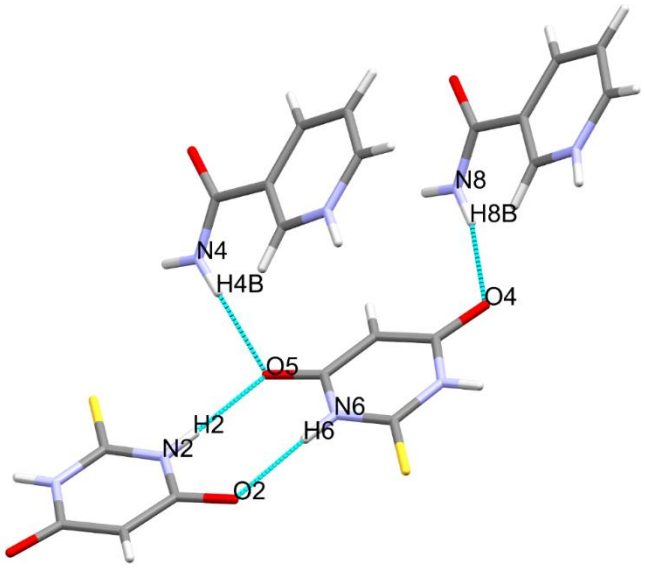

Figure 6.21: The asymmetric unit of the TBANAM salt system.

Throughout the crystal structure the dimer of hydrogen bonds formed between adjacent TBA molecules within the asymmetric unit gives rise to a one-dimensional TBA chain network, as was seen in the TBAISNAM structure. The TBA ion that is not involved with any inter-asymmetric unit TBA - nicotinamide hydrogen bonds forms two hydrogen bonds with two nicotinamide units from an adjacent asymmetric unit. These hydrogen bonds are formed between the carbonyls of the TBA ion and the protonated NH^+ of the nicotinamide pyridine rings (N7-H7A···O1 and N3-H3···O2). The formation of these hydrogen bonds gives rise to the formation of an extended chain network, where the TBA chains act as a backbone, as shown in Figure 6.22.

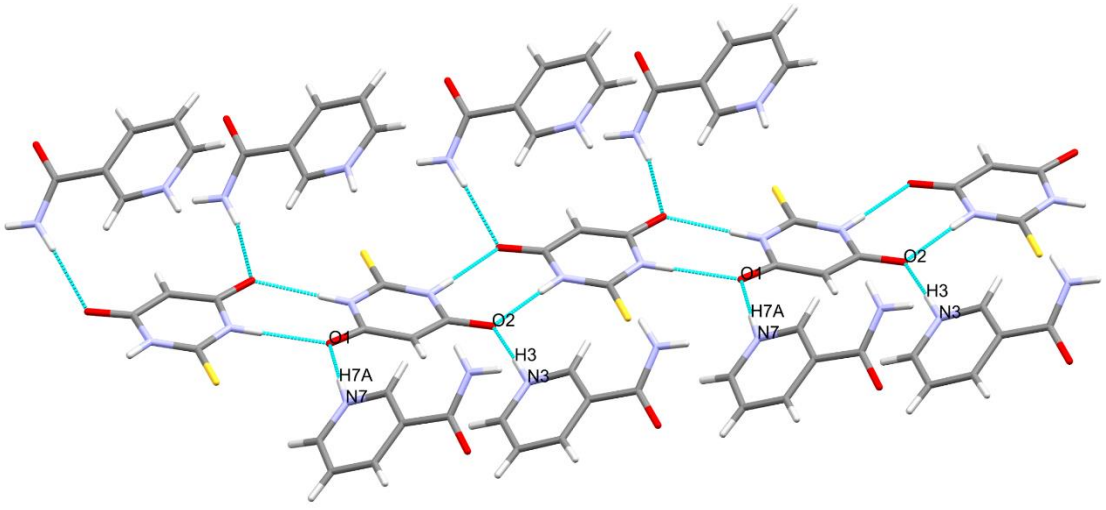

Figure 6.22: Extended chain network in the TBANAM crystal structure.

These extended chain networks are linked to one another by the formation of hydrogen bonds between adjacent nicotinamide units; each nicotinamide ion forms a hydrogen bonded dimer with an adjacent nicotinamide unit (that forms part of a separate chain network). The dimer forms between the amide groups of the two ions (N8-H8A···O3

and N4-H4A···O6; Figure 6.23). Figure 6.23 demonstrates how each nicotinamide hydrogen bonded dimers links together four TBA chain networks which results in the formation of two-dimensional 'sheets' within the crystal structure (Figure 6.24 (a)). These sheets lie parallel to the *c* axis of the unit cell and result in a wave-like packing arrangement (Figure 6.24 (b)).

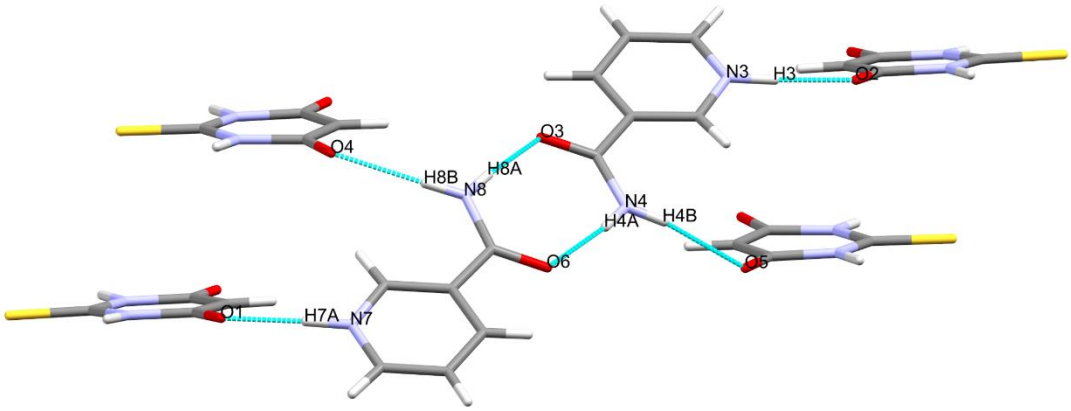

Figure 6.23: Hydrogen bonded nicotinamide dimer present in the TBANAM crystal structure.

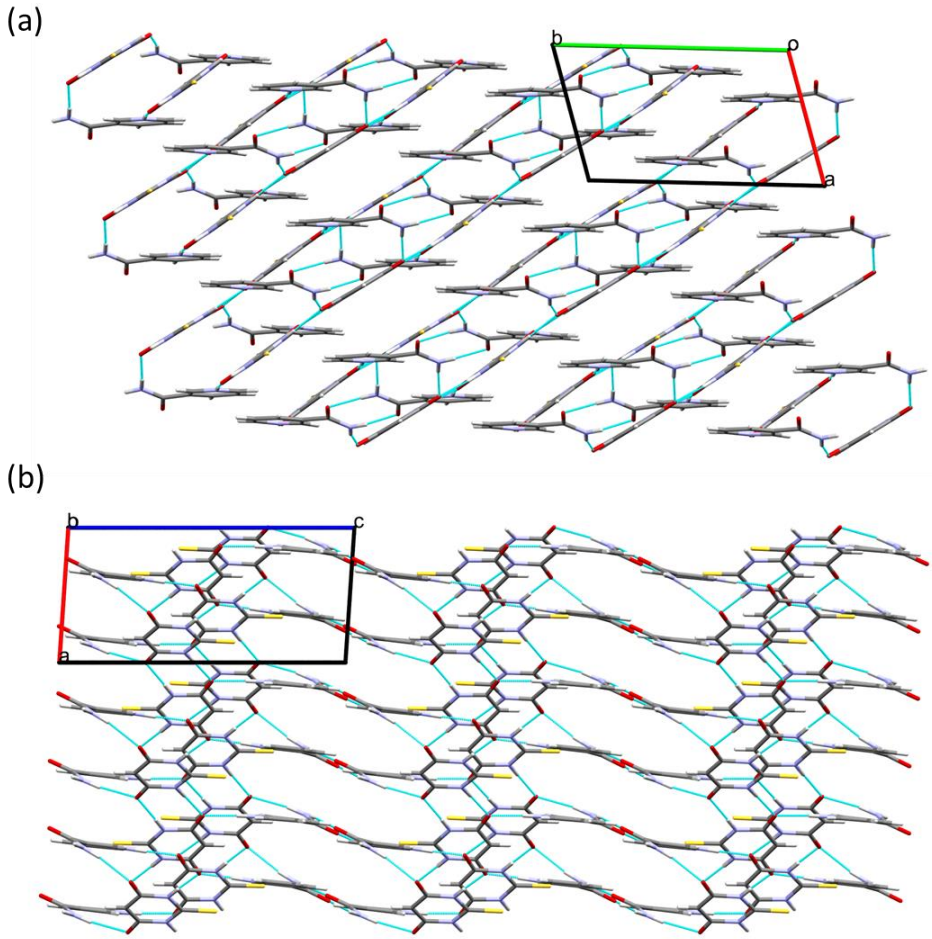

Figure 6.24: Packing in the TBANAM crystal structure as viewed along the c axis (a) and b axis (b).

The single crystal structure obtained from this work was used to calculate a PXRD pattern for the salt system. This was in turn compared to the experimental PXRD pattern of the solid obtained from small scale evaporative crystallisation experiments (Figure 6.25). It can be seen that the calculated and experimental patterns are a close match, however the PXRD pattern of the experimental system does not clearly exhibit every peak seen in the calculated pattern.

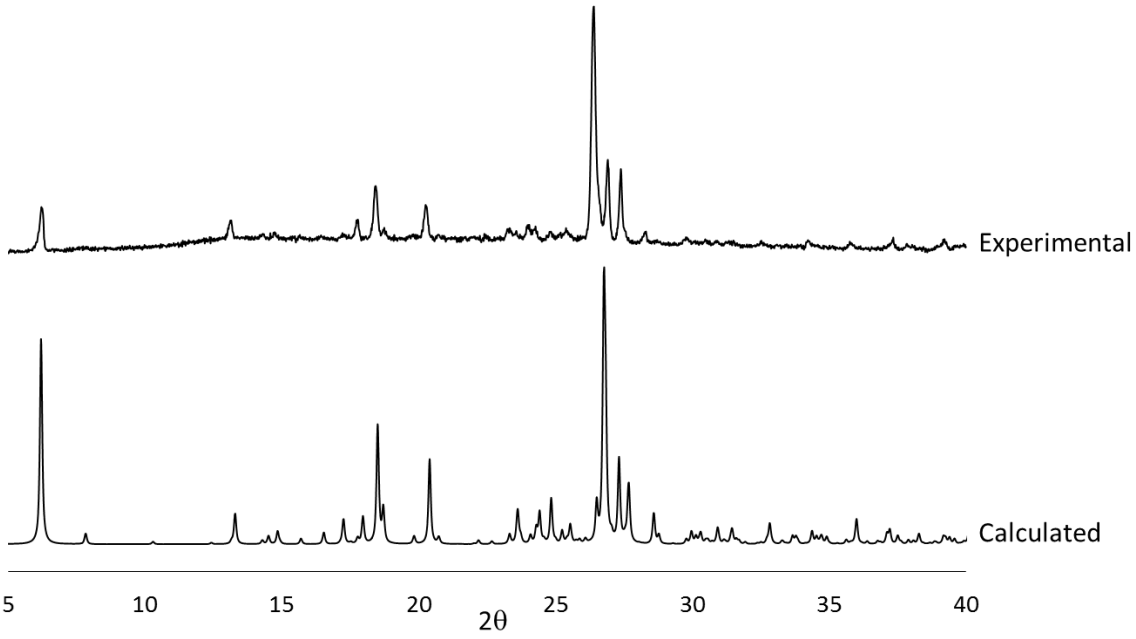

Figure 6.25: Calculated and experimental PXRD pattern of the TBANAM salt system (experimental pattern obtained from evaporative crystallisation of the sample from water at RT.

6.4.3 The Thermal Behaviour of the TBANAM Salt System.

One of the ways in which the novel salt system was identified was by DSC analysis of the evaporative crystallisation products: the thermal behaviour for the novel system was significantly different to that of the starting components (Figure 6.26). The DSC trace for the TBANAM salt system exhibits a single endothermic event at 215 °C immediately followed by a small exothermic event. This suggests that upon heating, the salt system melts at 215 °C and a high temperature solid form crystallises from this melt. As the melting point for TBA is 245 °C it is likely that upon the melting of the salt system the TBA molecules come together and recrystallise as a single component system, with the nicotinamide remaining in the liquid phase.

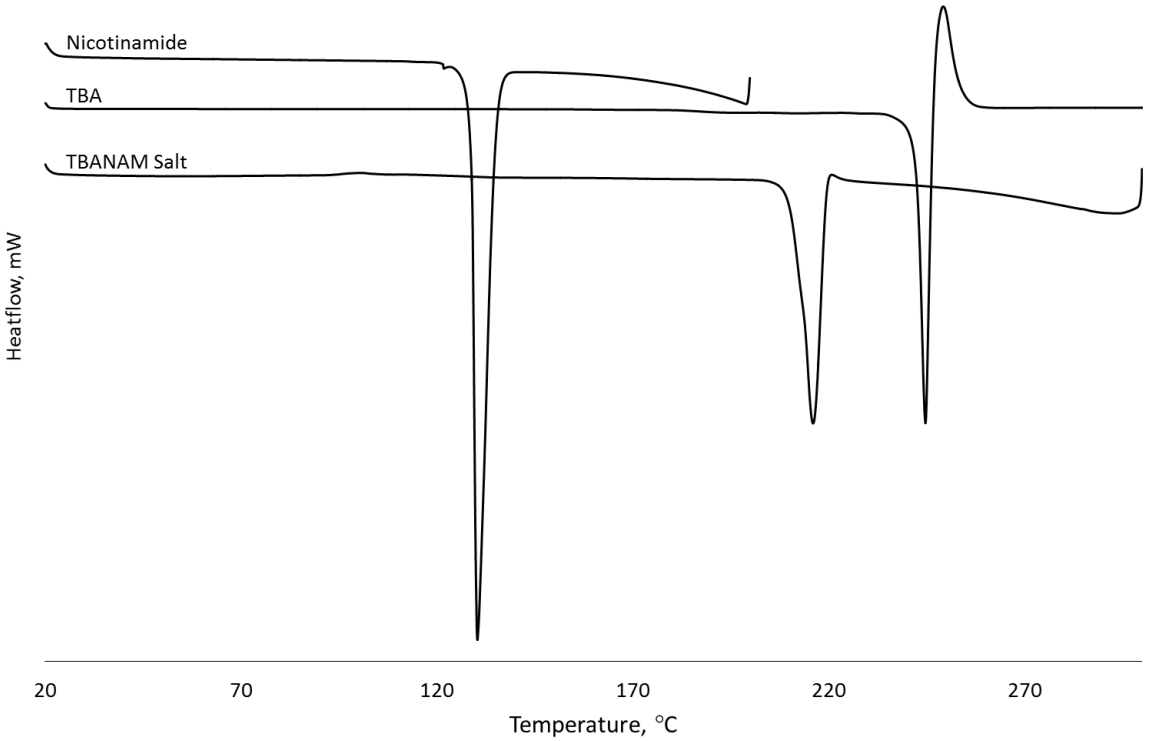

Figure 6.26: DSC traces of nicotinamide, TBA and the TBANAM salt system (10 °C min^{-1} heating rate).

6.4.4 Solution-mediated Multi-Component Phase Transformations (Slurry Techniques) for the Access of the TBANAM Salt System.

Small scale slurry experiments were conducted using both TBA and nicotinamide in order to investigate whether the salt system could be accessed under these conditions. As the salt system was accessed using four solvents in the evaporative crystallisation studies, each of these solvents was tested in the slurrying environment. A 1:1 molar ratio of the starting materials (150 mg of TBA) was used with 2 mL of solvent. The systems were left mixing at 250 rpm on a Drysyn hotplate set to 30 °C for a period of one week. The solid product was isolated using vacuum filtration and left to dry at room temperature before being analysed using PXRD and DSC.

The PXRD patterns for the resultant slurry products can be seen in Figure 6.27. When water, ethanol and IPA were used as the solvent media it can be seen that the TBANAM salt was accessed, with no remaining starting components being apparent in the solid product. However, some peak shift can be observed and it can be seen that the PXRD peaks for the slurry products are much broader than the calculated pattern. The water mediated slurry product PXRD pattern has sharper peaks than the alcohol mediated patterns. The methanol mediated slurry, however, did not produce the desired TBANAM salt, with the PXRD pattern not matching that if the salt system or the starting materials, suggesting that a novel solid form had been accessed under these conditions.

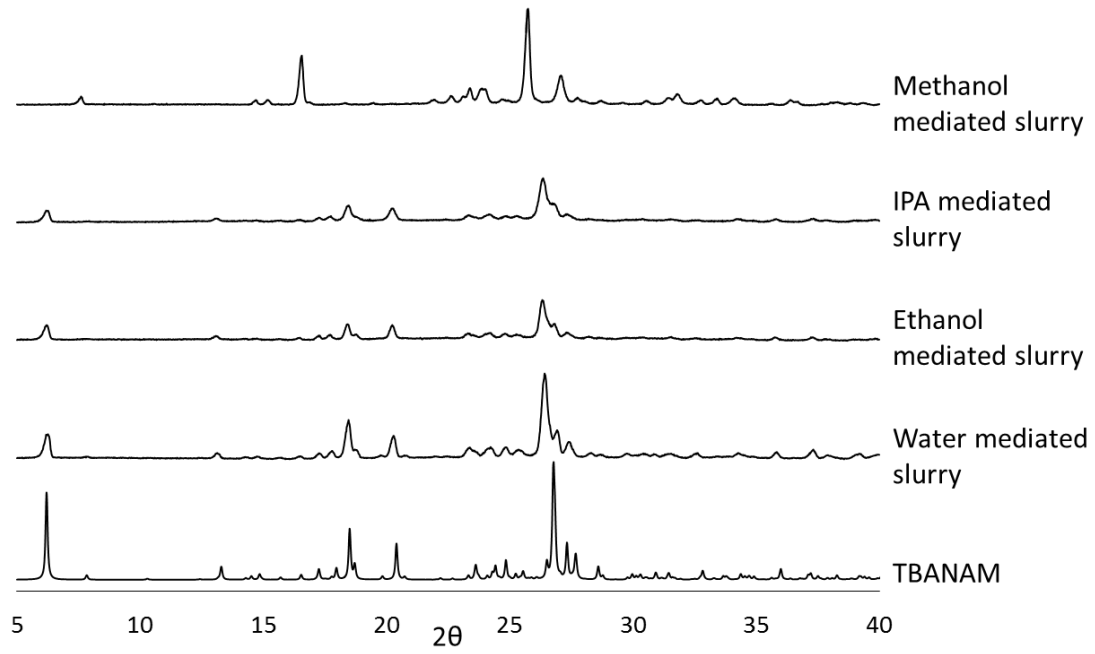

Figure 6.27: PXRD patterns of the TBA nicotinamide slurry products.

The DSC traces for the slurry products all display endothermic events at approximately 215 °C providing further evidence that the multi-component salt system had been accessed (Figure 6.28). For the IPA mediated slurry product a shoulder can be seen in the endothermic peak at approximately 206 °C. This shoulder may be due to small amounts of an additional solid in the slurry product that was not observed by PXRD. The DSC trace for the water mediated slurry product exhibits a broad and shallow peak around 76 °C, this is likely arising from residual water in the solid evaporating.

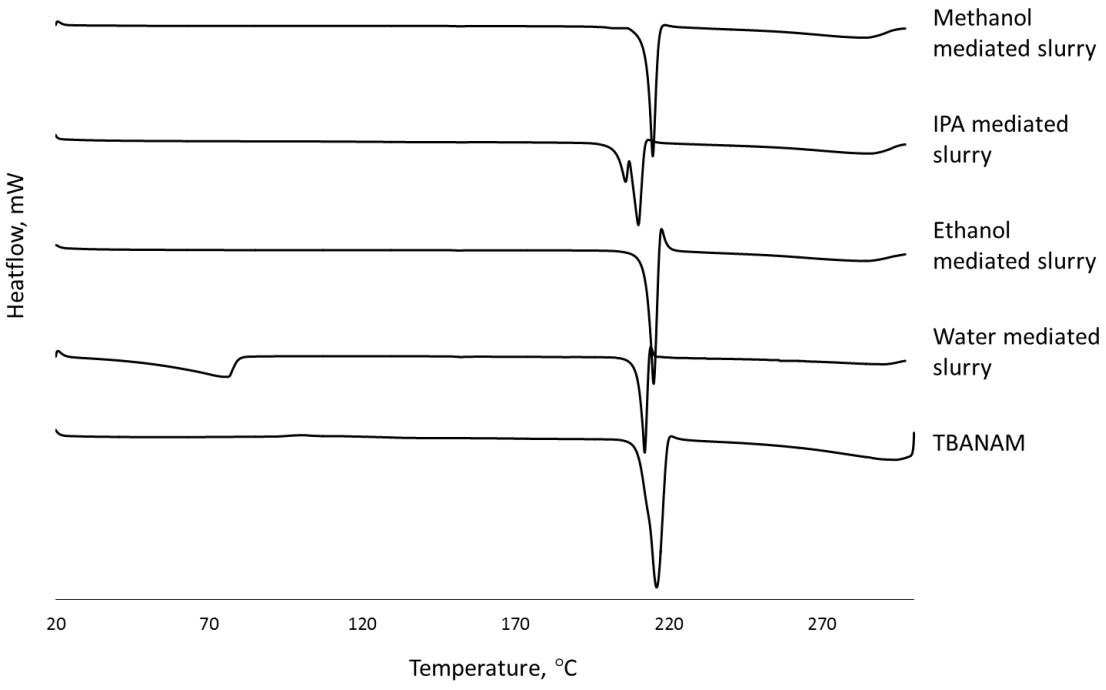

Figure 6.28: DSC traces of the TBA nicotinamide slurry products.

6.4.5 Mechano-chemical Grinding Experiments for the Access of the TBANAM Salt System

Due to the selective access of the TBANAM salt system using both evaporative crystallisation and slurrying techniques, investigations into grinding were conducted. Grinding experiments using both a pestle and mortar and a ball mill were carried out using a 1:1 ratio of the starting components. For the experiment using a pestle and mortar 40 mg of TBA was used, with 34 mg of nicotinamide. The samples were ground by hand for 15 minutes before being analysed using both PXRD and DSC.

PXRD analysis of the products showed that the salt system was accessed when using the pestle and mortar to grind the sample by hand (Figure 6.29), however the pattern possesses a lot of noise suggesting that the sample has become slightly amorphous during the grinding experiments.

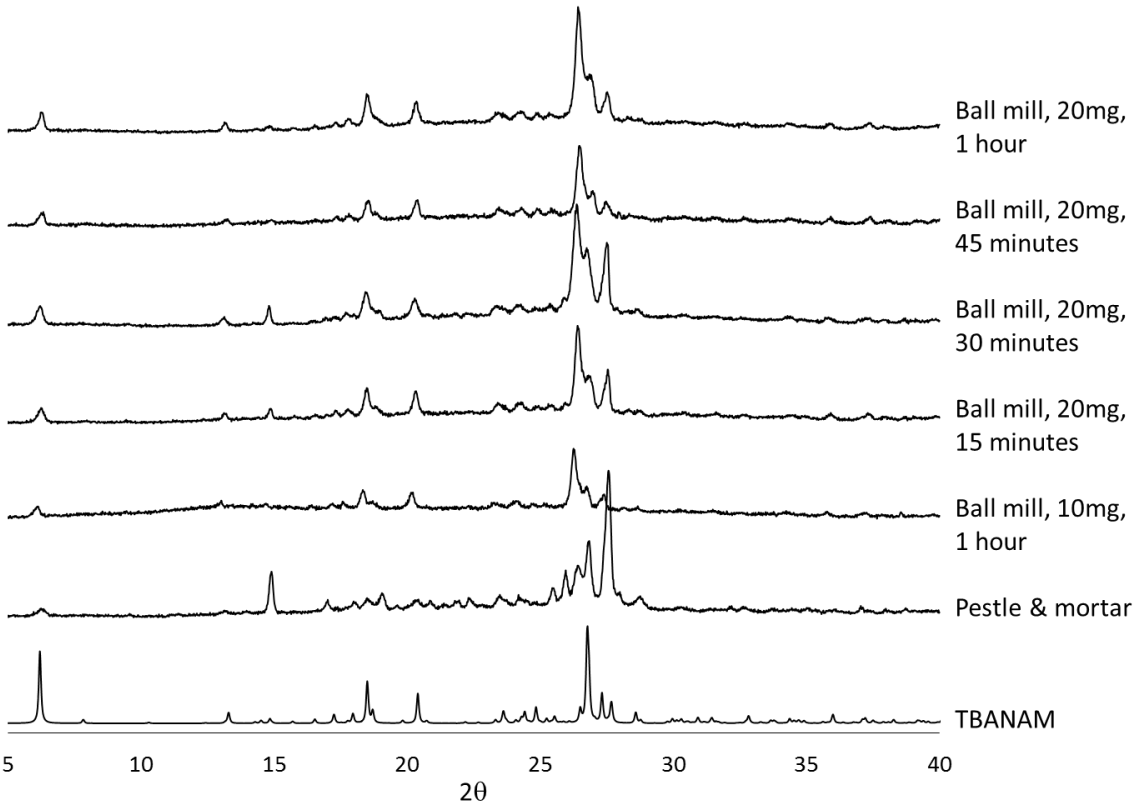

Figure 6.29: PXRD patterns of the TBA nicotinamide grinding experiment products.

Upon transfer of the grinding from the pestle and mortar to the ball mill, an initial experiment was conducted using 10 mg of TBA and 8.5 mg of nicotinamide. The system was placed in the ball mill for a period of 1 hour. The PXRD data suggests that the resultant solid is the desired salt system, however there are rather few peaks, suggesting that the sample is largely amorphous. The intensities of the peaks are also different to those in the calculated PXRD pattern, but do appear at angles corresponding to peaks for the salt system. Subsequent experiments were conducted using 20 mg of TBA and 17 mg of nicotinamide and investigated the effect that the experiment duration had on

the solid form outcome. The PXRD data implies that after grinding for 15 minutes the salt system was formed, however the pattern is very similar to that of the initial ball mill experiment. Upon increasing the experimental time it can be see that the PXRD patterns do not change significantly. This suggests that there is full conversion of the starting components to yield the salt within 15 minutes: no peaks are visible corresponding to the starting components. However, the resultant patterns possess very high levels of noise and peak broadness and it can therefore be concluded that upon grinding the sample in the ball mill the solid quickly loses some crystallinity.

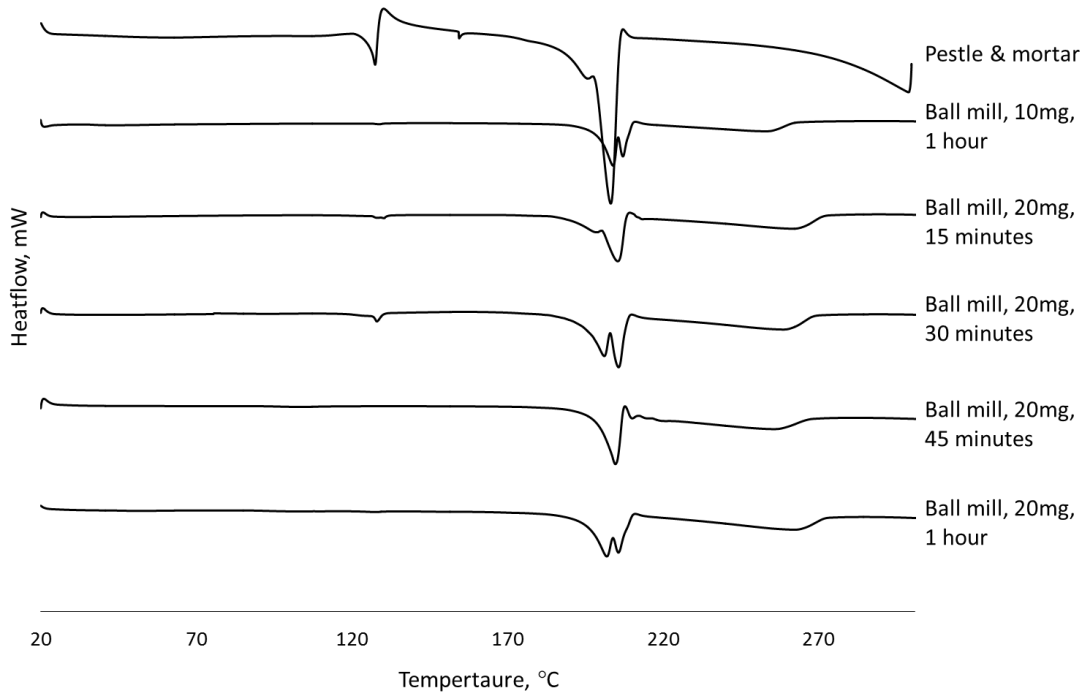

Figure 6.30: DSC traces of TBA nicotinamide grinding experiment products.

Each solid product was also subject to DSC analysis in order to further clarify which solid form had been accessed (Figure 6.30). It can be seen that the DSC trace for the product obtained from the pestle and mortar experiment has an endothermic peak at approximately 128 °C, the temperature at which nicotinamide melts. This indicates that complete conversion of the starting components to yield TBANAM has not occurred in this experiment. The presence of nicotinamide in this solid product was not observed in the PXRD pattern; PXRD is not as sensitive as DSC and as a result DSC picks up trace amounts of impurities in the solid. It can be seen that upon transfer to the ball mill, with 10 mg of TBA being used, complete conversion is almost achieved, with only a very small blip in the DCS trace being observed at 128 °C. It can be seen, however, that the endotherm at approximately 215 °C, where the salt melts, is split into two. This may be due to different particle sizes being present in the sample, resulting in different onset temperatures for their melting. Another reason for this split in the endotherm may be that an additional solid form is being accessed during the grinding experiments which melts at a similar temperature to that of the targeted salt form resulting in overlapping melting events. This additional solid form could be the novel form accessed via methanol

mediated slurry experiments as discussed in Section 6.4.4. This same shape is also seen with the 15 minute, 30 minute and 1 hour ball mill experiments using 20 mg, but not in the 45 minute ball mill sample.

The DSC data further confirms that the salt system can be accessed from the starting components using grinding techniques, however there are significant issues with loss of crystallinity using this technique.

6.4.6 Solubility Analysis of the TBANAM Salt System

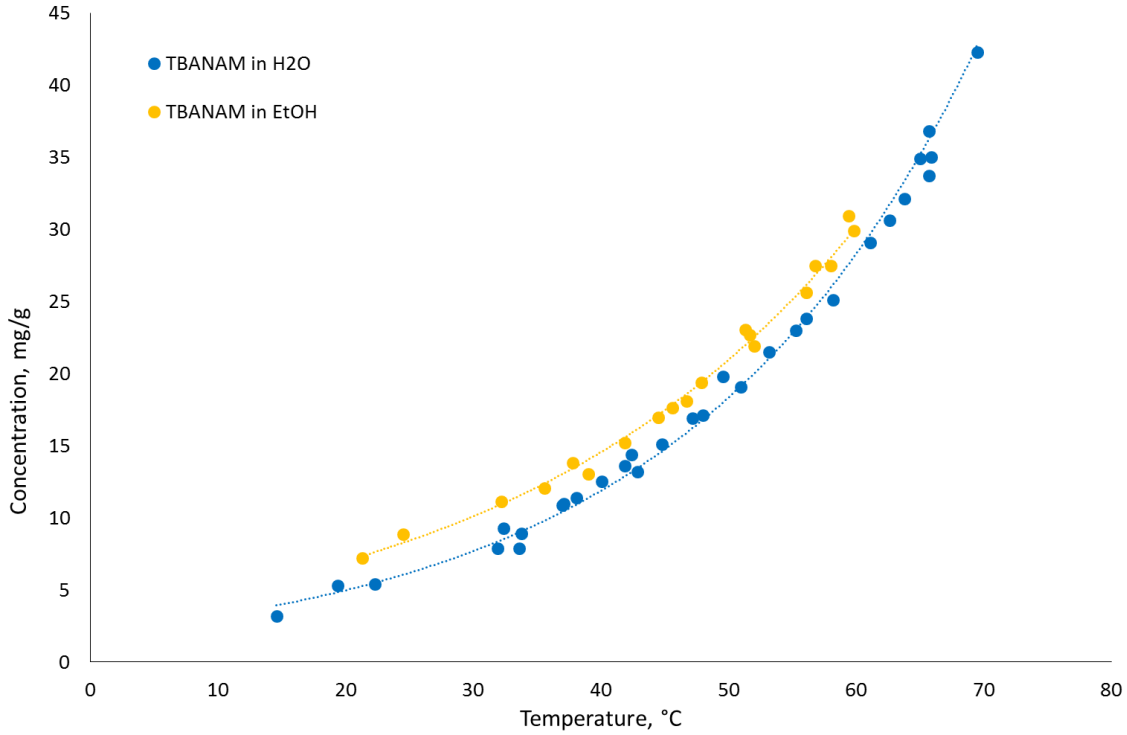

Figure 6.31: Solubility of TBANAM in water (blue) and ethanol (yellow) obtained using the Crystal16.

Solubility measurements of the thiobarbituric acid salt system were obtained using the Crystal16 at the University of Strathclyde in order to design subsequent cooling crystallisation experiments. The data were collected using a heating rate of 1 °C min^{-1} and the turbidity measurements were taken in both water and ethanol. Figure 6.31 shows the obtained solubility curves; it can be seen that the solubility of the salt system in ethanol is slightly greater than in water.

6.4.7 Batch Cooling Crystallisation of the TBANAM Salt System

Investigations into the transfer of the crystallisation of TBANAM into batch cooling crystallisation and the subsequent scale up of this process were conducted by a final year MChem student, Richard Wilkinson, under the supervision of the author.

6.4.7.1 1 mL Cooling Crystallisations of TBANAM from Water

Small scale cooling crystallisation (1 mL) experiments from water were conducted using the CRD Polar Bear Plus. Experiments using saturation temperatures of 50 °C and 60 °C, corresponding to solution concentrations of 18 mg/g and 27 mg/g respectively, were conducted. All systems were heated to 70 °C and left to dissolve for 30 minutes before being cooled to 5 °C at a rate of 1 °C min^{-1}. The systems were left at the final temperature for 30 minutes before being isolated by vacuum filtration and left to dry at room temperature. Each system was tested for solid form identity using PXRD. The PXRD data shows that the desired salt system was accessed selectively regardless of the saturation temperature used (Figure 6.32).

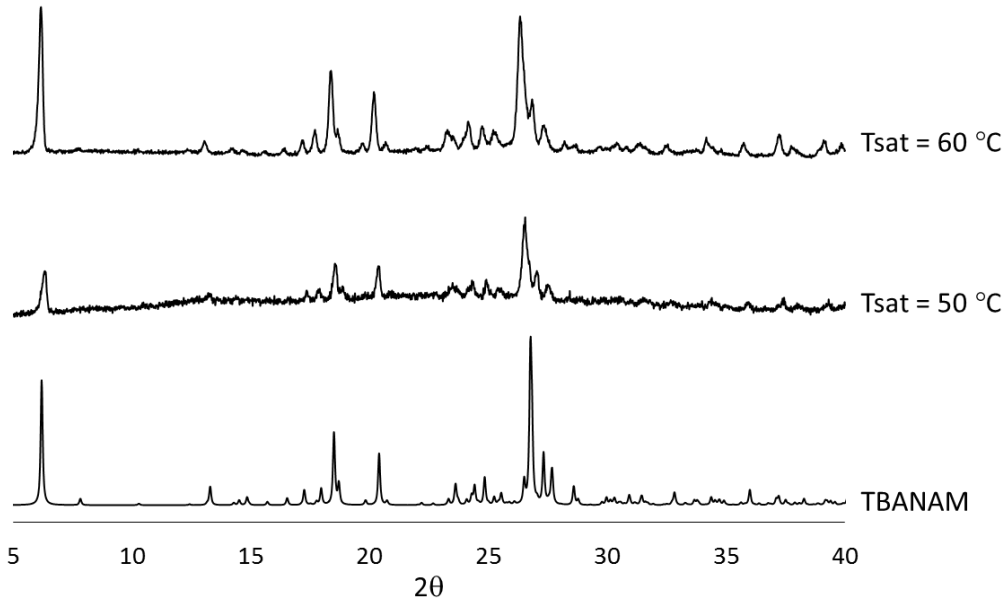

Figure 6.32: PXRD patterns of solid obtained from 1 mL cooling crystallisations of thiobarbituric acid nicotinamide from water.

6.4.7.2 Scale up of Cooling Crystallisations of TBANAM from Water to 150 mL

TBANAM was shown to be accessed selectively from 1 mL cooling crystallisation from water using two saturation temperatures (T_{sat} = 50 °C and 60 °C). The crystallisations were subsequently scaled up to 150 mL. During this study, several intermediate scales were used in order to ensure that the salt system was being accessed selectively from the process. Experiments at 5 mL, 10 mL, 50 mL and 150 mL were all conducted using the same saturation temperatures and cooling profile as the 1 mL system. Upon moving from the 10 mL scale to the $\geq$ 50 mL scale the crystallisations were no longer conducted using flat bottom vials with magnetic bottom stirring, and instead RBFs were used with overhead stirring. Product from each crystallisation was isolated via vacuum filtration and left to dry at room temperature before being analysed for solid form identity.

PXRD analysis of the solid product (Figure 6.33) shows that the TBANAM salt system was accessed selectively at each scale and was the sole product from each crystallisation. Repeat experiments showed that the crystallisation was reproducible and robust.

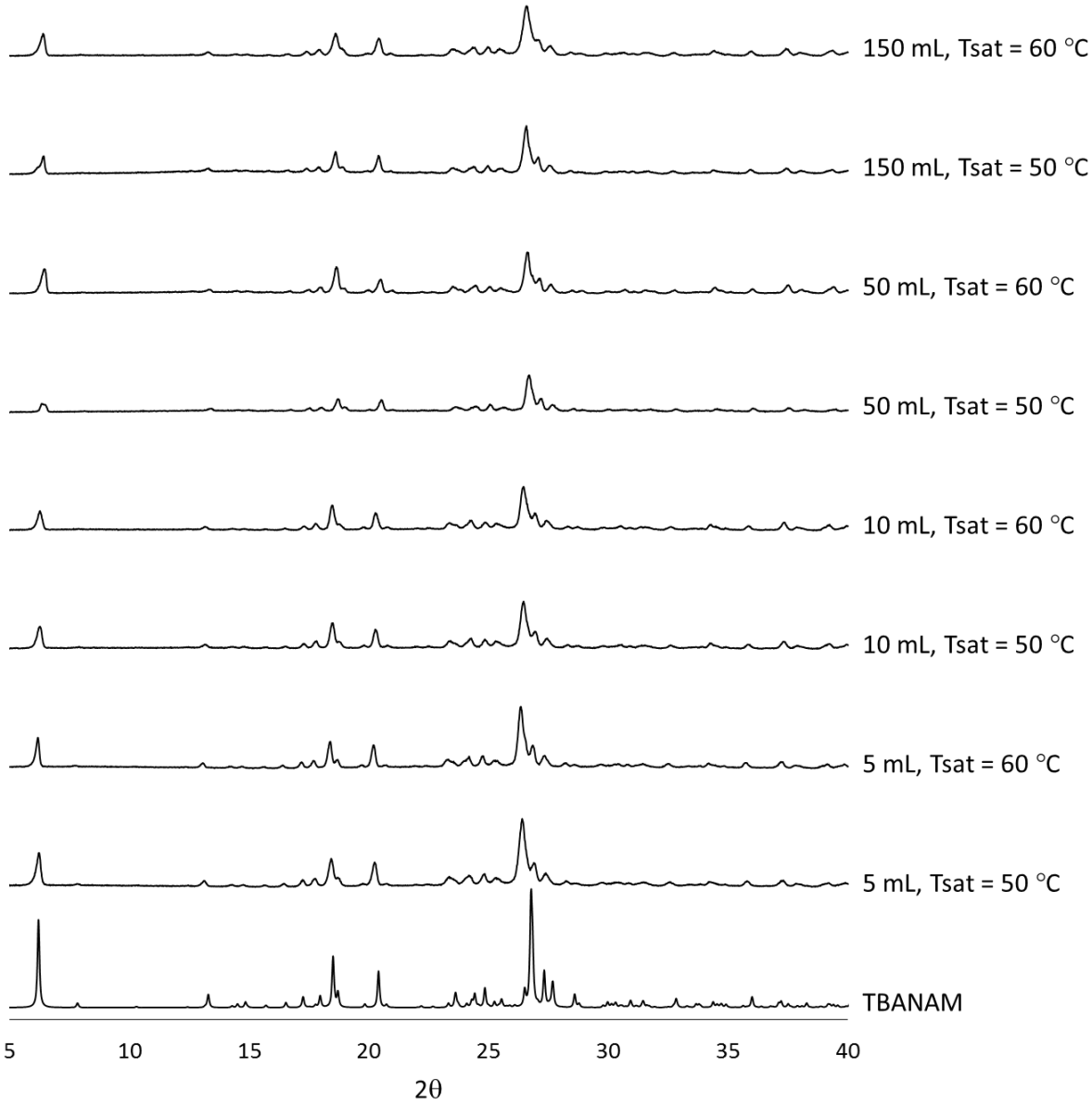

Figure 6.33: PXRD patterns of product from 5 mL - 150 mL batch cooling crystallisations of TBA and nicotinamide from water.

6.4.8 Continuous Cooling Crystallisation of the TBANAM Salt System

Due to success of accessing TBANAM from batch cooling crystallisation from water at a scale of 150 mL, investigations into continuous cooling crystallisation from water were conducted using both the COBC and the KRAIC platforms.

6.4.8.1 Continuous Cooling Crystallisation using the COBC

TBANAM COBC 1

For the transfer of the cooling crystallisation of TBANAM from water from batch to continuous methods using the COBC, a saturation temperature of 50 °C was taken forward. This corresponds to a solution concentration of 18 mg/g. Table 6.9 summarises

the experimental parameters chosen for the cooling crystallisation; the oscillation parameters and hence Reynolds numbers and Strouhal number are the same as for the UBA COBC runs presented in Chapter 5 as summarised in Table 5.9.

Table 6.9: Experimental parameters used for TBANAM COBC 1.

Feed concentration	18 mg/g
Flow rate	50 mL min^{-1}
Residence time (RT)	33 minutes 12 seconds
Feed temperature	60 °C
Straights 1 – 2 temperature	50/45†/35††/25‡ °C
Straights 3 – 6 temperature	15/10‡/7.5‡‡/2.5‡ °C
Straights 7 – 10 temperature	10/7.5‡‡/2.5‡ °C
Straights 11 – 12 temperature	10/7.5‡‡/2.5‡ °C

‡ Temperature reduce at 36 minutes into run
† Temperature reduced at 54 minutes into run
†† Temperature reduced at 1 hour 6 minutes into run
‡‡ Temperature reduced at 1 hour 10 minutes into run
‡ Temperature reduced at 1 hour 28 minutes into run

The continuous crystallisation was run for four RTs (approximately 2 hours and 13 minutes) with solid from the first three RTs being collected. The initial temperatures for the straights were based on the previous continuous cooling crystallisations conducted using the TBAISNAM salt system above. As no nucleation occurred in the system, the temperatures of all 12 straights were periodically reduced in an attempt to induce nucleation. After 36 minutes straights 3 – 6 were reduced to 10 °C with straights 1 -2 being reduced firstly to 45 °C at 54 minutes, and then to 35 °C at 1 hour and 6 minutes. This reduction in temperature did not induce any nucleation and as a result, straights 3 – 12 were subsequently reduced to 7.5 °C. After 1 hour and 28 minutes no crystals could be seen in the crystalliser; consequently straights 1 – 2 were reduced to 25 °C and straights 3 – 12 to 2.5 °C. After 1 hour and 40 minutes some very fine crystals could be observed on the filter paper as well as in the exit tubing. After two hours the nucleation in the system had not progressed to an earlier point in the crystalliser, even with the significant reduction in temperature of the system. Some large crystals could be seen in the end piece; these seemed to be remaining in the end piece and not exiting the crystalliser. After 2 hours and 12 minutes the run was terminated.

Unfortunately, even with the significant reduction in temperature the system did not nucleate until very late on in the run and very little solid was collected. The solid that was collected was subject to PXRD in order to determine the solid form identity. It can be seen that the desired TBANAM salt system was accessed during the continuous cooling crystallisation (Figure 6.34).

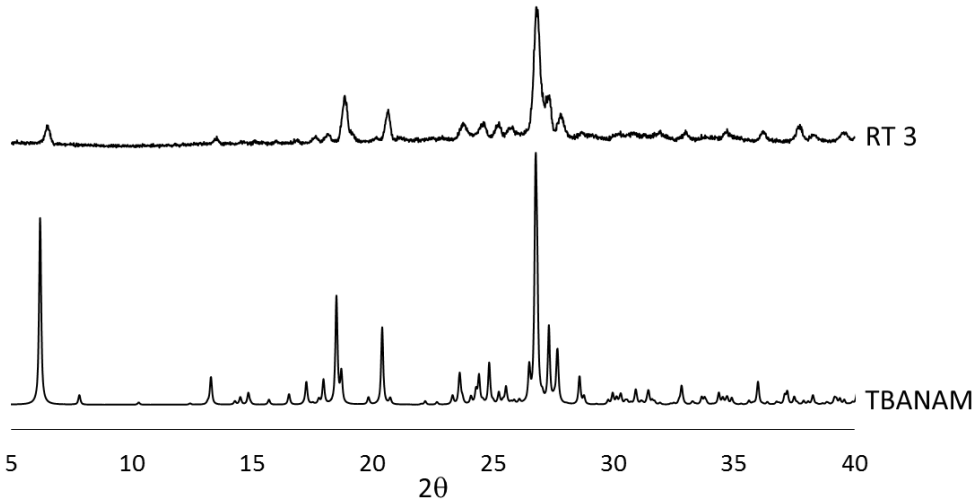

Figure 6.34: PXRD pattern of solid obtained from RT 3 of the continuous cooling crystallisation of TBA nicotinamide using the COBC.

TBANAM COBC 2

Table 6.10: Summary of experimental parameters used for TBANAM COBC 2.

Feed concentration	23 mg/g
Flow rate	50 mL min^{-1}
Residence time (RT)	33 minutes 12 seconds
Feed temperature	60 °C
Straights 1 – 2 temperature	30 °C
Straights 3 – 6 temperature	5 °C
Straights 7 – 10 temperature	5 °C
Straights 11 – 12 temperature	5 °C

As the system did not nucleate until the end piece of the crystalliser in the first COBC experiment, a second experiment was conducted using a slightly higher solution concentration (T_{sat} = 55 °C, concentration = 23mg/g). The initial temperature of the straights was also significantly reduced in comparison to COBC 1 due to the temperatures having to be reduced significantly in the previous run. The overall parameters for the run COBC 2 can be seen in Table 6.10.

During the run issues with air bubbles getting into the straights were encountered and these were unable to be removed; the cause of the air was unclear. After one RT (33 minutes and 12 seconds) some crystals were observed in/around an air bubble in straight 5 (Figure 6.35 (a)) and soon resulted in 'loose' crystals being seen in this straight. The nucleation at this point in the crystalliser is likely due to the presence of the air bubble prompting heterogeneous nucleation in the system. 36 minutes into the run crystals were then observed in straight 6 with nucleation occurring on air bubbles in straight 9. After 38 minutes crystals could be seen in straights 10, 11 and 12. However, issues with encrustation were encountered 41 minutes into the run, with straights 4 – 12 being affected. After 1 hour the encrustation in straights 3 and 4 was quite severe and there was an observed difference in colour of the solid obtained in earlier straights (a pale coral) when compared with later straights (cream/off-white) as can be seen in Figure 6.35. This variation in colour throughout the length of the crystalliser could be arising from the presence of different solid forms. It could be that a metastable form is accessed initially in the process which then transforms to the isolated salt form, changing form coral to cream/off-white.

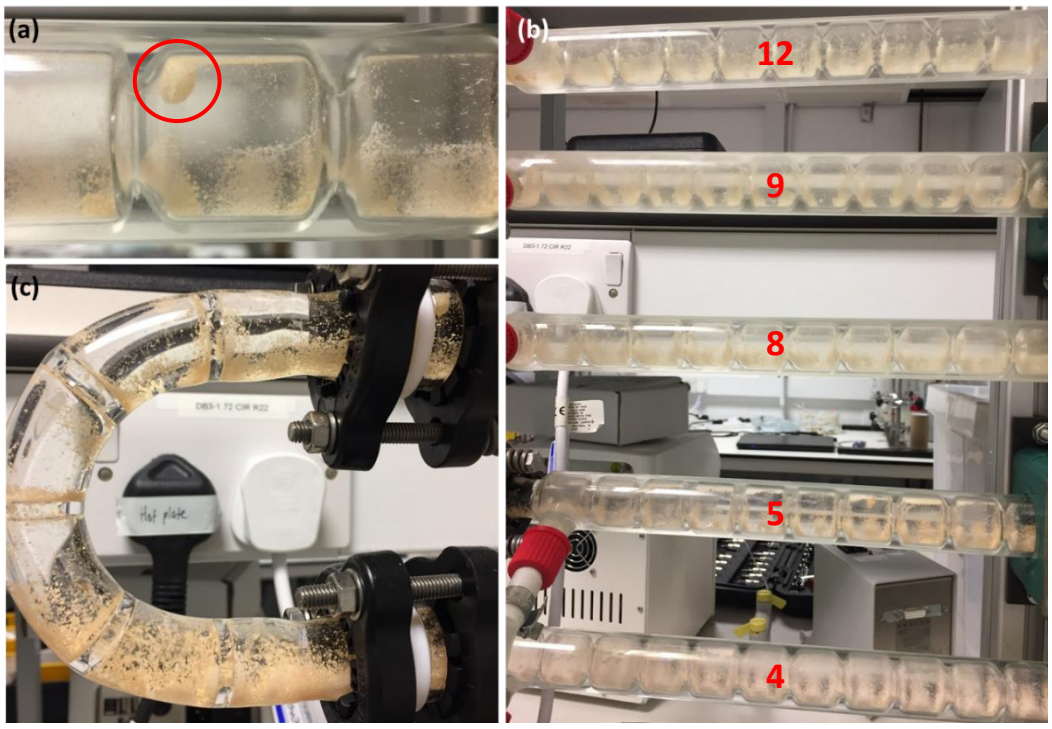

Figure 6.35: Images of TBANAM COBC 2: (a) crystallisation around air bubble in straight 5, (b) encrustation in COBC (straights 4, 5, 8, 9, and 12) and (c) sedimentation in bend between straights 8 and 9.

After 1 hour and 6 minutes (2 RTs) the input was changed to the primer solution. It appeared that there were no longer any free crystals in straights 3 and 4 and that the straights were severely encrusted. Straights 5 to 6 appeared to have relatively low solid loading in terms of free crystals and the solid loading appeared to increase moving from straights 6 to 12. Issues with sedimentation in the bends were also observed after 1 hour of run time, with sedimentation seen in bends between 5 and 6, 7 and 8, and 9 and 10 (Figure 6.35 (c)). Sedimentation was also observed in the exit tubing. After 3 RTs (1 hour

39 minutes) the flow was maximised in order to collect all the remaining solid that was trapped inside the crystalliser and the process was terminated.

Solid form analysis conducted on material collected from RT 1 and 2 was conducted using PXRD and the patterns show that the desired TBANAM salt system was obtained in each RT. It can be seen that some peak broadening and peak splitting is apparent in the patterns, with the peak sharpness and intensity increasing with later RTs. This is likely a consequence of the system heading towards steady state and accessing more crystalline particles as the system settles.

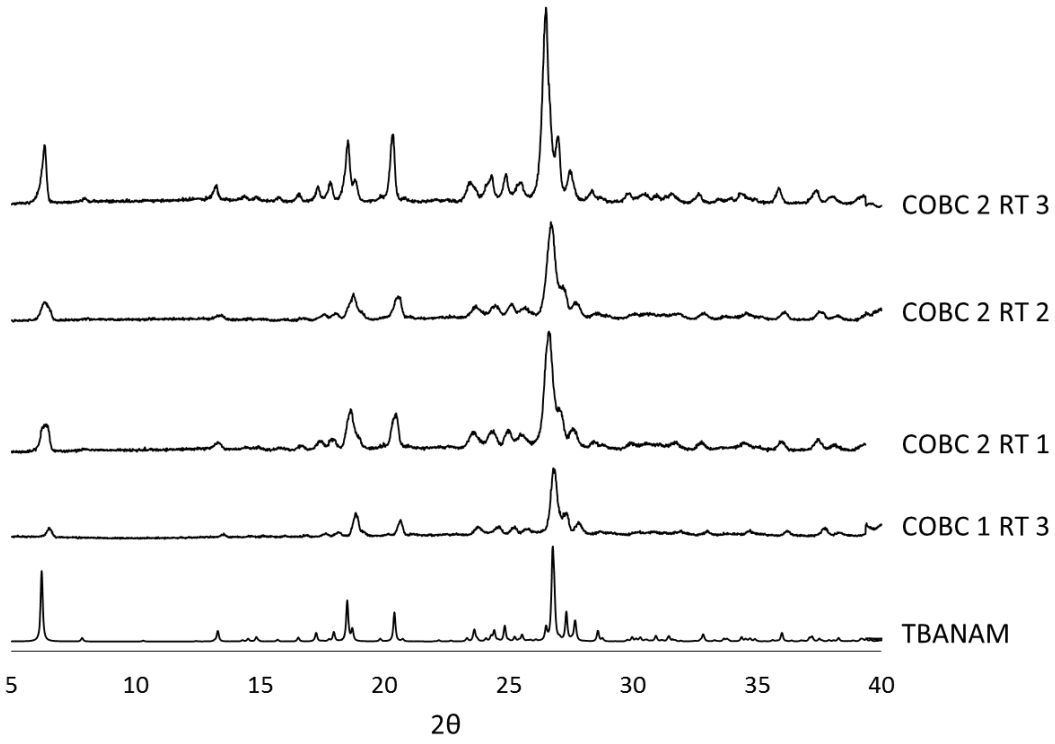

Figure 6.36: PXRD patterns of solid obtained from TBANAM COBC 1 and COBC 2.

Evidently, this continuous cooling crystallisation requires significant optimisation in order to access nucleation earlier in the process without causing severe encrustation. Subsequent experiments should be conducted with the straights being set to intermediate temperatures alongside a longer RT. This could allow the system more time to cool at a slower cooling rate and allow for a longer time for nucleation to occur. The longer RT could be achieved by reducing the flow rate of the system, however, this could lead to the system no longer mimicking plug flow. Another way in which to increase the RT would be to increase length of the crystalliser to allow for a larger volume. This could allow for significant increase in RT without affecting the flow properties. Further experiments could also be conducted using a higher saturation temperature, such as 60 °C, with higher temperatures used in the straights.

6.4.8.2 Continuous Cooling Crystallisation using the KRAIC

TBANAM KRAIC 1

The KRAIC platform was also investigated for the continuous cooling crystallisation of TBANAM from water. For this study, a saturation temperature of 60 °C was used, corresponding to a concentration of 27 mg/g. Table 6.11 below summaries the experimental parameters used for the first run conducted for this system.

Table 6.11: Summary of experimental parameters for TBANAM KRAIC 1.

Parameters	TBANAM KRAIC 1
Feed concentration	27 mg/g
Feed flow rate	2 mL min^{-1}
Carrier fluid flow rate	4.18 mL min^{-1}
Air flow rate	6.26 mL min^{-1}
Residence time (RT)	18 minutes 20 seconds
Feed temperature	65 °C
Transfer tube temperature	50/45†/40††/45‡‡/48‡ °C
Mixer bath temperature	45/40†/35‡/40‡‡/43‡/45‡‡ °C

† Temperature reduced 22 minutes into run
†† Temperature reduced 36 minutes into run
‡ Temperature reduced 47 minutes into run
‡‡ Temperature increased 53 minutes into run
‡ Temperature increased 1 hour into run
‡‡ Temperature increased 1 hour 11 minutes into run

It can be seen that for this run the RT was 18 minutes and 20 seconds. The feed temperature was set at 5 °C higher than the chosen saturation temperature (65 °C), but the temperature of the jacketed transfer tube was set at 50 °C, 10 °C below the saturation temperature. This was done in an attempt to cool down the solution before it reached the mixer piece and segmentation occurred. In the COBC set up it was seen that the temperature needed to induce the nucleation of the system was very low and the induction time was relatively long. As a result the temperature for the jackets, transfer tube and water bath in the KRAIC 1 run were chosen to be significantly lower than that of the saturation point in order to promote nucleation relatively early on in the crystallisation process. However, 22 minutes into the run no crystals had been observed and as a result the temperature of the transfer tube and the mixer bath were reduced to 45 °C and 40 °C, respectively. After 36 minutes nucleation had still not been induced in the crystalliser and the transfer tube temperature was further reduced to 40 °C, however this failed to induce nucleation and as a result the temperature of the mixer bath was further reduced to 35 °C 47 minutes into the run. These reductions in

temperature were substantial enough to induce nucleation; at 49 minutes (RT 3) some very small crystals were observed at the end of the crystalliser. The point of nucleation within the process continued to progress backwards with crystals being observed in the third rung of coil 2 at 51 minutes. After 53 minutes the point of nucleation had moved significantly and crystals could be seen as soon as the slugs left the mixer bath. As a result of this very early nucleation point, the temperature of the transfer tube and water batch were increased to 45 °C and 40 °C, respectively. After 59 minutes the increase in temperatures of the transfer tube and mixer bath had not resulted in preventing the nucleation occurring so early in the process and the temperatures were increased further to 48 °C and 43 °C, respectively.

The crystallisation progressed smoothly from this point onwards and only a few crystals were observed in a small proportion of slugs upon their exit of the mixer bath. The run was continued until 5 RTs worth of feed had been pumped into the platform (1 hour 35 minutes) and the feed was then changed to primer fluid to allow for the final RT to be collected. The crystallisation process was terminated after 6 RTs (1 hour 49 minutes).

All collected solid (for RTs 4 – 5) was subject to PXRD for solid form analysis. It can be seen (Figure 6.37) that during the continuous crystallisation, the resultant solid accessed in both RTs was relatively amorphous in nature. However, one peak sharp at 2θ = 6.2 ° can be seen in the patterns for both RT suggesting that some of the salt has been obtained.

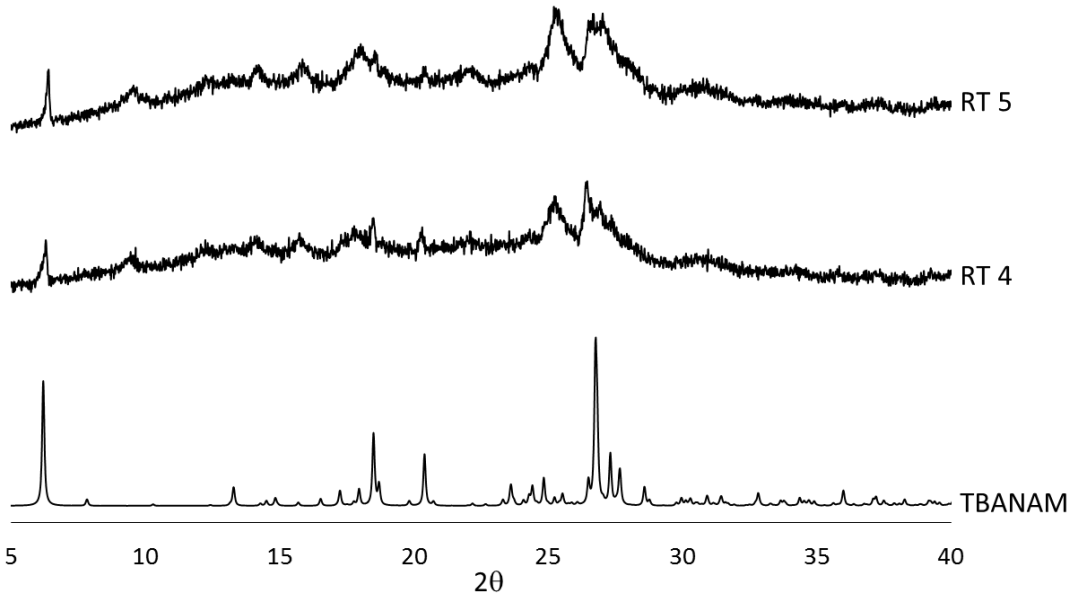

Figure 6.37: PXRD patterns of solid from RT 4 and RT 5 of TBANAM KRAIC 1.

TBANAM KRAIC 2

A second KRAIC experiment was conducted on the TBANAM system; the parameters used are summarised in Table 6.12. The same saturation temperature (T_{sat} = 60 °C) was used as with the first KRAIC run, but the temperatures of the transfer tube and mixer

bath were reduced due to issues with nucleation induction observed with the first run. Some slight changes were made with the flow rate for all three pumps, due to observed differences with the slug formation. The flow rates were chosen as to best mimic the slug formation observed in the first run. The issues were likely arising due to not enough air being pumped through the gear pump. The alteration in the flow rates, did however result in a significant reduction in the residence time for the system from 18 minutes 20 seconds to 12 minutes 30 seconds.

Table 6.12: Summary of experimental parameters for TBANAM KRAIC 2.

Parameters	TBANAM KRAIC 2
Feed concentration	27 mg/g
Feed flow rate	1.8 mL min^{-1}
Carrier fluid flow rate	6.26 mL min^{-1}
Air flow rate	8.34 mL min^{-1}
Residence time (RT)	12 minutes 30 seconds
Feed temperature	65 °C
Transfer tube temperature	45/40†/45††/48‡/52‡‡/55‡/52.5‡‡°C
Mixer bath temperature	40/35†/40††/45‡/50‡‡/45‡/40‡‡ °C

† Temperature reduced 12 minutes into run
†† Temperature increased 16 minutes into run
‡ Temperature increased 25 minutes into run
‡‡ Temperature increased 37 minutes into run
‡ Temperature increased 55 minutes into run
‡‡ Temperature changed 1 hour 27 minutes into run

During the first RT of the run no nucleation was observed and as a result the temperature for the transfer tube was reduced to 40 °C and the mixer bath temperature reduced to 35 °C. This reduction in temperature induced nucleation in the system and crystals were observed as early as the first rung in coil 1 after 16 minutes. The temperature of both the transfer tube and the mixer bath were then increased back to their original temperatures of 45 °C and 40 °C, respectively. 17 minutes 30 seconds into the run, crystals were observed in slugs as soon as they exited the mixer bath and as a result the mixer bath temperature was increased to 43 °C. After 25 minutes it was observed that air bubbles were being trapped in the solution slugs and segmentation was not occurring as it should. The presence of these air bubbles resulted in more nucleation in the slugs, and crystals were still observed in slugs as soon as they left the mixer bath. The temperature of the water bath was then increased to 45 °C and the transfer tube increased to 48 °C. The issues with air bubbles in the solution slugs continued and as a result the solution pump was reduced to 1.7 mL min^{-1} and the water bath and transfer tube were increased to 50 °C and 52 °C respectively. 46 minutes into the run a blockage was observed in the tubing at the solution pump (Figure 6.38). The

temperature of the transfer tube was increased to 65 °C and the inlet was transferred from the feed solution to the primer in an attempt to remove the blockage. After 48 minutes the blockage still remained; consequently the transfer tube temperature was increased to 70 °C and the solution pump rate was increased to 2 mL min^{-1}. After 55 minutes the blockage had been removed by dissolution and the inlet was changed back to the feed solution. The transfer tube temperature was reduced to 55 °C and the mixer bath to 45 °C. As a result of removing the blockage the amount of air bubbles observed in the solution slugs was greatly reduced.

Figure 6.38: Blockage in peristaltic pump tubing (TBANAM KRAIC 2).

Once the inlet had been changed back to the feed solution, no subsequent nucleation had occurred within the system. 1 hour and 6 minutes into the run the water bath was reduced back to 40 °C, with the transfer tube being reduced to 52.5°C after 1 hour and 9 minutes in an attempt to induce nucleation. However, 1 hour and 21 minutes into the run, there were still no crystals observed and the transfer tube temperature was reduced to 48 °C. Cold water was added to the mixer bath in an attempt to increase the rate at which it cooled to 40 °C. At 1 hour and 28 minutes the transfer tube was further reduced in temperature to 45 °C and two minutes later, small crystals were observed in the first rung of coil 1. The temperature of the transfer tube was then increased back to 50 °C.

However, at 1 hour and 27 minutes it appeared that there was a small blockage at the solution pump as was observed earlier in the run. As a result the feed solution temperature was increased to 70 °C and that of the transfer tube temperature was increased to 52.5 °C. At 1 hour and 40 minutes the inlet was changed to the primer solution and solid from the final RT (RT 8) was collected.

Solid collected from each RT (where available) was analysed using PXRD. It can be seen from the patterns that in each RT the desired TBANAM salt product was accessed selectively in RT 1 – 4 (Figure 6.39). However, significant issues were encountered during this run, both with difficulty in inducing nucleation and then subsequent early nucleation and blockages and as a result no solid was obtained for RT 5 or 6. Once the blockage had

been cleared and nucleation had once again been induced in the system it can be seen that the solid from RT 7 and RT 8 exhibits less crystallinity with much less well defined peaks. However, the PXRD patterns obtained from this run are significantly better in terms of peak sharpness and signal to noise when compared with those obtained from the KRAIC 1 run.

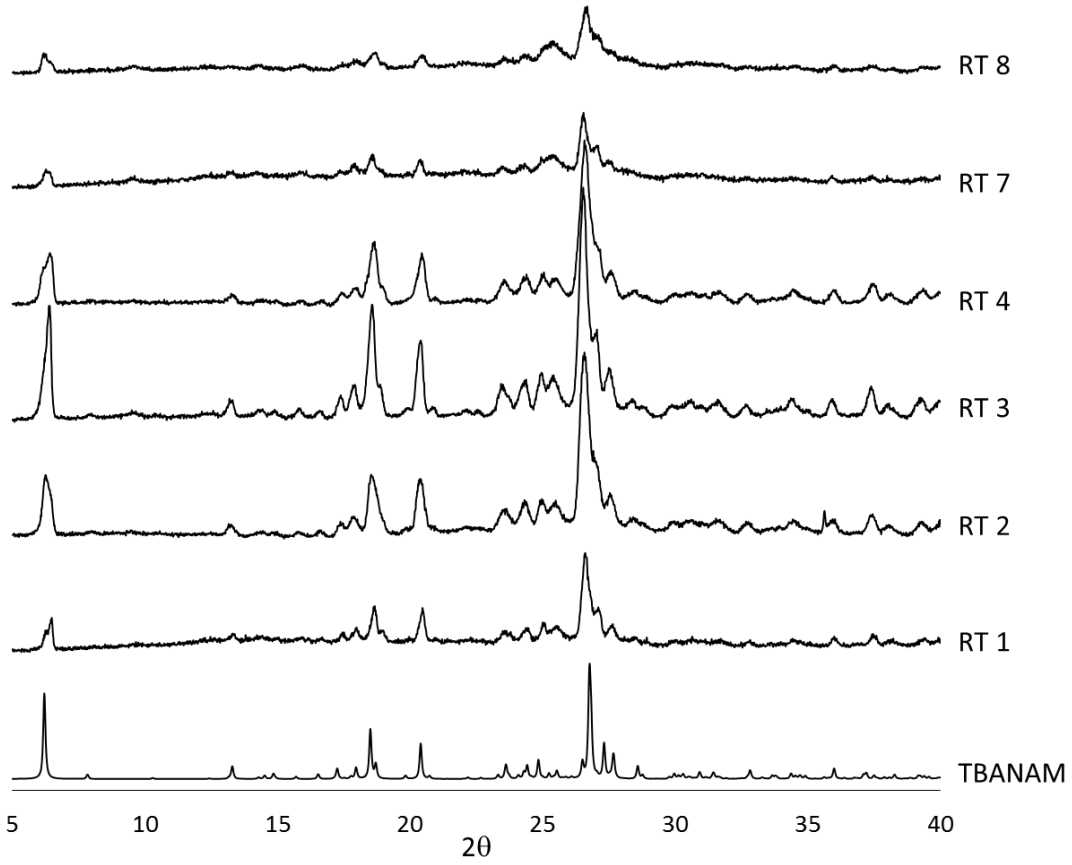

Figure 6.39: PXRD patterns of solid obtained from TBANAM KRAIC 2.

It is clear that further work needs to be conducted on this system with this platform in order to optimise both the flow and temperature profile of the system to allow for controllable nucleation within the system. One way in which this could be achieved would be to keep the temperature of the transfer tube and mixer bath at a closer value to that of the feed solution to avoid any crystallisation in the pumps and during segmentation, and then introduce a cold tube after the mixer bath. The cold tube could allow for efficient cooling of the crystallisation at a determined point within the crystalliser and allow for nucleation to be induced at a set point, post segmentation.

6.5 Chapter Conclusions

Evaporative multi-component screening was conducted with thiobarbituric acid as the target compound in aim to produce novel multi-component systems. As a result of this work, two novel salt systems were discovered with nicotinamide and isonicotinamide acting as counter ions.

The two salt systems display the same hydrogen transfer (deprotonation of the TBA hydroxyl group with protonation of the pyridine nitrogen in the counter-ion) with the thiobarbituric acid isonicotinamide (TBAISNAM) salt system crystallising in the $P2_1/c$ space group and the thiobarbituric acid nicotinamide (TBANAM) system crystallising in $P\bar{1}$. Both systems display very similar thermal behaviour, both melting at approximately 215 °C, an intermediate value between the melts of the individual starting components.

For both salt systems investigations into the transfer of their crystallisation from evaporative into grinding techniques was conducted. When TBA and isonicotinamide were ground by hand in the pestle and mortar the salt was accessed, but DSC analysis showed the presence of residual starting components. Upon transfer from hand grinding to mechanical, using the ball mill, the salt could be formed more selectively. When 10 mg TBA was ground with 8.5 mg of isonicotinamide for one hour the DSC showed only a small amount of residual isonicotinamide remained. Increasing the mass of the starting components resulted in an hour not being adequate to achieve sufficient phase transformations and a significant amount of starting material remained as shown by the DSC analysis. For the TBANAM salt system, grinding the starting components by hand led to the formation of the salt system, however the PXRD data showed that the resultant product had a relatively low level of crystallinity. Transfer into mechanical grinding using the ball mill allowed the salt system to be accessed, but again the resultant products were relatively amorphous in comparison to the product obtained from evaporative and slurrying techniques.

Turbidity solubility data for the novel salts in both water and ethanol was collected allowing for cooling crystallisations to be designed for each form. The experiments showed that each salt could be accessed via cooling crystallisation from water. The crystallisations were successfully scaled up from 1 mL to 150 mL using the CRD Polar Bear Plus crystalliser. It was seen that the saturation temperature (50 °C or 60 °C) had no effect on the solid form outcome obtained from the crystallisations and TBAINSAM and TBANAM could be accessed using both saturation temperatures.

Using the knowledge gained from the work conducted on the UBA co-crystal system, the transfer of the crystallisation of these novel salt systems from batch cooling to continuous cooling crystallisation was successfully achieved, with TBAISNAM being successfully accessed from continuous cooling crystallisation from water using the COBC. However, the process requires further optimisation as the system had a very long nucleation induction time resulting in the temperatures of the straights having to be reduced significantly which led to issues with encrustation. The same issues were observed with the continuous cooling of TBANAM. This system also required very low temperatures to induce nucleation which then led to encrustation issues.

Continuous crystallisation of the two forms was also investigated using the KRAIC. In this platform it was found that each salt could be crystallised selectively from water. For each system the nucleation induction time was again, as with the COBC, very long and as a result the temperature of the systems had to be reduced. Once the temperatures

had been optimised and nucleation occurred in the crystalliser the solid form which resulted was shown to be the desired salt. Further optimisation of the process for both is required in order to determine the best temperatures for the feed, transfer tube and mixer bath so that no modification during the run is required. The TBAISNAM runs ran smoothly with no encrustation or blockages, however for the TBANAM system, some issues with small blockages in the peristaltic were encountered.

Overall, two novel thiobarbituric acid salt systems have been discovered and their crystallisation has been transferred successfully form small scale evaporative to larger scale batch cooling crystallisation and into continuous crystallisation using two continuous crystallisation platforms.

Chapter 7 – Conclusions and Future Work

7.1 Conclusions

Investigations of urea barbituric acid (UBA) presented here have tackled two main research targets: determining which of its solid forms is most stable and developing a range of approaches to isolate the metastable form, in both batch and continuous crystallisation environments.

The previously unresolved issue of which form of UBA, form I or form III, is the thermodynamically stable form, has been investigated by a wide range of experiments that were conducted in order to determine their relative stability behaviour. Solubility analysis of the two forms highlighted the difficulty of accessing reliable and accurate solubility data for co-crystal forms with different methods yielding different solubility curves. From the solubility analysis the curves obtained from observation methods were deemed the most accurate and as a result it was these solubility curves that were used for subsequent work during this project. The solubility data of UBA form I and form III suggested that the two forms are enantiotropic in nature, with form I being the stable form at lower temperatures and form III becoming the stable form at higher temperatures. The transition temperature, T_t, estimated from the solubility curves was in the range of 35 °C – 42 °C. However, this value is called into question by competitive slurry experiments where it was shown that UBA form I is the thermodynamically stable polymorph up to temperatures of at least 75 °C; competitive slurries at 20 °C, 40 °C, 50 °C and 75 °C all showed conversion of a 1:1 mixture for form I and form III to yield form I within 24 - 48 hours. The value of the transition temperature is discussed further below.

When looking into the thermal behaviour of the two forms, it was shown that the co-crystals undergo a decomposition to the individual components, upon which the urea vaporises and decomposes. The resultant barbituric acid component then crystallises in a high temperature form which subsequently decomposes. The temperature at which the co-crystal decomposition happens is approximately 8 °C higher for UBA form III than for UBA form I, providing further evidence that the two systems are enantiotropic; as form III decomposes at a higher temperature it is likely the thermodynamically stable form at these elevated temperatures. During VT PXRD analysis of both UBA form I and form III it was seen that UBA form I undergoes a partial solid state transformation to yield form III upon heating: at 170 °C the PXRD pattern showed that a mixture of the two forms was present. These data highlighted the enantiotropic relationship between the two forms and indicated that T_t must lie in the range of 75 °C - 170 °C, however the exact value of T_t has yet to be determined.

Analysis of the crystal structures of form I and form III allowed for some justification of the stability relationship between the two forms. UBA form I has a marginally higher calculated density than UBA form III, suggesting that this may be the more stable form. UBA form I and form III both possess urea-urea hydrogen bonded dimers, that the highly metastable form III does not, which may be a reason as to why these two forms are more stable in comparison to the highly metastable UBA form II. The urea-urea dimers differ between the two forms, with the dimer in UBA form I being made up of hydrogen bonds of equal strength, and the dimer in UBA form III being made of two unique hydrogen bonds. The bond distances and angles also vary, with the form I dimer having a slightly shorter and more linear bond, suggesting that the dimer in form I is stronger than that of form III. When looking at the packing arrangements of form I and form III, form I is seen to have hydrogen bonds extending in three dimensions throughout the structure. However, form III only has one dimensional hydrogen bonding in the structure, again giving some justification as to why form I is the more stable form. Form I was also shown to satisfy more of the hotspots in the full interaction map than form III, again giving some further justification for form I being the more stable form.

During this work a novel solid form of UBA was discovered. Slurrying a 2:1 ratio of urea: barbituric acid in either ethanol or methanol for 24 hours results in the formation of this solid form. The slurry products displayed unique PXRD patterns and thermal behaviour. ^{13}C NMR analysis of the novel solid form indicated that both urea and barbituric acid are present in the crystal structure in a 1:1 ratio, and that no solvents are present. This, coupled with the thermal behaviour, suggested that the novel solid form is a new polymorph of UBA. The thermal behaviour showed that the new form decomposes into the individual components, as was seen with UBA form I and form III, but that the temperature at which this occurs for the new form is approximately 50 °C lower than the known forms. Competitive slurries of the novel solid form with UBA form I and form III did not lead to the conversion of the novel solid form to form I or form III, however. Instead the systems remained as mixtures even after a slurry time of two weeks.; it was concluded from this that the kinetic barrier between the novel solid form and form I and form III is too high to be overcome under these experimental conditions.

UBA form III has been shown to be a metastable form in comparison to UBA form I to a temperature of at least 75 °C. This is likely a reason as to why the selective crystallisation of UBA form III has been difficult to achieve in the past. During this work it was shown that reducing the solubility of the system, by increasing the size of the alcohol solvent used, allowed for more selectivity towards the metastable form III. Slurry experiments of urea and barbituric acid showed that form III was accessed initially and then converted to the thermodynamically stable form, form I. When methanol was used, this conversion occurred at a faster rate than with ethanol, with form I being accessed selectively after 16 hours in methanol, but 36 hours in ethanol. As a result, slurry times of 16 – 24 hours (using ethanol as the solvent medium) allow for access of UBA form III to high polymorphic purity.

Upon transfer of the crystallisation of urea and barbituric acid from ethanol into cooling crystallisation techniques, UBA form III was accessed selectively in batch crystallisation techniques using the CRD Polar Bear Plus up to a scale of 150 mL. However, a Design of Experiments study (at 50 mL), along with further repeat experiments at other scales (100 – 150 mL) highlighted a significant lack of reproducibility of the process, with a significant number of experiments containing form I impurities. Investigations into seeding in order to attain solid form selectivity, conducted at GSK Stevenage, were unsuccessful with the results showing that the seeds did not take to the solution. The experiments showed that to access form I selectively from the seeded experiments a seed loading of 5 % was required, regardless of the cooling rate used (0.5 °C min^{-1} or 1 °C min^{-1}). For form III, a seed loading of 20 % was required, again regardless of the cooling rate used (0.5 °C min^{-1} and 1 °C min^{-1}). The apparent solid form control however, was not as a result of the added seed growing or inducing secondary nucleation within the system. The FBRM and concentration profiles indicated that the seeds did not absorb any of the supersaturation upon their addition and seed hold, resulting in the systems acting largely as if unseeded; all displayed a nucleation event at approximately 45 °C, the temperature at which spontaneous nucleation occurs in the unseeded systems. It was concluded that the apparent solid form control from seeding with form I was due to the presence of form I accelerating the conversion of form III to form I in the process once the subsequent nucleation events had occurred. The solid form control under form III seeding was concluded to be due to the significant amount of form III (20 % seed loading) 'drowning out' any form I and hence appearing as if the high seed loading is allowed for form III to be accessed selectively.

Investigations into the continuous crystallisation of UBA from ethanol targeted the selective crystallisation of the metastable form III, not previously achieved. These investigations showed that selectivity and reproducibility of pure form III crystallisation could be accessed using the KRAIC continuous crystallisation platform: in each RT of each run (KRAIC 1 - 3) UBA form III was accessed selectively. The crystallisation requires further optimisation in terms of the temperature profile used in order to eradicate the blocking issues observed in the mixer piece. However, the crystallisation was shown to be robust, with form III being accessed across a wide range of temperatures used in the continuous crystallisation runs. Upon transfer of the crystallisation to the COBC platform, form III was not accessed selectively, with either form I being the resultant product (COBC 1 - 2) or a mixture of form I and III being obtained (COBC 3). It was shown that increasing the saturation of the feed solution as well as reducing the temperature of the straights of the COBC allowed for form III to be accessed alongside form I. This result suggests that further optimisation of the process could have the potential to yield form III selectively.

Due to the lack of reproducibility accessed in batch crystallisation using ethanol as the solvent medium, investigations into IPA were conducted. The solubility of UBA was shown to be reduced in IPA in comparison to ethanol. Slurry experiments indicated that this reduction in solubility resulted in a subsequent reduction in the rate of form III to

form I conversion. Slurry experiments also showed the presence of UBA form II, the highly metastable form, in slurries with 24 hour experiment times. Form II had never been witnessed before, other than in small scale evaporative crystallisations, and so its presence in the slurry products indicated that the solution mediated phase transformations occurring in IPA are significantly slower than those occurring in ethanol and methanol. Transfer of the system into cooling crystallisation techniques showed that UBA form III could be accessed selectively in batch crystallisation techniques from IPA solution, with a much higher level of reproducibility than was observed in the ethanol mediated system; this is likely due to the significant reduction in rate of the solution mediated phase transformations.

Again, as with the ethanol system, seeding experiments were conducted in order to investigate whether full solid form control could be accessed. When UBA form I seed was used a 1 % seed loading resulted in pure form I with both cooling rates (0.5 °C min^{-1} or 1 °C $min^{-1)}$. The FBRM data and concentration profiles indicated that at low seed loadings the seed did not absorb all the supersaturation and high seed loadings were required in order to control the process in terms of additional nucleation events. When the system was seeded with UBA form III, a seed loading of 5 % was required to access solid form control with the faster cooling rate of 1 °C min^{-1} and 20 % for the slower cooling rate of 0.5 °C min^{-1}. As with the seeding in the ethanol system, the FBRM and concentration profiles when UBA form III seed was used indicated that the seed did not take to the solution and the systems acted largely as if unseeded. Each UBA form III seeded experiment, regardless of seed loading and cooling rate used, displayed a nucleation event at approximately the same temperature at which spontaneous nucleation occurs in the unseeded system. Although the addition of UBA form III seed did not result in any growth of the seed particles or induce any secondary nucleation within the system, solid form control was achieved. However, as for the form III seeded crystallisations from ethanol, this is likely due to the large amount of UBA form III being present in the system 'drowning out' any form I and resulting in apparent solid form control.

Transfer of the crystallisation of UBA from IPA from batch to continuous methods was investigated using the KRAIC platform and it was shown that UBA form III could be accessed selectively using this set up. All experiments resulted in pure UBA form III being accessed in each RT. Using this solvent medium also removed the issues encountered with blocking in the mixer piece observed with ethanol as the solvent system, and the continuous crystallisations ran smoothly.

This work also investigated the discovery of novel solid forms of systems related to UBA, with the aim of characterising these fully and seeking to transfer their crystallisation from small-scale evaporative batch, as used in materials discovery, to continuous crystallisation in the available platforms.

From these investigations, two novel salt systems of thiobarbituric acid were discovered, one with nicotinamide as the counter ion (TBANAM) and the other with isonicotinamide

(TBAISNAM). Each salt system contained a 1:1 molar ratio of the individual components and the solid state structures displayed hydrogen transfer from the hydroxyl group of the TBA entity (enol tautomer) to the pyridine nitrogen of the counter ion. Each system was shown to melt at approximately 215 °C, an intermediate value between the melting points of the starting components of each system.

Further investigation into the crystallisation of these systems showed that the novel systems, which were discovered using small scale evaporative crystallisation techniques, could also be accessed using slurrying methods (in water, ethanol, methanol and IPA) and grinding methods. The systems were also shown to be accessed using cooling crystallisation from water with a 1:1 ratio of the starting components. The cooling crystallisation was successfully scaled from 1 mL to 150 mL in batch methods using the CRD Polar Bear Plus, before being transferred to continuous methods using the COBC and KRAIC platforms. The COBC experiments indicated that under these conditions the induction time for nucleation, for both systems, was long and as a result the temperatures of the straights had to be significantly reduced to induce nucleation. It was also seen that in both systems encrustation occurred in both the exit tubing and end piece, with fouling being observed in the later straights of the platform as the experiment went on.

During the KRAIC experiments it was again seen that both systems had long induction times, and as a result for the TBAISNAM system ice bags were implemented in order to reduce the temperature in coil 3. Once nucleation had occurred within the process, the salt was selectively achieved. For the TBANAM system the same issues with long induction times were observed and optimisation of the feed, transfer tube and mixer bath temperatures. However, once nucleation had been induced in the experiments, TBANAM was accessed selectively in the remaining RTs.

These investigations have shown that the approach and methodology developed in this work is well suited to allowing transfer of newly discovered multi-component systems both into larger scale batch crystallisation and into continuous crystallisation environments.

7.2 Future Work

It has been shown that UBA form III is metastable under ambient conditions with experiments suggesting that form I and form III are enantiotropic, with form III becoming the thermodynamically stable form at elevated temperatures. Future work should focus on determining the transition temperature for form I and form III. Investigations into attaining a single crystal structure of the novel solid of UBA, which was discovered during this work, should also be conducted to allow for a further understanding of the solid form. Knowing the crystal structure could also allow for structure comparison with the known solid forms which may allow for further understanding and justification of its stability behaviour in comparison to the known forms.

The selective crystallisation of UBA form III has been achieved using batch cooling crystallisation techniques, with both ethanol and IPA as solvent media. However, the process displayed a lack of robustness, with some experiments yielding form I impurities. Future work utilising Rietveld refinement and Pawley-fitting should be conducted in order to quantify the amount of UBA form I impurity as well as for further phase identification.

The reported investigation into seeding for solid form control in both IPA and ethanol, with both UBA form I and form III seeds, were unsuccessful in the fact that in the majority of experiments the seed did not take to solution. A widely adopted method in industrial crystallisation, the seeding experiments are a significant area upon which future work should be focused. There are many factors that could be investigated in these experiments in order to try and attain solid form control, such as the seed size, the point of seed addition, seed age length and the addition of seed in a slurry as opposed to dry seed.

Future work for the UBA system should also focus on the continuous crystallisation. It was shown that the KRAIC allowed for reproducible and selective access of UBA form III using both ethanol and IPA, however issues with blockages in the mixer piece were observed for the ethanol mediated system. Experiments to attempt to optimise the temperature profile of the KRAIC for this system could allow for a robust method of accessing UBA form III selectively without encrustation and blocking issues. When the COBC was used for the crystallisation of UBA from ethanol, selective crystallisation of UBA was not achieved. However, the work indicated that higher saturations and a 'harsher' cooling profile may favour the production of UBA form III over form I. Further work could investigate different cooling profiles and saturations for this system to attempt to access pure form III. Investigations into using shorter RTs could also be conducted, looking at both faster flow rates and decreasing the length of the crystalliser: this would give the system less time to transform from form III to form I, allowing for more selectivity to the metastable form.

Further work is required for the continuous crystallisation of the novel TBA salt systems in both the COBC and KRAIC. For both systems, issues were seen with long induction times in the COBC, resulting in nucleation only occurring at the very end of the crystalliser. Changing the feed saturation as well as further reducing the temperature of the COBC straights may allow for nucleation to be accessed earlier on in the process, giving more time for growth. Investigations into increasing the RT could also be conducted by increasing the length of the crystalliser. This may allow for less 'harsh' cooling rates to be used which may in turn reduce the level of encrustation observed.

Long induction times were also observed for the two salt systems in the KRAIC. The implementation of a cold tube after the mixer bath may allow for rapid cooling of the slugs and result in nucleation occurring earlier on in the crystalliser. Using a cold tube may also allow for higher temperatures to be used for the feed, transfer tube and mixer

bath resulting in a reduced risk of encrustation and blockages occurring at the pumps and mixer piece.

More generally, the methodology developed towards transferring novel solid-state systems from small-scale, often evaporative, discovery environments into larger scale batch cooling and continuous crystallisation methods should be investigated further in a wide range of systems. This could lead to establishment of protocols that allow a wider range of systems to be developed towards larger scale production in this way; this aspect of the work maps directly onto some of the main aims of the CMAC Future Manufacturing Hub, towards establishing rapid manufacturing methods for new crystalline products in the pharmaceutical and related industries.

Chapter 8 - References

1. B. M. Couillaud, P. Espeau, N. Mignet and Y. Corvis, *ChemMedChem*, 2019, **14**, 8-23.
2. H.-H. Tung, E. L. Paul, M. Midler and J. A. McCauley, *Crystallization of Organic Compounds: An Industrial Perspective*, John Wiley & Sons, Inc., United States of America, 2009.
3. J. W. Mullin, *Crystallisation*, Butterworth-Heinemann, United States, Fourth edn., 2001.
4. D. Wieckhusen, in *Crystallization: Basic Concepts and Industrial Applications*, ed. W. Beckmann, Wiley-VCH Verlag GmbH & Co. KGaA., Germany, 2013, ch. 10, Development of Batch Crystallizations, pp. 187-202.
5. D. Erdemir, A. Y. Lee and A. S. Myerson, *Accounts of Chemical Research*, 2009, **42**, 621-629.
6. B. Y. Shekunov and P. York, *Journal of Crystal Growth*, 2000, **211**, 122-136.
7. Z. K. Nagy, G. Fevotte, H. Kramer and L. L. Simon, *Chemical Engineering Research & Design*, 2013, **91**, 1903-1922.
8. Z. Q. Yu, J. W. Chew, P. S. Chow and R. B. H. Tan, *Chemical Engineering Research and Design*, 2007, **85**, 893-905.
9. H.-H. Tung, E. L. Paul, M. Midler and J. A. McCauley, in *Crystallization of Organic Compounds: An Industrial Perspective*, John Wiley & Sons, Inc., New Jersey, 2009, ch. 7, pp. 137-166.
10. *Handbook of Industrial Crystallization*, Butterworth-Heinemann, United states of America, Second edn., 2002.
11. *Industrial Crystallization*, Plenum Press, United States of America, 1976.
12. *Polymorphism in the Pharmaceutical Industry*, Wiley - VCH, Germany, 2006.
13. E. Grothe, H. Meekes, E. Vlieg, J. H. ter Horst and R. de Gelder, *Crystal Growth & Design*, 2016, **16**, 3237-3243.
14. R. Hilfiker, *Polymorphism: In the pharmaceutical Industry*, Wiley-VCH Verlag GmbH & Co., Germany, 2006.
15. *Polymorphism in Pharmaceutical Solids*, Informa Healthcare USA, New York, Second edn., 2009.
16. R. Hilfiker, in *Crystallization: Basic concepts and Industrial Applications*, ed. W. Beckmann, Wiley-VCH Verlag GmbH & Co. KGaA., Germany, First edn., 2013, ch. 5, pp. 85-104.
17. S. P. F. Miller, A. S. Raw and L. X. Yu, in *Polymorphism in the Pharmaceutical Industry*, ed. R. Hilfiker, WILEY_VCH Verlag GmbH & Co. KGaA, Germany, 2006, ch. 15, pp. 385-403.
18. R. Davey, in *From Molecules to Crystallizers an Introduction to Crystallization*, ed. L. F. Gladden, Oxford University Press, United States, 2006, ch. 6, pp. 44-42.
19. H. Lorenz, in *Crystallization: Basic Concepts and Industrial Applications*, ed. W. Beckmann, Wiley-VCH Verlag GmbH & Co. KGaA., Germany, First edn., 2013, ch. 3, pp. 35-74.
20. H.-H. Tung, E. L. Paul, M. Midler and J. A. McCauley, in *Crystallization of Organic Compounds: An Industrial Perspective*, 2009, ch. 2, pp. 13-48.
21. H. G. Brittain, in *Polymorphism in Pharmaceutical Solids*, ed. H. G. Brittain, Informa Healthcare USA, Inc., United States of America, 2009, ch. 1, pp. 1-23.
22. H. G. Brittain, in *Polymorphism in Pharmaceutical Solids*, ed. H. G. Brittain, Informa Healthcare USA, Inc., United States of America, 2009, ch. 2, pp. 24-51.

23. J. Bauer, S. Spanton, R. Henry, J. Quick, W. Dziki, W. Porter and J. Morris, *Pharmaceutical Research*, 2001, **18**, 859-866.
24. S. L. Morissette, S. Soukasene, D. Levinson, M. J. Cima and O. Almarsson, *Proceedings of the National Academy of Sciences of the United States of America*, 2003, **100**, 2180-2184.
25. S. R. Chemburkar, J. Bauer, K. Deming, H. Spiwek, K. Patel, J. Morris, R. Henry, S. Spanton, W. Dziki, W. Porter, J. Quick, P. Bauer, J. Donaubauer, B. A. Narayanan, M. Soldani, D. Riley and K. McFarland, *Organic Process Research & Development*, 2000, **4**, 413-417.
26. G. U. J., in *Polymorphism in the Pharmaceutical Industry*, ed. R. Hilfiker, WILEY-VCH Verlag GmbH & Co. KGaA, Germany, 2006, ch. 8, pp. 211-234.
27. J. W. Mullin, in *Crystallization*, First edn., 1961, ch. 2, pp. 21-43.
28. S. Lohani and D. J. W. Grant, in *Polymorphism in the Pharmaceutical Industry*, ed. R. Hilfiker, WILEY-VCH Verlag GmbH & Co. KGaA, Germany, 2006, ch. 2, pp. 21-42.
29. D. Giron, *Journal of Thermal Analysis and Calorimetry*, 2003, **73**, 441-457.
30. C. Saal and A. Becker, *European Journal of Pharmaceutical Sciences*, 2013, **49**, 614-623.
31. N. K. Duggirala, M. L. Perry, O. Almarsson and M. J. Zaworotko, *Chemical Communications*, 2016, **52**, 640-655.
32. P. W. Cains, in *Polymorphism in Pharmaceutical Solids*, ed. H. G. Brittain, Informa Healthcare USA, Inc., United States of America, Second edn., 2009, ch. 4, pp. 76-138.
33. S. Cherukuvada, R. Kaur and T. N. G. Row, *Crystengcomm*, 2016, **18**, 8528-8555.
34. E. A. Losev and E. V. Boldyreva, *CrystEngComm*, 2018, **20**, 2299-2305.
35. A. T. M. Serajuddin, *Advanced Drug Delivery Reviews*, 2007, **59**, 603-616.
36. K. K. Arora and M. J. Zaworotko, in *Polymorphism in the Pharmaceutical Industry*, ed. H. G. Brittain, Informa Healthcare USA, Inc, United States of America, Second edn., 2009, ch. 8, pp. 282-318.
37. S. Aitipamula, R. Banerjee, A. K. Bansal, K. Biradha, M. L. Cheney, A. R. Choudhury, G. R. Desiraju, A. G. Dikundwar, R. Dubey, N. Duggirala, P. P. Ghogale, S. Ghosh, P. K. Goswami, N. R. Goud, R. Jetti, P. Karpinski, P. Kaushik, D. Kumar, V. Kumar, B. Moulton, A. Mukherjee, G. Mukherjee, A. S. Myerson, V. Puri, A. Ramanan, T. Rajamannar, C. M. Reddy, N. Rodriguez-Hornedo, R. D. Rogers, T. N. G. Row, P. Sanphui, N. Shan, G. Shete, A. Singh, C. Q. C. Sun, J. A. Swift, R. Thaimattam, T. S. Thakur, R. K. Thaper, S. P. Thomas, S. Tothadi, V. R. Vangala, N. Variankaval, P. Vishweshwar, D. R. Weyna and M. J. Zaworotko, *Crystal Growth & Design*, 2012, **12**, 2147-2152.
38. C. Zhang, Y. Xiong, F. Jiao, M. Wang and H. Li, *Crystal Growth & Design*, 2019.
39. N. Qiao, M. Li, W. Schlindwein, N. Malek, A. Davies and G. Trappitt, *International Journal of Pharmaceutics*, 2011, **419**, 1-11.
40. C. B. Aakeroy, S. Forbes and J. Desper, *Journal of the American Chemical Society*, 2009, **131**, 17048-+.
41. T. Friscic and W. Jones, *Journal of Pharmacy and Pharmacology*, 2010, **62**, 1547-1559.
42. A. V. Trask, W. D. S. Motherwell and W. Jones, *Crystal Growth & Design*, 2005, **5**, 1013-1021.
43. A. Kumar, S. Kumar and A. Nanda, *Advanced pharmaceutical bulletin*, 2018, **8**, 355-363.
44. FDA, Regulatory Classification of Pharmaceutical Co-Crystals Guidance for Industry, https://www.govinfo.gov/content/pkg/FR-2018-02-15/pdf/2018-03133.pdf, (accessed 29.01.2019, 2019).
45. S. Aitipamula, P. S. Chow and R. B. H. Tan, *Crystengcomm*, 2014, **16**, 3451-3465.
46. A. Lemmerer, D. A. Adsmond, C. Esterhuysen and J. Bernstein, *Crystal Growth & Design*, 2013, **13**, 3935-3952.
47. A. J. Cruz-Cabeza, S. M. Reutzel-Edens and J. Bernstein, *Chemical Society Reviews*, 2015, **44**, 8619-8635.

48. G. R. Desiraju, *Crystal Engineering The Design of Organic Solids*, Elsevier, The Netherlands, 1989.
49. C. B. Aakeroey, T. K. Wijethunga, J. Benton and J. Desper, *Chemical Communications*, 2015, **51**, 2425-2428.
50. C. B. Aakeroey, T. K. Wijethunga and J. Desper, *Chemistry-a European Journal*, 2015, **21**, 11029-11037.
51. C. B. Aakeroey, S. Forbes and J. Desper, *Crystengcomm*, 2014, **16**, 5870-5877.
52. G. R. Desiraju, *Journal of the American Chemical Society*, 2013, **135**, 9952-9967.
53. N. Blagden, M. de Matas, P. T. Gavan and P. York, *Advanced Drug Delivery Reviews.*, 2007, **59**, 617-630.
54. G. R. Desiraju, *Journal of Chemical Sciences*, 2010, **122**, 667-675.
55. J. G. P. Wicker, L. M. Crowley, O. Robshaw, E. J. Little, S. P. Stokes, R. I. Cooper and S. E. Lawrence, *CrystEngComm*, 2017, **19**, 5336-5340.
56. M. K. Corpinot and D.-K. Bučar, *Crystal Growth & Design*, 2019, **19**, 1426-1453.
57. G. A. Jeffrey, *An introduction to hydrogen bonding*, Oxford University Press, United States of America, 1997.
58. G. R. Desiraju, *Accounts of Chemical Research*, 2002, **35**, 565-573.
59. J. Emsley, *Chemical Society Reviews*, 1980, **9**, 91-124.
60. G. R. Desiraju, *Crystal Growth and Design*, 2011, **11**, 896-898.
61. C. R. Martinez and B. L. Iverson, *Chemical Science*, 2012, **3**, 2191-2201.
62. C. A. Hunter and J. K. M. Sanders, *Journal of the American Chemical Society*, 1990, **112**, 5525-5534.
63. R. Thakuria, N. K. Nath and B. K. Saha, *Crystal Growth & Design*, 2019.
64. W. Beckmann, in *Crystallization: Basic Concepts and Industrial Applications*, ed. W. Beckmann, Wiley-VCH Verlag GmbH & Co. KGaA., Germany, First edn., 2013, ch. 2, pp. 7 - 33.
65. R. Davey and J. Garside, *From Molecules to Crystallizers: An Introduction to Crystallization*, Oxford University Press, United States, 2000.
66. R. Boistelle and J. P. Astier, *Journal of Crystal Growth*, 1988, **90**, 14-30.
67. A. M. Schwartz and A. S. Myerson, in *Handbook of Industrial Crystallization (Second Edition)*, ed. A. S. Myerson, Butterworth-Heinemann, Woburn, 2002, pp. 1-31.
68. *Crystallization Basic Concepts and Industrial Applications*, WILEY-VCH Verlag GmbH & Co. KGaA, Germany, 2013.
69. J. W. Mullin, *Crystallization*, Butterworth-Heinemann, Great Britain, Third edn., 1992.
70. D. Mangin, F. Puel and S. Veesler, *Organic Process Research & Development*, 2009, **13**, 1241-1253.
71. J. W. Mullin, in *Crystallization*, Butterworth & Co. Limited, Great Britain, First edn., 1961, ch. 5, pp. 101-135.
72. J. Chen, B. Sarma, J. M. B. Evans and A. S. Myerson, *Crystal Growth & Design*, 2011, **11**, 887-895.
73. H.-H. Tung, E. L. Paul, M. Midler and J. A. McCauley, in *Crystallization of Organic Compounds: An Industrial Perspective*, John Wiley & Sons, Inc., United States of America, 2009, ch. 4, pp. 77-100.
74. P. G. Vekilov, *Journal of Crystal Growth*, 2005, **275**, 65-76.
75. R. Davey and J. Garside, in *From Molecules to Crystallizers an Introduction to Crystallization*, Oxford University Press, United States, 2006, ch. 3, pp. 15-25.
76. S. G. Agrawal and A. H. J. Paterson, *Chemical Engineering Communications*, 2015, **202**, 698-706.
77. R. Davey and J. Garside, in *From Molecules to Crystallizers an Introduction to Crystallization*, ed. L. F. Gladden, Oxford University Press, United States, 2006, ch. 4, pp. 26-35.

78. J. W. Mullin, in *Crystallization*, Butterworth-Heinemann, Great Britain, Fourth edn., 2001, ch. 6, pp. 216-288.
79. F. C. Frank, *Discussions of the Faraday Society*, 1949, 48-54.
80. W. K. Burton, N. Cabrera and F. C. Frank, *Philosophical Transactions of the Royal Society of London Series a-Mathematical and Physical Sciences*, 1951, **243**, 299-358.
81. R. Davey and J. Garside, in *From Molecules to Crystallizers an Introduction to Crystallization*, ed. L. F. Gladden, Oxford University Press, United States, 2006, ch. 5, pp. 36-42.
82. Z. Berkovitch-Yellin, J. van Mil, L. Addadi, M. Idelson, M. Lahav and L. Leiserowitz, *Journal of the American Chemical Society*, 1985, **107**, 3111-3122.
83. A. R. Klapwijk, E. Simone, Z. K. Nagy and C. C. Wilson, *Crystal Growth & Design*, 2016, **16**, 4349-4359.
84. P. Dandekar, Z. B. Kuvadia and M. F. Doherty, *Annual Review of Materials Research*, 2013, **43**, 359-386.
85. W. M. L. Wood, *Powder Technology*, 2001, **121**, 53-59.
86. M. O. Besenhard, P. Neugebauer, C. Ho and J. G. Khinast, *Crystal Growth and Design*, 2015, **15**, 1683-1691.
87. A. Chianese and H. Kramer, J. M., *Industrial Crystallization Process Monitoring and Control*, Wiley-VCH & Co., Singapore, 2012.
88. D. Wieckhusen, in *Crystallization: Basic Concepts and Industrial Applications*, ed. W. Beckmann, Wiley-VCH Verlag GmbH & Co. KGaA., Germany, First edn., 2013, ch. 10, pp. 187-202.
89. R. Davey and J. Garside, in *From Molecules to Crystallizers An Introduction to Crystallization*, Oxford University Press, United States, 2006, ch. 2, pp. 6-13.
90. H.-H. Tung, E. L. Paul, M. Midler and J. A. McCauley, in *Crystallization of Organic Compounds: An Industrial Perspective*, John Wiley & Sons, Inc., New Jersey, 2009, ch. 8, pp. 167-178.
91. G. G. Z. Zhang, R. F. Henry, T. B. Borchardt and X. C. Lou, *Journal of Pharmaceutical Sciences*, 2007, **96**, 990-995.
92. P. T. Cardew and R. J. Davey, *Proceedings of the Royal Society of London Series a-Mathematical Physical and Engineering Sciences*, 1985, **398**, 415-428.
93. W. Du, Q. X. Yin, H. X. Hao, Y. Bao, X. Zhang, J. T. Huang, X. Li, C. Xie and J. B. Gong, *Industrial & Engineering Chemistry Research*, 2014, **53**, 5652-5659.
94. E. Garcia, C. Hoff and S. Veesler, *Journal of Crystal Growth*, 2002, **237**, 2233-2239.
95. T. Friščić and W. Jones, *Crystal Growth & Design*, 2009, **9**, 1621-1637.
96. S. L. James, C. J. Adams, C. Bolm, D. Braga, P. Collier, T. Friščić, F. Grepioni, K. D. M. Harris, G. Hyett, W. Jones, A. Krebs, J. Mack, L. Maini, A. G. Orpen, I. P. Parkin, W. C. Shearouse, J. W. Steed and D. C. Waddell, *Chemical Society Reviews*, 2012, **41**, 413-447.
97. D. Braga, L. Maini and F. Grepioni, *Chemical Society Reviews*, 2013, **42**, 7638-7648.
98. M. Kitamura, *CrystEngComm*, 2009, **11**, 949-964.
99. R. Hilfiker, S. M. De Paul and M. Szelagiewicz, in *Polymorphism: in the Pharmaceutical Industry*, ed. R. Hilfiker, Wiley-VCH Verlag GmbH & Co. KGaA., Germany, 2006, ch. 11, pp. 287-308.
100. M. Kitamura, *Journal of Crystal Growth*, 2002, **237–239, Part 3**, 2205-2214.
101. H. Takiyama, *Advanced Powder Technology*, 2012, **23**, 273-278.
102. M. Kitamura, Y. Hayashi and T. Hara, *Journal of Crystal Growth*, 2008, **310**, 3067-3071.
103. T. Threlfall, *Organic Process Research & Development*, 2000, **4**, 384-390.
104. L. R. Agnew, D. L. Cruickshank, T. McGlone and C. C. Wilson, *Chemical Communications*, 2016, **52**, 7368-7371.
105. J. Li, S. A. Bourne and M. R. Caira, *Chemical Communications*, 2011, **47**, 1530-1532.
106. M. Karanam, S. Dev and A. R. Choudhury, *Crystal Growth & Design*, 2012, **12**, 240-252.

107. C. Heffernan, M. Ukrainczyk, J. Zeglinski, B. K. Hodnett and Å. C. Rasmuson, *Crystal Growth & Design*, 2018, **18**, 4715-4723.
108. R. Hilfiker, F. Blatter and M. von Raumer, in *Polymorphism in the Pharmaceutical Industry*, ed. R. Hilfiker, WILEY- VCH Verlag GmbH & Co. KGaA, Germany, 2006, ch. 1, pp. 1-19.
109. H.-H. Tung, E. L. Paul, M. Midler and J. A. McCauley, in *Crystallization of Organic compounds an Industrial Perspective*, John Wiley & Sons, Inc., New Jersey, 2009, ch. 5, pp. 101-116.
110. W. Beckmann, *Organic Process Research & Development*, 2004, **4**, 372-383.
111. A. Cote, G. Zhou and M. Stanik, *Organic Process Research & Development*, 2009, **13**, 1276-1283.
112. W. Beckmann, W. Otto and U. Budde, *Organic Process Research & Development*, 2001, **5**, 387-392.
113. A. J. Florence, N. E. B. Briggs, U. Schacht, V. Raval, T. McGlone and J. Sefcik, *Organic Process Research & Development*, 2015, **19**, 1903-1911.
114. L. Nicoud, F. Licordari and A. S. Myerson, *CrystEngComm*, 2019, **21**, 2105-2118.
115. R. J. P. Eder, E. K. Schmitt, J. Grill, S. Radl, H. Gruber-Woelfler and J. G. Khinast, *Crystal Research and Technology*, 2011, **46**, 227-237.
116. B. L. M. Lung-Somarriba, M. Moscosa-Santillan, C. Porte and A. Delacroix, *Journal of Crystal Growth*, 2004, **270**, 624-632.
117. M. W. Girolami and R. W. Rousseau, *Industrial & Engineering Chemistry Process Design and Development*, 1986, **25**, 66-70.
118. P. W. Voorhees, *Journal of Statistical Physics*, 1985, **38**, 231-252.
119. J. S. Srai and L. S. Alinaghian, *Global Strategy Journal*, 2013, **3**.
120. J. S. Srai, T. Harrington, L. Alinaghian and M. Phillips, *Chemical Engineering and Processing*, 2015, **97**, 248-258.
121. N. Shah, *Computers & Chemical Engineering*, 2004, **28**, 929-941.
122. S. L. Lee, T. F. O'Connor, X. Yang, C. N. Cruz, S. Chatterjee, R. D. Madurawe, C. M. V. Moore, L. X. Yu and J. Woodcock, *Journal of Pharmaceutical Innovation*, 2015, **10**, 191-199.
123. B. Wood, K. P. Girard, C. S. Polster and D. M. Croker, *Organic Process Research & Development*, 2019, **23**, 122-144.
124. S. Mascia, P. L. Heider, H. Zhang, R. Lakerveld, B. Benyahia, P. I. Barton, R. D. Braatz, C. L. Cooney, J. M. B. Evans, T. F. Jamison, K. F. Jensen, A. S. Myerson and B. L. Trout, *Angewandte Chemie*, 2013, **125**, 12585-12589.
125. J. S. Srai, C. Badman, M. Krumme, M. Futran and C. Johnston, *Journal Of Pharmaceutical Sciences*, 2014.
126. J. S. Srai, T. Harrington and L. Alinaghian, *Chimica Oggi - Chemistry Today*, 2014, **32**, 27-32.
127. WHO, WHO List of Essential Medicines 20th List, https://www.who.int/medicines/publications/essentialmedicines/20th_EML2017.pdf?ua=1, (accessed 07/01/2019, 2019).
128. W. Bolton, *Acta Crystallographica*, 1963, **16**, 166-173.
129. T. C. Lewis, D. A. Tocher and S. L. Price, *Crystal Growth & Design*, 2004, **4**, 979-987.
130. G. A. Jeffrey, S. Ghose and J. O. Warwicker, *Acta Crystallographica*, 1961, **14**, 881-887.
131. G. S. Nichol and W. Clegg, *Acta Crystallographica Section B*, 2005, **61**, 464-472.
132. S. Millefiori and A. Millefiori, *Journal of Heterocyclic Chemistry*, 1989, **26**, 639-644.
133. M. Gryl, A. Krawczuk and K. Stadnicka, *Acta Crystallographica Section B-Structural Science*, 2008, **64**, 623-632.
134. M. Gryl, A. Krawczuk-Pantula and K. Stadnicka, *Acta Crystallographica Section B*, 2011, **67**, 144-154.

135. K. E. Wittering, PhD, University of Bath, 2015.
136. K. A. Powell, G. Bartolini, K. E. Wittering, A. N. Saleemi, C. C. Wilson, C. D. Rielly and Z. K. Nagy, *Crystal Growth & Design*, 2015, **15**, 4821-4836.
137. M. R. Chierotti, L. Ferrero, N. Garino, R. Gobetto, L. Pellegrino, D. Braga, F. Grepioni and L. Maini, *Chemistry-a European Journal*, 2010, **16**, 4347-4358.
138. M.-R. Calas and T. J. Martinez, *Acad. Sc. Ser*, 1967, **265**, 631.
139. O. Shemchuk, D. Braga and F. Grepioni, *Chemical Communications*, 2016, **52**, 11815-11818.
140. G. H. W. Milburn, *X-ray Crystallography*, Butterworth & Co Ltd, Great Britain, 1973.
141. G. H. Stout and L. H. Jenson, *X-ray Structure Determination: A Practical Guide*, John Wiley & Sons, United States of America, Second edn., 1989.
142. W. Clegg, in *X-ray Crytsallography*, Oxford University Press, United States of America, Second edn., 2015, ch. 1, pp. 1-34.
143. W. Clegg, *Crystal Structure Determination*, Oxford University Press, United States, First edn., 1998.
144. C. Hammond, *The Basics of Crystallography and Diffraction.*, Oxford University Press, United States, Third edn., 2009.
145. C. Hammond, in *Introduction to Crystallography*, Oxford University Press, United States of America, 1992, ch. 7, pp. 79-101.
146. M. Mahon, X-ray Crytsallography, Univeristy of Bath Lecture notes 2019.
147. M. J. Buerger, in *X-ray Crystallography*, John Wiley & Sons, Inc., United States of America, 1966, ch. 6, pp. 107-127.
148. C. Hammond, in *Introduction to Crystallography*, Oxford University Press, United States, 1992, ch. 6, pp. 70-87.
149. C. Hammond, in *The Basics of Crystallography and Diffraction*, Oxford University Press, United States of America, 1997, ch. 9, pp. 135-170.
150. C. Hammond, in *The Basics of Crystallography and Diffraction*, Oxford University Press, United States of America, 1997, ch. Appendix 6, pp. 224-231.
151. G. H. Stout and L. H. Jensen, in *X-ray Structure Determination. A Practical Guide*, John Wiley & Sons, Inc., United States of America, Second edn., 1989, ch. 5, pp. 140-149.
152. G. H. Stout and L. H. Jensen, in *X-ray Structure Determination. A Practical Guide.*, John Wiley & Sons, Inc., United States of America, Second edn., 1989, ch. 12, pp. 279-291.
153. W. Clegg, A. J. Blake, R. O. Gould and P. Main, in *Crystal Structure Analysis: Principles and Practice*, ed. W. Clegg, Oxford University Press, United States, 2001, ch. 8, pp. 90-100.
154. G. H. Stout and L. H. Jensen, in *X-ray structure Determination: A Practical Guide*, John Wiley & Sons, Inc., United States of America, Second edn., 1989, ch. 11, pp. 248-278.
155. V. Elser, *Acta Crystallographica Section A*, 2003, **59**, 201-209.
156. L. Palatinus, Durham Crystallography School 2019.
157. L. Palatinus, *Acta Crystallographica Section B*, 2013, **69**, 1-16.
158. L. Palatinus and G. Chapuis, *Journal of Applied Crystallography*, 2007, **40**, 786-790.
159. W. Clegg, in *Crystal Structure Determination*, Oxford University Press, Great Britain, 1998, ch. 2, pp. 27-49.
160. W. Clegg, in *X-ray Crystallography*, Oxford University Press, Great Britain, Second edn., 2015, ch. 4, pp. 93-105.
161. W. Clegg, in *Crystal Structure Determination*, Oxford University Press, Great Britain, 1998, vol. 60, ch. 4, pp. 70-80.
162. M. M. Woolfson, in *An Introduction to X-ray Crystallography*, Cambridge University Press, United Kingdom, Second edn., 1997, ch. 5, pp. 108-155.
163. D. Q. M. Craig, in *Polymorphism in the Pharmaceutical Industry*, WILEY-VCH Verlag GmbH & co. KGaA, Germany, ch. 3, pp. 43-80.

164. S. Bhattacharya, H. G. Brittain and R. Suryanarayanan, in *Polymorphism in Pharmaceutical Solids*, ed. H. G. Brittain, Informa Healthcare USA, Inc., United States of America, Second edn., 2009, ch. 9, pp. 318-346.
165. FDA, Guidance for Industry PAT - A Framework for Innovative Pharmaceutical Development, Manufacturing, and Quality Assurance, https://www.fda.gov/AboutFDA/CentersOffices/OfficeofMedicalProductsandTobacco/CDER/ucm088828.htm).
166. D. C. Hinz, *Analytical and Bioanalytical Chemistry*, 2006, **384**, 1036-1042.
167. G. L. Reid, H. Ward II, W., A. S. Palm and K. Muteki, Process Analytical Technology (PAT) in Pharmaceutical Development, (accessed 23/01/2019, 2019).
168. H. Wu, Z. Dong, H. Li and M. Khan, *Organic Process Research & Development*, 2015, **19**, 89-101.
169. A. R. Heath, P. D. Fawell, P. A. Bahri and J. D. Swift, *Particle & Particle Systems Characterization*, 2002, **19**, 84-95.
170. Mettler Toledo, FBRM Method of Measurement, https://www.mt.com/us/en/home/library/videos/automated-reactors/Lasentec-FBRM-Method-of-Measurement.html, (accessed 23/01/2019, 2019).
171. X. Ni, *Innovations in Pharmaceutical Technology,* 2006, **20**, 90-96.
172. S. Lawton, G. Steele, P. Shering, L. Zhao, I. Laird and X. Ni, *Organic Process Research & Development*, 2009, **13**, 1357-1363.
173. Q. Su, Z. K. Nagy and C. D. Rielly, *Chemical Engineering and Processing: Process Intensification*, 2015, **89**, 41-53.
174. J. Li, B. L. Trout and A. S. Myerson, *Organic Process Research & Development*, 2016, **20**, 510-516.
175. A. J. Alvarez, A. Singh and A. S. Myerson, *Crystal Growth & Design*, 2011, **11**, 4392-4400.
176. P. Stonestreet and A. P. Harvey, *Chemical Engineering Research and Design*, 2002, **80**, 31-44.
177. T. McGlone, N. E. B. Briggs, C. A. Clark, C. J. Brown, J. Sefcik and A. J. Florence, *Organic Process Research & Development*, 2015, **19**, 1186-1202.
178. X. Nogueira, B. J. Taylor, H. Gomez, I. Colominas and M. R. Mackley, *Computers & Chemical Engineering*, 2013, **49**, 1-17.
179. R. Kacker, S. I. Regensburg and H. J. M. Kramer, *Chemical Engineering Journal*, 2017, **317**, 413-423.
180. NiTech Solutions, About Us, http://www.nitechsolutions.co.uk/about-us/, (accessed 24/01/2019, 2019).
181. NiTech Solutions, Crystallisation, http://www.nitechsolutions.co.uk/technology/crystallisation/, (accessed 24/01/2019, 2019).
182. NiTech Solutions, Crystallisation in the NiTech Crystalliser, http://www.nitechsolutions.co.uk/technology/presentations-and-papers/, (accessed 24/01/2019, 2019).
183. X.-W. Ni, A. Valentine, A. Liao, S. B. C. Sermage, G. B. Thomson and K. J. Roberts, *Crystal Growth & Design*, 2004, **4**, 1129-1135.
184. K. Robertson, P.-B. Flandrin, A. R. Klapwijk and C. C. Wilson, *Crystal Growth & Design*, 2016, **16**, 4759-4764.
185. R. Vacassy, J. Lemaître, H. Hofmann and J. H. Gerlings, *AIChE Journal*, 2000, **46**, 1241-1252.
186. A. M. Nightingale and J. C. deMello, *Advanced Materials*, 2013, **25**, 1813-1821.
187. B. K. H. Yen, A. Günther, M. A. Schmidt, K. F. Jensen and M. G. Bawendi, *Angewandte Chemie International Edition*, 2005, **44**, 5447-5451.

188. S. Guillemet-Fritsch, M. Aoun-Habbache, J. Sarrias, A. Rousset, N. Jongen, M. Donnet, P. Bowen and J. Lemaître, *Solid State Ionics*, 2004, **171**, 135-140.
189. L. Agnew, Ph.D., University of Bath, 2017.
190. A. R. Klapwijk, Ph.D., University of Bath, 2016.
191. P. M. Murray, S. N. G. Tyler and J. D. Moseley, *Organic Process Research & Development*, 2013, **17**, 40-46.
192. L. Eriksson, E. Johansson, N. Kettaneh-Wold, C. Wikstrom and S. Wold, 2008.
193. G. Sheldrick, *Acta crystallographica*, 2008, **64**, 112-122.
194. L. J. Farrugia, *Journal of Applied Crystallography*, 2012, **45**, 846-854.
195. C. F. Macrae, I. J. Bruno, J. A. Chisholm, P. R. Edgington, P. McCabe, E. Pidcock, L. Rodriguez-Monge, R. Taylor, J. van de Streek and P. A. Wood, *Journal*, 2008, **1**.
196. *Journal*, 2013.
197. X. Zhang, J. Yang, Y. Wu and X. Zhou, *Journal of Crystal Growth*, 2018, **502**, 45-53.
198. L. C. Thomas and S. J. Schmidt, "Apparent Melting": A New Approach to Characterizing Crystalline Structure in Pharmaceutical Materials, https://www.tainstruments.com/pdf/literature/TA401.pdf, (accessed 15/03/2019, 2019).
199. B. Wunderlich, in *Thermal Analysis*, Academic Press, San Diego, CA, First edn., 1990, ch. 3, pp. 79-121.
200. P. M. Schaber, J. Colson, S. Higgins, D. Thielen, B. Anspach and J. Brauer, *Thermochimica Acta*, 2004, **424**, 131-142.
201. M. Pudipeddi and A. T. M. Serajuddin, *Journal of Pharmaceutical Sciences*, 2005, **94**, 929-939.
202. A. Kitaigorodskii, *Acta Crystallographica*, 1965, **18**, 585-590.
203. CCDC, Understanding Polymorph Stability using Full Interaction Maps, https://www.ccdc.cam.ac.uk/support-and-resources/ccdcresources/sulfathiazole_note.pdf, (accessed 10/05/2019, 2019).
204. P. A. Wood, T. S. G. Olsson, J. C. Cole, S. J. Cottrell, N. Feeder, P. T. A. Galek, C. R. Groom and E. Pidcock, *CrystEngComm*, 2013, **15**, 65-72.
205. I. J. Bruno, J. C. Cole, J. P. M. Lommerse, R. S. Rowland, R. Taylor and M. L. Verdonk, *Journal of Computer-Aided Molecular Design*, 1997, **11**, 525-537.

Chapter 9 – Appendices

9.1 Chapter 2 Appendix

Table 9.1: Systematic absences for centred unit cells.

Centring	Points equivalent to 0,0,0	Condition for observed intensity	Fraction of observed data
P	None	None	1
A	0, ½, ½	$k + l = 2n$	½
B	½, 0, ½	$h + l = 2n$	½
C	½, ½, 0	$h + k = 2n$	½
I	½, ½, ½	$h + k + l = 2n$	½
F	0, ½, ½ and ½, 0, ½ and ½, ½, 0	*h, k, l* all odd or all even	¼
R	$^1/_3, ^2/_3, ^2/_3$ and $^2/_3, ^1/_3, ^1/_3$	$-h + k + l = 3n$	$^1/_3$

Table 9.2: Systematic absences for glide planes.

Normal to glide plane	Reflections affected	Glide plane symbol	Translation Vector	Condition for observed intensity
a axis [100]	0*kl*	*b* *c* *n* *d*	**b**/2 **c**/2 (**b**+**c**)/2 (**b**+**c**)/4	$k = 2n$ $l = 2n$ $k + l = 2n$ $k + l = 4n$
b axis [010]	*h*0*l*	*a* *c* *n* *d*	**a**/2 **c**/2 (**a**+**c**)/2 (**a**+**c**)/4	$h = 2n$ $l = 2n$ $h + l = 2n$ $h + l = 4n$
c axis [001]	*hk*0	*a* *b* *n* *d*	**a**/2 **b**/2 (**a**+**b**)/2 (**a**+**b**)/4	$h = 2n$ $k = 2n$ $h + k = 2n$ $h + k = 4n$
[110]	*hhl*	*c* *d*	**c**/2 (**a**+**b**+**c**)/4	$l = 2n$ $2h + l = 4n$

Table 9.3: Systematic absences for screw axes: conditions for observed intensity.

Parallel to	Reflections affected	Condition for 2_1, 4_2 or 6_3	Condition for 3_1, 3_2, 6_2 or 6_4	Condition for 4_1 or 4_3	Condition for 6_1 or 6_5
a	*h*00	*h* = 2n	*h* = 3n	*h* = 4n	*h* = 6n
b	0*k*0	*k* = 2n	*k* = 3n	*k* = 4n	*k* = 6n
c	00*l*	*l* = 2n	*l* = 3n	*l* = 4n	*l* = 6n

9.2 Chapter 4 Appendix

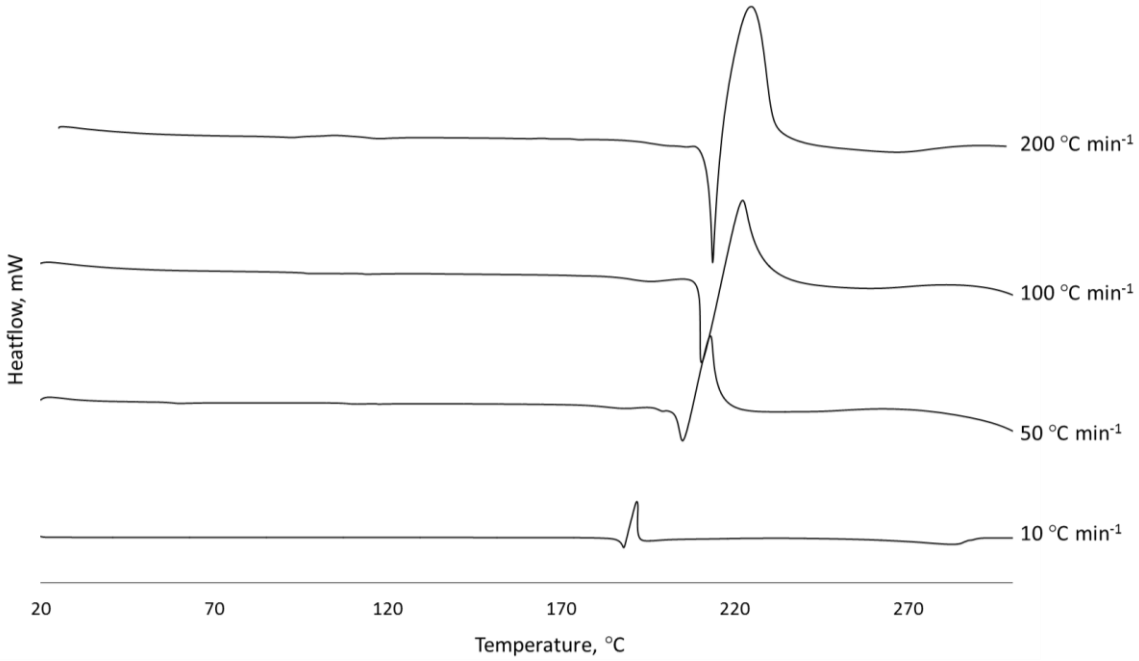

Figure 9.1: DSC traces of UBA form I collected using a variety of heating rates.

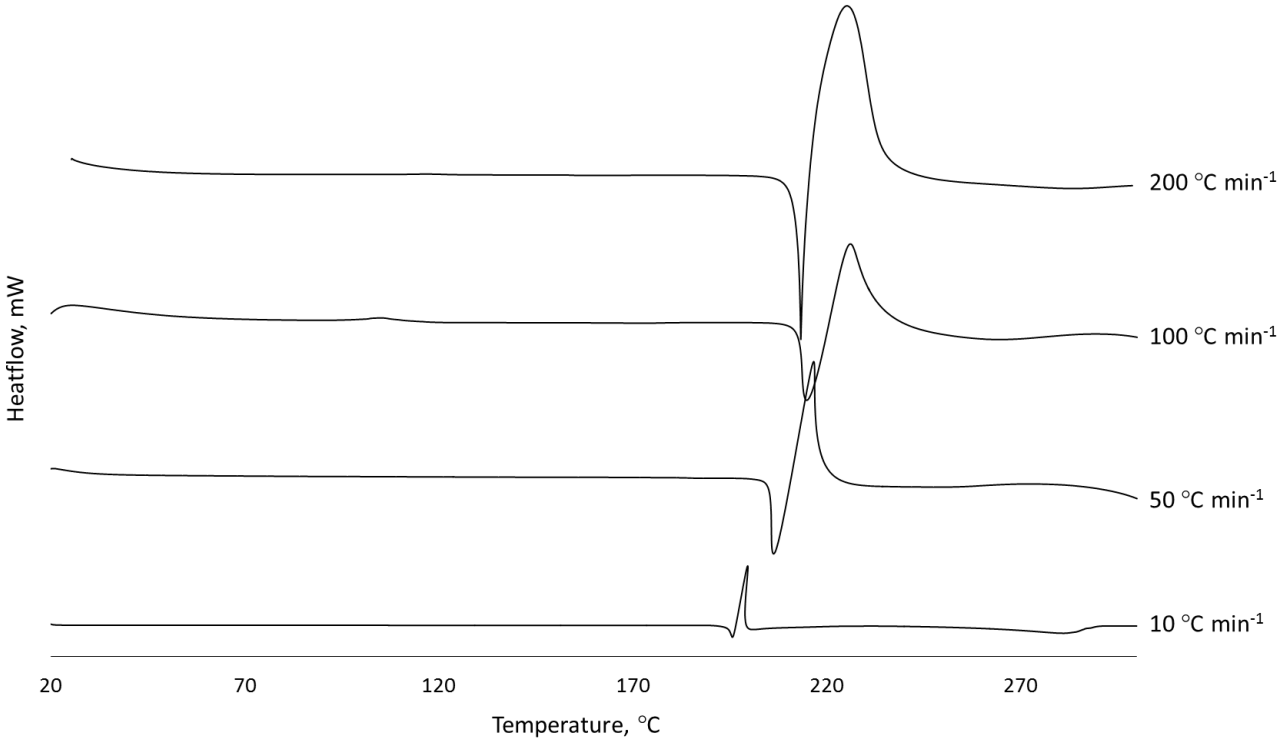

Figure 9.2: DSC traces of UBA form III collected using a variety of different heating rates.

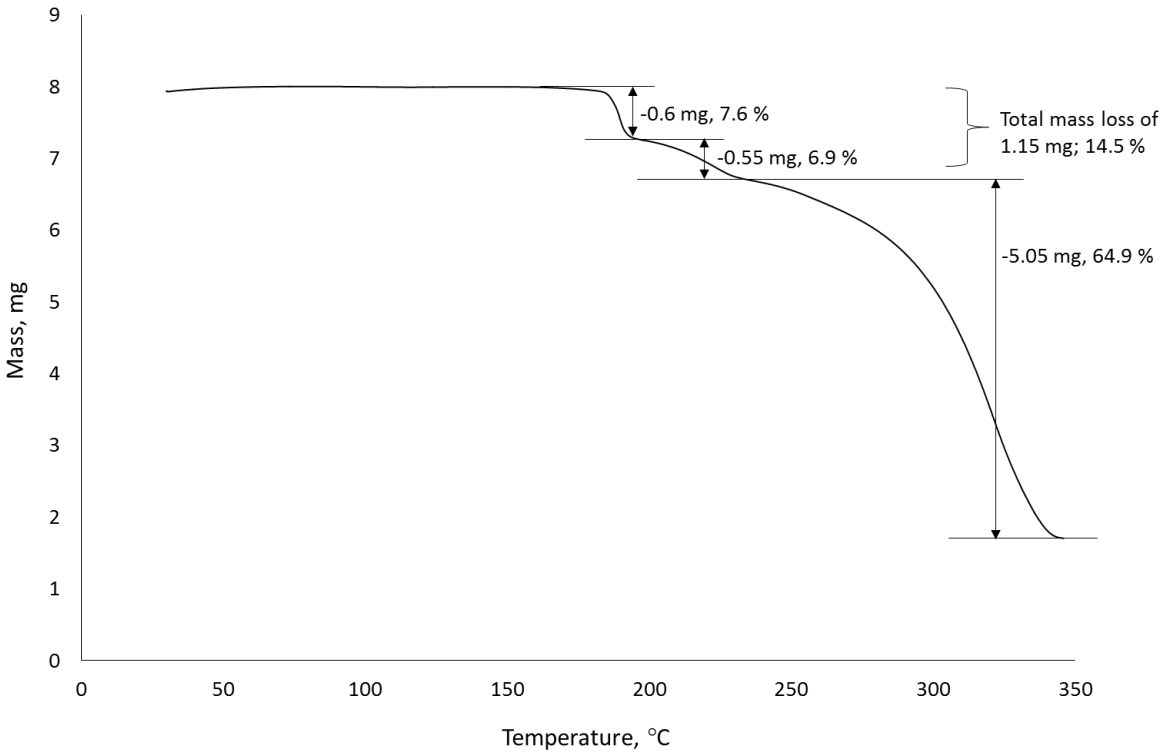

Figure 9.3: TGA trace of UBA form I (10 °C min^{-1}).

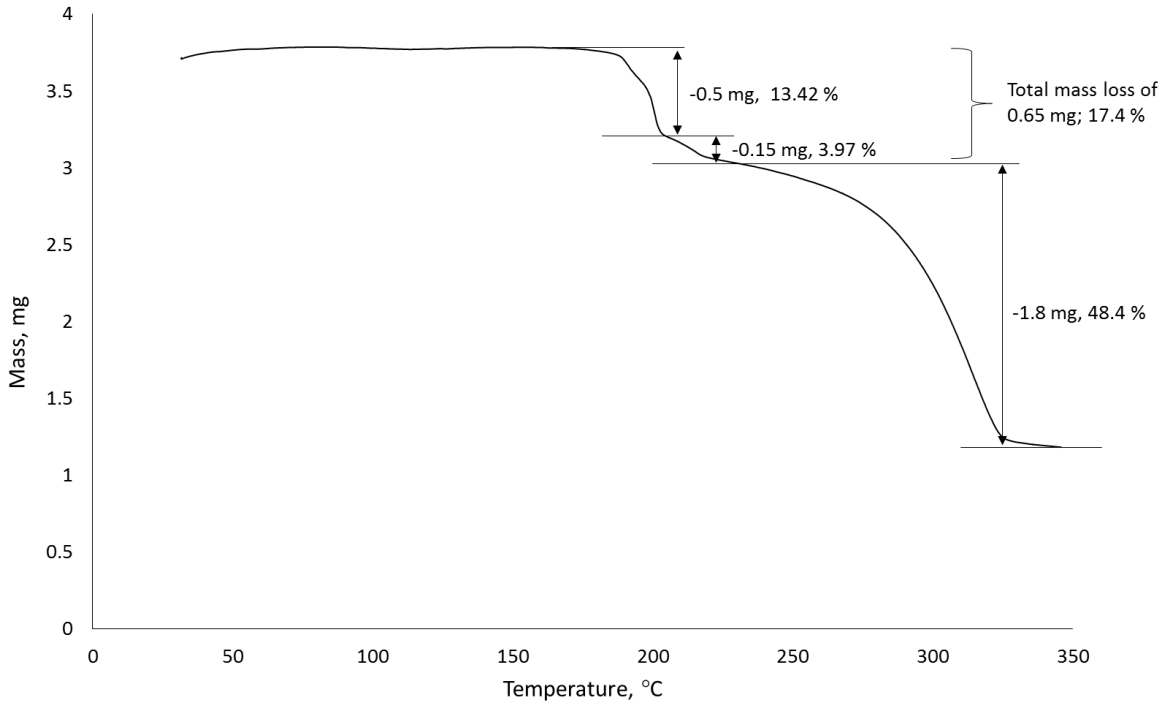

Figure 9.4: TGA trace of UBA form III (10 °C min-1).

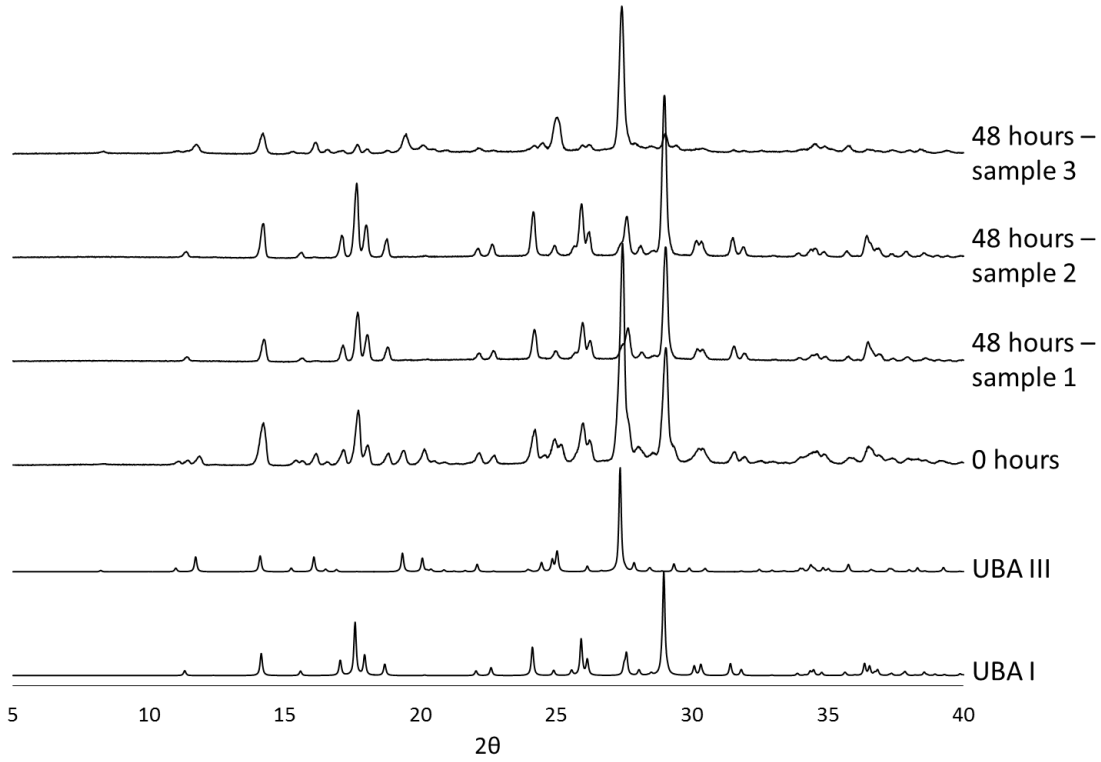

Figure 9.5: PXRD patterns of UBA form I and form III competitive slurry in ethanol at 75 °C.

9.3 Chapter 5 Appendix

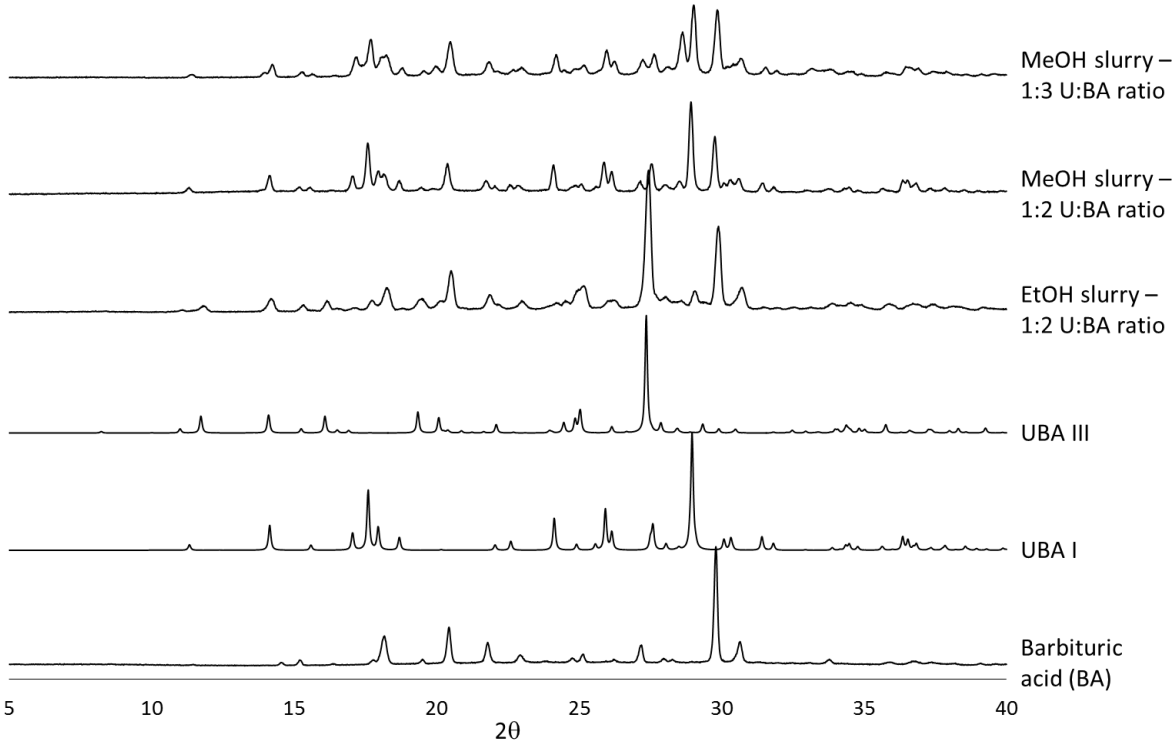

Figure 9.6: PXRD patterns of small scale 24 hour slurries using ethanol and methanol as solvent medium and 1:2 and 1:3 ratios of urea: barbituric acid.

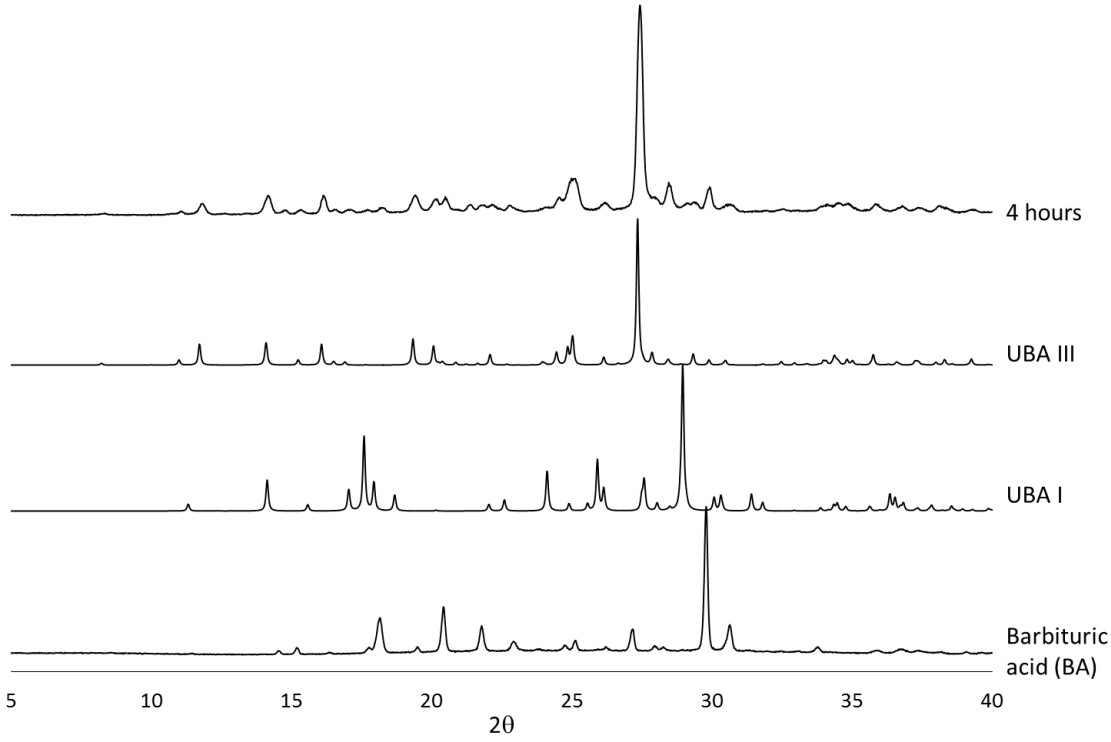

Figure 9.7: PXRD pattern of 4 hour 1:1 urea: barbituric acid slurry - 400 mg urea, 852 mg barbituric acid, 3 mL ethanol.

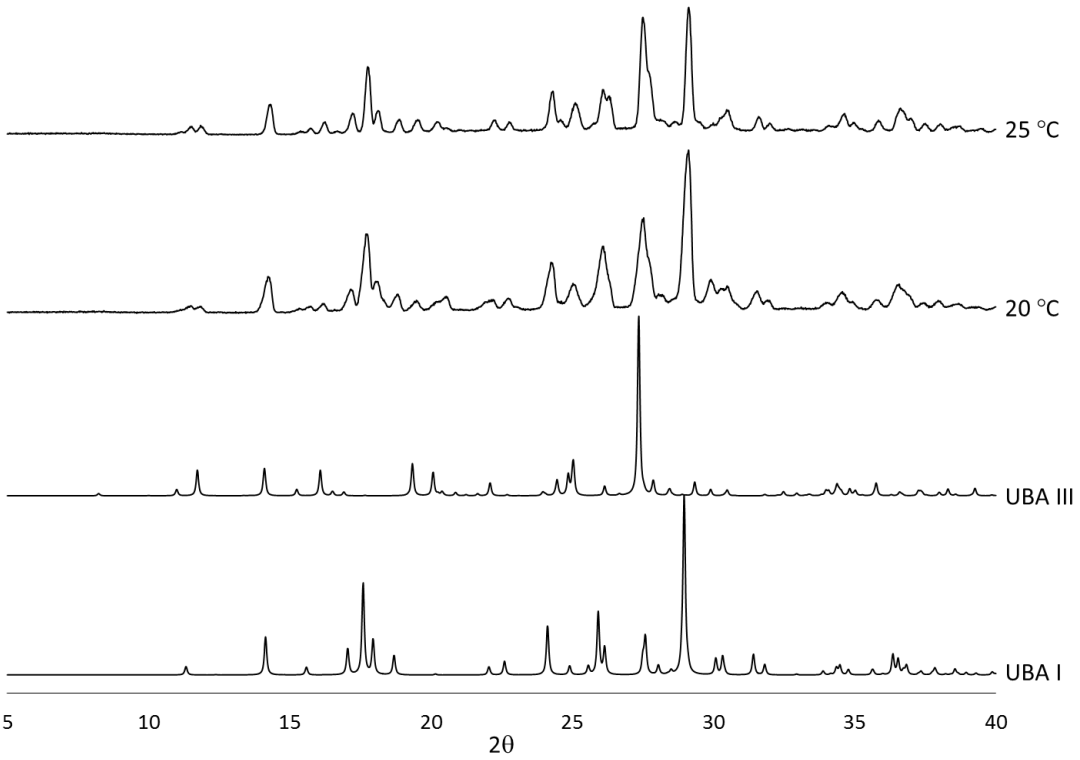

Figure 9.8: PXRD pattern of 50 mL ethanol mediated slurries with a 1:1 ratio of urea: barbituric acid.

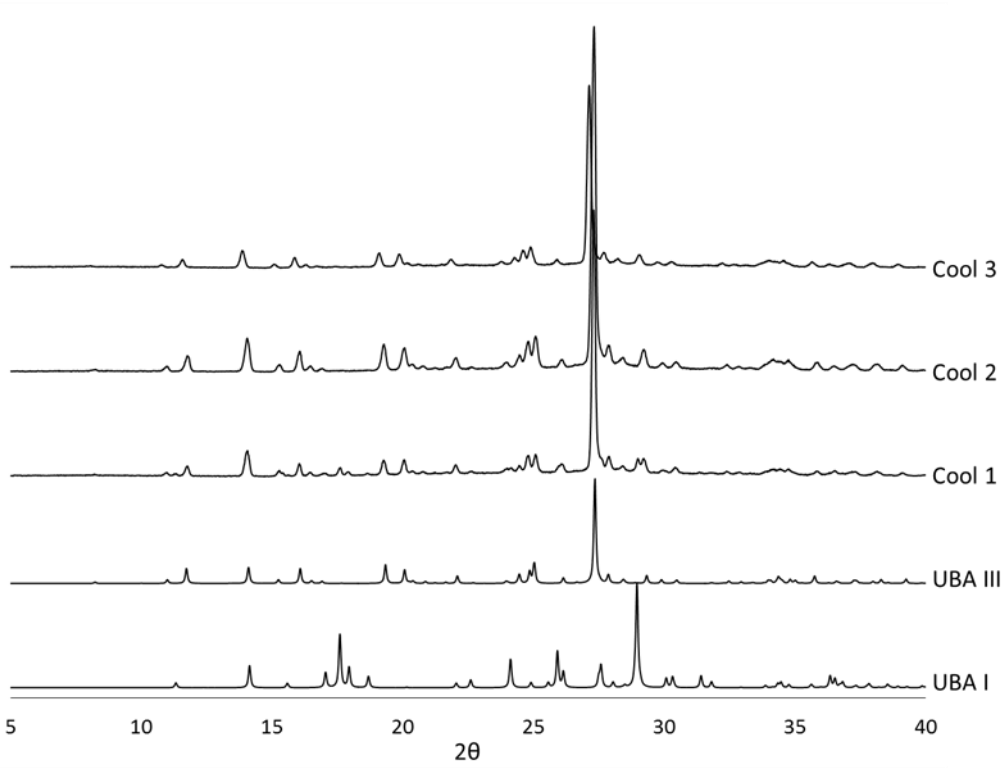

Figure 9.9: PXRD patterns for the subsequent unseeded 50 mL cooling crystallisations of UBA from ethanol - post DoE study.

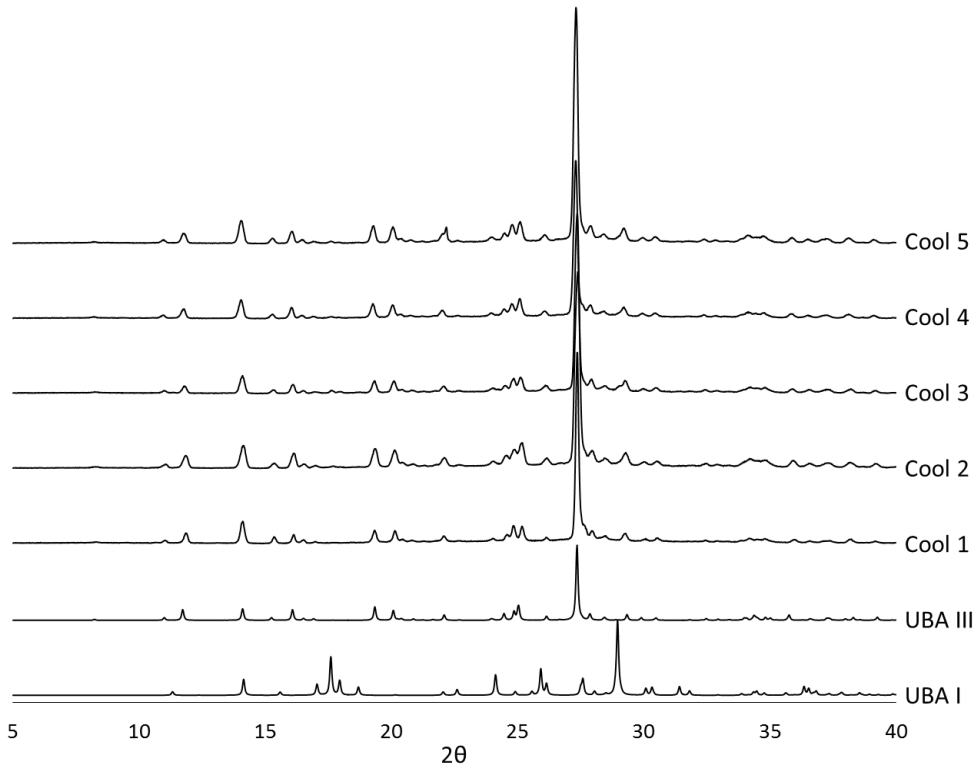

Figure 9.10: PXRD patterns of unseeded 150 mL cooling crystallisations of UBA from ethanol.

Table 9.4: Summary of all Easymax cooling crystallisation experiments conducted at GSK, Stevenage. Solid did not dissolve in crossed out experiments (EZM1 & EZM2).

Easymax experiment	Date	Solvent	Cooling , °C/min	Seed type	Seed loading, %	Overnight hold	Outcome
~~1~~	~~2018.05.14~~	~~IPA~~	~~1~~	~~none~~	~~0~~	~~no~~	~~none~~
~~2~~	~~2018.05.14~~	~~IPA~~	~~1~~	~~none~~	~~0~~	~~no~~	~~none~~
3	2018.05.15	IPA	1	none	0	no	UBA III
4	2018.05.17	IPA	0.5	none	0	no	UBA I & III
5	2018.05.21	IPA	0.5	none	0	yes	UBA III
6	2018.05.22	IPA	0.5	UBA III	1	no	UBA I & III
7	2018.05.22	IPA	1	none	0	yes	UBA I & III
8	2018.05.23	IPA	0.5	UBA III	5	no	UBA I & III
9	2018.05.23	IPA	1	UBA III	1	no	UBA I & III
10	2018.05.24	IPA	0.5	UBA III	20	no	UBA III
11	2018.05.24	IPA	1	UBA III	5	no	UBA III
12	2018.05.25	IPA	0.5	UBA I	1	no	UBA I
13	2018.05.25	IPA	1	UBA III	20	no	UBA III
14	2018.05.29	IPA	0.5	UBA I	5	no	UBA I
15	2018.05.29	IPA	1	UBA I	1	no	UBA I
16	2018.05.30	IPA	0.5	UBA I	20	no	UBA I
17	2018.05.30	IPA	1	UBA I	5	no	UBA I
18	2018.05.30	IPA	1	UBA I	20	no	UBA I
19	2018.08.06	EtOH	0.5	none	0	yes	UBA I, III & BA
20	2018.08.07	EtOH	1	none	0	yes	UBA III & BA
21	2018.08.08	EtOH	0.5	none	0	no	UBA III & I
22	2018.08.08	EtOH	1	none	0	no	UBA III & I/BA
23	2018.08.09	EtOH	0.5	UBA I	1	no	UBA I & III
24	2018.08.09	EtOH	1	UBA I	1	no	UBA I & III
25	2018.08.10	EtOH	0.5	UBA I	5	no	UBA I
26	2018.08.10	EtOH	1	UBA I	5	no	UBA I
27	2018.08.13	EtOH	0.5	UBA I	20	no	UBA I
28	2018.08.13	EtOH	1	UBA I	20	no	UBA I
29	2018.08.16	EtOH	0.5	UBA III	1	no	UBA III & I
30	2018.08.23	EtOH	1	UBA III	1	no	UBA III & trace I
31	2018.08.17	EtOH	0.5	UBA III	5	no	UBA III & trace I
32	2018.08.17	EtOH	1	UBA III	5	no	UBA III & trace I
33	2018.08.20	EtOH	0.5	UBA III	20	no	UBA III
34	2018.08.20	EtOH	1	UBA III	20	no	UBA III
35	2018.08.21	IPA	0.5	UBA III	20	yes	UBA III
36	2018.08.22	IPA	1	UBA III	5	yes	UBA III & I

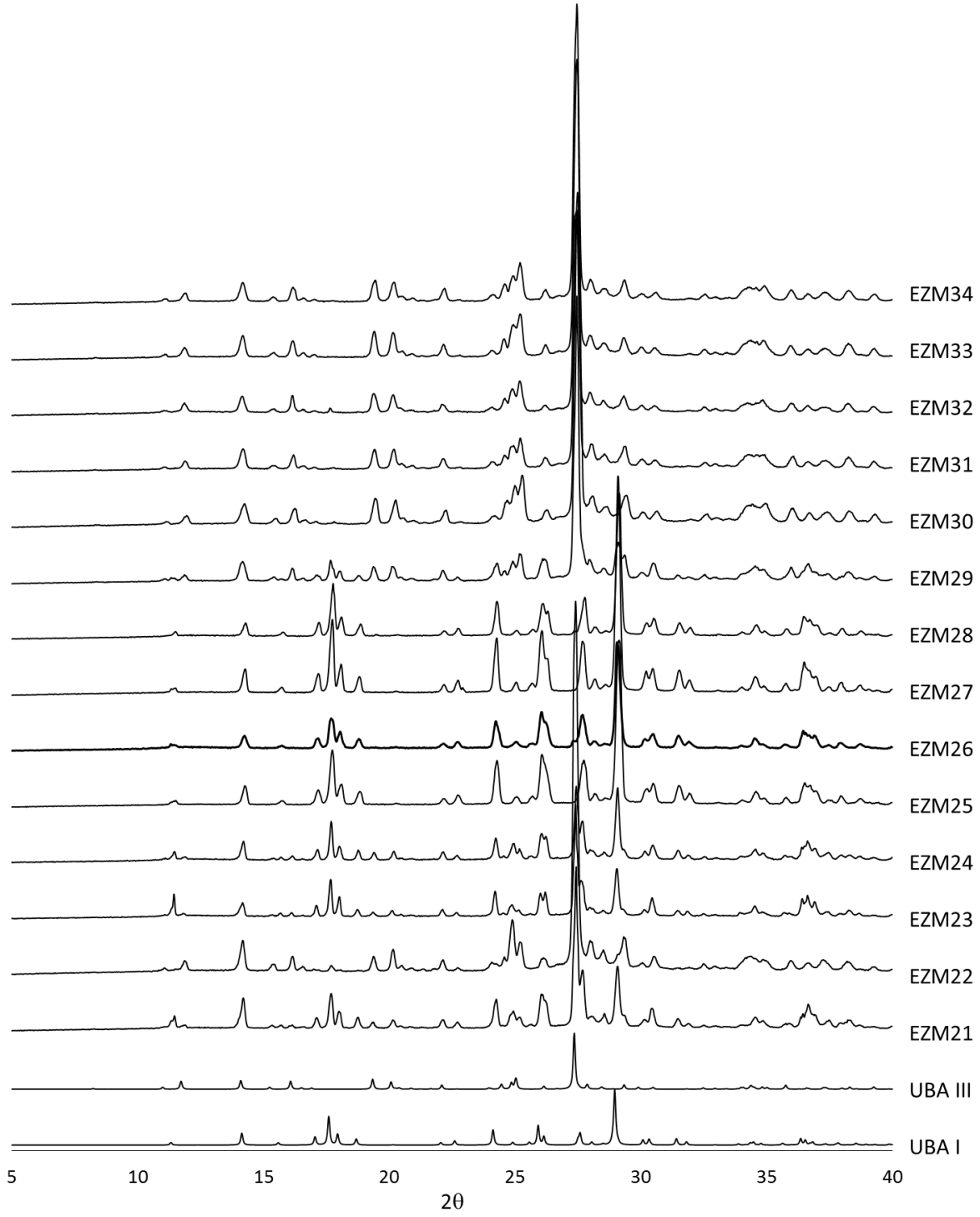

Figure 9.11: PXRD patterns for the ethanol mediated Easymax cooling crystallisation products.

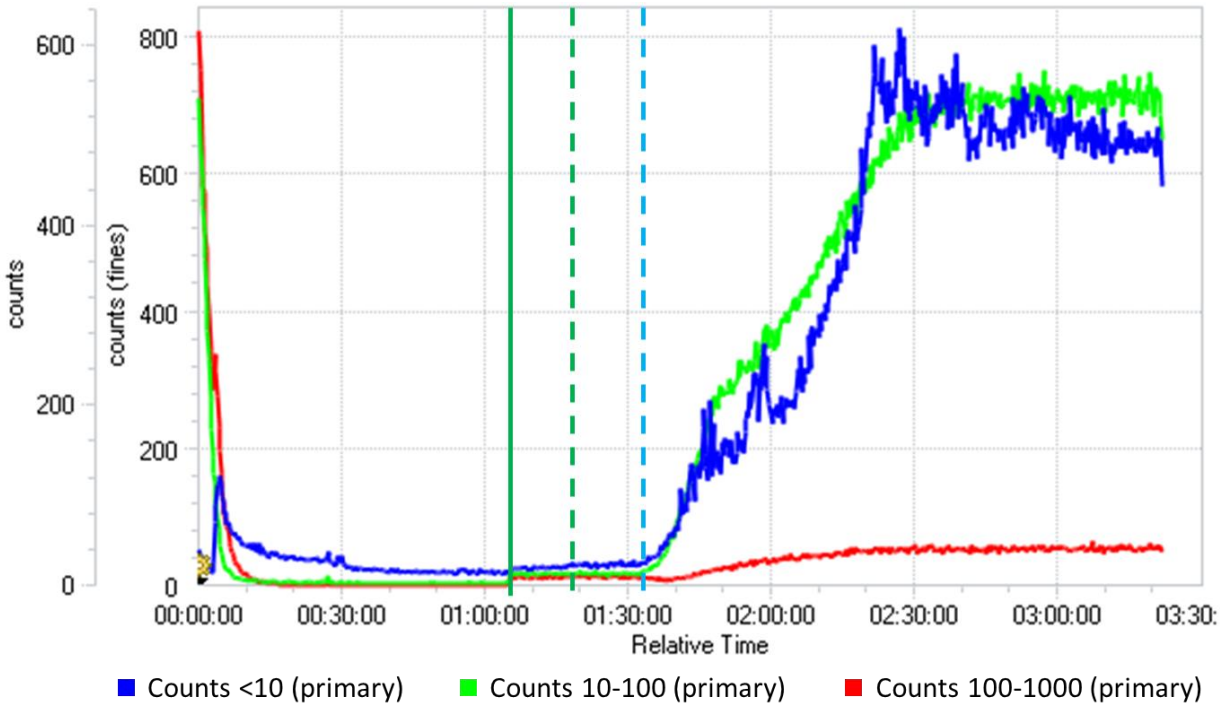

Figure 9.12: FBRM trace of 1 % UBA form I seeded Easymax cooling crystallisation of UBA from ethanol; 1 °C min^{-1} cooling rate. Solid green line represents seed addition, dashed green line shows end of seed hold and the dashed blue line shows the start of the nucleation event.

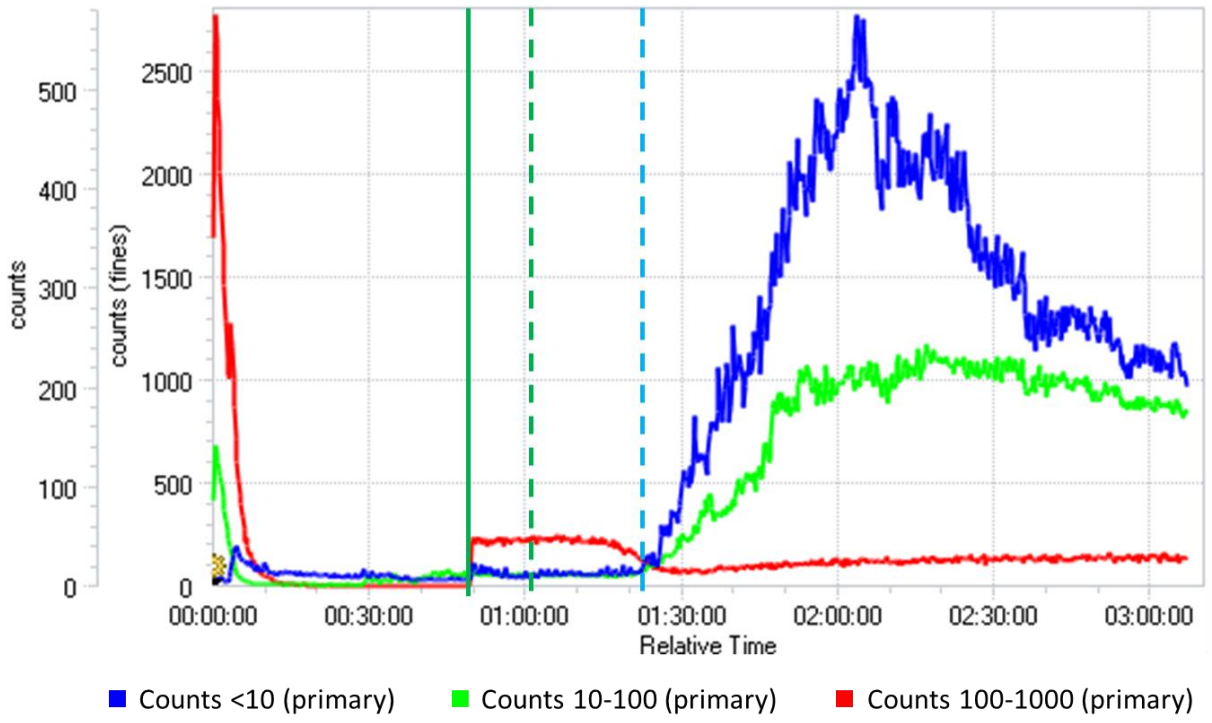

Figure 9.13: FBRM trace of 5 % UBA form I seeded Easymax cooling crystallisation of UBA from ethanol; 1 °C min^{-1} cooling rate. Solid green line represents seed addition, dashed green line shows end of seed hold and the dashed blue line shows the start of the nucleation event.

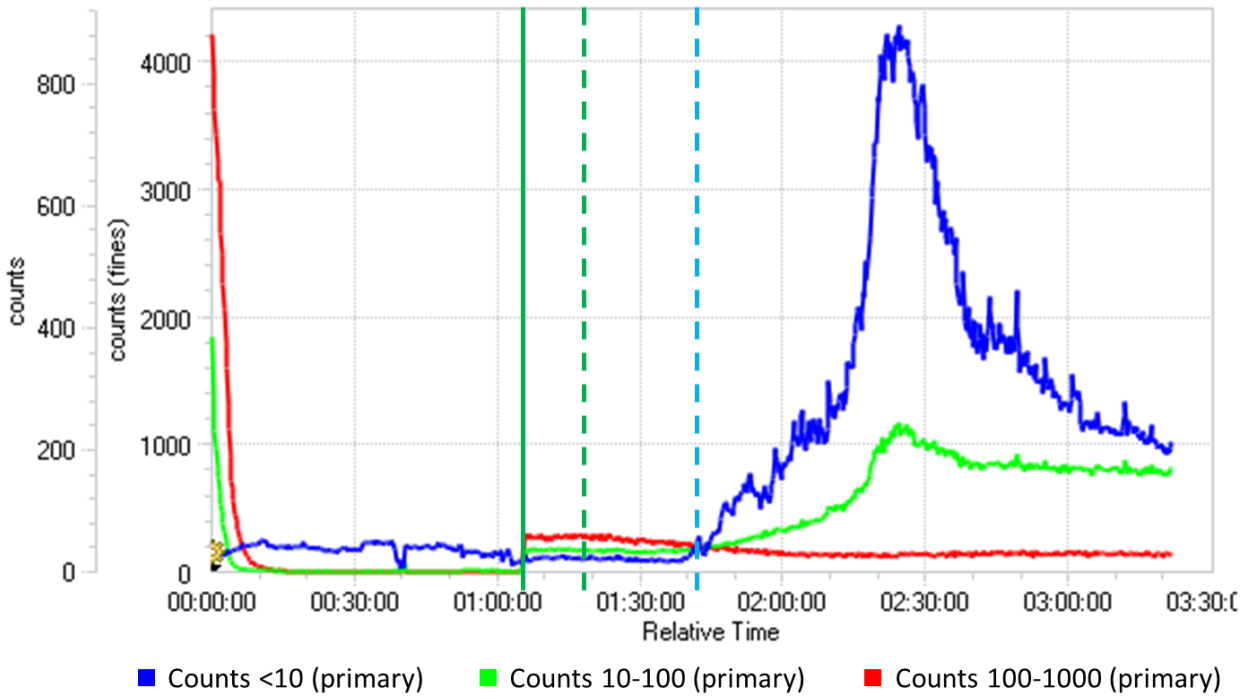

Figure 9.14: FBRM trace of 20 % UBA form I seeded Easymax cooling crystallisation of UBA from ethanol; 1 °C min^{-1} cooling rate. Solid green line represents seed addition, dashed green line shows end of seed hold and the dashed blue line shows the start of the nucleation event.

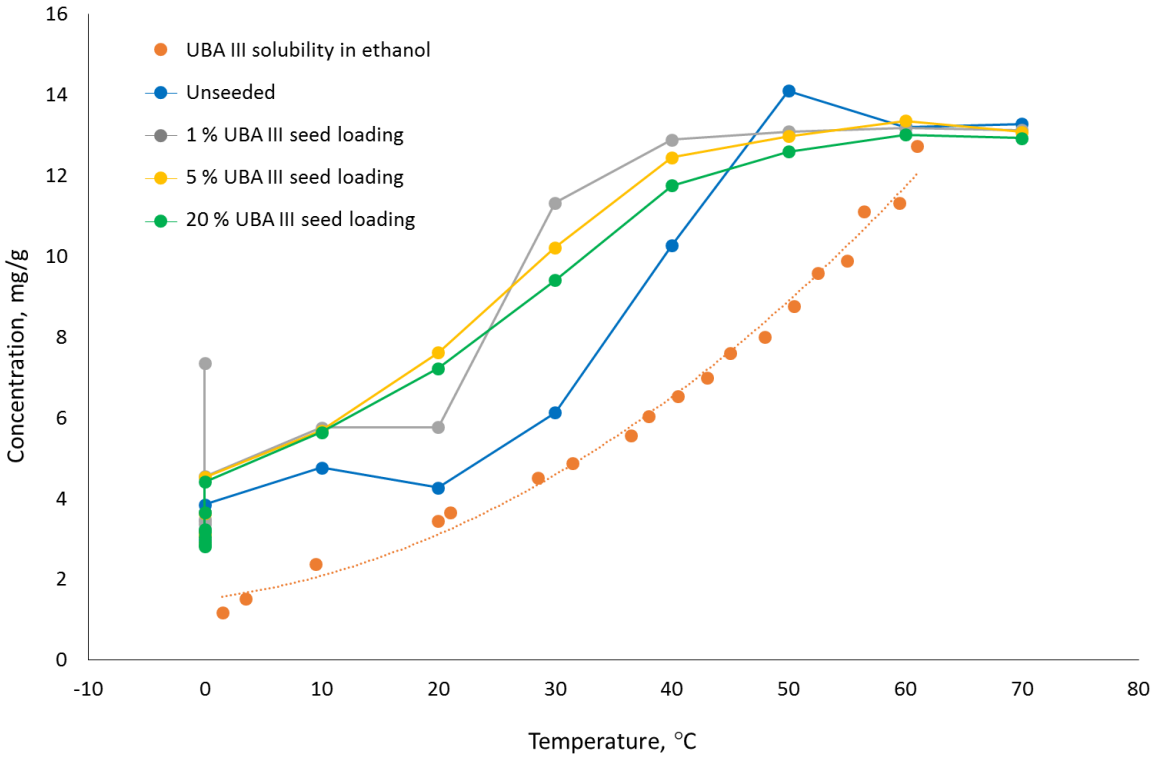

Figure 9.15: Concentration profiles for UBA form I seeded cooling crystallisations from ethanol with a cooling rate of 1 °C min^{-1}.

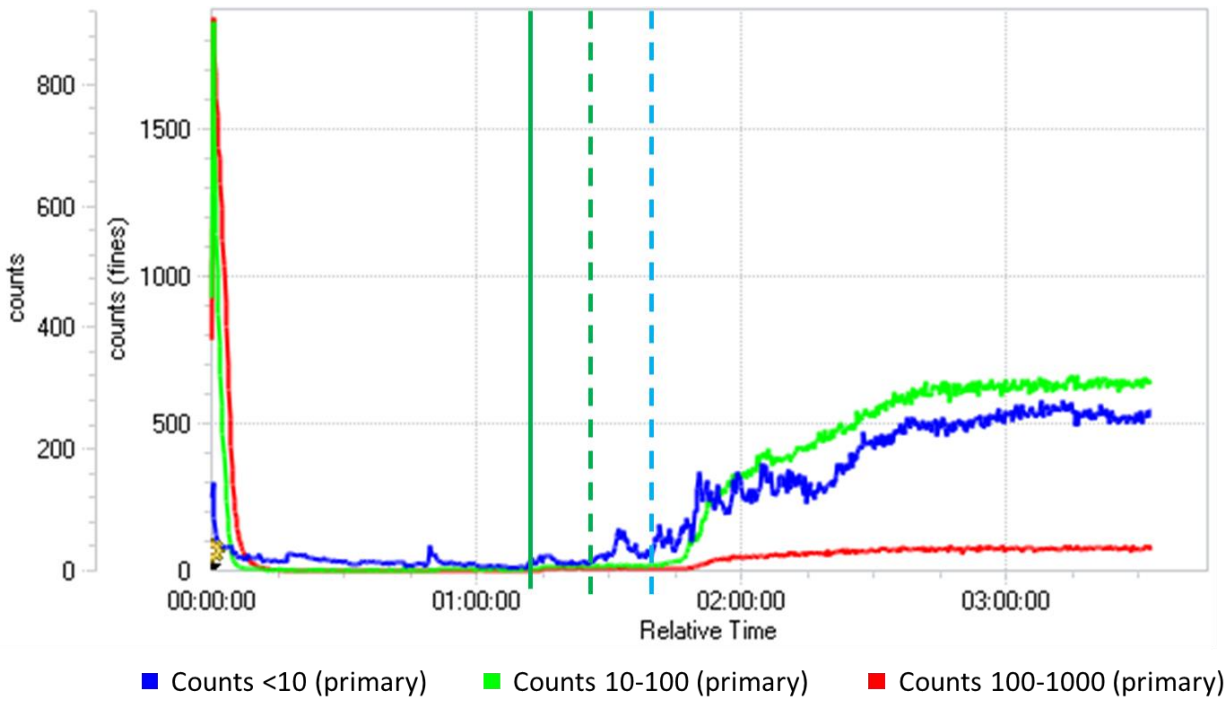

Figure 9.16: FBRM trace of 1 % UBA form III seeded Easymax cooling crystallisation of UBA from ethanol; 1 °C min^{-1} cooling rate. Solid green line represents seed addition, dashed green line shows end of seed hold and the dashed blue line shows the start of the nucleation event.

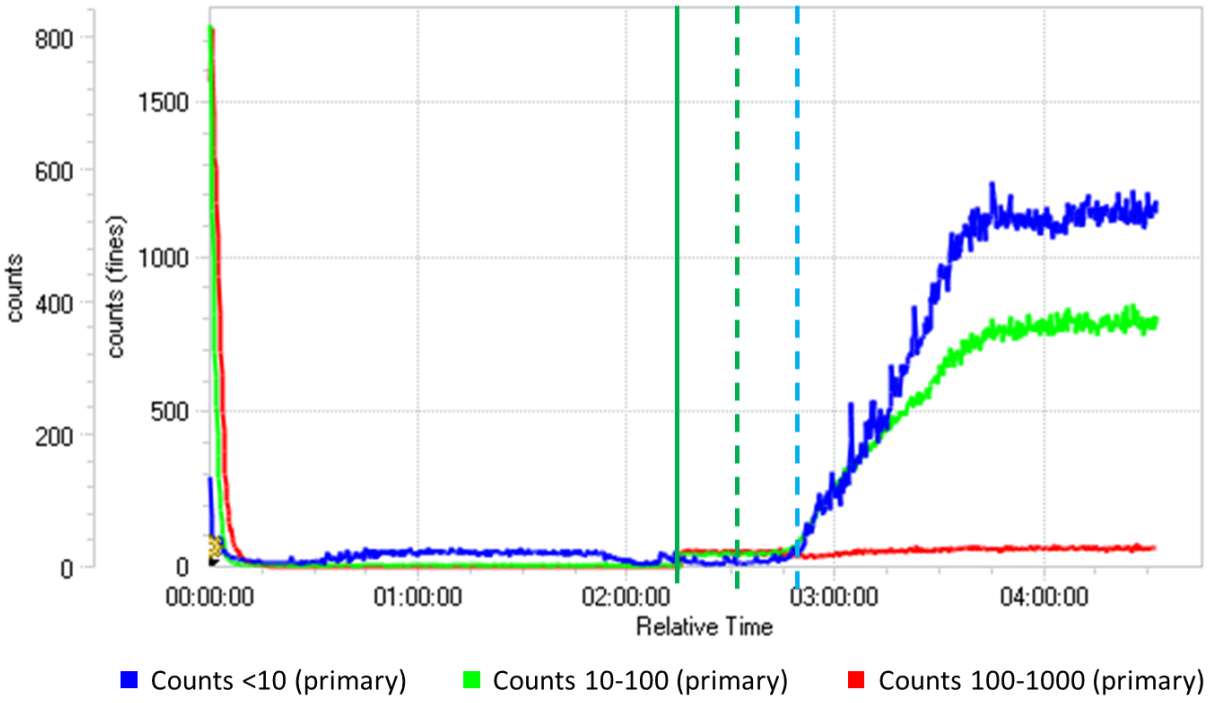

Figure 9.17: FBRM trace of 5 % UBA form III seeded Easymax cooling crystallisation of UBA from ethanol; 1 °C min^{-1} cooling rate. Solid green line represents seed addition, dashed green line shows end of seed hold and the dashed blue line shows the start of the nucleation event.

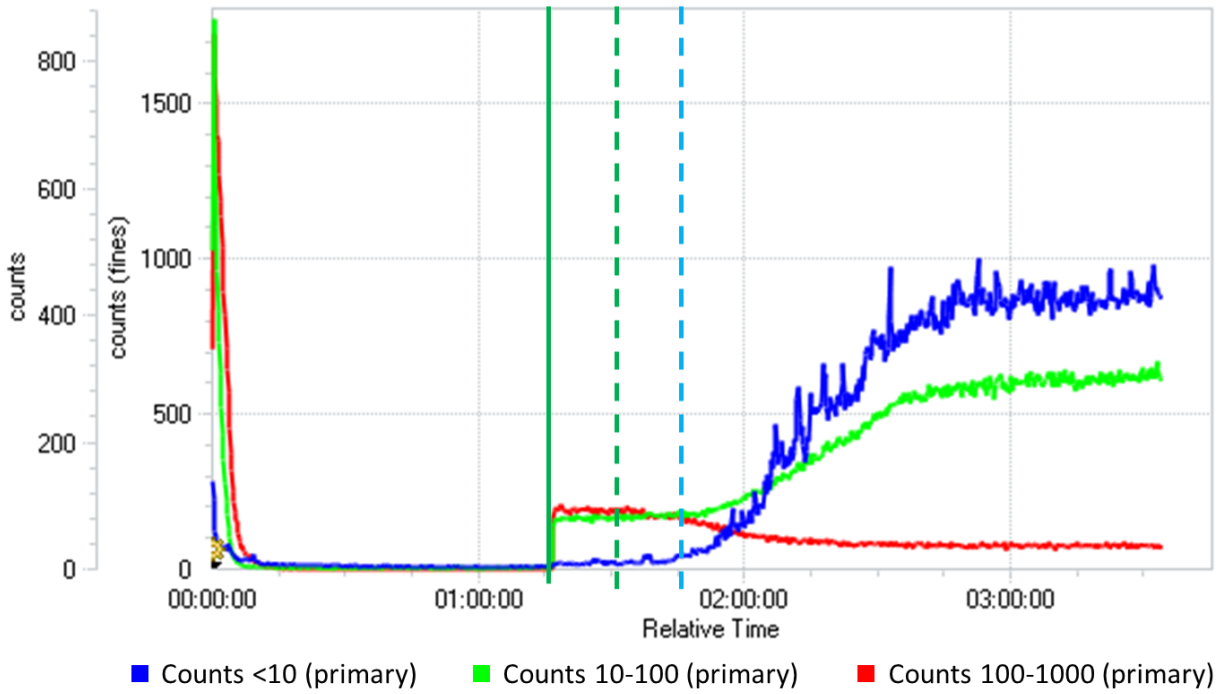

Figure 9.18: FBRM trace of 20 % UBA form III seeded Easymax cooling crystallisation of UBA from ethanol; 1 °C min^{-1} cooling rate. Solid green line represents seed addition, dashed green line shows end of seed hold and the dashed blue line shows the start of the nucleation event.

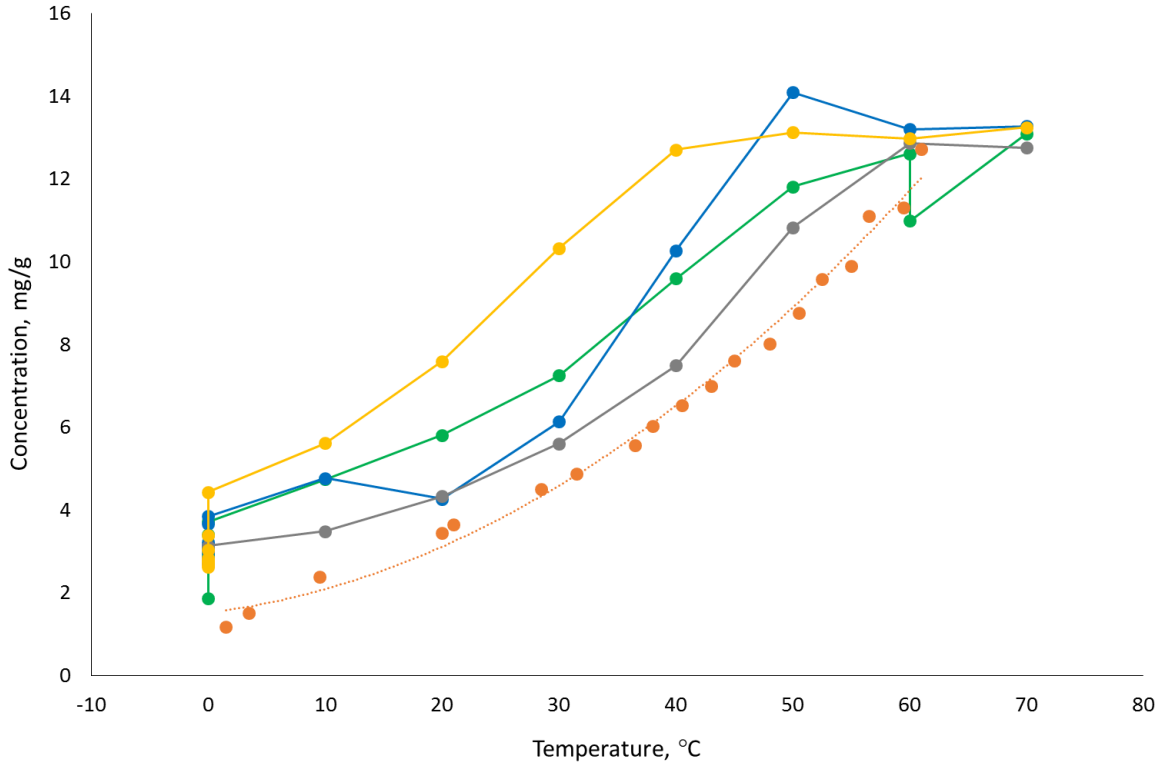

Figure 9.19: Concentration profiles for UBA form III seeded cooling crystallisations from ethanol with a cooling rate of 1 °C min^{-1}.

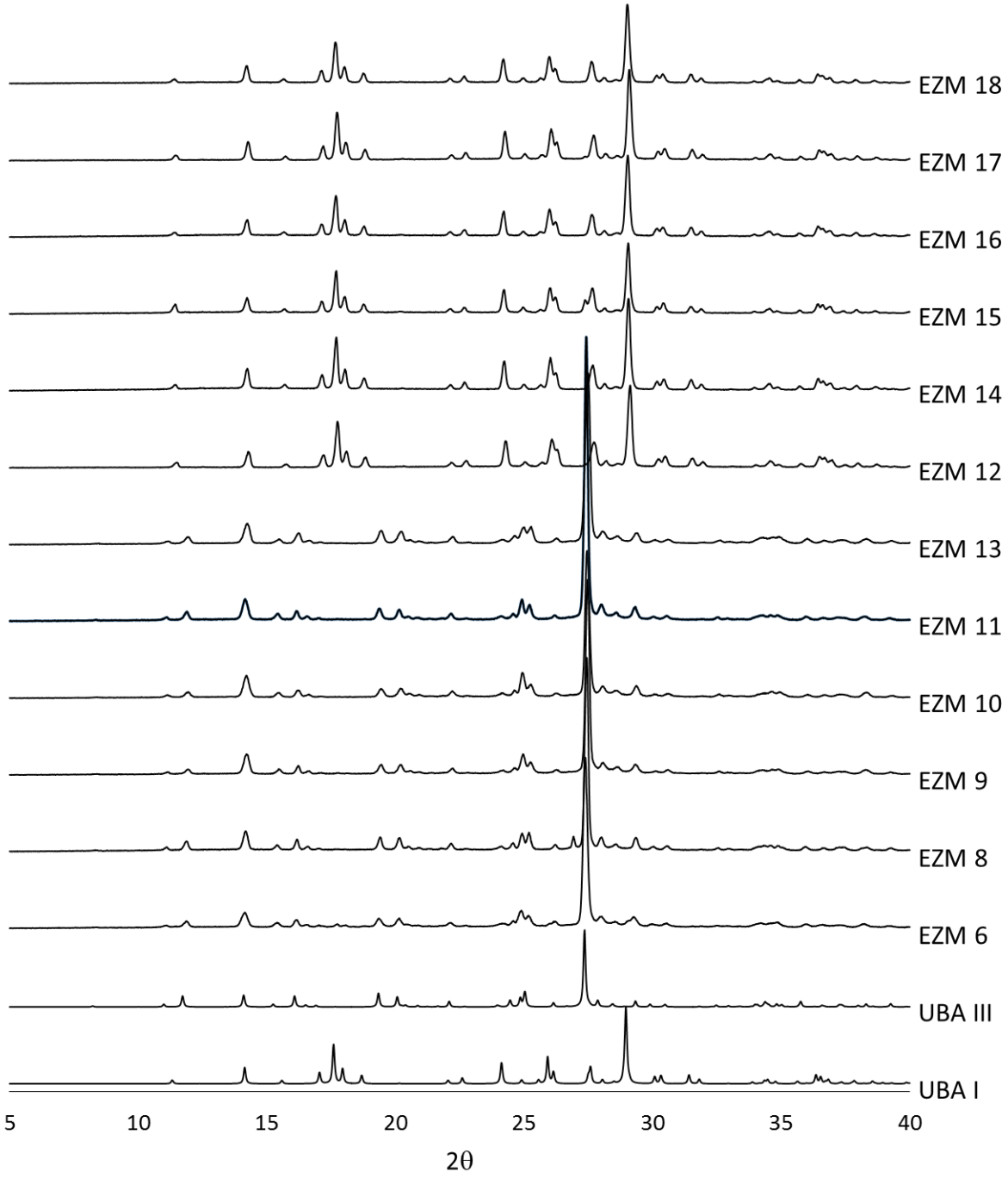

Figure 9.20: PXRD patterns of the UBA form I and form III seeded Easymax cooling crystallisations of UBA from IPA.

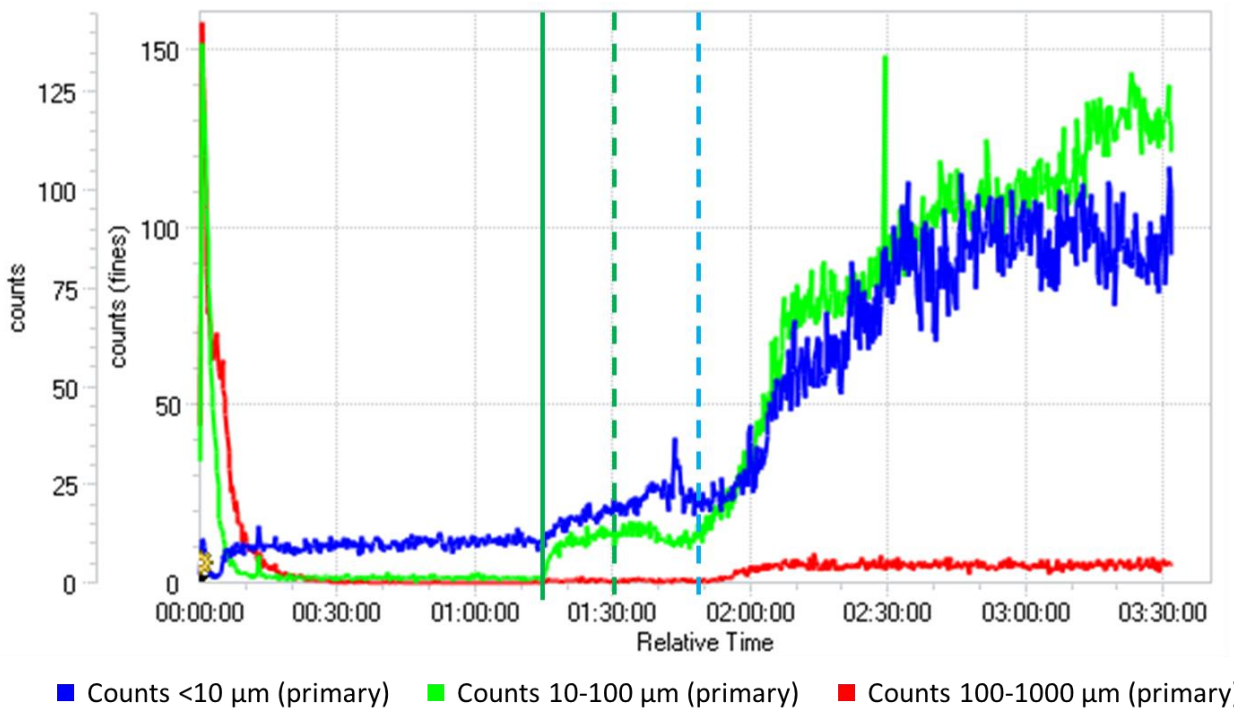

Figure 9.21: FBRM trace obtained from the 1 % UBA form I seeded Easymax cooling crystallisation of UBA from IPA, 1 °C min^{-1} cooling rate. Solid green line shows point of seed addition, dashed green line shows end of seed hold and the dashed blue line shows nucleation event.

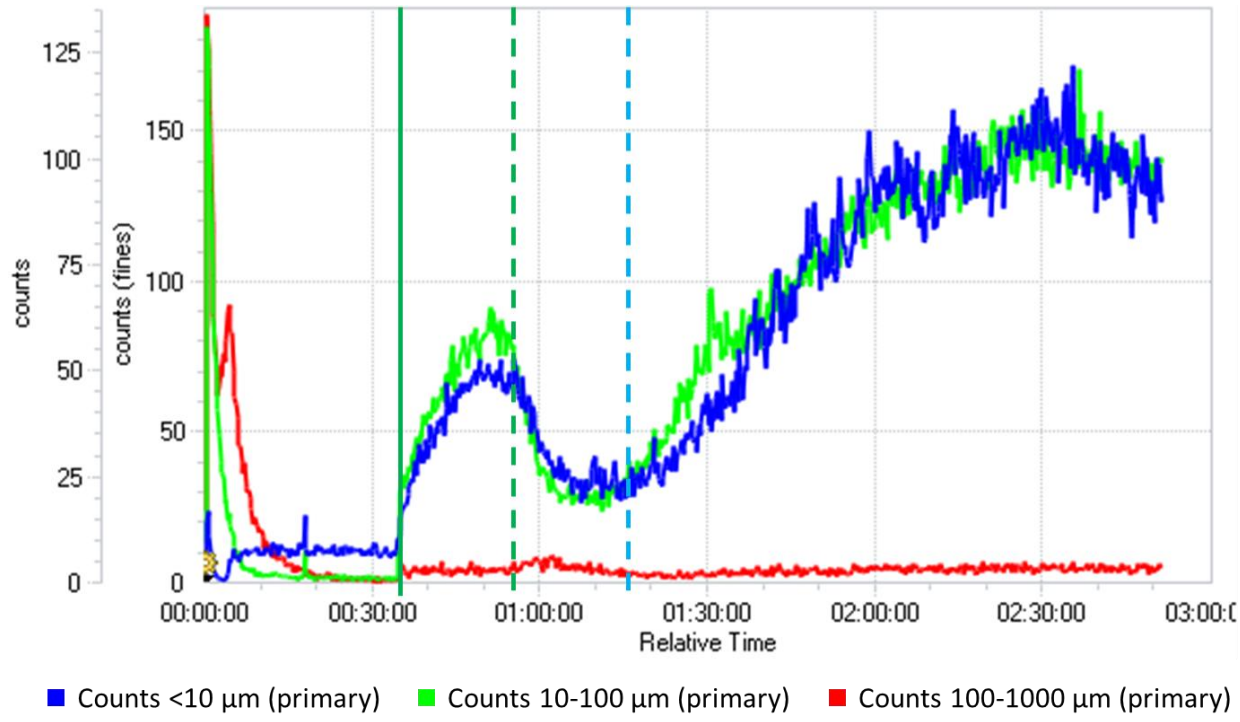

Figure 9.22: FBRM trace obtained from the 5 % UBA form I seeded Easymax cooling crystallisation of UBA from IPA, 1 °C min^{-1} cooling rate. Solid green line shows point of seed addition, dashed green line shows end of seed hold and the dashed blue line shows nucleation event.

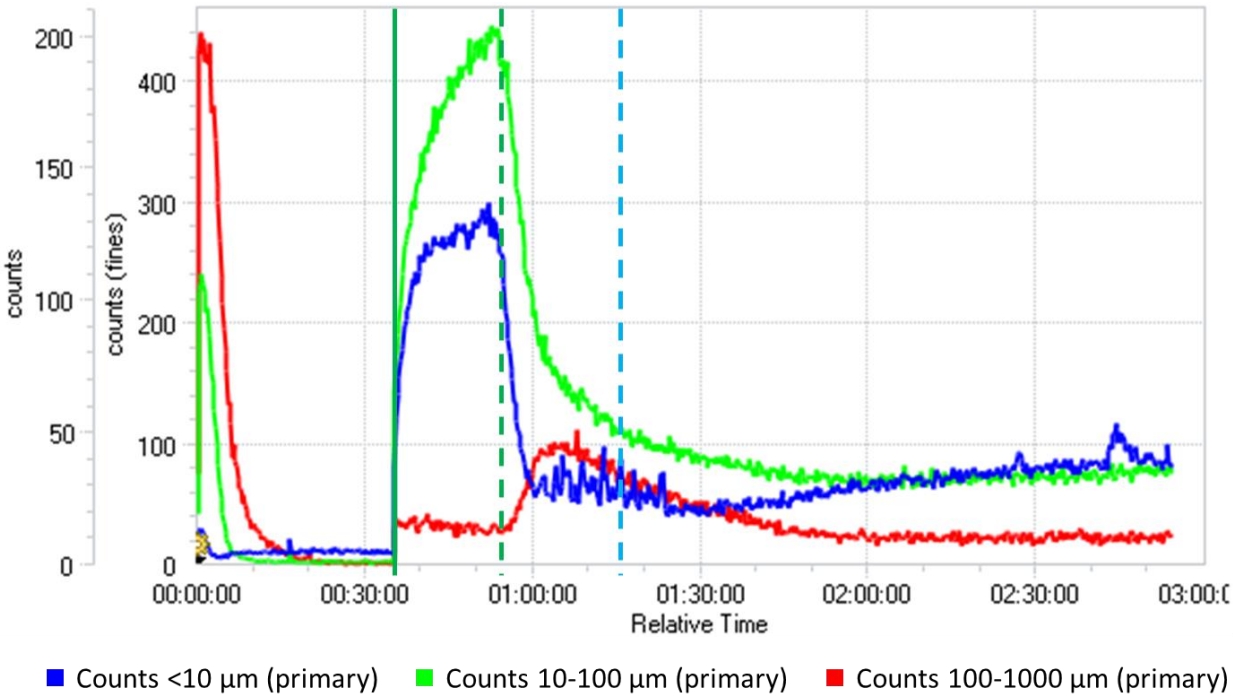

Figure 9.23: FBRM trace obtained from the 20 % UBA form I seeded Easymax cooling crystallisation of UBA from IPA, 1 °C min^{-1} cooling rate. Solid green line shows point of seed addition, dashed green line shows end of seed hold and the dashed blue line shows the point at which the system reaches approximately 40 °C.

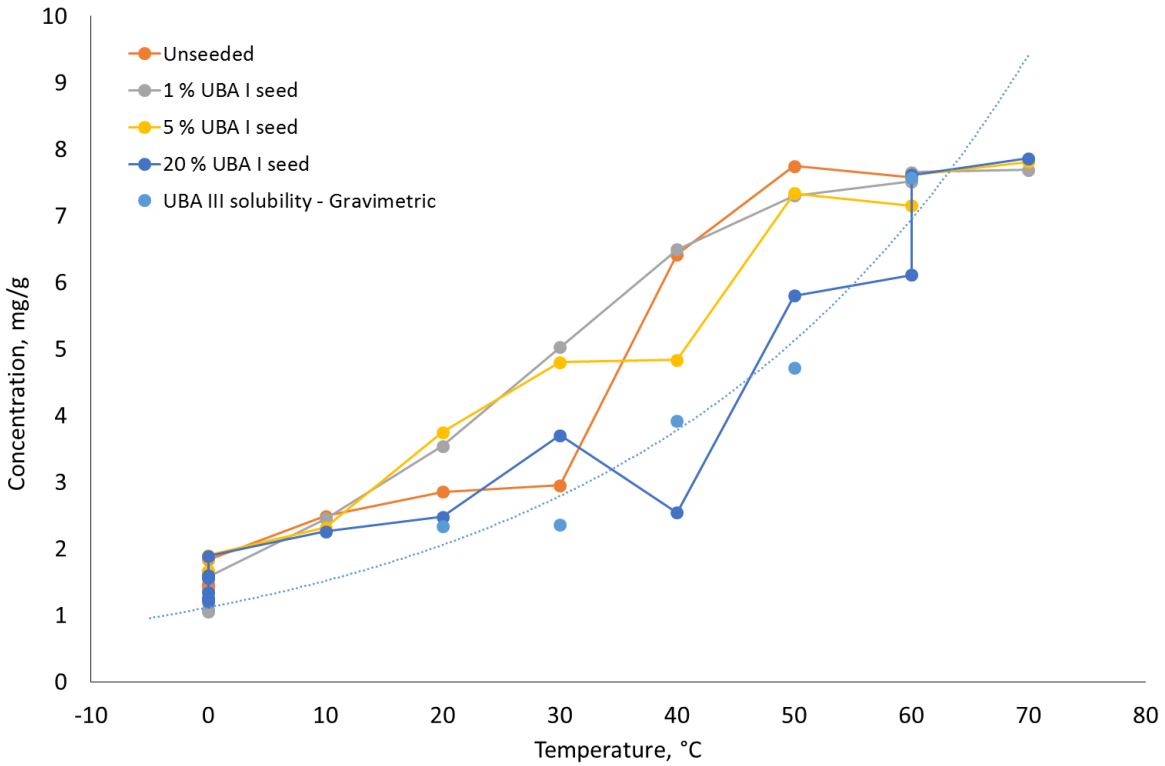

Figure 9.24: Concentration profile of UBA form I seeded and unseeded Easymax cooling crystallisation of UBA from IPA, 1 °C min^{-1} cooling rate.

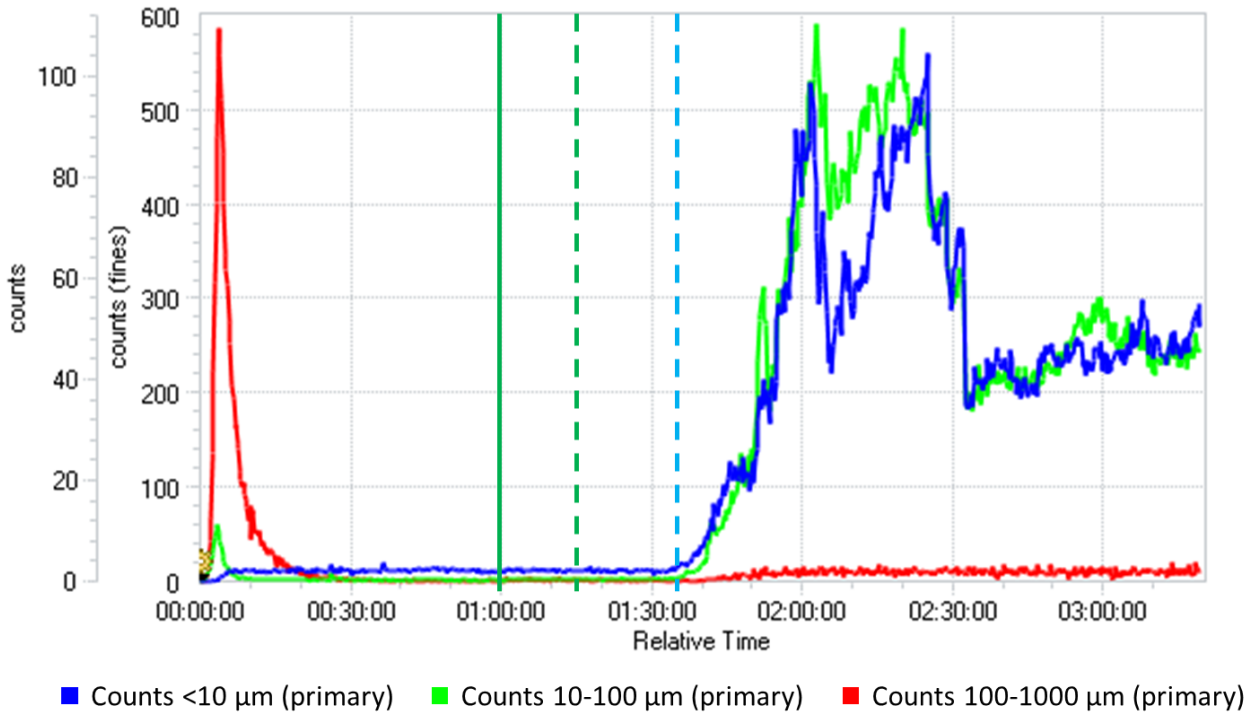

Figure 9.25: FBRM trace obtained from the 1 % UBA form III seeded Easymax cooling crystallisation of UBA from IPA, 1 °C min^{-1} cooling rate. Solid green line shows point of seed addition, dashed green line shows end of seed hold and the dashed blue line shows nucleation event.

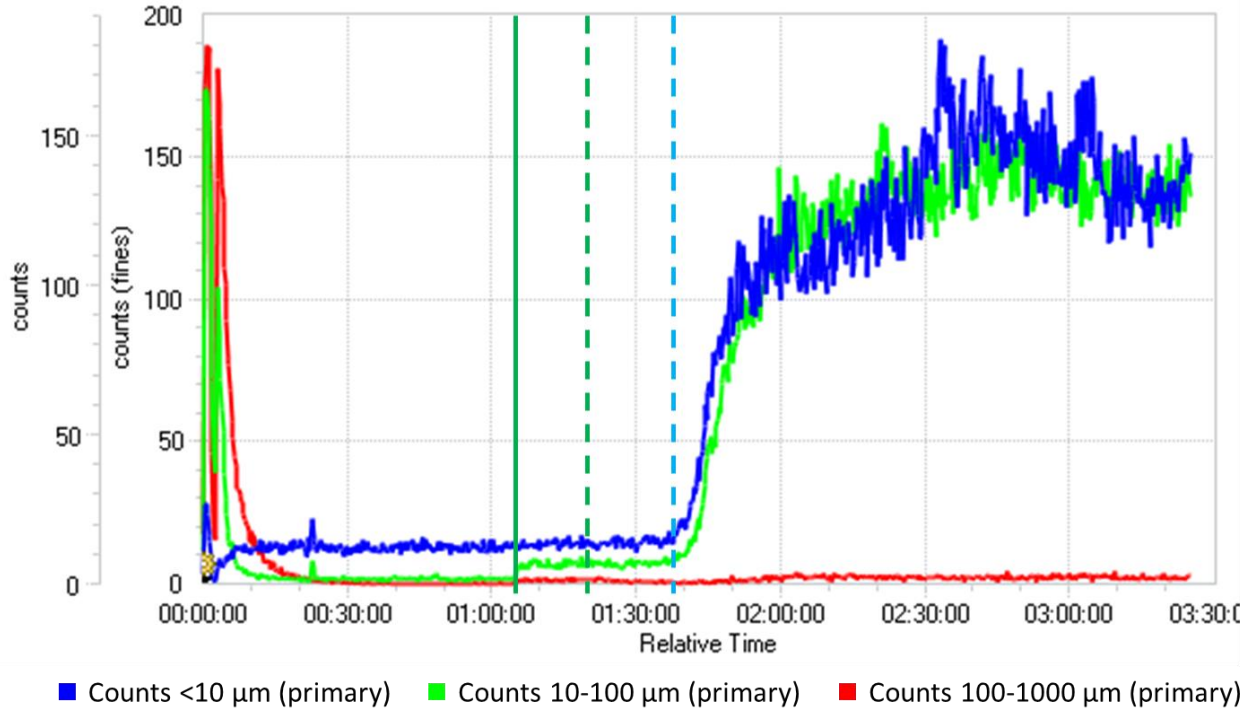

Figure 9.26: FBRM trace obtained from the 5 % UBA form III seeded Easymax cooling crystallisation of UBA from IPA, 1 °C min^{-1} cooling rate. Solid green line shows point of seed addition, dashed green line shows end of seed hold and the dashed blue line shows nucleation event.

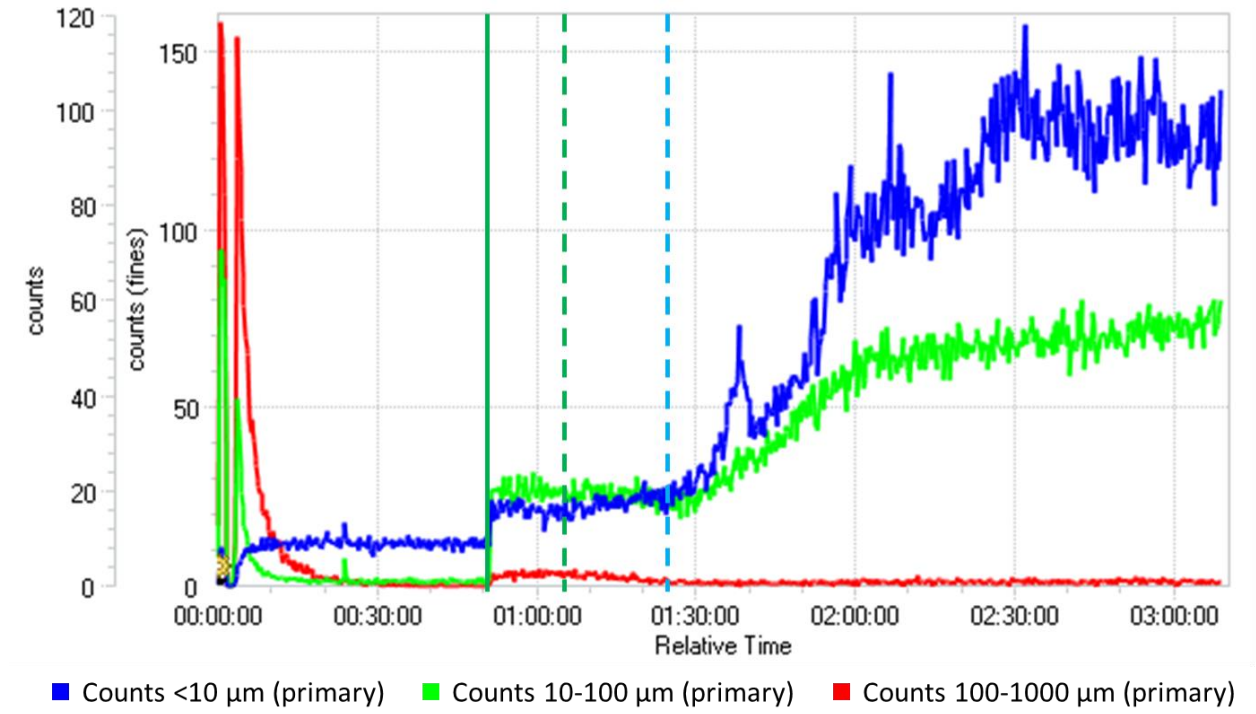

Figure 9.27: FBRM trace obtained from the 5 % UBA form III seeded Easymax cooling crystallisation of UBA from IPA, 1 °C min^{-1} cooling rate. Solid green line shows point of seed addition, dashed green line shows end of seed hold and the dashed blue line shows nucleation event.

9.4 Chapter 6 Appendix

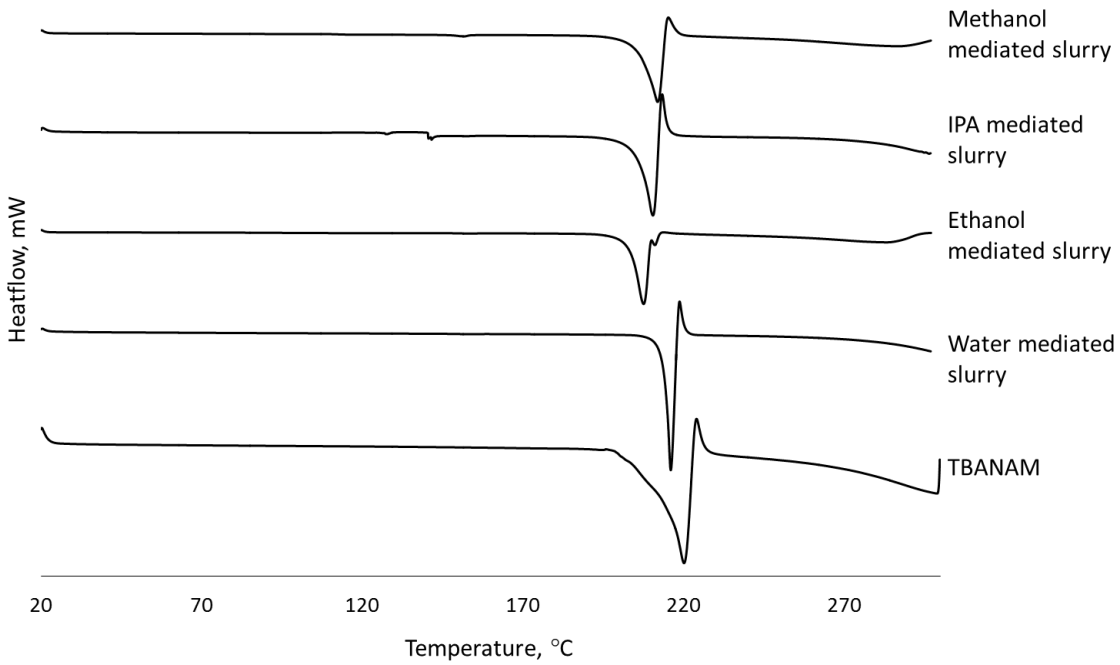

Figure 9.28: DSC traces for thiobarbituric acid isonicotinamide slurry products.